PB2002-100073

Fundamental Properties of Asphalts and Modified Asphalts, Volume 1: Interpretive Report

FHWA-RD-99-212

October 2001

REPRODUCED BY:
U.S. Department of Commerce
National Technical Information Service
Springfield, Virginia 22161

NTIS

FOREWORD

Public Law 102-240, the Intermodal Surface Transportation Efficiency Act (ISTEA) of 1991, directed the Federal Highway Administration in Section 6016 to enter into a 5-year contract research program with the Western Research Institute (WRI) of the University of Wyoming. The title of this research program is Fundamental Properties of Asphalts and Modified Asphalts, Contract No. DTFH61-92-C-00170. As part of this contract, "Fundamental Properties of Asphalts and Modified Asphalts – Volume I – Interpretive Report" is hereby presented.

This report presents the results of a comprehensive investigation of the physical and organic chemistry, and the chemical reactions of a wide variety of petroleum asphalts. Petroleum asphalts, even those of the same PG grade, have been shown to react with oxygen (air), water and aggregate differentially. This results in roadway asphalts developing widely variable physical properties with the passage of time. The primary mission was to identify those compositional factors that affect Long Term Pavement Performance (LTPP)—factors which are not part of the current Superpave® binder specification. New test methods that were developed during this project are reported in Volume II of this report. This report is of interest to asphalt users who want to improve the selection of asphalts for roadway construction, to producers to improve the predictability of their products, and to highway research personnel who seek to develop more distinctive test methods to classify asphalts by their long-term performance characteristics.

T. Paul Teng, P.E.
Director, Office of Infrastructure
Research and Development

NOTICE

This document is disseminated under the sponsorship of the Department of Transportation in the interest of information exchange. The United States Government assumes no liability for its contents or use thereof. This report does not constitute a standard, specification, or regulation.

The United States Government does not endorse products or manufacturers. Trade and manufacturers' names appear in this report only because they are considered essential to the object of the document.

Technical Report Documentation Page

1. Report No.	2. Government Accession No.	3. Recipient's Catalog No.
FHWA-RD-99-212		

4. Title and Subtitle

FUNDAMENTAL PROPERTIES OF ASPHALTS AND MODIFIED ASPHALTS
VOLUME I INTERPRETIVE REPORT

5. Report Date
October 2001

6. Performing Organization Code

8. Performing Organization Report No.

7. Author(s)
Authors listed below abstract

9. Performing Organization Name and Address
WESTERN RESEARCH INSTITUTE
365 North 9th Street
Laramie, WY 82072-3380

10. Work Unit No. (TRAIS)

11. Contract or Grant No.
DTFH61-92C-00170

12. Sponsoring Agency Name and Address
Special Projects Division, Federal Highway Administration
Turner-Fairbank Highway Research Center
6300 Georgetown Pike
McLean, VA 22101-2296

13. Type of Report and Period Covered
Final Report
August 1992-December 1998

14. Sponsoring Agency Code

15. Supplementary Notes
Contracting Officer's Technical Representative (COTR) - Dr. Ernest J. Bastian, Jr., HRDI-11

16. Abstract

The Superpave® binder specification developed during the Strategic Highway Research Program (SHRP) from 1987-93 classifies construction grade asphalts into rheologically similar groups. All asphalts in a given grade have the same rheological properties to within 6°C. The mission of this project was to improve the understanding of the expected performance of petroleum asphalts under service conditions. These conditions include physical behavior of thin asphalt films in contact with aggregate, rheology and oxidative aging of wet asphalt, behavior of asphalt after extended aging, and propensity of asphalt films to reconsolidate ("heal") after microcracking. These phenomena are not described by the current binder specification. The results of said exposures are included in this document and have been used to produce a comprehensive chemical model of petroleum asphalt. Finally, the results have been used to develop new analytical methods that improve the capability to predict performance of asphalt in roadway service. These 16 new tests are described in Volume II of this report.

This volume is the first in a series. The other volume in the series is:
FHWA-RD-99-213 Volume II: Final Report: New Methods

Authors: Raymond E. Robertson, Jan F. Branthaver, P. Michael Harnsberger, J. Claine Petersen, Samuel M. Dorrence, John F. McKay, T. Fred Turner, A. Troy Pauli, Shin-Che Huang, Jung-Do Huh, Jane E. Tauer, Kenneth P. Thomas, Daniel A. Netzel, Francis P. Miknis, Theresa Williams, John J. Duvall, F. Alan Barbour, and Christine Wright

17. Key Words	18. Distribution Statement
Asphalt, aggregate, asphalt model, aging, age hardening, oxidation, microdamage healing, service conditions, performance predictive tests, low temperature and fatigue cracking, permanent deformation and moisture damage.	No restrictions. This document is available to the public through the National Technical Information Service, Springfield, Virginia 22161.

19. Security Classif. (of this report)	20. Security Classif. (of this page)	21. No. of Pages	22. Price
Unclassified	Unclassified	496	

SI* (MODERN METRIC) CONVERSION FACTORS

APPROXIMATE CONVERSIONS TO SI UNITS

Symbol	When You Know	Multiply By	To Find	Symbol
	LENGTH			
in	inches	25.4	millimeters	mm
ft	feet	0.305	meters	m
yd	yards	0.914	meters	m
mi	miles	1.61	kilometers	km
	AREA			
in^2	square inches	645.2	square millimeters	mm^2
ft^2	square feet	0.093	square meters	m^2
yd^2	square yards	0.836	square meters	m^2
ac	acres	0.405	hectares	ha
mi^2	square miles	2.59	square kilometers	km^2
	VOLUME			
fl oz	fluid ounces	29.57	milliliters	mL
gal	gallons	3.785	liters	L
ft^3	cubic feet	0.028	cubic meters	m^3
yd^3	cubic yards	0.765	cubic meters	m^3
NOTE: Volumes greater than 1000 l shall be shown in m^3.				
	MASS			
oz	ounces	28.35	grams	g
lb	pounds	0.454	kilograms	kg
T	short tons (2000 lb)	0.907	megagrams (or "metric ton")	Mg (or "t")
	TEMPERATURE (exact)			
°F	Fahrenheit temperature	5(F-32)/9 or (F-32)/1.8	Celcius temperature	°C
	ILLUMINATION			
fc	foot-candles	10.76	lux	lx
fl	foot-Lamberts	3.426	candela/m^2	cd/m^2
	FORCE and PRESSURE or STRESS			
lbf	poundforce	4.45	newtons	N
lbf/in^2	poundforce per square inch	6.89	kilopascals	kPa

APPROXIMATE CONVERSIONS FROM SI UNITS

Symbol	When You Know	Multiply By	To Find	Symbol
	LENGTH			
mm	millimeters	0.039	inches	in
m	meters	3.28	feet	ft
m	meters	1.09	yards	yd
km	kilometers	0.621	miles	mi
	AREA			
mm^2	square millimeters	0.0016	square inches	in^2
m^2	square meters	10.764	square feet	ft^2
m^2	square meters	1.195	square yards	yd^2
ha	hectares	2.47	acres	ac
km^2	square kilometers	0.386	square miles	mi^2
	VOLUME			
mL	milliliters	0.034	fluid ounces	fl oz
L	liters	0.264	gallons	gal
m^3	cubic meters	35.71	cubic feet	ft^3
m^3	cubic meters	1.307	cubic yards	yd^3
	MASS			
g	grams	0.035	ounces	oz
kg	kilograms	2.202	pounds	lb
Mg (or "t")	megagrams (or "metric ton")	1.103	short tons (2000 lb)	T
	TEMPERATURE (exact)			
°C	Celcius temperature	1.8C + 32	Fahrenheit temperature	°F
	ILLUMINATION			
lx	lux	0.0929	foot-candles	fc
cd/m^2	candela/m^2	0.2919	foot-Lamberts	fl
	FORCE and PRESSURE or STRESS			
N	newtons	0.225	poundforce	lbf
kPa	kilopascals	0.145	poundforce per square inch	lbf/in^2

* SI is the symbol for the International System of Units. Appropriate rounding should be made to comply with Section 4 of ASTM E380.

(Revised September 1993)

TABLE OF CONTENTS

Page

CHAPTER 1: THE RELATIONSHIP OF ASPHALT COMPOSITIONAL PROPERTIES WITH PERFORMANCE-RELATED PHYSICAL PROPERTIES PRIOR TO 1993 1

SYNOPSIS 1
SUMMARY OF PRE-STRATEGIC HIGHWAY RESEARCH PROGRAM RESEARCH ON ASPHALT COMPOSITION 1
ASPHALT SUPPLY LINE HISTORY 13
WORK IN STRATEGIC HIGHWAY RESEARCH PROGRAM—SIGNIFICANT FINDINGS 16
REFERENCES 19

CHAPTER 2: OBJECTIVES AND SUMMARY OF ACCOMPLISHMENTS 23

OBJECTIVES OF THIS PROJECT 23
SUMMARY OF ACCOMPLISHMENTS DURING THIS PROJECT 24

CHAPTER 3: DEVELOPMENTS IN MODEL OF ASPHALT STRUCTURE SINCE STRATEGIC HIGHWAY RESEARCH PROGRAM 27

SYNOPSIS 27
INTRODUCTION TO DISPERSED SYSTEMS 28
Equations Developed for Model Systems 28
Studies of Petroleum Resids by Storm, Sheu, and Associates 34
Relationship of Relative Viscosity of Asphalts with Compatibility 38
DESCRIPTION OF SEPARATION METHODS FOR ASPHALTS 52
General Considerations 52
Solvent Precipitation Separations 53
Separations Based on Molecular Size 54
Separations Based on Polarity, Acidity, and Basicity 55
Comparison of Three Separation Methods 58
SEPARATION, CHARACTERIZATION, AND REASSEMBLY OF ASPHALT FRACTIONS 61
Fractionation of Strongest Molecular Associations 61
Reassembly of Asphalt Size Exclusion Fractions 65
Studies of Asphalt Ion Exchange Chromatography Neutral Fractions 69
Studies of Waxes in Asphalts 75

TABLE OF CONTENTS (continued)

Page

Asphaltene-Maltene Crossblends 78
Supercritical Fluid Extractions 84
SUMMARY OF SEPARATION RESULTS 129
LOW TEMPERATURE PROPERTIES 130
Introduction to Low Temperature Properties 130
Differential Scanning Calorimetry and Modulated Differential Scanning Calorimetry 131
Glass Transition Properties 132
Measurements on Strategic Highway Research Program Core Asphalts 133
Measurements on Asphalt Components 135
Low Temperature Molecular Dynamics of Asphalts as Determined by Solid State Nuclear Magnetic Resonance 143
Temperature Profile of Molecular Mobility in Asphalts 145
Crystalline, Interfacial, and Amorphous Phases 147
SUMMARY OF CHAPTER 3 177
REFERENCES 180

CHAPTER 4: OXIDATION AND OXIDATIVE AGING 187

SYNOPSIS 187
INTRODUCTION 188
OXIDATION AND ITS EFFECTS ON PERFORMANCE-RELATED PHYSICAL PROPERTIES 190
Microstructural Model of Asphalt Composition as Related to Asphalt Oxidation 190
Effects of Temperature and Oxygen Pressure on Oxidation Kinetics 191
Effects of Oxidation Products on Physical Properties 195
Effects of Aggregate on Asphalt Oxidation 203
ASPHALT OXIDATION MECHANISMS 225
Historical Background 225
Effects of Asphalt Composition on Oxidation Kinetics 227
Oxidation Kinetics in the Pavement Temperature Range 228
Proposed Oxidation Mechanisms 229
NUCLEAR MAGNETIC RESONANCE IMAGING INVESTIGATION OF ASPHALTENE PRECIPITATION IN AGED AND UNAGED ASPHALTS 248
USE OF INVERSE GAS LIQUID CHROMATOGRAPHY TO STUDY ASPHALT OXIDATIVE AGING 260

TABLE OF CONTENTS (continued)

Page

HIGH PRESSURE LIQUID CHROMATOGRAPHY USING SIZE EXCLUSION RESINS TO ANALYZE OXIDIZED ASPHALTS 267
REFERENCES 272

CHAPTER 5: ASPHALT IN CONTACT WITH AGGREGATE AND WATER 277

SYNOPSIS 277
STERIC HARDENING OF ASPHALTS AND MASTICS 278
SLIDING PLATE MICROVISCOMETER STUDIES OF ASPHALT-AGGREGATE INTERACTIONS 295
INTERFACIAL ADHESION STRENGTH OF MASTICS MEASURED BY PENETRATION 308
THE IMPACT OF MOISTURE ON ASPHALT RHEOLOGY AND AGING 313
Treatment of Asphalts with Water 314
Infrared Reflectance Spectroscopic Study 318
ENVIRONMENTAL SCANNING ELECTRON MICROSCOPE OBSERVATIONS OF ASPHALT-WATER AND ASPHALT-AGGREGATE-WATER INTERACTIONS 326
Use of the ESEM to Study Water Penetration into Neat and Aged Asphalt Surfaces 326
Use of the ESEM to Study Asphalt-Aggregate Interfaces before and after Freeze-Thaw Treatments 329
NUCLEAR MAGNETIC RESONANCE IMAGING INVESTIGATION OF ASPHALT-WATER-AGGREGATE INTERACTIONS 344
TIME-DEPENDENT MOLECULAR STRUCTURING 350
PYRIDINE DESORPTION TEST FOR MOISTURE SUSCEPTIBILITY (STRIPPING) OF AGGREGATES 355
REFERENCES 379

CHAPTER 6: THE EVALUATION OF MODIFIED ASPHALTS 387

SYNOPSIS 387
SHALE OIL-MODIFIED ASPHALT TEST STRIP 388
SHRP (AASHTO) Testing and Evaluation of Original Paving Materials 390
Continued Monitoring of the Pavement Sections 393
Summary of the Environmental Analyses 396

TABLE OF CONTENTS (continued)

Page

CRUMB RUBBER-MODIFIED ASPHALT 406
Evaluation of Variables that Are Related to the Use of Crumb Rubber 406
Nuclear Magnetic Resonance Imaging of Crumb Rubber-Modified Asphalt 412
REFERENCES 431

CHAPTER 7: PREDICTION OF FATIGUE IN PAVEMENT 435
UTILITY OF MICROMECHANICAL ANALYSIS TO ASPHALT CONCRETE PAVEMENT DESIGN 435
DEVELOPMENT OF A MECHANISTIC FATIGUE PREDICTION MODEL FOR AGING ASPHALT-AGGREGATE MIXTURES 442

CHAPTER 8: PREDICTION OF PERFORMANCE 447
SYNOPSIS 447
INTRODUCTION 447
THERMAL CRACKING 447
MOISTURE DAMAGE 450
PERMANENT DEFORMATION 452
FATIGUE 453
SUMMARY 454
REFERENCES 457

CHAPTER 9: VALIDATION 459

PROTECTED UNDER INTERNATIONAL COPYRIGHT
ALL RIGHTS RESERVED
NATIONAL TECHNICAL INFORMATION SERVICE
U.S. DEPARTMENT OF COMMERCE

Reproduced from best available copy.

LIST OF FIGURES

Figure		Page
3-1	$K = K_F K_S$ values calculated from Pal-Rhodes equation (equation 3-9) versus Heithaus parameters p_a and P	50
3-2	Idealized diagram of asphaltene molecular associations and floc particles	51
3-3	Structural formulae of alkanes used in the precipitation of asphaltenes	59
3-4	Flow sheet for separation of asphalts into neutral, acid, base, and amphoteric fractions by ion exchange chromatography	60
3-5	Flow sheet for size exclusion chromatography separation of asphalts	115
3-6	Black plot of G* vs. δ for mixtures of SEC Fraction-II of AAA-1 (78.3%) with SEC Fraction-I (21.7%) of eight SHRP core asphalts	116
3-7	Black plot of G* vs. δ for mixtures of SEC Fraction-II of AAB-1 (79.2%) with SEC Fraction-I (20.8%) of eight SHRP core asphalts	116
3-8	Black plot of G* vs. δ for mixtures of SEC Fraction-II of AAC-1 (86.4%) with SEC Fraction-I (13.6%) of eight SHRP core asphalts	117
3-9	Black plot of G* vs. δ for mixtures of SEC Fraction-II of AAD-1 (78.8%) with SEC Fraction-I (21.2%) of eight SHRP core asphalts	117
3-10	Black plot of G* vs. δ for mixtures of SEC Fraction-II of AAF-1 (86.7%) with SEC Fraction-I (13.3%) of eight SHRP core asphalts	118
3-11	Black plot of G* vs. δ for mixtures of SEC Fraction-II of AAG-1 (88.8%) with SEC Fraction-I (11.2%) of eight SHRP core asphalts	118
3-12	Black plot of G* vs. δ for mixtures of SEC Fraction-II of AAK-1 (75.2%) with SEC Fraction-I (24.8%) of eight SHRP core asphalts	119
3-13	IR spectra of: (a) IEC neutrals of AAD-1; (b) wax from AAD-1 neutrals; and (c) dewaxed IEC neutrals of AAD-1	120
3-14	G*sin δ 25°C vs. G*/sin δ 60°C at 10.0 rad/s for unaged and aged crossblended mixtures of maltenes and asphaltenes of AAD-1 and AAF-1	121

LIST OF FIGURES (continued)

Figure		Page
3-15	Black plot of G* vs. δ at 25°C and 10.0 rad/s for unaged and aged crossblended mixtures of maltenes and asphaltenes of AAD-1 and AAF-1	121
3-16	Black plot of G* vs. δ at 60°C and 10.0 rad/s for unaged and aged crossblended mixtures of maltenes and asphaltenes of AAD-1 and AAF-1	122
3-17	G*sin δ 25°C vs. G*/sin δ 60°C for unaged and aged crossblended mixtures of maltenes and asphaltenes of AAD-1 and AAG-1	122
3-18	Black plot of G* vs. δ at 25°C and 10.0 rad/s for unaged and aged crossblended mixtures of maltenes and asphaltenes of AAD-1 and AAG-1	123
3-19	Black plot of G* vs. δ at 60°C and 10 rad/s for unaged and aged crossblended mixtures of maltenes and asphaltenes of AAD-1 and AAG-1	123
3-20	G*sin δ 25°C vs. G*sin δ 60°C for unaged and aged crossblended mixtures of maltenes and asphaltenes of AAF-1 and AAG-1	124
3-21	Black plot of G* vs. δ at 25°C and 10.0 rad/s for unaged and aged crossblended mixtures of maltenes and asphaltenes of AAF-1 and AAG-1	124
3-22	Black plot of G* vs. δ at 60°C and 10.0 rad/s for unaged and aged crossblended mixtures of maltenes and asphaltenes of AAF-1 and AAG-1	125
3-23	Percent of SFE fractions extracted from core asphalts by CO_2 and THF modified CO_2	126
3-24	Heteroatom distribution in fractions obtained by SFE extraction of asphalt-aggregate mixtures and solvent extracts of asphalt-aggregate mixtures after SFE extraction	127
3-25	Comparison of experimental extraction yields with that of linear model based on heteroatom content	128
3-26	Temperatures at which S=300 MPa and m=0.3 as functions of DSC-derived glass transition temperatures	153
3-27	Relationship between wax content of asphalts and whether S or m controls the low-temperature SHRP specification	154

LIST OF FIGURES (continued)

Figure		Page
3-28	Correlation of specification controlling temperature to a linear combination of glass transition temperature and wax or crystallizable fraction	155
3-29	Asphalt fractionation by solvent, molecular size, and polarity	156
3-30	Fox-Flory behavior of IEC neutral fraction	157
3-31	Variation of SEC fraction glass transition temperatures with molecular weight	158
3-32	Glass transition temperatures of SEC Fraction-I/SEC Fraction-II blends	159
3-33	Glass transition parameter changes with asphaltene concentration for five SHRP asphalts	160
3-34	Glass transition temperatures in heptane asphaltene-maltene blends	161
3-35	Glass transition temperature dependence on supercritical fluid extraction pressure	162
3-36	Variation of glass transition temperature of SFE fractions with molecular weight	163
3-37	Crystallizable fractions of waxes, wax-doped asphalts, dewaxed asphalts, and asphalts compared with sample wax contents	164
3-38	Additive behavior of waxes in asphalts	165
3-39	Variations of dopant efficiency as a function of dopant carbon number for asphalt AAG-1	166
3-40	Relationship of asphalt and component glass transition temperatures to viscosity	167
3-41	Glass transition temperature prediction for heptane maltenes, iso-octane maltenes, SEC Fraction-II, and two weak neutral fractions based on polar component concentrations	168
3-42	Correlation of glass transition temperatures of heptane maltenes, iso-octane maltenes, SEC Fraction-II, weak neutrals, and neutrals with IEC polar components	169

LIST OF FIGURES (continued)

Figure		Page
3-43	Schematic representation of the types of molecular motions in a complex "asphalt-like" molecule	170
3-44	Carbon-13 CP/MAS NMR signal enhancement as a function of temperature for asphalts AAA-1, AAB-1, and AAM-1	171
3-45	NMR molecular-mobility/temperature profile and DSC plots of the total carbons in asphalt AAA-1	172
3-46	NMR molecular-mobility/temperature profile and DSC plots of the total carbons in asphalt AAB-1	173
3-47	NMR molecular-mobility/temperature profile and DSC plots of the total carbons in asphalt AAM-1	174
3-48	CP/MAS carbon-13 NMR spectrum of the aliphatic carbons in asphalt AAM-1 at 20°C	175
3-49	Carbon-13 dipolar-dephasing NMR relaxation rates in asphalts AAA-1, AAB-1, and AAM-1 at -45°C: (a) terminal methyl carbons (14 ppm), (b) methylene carbons (30 ppm) in the interfacial and amorphous phases, (c) methylene carbons (32 ppm) in the crystalline phase	176
4-1	Pictorial diagrams of the microstructural model of asphalt	210
4-2	Diagrammatic representation of the effects of composition on the physical properties of asphalts	210
4-3	Comparison of TFO/PAV and TFAAT aging of asphalt AAG-1	211
4-4	Comparison of TFO/PAV and TFAAT aging of asphalt AAM-1	212
4-5	Comparison of TFO/PAV and TFAAT aging of asphalt AAF-1	213
4-6	Comparison of TFO/PAV and TFAAT aging of asphalt AAA-1	214
4-7	Effects of association of polar components on effective molecular weight	215
4-8	Comparison of TFO/PAV and TFAAT aging of asphalt AAG-1	216

LIST OF FIGURES (continued)

Figure		Page
4-9	Comparison of TFO/PAV and TFAAT aging of asphalt AAM-1	217
4-10	Comparison of TFO/PAV and TFAAT aging of asphalt AAF-1	218
4-11	Comparison of TFO/PAV and TFAAT aging of asphalt AAA-1	219
4-12	Effect of temperature on the viscosity sensitivity of PAV oxidized asphalt AAD-1 to ketone oxidation products	220
4-13	Bending beam stiffness values of 60, 80, and 100°C TFO/PAV-aged asphalt AAG-1	221
4-14	Bending beam m-values of 60, 80, and 100°C TFO/PAV-aged asphalt AAG-1	221
4-15	Bending beam stiffness values of 60, 80, and 100°C TFO/PAV-aged asphalt AAM-1	222
4-16	Bending beam m-values of 60, 80, and 100°C TFO/PAV-aged asphalt AAM-1	222
4-17	Bending beam stiffness values of 60, 80, and 100°C TFO/PAV-aged asphalt AAF-1	223
4-18	Bending beam m-values of 60, 80, and 100°C TFO/PAV-aged asphalt AAF-1	223
4-19	Bending beam stiffness values of 60, 80, and 100°C TFO/PAV-aged asphalt AAA-1	224
4-20	Bending beam m-values of 60, 80, and 100°C TFO/PAV-aged asphalt AAA-1	224
4-21	Ketones and sulfoxides formed during and after oxidation spurt on TFO/PAV oxidation at 2.07 MPa (20 atmospheres) pressure	238
4-22	Ketones and sulfoxides formed during TFO/PAV oxidation at 60°C and 100°C at 2.07 MPa (20 atmospheres) pressure	239
4-23	Ketones and sulfoxides formed during and after oxidation spurt on TFAAT oxidation at atmospheric pressure	240
4-24	Ketones and sulfoxides formed during TFAAT oxidation at 85°C and 113°C at atmospheric pressure	241

LIST OF FIGURES (continued)

Figure		Page
4-25	Kinetic data for the formation of ketones and sulfoxides in Shell Wood River Asphalt during thin film ambient pressure oxidation at 45°C	242
4-26	Reaction sequences for oxidation of proposed polycyclic hydroaromatics in asphalt during oxidation spurt, illustrated for dihydroanthracene	243
4-27	Possible reaction sequences for ketone and sulfoxide formation during oxidation of asphalt benzylic carbon	244
4-28	Comparison of kinetics of ketone formation in asphalt AAG-1 from PAV oxidation at 60°C with TFAAT oxidation at 130°C	245
4-29	Comparison of kinetics of ketone formation in asphalt AAD-1 from PAV oxidation at 60°C with TFAAT oxidation at 130°C	246
4-30	Thin film GC column oxidation of Boscan asphalt with and without triphenyltin hydroxide	247
4-31	Illustration of slice geometry used in magnetic resonance imaging experiments	253
4-32	NMR images illustrating effects of aging and stirring on asphaltene precipitation. Times listed are settling times and refer to the time elapsed between addition of isooctane and the time when the image was recorded	254
4-33	NMR images illustrating time evolution of interface layer in aged asphalt. Times listed are settling times	255
4-34	Radial NMR images at different depths illustrating spherical globules in the solvent interface layer	256
4-35	NMR images illustrating the effect of aging on asphaltene settling	257
4-36	NMR images of aged asphalts after stirring. AAK-1 (top row) and AAE-1 (bottom row). In (a) asphalt AAK-1 had been setting undisturbed for 2,500 hr after addition of isooctane. In (d) asphalt AAE-1 had been setting undisturbed for 1,488 hr after addition of isooctane. The images in (b) and (e) were taken immediately after the surfaces of these samples were disrupted by stirring. The images in (c) and (f) were taken 24 hr after the samples were stirred.	258

LIST OF FIGURES (continued)

Figure		Page
4-37	NMR images illustrating breakup of interface layer with stirring. a), b) Longitudinal cross-section images at different positions, c), d) Radial cross-section images at different positions	259
4-38	Butanol interaction coefficient of 6 hour column aged asphalts vs. titratable total base in TFOT/POV (60°C, 1,000 hour, 300 psi oxygen) residue	263
4-39	Phenol interaction coefficient of 6 hour column aged asphalts vs. the amount of titratable weak base increase due to TFOT/POV (60°C, 1,000 hour, 300 psi oxygen)	264
4-40	Phenol interaction coefficient of 6 hour column aged asphalt vs. sulfoxide concentration in TFOT/POV (80°C, 144 hour, 300 psi oxygen) residue	265
4-41	Amount of titratable weak base formed by TFOT/POV (60°C, 1,000 hour, 300 psi oxygen) vs. the amount of sulfur in the unaged asphalt in sulfide form	266
4-42	HPLC/SEC DRID chromatograms of asphalt AAF-1 TFO/PAV aged for 0, 12, 20, or 36 hours with molecular weights estimated from the calibration curve; gravimetrically determined F-I cutpoint = 22.59 min	270
4-43	HPLC/SEC DRID chromatograms of asphalt AAK-1 TFO/PAV aged for 0, 12, 20, or 36 hours with molecular weights estimated from the calibration curve; gravimetrically determined F-I cutpoint = 22.95 min	270
4-44	Integrals, normalized to a total integral of 100,000, versus aging time for asphalt AAF-1 HPLC/SEC fractions; F-I cutpoint used is from DRID area % equal to preparative SEC weight % F-I	271
4-45	Integrals, normalized to a total integral of 100,000, versus aging time for asphalt AAM-1 HPLC/SEC fractions; F-I cutpoint used is from DRID area % equal to preparative SEC weight % F-I	271
5-1	Normalized G* data at 0.50 rad/s for unoxidized asphalt AAD-1 at 25°C	285
5-2	Normalized G*sin delta data at 10 rad/s for RTFO/PAV-oxidized asphalt AAM-1 at 25°C	286
5-3	G* data at 0.50 rad/s for asphalt AAG-1 at three levels of oxidation for isothermal hardening and heat treatment	287

LIST OF FIGURES (continued)

Figure		Page
5-4	G* data at 0.50 rad/s for asphalt AAD-1 at three levels of oxidation for isothermal hardening and heat treatment	288
5-5	G* data at 0.50 rad/s for asphalt AAK-1 at three levels of oxidation for isothermal hardening and heat treatment	289
5-6	G* data at 0.50 rad/s for asphalt AAM-1 at three levels of oxidation for isothermal hardening and heat treatment	290
5-7	Compression strength of unoxidized and oxidized mastics RD-AAM-1 as a function of time	291
5-8	Modulus of unoxidized and oxidized mastics RC-AAD-1 as a function of time	292
5-9	Compression strength at failure of mastic briquettes prepared from aggregates RB, RC, RD and unoxidized asphalt AAD-1 as a function of time	293
5-10	Compression strength at failure of mastic briquettes prepared from aggregates RB, RC, RD and oxidized asphalt AAM-1 as a function of time	294
5-11	Viscosity versus shear rate relationship for AAD-1 at 25°C using glass plates and limestone plates at different film thicknesses	301
5-12	Viscosity versus shear rate relationship for AAG-1 at 25°C using glass plates and limestone plates at different film thicknesses	302
5-13	Comparison of viscosity measurements by glass sliding plate (SPM) and dynamic shear rheometer (DSR) using 10 SHRP asphalts at 25°C	303
5-14	Viscosity versus film thickness for asphalt AAD-1 with both glass plates and limestone plates at 25°C	303
5-15	Viscosity versus film thickness for asphalt AAK-1 with both glass plates and limestone plates at 25°C	304
5-16	Viscosity versus film thickness for asphalt AAG-1 with both glass plates and limestone plates at 25°C	304
5-17	Interaction index at different film thicknesses for SHRP core asphalts AAD-1, AAG-1, and AAK-1	305

LIST OF FIGURES (continued)

Figure		Page
5-18	Viscosity versus film thickness for asphalt AAD-1 with both glass plates and limestone plates before and after storage at 25°C	306
5-19	Viscosity versus film thickness for asphalt AAG-1 with both glass plates and limestone plates before and after storage at 25°C	306
5-20	Hardening index for SHRP core asphalts AAD-1 and AAG-1 over extended time period of storage at 25°C	307
5-21	Penetration test data for mastic made of 17 mass percent AAA-1 (PG 58-28) and 83 mass percent, – #200 RD filler at 40°C	310
5-22	Comparison of the penetration test data at 25°C for unaged AAD-1 (PG 58-28), AAG-1 (originally graded as PG 58-10, now graded PG 64-10) and AAM-1 (PG 64-10) mastics made of 85 mass percent, – #200 RD filler	311
5-23	Comparison of the penetration test data at 40°C for unaged AAD-1 (PG 58-28), AAG-1 (originally graded as PG 58-10, now graded PG 64-10) and AAM-1 (PG 64-10) mastics made of 85 mass percent, – #200 RD filler	312
5-24	The change in G* with time for asphalt AAD-1 following various treatments	321
5-25	The impact of the environment at 60°C on G* of unaged AAD-1, AAG-1, and AAM-1	321
5-26	The impact of the environment at 60°C on G* of RTFO/PAV-aged AAD-1, AAG-1, and AAM-1	322
5-27	A comparison of the normalized percent change in G* with time for RTFO/ PAV-aged samples. All samples stored at 60°C	322
5-28	The thickness of the water layer at the asphalt/silicious substrate interface as a function of exposure time in water for unaged asphalts (from Nguyen et al. [1994])	323
5-29	A plot showing the amount of water incorporated into various unaged asphalts stored at 60°C	323
5-30	A plot showing the amount of water incorporated into several RTFO/PAV-aged asphalts stored at 60°C	324

LIST OF FIGURES (continued)

Figure		Page
5-31	The impact of the presence of water during PAV aging at 80°C on G* of RTFO-aged SHRP asphalts	324
5-32	A plot of the ratios of the amounts of carbonyl versus alkanes with time for unaged asphalts AAD-1 and AAG-1. (The asphalts were stored in argon.)	325
5-33	A plot of the ratios of the amounts of sulfoxide versus alkanes with time for unaged asphalts AAD-1 and AAG-1. (The asphalts were stored in argon.)	325
5-34	ESEM photomicrographs of cross-sections of asphalt AAM-1 showing water penetration into the neat sample: (a) before soaking in water at 50°C (122°F), (b) after 8 weeks, (c) after 16 weeks, and (d) RTFO PAV aged sample after 16 weeks	334
5-35	ESEM photomicrographs of cross-sections of asphalt AAA-1 showing water penetration into the RTFO PAV aged sample after soaking in water at 50°C (122°F) for (a) 2 weeks, (b) 8 weeks, and (c) 16 weeks, and (d) the neat sample after 14 weeks	335
5-36	ESEM photomicrographs of cross-sections of asphalt AAB-1 showing water penetration after soaking in water at 50°C (122°F): (a) neat after 4 weeks and (b) 8 weeks, and (c) RTFO PAV aged after 8 weeks and (d) 16 weeks	336
5-37	ESEM photomicrographs of cross-sections of asphalt AAG-1 showing water penetration after soaking in water at 50°C (122°F): neat for (a) 4 weeks and (b) 16 weeks, and RTFO PAV aged for (c) 8 weeks and (d) 16 weeks	337
5-38	ESEM photomicrographs showing interface of aggregate RD and asphalt AAD-1 before and after freeze-thaw cycling: (a) dry RD before, (b) dry RD after 10 cycles, (c) wet RD before, and (d) wet RD after 10 cycles	338
5-39	ESEM photomicrographs showing interface of aggregate RD and asphalt AAG-1 before and after freeze-thaw cycling: (a) wet RD before, (b) wet RD after one cycle, (c) dry RD before, and (d) dry RD after one cycle	339
5-40	ESEM photomicrographs showing interface of wet aggregate RD and asphalt AAM-1 (a) before and after (b) 1, (c) 3, and (d) 10 freeze-thaw cycles.	340
5-41	ESEM photomicrographs showing interface of dry aggregate RA and asphalt AAD-1 (a) before and after (b) 3, (c) 4, and (d) 10 freeze-thaw cycles	341

LIST OF FIGURES (continued)

Figure		Page
5-42	ESEM photomicrographs showing interface of aggregate RA and asphalt AAG-1 before and after freeze-thaw cycling: (a) dry RA before, (b) dry RA after one cycle, (c) wet RA after four cycles, and (d) wet RA after five cycles	342
5-43	ESEM photomicrographs showing interface of aggregate RA and asphalt AAM-1 before and after freeze-thaw cycling: (a) wet RA before, (b) wet RA after 1 cycle, (c) dry RA before, and (d) dry RA after 10 cycles.	343
5-44	Spin echo XZ planar images of SHRP asphalt AAA-1 and MRL aggregate RE in water after successive freeze thaw cycles. Images are for slice 4 after: (a) 0, (b) 3, (c) 4, and (d) 7 freeze thaws	347
5-45	Spin echo XZ planar images of SHRP asphalt AAM-1 and MRL aggregate RE in water after successive freeze thaw cycles. Images are of slice 5 after: (a) 0, (b) 4, (c) 6, and (d) 13 freeze thaws	348
5-46	Spin echo XZ planar images of SHRP asphalt AAM-1 and MRL aggregate RE in water after successive freeze thaw cycles. Images are of slice 6 after: (a) 0, (b) 4, (c) 6, and (d) 13 freeze thaws.	349
5-47	Carbon-13 CP/MAS NMR spectra of the aliphatic carbons in asphalt AAM-1: (a) initial spectrum at 20°C, (b) 2 years later at 20°C, (c) heated to 40°C for 4 hours then cooled to 23°C, (d) heated to 90°C for 1/2 hour then cooled to 23°C, and (e) heated to 95°C for 2 hours then cooled to 23°C	353
5-48	Carbon-13 CP/MAS NMR spectra of the aromatic carbons in asphalt AAM-1: (a) initial spectrum at 20°C, (b) 2 years later at 20°C, (c) heated to 40°C for 4 hours then cooled to 23°C, (d) heated to 90°C for 1/2 hour then cooled to 23°C, and (e) heated to 95°C for 2 hours then cooled to 23°C.	354
5-49	Thermal desorption characteristics of nitrogen-containing compounds from 70-80 mesh Idaho Lottman aggregate	370
5-50	Thermal desorption characteristics of nitrogen-containing compounds from 70-80 mesh Colorado Lottman aggregate	371
5-51	Thermal desorption characteristics of nitrogen-containing compounds from 70-80 mesh Arizona Lottman aggregate	372

LIST OF FIGURES (continued)

Figure		Page
5-52	Thermal desorption characteristics of nitrogen-containing compounds from 70-80 mesh Montana Lottman aggregate	373
5-53	Thermal desorption characteristics of nitrogen-containing compounds from 70-80 mesh Virginia Lottman aggregate	374
5-54	Thermal desorption characteristics of nitrogen-containing compounds from 70-80 mesh Georgia Lottman aggregate	375
5-55	Correlation of Lottman II TSR data and pyridine thermally desorbing 470-650°C. R-squared value is 0.50	376
5-56	Correlation of Lottman II TSR data and pyridine/water washed sample desorbing 470-650°C. R-squared value is 0.01	377
5-57	Meq/g of Indole-3-acetic acid consumed after reaction with 5 grams of 11 different SHRP aggregates (80-100 mesh) for 2 days	378
6-1	Aggregate grading chart for the averages of the two mixes used in Grand Teton National Park (NCE data). (The Superpave® gradation requirements are shown.)	398
6-2	Aggregate grading chart for the averages of the two mixes used in Grand Teton National Park (WFLHD data). (The job mix formula target values are shown.)	398
6-3	A plot showing the relationship between oxidation with time (in-service aging) and a rheological property of the asphalts	399
6-4	A plot of the change in G*sin delta of the asphalts versus time in service	399
6-5	The indirect tensile strength (wet) versus the percentage of air voids for cores taken from sections of the two pavements	400
6-6	Average elevation change from the base (1993) for sections C1 and S1 of U.S. 89	401

LIST OF FIGURES (continued)

Figure		Page
6-7	Contour map showing the change in elevation in centimeters for section C1 of U.S. Highway 89 (Base to 1996). The vertical lines denote a 1.8-m (6-ft) wheelpath	402
6-8	Contour map showing the change in elevation in centimeters for section S1 of U.S. Highway 89 (Base to 1996). The vertical lines denote a 1.8-m (6-ft) wheelpath	403
6-9	Crack map for sections C1 and S1, 1995 (C1 is in the southbound and S1 is in the northbound lane).	404
6-10	Crack map for sections C1 and S1 for 1996 (C1 is in the southbound and S1 is in the northbound lane).	405
6-11	Asphalt AAD-1 and CRM1 at 6, 12, and 18% by total weight of binder	418
6-12	Asphalts AAD-1, AAG-1, and AAM-1 with 18% CRM4 by total weight of binder	418
6-13	Asphalt AAG-1 and 18% CRM's or Teflon by total weight of binder	419
6-14	Asphalt AAD-1 and 12% CRM1 by total weight of binder, 60°C data	419
6-15	Asphalt AAG-1 and 12% CRM1 by total weight of binder, 60°C data	420
6-16	Asphalt AAM-1 and 12% CRM1 by total weight of binder, 60°C data	420
6-17a	NMR spectra of natural tire rubber	421
6-17b	NMR spectra of CRM rubber	421
6-18	HPLC/SEC DRID chromatograms of core asphalt AAB-1 with NR, heated for various times	422
6-19	HPLC/SEC DRID chromatograms of asphalt ABD with NR, heated for various times	422
6-20	HPLC/SEC DRID chromatograms of core asphalt AAB-1 with CRM4, heated for various times	423

LIST OF FIGURES (continued)

Figure		Page
6-21	HPLC/SEC DRID chromatograms of asphalt ABD with CRM4, heated for various times	423
6-22	HPLC/SEC DRID chromatograms of unmodified core asphalt AAB-1, heated for various times	424
6-23	HPLC/SEC DRID chromatograms of unmodified asphalt ABD, heated for various times	424
6-24	Shear modulus for asphalt AAB-1, carboxylic acid-modified AAB-1, and CRMA's, 60°C data	425
6-25	Asphalt AAB-1, carboxylic acid-modified AAB-1, and CRMA's stored at 156°C, data measured at 60°C	426
6-26	Asphalt AAB-1, carboxylic acid-modified AAB-1, and CRMA's stored at 200°C, data measured at 60°C	426
6-27	Asphalt AAB-1 with CRM4, and AAB-1 with CRM4 modified with 0.03 molar 9-anthranoic acid stored at 156°C, 60°C data	427
6-28	Asphalt AAB-1 with CRM4, and AAB-1 with CRM4 modified with 0.03 molar stearic acid stored at 156°C, 60°C data	427
6-29	NMR images showing the cross-section of a conical piece of natural tire rubber taken after heating at 170°C for (a) 0, (b) 2, (c) 8, and (d) 24 hr. In the top set of four images, the natural rubber was heated in the absence of asphalt. In the middle set of four images, the natural rubber was heated in the presence of asphalt. Both sets of images were acquired when the sample was at room temperature. In the bottom set of four images, the natural rubber was heated in the presence of asphalt and imaged while the sample cooled to room temperature	428
6-30	NMR images showing the cross-section of a triangular prism-shaped piece of styrene-butadiene tire rubber taken after heating at 170°C for (a) 0, (b) 2, (c) 8, and (d) 24 hr. In the top set of four images, the styrene-butadiene rubber was heated in the absence of asphalt. In the middle set of four images, the styrene-butadiene rubber was heated in the presence of asphalt. Both sets of images were acquired when the sample was at room temperature. In the bottom set of	

LIST OF FIGURES (continued)

Figure		Page
	four images, the styrene-butadiene rubber was heated in the presence of asphalt and imaged while the sample cooled to room temperature	429
6-31	Plot of the fraction of NMR signal remaining versus time of heating for natural and styrene-butadiene tire rubber heated in the presence and absence of asphalt	430
6-32	Plot of the swelling ratio versus time of heating for natural and styrene-butadiene tire rubber heated in the presence and absence of asphalt	430
8-1	A plot of fracture temperature versus flexible aliphatic carbon content	456
8-2	A plot of the limiting stiffness temperature versus flexible aliphatic carbon content	456

LIST OF TABLES

Table		Page
3-1	Whole asphalt (η) and n-heptane maltene (η_0) dynamic viscosities measured at 25°C and 0.1 rad/s, relative viscosities (η_{rel}), and n-heptane asphaltene volume fractions ($\phi_{n\text{-heptane}}$) for 16 SHRP asphalts	45
3-2	Heithaus parameters measured for SHRP asphalts using the Automated Heithaus Titration test with iso-octane as titrant and $K_S K_F$ values	46
3-3	Values of flocculation factor $K_F = 1/(1 - p_a)$ and values of solvation factor = K_S calculated from equation 3-15 for 16 SHRP asphalts	47
3-4	Values of iso-octane asphaltene volume fractions ($\phi_{iso\text{-}octane}$) and K' values for 16 SHRP asphalts	48
3-5	K_S values calculated from equation 3-17 and other quantities for 16 SHRP asphalts	48
3-6	Absolute asphalt compatibility indices (ACI_{abs}) and K_S/ACI_{abs} values calculated for 16 SHRP asphalts at 25°C	49
3-7	Preparative SEC separation of SEC Fraction-I of SHRP asphalts, 4.0 g/160 mL	87
3-8	Elemental composition of SEC Fraction-I subfractions	88
3-9	Relative amounts of aliphatic and aromatic carbon atoms in SEC Fraction-I subfractions SHRP core asphalts by ^{13}C NMR	89
3-10	Molecular weights of SEC Fraction-I-1 subfractions by membrane osmometry	90
3-11	Molecular weights of SEC Fraction-I-2 subfractions by membrane osmometry and vapor phase osmometry, both at 39°C	91
3-12	Molecular weights by vapor phase osmometry at 39°C of SEC Fraction-I-3 and I-4 subfractions of eight asphalts	93
3-13	Molecular weights by VPO of AAD-1 SEC Fraction-I subfractions	94
3-14	Rheological properties of mixtures of AAD-1 SEC Fraction-II (95%) with AAD-1 SEC Fraction-I subfractions (5%) at 25°C	95

LIST OF TABLES (continued)

Table		Page
3-15	Rheological properties of mixtures of AAD-1 SEC Fraction-II (90%) with AAD-1 SEC Fraction-I subfractions (10%) at 25°C	95
3-16	Rheological properties of mixtures of AAD-1 SEC Fraction-II (85%) with AAD-1 SEC Fraction-I subfractions (15%) at 25°C	96
3-17	Rheological properties of mixtures of AAD-1 SEC Fraction-II (80%) with AAD-1 SEC Fraction-I subfractions (20%) at 25°C	96
3-18	Yields of SEC fractions of eight SHRP asphalts and viscosities of SEC Fraction-II	97
3-19	Viscosities (Pa·s) of crossblended mixtures of SEC fractions of asphalts, 25°C, 1.0 rad/s	97
3-20	Reduced specific viscosity values of crossblended mixtures of SEC fractions of asphalts, 25°C, 1.0 rad/s	98
3-21	Solubility parameters of 10 solvents [Barton 1975]	98
3-22	Solubilities of IEC neutral fractions in acetone and in ethyl acetate	99
3-23	Surface tensions, densities, molecular weights, and solubility parameters of eight IEC neutral fractions at 60°C	99
3-24	Solubility parameters of SHRP core asphalts at 60°C calculated from surface tensions, densities, and molecular weights	100
3-25	Activation energies of viscous flow and solubility parameters (δ) of SHRP core asphalts	100
3-26	Masses of waxes in IEC neutral fractions of asphalts	101
3-27	Wax contents of IEC neutral fractions of TFO/PAV (60°C - 144 hr) aged asphalts	102
3-28	Effect of wax content on asphalt rheological properties	102
3-29	Rheological properties of mixtures of AAD-1 maltenes and asphaltenes with AAF-1 maltenes and asphaltenes, 25°C and 60°C, 1.0 rad/s	103

LIST OF TABLES (continued)

Table		Page
3-30	Selected rheological properties of mixtures of AAD-1 maltenes and asphaltenes with AAF-1 maltenes and asphaltenes, 25°C and 60°C, 10.0 rad/s	104
3-31	Rheological properties of mixtures of AAD-1 maltenes and asphaltenes with AAF-1 maltenes and asphaltenes, TFO/PAV aged	105
3-32	Selected rheological properties of mixtures of AAD-1 maltenes and asphaltenes with AAF-1 maltenes and asphaltenes, TFO/PAV aged, 25°C and 60°C, 10.0 rad/s	106
3-33	Rheological properties of mixtures of AAD-1 maltenes and asphaltenes with AAG-1 maltenes and asphaltenes, 25°C and 60°C, 1.0 rad/s	107
3-34	Selected rheological properties of mixtures of AAD-1 maltenes and asphaltenes with AAG-1 maltenes and asphaltenes, 25°C and 60°C, 10.0 rad/s	108
3-35	Rheological properties of mixtures of AAD-1 maltenes and asphaltenes with AAG-1 maltenes and asphaltenes, TFO/PAV aged	109
3-36	Selected rheological properties of mixtures of AAD-1 maltenes and asphaltenes with AAG-1 maltenes and asphaltenes, TFO/PAV aged, 25°C and 60°C, 10.0 rad/s	110
3-37	Rheological properties of mixtures of AAF-1 maltenes and asphaltenes with AAG-1 maltenes and asphaltenes, 25°C and 60°C, 1.0 rad/s	111
3-38	Selected rheological properties of mixtures of AAF-1 maltenes and asphaltenes with AAG-1 maltenes and asphaltenes, 25°C and 60°C, 10.0 rad/s	112
3-39	Rheological properties of mixtures of AAF-1 maltenes and asphaltenes with AAG-1 maltenes and asphaltenes, TFO/PAV aged	113
3-40	Selected rheological properties of mixtures of AAF-1 maltenes and asphaltenes with AAG-1 maltenes and asphaltenes, TFO/PAV aged, 25°C and 60°C, 10.0 rad/s	114
3-41	Summary of asphalt thermal properties	151
3-42	Dipolar dephasing relaxation times for methyl and methylene carbons in asphalts AAA-1, AAB-1, and AAM-1 at -45°C	152

LIST OF TABLES (continued)

Table		Page
3-43	Solid-state ^{13}C isotropic chemical shift values for selected *n*-alkanes [VanderHart 1981]	152
4-1	Viscosity sensitivity to ketones for selected SHRP asphalts oxidized by both PAV and TFAAT methods	205
4-2	Results from 5 mass % asphalt coated on aggregate aging experiments using the PAV method at 60°C for 144 hours. Asphalts extracted from aggregates. 60°C aging indices.	206
4-3	Results from 5 mass % asphalt coated on aggregate aging experiments using the PAV method at 60°C for 144 hours. Asphalts extracted from aggregates. 25°C aging indices.	207
4-4	Infrared analysis of aged asphalts recovered from 5 mass % asphalt coated on aggregate aging experiments using the PAV method at 60°C for 144 hours. Asphalts extracted from aggregates.	208
4-5	Results from 5 mass % asphalt coated on aggregate aging experiments using the PAV method at 100°C for 20 hours. Asphalts extracted from aggregate.	209
4-6	Summary of chemical properties of selected asphalts	252
5-1	Depth in microns of concentrated layer of voids resulting from soaking asphalt samples in distilled water at 50°C for different periods of time	333
5-2	Summary of aggregate test data, including pyridine sorption/thermal desorption data and pyridine water-stripping data	363
5-3	Potentiometric titration test results ranking the amount of model carboxylic acid (indole-3-acetic acid) consumed by SHRP aggregates	366
5-4	Elemental analyses of solutions resulting from the reaction of indole-3-acetic acid with SHRP aggregates, run 1	366
5-5	Elemental analyses of solutions resulting from the reaction of indole-3-acetic acid with SHRP aggregates, run 2	367
5-6	Potentiometric titration of carboxylic acids in asphalts	367

LIST OF TABLES (continued)

Table		Page
5-7	Moisture sensitivity test results for SHRP asphalt-aggregate combinations	368
5-8	Sorted WST data. Same data as in table 5-7 above, but sorted by freeze-thaw cycles-to-failure	369
6-1	An accounting of the number of times the low-temperature limit has been exceeded	397
6-2	Asphalt and natural tire rubber storage time at 200°C	416
6-3	Asphalt and natural tire rubber storage time at 156°C	417
8-1	Amount of flexible aliphatic carbons in SHRP core asphalts at 23°C using cross polarization-magic angle spinning-dipole dephasing NMR (contact time = 0.5 ms)	455

LIST OF ABBREVIATIONS

There are two lists of abbreviations below. The first list consists of what are commonly known as acronyms. The terms which the acronyms abbreviate are spelled out on first use. The second list consists of some symbols for rheological terms that are used throughout the report. Other common symbols for scientific terms are defined in the text on first use.

The Strategic Highway Research Program (SHRP) asphalts are described by a coding system that consists of three capital letters usually followed by a hyphen and a number. The asphalt designations (AAA-1, AAB-1, ABD, etc.) are not acronyms. The SHRP aggregates are described by a code consisting of two capital letters (RA, RB, etc.).

AAPT ..... Association of Asphalt Paving Technologists
AASHTO ..... American Association of State Highway and Transportation Officials
AC ..... asphalt concrete
ACI ..... asphaltene compatibility index
AI ..... aging index
ALF ..... Accelerated Loading Facility
ASTM ..... American Society for Testing Materials
ATR ..... attenuated total reflectance
CDOT ..... Colorado Department of Transportation
CF ..... crystallizable fractions
COTR ..... Contracting Officers Technical Representative
CPG ..... continuous performance grading
CP/MAS ..... cross polarization/magic angle spinning
CR ..... crumb rubber
CRM ..... crumb rubber modifier
CRMA ..... crumb rubber modified asphalt
DRID ..... differential refraction index detection
DSC ..... differential scanning calorimetry
DSR ..... dynamic shear rheometer
ESEM ..... environmental electron scanning microscope
FHWA ..... Federal Highway Administration
FOV ..... field of view
GLC ..... gas-liquid chromatography
GPC ..... gel permeation chromatography
HPLC ..... high pressure liquid chromatography
IEC ..... ion exchange chromatography
IGLC ..... inverse gas-liquid chromatography
IR ..... infrared
IRRS ..... infrared reflectance spectroscopy
ISTEA ..... Intermodal Surface Transportation Efficiency Act of 1991
LTA ..... long term aging

LIST OF ABBREVIATIONS (continued)

LTPP ..... Long Term Pavement Performance
MDSC ..... modulated differential scanning calorimetry
MPL ..... modified power law
MRL ..... Materials Reference Library
MSD ..... molecular size distribution
NAPT ..... nonaqueous potentiometric titration
NCE ..... Nichols Consulting Engineers
NMR ..... nuclear magnetic resonance
NMRI ..... nuclear magnetic resonance imaging
NR ..... natural rubber
OD ..... outer diameter
OSHA ..... Occupational Safety and Health Administration
PAV ..... pressure aging vessel
PG ..... performance grade
RTFOT ..... rolling thin film oven test
SEA ..... sulfur extended asphalt
SEC ..... size exclusion chromatography
SEM ..... scanning electron microscopy
SFC ..... supercritical fluid chromatography
SFE ..... supercritical fluid extraction
SHRP ..... Strategic Highway Research Program
SOM ..... shale oil modifier
SOMAT ..... shale oil modified asphalt
SPM ..... sliding plate microviscometer
SPS ..... special pavement section
STA ..... short term aging
TCLP ..... Toxicity Characteristic Leaching Procedure
TFAAT ..... thin film accelerated aging test
TFO/PAV ..... thin film oven/pressure aging vessel
TFOT ..... thin film oven test
TFOT/POV ..... thin film oven test/pressure aging vessel
T_g ..... glass transition temperature
THF ..... tetrahydrofuran
TSR ..... tensile strength ratio
UV ..... ultraviolet
VPO ..... vapor phase osmometry
WFLHD ..... Western Federal Lands Highway Division
WLF ..... Williams-Land-Ferry
WRI ..... Western Research Institute
WST ..... water susceptibility test

LIST OF ABBREVIATIONS (continued)

η^* ..... dynamic viscosity
G' ..... storage modulus
G'' ..... loss modulus
G^* ..... complex modulus
tan G''/G' ..... tan delta

EXECUTIVE SUMMARY

The Superpave® binder specification developed during the Strategic Highway Research Program (SHRP) from 1987-93 classifies tank asphalts used in roadway construction into groups that have similar (to within 6°C; 10.8°F) rheological properties at high to low service temperatures. This represents a significant improvement over previous classification, or grading, systems that ignored low temperature properties of asphalts. However, with the exception of measuring the effects of mild oxidation on intermediate and low temperature physical properties, the Superpave® binder specification does not account for major changes in physical properties that occur when asphalts are placed into roadway service conditions. These unpredictable changes in physical properties result from chemical reactions of asphalts in the pavement and/or from exposure to service environments.

The mission of the project reported here was to improve the understanding of the fundamental properties of petroleum asphalts used in roadway construction in order to better classify them into distinctive performance groups. Particular emphasis was placed on characterizing asphalts while exposed to realistic and long-term service environments.

The approach used in this project was fourfold. The first objective was to continue to refine a comprehensive, fundamentally based, chemical model of petroleum asphalt that explains its expected behavior in all types of roadway-use situations. The second objective was to challenge the current Superpave® binder specification to determine where it is and is not predictive of performance. The third objective was to explore, in greater detail, those phenomena that alter asphalt behavior in service, but that are not predicted by the Superpave® binder specification; i.e., this was a search for "holes" in the specification. The fourth objective was to convert predictive methodology into fast, user-friendly test methods. The objectives were fulfilled and are reported in the nine chapters that follow in this volume. Each chapter begins with a synopsis that summarizes the technical results for the chapter subject. There is a second volume that presents the details for conduct of newly developed analytical methods and, separate from both, a computerized database for the large volume of data generated in this project.

The results of this project show that asphalts classified into the same Superpave® binder grade often exhibit significantly different physical properties from each other once placed in one or more of the realistic service environments. These environments include exposure of asphalts to water, exposure to oxygen to simulate long-term pavement aging, exposure of thin films of asphalt to mineral surfaces, long-term storage at low temperature, and a measure of the ability of asphalt to "heal" after having been fractured. In most of these cases, two or more methods were used to study the phenomenon and good agreement among methods was observed. New performance predictive methods that are fast (½ to 4 hours) emerged during this project. Other performance predictive methods emerged that are too time consuming to be useful as specification methods. Surrogate methods will be needed if these phenomena are to be considered in a performance-related classification of asphalts. A logical sequence starting with the comprehensive model to the various bench experimental methods to development of fast, user-friendly tests is described. Several new test methods are recommended. Each

recommendation addresses a source (composition) dependent performance variable that is not or cannot be measured (distinguished) by the Superpave® binder specification. Each of these new test methods has been presented to the Superpave® binder specification Expert Task Group with the emphasis that these methods will improve the truly blind-to-source nature of the specification. Source, in this context, means the source of crude oil used to produce asphalt and does not mean the point of purchase. A single producer may very well prepare asphalts from crude oils that have major differences in composition.

Validation of results (new tests) remains an all important task. Validation of the greatest utility is to demonstrate that new test methods do predict observed performance (or failure) in roadways where all variables are kept as similar as possible except the source of asphalt. With the same objectives as the WesTrack experiment near Reno, Nevada, which tested the effects of variation of design on performance, the variability of performance that can be attributed to variation in asphalt source also needs to be tested with controlled experiments. This would involve multiple road sections where the asphalt source is the only significant variable. A search was made throughout the United States, Canada, and western Europe for construction sites where multiple sources of asphalt were used, including the requirement that original asphalts must be available. The latter requirement is necessary because prediction does have to be made using asphalt as it is produced at the refinery. Anything else is after-the-fact observation. Sites of the above described configuration that also are old enough to be distinctive, i.e., sites that are useful for validation of source-dependent performance prediction, because they may demonstrate performance differences (distresses being of particular interest) are VERY SCARCE. What is needed for validation is the type of field experiment described by the Federal Highway Administration (FHWA) as Long Term Pavement Performance (LTPP) Special Pavement Studies (SPS), experiment type 9a [LTPP SPS 9a]. More such sites, SPS 9a or otherwise, are needed to validate, refine, and quantitate test methods that predict source-dependent performance variability that cannot be predicted by the current Superpave® binder specification.

A significant portion of the work in this project was contracted to outside organizations that have specialized expertise to address subjects that range from the elucidation of very fundamental asphalt properties to development of new test methods that are available for immediate use. Numerous publications from all organizations involved in this project have resulted. These are principally in the *Transportation Research Record*, the *Journal of the Association of Asphalt Paving Technologists*, American Chemical Society journals, and in *Petroleum Science and Technology* (formerly *Fuel Science and Technology International*).

PROJECT MANAGEMENT

The project management at Western Research Institute was as follows: Dr. Raymond E. Robertson, Principal Investigator; Dr. Jan F. Branthaver, Co-Principal Investigator for chemical studies; P. Michael Harnsberger, Co-Principal Investigator for physical property studies; Dr. J. Claine Petersen, Consultant; Dr. Samuel M. Dorrence, Technical Administrator for Subcontracts; Jane E. Tauer, Computerized Database Manager; David C. Coletti, Subcontract Manager; Dawn K. Geldien, Program Administrator; and Jackie Greaser, Project Secretary.

AUTHORS

The authors of this report are Dr. Raymond E. Robertson, Dr. Jan F. Branthaver, P. Michael Harnsberger, Dr. J. Claine Petersen, Dr. Samuel M. Dorrence, Dr. John F. McKay, T. Fred Turner, A. Troy Pauli, Dr. Shin-Che Huang, Dr. Jung-Do Huh, Jane E. Tauer, Dr. Kenneth P. Thomas, Dr. Daniel A. Netzel, Dr. Francis P. Miknis, Theresa Williams, Dr. John J. Duvall, F. Alan Barbour, and Christine Wright. Those responsible for editing and assembling this document are Dr. Raymond E. Robertson, Dr. Jan F. Branthaver, P. Michael Harnsberger, Dr. John J. Duvall, Dr. J. Claine Petersen, Dr. Samuel M. Dorrence, Dr. John F. McKay, Dr. Shin-Che Huang, Dr. Kenneth P. Thomas, and T. Fred Turner.

ACKNOWLEDGMENTS

The authors gratefully acknowledge the Federal Highway Administration, U. S. Department of Transportation, for financial support for this project. Thanks is expressed to Dr. Ernest J. Bastian, Jr., Contracting Officer's Technical Representative (COTR), and his reviewer team from the FHWA Special Projects and Engineering Division and several engineering groups for many helpful suggestions and continual encouragement. Thanks is expressed for advice and encouragement from Mr. Derek Karis, Mr. John Hardy, and Ms. Linda Hooks, all of whom served as FHWA Contracting Officers during this project.

The authors gratefully acknowledge the untiring efforts of the scientists and technicians who produced most of the samples and acquired most of the data during this project. They are Dr. Sang-Soo Kim, Stephen Salmans, Gerald Gardner, Joseph Rovani, Janet Wolf, Felicia Reid, Craig Brommer, Gerald Forney, Paul Holper, Bruce Thomas, Alana Hansert, Charles Collier, III, Julie Miller, Randall Blake, Jan Hart, Deborah Colgin, and George Miyake. University of Wyoming students who worked part time on Nuclear Magnetic Resonance spectroscopy experiments are Michelle Serres, Jeni Soule, Arland Taylor, Cal Wallace, and Clint Butcher.

Finally, the authors express special thanks to Jackie Greaser, Project Secretary, who typed and maintained a well-organized file of virtually all the publications and documentation produced during this project, and to Anthony Munari who prepared the graphics throughout this project.

CHAPTER 1: THE RELATIONSHIP OF ASPHALT COMPOSITIONAL PROPERTIES WITH PERFORMANCE-RELATED PHYSICAL PROPERTIES PRIOR TO 1993

SYNOPSIS

Asphalts are petroleum residua and therefore are mixtures of a large number of organic compounds having diverse properties. The relationship between asphalt chemical and physical properties is not straightforward. This chapter describes the efforts of researchers to understand the nature of asphalt before the Strategic Highway Research Program (SHRP). The development of a model of asphalt structure is described. The evolution of testing methods for evaluating asphalts also is described.

A summary of the results of the SHRP Binder Characterization and Evaluation Program is presented. The changes in asphalt supply patterns over the years also is discussed.

SUMMARY OF PRE-STRATEGIC HIGHWAY RESEARCH PROGRAM RESEARCH ON ASPHALT COMPOSITION

Many years ago Hveem [1943] observed that asphalts are perceived differently by highway engineers than by chemists. To the highway engineer, asphalt is a substance that causes particles of sand, gravel, and crushed stone to stick together to form a pavement that will withstand the abrasion of vehicle tires, resist deformation under the weight of vehicles, and withstand the deteriorating effects of rain and sun. To a chemist, asphalt is (with the exception of natural asphalt) a residue of the distillation of petroleum or a product of solvent extraction of petroleum. It is a complex mixture of thousands of different organic compounds mutually dissolved or dispersed.

Early in this century, most pavement asphalts were native asphalts. Later, when refinery-produced asphalts began to be used in pavement construction in addition to natural asphalt, it became obvious that there was considerable variability in the properties of the manufactured materials. This variability was reflected in binder performance in pavements. Therefore, from the beginning of the use of asphalts in road building, methods for evaluation of asphalts have been in demand and have been utilized. The earliest methods were empirical, involving qualitative estimates of viscosity, ductility, and softness. Enough information was obtained from these crude tests to provide those who designed pavements with a vague notion of how the pavement mixtures might be expected to perform. Standard testing methods eventually evolved, including more accurate determinations of viscosity and penetration. Some chemical tests based on solubility also were used [Hveem 1943]. Unfortunately, according to Hveem [1943], "anyone having more than a casual knowledge of the behavior and characteristics of asphaltic paving materials is aware that most of the standard tests do not indicate quality. Asphalts which meet all of the usual specification requirements may prove to be more or less unsatisfactory and, conversely, cases have been known where materials which do not comply have given excellent performance." Hveem [1943] concluded that the reason for the imperfect performance

predictions of the standard tests is that the tests did not rest on well-founded bases. The situation did not improve greatly from 1943 until the inception of the Strategic Highway Research Program in the late 1980's.

In his 1943 paper, Hveem pointed out that there was then a tendency among highway engineers to blame pavement failures on "chemical action" in the asphalt. Hveem cautioned that such judgments are not always accurate, and that pavement failures cannot necessarily be attributed to deficiencies of the asphalt. It is necessary to identify those pavement troubles, or failure modes, for which the asphalt alone is responsible. Obviously, if "chemical action" in asphalt is crucially important to performance, knowledge of chemical differences among asphalts is essential. Hveem then attempted to determine what information was required to evaluate binders properly. He stated that there are four properties of asphalts that are crucial to prediction of pavement performance. The properties he listed are consistency, durability, curing rate, and resistance to water action. All other properties were deemed to be inconsequential. Meaningful tests of asphalts must, according to Hveem, provide information about these four properties and must rest on well-founded bases. The meaning of these terms as Hveem used them in his 1943 article may not be entirely clear to some modern readers. By consistency, Hveem meant hardness and flow properties of asphalts at service and mix plant temperatures, i.e., the overall rheological properties of asphalts. The term durability as used by Hveem refers to the changes brought about in asphalt by reaction with oxygen and the rate at which these changes occur. Sixty years ago it was known that some asphalts became excessively brittle early in their service lives as a result of oxygen incorporation. It also was known that some asphalts that were unreactive to oxygen failed to cure and tended to strip. In 1943 and for many years afterward, problems arising as a result of reaction with oxygen were the principal causes of failure in asphalt pavements. Hveem's concern with curing rates involved less viscous materials such as road oils and cutback stocks. Improper curing appeared to be more of a problem with materials produced from thermally cracked crudes. It is to be noted that thermal cracking is currently being used to produce binders that meet recently promulgated SHRP specifications. The term resistance to water action as used by Hveem meant resistance to moisture damage and resulting stripping.

The conclusions of Hveem would be seconded by most asphalt researchers, engineers, as well as chemists. A great deal of experience since 1943 has shown that asphalts from different sources, but of identical viscosity grade, behave very differently in pavements. Qualitative data on the effect of asphalt source on performance were obtained during the Zaca-Wigmore Road Test [Hveem et al. 1959], in which construction variables were carefully controlled and asphalt source was intentionally varied. These results, and others of a similar nature, must be considered in the design of any standard binder tests.

Earlier, it was stated that engineers perceive asphalt as an adhesive binder holding the aggregate particles together. Therefore testing methods designed by engineers will tend to favor measurements of physical properties that are used to evaluate pavements. Chemists view asphalts as complex chemical mixtures. Therefore, chemists will tend to devise testing methods that demonstrate how asphalt chemical composition influences physical properties and how asphalts differ from one another in composition. Both kinds of tests, if based on fundamental properties, should relate to one another.

Many of the earliest developed tests for asphalts were performed on whole asphalts under specified conditions. Examples of these are viscosity determination at 60°C (140°F), penetration determinations, glass transition temperatures, elemental composition, etc. Viscosity at 60°C (140°F) was the basis for the long-used viscosity grading system. Asphalts were designated AC-10, AC-20, etc., meaning that their 60°C (140°F) viscosities were 1,000 poises, 2,000 poises, etc. The data obtained from these tests are useful for pavement design and construction, but are not sufficient for prediction of performance.

The problem with grading asphalts based on one physical property measurement, using viscosity at 60°C (140°F) as the example, is that asphalts having the same viscosity grading, but produced from different crude sources, are observed to perform differently. The differences in performance may be attributed to the unique chemical composition of a given crude oil, which is reflected in any asphalt residuum from that crude. Asphalts that differ significantly in chemical composition may have the same viscosity at 60°C (140°F). Viscosity at this temperature is a made to order property at the refinery. Also, asphalts with identical 60°C (140°F) viscosities are observed to have viscosities quite different from each other at other temperatures. Thus, it is not reasonable to extrapolate from this one physical measurement to other performance-related chemical and physical properties. On the other hand, with the development of more sophisticated apparatus for measuring rheological properties, it is now possible to measure viscosities and other rheological properties of asphalts over a wide temperature range at various rates of shear. Individual rheological profiles may be obtained for asphalts that classify them into rheologically similar groups of materials. This is the basis for the current Superpave® binder specification. It was anticipated that this new specification would be helpful in predicting certain aspects of performance, but this remains unproven. Rheologically similar asphalts may still have other physical properties that are different and thus not behave alike under service conditions. A specific rheological profile may include asphalts with many different chemical compositional variations.

In principle, it is conceivable that detailed physical property measurements (rheological, differential scanning calorimetric, etc.) may be correlated with asphalt failure modes without any knowledge of asphalt composition. In practice, such an approach is expensive and time-consuming. This is because asphalt properties are altered by interactions with other substances, and the results of such interactions may not be easily predicted from physical properties of individual asphalts. Some asphalt failure modes are the direct result of physical interaction with water and chemical reactions of binders with oxygen. It is also likely that binders react with certain minerals in aggregates. These reactions affect binder durability and were a focus of research efforts of early investigators. Therefore, it is useful to review the overall chemical composition of asphalts and some earlier investigations that studied the influence of chemical composition on physical properties.

Asphalts are composed of carbon, hydrogen, oxygen, nitrogen, sulfur, and trace amounts of many other elements. Carbon values vary from 83-87 percent, hydrogen values from 9-11 percent, oxygen values from 0.1-1.0 percent, nitrogen values from 0.2-1.2 percent, and sulfur values from 1.0-7.0 percent [Plancher et al. 1976]. The relative amount of carbon and hydrogen in asphalts provides some useful information about asphalt properties. Heteroatom (nitrogen,

oxygen, sulfur) contents provide more information. An asphalt having a high oxygen concentration is likely to have been subjected to aging conditions either in the laboratory or in the field. Asphalts that are high in sulfur have different physical properties and oxidative aging characteristics than low sulfur asphalts. The reason for this is discussed in chapter 4. High nitrogen values may influence adhesion on aggregates and thus moisture resistance of pavements. Bulk chemical composition data are useful in classifying asphalts into certain categories, but still are limited in their value in predicting binder performance.

Any detailed analysis of asphalts reveals the presence of many thousands of individual compounds, mostly present at the level of a fraction of a percent. Many of these compounds are hydrocarbons (compounds consisting solely of hydrogen and carbon). Examples of hydrocarbons found in asphalts are normal alkanes (paraffins), iso-alkanes, branched alkanes, cycloalkanes, and various aromatic compounds. Structures of these compound types may be found in any textbook of petroleum chemistry, e.g., Speight [1980]. Other compounds present in asphalts contain, in addition to carbon and hydrogen, one or more of the heteroatoms listed above. The chemical and physical properties of these organic compounds may differ markedly. One such property is polarity.

The concept of polarity refers to charge separation within a molecule, resulting in positive and negative centers at different atoms within a molecule. Thus polar molecules have measurable dipole moments. The charge separation results from the fact that some atoms, e.g., nitrogen and oxygen, attract electrons more strongly than carbon or hydrogen. Molecules containing nitrogen and oxygen tend to have centers of electron density at these atoms, and centers of positive charge elsewhere. Substituted aromatic hydrocarbons also have dipole moments and are therefore polar. Polar molecules attract one another by electrostatic forces, which are moderately strong. For molecules having no dipole moments, e.g., non-polar hydrocarbons such as alkanes and cycloalkanes, these kinds of attractive interactions do not take place. However, even those non-polar molecules interact with—and therefore attract—one another to some degree. For most of the non-aromatic hydrocarbons in asphalt, the strength of intermolecular interactions (by means of so-called Vander Waal's forces) is weak at ambient temperatures. For aromatic hydrocarbons, most of which are weakly polar, intermolecular interactions may be somewhat stronger. Interactions among more polar molecules are stronger yet, as stated above. The intermolecular interactions among asphalt components greatly influence asphalt properties. The main reason is that more energy, usually in the form of heat and shear, is required to break up the stronger polar associations compared with the weak interactions of non-polar compounds.

A large number of asphalt molecules contain one or more sulfur atoms. These molecules for the most part are relatively non-polar. However, many of these sulfur compounds are readily oxidized to more polar compounds.

The components of asphalts that contain nitrogen, oxygen, or both are usually highly polar. They will interact with one another strongly and may form extensive molecular associations. Because many of the physical properties of asphalts are a function of the size of

molecular associations, highly polar molecules exert a disproportionate influence on these properties.

Although relative amounts of total hydrogen and carbon in asphalts do not vary widely, the relative amounts of aromatic and aliphatic carbons and hydrogens do vary significantly. The amounts of substituted aromatics are important factors affecting property changes in asphalt oxidation. Estimates of aromatic carbons may be obtained by nuclear magnetic resonance (NMR) spectroscopy. For most asphalts, aromatic carbons are 25-35 percent of total carbon [Ramsey et al. 1967].

The initial attempts to correlate overall chemical compositional features (global parameters) of unaged asphalts with pavement performance proved to be of limited success, as stated above. So attempts were made to fractionate asphalts into significantly different chemical components. It was hoped to demonstrate that different chemical components influenced physical properties in different ways. In a mixture that contains tens of thousands of different compounds, it is obviously impractical to isolate each one. Therefore, the fractions that are isolated from asphalts must each have some common compositional factor that exerts an influence on some important property. In order to do this, the earliest separations were based on relative polarity.

Parenthetically, the use of NMR data on whole asphalts, discussed later in this report, refutes the previous statement that overall chemical properties of unaged asphalts are not particularly useful in predicting performance. However, NMR instruments were not readily available in the early days of asphalt research. Additionally, analysis of some global chemical properties of oxidatively aged asphalts can be useful in the correlation of data from laboratory aged asphalts with binders extracted from pavements. The use of infrared (IR) spectrometry in the analysis of aged asphalts is discussed in chapter 4.

As stated earlier in this introduction, the organic compounds in asphalts vary widely in polarity, some being non-polar, others strongly polar, and most weakly polar. In the 19th century, it was observed that when crude oils were treated with several volumes of alkane solvents such as propane, n-pentane, –hexane, n-heptane, etc., black friable solids designated as asphaltenes were precipitated. These solids were easily separated from the remainder of the crude oil by filtration. The filtrates, after solvent removal, were designated maltenes or petrolenes. Almost all crude oils were observed to contain a percent or two of asphaltenes, and some heavy crudes contain several percent. Because asphaltenes are involatile, they become concentrated in asphalts manufactured by distillation. Most asphalts contain 5-25 percent asphaltenes as defined by n-heptane precipitation.

Yields of asphaltenes are a function of the precipitating solvent [Girdler 1965]. Asphaltenes from all crude sources are much more aromatic (H/C atomic ratio = 1.15 ± 0.05 for n-heptane asphaltenes from a large number of crude oils) than the parent crude oils or asphalts. The heteroatoms N, O, and S are concentrated in asphaltenes. Asphaltenes are the viscosity-building components of asphalts. Maltenes are much less viscous than their parent asphalts. Thus, it appeared obvious to many of the earlier researchers that asphaltene precipitation should

be part of any rational separation scheme, particularly because it is so readily accomplished. Asphaltene precipitation then was followed by other operations on the maltenes. At the end of each separation method, three, four, or five generic fractions were produced. The generic fractions ranged from non-polar to moderately polar to highly polar overall. For example, the method of Hubbard and Stanfield [1948] separated maltenes into oils and resins by selective desorption from activated alumina. Thus, in this separation method, three generic fractions are obtained, asphaltenes, resins, and oils. They were weighed, and the weights were recorded on triangular plots. For each asphalt, there corresponds a unique point on such a plot. The goal of the separation was to accumulate large numbers of data points for different asphalts and hopefully find trends relating them to performance.

The Corbett method [1970] is the separation procedure that historically has been most commonly used by asphalt chemists. Maltenes obtained by asphaltene precipitation are fractionated into saturates, naphthene aromatics, and polar aromatics by adsorption chromatography on alumina. The four generic fractions generated by the Corbett method serve to "fingerprint" asphalts. The fractions are chemically distinct from one another in many ways. Saturates contain only saturated hydrocarbons and sulfur compounds, and are non-polar. Naphthene aromatics are weakly polar. Polar aromatics are moderately polar, as the name suggests, and are rich in heteroatom-containing compounds. Using the Corbett method to analyze asphalts from cores of the Michigan Road Test [Corbett and Merz 1975], it was found that oxidative aging resulted in the buildup of asphaltenes at the expense of naphthene aromatics and polar aromatics. Saturates were observed to be unchanged. Since each generic fraction influences different properties of asphalts, the gradual conversion of mildly polar components into asphaltenes served to rationalize the change of asphalt properties as a result of oxidative aging. The Corbett procedure illustrates one of the goals of chemists in asphalt research, namely to fractionate a highly complex mixture into components that are less complex and that impact differently on asphalt properties.

Other methods of separation developed in the early years of asphalt research are based on successive solvent precipitation [Traxler and Schweyer 1953] and chemical treatment of maltenes [Rostler and White 1962], among others. Some of these methods were designed for specific research needs and are not suitable for general use. A major weakness of all the above described separation procedures is that they yield only mass fraction data. The individual maltene subfractions are not as varied in chemical properties as their parent maltenes, but are still highly complex. Also the asphaltenes, which are known to strongly influence asphalt physical properties, are not further studied or fractionated. Partly, this is because asphaltenes are very difficult to work with using classical chemical separation methods.

The above separation methods have been evaluated by Goodrich et al. [1986] and by Petersen [1984]. It was concluded that the methods are useful in demonstrating that, in order to be durable, there must be some sort of balance among the generic fractions. For example, in the Corbett fractionation, it is observed that saturates and asphaltenes are not mutually soluble. Too much of either of these materials results in an unstable system. That is apparently what happens during oxidative aging, which involves buildup of asphaltenes. Nevertheless, despite

considerable efforts, the above methods are of limited utility in diagnosis of asphalt failure modes. Physical property measurements appear to be superior [Goodrich et al. 1986].

The observation that asphalts resemble simple amorphous polymers in their viscoelastic behavior was made many years ago [Schmidt and Barrall 1965]. The implications of this observation will be discussed in more detail below. Yet the first investigations of asphalt components indicated that few, if any, macromolecules are present in asphalts. Attempts to explain this behavior have been one of the priorities of asphalt researchers for many years. In polymers, it is known that molecular weight values and molecular weight distributions determine rheological properties. Therefore it is logical to measure the molecular weights and molecular weight distributions in asphalts. One technique that may be used to fractionate asphalts into components of various molecular weights is size exclusion chromatography (SEC), also earlier known as gel permeation chromatography (GPC). A more detailed discussion of this technique is given in chapter 3. The SEC method may be analytical or preparative. The earliest SEC findings showed that asphalt molecular weight distributions varied considerably, and that the process of oxidative aging results in the buildup of entities having high apparent molecular weight values. Many workers have studied SEC fractionations of asphalts, and there are a large number of publications in this field. Some are referenced in chapter 3.

The SEC, solvent precipitation, and chromatographic methods yield fractions that are defined by properties such as molecular size, solubility, adsorption behavior (a function of polarity), etc., but are not necessarily defined by specific chemical composition. One separation method that does separate asphalts into defined chemical fractions is ion exchange chromatography (IEC). This method was long used to separate crude oils and shale oils into defined chemical fractions [McKay et al. 1978] and was applied to asphalts by Boduszynski et al. [1977]. In this technique, asphalt non-polar components are completely separated from the polar components. The latter then are fractionated into acidic and basic subfractions of various strengths. It is not necessary to perform an initial asphaltene precipitation in an IEC separation. Detailed chemical compositional information about asphalts may be obtained using IEC that cannot be had using other separation methods. The IEC method also may be preparative. However, in addition to being tedious and time-consuming, the IEC method has the disadvantage that material recoveries are often less than quantitative.

The effects of embrittlement caused by oxidative age hardening of asphalts have long been of concern to asphalt researchers. This process is the result of reaction of asphalt over time with atmospheric oxygen and is manifested in the familiar "alligator" fatigue cracking patterns in pavements. This failure mode is thus in part the result of a chemical reaction. Of course, loading due to traffic also contributes to this type of distress. Much effort has been expended in understanding the mechanism of the oxidation reaction and designing laboratory tests that simulate field results. Petersen [1984] and co-workers have demonstrated that IR spectra of asphalts aged in the field and by various laboratory methods exhibit peaks corresponding to carbonyl and sulfoxide functional groups. These functional groups are the result of the reaction of alkyl or aryl sulfides and benzylic carbon atoms with oxygen, as discussed in chapter 4. The result of this process is the conversion of relatively non-polar molecules into polar ones. Consequently, oxidative aging causes asphalt viscosity to increase. Extensively aged asphalts

become brittle, leading to pavement failure. Obviously it is a matter of great importance to understand the nature of asphalt oxidation, because it may prove possible to retard the process by such means as blending to alter component compatibility, or by chemical means.

The California Zaca-Wigmore experimental road test [Hveem et al. 1959] was the first major pavement test to evaluate the effects of differences in asphalt composition in pavement performance. In this extensive, carefully controlled test, eight different test sections were built end to end on the same road using the same aggregate and construction methods, the only variable being that the asphalts — all meeting specifications — were from different crude oil sources. Performance was evaluated by the amount of alligator-type fatigue cracking, partly the result of asphalt oxidative aging, that appeared in the pavements over a five-year period. The highly important conclusion of this test was that variations in the composition of asphalts all meeting the then current specifications had a major effect on pavement performance. Some pavement sections completely failed in a few years while other sections were in excellent condition at the end of the test. That asphalt chemical composition played a major role in the variable performance of these test pavements was confirmed using a unique chromatographic technique called inverse gas-liquid chromatography (IGLC) in which asphalt serves as the stationary chromatographic phase and can be oxidized *in situ* in the column [Davis and Petersen 1967]. The interaction of phenol as an IGLC test compound with the oxidized Zaca-Wigmore asphalts showed an excellent correlation with pavement performance as evaluated by crack density in the pavement test sections after five years of service. This strongly implicated the polar, associating components of asphalt, both those initially present and those formed on oxidation, as major contributors to asphalt embrittlement. Phenol was chosen as the standard test compound because it contains hydrogen bonding functionality, an electronegative oxygen atom, and aromaticity in its molecular structure. The phenol interaction coefficient is believed to provide a relative measure of the total polar associating components of asphalt. Further discussion of the IGLC method is in chapter 4.

The physical property and chemical compositional data described above have stimulated much speculation about the microstructure of asphalts. Asphalts, which are highly complex mixtures of organic compounds, have unusual physical properties. To give one example, the large variations in viscosity with temperature that characterize asphalts are not observed in most mixtures of organic materials. It is natural to inquire what chemical compositional factors give rise to these features. To quote two of the most prominent contemporary asphalt researchers, "The key to understanding the mechanical behavior of any material is understanding its structure" [Christensen and Anderson 1991]. Therefore, asphalt scientists have proposed plausible models of asphalt microstructure. If the models prove to be valid, more fruitful areas of research result. Good models stimulate good science.

Parenthetically, the term model does not necessarily mean the same thing to engineers and chemists. To many engineers, a model comprises an equation or set of equations into which numbers are inserted and predictions emerge. The equation or equations need not be concerned with causes of physical behavior of systems. To many chemists, a model is a simplified two- or three-dimensional representation of physical reality from which mathematical relationships may

be derived. These mathematical relationships should relate the structure of a system with its behavior.

From the earliest days of asphalt research, most chemists studying asphalts have concluded that asphalts are not simple solutions at service temperatures. In 1915, Richardson [quoted in Traxler 1961] observed that many properties of asphalts resemble those of colloids. Colloids are systems in which one or more of the components has at least one dimension within the range of 1.0 nm to 1,000 nm [Shaw 1980] although the larger number is probably more typical for colloids. Thus, colloidal systems contain large molecules or small particles. These entities may be long, rod-like structures (only one dimension in the required size range), flat discs (two dimensions in the required size range), or spherical-ellipsoidal (all three dimensions in the required size range). The larger entities usually are dispersed in a solvent medium consisting of much smaller molecules. The dispersing medium may be a liquid, a gas, or a solid.

In simple mixtures of small molecules, every part of a specific molecule may interact with every part of other molecules. As an example, in a solution of sugar in water, all functional groups of the solute (sugar) interact with the solvent (water). For solutions of very large molecules (polymers) and dispersions of small particles, this is not the case [Mysels 1959]. Only certain portions of the large molecules and those molecules comprising the surface of the particles interact with solvent. Significant portions of large molecules, and those molecules buried deeply within particles, do not interact with solvent molecules. Thus, colloidal systems are microheterogeneous.

Obviously, there is no sharp dividing line between colloidal and non-colloidal systems. Solutions of molecules having dimensions of 0.95 nm would not be colloidal according to the definition given earlier. If the dissolved molecules were slightly larger, the solution would be considered to be colloidal.

Currently, colloids are classified into three major categories. These are colloidal dispersions, solutions of macromolecules, and association colloids.

Colloidal dispersions consist of dispersed particles in a dispersion medium. The dispersed particles are a separate phase from the dispersion medium. The properties of dispersions are strongly influenced by the surfaces that separate the dispersed phase from the dispersion medium. Colloidal dispersions are thermodynamically unstable. After phase separation, colloidal dispersions are not readily reconstituted. Two of the most common types of colloidal dispersions are sols and emulsions. Examples of sols are dispersions of very fine sulfur or gold particles in water. Emulsions are mixtures of liquids that are mutually immiscible or slightly miscible. Examples are oil-in-water or water-in-oil emulsions. It is noteworthy that examples of these two emulsion types may have similar compositions, yet have entirely different properties, depending on which of the two liquids is the dispersed and dispersing medium.

Solutions of macromolecules, typically solutions of polymers, are true solutions and are thermodynamically stable. Many polymers are linear in shape and tend to form what are termed random coils in solution. These coils entangle one another and immobilize some of the much

smaller solvent molecules. The extent of the entanglements affects the physical properties of the solutions. Not all macromolecules are linear. Some may be sheetlike or spherical. Some macromolecules are so large that they rival small particles in size, and similarly affect properties of solutions.

Association colloids are composed of molecular associations of relatively small molecules. Classical examples of association colloids are various soap solutions. Soaps are salts of long chain carboxylic acids. Thus a soap molecule has a polar end and a non-polar "tail." When in dilute solution, soaps behave as ordinary solutes. At a certain critical concentration, soap molecules associate to form spherical structures called micelles. In these micelles, the polar ends comprise the surface, and the hydrocarbon "tails" the interior. The interior of the micelle can solubilize oily molecules that would not ordinarily be soluble in water; hence the cleaning action of soaps.

Unlike colloidal dispersions, association colloids are thermodynamically stable.

Two important terms used in discussions of colloidal systems are lyophilic and lyophobic. The term lyophilic (liquid loving) means that the surface of the dispersed material has a close affinity with the solvent medium. Lyophobic means the reverse. Although the two terms are commonly encountered, they are somewhat illogical, as pointed out by Shaw [1980]. No dispersed material could possibly be totally lyophobic and form a colloid, and lyophobic regions may exist in dispersed phases of lyophilic colloids.

Nellensteyn [1924] proposed that asphalts are, in fact, colloids. He implied that asphalts consist of dispersions of discrete particles in a continuous phase. It was suggested that the dispersed components of asphalts have a graphitic core. The graphitic core, in this model, is surrounded by aromatic molecules that Nellensteyn termed "protective" bodies. It is now known that this model is incorrect, as no measurable amounts of elemental carbon exist in asphalts. However, Nellensteyn's concept of a particulate-like body dispersed in a solvating medium by the adsorption of "protective" bodies still forms the fundamental basis for some current models of asphalt structure.

Traxler [1961] discusses the flow properties of asphalts and claims that some sort of colloidal model best fits the data. Following Mack [1932], who stated that asphalts are lyophilic sols, and Labout [1950], Traxler suggests that asphalts may be viewed as dispersions of asphaltene micellar structures in a maltene solvent phase. Maltenes and asphaltenes were described earlier in the discussion of separation methods. The effectiveness by which the asphaltenes are dispersed in the maltenes will determine the properties of the asphalt. That fraction of the maltenes that is crucial to this stabilization is termed resins. These materials are presumed to behave like soap molecules in association colloids. Resins are the most polar and aromatic components of the maltenes. Using this model, Traxler classifies asphalts into sol, gel, or sol-gel types. Sol-type asphalts have relatively few asphaltenes and many resins. Thus, the asphaltenes are well-dispersed, and the system is said to be compatible. Sol asphalts are characterized by high variation of viscosity with temperature, high ductility, and low elasticity. Gel asphalts contain relatively few resins and large amounts of asphaltenes, which are less well-

dispersed. They are not as compatible as sol asphalts. Gel asphalts are elastic, not very ductile, and have a relatively low variation of viscosity with temperature. In Traxler's model, a specific set of chemical properties is correlated with a specific set of physical properties.

Pfeiffer and Saal [1940] proposed a model of asphalt structure similar to that described by Traxler. They claimed that the dispersed component in asphalts consists of spherical entities that have at their centers highly aromatic molecules. These molecules are surrounded by a layer of slightly less aromatic molecules. The next layer of molecules is even less aromatic. Thus there is an aromaticity gradient from the center of the dispersed phase entities to their outer boundaries. At the boundaries, there is not even a sharp demarcation between the outermost molecules of the dispersed materials and the solvent phase, and therefore no distinct surfaces. So it may not be proper to refer to the dispersed entities as colloids. Not surprisingly, the Pfeiffer-Saal model has been nicknamed the onion-skin model. The dispersed structures were believed to be large in gel-type asphalts and small in sol-type asphalts. The dispersed structures are assumed to be equivalent to the asphaltene component of an asphalt, and their molecular weight values were thought to be in the 2,000-30,000 dalton range. Obviously, the dispersing medium is equivalent to the maltenes. Heating and shearing of asphalts causes reduction of the size of the asphaltene structures, according to this model, thus accounting for the great changes in rheological properties with temperature. Gel asphalts become more sol-like at high temperatures due to solubilization of the dispersed structures in the solvent medium.

The model of Pfeiffer and Saal is based on the observation that molecules of similar structure tend to interact preferentially with one another. In their studies of asphalts, Pfeiffer and Saal emphasized interactions between aromatic molecules. While the interaction forces among aromatics are small, they are enough to promote weak molecular associations, particularly "stacks" of aromatic molecules. Pfeiffer and Saal did not consider the interactions among heteroatom-containing molecules, which also engage in molecular associations through polar interactions. Hydrogen bonding interactions and acid-base interactions probably are stronger than the interactions among aromatic molecules. Some asphalt components are aromatic and contain heteroatoms, so they may interact with other molecules in several ways. Thus, the presence of more than one type of interacting chemical functionality on the same molecule can intensify the molecular interactions. The important feature of the Pfeiffer-Saal model is the recognition that while all molecules attract each other to some degree, aromatic (and especially polar) interactions are relatively strong (although not nearly as strong as the bonding forces that hold individual molecules together) and result in the formation of stable molecular associations of these kinds of molecules.

Petersen [1984] refined the Pfeiffer-Saal model to account for heteroatom-containing molecules, which are numerous in asphalts. These molecules contain one or more of the atoms nitrogen, oxygen, or sulfur. Some are highly polar and may interact to form strong molecular associations. During service lifetimes, asphalts chemically react with atmospheric oxygen, resulting in oxidative age hardening. When asphalts react with oxygen, sulfoxide and ketone buildup is observed. These are polar molecules. Inevitably, asphalts become more gel-like, according to Traxler's terminology, with increased service time. Sol asphalts, which contain fewer asphaltenes to begin with, exhibit less pronounced rheological effects as a result of

reaction with oxygen. According to the model, there are enough resins present in these sol-like systems to disperse additional asphaltenes. In gel-type asphalts, this is not the case, and reaction with oxygen results in large changes in rheology, as the dispersed component increases in concentration and is not readily solubilized by limited amounts of resins.

The models of Pfeiffer and Saal, Traxler, and Petersen identify asphaltenes formed by solvent precipitation with dispersed phase associations. The problem with this simplistic approach is that asphaltene yields are a function of the solvent used to precipitate them, and so the question arises as to what kind of asphaltenes (precipitated by n-heptane, n-hexane, –pentane, etc.) are the dispersed component. This dilemma has led some critics to doubt the existence of any substantially large entities in asphalts resulting from molecular associations. In other words, it is proposed that asphalts are nothing more than a simple solution of a large number of different molecules, and that there is no ordering beyond the molecular level.

The simple solution model does not explain certain asphalt physical properties, particularly the large variation of viscosity with temperature. It also does not explain the phenomenon of steric hardening, which is a viscosity increase over time that can be reversed by heat and shear. Steric hardening is distinct from oxidative age hardening. In the latter phenomenon, viscosity increases are much larger and are irreversible. Thelen [1964] rationalizes steric hardening by invoking a colloidal model. He claims that when asphalts are heated to very high temperatures, the arrangement of individual molecules is random, and a true solution exists. This random state is not thermodynamically stable at lower temperatures. Upon cooling, the more polar, and/or aromatic molecules tend to form molecular associations that are impediments to flow of the molecules in the solvent phase. Hence, the viscosity of an asphalt may rise isothermally over time as the various molecular components rearrange into the most thermodynamically stable state.

There is a considerable amount of direct evidence for the existence of molecular associations in crude oils. Dwiggins [1978] claimed to observe colloidal particles in heavy crude oils using x-ray diffraction. Crude oils also may be separated into various components by ultrafiltration and centrifugation. These separations would be impossible if the oils were simple molecular solutions of small molecules, and the results strongly support the existence of discrete dispersed entities of considerable size. Altgelt and Harle [1975] manufactured artificial asphalts by mixing asphaltenes of selected asphalts with maltenes of other asphalts. Rheological properties of the mixtures could not be predicted from asphaltene concentrations alone, demonstrating that the manner in which the asphaltenes are dispersed by maltenes is important in determining rheological properties. More evidence for the existence of discrete dispersed entities in asphalts has been published since the beginning of SHRP, and will be discussed in chapter 3.

Thus, prior to SHRP, there existed a fairly satisfactory model (at least to chemists) of asphalt structure. The model was developed over many years and is supported by a considerable body of experimental evidence. It also explains asphalt physical properties in a qualitative manner. It rationalizes the empirical classification of asphalts into the extremes of gel-like and sol-like, which is based on physical properties that influence pavement performance. One common test, the Heithaus Test [1962], uses the features of the model to classify asphalts rapidly

according to compatibility. The test has considerable practical value [Dybalski 1995] and will be discussed at length in chapter 3. Development of practical tests is one result (although not proof of) of a valid model.

Nevertheless, the colloidal model was, at the beginning of SHRP, a qualitative, descriptive model and hardly adequate for predicting the effect of chemical composition and chemical changes on asphalt physical properties [King 1991]. One of the principal objectives of SHRP and this program was and is challenging the above model and refining it so that it will be of more practical value.

ASPHALT SUPPLY LINE HISTORY

This section is a commentary on the history of purchase specification development. It is framed in terms of major historical events experienced by suppliers (refiners). All too often, the significance of these events went unnoticed for a time by users. At times this discussion is rather pointed, but is not intended to criticize any specific discipline. Rather, it is to establish the current position in the overall development of a truly blind-to-source performance specification. Finally, it is intended to raise attention to performance measurables that are not yet part of the specification.

Historically, the asphalt user community enjoyed the luxury of relatively consistent supplies of cheap asphalt, at least until the early 1970's. Prior to that time, the specifications imposed on asphalts were little more than a quality control verification of the refiner's product. The user became familiar with local or regional asphalt supplies and learned to build roadways with available asphalts. Some in the highway engineering community were well aware that the specifications did not specify performance. The literature of the time contains many technical papers dealing with variations in physical properties of asphalts of the same grade, and the resulting effect on performance. However, it was largely ignored that asphalts graded as, for example, AC-20, or as 85/100 pen, were substantially different from each other in different regions of the United States. The specification of AC-20 or AC-10 or 85/100 pen, etc., did not mean that asphalt of any given grade was interchangeable with asphalt of the same grade from a different crude oil source with respect to performance. The viscosity or penetration grading system simply ensured that any given asphalt met certain physical property requirements, with large tolerances at that, but in other properties asphalt reflected the nature of the crude oil from which it was prepared. Anderson et al. [1983] and Plummer and Zimmerman [1984] clarified this position well, but both also point out that the gradual change from penetration to viscosity grading further contributed to a lack of blind-to-source predictability. The penetration and asphalt concrete (AC) specifications were not at all blind-to-source, but then in most cases they did not need to be because refiners supplied asphalts consistently from specific oil fields.

There are notable exceptions to the above generalization that have become common stories. In some circumstances, the California Department of Transportation (Cal Trans) has blended asphalts from San Joaquin Valley crudes with those from southern California coastal crudes. The asphalt from one crude (coastal) age hardened too rapidly during service while the

other hardened so slowly that its setting characteristics were poor. Fortunately, the blends gave materials that had more desirable properties than either asphalt alone. However, this situation was experience-based and specific to two known crude sources, i.e., definitely NOT blind-to-source! In a somewhat different case, there is little doubt that J. J. Heithaus developed the well-known Heithaus compatibility test to ensure that blended asphalts from the Shell Wood River, Illinois, refinery were somewhat consistent to the user. But then there was little choice considering that Wood River is fed by a spider web of supply lines (different sources). This is an early example of blinding the source, but it was self-imposed onto the refiner by the refiner and viewed by the refiner as necessary to please the buyers (principally the Missouri and Illinois Departments of Transportation). It was NOT part of the buyers' specification; instead it was marketing strategy that was seen by the refiner as desirable or even necessary. In summary, to this point in history, there was essentially no requirement to purchase asphalts on a truly blind-to-source basis (unless the refiner chose to make it such) but neither was truly blind-to-source an important issue.

Then came the year 1973. Oil embargo! Scrambled supplies and rising crude oil prices were followed by sharp price differentials between light and heavy crude oils. Soon cokers, which convert asphalt from the cheaper heavy crudes into distillable fuel and solid coke (solid fuel), competed for large amounts of resids (asphalts), and with that event, asphalt prices skyrocketed. The widespread use of cokers set the price of asphalt almost 10 times higher than any time in history. The historical crude oil source reliability was gone and rude surprises in performance became commonplace in roadways. Yet the asphalts on the market at that time met the viscosity specification requirements. The situation was bleak. Prices were greatly increased and predictability greatly diminished.

Something had to be done, and soon. Something was done. At first it was called Strategic Transportation Research Study. Later it was renamed the Strategic Highway Research Program (SHRP). The mission: develop a blind-to-source, performance-sensitive purchase specification for roadway asphalts. The idea of a new specification had to be sold. The SHRP contractors were informed repeatedly that one of the selling points for SHRP was the suspicion that refiners were removing so-called "goodies" and "stickies" from asphalt. This story circulated fairly widely and is apparently what sociologists call an "Urban Legend." It was brought up in formal discussions at scientific meetings, as mentioned in the next paragraph. Just what "stickies" and "goodies" were was never defined, nor was there any appreciation of what effects on refining operations their removal (whatever they are) would have. Consider that refiners purchase crude oil and have no choice but to sell or use all parts of the crude after it has been separated into several products. Suppose the refiners at the time of the oil embargo went to the trouble and expense of isolating "stickies." In which product stream would they have been put? No refinery product except asphalt can tolerate sticky components. The simple fact is that some crude oils have little or no sticky materials. In any event, the fear that refiners were altering their operations to the disadvantage of asphalt users did stimulate the development of specifications based on new criteria.

Professor David Anderson et al. [1983, p. 291] stated: "The composition and properties of asphalt are dependent on the crude used in its manufacture; . . . . ". A year later Mr. Richard

Davis shed some interesting light on this subject in a recorded discussion with Dr. Mark Plummer at the Association of Asphalt Paving Technologists [Plummer and Zimmerman 1984]. The essence of these papers and discussions was that the behavioral properties of asphalt can be expected to differ with source. Further, as Mr. Davis points out, the gradual change from penetration to viscosity grading of the previous 20 years had more or less demanded a reduction in stickiness ("stickies") by requiring viscosities that were about four times higher than those used several years earlier. There are several reasons for specifying higher viscosities, and Mr. Davis made it clear that it did happen. Both experts were clear that user-imposed changes in refinery practices should be expected to give materials with new and different properties. They also made it clear that source dependence of asphalt performance properties was a known phenomenon. Neither covered one other possibility. Some crude oils have resids (i.e., undistillable materials) that simply do not adhere satisfactorily to many aggregates, i.e., are not "sticky." But then, why was this even a subject of concern? The historical purchase specifications never did include the word "sticky" or any other term to set a minimum requirement for adhesion of asphalt to aggregate. By the way, neither does the current performance grading (PG) system for asphalt cements call for any measure of adhesive quality. Almost certainly a properly designed mixture test would find differences of adhesion, but mixture tests are NOT part of any binder purchase specification.

Yes, something was done. A performance grading system for public purchase of asphalts was invented and is now going into common use. Tank car loads of asphalts (bulk liquids) that are graded alike no doubt are interchangeable with respect to physical properties over the entire service temperature range and with respect to some measure of maximum aging sensitivity. This represents a major advance in the purchasing system.

Asphalt in asphalt concrete (in roadways) does not experience the same conditions as a tank car (or even a tin can) full of asphalt. Asphalt in concrete exists as very thin layers, exposed to atmospheric oxygen all the time. Oxidation occurs and this changes both in-place stiffness and moisture sensitivity. Asphalt in concrete experiences high shear when it is very hot, when it is very cold, and when temperatures fluctuate greatly. Add water and the service environment is further complicated. All of these are the real service conditions in which asphalt is to have or should have predictable performance. What assurance is there that asphalts graded alike will still have the same stiffness as thin films? What assurance does the PG system offer that asphalts graded alike will have the same stiffness or adhesive quality when soaked in water? Or what assurance is there that oxidation will not cause major differences in water sensitivity between one asphalt and the next after a few years in service? What assurance is there that oxidation will not cause differential embrittlement (because of the influence of aggregate on oxidized asphalt) after one-fourth or one-half of the expected road lifetime? The intent of the Superpave® binder specification was to address these subjects, but there is essentially no answer to any of the above questions based on actual field trials where asphalt source is the principal variable. The current Superpave® binder performance grading system does not speak to these questions and offers no assistance in selecting appropriate asphalts to perform predictably in the above stated real world roadway environments. The questions above cannot be answered by the current specification. The Superpave® performance grading system is a major improvement over any previous grading system, but still has several "holes" if true in-service performance prediction is to be achieved.

This report, starting with chapter 3, poses an updated model of petroleum asphalt that is useful to identify "holes" in the specification. The model describes not only bulk material, but also considers asphalts exposed to roadway service conditions. The chapters that follow provide the details for the model of asphalt in service as well as to point out "holes" in the specification to the practitioner. Finally, the report concludes with recommendations of ways to improve predictability of asphalts without having to consider asphalt source.

WORK IN STRATEGIC HIGHWAY RESEARCH PROGRAM — SIGNIFICANT FINDINGS

The SHRP involved a large number of research groups working on a wide variety of projects. The project most closely involved with investigating the relationship between binder chemical and physical properties was Binder Characterization and Evaluation, Contract A-002A. Western Research Institute (WRI) and subcontractors from The Pennsylvania State University, SRI International, and Texas A&M University worked in the area from 1987 to 1992. Reports summarizing research results of this project have been published [SHRP 1993; SHRP 1994a, 1994b, 1994c].

The objective of the research in SHRP A-002A was to increase the understanding of the fundamental properties of asphalt that influence performance and thus provide a rational basis for the development of performance-based specifications that would more closely relate to the actual performance of asphalt in pavements. To achieve this objective, various techniques were developed or improved to identify important chemical and physical properties. As the project progressed, performance-related tests were developed. At the beginning of the program, many different binders were selected for study. All of them had been used in building roads, and their performance characteristics varied considerably. Eight of these binders, the so-called "core asphalts," were studied most intensively. This was done because of criticisms of much previous asphalt research involving "pet" asphalts of individual investigators.

Throughout SHRP A-002A, the model of asphalt structure described in the previous section of this chapter was challenged. Asphalts were separated into components by IEC and by SEC. According to the model, both techniques should separate asphalts into components that approximate in properties the dispersed and solvent components of asphalts. Chemical properties of the component fractions were found to differ from each other and differ among asphalts.

An IEC method was developed that separates asphalts into polar and non-polar (neutral) fractions, and further subdivides the polar moiety into acidic, basic, and amphoteric (molecules having both acidic and basic functional groups) fractions. The IEC neutral fractions comprise 50-60 percent of a given asphalt and thus, according to the model, must comprise the bulk of the asphalt solvent component. The relative amounts of acids, bases, and amphoterics also vary among asphalts. The properties of the IEC neutral fractions were intensively studied. They were found to be much less viscous than the parent asphalts. There was an almost linear relationship between number-average molecular weights of the neutral fractions and their viscosities, which is

not true for the parent asphalts. The glass transition temperatures of the IEC neutral fractions, which are much lower than glass transition temperatures of whole asphalts, also correlate fairly well with the viscosities of the IEC neutral fractions.

The amphoteric fractions are the most polar and most aromatic of asphalt components. They are the viscosity building components of asphalts. Of the three IEC polar fractions, the amphoterics are the most abundant in all the asphalts studied. They comprise 15-25 mass percent of whole asphalts. The amount of amphoterics in an asphalt increases as a result of oxidative aging.

Amphoteric molecules are by definition polyfunctional. That is to say, they have two or more polar functional groups per molecule, at least one functional group being acidic and at least one basic. Thus, amphoteric molecules may interact with one or more other polyfunctional molecules by means of moderately strong forces to form extended molecular associations. The extent of these molecular associations and the strength of the bonds by which they are held together are believed to strongly influence rheological properties of asphalts. Monofunctional acids and bases cannot, by means of polar interactions, associate with more than one other polar molecule, so that by themselves they cannot form extended molecular associations. By interacting with amphoteric functional groups they can limit the size of the amphoteric molecular associations. To verify these observations, model compounds were added to asphalts at low levels and rheological properties of the mixtures were measured. Amphoteric model compounds caused significant increases in viscosity when added to asphalts. Non-polar compounds and monofunctional acids and bases caused decreases in viscosity.

Polarity factors were assigned to the IEC fractions of asphalts. These polarity factors were calculated from mass percent data and estimated relative polarities. Using these factors and the viscosity of the IEC neutral fractions, viscosities of asphalts could be predicted. A relationship between activation energy of viscous flow and total polarity determined by IEC was found for several asphalts.

Asphalts also were fractionated using SEC. A gravimetric analytical method and a preparative method were developed to separate the solvent and dispersed components of asphalts, the cutpoint between the two fractions being based on non-fluorescence of the dispersed components, while the solvent component exhibits fluorescence. The non-fluorescent components (designated SEC Fraction-I) resembled asphaltenes in their appearance. The fluorescent eluates (SEC Fraction-II) were liquids that were less viscous than the parent asphalts. Relative amounts of the two fractions varied among asphalts and could be related to the phase angle, δ, measured at 25°C (77°F) of the parent asphalt.

A non-aqueous potentiometric titration (NAPT) method was investigated for the rapid determination of acidic and basic components in aged and unaged asphalts. The NAPT for bases was fully developed and development of a method to determine acids was started during SHRP. It was found that asphalts varied considerably in relative abundances of weak and moderately strong bases. Upon oxidation, weak bases become more abundant, but moderately strong bases become less abundant. This is due to the formation of sulfoxides, which are primary products of

oxidation (chapter 4) and which are weak bases. The reason for the decrease in moderately strong bases is not clear.

A study of the mechanism of asphalt oxidation was begun in SHRP. From chemiluminescence studies [SHRP 1993], it was shown that peroxy radicals exist in asphalts exposed to oxygen. Asphalts contain natural oxidation inhibitors, probably phenols, which inhibit oxidation of model compounds such as cumene. Paradoxically, asphalts also were shown to contain catalysts that facilitate oxidation of organic sulfides. From these studies, it was speculated that some sort of peroxy intermediate forms during asphalt oxidation.

A new aging test was developed using pressure vessel aging to simulate as nearly as possible oxidative aging in pavements and thus provide laboratory samples for studying the effects of oxidative aging on physical properties. The component compatibility of asphalts was found to be a major factor influencing the changes in physical properties on oxidation. The temperature-sensitive microstructure of asphalt was found to inhibit the oxidation in asphalts via molecular immobilization. Thus a test to simulate and predict pavement aging must be run as nearly as possible to actual pavement temperatures. The present pressure aging vessel (PAV) test, now conducted considerably above pavement temperature, needs further refinement and validation to be reliable in simulating and predicting asphalt aging in pavements. Relationships between asphalt chemical composition, oxidation products, and performance-related physical properties were found. Further elucidation was made of the mechanisms of asphalt oxidation, particularly sulfoxide formation.

To develop quantitative relationships between field performance and asphalt chemical and physical properties, a quantitative model was proposed to characterize the stiffness of asphalts as a function of loading time and temperature. This rheological model was used to relate asphalt physical and chemical properties to one another.

Measurements of rheological properties of asphalts were emphasized in the SHRP A-002A Project. The dynamic shear rheometer was studied intensively as one of the primary test devices for characterizing asphalts. Using this instrument and parallel plate geometry, many thousands of stiffness measurements of asphalts were performed. These measurements were used in the development of binder specifications. At lower temperatures, the bending beam rheometer was used to measure stiffness. The two instruments can be used to obtain most necessary rheological data for asphalts in the service temperature range [SHRP 1994b].

Properties of asphalts at low temperatures were studied during SHRP. The phenomenon of low-temperature physical hardening was identified in asphalts. It was speculated that the phenomenon was related to wax content, and may, therefore, be source-related.

Fatigue and fracture properties of asphalts also were studied during SHRP. Considerable work on a direct tension test to measure fatigue was done. Detailed descriptions of the work outlined above, including experimental procedures, have been published [SHRP 1994a; SHRP 1993; SHRP 1994b; SHRP 1994c].

REFERENCES

Altgelt, K. H., and O. L. Harle, 1975, The Effect of Asphaltenes on Asphalt Viscosity. *Industrial Engineering Chemistry, Product Research Development*, 14: 240-256.

Anderson, D. A., E. L. Dukatz, and J. L. Rosenberger, 1983, Properties of Asphalt Cement and Asphaltic Concrete. *Proceedings, Association of Asphalt Paving Technologists*, 53: 291-324.

Boduszynski, M. M., B. R. Chadha, and T. S. Pochopien, 1977, Investigations on Romashkino Asphaltic Bitumen. 3. Fractionation of Asphaltenes Using Ion Exchange Chromatography. *Fuel*, 56: 432-436.

Christensen, D. W., and D. A. Anderson, 1991, Molecular Structure in Asphalt Cements. *Proceedings, International Symposium - Chemistry of Bitumens*, Rome, Italy, June 5-8, 1991, 2: 529.

Corbett, L. W., 1970, Relationship Between Composition and Physical Properties of Asphalt. *Proceedings, Association of Asphalt Paving Technologists*, 39: 481-491.

Corbett, L. W., and R. E. Merz, 1975, Asphalt Binder Hardening in the Michigan Test Road After 18 Years of Service. *Transportation Research Record* 544, 27-34.

Davis, T. C., and J. C. Petersen, 1967, An Inverse GLC Study of Asphalts Used in the Zaca-Wigmore Experimental Road Test. *Proceedings, Association of Asphalt Paving Technologists*, 36: 1-15.

Dwiggins, C. W., 1978, Study of the Colloidal Nature of Petroleum with an Automated Bonse-Hart X-Ray Small-Angle Scattering Unit. *Applied Crystallography*, 11: 615-619.

Dybalski, J., 1995, Personal Communication.

Girdler, R. B., 1965, Constitution of Asphaltenes and Related Studies. *Proceedings, Association of Asphalt Paving Technologists*, 34: 45-79.

Goodrich, J. L., J. E. Goodrich, and W. J. Kari, 1986, Asphalt Composition Tests: Their Application and Relation to Field Performance. *Transportation Research Record* 1096, 146-167.

Heithaus, J. J., 1962, Measurement of Significance of Asphaltene Peptization. *Journal of the Institute of Petroleum*, 48: 45-53.

Hubbard, R. L., and K. E. Stanfield, 1948, Determination of Asphaltenes, Oils, and Resins in Asphalt. *Analytical Chemistry*, 20: 460.

Hveem, F. N., 1943, Quality Tests for Asphalts - A Progress Report. *Proceedings, Association of Asphalt Paving Technologists*, 15: 111-152.

Hveem, F. N., E. Zube, and J. Skog, 1959, Progress Report on the Zaca-Wigmore Experimental Asphalt Test Project. *ASTM Special Technical Publication*, 277: 1-45.

King, G. N., 1991, Using Rapid Analytical Methods to Define Bitumen Chemical Structure: A Refiner's Approach. *Proceedings, International Symposium - Chemistry of Bitumens*, Rome, Italy, June 5-8, 1991, 2: 742-769.

Labout, J. W. A., 1950, Constitution of Asphaltic Bitumen. In Pfeiffer, J. P., ed., *The Properties of Asphaltic Bitumen*. Elsevier, New York, NY, 13-48.

Mack, C. J., 1932, Colloid Chemistry of Asphalts, *Journal of Physical Chemistry*, 36: 2901-2914.

McKay, J. F., P. J. Amend, T. E. Cogswell, P. M. Harnsberger, R. B. Erickson, and D. R. Latham, 1978, Petroleum Asphaltenes: Chemistry and Composition. In Uden, P., S. Siggia, and H. P. Jensen, eds., *Analytical Chemistry of Liquid Fuel Sources*. Advances in Chemistry Series 170, American Chemical Society, Washington, D. C., 128-142.

Mysels, K. J., 1959, *Introduction to Colloid Chemistry*. Interscience Publishers, Inc., New York.

Nellensteyn, F. J., 1924, The Constitution of Asphalt. *Institute of Petroleum Technology*, 14: 134-138.

Petersen, J. C., 1984, Chemical Composition of Asphalt as Related to Asphalt Durability: State of the Art. *Transportation Research Record* 999, 13-30.

Pfeiffer, J. P., and R. N. Saal, 1940, Asphaltic Bitumen as Colloidal System. *Journal of Physical Chemistry*, 44: 139-149.

Plancher, H., E. L. Green, and J. C. Petersen, 1976, Reduction of Oxidative Hardening of Asphalts by Treatment with Hydrated Lime - A Mechanistic Study. *Proceedings, Association of Asphalt Paving Technologists*, 45: 1-24.

Plummer, M. A., and C. C. Zimmerman, 1984, Asphalt Quality and Yield From Crude Oil Analysis. *Proceedings, Association of Asphalt Paving Technologists*, 53: 138-159, Mr. Davis' discussion p. 150.

Ramsey, J. W., F. R. MacDonald, and J. C. Petersen, 1967, Structural Study of Asphalts by Nuclear Magnetic Resonance. *Industrial Engineering Chemistry, Product Research Development*, 6: 231-236.

Rostler, F. S., and R. M. White, 1962, Composition and Changes in Composition of Highway Asphalts, 85-100 Penetration Grade. *Proceedings, Association of Asphalt Paving Technologists*, 31: 35-89.

Schmidt, R. J., and E. J. Barrall, 1965, Asphalt Transitions. *Journal of the Institute of Petroleum*, 51: 162-168.

Shaw, D. J., 1980, *Introduction to Colloid and Surface Chemistry.* Butterworths, London, Chapter 1.

SHRP, 1993, *SHRP-A-368, Binder Characterization and Evaluation, Volume 2: Chemistry.* Strategic Highway Research Program, National Research Council, Washington, D. C.

SHRP, 1994a, *SHRP-A-367, Binder Characterization and Evaluation, Volume 1.* Strategic Highway Research Program, National Research Council, Washington, D. C.

SHRP, 1994b, *SHRP-A-369, Binder Characterization and Evaluation, Volume 3: Physical Characterization.* Strategic Highway Research Program, National Research Council, Washington, D. C.

SHRP, 1994c, *SHRP-A-370, Binder Characterization and Evaluation, Volume 4: Test Methods.* Strategic Highway Research Program, National Research Council, Washington, D. C.

Speight, J. G., 1980, *The Chemistry and Technology of Petroleum.* Marcel Dekker Inc., New York, NY, Chapter 3.

Thelen, E., 1964, Asphalt Composition, Rheological Properties, and Syneresis. *American Chemical Society Division of Petroleum Chemistry Preprints*, 9(2): B-5 - B-14.

Traxler, R. N., and H. E. Schweyer, 1953, Separating Asphalt Materials - Butanol Acetone Method. *Oil and Gas Journal*, 52: 158.

Traxler, R. N., 1961, *Asphalt.* Reinhold Publishing Co., New York, NY, Chapter 5.

CHAPTER 2: OBJECTIVES AND SUMMARY OF ACCOMPLISHMENTS

OBJECTIVES OF THIS PROJECT

Several objectives were set at the beginning of this project. These objectives were oriented toward answering practical questions of prediction of rutting, fatigue, thermal cracking, effects of oxidation, and ill-effects of water (other than outright stripping) in pavement. In the main, the objectives were set by work that had not been completed or, in some cases, was impossible to start during the SHRP. The objectives can be placed into four main categories: (1) improvement of the structural and rheological models of petroleum asphalt, (2) a challenge and/or validation of current purchase (Superpave®) specifications, (3) a systematic search for performance-related properties of asphalts for which there is no specification (i.e., a search for "holes" in the current specification), and (4) to convert time-consuming specification or potential specification laboratory methods into relatively straightforward and very rapid methods.

A comprehensive model that considers all significant behavioral characteristics of any system is always useful for predictive purposes and is especially useful when accurate quantitation accompanies the model. A comprehensive model is simply a complete description of behavior, the ultimate goal of any material specification. In this project, attention has been focused on the properties of asphalt in its use environment as well as on its properties as a dry, bulk material. For a system such as petroleum asphalt, many characteristics have never been considered seriously when predicting pavement performance. The only chemistry considered in the current version of the Superpave® binder specification is the effect of oxidative aging on intermediate and low temperature properties. However, the analytical data presented in the following chapters show that there are many variations in the chemistry of asphalt that are related to asphalt source. Further, the model described in these chapters explains how these variations should affect, or influence, performance of asphalt in pavement. For example, as shown in detail in chapter 6, the chemistry of asphalt has a major influence on crumb rubber modification. Asphalts from two different sources, but prepared to the same PG grade, often become two totally different binders when reacted with crumb rubber, even when all conditions of rubber source, particle size, asphalt/rubber ratio, reaction time, and temperature are identical. It is a readily measurable chemical property of asphalt that controls the level of "digestion" of rubber and, hence, controls the final crumb rubber modified asphalt physical properties. The effects of this chemical reaction CANNOT be predicted from any of the Superpave® binder measurements. Other examples of phenomena that should be able to be predicted for roadway performance include the effects of aggregate, water, high temperature oxidation conditions (the PAV test is somewhat helpful here), steric hardening, and differential shrinkage of asphalt away from aggregate. All of the above were "holes" in the knowledge of prediction of the behavior of asphalt in a pavement environment at the end of the SHRP.

SUMMARY OF ACCOMPLISHMENTS DURING THIS PROJECT

Several advances have been made during this project to improve prediction of the behavior of asphalt in pavement. A chemical structural model of asphalt has been developed (refined since SHRP) that accommodates observed behavior over the entire service temperature range and other service environments of pavement. Improvements were made in the rheological model that was used to develop the Superpave® binder specification. Both have been reported to the FHWA Binder Expert Task Group on a regular basis. More specific examples of accomplishments during this project are as follows. It was shown that the naturally occurring acid content of asphalt must be known in order to predict the properties of crumb rubber modified asphalt and, further, the ratio of natural to synthetic rubber in crumb rubber modifier (CRM) must also be known. Separately, a rapid (30 minutes) analytical method for determining acid content in asphalt (adapted from NAPT) was developed. The utility of solid-state NMR spectroscopy as a reliable method to determine natural rubber-synthetic rubber ratios in about an hour was demonstrated.

The effects of variation in asphalt composition under the influence of aggregate have been demonstrated during this project. As with previous examples, asphalts that are classified alike by the Superpave® binder specification actually have significantly varied properties as thin films of asphalts between aggregate surfaces at 20 and less micron film thicknesses. This phenomenon is not observed with thin films of asphalt on glass plates. Likewise, asphalts of the same PG grade show different yield stresses while in contact with high percentages of mineral filler. Yield stress is an indication of permanent deformation propensity. Again, the composition of the asphalt, especially the 2-quinolones and carboxylic acids, strongly affects its physical properties in thin films on aggregate, but these effects of composition on performance are not considered in the Superpave® binder specification.

Another significant result from this project is the determination of the effect of water on the binder. Again, like above examples, asphalts graded as being alike by the PG system become quite different from each other once they are saturated with water. Before asphalt is even a constituent of a pavement, there is a large differential water sensitivity that varies with source! An environmental electron scanning microscope (ESEM) has been employed to examine asphalt-aggregate interfaces. This has been done with freeze-thaw cycling with dry (control) and water-soaked samples. The ESEM records a photomicrograph (greatly enlarged "picture") of the interface. Striking differences of adhesion of asphalt to aggregate were observed for asphalts that were graded as being alike. The loss of adhesion clearly leads to reduced strength. Differences in failure by fatigue could be expected as well as major differences in the time to failure as a result of stripping.

Low temperature properties have been studied using two techniques. Modulated differential scanning calorimetry (MDSC) is a method that detects changes in heat capacity and, consequently, changes in physical form(s) of materials. It was applied to petroleum asphalt during this project, and the results show that the amount of the crystallizable fraction of neutral materials (the non-polar components of asphalts are largely amorphous, but some of them form crystals) and the acid content in tank asphalts are the factors of a constitutive relationship that

correlates very well with the bending beam low temperature specification method. However, the MDSC is a much faster method than bending beam (or direct tension) measurements made on artificially aged asphalts. The refiners are certainly interested in this area for certification purposes if for nothing else.

Simulation of embrittlement that takes place in hot climates is not considered in the PG system. There is a specification requirement to protect against rutting that a plant mix simulation be imposed and that the resulting asphalt meet a minimum stiffness to achieve a given high temperature grade. But there is no differentiation in the purchase criteria between asphalts that will harden just enough to pass the rutting requirement (PAV residue having $G^*/\sin \delta = 2.2$ kPa minimum) from those that will harden greatly in a hot (oxidative) climate. The results given in successive chapters show that stiffening of oxidized asphalt in contact with a given aggregate varies sharply with asphalt source. Current testing methods measure oxidative aging effects on the binder alone.

The plant mix simulation mentioned above is, of course, the rolling thin film oven test (RTFOT), a tedious process. One faster method reported herein is to mimic the RTFOT using the methodology of the German Rolling Flask method. The work reported herein describes a recipe that will produce 200 g of simulated plant mix asphalt at once rather than a few grams at a time in each of several RTFOT bottles.

Simulation of oxidative aging is a bottleneck in the Superpave® specification process. It requires 20 hours processing (oxidation) time and this is a compromise with the original 6-day, 60°C (140°F) test developed during SHRP. The 6-day test is considered to simulate road aging better than the 20-hour test. In a cooperative venture with the Kansas Department of Transportation, a microwave-promoted oxidative aging method that simulates results of the 6-day test in less than 6 hours is being developed.

Fatigue is the almost undefinable failure mode in asphalt concrete. A major advance has been made in this project by Texas A&M and North Carolina State Universities to describe and measure fatigue in terms of microdamage and its attendant healing. Improvements in accuracy of rheological characterization of asphalts have been made by Pennsylvania State University as part of this project.

A shale oil modified asphalt concrete (SOMAT) test road, with polymer modified control sections, was built near Jackson, Wyoming, as part of US Hwy 89. The performance and environmental impact are being monitored as part of this project. The environmental monitoring shows no detectable leaching and the performance of the test and control sections are similar. The test and control sections both show modest amounts of thermal cracking (total cracking minus reflective cracking), but both asphalts are four low temperature grades higher than recommended for the area, i.e., both are -22°C grade and -46°C is recommended. This draws serious questions about the need for a -46°C material in this climate. Distress surveys were conducted by Nichols Consulting Engineers, Chtd., Reno, Nevada.

Eighteen sulfur extended asphalt (SEA) highways that range from 15 to 20 years in age were evaluated during this project by Brent Rauhut Engineering, Austin, Texas. A manuscript reporting the results was submitted to FHWA and was accepted for publication. Generally, the sulfur can be viewed as a spectator. The road performances were affected very little by the presence of sulfur, i.e., no significant performance advantages or disadvantages were observed. However, caution is drawn to the recyclability of SEA. While recycling of SEA was not considered in this project, data from other sources suggest the process could produce hazardous off gases.

Separately, efforts are under way to speed up and/or improve test methods. These include development of a faster plant mix aging simulation and a faster oxidative aging simulation, as described above. Work also has been done on the development of a fast (1-2 hr) size exclusion chromatographic separation method (a predictor of viscoelastic properties), development of a rapid, operator independent version of the classical Heithaus compatibility test, and a rapid method to measure strengths and quantities of acids in asphalt.

In summary, the source dependence that causes variable behavior of asphalt under several service conditions has been demonstrated. The source dependencies not identified by the current PG system include effects of water, the effects of aggregate on thin asphalt films, the oxidative aging propensity of binders in contact with aggregates at high temperature, the "digestive" power asphalt has for crumb rubber, and the expected low temperature properties when asphalt is in a cold environment for prolonged periods.

The effects of water on various properties, of neutral materials on low temperature properties, of acids on crumb rubber digestion, the behavior of asphalts in thin films, the changes observed during high temperature oxidation, and healing propensity have all been demonstrated to vary sharply with source in this project. Yet none are considered in the current purchase specification. New methods to predict these source dependencies are available. Quantitation of their effects in pavement situations (validation) is needed next. Following that, implementation into the purchase specification is recommended for those methods that truly reduce the source sensitivity.

CHAPTER 3: DEVELOPMENTS IN MODEL OF ASPHALT STRUCTURE SINCE STRATEGIC HIGHWAY RESEARCH PROGRAM

SYNOPSIS

The first section of this chapter describes a model of asphalt structure from the perspective of rheology. The work of Storm, Sheu, and associates is described. Then, based upon theoretical considerations, a relationship between relative viscosities of asphalts at 25°C (77°F) and 0.1 rad/s and compositional features is developed.

One of the primary objectives of this program is to determine the relationships between various asphalt components and specific physical and chemical properties. Toward this end, asphalts have been separated into maltenes and asphaltenes, into defined chemical fractions by ion exchange chromatography, and into fractions of varying molecular size by size exclusion chromatography. The details of these separations are described in the second section of the chapter. It was found that solubility parameters of the neutral fractions isolated by ion exchange chromatography are surprisingly low. An excellent linear correlation exists between number-average molecular weights of this fraction and their glass transition temperatures. The glass transition temperature of an asphalt was found to be a function of the glass transition temperature of the non-polar component as represented by neutral or low molecular weight size exclusion chromatographic fractions and the amount (but not the nature) of polar components. Waxes were isolated from neutral fractions and were found to have varying influences on physical properties, depending on the nature of the waxes.

The most polar, aromatic components of asphalts were isolated by size exclusion chromatography. These materials were found to have effective molecular weights of up to 40,000 daltons by membrane osmometry. The molecular sizes of these entities are a function of association phenomena, which persist in solution. Rheological properties of asphalts are strongly influenced by these materials.

The third section of this chapter describes research on low temperature properties of asphalts using modulated differential scanning calorimetry and various NMR techniques. The formation of crystallizable phases, almost certainly waxes, was demonstrated by both techniques. These phases must have a great impact on low temperature properties. Experiments were performed using additives to alter glass transition temperatures and crystal formation. Specific kinds of molecular motions in asphalts that affect low temperature behavior were monitored using solid state carbon-13 NMR from ambient temperatures to below glass transition temperatures.

INTRODUCTION TO DISPERSED SYSTEMS

Equations Developed for Model Systems

In chapter 1, a model of asphalt structure was described. The historical development of this model from about 1920 to 1985 was presented. It was shown that the model was based on a variety of observations, some based on asphalt physical properties and some based on the chemical nature of asphalts. In the section below, implications of asphalt rheological properties on any model of asphalt structure are outlined. Some of the material in chapter 1 is repeated below for purposes of exposition.

Rheology is the study of the flow properties of materials. It is a science of great practical importance, particularly with respect to asphalt. The rheological properties of asphalts strongly influence pavement performance characteristics such as rutting and resistance to cracking.

One of the most important rheological properties of a fluid is its viscosity (or coefficient of viscosity), usually denoted by the Greek letter eta (η). For any fluid, the viscosity is defined as the force (in dynes) required, per square centimeter, to maintain a relative velocity of one centimeter per second between two planes separated by one centimeter of the fluid [Mysels 1967]. The force per unit area (F/A) is defined as the shearing stress. The velocity per unit of spacing between planes (dv/dx) is defined as the rate of shear. Thus,

$$\eta = \frac{\text{shearing stress}}{\text{rate of shear}} = \frac{(F/A)}{(dv/dx)} \qquad (3\text{-}1)$$

Absolute viscosity (η) in centimeter-gram-second units is reported in poises. In Standard International units, viscosities are reported in pascal-seconds, abbreviated Pa·s. One pascal-second is equivalent to 10 poises.

Viscosity is the measure of the resistance of a fluid to flow. One objective of rheological studies of liquids is to determine the relationship between the two components of viscosity, which are rate of shear and shearing stress [Severs 1962]. For many pure liquids and dilute solutions, absolute viscosity at a given temperature and pressure is independent of rate of shear. Such materials are referred to as Newtonian. A plot of rate of shear versus shearing stress for a Newtonian fluid will be a straight line intersecting the origin.

For many concentrated solutions and colloidal dispersions, viscosity is not independent of shear. Such liquids are designated as non-Newtonian. A plot of rate of shear versus shearing stress for a non-Newtonian liquid is non-linear. Viscosities of these liquids are termed apparent viscosities or shear-dependent viscosities. It should be noted that a liquid may exhibit non-Newtonian behavior at one temperature and Newtonian behavior at a higher temperature. Some asphalts behave in this manner. The main causes of non-Newtonian behavior appear to be (1) shear-induced orientation in solutions and suspensions of asymmetric particles, and (2) formation of microstructures that immobilize solvent molecules in systems in which solute particles are much larger than solvent molecules [Shaw 1980].

The viscosities and apparent viscosities of Newtonian and non-Newtonian liquids are dependent on temperature and pressure. The dependence of viscosity on these two variables is substance specific. For example, the viscosity of water is halved between 0°C (32°F) and 25°C (77°F). It is halved again between the latter temperature and 63°C (145.4°F) [Mysels 1967]. Asphalt viscosities vary much more than this over the same temperature range.

When liquids solidify, they become glassy (amorphous) or crystalline solids. Typically, solid materials deform slightly when subjected to shearing stress. The deformation is proportional to the applied stress. When the stress is removed, the solid immediately reverts to its original shape. The applied stress imparts energy to the solid, and this energy is released when the stress ceases to act on the solid. Solids that behave in this manner are elastic solids. In Newtonian liquids, the energy imparted by applied stresses is dissipated as heat, and the liquid does not revert to its original condition when stress is removed. Newtonian liquids are perfectly viscous. Some materials, which may even appear to be solid, exhibit behavior intermediate between viscous liquids and elastic solids. They deform continuously when subjected to stresses, but revert only partly to their original form when the stress is removed. These viscoelastic materials tend to exhibit elastic behavior when subjected to rapid deformations, but exhibit viscous behavior when stressed for longer periods of time. Asphalts in the service temperature range above glass transition temperatures are viscoelastic, and this behavior is critical to their utilization in pavements. Other examples of viscoelastic materials are various polymers and solutions of polymers. An unusual property of viscoelastic materials is that flow tends to occur at right angles to applied forces [Shaw 1980].

Shaw [1980] points out that there are two general approaches to describing rheological properties of materials. One, the engineering approach, is to derive equations that describe flow behavior for each material. A second, the physical-chemical approach, is to correlate flow behavior with a model of the structure of a material under investigation. If the structural model is correct, it should be possible to derive equations that accurately describe flow behavior and correlate observed behavior with structure. Both approaches have been used in the case of asphalts.

The rheological behavior of viscoelastic materials is complex and not completely understood. Mechanical spectrometers are used to study viscoelastic materials. A mechanical spectrometer is a research instrument in which a substance (such as an asphalt) is subjected to sinusoidal deformations. The response of the substance is monitored. Stress curves as a function of applied strain are obtained. These curves differ from one substance to another, and among asphalts. A complex modulus $|G^*|$ is obtained from the data. This entity is a combination of a viscous component G'' and an elastic component G', i.e., $|G^*| = [(G')^2 + (G'')^2]^{1/2}$. The quantity $|G^*|$ divided by the frequency of the oscillating deformation, ω, is equivalent to the apparent viscosity or shear dependent viscosity, or as the quantity also is known, the complex viscosity, η^*. Complex viscosities measured on the mechanical spectrometer also are referred to as dynamic viscosities. The latter term indicates that measurements were performed on an oscillatory apparatus. At a frequency of 1.0 radians/s, η^* is equivalent to $|G^*|$. A mechanical spectrometer provides a scan of $|G^*|$ over a wide range of frequencies. When G'' is divided by G', the quantity tan δ is obtained, δ being the phase angle. Tan δ is known as the loss tangent

and measures the viscoelastic character of an asphalt or other substance. Large values of tan δ indicate that the material is highly viscous (Newtonian), whereas low tan δ values are characteristic of an elastic material. Mechanical spectrometers allow detailed investigation of the processes of energy dissipation in substances such as asphalts. Information about asphalt structure and intermolecular interactions also can be obtained. The results of these studies should be useful in determining limiting performance conditions for asphalts.

It is emphasized many times in this report that the rheological properties of asphalt strongly influence the performance of asphalts in roads. Among the rheological properties of asphalt that are of interest are the temperature susceptibility and shear susceptibility. These properties are measures of the variation of rheological properties with temperature and rate of shear, respectively. For example, above their glass transition temperatures, which are usually well below 0°C (32°F), asphalt complex viscosities vary greatly with temperature. Asphalts are quite fluid and essentially Newtonian at mix plant temperatures (160°C [325°F]), but become viscoelastic and stiff at normal service temperatures. Asphalt viscosities at service temperatures are a function of shear, so it is appropriate to refer to the quantity as the apparent, shear dependent, or complex viscosity η^*, as for all non-Newtonian materials. It is the viscoelastic behavior of asphalts at service temperatures that is of such great interest to pavement technologists. These properties, known as complex flow in the older literature, have been instrumental in developing standards for asphalt selection. Obviously, any model of asphalt structure must account for the characteristic rheological behavior of asphalt.

Theories of viscosities of liquids have been advanced by Andrade [1934] and by Eyring [1936]. Andrade showed that the flow of liquids could be modeled by relative motions of layers of molecules, and that energy exchanges between layers would result from molecular vibrations. He reasoned that energy exchange by translational motion, important in gases, was not important in liquid flow. This is because molecules in the liquid state do not have the three-dimensional degrees of freedom possessed by molecules in the gaseous state. Eyring treated flow in liquids as a rate process involving molecules surmounting activation energy barriers. Ewell and Eyring [1937] review various properties of liquids composed of small, non-polar molecules. For example, all such liquids have the same viscosity (0.002 Pa·s) at the melting point. The viscosity-temperature relationship of these liquids is straightforward, and is sufficiently described by the Arrhenius equation [Severs 1962]. The relationship of the natural logarithm of viscosity plotted versus the reciprocal of absolute temperature is a straight line. Ewell and Eyring view the flow of liquids on the molecular level as one in which individual molecules move into suitably sized holes. They note that for small spherical molecules, activation energies of viscous flow in the liquid state are approximately one-third of the energy of vaporization, so that viscous flow may be considered to be vaporization in one degree of freedom. The flow of larger molecules cannot be treated so simply, as creation of large holes is unlikely. These molecules are believed to flow as sub-units of fixed size. Eyring explains non-Newtonian behavior as arising when work required for molecules to surmount energy barriers to flow is significant in magnitude compared with the product of the Boltzman constant, k_B, and the absolute temperature, T. In liquids composed of small, non-polar molecules, energy barriers to the flow are small compared with k_BT.

Most liquids, including asphalts, are composed of molecules that are not small, non-polar, and spherical. Some liquids contain large molecules. Others contain polar molecules, which can interact to form molecular associations. These molecular associations may affect rheological properties of liquids in the same manner as large molecules. The difference between large molecules and molecular associations of polar molecules is that the latter are held together by weak forces. The large molecules and the individual polar molecules are held together by strong chemical bonds that are not broken except by large energy inputs. Thus, the size of a particular molecular association is a function of temperature and mechanical energy input. Moderate heating and agitation reduce the sizes of molecular associations. Very high temperatures are required to break bonds between atoms within molecules, the so-called covalent bonds.

Many familiar liquids are dispersions of large molecular entities (either large molecules or associations of smaller molecules) in a bulk solvent. Such dispersions are often termed colloids. An early attempt to model the rheological properties of dispersions is that of Einstein [1906]. He deduced a relationship between the volume fraction of the dispersed particles and the relative viscosity of the whole liquid (dispersion):

$$\eta_{rel} \equiv \frac{\eta}{\eta_o} = 1 + 2.5\phi \tag{3-2}$$

In equation 3-2, the relative viscosity (η_{rel}) is defined as the viscosity of the dispersion (η) divided by the viscosity of the solvent (η_0). For the Einstein equation to be valid, the volume fraction of the dispersed particles, ϕ, must be low (< 0.05). Therefore, they are essentially non-interacting. They also must be nearly spherical and perfectly rigid. The size of the dispersed particles is very large compared with the individual molecules comprising the solvent. Equation 3-2 establishes a relationship between the composition of a dispersion of particles (ϕ is a compositional property) and a rheological property, η_{rel}, of the dispersion. The relative viscosity of the dispersion is dependent on ϕ but is independent of the nature or size of the non-interacting spherical particles. Thus, from a simple model of dilute spherical particles dispersed in a uniform fluid medium, Einstein derived an equation that accurately relates two properties of certain kinds of dispersions.

Eilers [1941] developed an empirical equation to relate ϕ to η_{rel} in bituminous emulsion systems as follows:

$$\eta_{rel} = \exp\left(1 + \frac{1.25\phi}{1 - k_E\phi}\right)^2 \tag{3-3}$$

Eilers found that values of the empirical parameter, k_E, which is an estimate of the packing efficiency of the emulsified particles, varied between 1.28 and 1.30, depending on the nature of the bitumen.

Mooney [1951] investigated dispersions of interacting spherical particles of various sizes at higher concentrations than the systems studied by Einstein. He proposed that the relationship

between relative viscosity and volume fraction of dispersed interacting spherical particles is as follows:

$$\eta_{rel} = \exp\left(\frac{2.5\phi}{1 - k_M\phi}\right) \tag{3-4}$$

In equation 3-4, k_M, the Mooney parameter, is designated as a crowding factor. Mooney states that k_M varies between the values of 1.35 and 1.91, depending on the system. In practice it is not easy to predict what the value of k_M should be for a given system.

Roscoe [1952] also investigated dispersions of spherical particles at higher concentrations. He noted that as the volume fraction of the spherical particles increases, relative viscosity is no longer independent of their size distribution. In equation 3-2, if η_{rel} is plotted versus ϕ, a straight line with a slope equal to 2.5 is observed for low values of ϕ. At higher values of ϕ, this relationship is no longer linear and slopes of up to 4.0 are observed. Dispersions in which spherical particles are uniform in size have higher η_{rel} values than dispersions consisting of spherical particles of non-uniform size. This is due to the more efficient packing of the particles of varying sizes. In each case, interacting spherical particles trap a portion of the solvent, resulting in a higher effective concentration of the dispersed component. Roscoe did not consider immobilization of solvent molecules on the particle surfaces, which would vary according to particle size. It was proposed that for dispersions of spherical particles of uniform size,

$$\eta_{rel} = \left(1 - \frac{\phi}{\phi_0}\right)^{-2.5} \tag{3-5}$$

where $\phi_0 = 0.74$, the packing fraction for a hexagonal close packed arrangement of spheres. For dispersions of spherical particles of very disperse sizes,

$$\eta_{rel} = (1 - \phi)^{-2.5} \tag{3-6}$$

The spheres of disperse sizes in theory may pack much more efficiently than uniform size spheres, and so these particles may occupy over 74 volume percent of a system. At very low values of ϕ, equations 3-5 and 3-6 give nearly identical numerical values of η_{rel} as does equation 3-2.

Maron and Fok [1953] applied the Mooney and Roscoe equations to concentrated dispersions of spherical glass beads (4 μm to 12 μm in diameter) in a glycerol-water medium. Neither equation successfully related relative viscosity values of the dispersions with the volume fraction of the glass beads. Maron proposed another equation, which appeared to successfully represent their data:

$$\log(\eta_{rel}) = \left(\frac{\beta\alpha\phi}{1 - \alpha\phi} \right) \qquad (3\text{-}7)$$

In equation 3-7, α and β are parameters related to the size distribution and shape of the particles. The volume fraction at which the viscosity of the dispersion becomes infinite is $1/\alpha$, which varies according to the size distribution of the spherical particles. For uniformly sized spheres, $1/\alpha$ should be 0.74, the packing fraction for a hexagonally close packed arrangement of spheres. In practice, $1/\alpha$ was found to vary from 0.68 to 0.88. The number $2.033\alpha\beta$ is the slope of the curve obtained when η_{rel} is plotted versus ϕ as ϕ approaches zero. For this system, the slope was found to range from 3.15 to 3.35, and is not 2.5. That is why the Mooney and Roscoe equations were not applicable to the system.

Pal and Rhodes [1989] applied equations 3-2 through 3-7 in an attempt to relate the relative viscosities of emulsions that they studied with the dispersed phase concentrations of the emulsions. Emulsions consist of one or more immiscible liquid components stabilized by emulsifying agents. In the case of a two-component emulsion, one liquid is considered to be dispersed in the form of very small droplets in the other liquid, which is the solvent. The emulsifying agent adsorbs on the droplet surfaces and prevents their coalescence and separation into two distinct macro phases. The emulsifying agent is chemically distinct from the two immiscible liquids, so that in reality such a two-component emulsion consists of at least three distinct chemical species. However, the concentration of the emulsifying agent is small compared with the dispersed liquid and the solvent. Each of the droplets of the dispersed liquid and the coating of emulsifying agent constitutes a distinct phase, different from the continuous solvent phase.

Pal and Rhodes found that equations 3-2 through 3-7 could not rationalize variations of η_{rel} with concentrations of dispersed phases (dispersed droplets) for a number of emulsions. Therefore, they proposed an equation of their own, based on a model of the structure of emulsions. At low concentrations of the dispersed phase, many emulsions are Newtonian. Non-Newtonian behavior is observed in more concentrated systems, due to the formation of flocs of dispersed phase droplets. Flocs are aggregations of the droplets, which weakly interact with one another, yet do not coalesce into larger droplets. Each floc immobilizes a portion of the continuous phase (solvent) by entrapment between the aggregated droplets, increasing the effective dispersed phase concentration. For this reason, non-Newtonian emulsions usually are more viscous than Newtonian emulsions at the same concentration. Shear breaks up flocs, liberating the immobilized solvent that is trapped between the droplets that comprise the flocs. This reduces the effective dispersed phase concentration, reducing viscosity. At very high shear rates, all flocs are broken up and the viscosity of the system reaches a constant value.

In addition to the effect of shear on the floc size, Pal and Rhodes considered solvation effects on the dispersed phase volume. Emulsifying agents absorbed on the dispersed droplets attract and immobilize some of the solvent, thus increasing the effective dispersed phase concentration. The solvation effect is operative whether or not the system is Newtonian or non-Newtonian. Pal and Rhodes assign a solvation factor K_S to emulsion systems. K_S will vary

according to emulsifier concentration and the nature of the dispersed and continuous phases. The effective dispersed phase concentration (ϕ_{eff}) for an emulsion, according to Pal and Rhodes is:

$$\phi_{eff} = K_S K_F \phi \tag{3-8}$$

where K_S is the solvation factor and K_F is the flocculation factor. K_F also is designated as $1/(1 - \alpha)$, where α is that fraction of the floc not occupied by the solvated particles (this α is not the same as α in equation 3-7). The flocculation factor K_F depends on shear. As shear rate increases, the size of the flocs and α decrease, hence K_F also decreases. At high shear rates, or in a Newtonian system, $\alpha = 0$ and $K_F = 1$. Pal and Rhodes propose the following equation to relate relative viscosity with the dispersed phase volume fraction, where K_F is a function of the shear rate, i.e., $K_F = K_F(d\gamma/dt)$.

$$\eta_{rel} = (1 - K_S K_F \phi)^{-2.5} \tag{3-9}$$

A plot of $(\eta_{rel})^{-0.4}$ versus ϕ at a given rate of shear should be a straight line with a slope of $K_S K_F$.

Studies of Petroleum Resids by Storm, Sheu, and Associates

Sheu and Storm [1995] have attempted to explain the rheology of petroleum residua using the models of dispersed systems described above. Their studies are applicable to asphalt rheology because most asphalts are residua from the distillation of petroleum. Before discussing Storm's results, it is necessary to review certain features of asphalt physical properties and their relation to composition.

The viscoelastic behavior of asphalts is known to resemble that of amorphous polymers. Schmidt and Barrall [1965] state that, although asphalts are much more heterogeneous, they may be treated rheologically as low molecular weight polymers. Polymers are very large molecules whose constituent atoms are held together by strong covalent bonds. A polymer molecule is formed from combinations of atoms known as repeating units. For example, one of the simplest organic polymers is polyethylene, in which the repeating unit is $-CH_2CH_2-$. To be classified as a polymer, a molecule must have 100 or more repeating units. Thus, the lowest molecular weight value for a true polymeric polyethylene would be 100 times the molecular weight of the repeating unit, 100 times 28, or approximately 2,800 daltons. From considerations of valence, such a polyethylene molecule (assuming each repeating unit to be part of a linear chain) must also have two CH_3 end groups. So the lowest molecular weight of a truly polymeric polyethylene would be 2,830 daltons. Other familiar organic polymers, such as rubber and cellulose, have much larger repeating units than polyethylene. The molecular weights of most organic polymers are greater than 20,000 daltons. Macromolecules differ from polymers in not being composed of large numbers of identical repeating units. Molecular weights of macromolecules are in the same range as polymers. Macromolecules are held together by strong covalent bonds. Asphalts are not known to contain molecules of sufficiently large size to qualify as true polymers. Few asphalt components are known to be composed of multiple repeating units. The largest molecular entities in asphalts might be considered to be macromolecules. A discussion of the

various methods used to determine asphalt molecular weights is provided in another section of this chapter. From the above considerations, it is of interest to determine what features of asphalt structure cause the rheological properties to resemble those of polymers.

It was mentioned in chapter 1 that asphalts consist of a very large number of different kinds of organic compounds. Some are non-polar hydrocarbons, and others are compounds of considerable polarity, such as phenols, carboxylic acids, quinolines, etc. The most polar and least polar constituents are not mutually soluble. Obviously asphalts must contain compounds of intermediate polarity that act in such a way that the system as a whole is stable at service temperatures.

The addition of large amounts of non-polar solvents (e.g., n-pentane, n-heptane, iso-octane) to asphalts disturbs the total polarity of the system and results in the precipitation of black, friable solids called asphaltenes. Asphaltenes can comprise upwards of 25 mass percent (and in some cases higher) of most unaged paving asphalts. The remainder of an asphalt, usually referred to as maltenes or petrolenes, is much less viscous than the original asphalt. Therefore asphaltenes are the viscosity-building components of asphalt. Asphaltenes from different asphalts vary in several characteristics, as do maltenes. Rheological properties of asphalts are influenced both by the nature and relative amounts of asphaltenes and maltenes [Altgelt and Harle 1975], which determine the manner in which the two components interact.

Asphaltenes have been considered by some authorities to be "operationally" defined entities. That is, presumably they do not exist as discrete units in asphalts, but are mobilized and then precipitated by the flocculation process [Boduszynski et al. 1980]. On the other hand, there is some evidence that discrete particulate species of some sort do exist in asphalts [Storm et al. 1993]. Small angle x-ray and neutron scattering techniques have been used to find evidence of such species in whole asphalts. The same techniques do not find evidence for discrete entities in maltenes [Storm et al. 1994]. Therefore, at least a part of the asphalt components known as asphaltenes must exist in asphalts as entities that are significantly larger than the molecules in the maltenes. Storm et al. [1994] have shown that the particles that are responsible for the scattering patterns of x-rays and neutrons in asphalts are in the size range of 60 to 120 Å in diameter. Hence asphaltenes, if they are assumed to be the entities detected by the x-ray and neutron scattering experiments, resemble some colloids in dimensions. Due to the large number of different kinds of molecules in asphaltenes, it follows that such entities, if they exist, must be polydisperse. That is, the dispersed entities are not identical in composition or size. Obviously, the nature and amount of these entities will influence the rheological properties of asphalts.

Sheu et al. [1991] studied the rheological properties of solutions of Ratawi vacuum residua asphaltenes in toluene. The asphaltenes were prepared by precipitation using n-heptane. The toluene solutions contained asphaltenes in amounts ranging from 0 to 40 mass percent. Relative viscosities (quotients of solution viscosities divided by the viscosity of toluene) of the solutions were determined at fairly high temperatures, and reciprocals of these values ($1/\eta_{rel}$) raised to various powers were plotted versus the volume fractions (ϕ) of asphaltenes to determine $K_S K_F$ (referred to as K in the 1991 publication of Sheu et al.) values from the Pal-Rhodes equation (equation 3-9). It was found that the exponent 0.4 gave the most linear plot,

with a y intercept of unity. Thus Sheu et al. [1991] concluded that asphaltene particles in toluene are nearly spherical (i.e., 1/0.4 = 2.5). It was also concluded that the Pal-Rhodes equation properly describes the rheological behavior of Ratawi asphaltenes in toluene. The K value was calculated to be approximately 2.8.

When η_{rel}, (and not $1/\eta_{rel}$) is plotted versus ϕ for solutions of Ratawi asphaltenes in toluene, a linear relationship is observed (in concurrence with the Einstein equation) for values of ϕ from 0 to 0.1, indicating that the asphaltene molecular entities are relatively non-interacting at low concentrations. At higher concentrations of asphaltenes, the relationship between η_{rel} and ϕ deviates from linearity, the deviation being more pronounced at higher ϕ values. Thus, interaction of asphaltene molecular units at ϕ values higher than 0.1 is implied. These results do not mean that molecular associations do not occur below ϕ values of 0.1, but that any associations that exist in dilute solution do not greatly affect solvent mobility.

Storm et al. [1991] diluted several vacuum resids with maltenes from each of their parent resids. This procedure yields mixtures having asphaltene concentrations ranging from 0 to the natural abundance level of the resid. Relative viscosities were calculated for each of the mixtures (the viscosities of the mixtures were divided by maltene viscosities, and not the viscosity of toluene). Using the relative viscosity data, intrinsic viscosities were calculated for each of the resids. Intrinsic viscosities [η] are calculated from relative viscosities, η_{rel}, as follows. First, unity is subtracted from each value of η_{rel} to give specific viscosities, η_{sp}, i.e.,

$$(\eta_{rel} - 1) = \eta_{sp} \tag{3-10}$$

Then, each value of η_{sp} is divided by c, the asphaltene concentration (based on mass) of the mixture, to yield the reduced specific viscosity, η_{red}, i.e.,

$$\eta_{red} = \eta_{sp}/c \tag{3-11}$$

The values of η_{red} are plotted versus c, and a line is drawn between the points and extrapolated to the y axis. The point at which the line intersects the y axis is the intrinsic viscosity, [η], which is a measure of molecular size of the dispersed entities [Severs 1962]. Storm et al. [1991] found that values of [η] for five vacuum resids ranged from 7 to 9, indicating that extensive associations are present in each of the systems. Storm et al. [1991] again used the Pal-Rhodes equation (equation 3-9) to calculate K values (the product $K_F K_S$) from η_{rel} and ϕ data for each of the series of maltene-diluted resids. The K values ranged from 1.9 to 2.9, indicating that the asphaltene associations immobilized considerable amounts of maltene solvent in each case, either by solvation or by trapping. The mixtures studied by Storm et al. [1991] do not involve solvents such as toluene, but are mixtures of asphaltenes with their natural solvents, the maltenes. Thus, the results are not open to the objection that the systems are largely artificial.

Storm and Sheu [1993], continuing their rheological analysis of Ratawi vacuum resid, observed that dividing the intrinsic viscosity, [η] = 7.3, by the 2.5 coefficient in the Einstein equation 3-2, gave a value of 2.9. This value corresponds to $K_S K_F$ in the Pal-Rhodes equation 3-9, which was determined by independent calculation. Storm and Sheu [1993] concluded that at

93°C (199.4°F), the temperature at which their measurements were performed, asphaltenes exist in vacuum residua as suspensions of polydisperse, spherical, solvated particles.

Storm et al. [1994] also measured the value of $K = K_S K_F$ of Ratawi resid at room temperature and found the value to be 3.7. They concluded that the forces responsible for solvation are weak, 1-2 kcal/mol required to escape the solvation shell. Storm et al. [1994] also discuss the significance of the x-ray scattering studies of Ratawi resid and the neutron scattering studies of Ratawi asphaltenes dissolved in deuterotoluene. It was observed that the scattering centers in the vacuum resid and the asphaltene-deuterotoluene solutions are nearly the same size and have similar size distributions. This implies that asphaltene particles are responsible for the scattering in both experiments, because the deasphaltened resid (maltenes) does not show evidence of the presence of particles in the x-ray analysis. In the neutron experiments, scattering results from the presence of hydrogen atoms in certain kinds of aromatic molecules. The asphaltenes alone have the type of hydrogens that interact with neutrons in the deuterotoluene experiments (the "heavy" hydrogen [deuterium] in deterotoluene does not interact with neutrons nor does the "light" hydrogen in the deasphaltened resid), so they must be responsible for the neutron scattering in the resids.

Storm et al. [1995a] refined their rheological analysis of Ratawi resid in a recent publication. At 93°C (199.4°F) the resid is relatively Newtonian. At lower temperatures, the solvation shells of the asphaltene particles become more extensive and begin to overlap, causing restriction of flow of the mobile portion of the resid and non-Newtonian behavior. At ambient temperatures, yield stress is observed in the resid. Earlier, Sheu et al. [1991] showed that the ratio of the volume of the solvated asphaltene particles ($V_{solvated}$) to the volume of the unsolvated asphaltene particles ($V_{unsolvated}$) was related to $K = K_S K_F$ as:

$$\frac{V_{solvated}}{V_{unsolvated}} = \left(\frac{R_0 + \Delta R}{R_0} \right)^3 = \frac{\rho_A}{\rho} K \qquad (3\text{-}12)$$

where R_0 is the radius of the unsolvated particle, ΔR is the apparent increase in the radius of the asphaltene particle due to the solvation shell, and ρ and ρ_A are the densities of the whole resid and the asphaltenes, respectively. Storm et al. [1995a] further pointed out that the magnitude of the quantity $R_0/\Delta R$ (which is the ratio of the radius of the hard-sphere particle to the difference in the radius between solvated and unsolvated asphaltene particle, or the thickness of the solvation shell) is directly related to the stability of the dispersed phase with respect to flocculation. Storm et al. [1995a] found the quality $R_0/\Delta R$ to be equal to 1.56 for Ratawi resids at 25°C (77°F). Thus, from rheological data, Storm, Sheu, and co-workers conclude that petroleum resids may be modeled as dispersions of core asphaltene particles that have a tendency to aggregate and immobilize portions of the continuous phase (maltenes) either by solvation or by trapping. As temperature decreases, the immobilization of continuous phase becomes more extensive, increasing the effective size of the interacting particles. This model explains the uniquely large temperature variation of viscosity of resids and, of course, asphalts.

The rheological analysis of resids by Storm, Sheu, and associates fits well with classical ideas about asphalt structure that were described in chapter 1. The classical model was developed from observations of other properties as well as rheological behavior [Traxler 1961]. In this model, asphaltenes are considered to be dispersed in a mobile solvent phase, identified with maltenes. The asphaltenes are stabilized against flocculation by a third kind of material designated as resins, some of which surround the asphaltenic particles and the remainder of which are dissolved in the solvent to an extent that depends on the temperature. At higher temperatures, more resins will be part of the solvent, reducing the effective size of the dispersed phase particles. Partitioning of resins between asphaltene particles and solvent explains why asphaltene yields are a function of the precipitating solvent. Some solvents will precipitate asphaltene particles and most of the resins. Other solvents cause most of the resins to remain in the maltenes. In the model of Storm, Sheu, and associates, a resid consists of asphaltene particles, mobile solvent, and immobilized solvent. The asphaltene particles include their surrounding resins.

Relationship of Relative Viscosity of Asphalts with Compatibility

It was stated in chapter 1 that asphalts long have been classified as gel or sol type. Gel type asphalts exhibit pronounced non-Newtonian behavior, whereas sol type asphalts are more Newtonian. Gel type asphalts generally contain large amounts of asphaltenes, and sol type asphalts are characterized by low asphaltene content. Therefore it would be expected that relative viscosity, η_{rel}, values (calculated as the quotient of asphalt viscosities divided by their maltene viscosities) of sol type asphalts would be much smaller than η_{rel} values of gel type asphalts. This is observed to be so. Thus a low value of η_{rel} serves to characterize a sol type asphalt, and a high value of η_{rel} a gel type asphalt. Using the classical asphalt science terminology, sol type asphalts are compatible, while gel type asphalts are incompatible asphalts.

There are other methods which, it is claimed, measure relative compatibilities of asphalts. If the methods are accurate and meaningful, they should be useful in predicting η_{rel} values, because the same property, compatibility, is being measured. In the preceding discussion, it was stated that η_{rel} values of asphalts vary directly with asphaltene contents. Obviously, asphaltene content provides some measure of compatibility.

One of the best known analytical methods for determining asphalt compatibility is the Heithaus test. The procedure was developed in the 1960's to improve prediction of the properties of asphalt blends [Heithaus 1962]. Solutions of asphalts in toluene (usually four or five in number) of various concentrations are titrated with a precipitating solvent such as n-heptane until flocculation is observed. The amounts of n-heptane titrant required for flocculation and the amount of solvent present in the solution are used to calculate a flocculation ratio, FR. Values of FR are defined as the volume fraction of solvent (toluene) in the solvent-titrant system, and are plotted versus the dilution concentration, C, which is the asphalt concentration in the total volume of titrant and solvent (toluene plus n-heptane) at the onset of flocculation for each solution. FR values are plotted on the y-axis and C values on the x-axis. A straight line is drawn through the four or five points and is extrapolated to the x and y axes. These intercept values, referred to as the flocculation ratio maximum, FR_{max}, and dilution concentration minimum, C_{min},

respectively, are used to calculate three Heithaus parameters: P (state of peptization of asphalt), p_a (peptizability of asphaltenes), and p_o (peptizing power of maltenes).

The Heithaus method implicitly models asphalts as dispersions of asphaltenes in a maltene solvent. High values of P indicate that an asphalt is compatible. High values of p_a indicate that asphaltenes are readily solubilized. High values of p_o indicate that maltenes are good solvents. Because Heithaus parameters measure compatibilities, there should be some relationship between them and relative viscosity, η_{rel}. In his paper, Heithaus [1962] shows that p_o does correlate with η_{rel} for the asphalts he studied. Therefore, it is of interest to determine whether or not Heithaus parameters can be related to some of the terms in either the Roscoe or Pal-Rhodes equations for the description of asphalt relative viscosities.

Relative viscosities at 25°C (77°F) were calculated for many SHRP asphalts from measurements of dynamic viscosities of whole asphalts and their n-heptane maltenes at a shear rate of 0.1 rad/s. The n-heptane maltenes are assumed to be the solvent in the asphalt systems, so η_{rel} for each asphalt is the quotient of the dynamic viscosity of the whole asphalt divided by the dynamic viscosity of the maltenes. The Heithaus test may be performed using either iso-octane or n-heptane as precipitating solvents. The values of the Heithaus parameters P, p_a, and p_o differ somewhat according to the solvent used. The data discussed below were obtained using a new automated method developed in this program and described in detail in Volume II, method 1.

Heithaus parameters can be related to compositional and rheological properties of asphalt as follows. Using the Pal-Rhodes equation (equation 3-9), individual values of K_SK_F (the product of the solvation factor K_S and the flocculation factor K_F) were calculated directly for each of 16 SHRP asphalts based on their dynamic relative viscosities and n-heptane asphaltene volume fractions ($\phi_{n\text{-heptane}}$). The volume fractions are calculated from asphaltene mass percent values as $\phi_{n\text{-heptane}}$ = [(asphaltene mass percent)/100]/ρ, where ρ, the density of asphaltenes, was measured to be approximately 1.1 g/mL. Table 3-1 lists values of relative viscosities calculated from dynamic viscosity values of whole asphalts and n-heptane maltenes, which are also listed in table 3-1, along with n-heptane asphaltene volume fractions, $\phi_{n\text{-heptane}}$. Table 3-2 lists Heithaus parameters P, p_a, and p_o obtained from titration experiments performed with iso-octane used as the titrant. The individual calculated values of K_SK_F (table 3-2) were plotted versus Heithaus parameters P, p_a, and p_o for each of the 16 asphalts. The two graphs in figure 3-1 show calculated values of K_SK_F plotted versus measured values of P and p_a, respectively. The Heithaus parameters P and p_a correlate fairly well with the product K_SK_F, and P values are of comparable magnitude to the calculated values of the product K_SK_F. The p_o parameter did not correlate with K_SK_F values. It was also observed that the definition of $K_F = 1/(1 - \alpha)$ by Pal and Rhodes is formally similar to the definition of the Heithaus parameter P as a function of p_a, i.e., P is a function of $1/(1 - p_a)$. Furthermore α values are numerically similar to p_a values, both of which range, in theory, from zero to unity. Parenthetically, it should be noted that α used here is not identical to the α used by Maron and Fok, equation 3-7. Therefore, it was speculated that if measured values of p_a could be substituted for α, individual values of K_S and K_F could be calculated for each asphalt. Thus, K_S values were calculated for 16 SHRP asphalts using the following relationships:

$$K_F = \left(\frac{1}{1 - p_a} \right) \tag{3-13}$$

and rearranging equation 3-9

$$K_S K_F = \frac{1 - \eta_{rel}^{-0.4}}{\phi_{n-heptane}} \tag{3-14}$$

so

$$K_S = (1 - p_a) \frac{1 - \eta_{rel}^{-0.4}}{\phi_{n-heptane}} \tag{3-15}$$

Table 3-3 lists calculated values of K_S from equation 3-15 for each of the 16 SHRP asphalts, along with measured values of $K_F = 1/(1 - p_a)$, for iso-octane titrated solutions of the asphalts dissolved in toluene. Values of K_S that were obtained using equation 3-15 were found to average around the value of 1.56 and range in value from 1.2 for AAM-1 to 1.8 for AAE. It is known that AAM-1 asphaltenes are not very polar, and AAE is an air-blown asphalt. Its asphaltenes should be highly polar. Thus solvation shells, which K_S measures, should be smallest in AAM-1 and largest in AAE. Earlier, it was mentioned that Storm, Sheu, and co-workers proposed that asphalts consist of solvated spherical particles dispersed in a solvent. The particles were considered to be roughly equivalent to asphaltenes. The ratio of the radii of the solvated and unsolvated particles were determined at several temperatures. Storm et al. [1996] found that the value of this ratio, essentially equivalent to K_S, at 25°C (77°F) is approximately 1.56 for Ratawi resids. If values of K_S calculated using equation 3-15 are real, one of the Heithaus parameters (p_a, the asphaltene compatibility parameter, a compositional factor) has been shown to be related to an asphalt rheological property, η_{rel}, by equation 3-15.

The values of the product $K_S K_F$ (table 3-2) vary considerably among the 16 SHRP asphalts when volume fractions of n-heptane asphaltenes are used to calculate $K_S K_F$. Assuming that the asphaltenes comprise a large proportion of asphalt dispersed components, then their properties presumably differ significantly from one asphalt to another. Degree of solvation (measured by solvation factor K_S) and tendency to trap solvent (measured by flocculation factor K_F) are two such properties.

It was then decided to determine how the quantity $K_S K_F$ (which is equal to the solvation constant K) varies when volume fractions of iso-octane asphaltenes are used to calculate this quantity instead of $\phi_{n\text{-heptane}}$. Obviously, the materials precipitated by n-heptane must be different from those precipitated by iso-octane. It is reasonable to assume that iso-octane precipitates all those materials precipitated by n-heptane plus more material that is somewhat less polar and of

lower molecular weight than the n-heptane asphaltenes. For the sake of argument, it may be assumed that these additionally precipitated materials are part of the resin component of asphalts. The η_{rel} values based on iso-octane maltenes are not available, so η_{rel} values based on n-heptane maltenes were used in the new calculations. The new solvation constant is designated K' to distinguish it from the solvation constant calculated from the n-heptane asphaltene volume fractions. Surprisingly, when iso-octane asphaltene volume fractions (table 3-4) are used to calculate K', the results vary somewhat narrowly, ranging from 3.36 to 4.17 and averaging 3.87. This value is close to that reported by Storm et al. [1995a] for Ratawi resid at 25°C (77°F) using a different method. When iso-octane asphaltene volume fractions are multiplied by 3.87 (the average K' value for the 16 asphalts), products are obtained that are listed in table 3-5. These products are numerically similar to the $(1-\eta_{rel}^{-0.4})$ values for each entry. Therefore, the quantity $3.87\,\phi_{iso\text{-}octane}$ may be used as an approximation for $(1-\eta_{rel}^{-0.4})$. Rearranging terms in equation 3-15, there are now two relationships involving $(1-\eta_{rel}^{-0.4})$:

$$3.87\phi_{iso\text{-}octane} = \left(1 - \eta_{rel}^{-0.4}\right) = \frac{K_S\phi_{n\text{-}heptane}}{1 - p_a} \tag{3-16}$$

It follows that:

$$K_S = 3.87\left(1 - p_a\right)\frac{\phi_{iso\text{-}octane}}{\phi_{n\text{-}heptane}} \tag{3-17}$$

Thus a solvation factor, K_S, can be approximately calculated entirely from compositional parameters. Values for the 16 asphalts calculated using equation 3-17 are listed in table 3-5. The values are fairly close to those listed in table 3-3 for K_S calculated as described earlier.

In addition to measuring the compatibility of an asphalt based on Heithaus parameters, an alternative method was developed involving calculation of asphaltene compatibility indices (ACI), described in Branthaver et al. [1991]. A variant of this method utilizes asphaltene volume fraction values of n-heptane and iso-octane asphaltenes, and yields what are termed absolute ACI values (ACI_{abs}). These quantities are defined as follows:

$$ACI_{abs} = \frac{\phi_{isooctane}}{\phi_{isooctane} + \phi_{n\text{-}heptane}} \tag{3-18}$$

The advantage of the absolute ACI scale is that it ranges from zero to unity in theory. For each of the 16 SHRP asphalts, ACI_{abs} values were calculated and are listed in table 3-6. When these values are divided into K_S values for each of the asphalts (table 3-3), the quotients are observed to average 2.63. Curiously, the value 2.6 is nearly that of the intrinsic viscosity ($[\eta] = 2.5$) for spherical particles.

The above relationships are consistent with a model of asphalt structure in which asphaltene molecular associations, each surrounded by a shell of solvating resins (for want of a better term) and immobilized solvent, are dispersed in a relatively non-polar solvent. Resin

molecules are in equilibrium between the surface of the asphaltene particles and the solvent. The asphaltene molecular associations are probably roughly spherical in shape and appear to be stable at asphalt service temperatures. The diverse composition of the polar components of asphalts requires that the asphaltene molecular associations are of varied composition. At mix plant temperatures, the asphaltene molecular associations are stabilized by fairly small amounts of adsorbed resins. Flocs of molecular associations are not large enough at higher temperatures to immobilize much of the solvent component. Lowering the temperature results in more resins adhering to the asphaltene molecular associations, thus increasing their effective volume and reducing the amount of free solvent volume. The nature of the solvent also changes, because the relatively polar resins become immobilized on the molecular associations. These resins are no longer part of the remaining free solvent. Floc formation also occurs at lower temperatures, immobilizing more solvent. Floc formation does not alter the nature of the remaining free solvent. Viscosities increase markedly as a result of these processes. Eventually the molecular associations of asphaltenes and their accompanying resins become the matrix of the system and probably assume configurations having considerable order at lower temperatures. Shearing disturbs the matrix, resulting in the liberation of trapped solvent, with an accompanying decrease in viscosity.

Figure 3-2 is a highly idealized diagram of the asphalt structural units described above. At the bottom of the diagram is a representation of three flocs, each consisting of seven asphaltene molecular associations. This number of molecular associations is purely arbitrary, and the representation is two-dimensional. Also, the natural situation will not be nearly as regular as in figure 3-2. In the middle of the figure, an enlarged view of an individual floc is shown. Again, no such regularity will be observed in nature. The enlarged floc shows the core of the asphaltene molecular association surrounded by solvating resins. This assemblage will have a solvation shell. Much solvent is physically trapped within the floc. At the top of figure 3-2 is a representation of an asphaltene molecular association according to Pfeiffer and Saal. In this diagram, highly aromatic nuclei are surrounded by less aromatic molecules, and the assemblage is dispersed in solvent molecules. The highly aromatic nuclei may be considered to be equivalent to n-heptane asphaltenes. They would be centers of electron density and would be detected in x-ray scattering experiments. The molecules surrounding the aromatic nuclei may be designated as resins, and the two entities together probably comprise iso-octane asphaltenes. In neat asphalts, there would be an equilibrium between resin molecules adhering to the nuclei and those dissolved in the solvent, and this equilibrium would be temperature dependent. More resins would be dissolved at higher temperatures. Those resins adhering to the nuclei are surrounded by a layer of immobilized solvent molecules. When several of these molecular associations interact with one another, floc formation occurs, resulting in trapping of solvent between the floc components. There is no distinct boundary between the solvent trapped within a floc and solvent adsorbed on the periphery of the individual molecular associations. The trapped solvent is immobilized by steric factors, and should be greatly affected by shear. The adsorbed solvent is weakly held, and should be affected by both temperature and shear.

What is not shown in figure 3-2 is that the size of molecular associations probably varies considerably within an asphalt. At high dispersed phase concentration, this factor will influence

packing efficiencies. Obviously, as dispersed phase concentrations become large, virtually all solvent will be immobilized by trapping or adsorption, which will be reflected in flow properties.

The most compatible asphalts have relatively few asphaltenes and large amounts of resins. Because of their polar nature, there should be some limited self association of resins within the solvent, mostly dimerization and trimerization. This results in a solvent having a high viscosity. Other resin components become adsorbed on the asphaltene molecular associations as temperatures decline, as with the less compatible asphalts. Buildup of the non-solvent matrix in compatible asphalts must involve trapping of relatively large amounts of solvent. Possibly compatible asphalts have asphaltene molecular associations that pack in such a way that solvent trapping is maximized. Otherwise, it is difficult to explain the high shear and temperature susceptibilities of these asphalts.

It should be noted that not all studies support the above model. Molecular associations of significant size in asphalts were not detected by the NMR studies of VanderHart, reported in Jennings, et al. [1991]. This study involved interpretation of solid-state proton NMR spectra of SHRP asphalts. VanderHart observed that number-average molecular weight differences among asphalts are too small to account for viscosity differences, so factors such as molecular shapes or formation of small (2-3 molecular diameters in at least one dimension) associations must be involved. The NMR experiments measure molecular mobilities, and there do not appear to exist in asphalts large domains of immobilized molecules detectable by NMR. It is claimed that most polar molecules should have flexible side chains that would disrupt intermolecular structures. VanderHart points out that NMR studies do not detect significant differences between oxidized and neat asphalts, although there are great differences in rheological properties between them. VanderHart detected a continuum of molecular mobilities by NMR. It was suggested that polar constituents of asphalts may themselves form a continuous phase, rather than discrete molecular associations. The inability of NMR to detect any large scale molecular organization in asphalts may provide some insights into the nature of asphalt structure. The NMR data do not by themselves refute the results of rheological, x-ray, IR, and other studies, all of which support a colloidal model of asphalt structure.

Anderson, in Christensen et al. [1996] has proposed that it may not be necessary to invoke anything as complex as a colloidal model to rationalize asphalt rheological properties. These authors observe that asphalt temperature dependence is well described by the Williams-Landel-Ferry (WLF) equation. Parenthetically, there is a vast literature on the application of WLF to paving grade asphalts, and so there will be no discussion of it here other than to point out that the form and coefficients of WLF are related to thermal expansion coefficients and free volume parameters of amorphous materials. Christensen et al. [1996] suggest that flow properties of asphalts may be described from considerations of free volume and what they designate as intermolecular friction, which is related to overall polarity of an asphalt. Free volume is a function of density. Asphalt densities are temperature dependent and do not vary greatly among asphalts. Asphalt polarities vary considerably and are a function of chemical composition. Christensen et al. [1996] suggest that asphalt rheological properties should be compared under conditions of equivalent free volumes, so that rheological differences observed are the result of intermolecular friction. This is why measuring rheological properties of asphalts

at a fixed temperature does not provide a proper comparison of those properties among asphalts. Free volumes differ among asphalts at a given temperature, except at the glass transition temperature.

The viscosities of most simple organic liquids do not vary greatly with temperature. Reid et al. [1977] have compiled kinematic viscosity data for a large number of compounds over wide temperature ranges. For example, the viscosity of toluene in centipoises at 110°C (230°F) is approximately 40 percent of the viscosity at 20°C (68°F). Changes in viscosity with temperature of similar magnitude are observed for many non-polar organic liquids. Polar liquids exhibit somewhat larger variations of viscosity with temperature. Phenol is one-fourth as viscous at 110°C (212°F) as at 50°C (122°F). Also, moderate increases in pressure do not greatly affect the viscosities of simple organic compounds [Reid et al. 1977]. It would be expected that for most simple organic compounds, viscosity would be largely a function of free volume, and therefore, of density.

Complex mixtures of organic compounds, such as petroleum residua, do not behave in such a simple manner. Variations of viscosities of asphalts from glass transition temperatures to mix plant temperatures are several orders of magnitude. Also, an increase in pressure on tar sand bitumens from atmospheric to 10 MPa causes significant viscosity increases, yet with very small accompanying changes in density [Mehrotra and Svrcek 1986]. Furthermore, the viscosity changes caused by increasing pressure are greater for more polar, asphaltenic tar sand bitumens. Tar sand bitumens are natural materials with properties similar to asphalts.

Asphalt in thin films can be much more viscous than in the bulk [Huang et al. 1998, and references therein]. It is not likely that there is a significant difference in density from the bulk asphalt in the films, so that the variation must be attributed to intermolecular friction. There also exist materials that are electrorheological. Application of an electrical field results in huge increases in viscosity in these materials, and removal of the field results in rapid viscosity reduction. Free volume considerations can hardly explain this phenomenon.

The colloidal model of asphalts does not preclude the free volume influence on viscosity. The model may be a more detailed way to explain intermolecular friction effects. If intermolecular friction is a function of polarity, then the suggestions of Christensen et al. [1996] are not greatly different from the ideas developed from the colloidal theory. The latter strives to explain how polar molecules interact to influence rheological properties of asphalts. These interactions are probably responsible for what is termed intermolecular friction.

Polar molecules comprise a very large proportion of asphalt components. The probability, in a randomly distributed system, of a polar molecule having one or two nearest neighbor molecules that also are polar is close to unity. Thus polar molecules will interact, whatever the temperature, to form loosely bonded molecular associations. Furthermore, as pointed out by VanderHart in Jennings et al. [1991], systems containing large numbers of molecules of different kinds will always contain groups of molecules that show a preference for each other. The formation of such molecular associations, which would probably differ in

composition, would affect rheology and their makeup would be a function of temperature and shear.

Based on the studies of tar sand bitumens by Mehrotra and Svrcek [1986], the polar molecular associations must be responding to pressure so as to increase viscosity, because densities hardly change. It may be that the polar molecular associations become packed in a different way, which of course might alter free volume. In any event, the polar molecules become more effective impediments to flow, probably by trapping more solvent as a result of the formation of more extended flocs.

Asphalts and asphalt fractions have been studied by a number of experimental techniques in the course of this program. A principal goal of these studies has been refining the above described model and gaining new insights into asphalt structure. The results of these efforts are reported in the remainder of this chapter.

Table 3-1. Whole asphalt (η) and n-heptane maltene (η_0) dynamic viscosities measured at 25°C and 0.1 rad/s, relative viscosities (η_{rel}), and n-heptane asphaltene volume fractions ($\phi_{n\text{-heptane}}$) for 16 SHRP asphalts.

Asphalt	η, Pa·s [1]	η_0, Pa·s [2]	η_{rel}	$\phi_{n\text{-heptane}}$ [3]
AAA-1	37,020	804	46	0.144
AAB-1	118,600	3,020	39	0.157
AAC-1	90,100	10,520	9	0.090
AAD-1	57,280	329	174	0.184
AAE-1	184,500	530	348	0.208
AAF-1	381,700	25,000	15	0.122
AAG-1	248,900	82,460	3	0.045
AAH-1	159,500	1,804	88	0.145
AAJ-1	201,100	15,251	13	0.096
AAK-1	251,700	1,620	155	0.183
AAM-1	364,400	101,800	4	0.034
AAN-1	122,700	3,720	33	0.143
AAS-1	164,100	734	224	0.167
AAV-1	46,700	5,334	9	0.088
AAW-1	288,700	8,962	32	0.163
AAX-1	275,900	24,057	12	0.109

[1,2] Standard deviation = ± 5%.

[3] $\phi_{n\text{-heptane}}$ = (mass fraction of n-heptane asphaltenes ÷ 1.1); Standard deviation ± 10%.

Table 3-2. Heithaus parameters (p_a = peptizability of asphaltenes; p_o = peptizing power of maltenes; P = state of peptization of asphalt) measured for SHRP asphalts with iso-octane as titrant and $K_S K_F$ values.

Asphalt	p_a [1]	p_o [2]	P [3]	$K = K_S K_F$
AAA-1	0.701	0.84	2.8	5.44
AAB-1	0.697	0.87	2.9	4.90
AAC-1	0.765	0.76	3.2	6.50
AAD-1	0.660	0.89	2.6	4.74
AAE-1	0.592	1.35	3.3	4.34
AAF-1	0.687	0.73	2.3	5.42
AAG-1	0.802	0.82	4.1	7.90
AAH-1	0.760	0.69	2.9	5.75
AAJ-1	0.752	0.95	3.8	6.68
AAK-1	0.692	0.98	3.2	4.74
AAM-1	0.902	0.76	7.7	12.52
AAN-1	0.692	0.95	3.1	5.27
AAS-1	0.704	0.92	3.1	5.30
AAV-1	0.759	0.81	3.4	6.64
AAW-1	0.624	0.93	2.5	4.60
AAX-1	0.741	0.89	3.4	5.66

[1] Range of standard deviations (0.001 to 0.015).
[2] Range of standard deviations (0.006 to 0.23).
[3] Range of standard deviations (0.002 to 0.38).

Table 3-3. Values of flocculation factor $K_F = 1/(1 - p_a)$ and values of solvation factor = K_S calculated from equation 3-15 for 16 SHRP asphalts.

Asphalt	$K_F = 1/(1 - p_a)$	K_S at 25°C [1]
AAA-1	3.34	1.63
AAB-1	3.30	1.48
AAC-1	4.26	1.53
AAD-1	2.94	1.61
AAE-1	2.45	1.77
AAF-1	3.19	1.70
AAG-1	5.05	1.56
AAH-1	4.17	1.38
AAJ-1	4.03	1.66
AAK-1	3.25	1.46
AAM-1	10.20	1.23
AAN-1	3.25	1.62
AAS-1	3.38	1.57
AAV-1	4.15	1.60
AAW-1	2.66	1.73
AAX-1	3.86	1.47
		1.56 ± 0.14 = Avg.

[1] Standard deviation range (0.1 to 0.3).

Table 3-4. Values of iso-octane asphaltene volume fractions ($\phi_{iso\text{-}octane}$) and K′ values for 16 SHRP asphalts.

Asphalt	Iso-octane asphaltenes, mass fraction (χ)	$\phi_{iso\text{-}octane}$ [1]	K′ [2]
AAA-1	0.221	0.201	3.91
AAB-1	0.224	0.204	3.77
AAC-1	0.155	0.141	4.15
AAD-1	0.274	0.249	3.51
AAE-1	0.259	0.235	3.85
AAF-1	0.187	0.170	3.89
AAG-1	0.102	0.093	3.82
AAH-1	0.242	0.220	3.79
AAJ-1	0.182	0.165	3.89
AAK-1	0.247	0.225	3.85
AAM-1	0.112	0.102	4.17
AAN-1	0.207	0.188	4.01
AAS-1	0.244	0.222	3.99
AAV-1	0.164	0.149	3.92
AAW-1	0.245	0.223	3.36
AAX-1	0.171	0.155	3.98

[1] Calculated by dividing entries in column 2 by 1.1.
[2] Calculated using $\phi_{iso\text{-}octane}$ in equation 3-15.

Table 3-5. K_S values calculated from equation 3-17 and other quantities for 16 SHRP asphalts.

Asphalt	$3.87 \times \phi_{iso\text{-}octane}$	$(1-\eta_{rel}^{-0.4})$ [1]	K_S
AAA-1	0.77	0.78	1.62
AAB-1	0.77	0.77	1.52
AAC-1	0.59	0.58	1.42
AAD-1	0.88	0.87	1.78
AAE-1	0.88	0.90	1.78
AAF-1	0.66	0.66	1.69
AAG-1	0.37	0.36	1.58
AAH-1	0.85	0.83	1.41
AAJ-1	0.63	0.64	1.65
AAK-1	0.85	0.87	1.47
AAM-1	0.40	0.40	1.14
AAN-1	0.74	0.75	1.57
AAS-1	0.88	0.89	1.52
AAV-1	0.59	0.58	1.58
AAW-1	0.74	0.75	1.99
AAX-1	0.63	0.62	1.43
			1.57 Avg.

[1] Calculated from η_{rel} values reported in table 3-1.

Table 3-6. Absolute asphalt compatibility indices (ACI_{abs}) and K_S/ACI_{abs} values calculated for 16 SHRP asphalts at 25°C.

Asphalt	ACI_{abs} [1]	K_S/ACI_{abs} [2]
AAA-1	0.58	2.81
AAB-1	0.56	2.64
AAC-1	0.61	2.51
AAD-1	0.58	2.77
AAE-1	0.53	3.34
AAF-1	0.58	2.93
AAG-1	0.67	2.32
AAH-1	0.60	2.30
AAJ-1	0.63	2.63
AAK-1	0.55	2.65
AAM-1	0.75	1.64
AAN-1	0.57	2.84
AAS-1	0.57	2.75
AAV-1	0.63	2.54
AAW-1	0.58	2.98
AAX-1	0.59	2.49
		2.63 Avg.

[1] Standard deviation range (0.02 to 0.05).
[2] Standard deviation range (0.06 to 0.13).

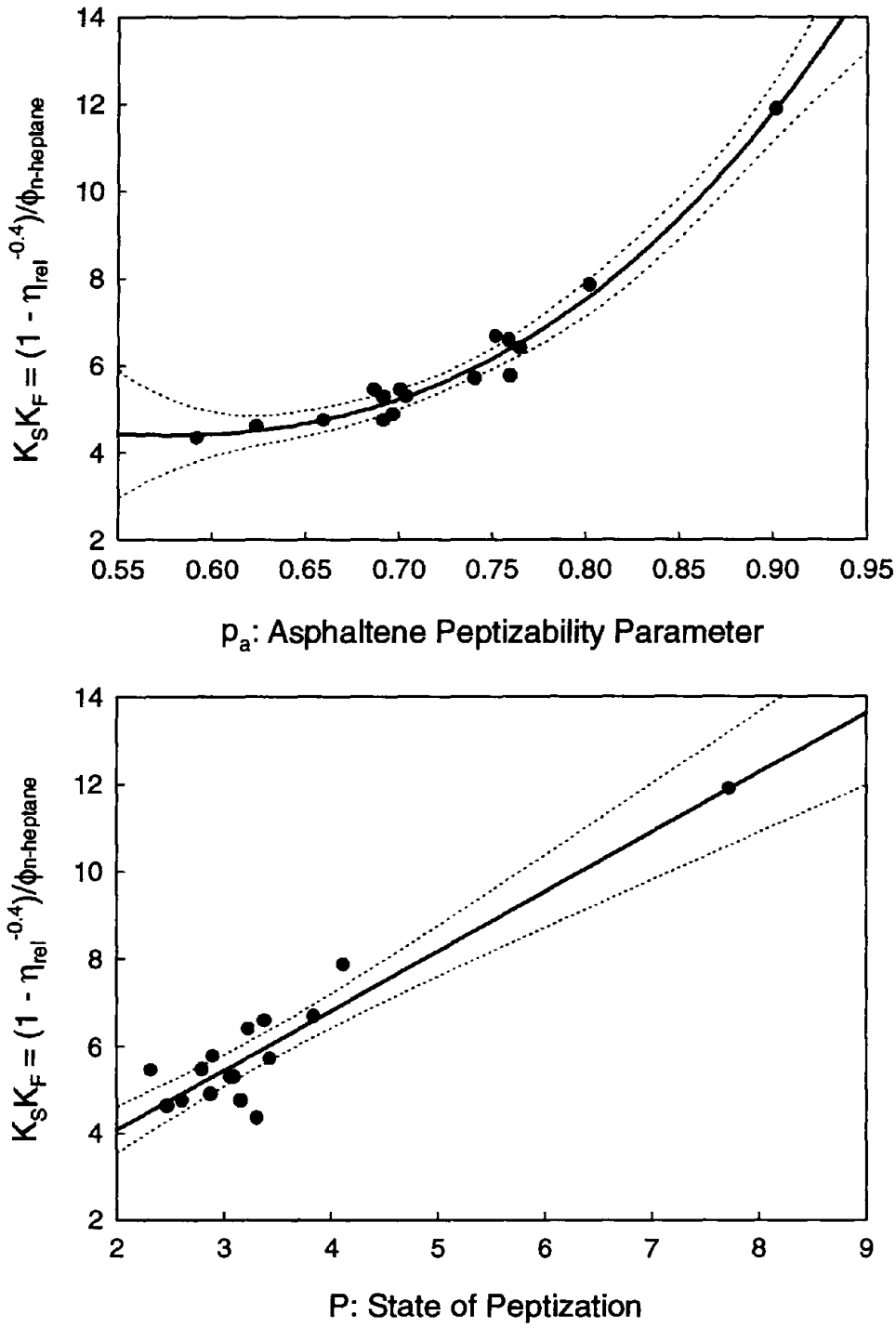

Figure 3-1. $K = K_F K_S$ values calculated from Pal-Rhodes equation (equation 3-9) versus Heithaus parameters p_a and P.

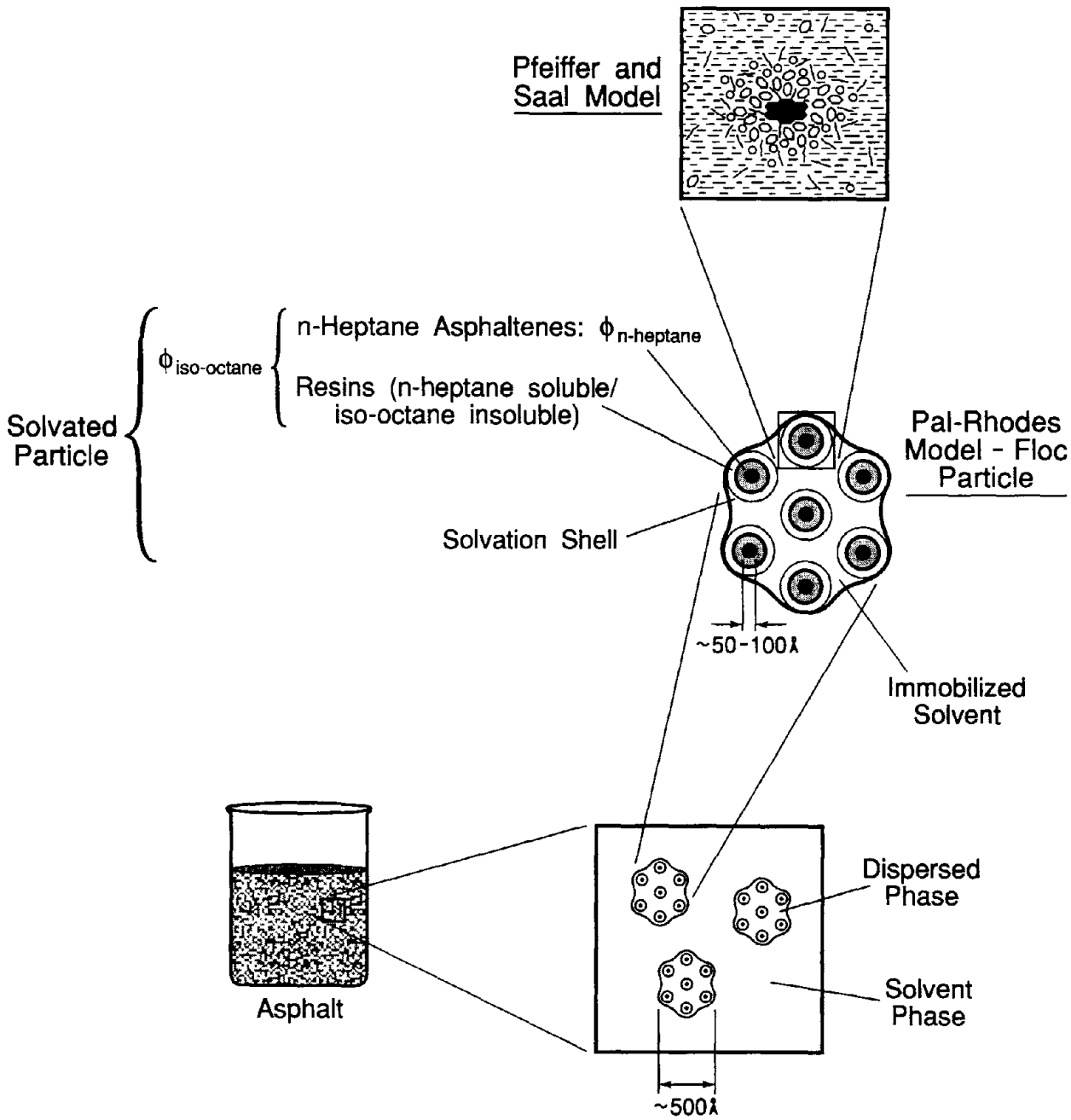

Figure 3-2. Idealized diagram of asphaltene molecular associations and floc particles.

DESCRIPTION OF SEPARATION METHODS FOR ASPHALTS

General Considerations

The separation of asphalts into components followed by their characterization is complicated by the chemical diversity of asphalts. Asphalts consist of thousands of different organic compounds. These compounds range from non-polar to highly polar and, thus, vary considerably in chemical and physical properties. In molecular size, asphalt components range from molecules with relatively low (approximately 15) carbon numbers to molecules containing over 100 carbons. It is likely that the single most abundant molecular species is present only as a fraction of a mass percent of the whole, and many species are present in trace amounts. Separation of such a mixture into individual molecular components is not practical. However, it is possible to separate asphalts into various compound classes, each of which is characterized by distinctive physicochemical properties. An objective of this program is to determine the influence of various chemical compound types present in asphalts on performance-related physical properties. Therefore, it is necessary to perform some fairly complex separations on asphalts, because the desired relationships cannot always be elucidated by model compound studies.

Separation methods for asphalts must be based on the nature of the materials. Because most asphalts are distillation residua of petroleum, separations involving volatilization cannot be utilized. This is unfortunate, because these methods are among the most efficient used by organic chemists. Asphalts contain large numbers of different kinds of organic compounds, but not every major compound type. For example, such common organic compounds as alcohols, nitriles, alkynes, and aldehydes appear to be absent, and alkenes nearly so. The most abundant compound types are hydrocarbons such as normal and branched alkanes, cycloalkanes, and a wide variety of aromatics. Of the non-hydrocarbons present, compounds containing the heteroatoms nitrogen, oxygen, or sulfur are prevalent. Among these are the nitrogen-containing pyrroles, indoles, and pyridines, the oxygen-containing carboxylic acids and phenols, and the sulfur-containing thiophenes and thioethers. Compounds containing two or more different heteroatoms also are known. Prominent among these are 2-quinolones, amides, and in aged asphalts, sulfoxides. In addition to compounds composed of carbon, hydrogen, nitrogen, oxygen, and sulfur, compounds containing the metals nickel, vanadium, and iron also may be present in significant quantities. These compounds are not inorganic salts, but are either metal chelates or metal salts of organic acids. That is, they are organic anions bonded to metal cations. Compounds containing other elements are present in asphalts in trace quantities. Each of the above compound types will be represented by a wide variety of methylene homologues, as is typical of petroleum. A methylene homologue is a member of a class of compounds differing from other members of the class by one or more $-CH_2-$ groups. An example of a homologous series is the class of compounds known as n-alkanes, or normal paraffins. In asphalts, the n-alkane having a carbon number of 18 is usually the lowest member of the series in molecular size. Normal alkanes having carbon numbers ranging from 25-40 are found in significant quantities in some asphalts. Normal alkanes of higher carbon number are not usually abundant in asphalts, but some normal alkanes having carbon numbers of over 100 have been identified. While they may not have large molecular abundances, they are relatively large molecules and

comprise a substantial proportion of total mass. In theory, the chemical properties of all members of a homologous series should be similar. Because the various members of a homologous series differ in molecular size, physical properties of the components will vary, particularly between the extremes of a series.

Thus, because of the nature of asphalts, while it is impractical to isolate any significant number of individual compounds, it may be possible to isolate specific compound types. The methods chosen to accomplish this end must be selected to account for the fact that the various compound types consist of a large number of homologues, and the fact that many asphalt components are polyfunctional, i.e., they may be classified as more than one compound type.

Separation methods also may be chosen with regard to the model of asphalt structure described earlier in this chapter and in chapter 1 of this report. In the model, asphalts are considered to be dispersions of polyfunctional, polar, and aromatic molecules in a non-polar, more aliphatic solvent. The dispersed components are believed to exist as molecular associations that may be of fairly large molecular size. If the model is valid, it should be possible to separate those components comprising the solvent from those comprising the dispersed moiety. Failure to be able to do this using well-tested separation methods would refute the model.

Solvent Precipitation Separations

The longest-used and best known method for asphalt fractionation is the precipitation of asphaltenes [Girdler 1965]. The procedure is simple and fairly rapid. It involves mixing a weighed amount of asphalt with a large excess (20-40 mL per gram of asphalt) of a low molecular weight normal alkane (propane, n-butane, n-pentane, –hexane, n-heptane, –octane) or a branched alkane such as 2,2,4-trimethyl pentane (iso-octane). Chemical structures of these compounds are illustrated in figure 3-3. The mixture of asphalt and hydrocarbon is allowed to stand for several hours. During this time, the mixture is agitated by swirling periodically. As a result of this process, black solids precipitate. These solids can be recovered by filtration and are known as asphaltenes. The hydrocarbon used to precipitate asphaltenes may be separated from the filtrate by evaporation. The non-asphaltenic component of an asphalt is known as the maltenes or petrolenes. Yields of asphaltenes are a function of the asphalt and of the hydrocarbon used. In the separation of asphalts into maltenes and asphaltenes, it has been claimed that the maltenes are roughly equivalent to the solvent moiety and asphaltenes approximate the dispersed component. Contrariwise, it has been stated that the separation is a function only of solubility characteristics, and that asphaltenes have no existence as such in asphalts. The controversy was discussed in this chapter and in chapter 1.

Whether or not either of the above arguments is valid, the separation is a useful one. It has been shown that asphaltenes are the viscosity-building components of asphalts. Maltene viscosities are much lower than whole asphalt viscosities at the same temperature. Also, asphalts having high (>15 percent) asphaltene contents differ in properties from those having lower asphaltene contents [Traxler 1961]. So the separation into maltenes and asphaltenes, while possibly arbitrary, is meaningful and has been used extensively in this program.

Separations Based on Molecular Size

SEC has been employed as a method for characterizing asphalts by numerous investigators [see Branthaver et al. 1992, and references therein]. In most cases, it has been used as an analytical method, and not a true separation, in which different fractions are separated, isolated, and collected. The SEC method separates asphalt components according to molecular size. The mechanics of SEC separation are described in Volume II, method 15 and will be briefly reviewed below.

In SEC, which was formerly termed GPC, the separation agent is a column of gel particles swelled in an appropriate solvent. The gel particles, when swelled, contain pores of varying diameters. For separation of organic mixtures such as asphalts, gels made of polystyrene crosslinked with divinyl benzene are used. The swelled gel beads are packed in glass columns. Originally, solutions of asphalts were poured over the top of a column and flowed through the gel bed to the bottom by gravity. Currently, the asphalt solutions are introduced into the bottom of the column and are pumped upward through the gel bed. Reversing the direction of flow was found to minimize channeling and improve reproducibility. After the asphalt solution has been introduced into the column, more solvent is pumped in until all asphaltic material has been eluted from (i.e., passed through from bottom to top) the column. The solvent chosen for preparative separations is toluene. As the asphalt solution proceeds through the column, smaller molecules enter the gel pore structure, retarding their progress. Larger molecules or associations of smaller molecules cannot enter much of the gel pore volume. If asphalt components are sufficiently large, they may not enter the gel pores at all, but merely percolate through the column between the gel beads. Thus, the largest molecules, or largest associations of smaller molecules, rapidly pass through the gel bed, and are eluted first in SEC separations. The smallest components in a mixture are eluted last. The various eluates (solutions collected from the top of an SEC column) may be collected in any number of fractions, depending on the objectives of the experimenter.

The fractionation pattern resulting from separation of any mixture in a given SEC method depends on the solvent used during the separation, flow rate, column temperature, and amount of material to be separated relative to the gel bed volume. Column dimensions also are a factor. Many different gels, each with characteristic pore size distributions, are available. Columns containing different gels may be connected in series. For example, the first column in a series may contain a gel with mainly large pores, and the next column (or columns) might contain gels with smaller pores. This arrangement of columns containing different gels in series permits more efficient separations of mixtures and is customary in analytical SEC.

All SHRP asphalts have been separated by preparative SEC into two or, in some cases, more fractions. The basis of the separation of asphalt solutions into two fractions is the observation that the initial eluates are relatively non-fluorescent to 350 mμ (ultraviolet - UV) radiation, while later eluates fluoresce. In most asphalts, the demarcation between the fluorescent and non-fluorescent zones is distinct. If eluates are collected in graduated cylinders, the two zones are easily visible. It is believed that the initial SEC eluates of asphalts consist of strong associations that are not broken up in toluene. The persistence of molecular associations is the reason for the suppression of fluorescence in the initial SEC eluates. Later eluates are not

strongly associated and, therefore, are fluorescent. The initial non-fluorescent eluates in SEC separations are designated SEC Fraction-I. The fluorescent eluates are designated SEC Fraction-II. Each asphalt contains unique amounts of the two fractions. For many asphalts, SEC Fraction-I is similar in amount to n-heptane asphaltene content, and SEC Fraction-II is similar in amount to n-heptane maltene content. For others, the amounts of the two SEC fractions are different from asphaltene and maltene contents. As is true of asphaltenes, SEC Fraction-I materials are black, friable solids. They are more aromatic and higher in molecular weight than the SEC Fraction-II components, which are viscous liquids. The SEC Fraction-I materials are the viscosity-building components and impart elastic properties to asphalts. The dynamic mechanical rheological property tan δ correlates with SEC Fraction-I concentration [SHRP 1993].

In some separations, SEC Fraction-II was subdivided into as many as seven subfractions by collecting equal volumes of eluates instead of collecting all of the SEC Fraction-II eluates in one large batch. The eluates containing the SEC Fraction-II subfractions were dried and the residues were weighed. Mass distributions of the subfractions vary among asphalts and are unique to each asphalt. This procedure allows construction of a characterization diagram for a given asphalt based on mass fraction data for the SEC Fraction-I and the SEC Fraction-II subfractions. In experiments to be discussed later, SEC Fraction-I was also separated into subfractions, but always in a second SEC separation.

The preparative SEC technique developed in this research processes 16 g asphalts in each run. Fractions are collected that are abundant enough for subsequent studies. In many of these studies, SEC Fraction-I materials are assumed to correspond to asphalt dispersed moieties, and SEC Fraction-II corresponds to the solvent. This assumption is reasonable if it is accepted that separation based on molecular size is less arbitrary than separation based on solvent precipitation. Furthermore, the fluorescence behavior of the two fractions indicates that indigenous asphalt molecular associations may survive in toluene and are isolatable by SEC. Work in the program has been directed toward studying effects of the nature and relative amounts of the two SEC fractions on asphalt physical properties.

In many applications, SEC fraction profiles are required without the need for subsequent analysis. Toward this end, a rapid instrumental analytical method was developed during this program. The analytical SEC method provides results similar to the preparative method and requires only small quantities of material. This method is described in detail in Volume II, method 2.

Separations Based on Polarity, Acidity, and Basicity

If the model of asphalt structure described in the previous section is correct, the asphalt dispersed component should differ from the solvent component in molecular size and polarity. The two components should be separable by methods that rely on chemical affinity as well as by methods separating asphalts according to molecular size. One method for effecting separation of asphalts into defined chemical fractions based on chemical affinity is IEC. In this separation procedure, a solution of an asphalt is pumped through a column or series of columns filled with

activated ion exchange resins. The resins are selected so that specific components of an asphalt are adsorbed by the resin bed and the remainder of the asphalt solution passes through. The adsorbed materials may be displaced from the resin bed by treatment with a desorbing agent. The portion of the asphalt not adsorbed by the resin may be recovered by solvent removal or may be pumped through a column filled with another variety of activated ion exchange resin.

During SHRP, preparative IEC separations were performed using Bio-Rad™ MP-1 (anion) and MP-50 (cation) resins. The MP-1 (anion) resin interacts with and adsorbs acidic components of asphalt solutions. The MP-50 (cation) resin interacts with and adsorbs basic components. In one of the IEC separation methods developed in SHRP, a solution of an asphalt in cyclohexane was pumped through two columns of activated ion exchange resin arranged in series. The first column contains activated MP-50 (cation) resin and the second contains activated MP-1 (anion) resin. The basic components of the asphalt solution are adsorbed on the first column and the acidic components are adsorbed on the second column. The asphalt components eluting from both columns are free from all strongly polar materials, and are referred to as the IEC neutral fraction. The second column is treated with formic acid to desorb the acid fraction of the asphalt, which can be recovered by distilling off the formic acid. The first column is desorbed by propylamine, yielding all components of the asphalt solution that contain basic functional groups. After removal of the propylamine by distillation, the eluates are redissolved in cyclohexane and pumped through a third column, filled with activated MP-1 (anion) resin. Molecules that contain only basic functional groups are not adsorbed. Many of the compounds that contain basic functional groups also contain acidic functional groups. That is, they are amphoteric. They will be adsorbed by the second column of MP-1 (anion) resin. In the initial separation, these compounds were adsorbed on the MP-50 (cation) resin. Desorption of the second MP-1 (anion) resin column by formic acid yields the amphoteric fraction. The materials not adsorbed by the second MP-1 (anion) resin column are the base fraction. A flow sheet for this process is illustrated in figure 3-4. It is emphasized that the designations acid, base, amphoteric, and neutral in this work are defined by interactions of asphalt components with ion exchange resins.

The four fractions isolated by this separation method are distinctly different from one another in chemical and physical properties. The IEC neutral fractions are non-Newtonian liquids at 60°C (140°F), much lower in viscosity than parent asphalts, and are relatively low in number-average molecular weight. The glass transition temperatures (T_g) of these materials are lower than those of their parent asphalts. The IEC neutrals comprise 50-60 percent of the mass of unaged asphalts. Acidic and basic fractions are relatively minor components of asphalts. They are tacky semisolids. Carboxylic acids, phenols, and pyrroles are abundant in the acid fractions. Bases contain metalloporphyrins, pyridines and, in aged asphalts, sulfoxides. The amphoteric fractions comprise 15-25 mass percent of unaged asphalts. They are the viscosity-building components of asphalts. They also impart elastic properties to asphalts. Some molecules in the amphoteric fraction are highly surface active. Of the four IEC fractions, they are highest in number-average molecular weight. The relative amounts and chemical composition of each IEC fraction is source dependent, so that this method of separation may be used as a characterization tool.

In the previous paragraph, differences in molecular weight values of the IEC fractions were commented on. At this point in this discussion, it is useful to elaborate on the concept of molecular weight and a method used to measure this property in asphalts. The term true molecular weight refers to the sum of the atomic weights of the atoms that make up a molecule. True molecular weights of molecules that do not engage in molecular associations are easily determined by several classical methods. However, many of these methods involve counting of individual submicroscopic particles. They cannot distinguish between an individual molecule and associations of molecules held together by weak bonds. As an example, the compound known as acetic acid, familiar as the acidic component of vinegar, has the formula $C_2H_4O_2$. The true molecular weight of this compound is 60 daltons. This is the sum of the atomic weights of the eight atoms held together by covalent bonds. However, in aqueous solutions of acetic acid, each molecule of acetic acid associates with another molecule by means of hydrogen bonding to form a dimer. The hydrogen bond is much weaker than a covalent bond, but the molecular association (dimer) persists except at high dilution. Thus, some methods used to determine molecular weights will report a value of up to 120 daltons for acetic acid. Others, depending on concentration, will yield values between 60 and 120 daltons. The values over 60 are apparent molecular weights, but they reflect the reality of acetic acid dimerization in aqueous solution, which the true molecular weight does not. Thus, under some circumstances the apparent molecular weight value is the more genuine, because many physical properties are a function of the extent and strength of molecular associations.

Molecular weight determinations of mixtures of compounds involve additional complications. The vapor phase osmometry (VPO) method applied to mixtures of non-interacting molecules yields number-average molecular weight values. If the molecular weights of the individual components of a mixture vary over a narrow range, VPO measurements should provide an accurate estimate of an average molecular weight value. If, however, the molecular weights of the individual components of a mixture vary widely, the VPO value will be skewed to lower values. For such a mixture, the existence of small amounts of large molecules might not be suspected from VPO measurements. Additionally, VPO measurements of mixtures of compounds that form molecular associations are strongly influenced by choice of solvent, concentration, and temperature at which measurements are performed. If molecular associations do not occur, VPO values should be essentially the same in different solvents, and at different concentrations and temperatures. Where there are molecular associations of varying strengths, VPO values measured in a solvent such as toluene will be considerably higher than those measured in the more polar solvents pyridine or nitrobenzene. Dilution and temperature also tend to break up molecular associations, and so VPO values in a given solvent will be lower at higher dilutions and temperatures.

Based on the model of asphalt structure discussed previously, the IEC neutrals may be considered to be the solvent. Amphoterics may be considered to be the dispersed phase, and acids and bases are the resins. The IEC neutrals of a large number of asphalts are characterized by a direct relationship between measured molecular weight values by VPO and viscosity, as would be expected for such materials. In systems in which strong molecular interactions do not occur, the true (as distinct from apparent) molecular weights should correlate directly with viscosities. When IEC neutrals are mixed with the polar, associating acids, bases, and

amphoterics, measured molecular weight values no longer correlate with viscosities [Kim and Branthaver 1996].

During SHRP, other IEC separation methods were employed, but will not be discussed here. A scaled-down IEC procedure using small samples that is useful for characterization studies was developed during this program and is described in Volume II, method 5. The use of a more rapid preparative IEC method (employing different resins) for isolation of neutral fractions only will be discussed later in this chapter and in Volume II, method 11.

The relatively new supercritical fluid extraction (SFE) method has been used to extract non-polar components from asphalts. This method is based on the observation that fluids at high temperatures and pressures (often approaching or exceeding the critical temperature and pressure) have the solvent power of a liquid but the viscosity of a gas. The supercritical fluid chromatography (SFC) extracts have been used mainly for studies of low temperature properties, so the procedure will be described in a later section of this chapter.

Comparison of Three Separation Methods

The three separation methods discussed in detail above (IEC, SEC, and asphaltene precipitation) separate asphalts into polar and relatively non-polar subunits. These subunits would be expected to correspond to some degree to the dispersed and solvent components of asphalts as predicted by the model. It is of interest to compare the relative amounts and properties of the most polar components generated by the three methods, namely asphaltenes, SEC Fraction-I, and amphoterics from IEC. All three of these materials are black, friable solids. They are the viscosity builders in all asphalts and have much higher molecular weight values than their parent asphalts. In some asphalts, the mass fractions of the parent asphalts of the three polar materials are nearly the same, so there must be much overlap among them. In other asphalts, the mass fractions of the three materials vary in amount by an order of magnitude. Usually, molecular weight values of amphoterics are lower than molecular weight values of the other two polar fractions for a given asphalt. Thus, separation of asphalts based on differential solubility, molecular weight distribution, and polarity do not yield identical subunits. Each method of separation does yield fractions that have properties of unique interest. Although they are difficult to generate, certain kinds of information can be obtained only from IEC neutral fractions, and not from maltenes or lower molecular weight SEC fractions. The fact that the very different separation methods do not yield the same subunits should not be surprising, due to the complexity of asphalts. Models of asphalt structure must take these results into account.

The fractions generated using the above described separation methods have been subjected to further studies in this program, and the results of these studies are described in the remainder of this chapter and in chapter 4 of this report.

Compound	Molecular Formula	Structural Formula	Molecular Weight (Daltons)
Propane	C_3H_8	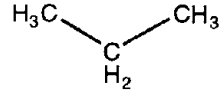	44
n-Butane	C_4H_{10}	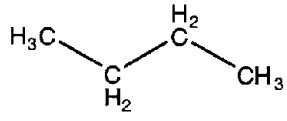	58
n-Pentane	C_5H_{12}	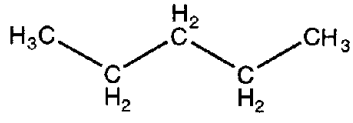	72
n-Hexane	C_6H_{14}	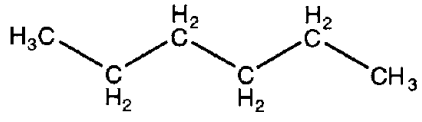	86
n-Heptane	C_7H_{16}	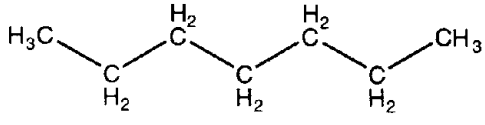	100
n-Octane	C_8H_{18}	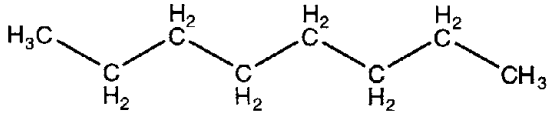	114
iso-Octane (2,2,4-Trimethyl Pentane)	C_8H_{18}	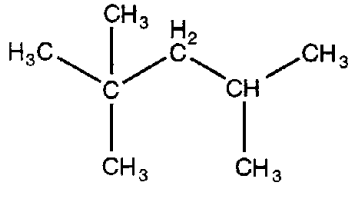	114

Figure 3-3. Structural formulae of alkanes used in the precipitation of asphaltenes.

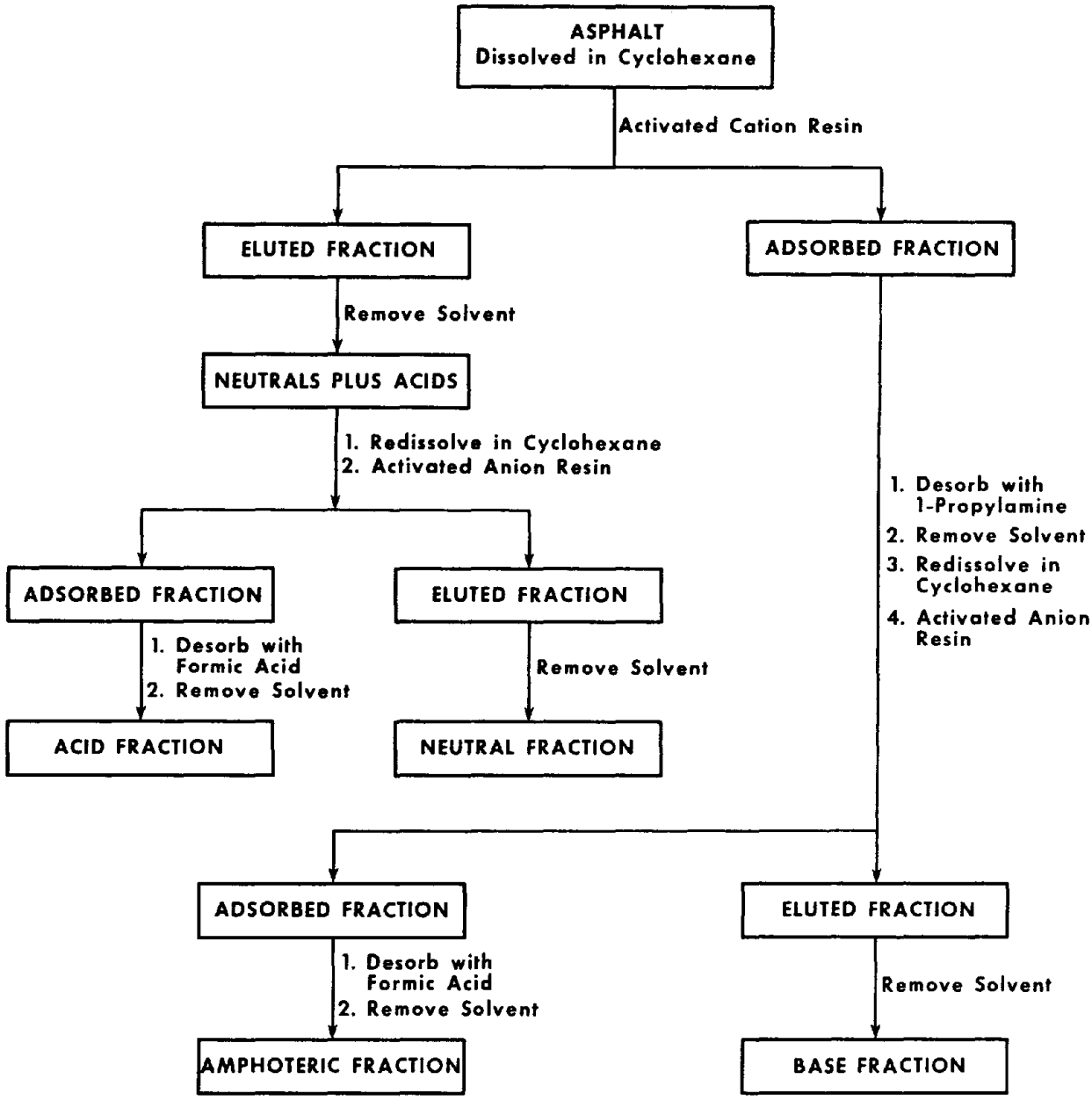

Figure 3-4. Flow sheet for separation of asphalts into neutral, acid, base, and amphoteric fractions by ion exchange chromatography.

SEPARATION, CHARACTERIZATION, AND REASSEMBLY OF ASPHALT FRACTIONS

Fractionation of Strongest Molecular Associations

Earlier in this chapter, it was mentioned that asphalts have rheological properties that resemble polymers in some ways [Schmidt and Barrall 1965]. The rheological properties of polymers are strongly influenced by molecular weight and molecular weight distribution. By definition, these molecular weight values must be several thousand or larger. Asphalts are not polymers. Number-average molecular weight values of asphalts are relatively low. When measured in toluene at 60°C (140°F) by VPO, the molecular weight values of eight SHRP core asphalts range from 700 to 1,300 daltons [SHRP 1993]. These values do not come close to those recorded for common polymers. Polymer molecular weights vary from a few thousand to over one million daltons. The connection between rheological properties and molecular weight values of polymers is well established [Manson 1982]. It is of great interest to determine what features of asphalts cause them to behave in polymer fashion, if not the property of molecular weight. Toward this end, the molecular weight distributions of asphalt polar fractions were investigated.

The model of asphalt structure described earlier in this report postulates that polyfunctional polar molecules in asphalts form molecular associations by means of polar attractions, hydrogen bonding, and aromatic stacking. These bonds are much weaker than the covalent bonds that hold individual molecules together. The weak bonds may be broken up by minor energy inputs in the form of heat and shear and by addition of solvents. Covalent bonds are stable to mild energy inputs. Number-average molecular weight values of asphalts are determined in very dilute solutions (most frequently in toluene) in which most molecular associations should be broken up. In neat asphalts, polar components could, according to the model, have high effective molecular weights, which would be reflected in rheological properties. The relatively low number-average molecular weight values of asphalts thus would not preclude the existence of extensive molecular associations in neat asphalts, or even small amounts of large molecules. It was pointed out earlier that number-average molecular weights of mixtures are skewed to the lower boundary of a molecular weight range.

One technique used for measuring molecular weight values of polymers, membrane osmometry, does not suffer from such a disadvantage. However, membrane osmometry is not useful for measuring any molecular weight values of entities below several thousand daltons. It is not known whether true molecular weight values (molecular weight values in the absence of effects caused by molecular interactions) of the vast majority of asphalt components exceed 2,500 daltons. Therefore membrane osmometry, if it were able to be used to study asphalt molecular weights, should be measuring extents of asphalt molecular associations. These associations would have to persist in toluene solution, because asphalts or asphalt fractions are dissolved in toluene to perform molecular weight determinations by membrane osmometry.

Vapor phase osmometry measurements in toluene of whole asphalt molecular weights yield relatively low values, as mentioned previously. However, similar measurements of asphaltenes, IEC amphoterics, and SEC Fraction-I materials yield values of up to 10,000 daltons.

The highest of these values is almost too low for membrane osmometry determination. Therefore, it was decided to refractionate SEC Fraction-I components of the eight SHRP core asphalts by SEC. By doing so, the relative heterogeneity, or lack thereof, of the SEC Fraction-I materials would be determined. Also, it might prove possible to gain some measure of the size of the largest molecular associations present in each asphalt. This goal is of considerable importance because such entities would be expected to influence rheological properties disproportionately.

Samples of SEC Fraction-I were dissolved in toluene and the solutions were injected into the same SEC columns on which the SEC Fraction-I materials were originally generated. The original SEC Fraction-I materials are the initial eluates in the separation of solutions of whole asphalts. They are separated from the rest of the asphalt by observing the onset of fluorescence in the eluates. For most asphalts, SEC Fraction-I corresponds to the initial 250-300 mL of eluates in the experimental procedure used in this study. In the refractionation of SEC Fraction-I, three equal portions of the initial eluates were collected up to the onset of fluorescence. Thus, if the original SEC Fraction-I materials were obtained from the first 300 mL of eluates, then in the refractionation, three 100 mL fractions would be collected. A fourth subfraction, consisting of materials eluting after the onset of fluorescence, also was collected. According to the model, if SEC Fraction-I consists of molecular associations, then some of the smaller units ought to be observed as tailing in the refractionation. The amount of materials collected in this last subfraction should be some indication of the strength of the forces holding together molecular associations in SEC Fraction-I. If little or no tailing materials are observed, the associations are presumably strongly held together and vice versa. So in the refractionation of SEC Fraction-I components of eight SHRP asphalts, four subfractions were collected and their properties studied. A flow sheet for this procedure is shown in figure 3-5.

Table 3-7 lists mass percentages of materials in each of the four subfractions of the eight asphalts. The data are averages of several runs. Reproducibilities between runs are not very good. Asphalt AAD-1 was intensively studied, and results for the SEC Fraction-I of this asphalt will be discussed in detail. The mass distribution of material among the four subfractions of AAD-1 is uneven. Subfraction I-2 is by far the largest, followed by subfractions I-1 and I-3. The amount of material in subfraction-I-4 is small. The same mass distribution pattern is observed for all other asphalts except AAM-1. In this unusual asphalt, the amounts of material in subfractions I-2 and I-3 are nearly equivalent, and contain more material than subfractions I-1 and I-4. The I-4 subfraction of AAM-1 contains much more material than equivalent subfractions of the other asphalts, and the I-1 subfraction much less. This observation indicates that molecular associations in AAM-1 are less extensive and more weakly held together than in other asphalts.

The model of asphalt structure proposed earlier would predict that the subfractions should differ in chemical properties. Because the I-1 subfractions presumably consist of the largest molecular associations, they also should be the most aromatic (lowest atomic ratio of hydrogen to carbon). Table 3-8 lists elemental composition data for the subfractions of all eight asphalts. For each of the asphalts, the I-1 subfraction is the most aromatic. However, these aromaticity values are not significantly different from aromaticity values of I-2 subfractions of the same asphalt.

The I-3 subfractions are much less aromatic than the I-1 and I-2 subfractions. The I-4 subfractions are nearly the same as the I-3 subfractions in aromaticity. These data suggest that there are two fundamentally different types of materials in SEC Fraction-I components of asphalts. Nitrogen and sulfur concentrations are high in all the subfractions.

To verify the relative aromaticities of the subfractions, NMR studies were performed on some of them. In those subfractions subjected to NMR analysis, ^{13}C resonances were measured. The ^{13}C resonance frequency of an aliphatic carbon differs from that of an aromatic carbon, so the relative amounts of each can be quantified. These NMR data are listed in table 3-9. The relative aromaticities in table 3-9 parallel those in table 3-8, which were calculated from hydrogen-to-carbon (H/C) atomic ratios. For example, the I-1 subfractions of AAB-1 and AAC-1 have nearly equivalent amounts of aromatic and aliphatic carbons, with slightly more of the latter. In table 3-8, the H/C ratios of these two subfractions are low. For almost all of the asphalts, aromaticities of the I-1 and I-2 subfractions measured by ^{13}C NMR are similar. The I-3 subfractions are considerably less aromatic. Aromaticity measurements by ^{13}C NMR were not performed on I-4 subfractions because of the small amounts of materials available.

The property of molecular weight should parallel aromaticity in the subfractions. The most aromatic subfractions should be the highest in molecular weight. Table 3-10 lists molecular weight values determined by membrane osmometry of I-1 subfractions of each of the eight asphalts. The I-1 subfractions of AAD-1 and AAK-1 have molecular weight values of nearly 40,000 daltons. These high values, which are in the low molecular weight polymer range, are doubtless the result of molecular associations, but the associations must be fairly strong to persist in toluene solution. These materials included in the SEC I-1 subfractions comprise about 4 mass percent of the whole asphalts for AAD-1 and AAK-1. They may be expected to exert disproportionately large influences on rheological properties of asphalts. The effective molecular weights of these materials may be even greater in neat asphalts than in toluene solution.

Membrane osmometry molecular weight values for I-1 subfractions of other asphalts are lower than molecular weight values for I-1 subfractions of AAD-1 and AAK-1. Values for AAM-1 I-1 subfraction are not even half as large as the values for the AAD-1 and AAK-1 materials. Also, there is much less material in the AAM-1 I-1 subfraction compared with the other seven asphalts (table 3-7). This relative lack of strong molecular associations may account for some of the unusual properties of AAM-1.

Molecular weight values for the I-2 subfractions are listed in table 3-11. These measurements were made using both membrane osmometry and VPO. The molecular weight values of the I-2 subfractions by membrane osmometry are considerably lower than molecular weight values of I-1 subfractions of the same asphalts. The vapor phase osmometry molecular weight values are considerably lower than the membrane osmometry molecular weight values for the I-2 subfractions. It was noted earlier that vapor phase osmometry molecular weights of mixtures are skewed toward the lowest molecular weight components, while this bias is not observed in the membrane osmometry determinations.

Molecular weights of the I-3 and I-4 subfractions were determined by vapor phase osmometry only. These values are listed in table 3-12. Values for the I-3 fractions are approximately two times larger than those of the I-4 subfractions. The molecular weight values of all eight I-4 subfractions are not greatly different.

Table 3-13 lists VPO molecular weight values of all four subfractions of asphalt AAD-1. These data were obtained from three different preparations of the subfractions. The I-2 and I-3 subfractions whose molecular weights are listed in table 3-13 are from different runs than those subfractions whose molecular weights are listed in tables 3-11 and 3-12. Therefore, AAD-1 subfraction molecular weights differ somewhat when values listed in tables 3-11 and 3-12 are compared with values listed in table 3-13. The molecular weight values of the subfractions vary seven-to-tenfold between subfractions I-1 and I-4. Interestingly, the VPO molecular weight of the I-1 subfraction of AAD-1 is three-fourths that of the membrane osmometry molecular weight. The relative magnitudes of molecular weights of the subfractions are detected by VPO, even though the values determined by the method are smaller than the membrane osmometry values of the same materials.

The above results establish the existence of significant amounts of polar, aromatic entities in asphalts that are probably molecular associations of high apparent molecular weight. Additionally, some macromolecules may be present. It is necessary to verify these findings by measuring the effects of the high apparent molecular weight materials on rheological properties.

Toward this end, the model of asphalt structure described above was modified somewhat to accommodate the findings from the SEC separations. Asphalts are considered to be composed of SEC Fraction-I materials dispersed in a solvent, assumed to be SEC Fraction-II. Based on the model of asphalt structure described earlier, the SEC Fraction-I materials should contain most of the asphaltene molecular associations. The solvent component and some resins should be included in SEC Fraction-II. Each asphalt is characterized by SEC fractions having unique properties and, perhaps more importantly, having unique natural abundances. For example, the relative abundance of the two SEC fractions in AAD-1 is approximately 25 percent SEC Fraction-I and 75 percent SEC Fraction-II.

The SEC Fraction-I subfractions of AAD-1 differ by up to a factor of 10 in molecular size. If the model of asphalt structure described earlier is valid, they should have disparate influences on rheological properties. To measure these influences, synthetic asphalts were prepared. Mixtures of the I-1, I-2, and I-3 subfractions with SEC Fraction-II of AAD-1 were prepared with subfractions consisting of 5 percent, 10 percent, 15 percent, and 20 percent of the mixtures. Mixtures containing 25 percent of the subfractions were not prepared because of apprehensions that such a mixture of the I-1 subfraction with SEC Fraction-II would be extremely difficult to work with. The small amounts of the I-4 subfraction limited the number of mixtures that could be prepared with this material. Only two mixtures with the I-4 subfraction, at the 5 percent and 15 percent level, were prepared. The mixtures were manufactured by dissolving weighed amounts of the materials in a solvent and removing the solvent. This process results in some loss of light ends, and so the solvent removal process is performed in a consistent manner among all the samples.

The viscosity of AAD-1 SEC Fraction-II (336 Pa·s at 1.0 rad/s) is much lower than that of the whole asphalt (approximately 40,000 Pa·s at 1.0 rad/s) at 25°C (77°F). When the SEC Fraction-I subfractions of AAD-1 are mixed with SEC Fraction-II at the 5 percent level, the mixtures are not much more viscous than SEC Fraction-II (table 3-14). The three subfractions I-1, I-2, and I-3 appear to have identical effects on viscosity. At the 5 percent level, SEC Fraction-II effectively disperses all of these materials. The mixtures are relatively undifferentiated.

At the 10 percent level, viscosities of the mixtures are much greater than the 5 percent level mixtures. The mixture containing the I-1 subfraction is considerably more viscous than the mixture containing the I-2 subfraction, which is more viscous than the mixture containing the I-3 subfraction (table 3-15).

When the subfractions are increased to the 15 percent level, viscosities of the mixtures are higher than viscosities of mixtures at the 10 percent level. In table 3-16, the mixture containing the I-2 subfraction is approximately as viscous as the mixture containing the I-3 subfraction. Except for the mixture containing the I-4 subfraction, tan δ values are 10 or lower.

At the 20 percent level (table 3-17), the mixture containing the I-1 subfraction has approximately the same viscosity as neat AAD-1, which contains 24-25 percent SEC Fraction-I. Tan δ of the mixture is 2-3, depending on shear rate. This indicates that the mixture has substantial elastic properties. The viscosities of the mixtures containing the I-2 and I-3 subfractions are lower than the mixture containing the I-1 subfraction, and are distinctly different from one another. Tan δ values of the mixtures rise with decreasing apparent molecular weight of the subfraction in each mixture.

The above results show that SEC Fraction-I materials consist of entities that have a wide range in apparent molecular weight, at least in toluene solution. The largest entities are probably extended molecular associations, and their effective molecular weights in toluene are polymeric in magnitude, about 30,000 to 40,000 daltons. Measuring number-average molecular weight values of whole asphalts by VPO cannot give any indication of the presence of these entities, which exist in substantial amounts in the asphalts studied. This is due to the nature of VPO determinations, as explained previously. The higher apparent molecular weight components influence rheological properties of asphalts more than the lower molecular weight components as would be expected from theoretical considerations. Size exclusion chromatography has been shown to be a valuable preparative technique for separation of asphalt solutions into components that differ from one another in many fundamental properties that depend on molecular size.

Reassembly of Asphalt Size Exclusion Fractions

It is not only of interest to isolate and characterize asphalt fractions of interest, but also of interest to determine how these fractions interact with one another. It is expected that asphalt properties will be influenced by the relative amounts of various compound types comprising an asphalt. It may or may not be true that properties are influenced by small differences in chemical makeup of the compound types.

Consider the separation of asphalts into two fractions by size exclusion chromatography. The two fractions are the high molecular weight solids designated SEC Fraction-I (the subfractionation of which was discussed in the immediately preceding section) and the low molecular weight semi-solid or liquid SEC Fraction-II. It may be arbitrarily assumed that the first fraction corresponds to the asphalt dispersed component, and the second to the solvent component. In SHRP, it was established that the SEC Fraction-I component is the viscosity-building component. Each asphalt is characterized by a unique natural abundance of the two SEC fractions. The SEC fractions of a given asphalt differ in chemical properties from equivalent fractions in other asphalts. It is known that relative amounts of the two fractions influence asphalt physical properties, but it is not known how the variations in chemical properties among the same SEC fractions of different asphalts influence physical properties. One way to determine this is to mix fractions from different asphalts to prepare artificial asphalts.

The artificial asphalts are referred to as crossblended mixtures. To manufacture them, each SEC Fraction-II of the SHRP core asphalts (with one exception) was mixed with the SEC Fraction-I of the eight SHRP core asphalts. That is, eight mixtures were prepared in which SEC Fraction-II of asphalt AAA-1 was mixed with eight different SEC-I fractions, and similarly for the SEC Fraction-II of AAB-1, AAC-1, AAD-1, AAF-1, AAG-1, and AAK-1. Natural abundances of the two fractions in each mixture were those of the parent asphalt of the SEC Fraction-II component. Thus, for each set of eight crossblended mixtures, one mixture reconstitutes the parent asphalt and serves as a control. The mixtures were prepared in a solvent, and some light ends are lost during solvent removal. After drying, rheological properties of the mixtures were determined.

Viscosities and other rheological properties of the crossblended mixtures were measured at 25°C (77°F) on a Rheometrics model 605 Mechanical Spectrometer. Table 3-18 lists natural abundance levels of the two SEC fractions of the eight SHRP core asphalts. These natural abundance levels determine the composition of the crossblended mixtures. Table 3-18 also lists viscosities of SEC Fraction-II of the eight core asphalts at 25°C (77°F). These values are used to calculate reduced specific viscosities (equation 3-11). Crossblends involving SEC Fraction-II of AAM-1 at the AAM-1 natural abundance level (31.8 percent) were not prepared because most of the mixtures would have viscosities so large at 25°C (77°F) that they could not be accurately measured.

The 25°C (77°F) viscosities of the crossblended mixtures are listed in table 3-19. Each column in table 3-19 represents a set of mixtures in which the SEC Fraction-II component is the same, as is the relative abundance of the two fractions. Only the source of the SEC Fraction-I component varies. Crossblended mixtures with all eight SEC Fraction-I components, including that of AAM-1, were prepared. It is observed that viscosities of the eight mixtures in each column vary greatly, depending on the nature of the SEC Fraction-II materials.

To make comparisons with previous research on asphalt compatibilities, reduced specific viscosities (η_{red}) were calculated. The manner in which η_{red} values are calculated was explained earlier (equation 3-11). Briefly, they are relative viscosities minus unity, and the differences divided by mass fractions of SEC Fraction-I components. Relative viscosities are viscosities of

the crossblends divided by SEC Fraction-II viscosities. The η_{red} values allow comparisons of mixtures in which SEC Fraction-II viscosities vary and in which relative abundances of the two fractions vary.

Table 3-20 lists η_{red} values of all of the crossblended mixtures at 25°C (77°F). Each column lists η_{red} values of mixtures having the same SEC Fraction-II component, but different SEC Fraction-I components. Within each column, natural abundances of the two fractions are the same. Reading down a column, the only variable is the nature of the SEC Fraction-I component of the crossblended mixture. In column 1, each mixture consists of 78.3 mass percent of SEC Fraction-II of asphalt AAA-1. It is obvious that there are very large differences among the η_{red} values of the mixtures. The mixture containing SEC Fraction-I of AAM-1 is compatible (η_{red} = 30), while the mixture containing SEC Fraction-I of AAD-1 (η_{red} = 1,610) is highly incompatible. SEC Fraction-I components of AAB-1, AAC-1, AAF-1, and AAK-1, when mixed with SEC Fraction-II of AAA-1, yield more or less similar mixtures (η_{red} varies from 820 to 920).

In column 2 (table 3-20) η_{red} values of mixtures containing SEC Fraction-II of AAB-1 are reported. The values range from 30 to 780. Again, the mixture containing SEC Fraction-I of AAM-1 is the most compatible mixture, and that containing SEC Fraction-I of AAD-1 is the least compatible. Five of the crossblends containing SEC Fraction-II of AAB-1 are lower in η_{red} values than equivalent mixtures in column 1, but three are either identical or the η_{red} value in column 2 is higher. This observation indicates that the SEC Fraction-II component of AAB-1 is usually a better solvent than that of AAA-1, but that there are specific interaction effects with particular SEC Fraction-I materials.

The η_{red} values in column 3 (table 3-20) are low compared with η_{red} values in columns 1 and 2. This is because of lower natural abundances of SEC Fraction-I in AAC-1.

The η_{red} values in column 4 (table 3-20) correspond to crossblended mixtures in which the SEC Fraction-II component is that of AAD-1. The relative abundance of the two fractions is similar to that of mixtures in columns 1 and 2. The η_{red} values in column 4 range from 40 to 830. Again, the mixture containing the SEC Fraction-II component of AAM-1 is most compatible, and reconstituted AAD-1 is least compatible.

Comparison of columns 1, 2, and 4, crossblends having similar relative amounts of the two SEC fractions, shows that the response of SEC Fraction-II of AAA-1, AAB-1, and AAD-1 to SEC Fraction-I of AAM-1 is similar. The same may be said about the SEC Fraction-I of AAG-1. The response of the three SEC Fraction-II materials to the SEC Fraction-I component of AAA-1 does not vary greatly. However, the interaction of the three SEC Fraction-II materials with the remaining four SEC Fraction-I components varies considerably. For example, SEC Fraction-II of AAA-1 forms much less compatible mixtures with SEC Fraction-I components of AAB-1, AAC-1, AAF-1, and AAK-1 than the other two SEC Fraction-II materials.

Columns 3 and 5 in table 3-20 list η_{red} values of crossblended mixtures in which the SEC Fraction-II components are those of AAC-1 and AAF-1, respectively. Natural abundances of the

two SEC fractions in these crossblended mixtures are nearly identical, so η_{red} values in each row may be directly compared. Each entry in column 3 is larger than the corresponding entry in column 5. For example, the two mixtures containing SEC Fraction-I of AAA-1 (row 1) have η_{red} values of 190 (column 3), and 80 (column 5), respectively. The only two mixtures in which the differences are not large are those in which the SEC Fraction-I component is AAM-1 (row 8). Comparison of the entries in columns 3 and 5 leads to the conclusion that SEC Fraction-II of AAF-1 is a much more effective solvent than SEC Fraction-II of AAC-1.

Entries in column 6 of table 3-20 consist of η_{red} values of crossblended mixtures in which the SEC Fraction-II component is that of AAG-1. Natural abundance levels of the SEC Fraction-II component are the highest of all of the crossblended mixtures. The relatively low η_{red} values in column 6 reflect low amounts of SEC Fraction-I components. Based on these values, it would appear that only the SEC Fraction-I component of AAD-1 is significantly less compatible with SEC Fraction-II of AAG-1 than the SEC Fraction-I materials in AAG-1 itself. It is observed that SEC Fraction-I of AAA-1 forms a highly compatible crossblended mixture ($\eta_{red} = 20$) with the SEC Fraction-II component of AAG-1.

Column 7, table 3-20, lists η_{red} values of mixtures in which the SEC Fraction-II component is that of AAK-1. These mixtures contain the largest natural abundances of SEC Fraction-I components of all the seven subgroups of the crossblends. Yet the η_{red} values in column 7 are not particularly larger than values in columns 1, 2, and 4. The SEC Fraction-II component of AAK-1 appears to be most incompatible with SEC Fraction-I of AAC-1 and AAG-1.

It may be concluded from the data in table 3-20 that the relative abundance of the two SEC fractions is a principal determinant of mixture compatibility. The nature of the SEC Fraction-I component also is an important determinant, even if the anomalous AAM-1 materials are excluded from consideration. Solvation power of the SEC Fraction-II also is a contributing factor. A fourth factor, the manner in which the two SEC fractions interact, also is important. This is evident upon ranking η_{red} values in order from one to eight for members in each column. When rankings of η_{red} values in one column are compared with those in another, it is observed that the rankings are not always identical.

The η_{red} data in table 3-20 may have practical consequences. It is known that asphalt AAG-1 is prone to rutting [Stroup-Gardiner 1996]. To reduce this tendency, it may be blended with another asphalt. Blending AAG-1 with an asphalt such as AAA-1 with which AAG-1 forms compatible mixtures (entry 1, row 6; entry 6, row 1) might not be effective, whereas mixing AAG-1 with AAD-1 (entry 4, row 6; entry 6, row 4) should be effective.

Other rheological data in addition to viscosities were obtained for the crossblended mixtures. Dynamic shear modulus (G*) values and phase angles (δ) over a wide range of shear rates were measured. For most measurements, 8 mm plates were used, and strain rates of 3-15 percent were employed. These data are exhibited in seven Black plots (figures 3-6 to 3-12). Individual data points are not listed in tables in this report. Each Black plot illustrates data from eight mixtures containing the same SEC Fraction-II component. In figure 3-6, the SEC

Fraction-II component is derived from AAA-1. The data for various crossblended mixtures corresponding to each SEC Fraction-I material with SEC Fraction-II of AAA-1 are represented by individual points, which coalesce to form identifiable lines. The lines corresponding to the mixtures containing SEC Fraction-I components of AAD-1, AAG-1, and AAM-1 are most distinctive. The mixture containing SEC Fraction-I of AAD-1 has lowest values of δ for a given G* value. This means that this mixture is the most elastic of the eight. Contrariwise, the mixture containing SEC Fraction-I of AAM-1 is least elastic. The slope of the line corresponding to the mixture containing SEC Fraction-I of AAG-1 is least steep, indicating that this mixture is most shear susceptible (greatest change in δ for a given change in G*). The mixtures containing SEC Fraction-I of AAA-1, AAB-1, and AAF-1 are rheologically similar. Of the eight mixtures, that containing SEC Fraction-I of AAK-1 is least shear susceptible (least change in δ for a given change in G*).

The above comments apply, to varying degrees, to the other six Black plots. In the more compatible mixtures, the lines are not as strongly separated, but the less compatible mixtures containing SEC Fraction-I of AAD-1 are most elastic, and the compatible mixtures containing SEC Fraction-I of AAM-1 are least elastic. In figure 3-10, all lines have identical slopes and none are clearly differentiated. These mixtures contain low relative abundances of SEC Fraction-I components (13.3 mass percent) and the SEC Fraction-II of AAF-1, a good solvent for SEC Fraction-I components at this abundance level. Figure 3-11 corresponds to mixtures in which the SEC Fraction-II component is that of AAG-1. The curves are not well differentiated and are unusual in shape compared with the curves in the other figures. The δ values decrease as G* increases until a value of $G^* = 1 \times 10^6$. The δ's reach a minimum and then increase. This phenomenon probably reflects unreliability of data at G* values greater than 1×10^6 for these particular mixtures.

The above data show that asphalt solvent and dispersed components may be expected to interact in unique ways. The relative abundance of the two components appears to be the most important factor in determining the rheological properties of crossblended mixtures, but the nature of the two fractions also is important. The solvent components of some asphalts are better at peptizing dispersed components than solvent components of other asphalts. These considerations indicate that properties of asphalt blends might not be so easily predicted in the absence of detailed chemical compositional data for asphalt components.

Studies of Asphalt Ion Exchange Chromatography Neutral Fractions

The above discussion described results from the study of asphalt fractions that are isolated according to molecular size. It is of interest to separate asphalts into fractions according to chemical functionality and compare these fractions with those obtained by SEC. In an earlier discussion in this chapter, such a comparison with respect to SHRP work was described.

Continuing studies begun during SHRP, IEC was used to separate asphalts into defined chemical fractions. It was decided that the fractions so obtained should be small in number yet constitute distinctive chemical assemblages. Fundamentally, it is desirable to be able to separate polar from non-polar groups of molecules. These two categories should correspond more or less

with dispersed and solvent components, respectively. The polar molecules comprise several fundamentally different compound types that may be readily separated from one another by IEC, and this was done. The polar components of asphalts were separated into fractions that are acidic, basic, or both acidic and basic (amphoteric). The non-polar components also comprise many different compound types, but are not separable by IEC. The non-polar components of asphalts are referred to as neutral materials. As does the SEC Fraction-II material, the IEC neutral fraction of an asphalt approximates the asphalt solvent component. Because the IEC neutral fraction comprises 50-60 percent of an unaged asphalt, it must be the bulk of the solvent component if the model of asphalt structure described earlier is meaningful.

It is necessary to characterize IEC neutral fractions for a number of reasons. According to the model, the solvent component should strongly influence several important asphalt physical properties, among them the glass transition temperature and temperature variation of viscosity, solubility parameter, and low temperature crystallization behavior. Therefore, there is a need to determine how IEC neutral materials vary among asphalts and how they vary with exposure to oxygen. Detailed compositional knowledge might allow design of additives to modify asphalt properties.

One of the most important properties of any solvent is the solubility parameter, δ. The Greek letter δ also is used to denote the phase angle in rheological measurements. The two terms should not be confused. The solubility parameter is the square root of the cohesive energy density of the material, $\Delta E/v$, where ΔE is the energy of vaporization and v is the molar volume. The molar volume of a substance is its molecular weight divided by its density, MW/ρ. Thus,

$$\delta = \left[\frac{\Delta E}{MW/\rho}\right]^{1/2} \tag{3-19}$$

According to this definition, the behavior of any material as a solvent is predictable from three properties that can be readily measured for many pure compounds. An explanation of why this is so is as follows.

All molecules in a solid or liquid experience forces of attraction among each other. Thus each molecule has an internal energy bond with other molecules, particularly with nearest neighbors. The existence of these bonds in a solid or liquid tend to prevent mixing with dissimilar substances.

When a solid or liquid vaporizes, the individual molecules are so far apart that internal bonding essentially disappears. To vaporize a substance, work must be done to overcome internal attraction forces. The energy required to do this is known as the heat of vaporization. These same internal bonds must be overcome when one substance is dissolved in another. The difference in energy between vaporization and dissolution is the work done through volume expansion to the vapor state.

When two or more substances are mixed, the equation

$$\Delta F = \Delta H - T\Delta S \tag{3-20}$$

determines whether or not they will form a solution. The ΔF term is the change in free energy of the process and must be negative for solubilization to occur. The ΔH term is known as the heat of mixing. The entropy change is reflected in the $T\Delta S$ term. If the molecules being mixed are nearly the same size and shape and of similar polarity, ΔH is nearly zero, and the molecules form a solution. In this case, little energy is required to overcome the forces of attraction between similar molecules. The ΔH term measures the energy required to overcome these forces. In the case of dissimilar molecules, the energy can be fairly large. Thus ΔF in equation 3-20 is positive, and solution does not occur.

Hildebrand showed that the magnitude of the heat of mixing (ΔH) is a function of the differences between the cohesive energy densities of the two kinds of molecules being mixed:

$$\Delta H = V\phi_1\phi_2\left[\left(\frac{\Delta E_1}{v_1}\right)^{1/2} - \left(\frac{\Delta E_2}{v^2}\right)^{1/2}\right]^2 \tag{3-21}$$

In equation 3-20, V is the total volume of solution, and ϕ_1, ϕ_2 are volume fractions of the two different molecular species. If the solubility parameter, δ, is the square root of the cohesive energy ($\Delta E/v$), equation 3-20 may be rewritten as:

$$\Delta H = V\phi_1\phi_2(\delta_1 - \delta_2)^2 \tag{3-22}$$

Units of δ are $cal^{0.5}/cm^{1.5}$. Obviously, as δ values approach each other, ΔH approaches zero. When δ values differ significantly, ΔH increases. If ΔH is large enough in equation 3-20 to cause ΔF to become positive, no solution will occur. This is the physicochemical basis for the aphorism "like dissolves like."

The value of δ increases with increasing ΔE and ρ, but decreases as molecular weight increases. Polar molecules, in general, have higher values of ΔE and ρ than non-polar molecules of equivalent molecular weight, so δ values of polar molecules will be higher than δ values of non-polar molecules. Solubility parameters of many common organic solvents are listed in table 3-21. The utility of the data in the table lies in the ability to predict solubility behavior. If it is desirable to dissolve a polar material in an organic solvent, inspection of table 3-21 will eliminate a large number of materials having low values of δ from consideration. Similarly, if it is desired to solubilize non-polar substances, one would choose a solvent with a low value of δ. As a generalization, two non-polymeric organic substances separated by more than 3.5 δ units will not be mutually soluble at normal temperatures and pressures [Burrell 1955].

Calculation of δ values for solvents containing more than one molecular species is complicated. This is because it is not easy to accurately measure molecular weights of mixtures, particularly if they contain many different compounds whose identities are not precisely known. Number-average molecular weight determinations tend to overemphasize smaller components of mixtures, as mentioned earlier. In mixtures such as asphalts, it is not possible to measure ΔE values because asphalt is not volatile. Therefore, δ values must be determined in other ways. In discussing solubility parameters of asphalts, it again needs to be pointed out that δ is not to be confused with phase angles in rheological measurements, which are denoted by the same Greek letter. Solubility parameters for such complex mixtures as asphalts will be averages of individual δ values on a mole fraction basis and would be expected to vary over a considerable range. These averages may not indicate the range of individual δ values present.

It is not only the solubility parameter values of whole asphalts that are of interest. Solubility parameters of IEC neutral fractions, which comprise the majority of asphalt solvent components, need to be determined. The δ values of IEC neutral fractions should be more meaningful than those of whole asphalts because there will be a much more restricted range of δ values of the components. It should be easier to measure δ values of IEC neutrals, and attempts to do so will be discussed before attempts to perform similar measurements on whole asphalts.

First, the miscibility of IEC neutral fractions with various polar solvents was measured. It is known that the neutral fractions are completely soluble in non-polar solvents such as iso-octane and n-heptane. The IEC neutral fractions of eight SHRP asphalts also are miscible with toluene, although dissolution is not rapid in all cases. The eight IEC neutral fractions are insoluble in polar solvents such as isopropyl alcohol and acetonitrile. Ethyl acetate is intermediate in polarity between toluene and acetonitrile. The IEC neutral fractions all exhibited partial to nearly complete solubility in ethyl acetate. The result of this experiment shows that the eight IEC neutral fractions differ in solubility behavior.

Quantitative solubility measurements of the eight IEC neutral fractions were performed using ethyl acetate ($\delta = 9.1$) and acetone ($\delta = 9.9$). These results are listed in table 3-22. Seven of the IEC neutral fractions are largely soluble in ethyl acetate, the IEC neutral fraction of AAM-1 being the exception. The solubility behaviors of the IEC neutral fractions are much better differentiated in acetone. The IEC neutral fraction of AAD-1 is almost 75 percent soluble in acetone, while that of AAM-1 is nearly insoluble. The IEC neutral fractions of the high wax (see next section) asphalts are the least soluble in acetone. IEC neutral fractions of low wax asphalts are over 50 percent soluble in acetone.

The above results show that acetone, $\delta = 9.9$, is near the high polar limit of IEC neutral fractions. The δ values of the IEC neutral fractions may be expected to be somewhat lower than this.

To measure δ values of involatile mixtures, for which ΔE of vaporization cannot be measured, other approaches are necessary. In theory, it is possible to use surface tension measurements in place of ΔE [Burrell 1955], using the formula:

$$\delta = 4.1\left(\frac{\gamma}{v^{1/3}}\right)^{0.43} \qquad (3\text{-}23)$$

where γ = surface tension and v = molecular volume, or molecular weight divided by density. The relationship is based on the fact that two substances are miscible if their interfacial tensions are zero. Obviously, values of γ and v must be divided by some standard state with similar units, because units taken to the 0.43 power are meaningless.

Surface tensions of the eight IEC neutral fractions were measured at 60°C (140°F) using a Du Nuoy ring tensiometer. These results are listed in table 3-23. Densities of the materials also were measured, and are listed in table 3-23. Molecular weights were determined during SHRP. From these data, δ values of the IEC neutral fractions were directly calculated, and these data also are listed in table 3-23. Because they were calculated from equation 3-23, they are reported as dimensionless.

The δ values in table 3-23 are low, ranging from 6.00 to 6.78. If these numbers are valid, then the IEC neutral fractions are markedly non-polar, equivalent to iso-octane. This result is somewhat surprising. However, the molecular weight values of the materials are fairly high, which means that surface tension values are divided by the cube roots of relatively large numbers. The surface tension values of the IEC neutral fractions are not much different from surface tensions of small organic molecules such as n-octane or toluene. Also, it is observed empirically that the IEC neutral fractions easily dissolve in iso-octane. Like dissolves like.

Therefore the IEC neutrals cannot be expected to be very compatible with polar molecules. In order for them to form stable systems with large amounts of polar species, peptizing agents will be required.

The same approach was used to calculate δ values of whole asphalts. Surface tensions and densities were measured at 60°C (140°F). The molecular weight values published in SHRP [1993] were used. These number-average determinations are not considered to be as reliable as the molecular weight values for the IEC neutral fractions. The IEC neutral fractions contain no polar molecules, so number average molecular weight values are not affected by strong molecular interactions, which is not true for the whole asphalts. Nevertheless, there appear to be no alternatives to using the SHRP values of molecular weight for the whole asphalts. The δ values of eight SHRP asphalts, calculated from surface tensions and number-average molecular weights, are listed in table 3-24. These values are somewhat higher than the δ values of the IEC neutral fractions, but still indicate that, at 60°C (140°F), asphalts as a whole are not very polar. Surface tensions of the eight SHRP asphalts are comparable in magnitude to surface tensions reported in Barth [1962] for other asphalts.

Many years ago, it was observed that surface tensions of whole asphalts are not very different from surface tensions of asphalt maltene fractions. This finding indicates that polar molecules are less concentrated in the surface layers of asphalts than they are in the bulk asphalt,

and is more support for the notion that polar molecules, to a large extent, exist in molecular associations.

Another, more indirect, method was used to calculate δ values of whole asphalts. Ewell and Eyring [1937] pointed out that, for many liquids, activation energies of viscous flow (E_a) are related to energies of vaporization by the factor 3.5. The term E_a is a measure of the energy required in a liquid to create a hole large enough to accommodate a unit of flow, which may be an entire small molecule or a segment of a larger molecule. Ewell and Eyring [1937] claim that the fact that ΔE is 3.5 times E_a for many liquids indicates that viscous flow may be considered to be vaporization in one degree of freedom. The values of E_a for eight SHRP asphalts have been determined. They are calculated from measurements of viscosities at 60°C (140°F) and 25°C (77°F). It would perhaps be best to calculate E_a values from viscosity measurements at temperatures that are closer together, but the viscosity determinations available are those made at 25°C (77°F) and 60°C (140°F). The E_a values are a measure of temperature susceptibility of viscosity over the aforementioned temperature range.

To calculate δ from $\Delta E = 3.5\ E_a$ in equation 3-19, number-average molecular weights were not used, because viscosities are measured at 25°C (77°F) as well as 60°C (140°F). Number-average molecular weights were determined at 60°C (140°F) only. Instead, weight average molecular weight values determined by summing individual molecular weights of SEC fractions were used. These values are believed to better approximate effective molecular weights of asphalts at lower temperatures. Solubility parameters at 25°C (77°F) calculated by this method (table 3-25) range from $\delta = 6.2$ to $\delta = 9.3$, a greater range than the values calculated using the surface tension method at 60°C (140°F). The δ values at 25°C (77°F) should be greater than those calculated from measurements made at the higher temperature. One reason for the wider range in δ values using $\Delta E = 3.5\ E_a$ in equation 3-19 is that the molecular weight factor is larger in that calculation. In the calculation using surface tensions, the cube root of molecular weight is used (equation 3-23).

The solubility parameter data reported above indicate that IEC neutral fractions are not very polar. This should not be surprising considering their substantial molecular weights and molecular weight ranges. In Volume II, Additional Test Results, Section A, the SEC fractionation of IEC neutral fractions of SHRP asphalts is reported. For example, the IEC neutral fraction of AAB-1 was separated by SEC into seven subfractions using the same cut points that were used in the SEC fractionation of the original asphalt. The molecular weights of these subfractions range from 340 to 2,760 daltons. The latter value is surprisingly high, considering the nature of the materials. These highest molecular weight materials comprise 5 mass percent of the IEC neutral fraction of AAB-1. Because there are no polar functional groups in IEC neutral fractions, the molecular weight values should be true molecular weights. The higher value reported above corresponds to a molecule having approximately 200 carbon atoms.

Infrared spectra of the IEC neutral subfractions show that there is a regular variation of compound types as well as molecular weights. The higher molecular weight subfractions appear to be predominantly aliphatic or cycloalkanic. The aromatic molecules present in these subfractions are highly substituted, probably multiring condensed aromatic molecules. Long

aliphatic side chains are observed to be present. These side chains may be connected to aromatic or cycloalkanic ring structures. The lower molecular weight SEC subfractions contain relatively more aromatic molecules, with less substitution than the higher molecular weight subfractions. The aromatic molecules in the lower molecular weight subfractions are probably one and two ring compounds. Long aliphatic side chains do not appear to be present in substantial amounts.

Thus, the IEC neutral fractions contain molecules that differ markedly in molecular weight, aromaticity, and other properties. Their ability to solubilize polar molecules should also vary greatly. The smaller aromatic molecules should be good solvents for polar molecules, but they comprise less than 30 mass percent of the IEC neutral fraction of AAB-1. The majority of the IEC neutral fraction comprises compounds that are not likely to be good solvents for polar molecules. Thus the δ values found for whole IEC neutral fractions may not reflect the substantial range in δ values of the various components.

The δ values of whole asphalts are equivalent to n-hexane or n-heptane. Obviously these average values do not accurately predict solubilities in real solvents, because asphalts are only partially soluble in these solvents, yet completely dissolve in toluene. The δ values for whole asphalts do not take into account the broad range of polarities among asphalt components. Nevertheless, the relative average non-polarity must be considered when asphalts are combined with additives such as polymers or antioxidants. The δ values of asphalts vary enough so that interaction with a given additive may be expected to vary among asphalts.

Studies of Waxes in Asphalts

Interest in the effect of native waxes on asphalt properties has increased in recent years. Anecdotal evidence suggests that asphalts that contain paraffin waxes are prone to low temperature cracking. Bahia and Anderson [1992] have shown that there is a relationship between asphalt low temperature properties (e.g., physical hardening) and wax content. Claudy et al. [1992] studied the effect of addition of waxes of known composition on asphalt physical properties. They concluded that waxes could be important factors in determining the tendencies of asphalts to crack in cold environments.

Waxes are a defined chemical compound class that are found in varying amounts in crude oils. Petroleum waxes are predominantly mixtures of n-alkanes ranging from carbon number 18 to above 100. Some alkanes with one methyl side chain may also be included in petroleum waxes. These compounds tend to form crystals in asphalts at low temperatures. During the distillation steps in the refining of petroleum, some alkenes (compounds with a carbon-carbon double bond) are generated, and they become incorporated in petroleum waxes if waxes are isolated as separate products. The higher molecular weight n-alkanes (which are classified as waxes) in a crude will become part of asphalts made from the crude. Usually, waxes comprise only a few mass percent of an asphalt. However, some asphalts are essentially wax-free, and some others contain substantial amounts. One objective of the current study is to determine the effects of defined chemical fractions of asphalts on performance-related physical properties. By doing so, failure modes may be related to specific chemical makeup, and ameliorative measures might be designed. Consequently, waxes have been isolated from unaged and aged asphalts.

Waxes of acceptable purity cannot be readily obtained from whole asphalts. Most wax separation methods involve solvent precipitation at cold temperatures in a single operation. When performed on whole asphalts, application of such a procedure results in asphaltene precipitation along with waxes. Therefore, preliminary separation of non-polar hydrocarbons from polar components is necessary in any scheme to isolate waxes. The initial step may be deasphaltening. However, it is known that high molecular weight paraffins precipitate with asphaltenes and would not be included in waxes isolated in a separation scheme involving deasphaltening. Asphalts also may be combined with an adsorbant and the mixture extracted with a non-polar solvent. The extracts, which do not contain polar molecules, then may be subjected to solvent precipitation. Obviously, waxes are to some extent operationally defined.

In the work reported here, waxes were obtained by solvent precipitation of IEC neutral fractions obtained from Amberlyst® - Amberlite® Resins, as described in Volume II, method 11. This procedure was designed to generate IEC neutral fractions more rapidly and less expensively than the SHRP procedure. It is not recommended for preparing acid, base, and amphoteric fractions. Because of their extreme non-polar nature, it may be assumed that waxes are found almost entirely in IEC neutral or SEC Fraction-II components. The neutral fractions then were dissolved in toluene, and 2-butanone (methyl ethyl ketone) was added to the toluene solution. After chilling, solid waxes were obtained by filtration. Details of the procedure are given in the Experimental Procedures Section of Volume II, method 12. Yields of waxes from each of the SHRP core asphalts are listed in table 3-26.

One simple method for characterizing waxes utilizes IR spectrometry. The IR spectrum of a wax features a prominent peak at 723 cm^{-1}. This peak corresponds to four $-CH_2-$ groups joined in succession in a molecule. Any compound having an unbranched long alkyl chain substituent will have an IR spectrum with a 723 cm^{-1} peak. Waxes, by definition, are long-chain organic compounds. The IR spectrum of waxes isolated from the IEC neutral fraction of AAD-1 is shown in figure 3-13. Also shown in figure 3-13, for purposes of comparison, is the IR spectrum of the parent IEC neutral fraction and that of the dewaxed neutral fraction. The 723 cm^{-1} peak is, at best, a shoulder in the IR spectra of these materials.

It was speculated that quantification of the 723 cm^{-1} peak might provide a simple method for quantification of waxes in asphalts. Accordingly, the model compound hexatriacontane ($C_{36}H_{74}$) was mixed with asphalt AAA-1 at 4 percent, 8 percent, and 10 percent levels. The IR spectrum of each mixture was recorded. Unfortunately, even at the 10 percent level, the enhancement of the 723 cm^{-1} peak by hexatriacontane is marginal. So it is probably not feasible to quantify waxes in asphalts using this IR method.

Inspection of table 3-26 shows that wax contents of the eight SHRP asphalts vary considerably. The entries in table 3-26 are based on amounts of waxes isolated from IEC neutral fractions and corrected for abundances of the neutral fractions in the asphalts. Asphalts AAA-1, AAD-1, and AAG-1 contain only small amounts of waxes (2 percent or less). Four of the asphalts, AAB-1, AAC-1, AAF-1, and AAK-1, contain significant amounts of waxes (3-8 percent). Asphalt AAM-1 appears to be about 25 percent wax!

Waxes obtained from all asphalts except AAM-1 were observed to be hard, brittle solids. They have the properties expected of paraffin waxes. On the other hand, waxes obtained from AAM-1 are gelatinous. They probably are microcrystalline waxes. According to Giavarini and Pochetti [1973], crystalline petroleum waxes range in carbon number from 18 to 40 and are mostly n-paraffins. Due to their crystalline nature, these materials are brittle solids at ambient temperatures. Microcrystalline waxes contain branched alkanes, and range in carbon number from 25 to 65. Alkanes of even higher carbon number may be present in either material.

When asphalts are subjected to oxidative aging, it is not expected that waxes should undergo reaction with oxygen. Normal alkanes do not react with molecular oxygen at ambient temperatures. However, there may be reaction with oxygen in the mix plant. Asphalts were aged using a combined thin film oven (TFO) pressure aging vessel (PAV) procedure (60°C [140°F]; 144 hours). This TFO-PAV combination was chosen because it simulates mix plant conditions, and a relatively mild oxidation regime in pavements. It is not the SHRP PAV oxidation protocol, which is carried out at 100°C (212°F) for 20 hours. The aged asphalts were separated using preparative IEC. The IEC neutral fractions then were dewaxed. Table 3-27 lists yields of IEC neutral fractions and wax yields. The yields of IEC neutral fractions from aged asphalts appear to be significantly lower than yields of the same materials from the parent asphalts. This would be expected, as oxidation causes non-polar compounds to be converted to polar compounds. However, total wax contents of the aged whole asphalts do not appear to differ much from total wax contents of the unaged asphalts, except for AAF-1. Wax yields from the IEC neutral fractions of aged AAF-1 are somewhat lower than from neutral fractions of the parent asphalt (table 3-26). The reason for the loss of waxes in AAF-1 is not evident. It may be an artifact of separation. If waxes are unchanged during oxidative aging, total wax contents of aged asphalts would be the same as the parent materials. During IEC separation, there is no reason to believe that waxes would end up in the three polar fractions. Thus, it is possible that some small amount of the waxes are oxidized during the TFO-PAV treatment of AAF-1. Some of the waxes may be long alkyl chains attached to ring structures and, thus, would have one carbon atom susceptible to oxidation. On the other hand, it is possible that asphalt oxidation involves a highly reactive intermediate that even reacts with n-alkanes. Thus, the course of oxidative age-hardening may, in some asphalts, partly vitiate whatever positive or negative effects waxes have on asphalt physical properties.

To investigate the effect of waxes on rheological properties of asphalts, mixtures of asphalts spiked with waxes were prepared. Each of three asphalts, AAA-1, AAD-1, and AAM-1, was mixed with three different kinds of waxes. The waxes were derived from the same asphalts. Nine mixtures were prepared. Each consisted of 95-96 mass percent of asphalt and 4-5 mass percent added wax. Thus, each spiked sample contains its own naturally occurring waxes plus the added waxes. A solvent was used to mix the materials, and the solvent was removed after mixing. In addition, control samples of each asphalt, solvent treated but with no added wax, also were prepared. Rheological properties of the mixtures then were determined. Some results are listed in table 3-28. When waxes from AAA-1 are added to the parent asphalt, the viscosity of the mixture is the same as that of the control. Waxes from AAD-1 cause an increase in the viscosity of AAA-1. When AAM-1 waxes are added to AAA-1, the viscosity of the mixture is less than that of the control. The effect of waxes on tan δ values of mixtures of AAA-1 is

opposite to the effect on viscosity. AAD-1 waxes enhance elasticity, while AAM-1 waxes diminish elastic properties.

Asphalt AAD-1 reacts differently to added waxes than AAA-1. Both the AAA-1 and AAD-1 waxes cause viscosity increases and tan δ decreases in asphalt AAD-1. Waxes from AAM-1 apparently cause no changes in the properties of AAD-1 at the 5 percent level.

The changes in properties of AAM-1 by added waxes are more dramatic. AAA-1 and, especially, AAD-1 waxes cause viscosity increases in AAM-1. Addition of its own waxes at approximately the 5 percent level results in a mixture one-fourth as viscous as AAM-1! Obviously, the AAA-1 and AAD-1 waxes are different in nature from the AAM-1 waxes. Also, asphalts react somewhat differently to added waxes. Therefore, if waxes are partly lost due to oxidative aging or other processes, responses would not be expected to be the same in all asphalts. Alterations in wax contents over time would have the greatest effect in high wax asphalts. If waxes significantly control low temperature properties or healing tendencies, then the practical importance of the wax component in asphalts is evident.

Waxes and wax-spiked asphalts were prepared for study for several other researchers.

Asphaltene-Maltene Crossblends

The separation of asphalts into maltenes and asphaltenes by solvent precipitation is rapid compared with SEC or IEC methods, but does not yield such distinctive fractions. Nevertheless, asphalts have been modeled as dispersions of asphaltenes in maltene for many years. Whether or not the model corresponds to reality has been debated for the same length of time. Storm et al. [1995b] provide direct evidence for the existence of polar, aromatic entities in distillation residua of petroleum. These researchers believe that the distinctive entities correspond to asphaltenes in part.

During a review of the program, interest was expressed in attempting to measure the influence of both the asphalt dispersed and solvent components on various physical properties and on the changes in these properties observed after oxidative aging. Asphalt AAD-1 has good fatigue properties, but is susceptible to oxidative age hardening. Asphalt AAF-1 has poor fatigue properties and also undergoes oxidative age hardening. Asphalt AAG-1 is susceptible to permanent deformation but not oxidative age hardening. It should be noted that age hardening does not measure oxidation per se, but the response of viscosity to oxidation. All three asphalts oxidize extensively in service, but the effect on the viscosity of AAG-1 is small compared with the effect on the other two. Oxidative age hardening is measured by the Aging Index (AI), which is the ratio of the dynamic viscosity of the aged asphalt to that of the parent, both measurements performed at 60°C (140°F) and 1.0 rad/s.

To determine the influence of maltenes and asphaltenes on fatigue and its response to aging, crossblended mixtures of the maltenes and asphaltenes of the three asphalts were prepared. For each pair of asphalts, eight crossblends were prepared. The reason for choosing eight crossblends is that three variables are being studied. These variables are the nature of the

asphaltenes, the nature of the maltenes, and the proportions of the two components in each crossblended mixture. The proportions chosen were the two natural abundances of asphaltenes and maltenes in each asphalt.

For example, consider the eight unaged crossblended mixtures of AAD-1 and AAF-1. Some rheological properties of these mixtures are listed in tables 3-29 and 3-30. The natural abundance ratio for AAD-1 is 21.1 percent asphaltenes and 79.9 percent maltenes. For AAF-1, the ratio is 14.2 percent asphaltenes and 85.8 percent maltenes. Two of the crossblended mixtures, designated I and V, reconstitute the parent asphalts. These two mixtures serve as controls. Four of the mixtures (I-IV) contain AAF-1 maltenes. Each of the four mixtures contains either AAF-1 or AAD-1 asphaltenes at one of the two levels, 14.2 percent or 21.1 percent. Similarly, mixtures V through VIII contain AAD-1 maltenes mixed with the two asphaltenes at the two levels. Rheological properties of the crossblends were determined, and the mixtures were oxidatively aged according to the SHRP protocol: TFO aging followed by PAV at 100°C (212°F) for 20 hours. Some rheological properties of the aged crossblends were then measured (table 3-31). Two more sets of eight crossblends also were prepared. One set consisted of combinations of asphaltenes and maltenes of AAD-1 and AAG-1, and the other consisted of asphaltenes and maltenes of AAF-1 and AAG-1. Their rheological properties were measured, and then the crossblended mixtures were oxidatively aged as above. Due to the aging of the crossblends, gains in properties that decrease permanent deformation were expected. Two questions of interest were: How much loss of properties that decrease fatigue performance would also occur during aging? and Which combinations of materials in which amounts would behave most favorably in the tradeoff between fatigue and permanent deformation? The hypothesis guiding the work is that the chemical driving factors involved in fatigue and permanent deformation (and changes brought about by aging) are not uniformly distributed throughout an asphalt, but tend to be concentrated in either the maltene or the asphaltene fractions. Additionally, these chemical driving factors will be influenced by the manner in which a given maltene interacts with a given asphaltene. Thus, it may be possible to adjust physical properties by proper selection and blending of maltene and asphaltene fractions. Because the maltene-asphaltene separation is a simple one, it may be possible to more specifically isolate chemical driving factors if significant effects are observed in these crossblends.

Table 3-29 lists rheological properties of eight crossblends of maltenes and asphaltenes of asphalts AAD-1 and AAF-1. Viscosities at 1.0 rad/s and two temperatures, tan δ values at 25°C (77°F), and reduced specific viscosities (η_{red}), also are listed in table 3-29 for the eight mixtures of asphaltenes and maltenes from AAD-1 and AAF-1. The reduced specific viscosity values are a measure of the compatibility (compatibility reflects the relative size and amount of the associated species, and the effectiveness by which they are solvated) of a mixture, a high value indicating less compatibility compared with a low value. Reduced specific viscosities were calculated by dividing absolute viscosities of the mixtures by the viscosities of the appropriate maltene fractions (each measurement being performed at the same temperature) to obtain relative viscosities (η_{rel}). Specific viscosities (η_{sp}) were calculated by subtracting unity from each η_{rel} value. The η_{red} values were obtained by dividing η_{sp} by the concentration of asphaltenes in each mixture, 0.211 in four mixtures, and 0.142 in the other four. Tan δ values also are indicators of compatibility. A large tan δ value indicates that a mixture is less compatible, and vice versa.

The η_{red} values indicate that mixture V, table 3-29, which is reconstituted AAD-1, is much less compatible than mixture I, reconstituted AAF-1. Tan δ and η_{red} values for mixtures containing 21.1 mass percent asphaltenes are much higher than corresponding values for mixtures containing 14.2 percent asphaltenes, as would be expected. The η_{red} values for most, but not all, mixtures are much lower at 60°C (140°F) than at 25°C (77°F).

Rheological data for the eight mixtures at 10.0 rad/s are listed in table 3-30. These data are included so that the mixtures may be evaluated according to the Superpave® binder specifications. These specifications stipulate a maximum G* sin δ value of 5,000,000 Pa at 10 rad/s and a minimum value of G*/sin δ of 2,200 Pa at 10 rad/s. At 25°C (77°F), mixtures II and IV (table 3-30) exceed the maximum permissible value of G* sin δ. AT 60°C (140°F) mixtures VI, VII, and VIII fall below the minimum value of G*/sin δ.

Data in table 3-29 also illustrate the relative effect of the nature of the asphaltenes and maltenes (and their relative proportions) on the viscosities of the mixtures. For example, comparison of the data for mixture I with mixture III, mixture II with mixture IV, mixture V with mixture VII, and mixture VI with mixture VIII shows that the viscosities of the mixtures are not greatly sensitive to the source of the asphaltenes. In each of these pairs of mixtures, the source of the maltenes and the relative abundance of the two fractions are the same. Mixtures I and III contain 85.8 mass percent maltenes of AAF-1. Mixtures II and IV contain 78.9 mass percent maltenes of AAF-1. Mixtures V and VII contain 78.9 mass percent maltenes of AAD-1, and mixtures VI and VIII contain 85.8 mass percent of maltenes of AAD-1. Within each of these pairs, only the source of asphaltenes varies. In all the above paired mixtures, the crossblended mixture containing AAF-1 asphaltenes is relatively more viscous at 25°C (77°F), but not greatly so. At 60°C (140°F), the trend is reversed. Reduced specific viscosities of these pairs of crossblends also show that at 25°C (77°F), for pairs of mixtures containing the same maltene component at the same abundance level, those mixtures containing AAF-1 asphaltenes are less compatible (η_{red} is larger) than those mixtures made up of AAD-1 asphaltenes. At this lower temperature, AAF-1 asphaltenes are not as readily solubilized by either of the maltenes as are AAD-1 asphaltenes. At 60°C (140°F), the trend appears to have reversed.

Relative amounts of maltenes and asphaltenes greatly influence viscosities of the mixtures, as would be expected. To illustrate this point, mixture I is compared with mixture IV, mixture II with mixture III, mixture V with mixture VIII, and mixture VI with mixture VII. In each of these pairs of mixtures, that with the greatest asphaltene content is much more viscous and has the larger η_{red} value.

The source of the maltenes has a substantial influence on the viscosities of the crossblended mixtures. This is necessarily true because the viscosity of AAF-1 maltenes is so much greater than the viscosity of AAD-1 maltenes (see note 2, table 3-29). The effect can be observed by comparing mixture I with mixture VI, mixture II with mixture V, mixture III with mixture VIII, and mixture IV with mixture VII. However, within these pairs, η_{red} values at 25°C (77°F) are not so greatly different. Nevertheless, within each pair, the mixture containing AAD-1 maltenes has a higher η_{red} value than corresponding mixtures containing maltenes of AAF-1. It may be concluded from these data that at 25°C (77°F), AAF-1 maltenes are the better

solvent compared with AAD-1 maltenes. At 60°C (140°F), the situation appears to be reversed. Thus warming AAD-1 maltenes improves their solvent properties compared with maltenes of AAF-1. In summary, properties of the crossblends of maltenes and asphaltenes of AAD-1 and AAF-1 are mostly influenced by the relative amounts of the two components. The influence of the sources of the two components are also important, and can be best determined by comparing η_{red} values. The influence of sources are temperature dependent. The data above indicate that at 25°C (77°F), maltenes of AAF-1 are superior as solvent to maltenes of AAD-1, and asphaltenes of AAD-1 are more readily dissolved than asphaltenes of AAF-1. Thus it would be predicted that at 25°C (77°F), the mixtures containing maltenes of AAF-1 and asphaltenes of AAD-1 (II and III) would have significantly lower η_{red} values than mixtures containing maltenes of AAD-1 and asphaltenes of AAF-1 (VI and VII). Among these two pairs, mixture II should be compared with mixture VII, and mixture III with mixture VI, because of different relative proportions of asphaltenes and maltenes in the crossblended mixtures. Inspection of table 3-29 shows that the prediction is confirmed. It would also be predicted that the situation is reversed at 60°C (140°F), as is also observed.

The eight mixtures were oxidatively aged using SHRP protocol. Viscosities of the aged mixtures at 25°C (77°F) and 60°C (140°F) and 1.0 rad/s are listed in table 3-31. AI's were calculated by dividing the 1.0 rad/s viscosities of the aged materials measured at 60°C (140°F) by viscosities of the parent, unaged materials measured under the same conditions. Both asphalts AAD-1 and AAF-1 are known to be susceptible to oxidative aging, so that it would be expected that combinations of their maltenes and asphaltenes also would readily undergo oxidative aging. The AI values for these mixtures range from 5.9 to 22.6. The AI values of mixtures I and V (table 3-31) (corresponding to parent asphalts AAF-1 and AAD-1) are 10.1 and 12.9, comparing reasonably well with other work in which the parent asphalts were oxidatively aged. Combinations of AAF-1 maltenes and AAD-1 asphaltenes (mixtures II and III) appear to be unusually susceptible to oxidative aging. Mixture VI, consisting of AAD-1 maltenes (85.8 percent) and AAF-1 asphaltenes (14.2 percent) does not oxidatively age to nearly the extent of the other mixtures. The AI values of the crossblended mixtures are almost entirely out of the limits set by AI values representing the two parent asphalts (I and V; AI = 10.1 and 12.9, respectively). It is known that asphalt component compatibility influences susceptibility to oxidation, and, therefore, the aging index. This phenomenon will be discussed at length in chapter 4. It was stated previously that at high temperatures, combinations of AAD-1 maltenes and AAF-1 asphaltenes are particularly compatible (but not at lower temperatures) and would be less susceptible to effects of oxidation than combinations of AAF-1 maltenes and AAD-1 asphaltenes. This is observed to be so.

Rheological properties at 10.0 rad/s of the aged mixtures are listed in table 3-32. The G* sin δ values at 25°C (77°F) and 10.0 rad/s relate to fatigue properties. The G*/sin δ values at 60°C (140°F) and 10.0 rad/s are a measure of resistance to permanent deformation. In figure 3-14, G* sin δ values are plotted against G*/sin δ values for all aged and unaged crossblends of AAD-1 and AAF-1. The data are plotted on logarithmic coordinates. For a given crossblend, relatively large G*/sin δ values at 60°C (140°F) compared with G* sin δ values at 25°C (77°F) are most desirable. Such an asphalt would have good rutting resistance, but not be too susceptible to cracking. Upon oxidative aging, both G*/sin δ and G*sin δ values increase, but it

is desirable for the former to increase relative to the latter. That is to say, there should not be too much of an increase in cracking propensities to compensate for increased rutting resistance.

In figure 3-14, oxidation of crossblends VI and VIII results in aged materials that seem to follow the general trend of the plot. Oxidation of V produces a material that is above the general trend of the plot (the line drawn in figure 3-14), which is desirable (larger increase in G*/sin δ compared with G*sin δ). Oxidation of VII produces a material that follows the general trend. Before oxidative aging, mixtures I through IV are represented in figure 3-14 by points well below and to the right of the general trend of the plot. This is not desirable. Oxidative aging of these crossblends results in mixtures that are definitely improved in G*/sin δ relative to changes in G* sin δ. Thus, the process of oxidative aging of the AAD-1/AAF-1 crossblends appears to be either neutral or beneficial based on the above considerations.

Dynamic moduli (G*) values for the unaged and aged crossblended mixtures at 25°C (77°F) and 10.0 rad/s are plotted vs. phase angles (Black plots) in figure 3-15. The 60°C (140°F) G* values are plotted versus phase angles in figure 3-16. In figure 3-15, two sets of points are observed. One set corresponds to those mixtures composed of AAD-1 maltenes and the other set to those mixtures composed of AAF-1 maltenes. The points corresponding to mixtures composed of AAD-1 maltenes are those with the smallest G* and largest δ values. A line with a relatively steep slope is drawn to approximate a trend for these points. The points corresponding to mixtures composed of AAF-1 maltenes have the highest G* values and lowest δ values. A line with a somewhat less steep slope is drawn to approximate a trend for these points. For the mixtures containing AAD-1 maltenes, oxidation results in somewhat greater increases in log G* for a given loss in phase angle compared with the mixtures containing AAF-1 maltenes. For the mixtures with AAF-1 maltenes, losses in phase angle upon oxidation seem to be accompanied by relatively smaller increases in log G*. Although these differences are not great, it appears that at 25°C (77°F), the source of the maltenes (and of course their relative abundance) appears to strongly influence rheological properties of the crossblends. Otherwise, the points would not all lie near one of two lines of different slopes. At 60°C (140°F) (figure 3-16) there is not such strong differentiation of slopes of lines on which the data points are plotted, suggesting that at 60°C (140°F) asphaltene molecular associations may be partially broken up and are dissolving in the maltenes, changing the properties of the latter and altering the size and nature of the asphaltene associations.

Next, properties of crossblended mixtures of asphaltenes and maltenes of asphalts AAD-1 and AAG-1 will be described. Asphalts AAG-1 and AAD-1 differ in a number of ways. Asphalt AAG-1 is susceptible to permanent deformation, but is less susceptible to oxidative age-hardening. Asphalt AAG-1 contains only a small amount of asphaltenes (6.0 mass percent). Asphalt AAD-1 contains large amounts of asphaltenes (21.0 percent) and is highly susceptible to oxidative age-hardening. Table 3-33 lists the composition and some rheological properties of eight crossblended mixtures of these two asphalts. In this set of crossblends, mixture I reconstitutes AAD-1, and VII reconstitutes AAG-1. Some of the mixtures (II and IV) obviously are not realistic asphalts because they are nearly fluid at 60°C (140°F). The values of η_{red} are, in general, lower than the AAD-1/AAF-1 mixtures. Table 3-34 lists rheological properties of the

mixtures at 10.0 rad/s and two temperatures. The G* sin δ values at 25°C (77°F) range over several orders of magnitude as do the G*/sin δ values at 60°C (140°F).

Table 3-35 lists some rheological properties of the aged AAD-1/AAG-1 mixtures. Of particular interest are the 60°C (140°F) AI values. These values range from 3.7 to 15.9. The value for reconstituted AAD-1 (mixture I) is 15.4 and that for reconstituted AAG-1 (mixture VII) is 4.2. The AI values of all the mixtures essentially fall within the range of values established by the two parent asphalts AAD-1 and AAG-1. The principal factor in determining AI values appears to be asphaltene content. This is because increasing the asphaltene content relative to a given maltene component increases the size and amount of strongly associating species, reducing the compatibility of the system and increasing the sensitivity of the asphalt properties to changes on oxidation. Thus compatibility, and therefore η_{red} of an unaged asphalt, should be predictive of susceptibility to effects of oxidative age hardening, as measured by AI of aged asphalts. The AI values of the aged crossblends correspond somewhat with η_{red} at 60°C (140°F) in table 3-33. Unaged crossblends with η_{red} values $\geq$ 200 yield materials with AI values $\geq$ 9.0 after oxidation. The unaged crossblends characterized by η_{red} values from 17 to 47 yield materials having AI values of 3.7 to 5.3 after oxidation.

Table 3-36 lists rheological properties of the aged mixtures at 10.0 rad/s and two temperatures. The G* sin δ values at 25°C (77°F) and G*/sin δ values at 60°C (140°F) in this table are plotted in figure 3-17. Those mixtures having small (6.0 percent) amounts of asphaltenes do not experience greatly increased resistance to permanent deformation upon oxidation, because the oxidation products formed are better solubilized by the maltenes. The points in figure 3-17 lie more or less on a line with the same slope as the points in figure 3-14.

Dynamic modulus (G*) and phase angle (δ) data obtained at 10.0 rad/s listed in tables 3-34 and 3-36 are plotted in figures 3-18 and 3-19. In figure 3-18, for the 25°C (77°F) data, the points corresponding to mixtures (aged or unaged) containing AAG-1 maltenes have higher G* values and lie on or near one line. The points corresponding to mixtures containing AAD-1 maltenes have lower G* values and lie on another line having a slightly steeper slope. The slope of this line is nearly identical to that in figure 3-15, in which data for mixtures of AAD-1 maltenes with AAD-1 and AAF-1 asphaltenes are plotted. Again, solubility properties of the maltenes appear to determine certain rheological behaviors at 25°C (77°F). In figure 3-19, in which rheological data (G* and δ) at 60°C (140°F) and 10.0 rad/s are plotted, the data points do not lie on two distinct lines, indicating that asphaltenes may be exerting an influence on the systems, probably by partial dissolution.

The third set of crossblended mixtures studied are combinations of maltenes and asphaltenes of AAF-1 and AAG-1. These asphalts have fewer asphaltenes than AAD-1. Asphalt AAF-1 has poor fatigue-related properties and is more susceptible to oxidative age-hardening. AAG-1 is susceptible to permanent deformation, and does not undergo extensive oxidative age-hardening under SHRP protocol conditions. Table 3-37 lists some rheological properties of these mixtures. In table 3-37, mixture I reconstitutes asphalt AAG-1, and mixture V reconstitutes AAF-1. The η_{red} values of the eight mixtures have the smallest range of the three sets of crossblended mixtures. Table 3-38 lists rheological data for the samples at 10.0 rad/s at two

temperatures. The crossblended mixtures were aged according to the SHRP protocol and rheological measurements again were performed. Aging indices are listed in table 3-39. The values are low, and all values lie between those for the reconstituted parent asphalts, mixtures I and V. It is noteworthy that although some of the aged crossblends have much higher viscosities than the aged parent asphalts (compare mixtures I and V with mixture IV in table 3-39), the aging indices of the crossblends are not greatly different from those of the reconstituted parent asphalts. Again, it is suggested that solubility properties of maltenes control component compatibilities and thus the aging tendencies of the mixtures. In the example cited above, increasing asphaltene content in AAG-1 above natural abundance level (mixture IV) resulted in a highly viscous mixture, but good solubility properties of AAG-1 maltenes enable solubilization of additional viscosity building oxidation products formed. This is consistent with reduced specific viscosity data obtained during SHRP, which showed that AAG-1 maltenes could effectively solubilize up to 2.5 times the natural abundance of AAG-1 asphaltenes.

Rheological data for the aged samples at 10.0 rad/s at two temperatures are listed in table 3-40. Values for G* sin δ at 25°C (77°F) and G*/sin δ at 60°C (140°F) in this table and table 3-38 are plotted in figure 3-20. The points in this graph trace a line whose slope is almost the same as the slopes in the lines in figures 3-14 and 3-17.

In figures 3-21 and 3-22, Black plots of G* values at 10.0 rad/s are plotted versus phase angles for each of the aged and unaged AAG-1/AAF-1 mixtures. As is the case for the other two sets of crossblended mixtures described earlier, points corresponding to mixtures containing the same maltene fraction appear to lie on different lines, regardless of the type of asphaltenes with which they are combined or the extent of oxidation. However, the two lines have similar slopes. This trend even extends to 60°C (140°F) for the AAF-1/AAG-1 mixtures (figure 3-22), unlike the other two mixtures. There may be minimal asphaltene dissolution in these mixtures.

The process of oxidative aging is accompanied by increased asphaltene content, so the above results should not be too surprising. These data suggest that oxidative behavior of asphalts measured by rheology at 25°C (77°F) may be simulated by preparing various (at least three) maltene-asphaltene mixtures of different compositions and then measuring their rheological properties. These measurements should establish the slope of the line of the G* value versus phase angle plot, and may be extrapolated. The slope of the line appears to be a function of the particular maltene fraction chosen, from which the speculation arises that the nature of maltene fraction in an asphalt greatly influences physical changes in asphalts resulting from oxidation.

The variation in slopes of the lines in the G* versus phase angle plots suggests that if G* measures stiffness and phase angle elasticity, some maltene fractions induce more gains in elastic properties with less increase in stiffness than others. This observation may prove to be of value in blending asphalts.

Supercritical Fluid Extractions

As part of this program, SFE using carbon dioxide and various modifiers was used in attempts to quantitatively extract binders from asphalt-aggregate mixtures. The objective of this

particular study was to find a replacement for the chlorinated solvents that historically have been used to extract binders from pavement cores. Supercritical carbon dioxide was able to extract only the least polar organic constituents from asphalt-aggregate mixtures, so it did not fulfill the requirements originally hoped for [Barbour et al. 1997]. However, the method is useful for the rapid isolation of non-polar materials from asphalts in amounts sufficient for physical property studies. The nature of the materials extracted are a function of temperature, pressure, and added modifier. Thus the solvent properties may be "fine tuned." The SFE extracts of asphalts were subjected to MDSC analysis, which will be discussed in a subsequent section, so a description of how they were obtained is appropriate at this point.

Asphalt-aggregate mixtures (6 mass percent asphalt-94 mass percent aggregate) were prepared from each of the SHRP core asphalts and SHRP aggregate RJ by heating both components to 150°C (302°F) for 20 minutes. The mixtures were stirred while cooling and then were placed in a 50-mL extraction vessel. Each sample was extracted sequentially using five increasingly more severe extraction conditions: (1) 200 atm (20.3 MPa) CO_2; (2) 300 atm (30.45 MPa) CO_2; (3) 400 atm (40.6 MPa) CO_2; (4) 500 atm (50.75 MPa) CO_2; and (5) 500 atm (50.75 MPa) CO_2 modified with 20 volume percent tetrahydrofuran (THF). All extractions were performed at 115°C (239°F). Portions of the asphalts not extracted by SFC were removed from the aggregate using dichloromethane.

Coating of asphalts on an aggregate support was essential for efficient extraction in the extractor. Comparison of the percent extracted data for each of the asphalts indicates that CO_2 combined with THF (THF modified conditions) always extracted the largest fraction of asphalt in any of the supercritical CO_2 extraction experiments. These data are depicted as a stacked bar graph in figure 3-23. The amount of material obtained by extraction with 400 atm (40.6 MPa) CO_2 appeared to be nearly constant for all of the asphalts except AAM-1. In figure 3-23, it is the increment from the top of the 300 atm increment to the bottom of the 500 atm increment that is nearly the same for seven of the SHRP core asphalts. The other fractions vary considerably from one asphalt to another. Another interesting observation is that the summation of all of the supercritical CO_2 extracted fractions for each asphalt (top of the 500 atm increment in figure 3-23; THF modified extracts not included) is approximately the same for most of the asphalts. Again, asphalt AAM-1 appears to stand out compared with the other asphalts.

There is a general increase in molecular weight in the SFE fractions as the severity of the extracting conditions increases. Evaluation of the fractions by SFC indicated that the 200 atm extracted fractions generally contained molecular species having an average of about 30 carbon atoms, while the last fraction (500 atm with THF) contained molecules having an average of about 70 carbon atoms. Determination of carbon numbers of asphalt fractions by SFC was discussed by Barbour and Branthaver [1992]. The molecular species in the remaining fractions generally increase in carbon number by approximately 10 carbons per fraction according to the severity of extraction. That is, if the average carbon number of the 200 atm (20.3 MPa) fraction is 30, that of the 300 atm (30.45 MPa) fraction will be approximately 40, and so on. Analysis of the fractions by Iatroscan [Bharati et al. 1994] to determine saturate, aromatic, polar aromatic, and asphaltene distribution indicated that the fractions extracted at 200, 300, and 400 atm (20.3, 30.45, and 40.6 MPa) contained mainly saturate and aromatic material. The more polar material

(polar aromatics and asphaltenes) was generally distributed between the 500 and 500 modified with THF fractions. Elemental analyses on the SFE fractions suggest that few of the heteroatoms (N, O, S) are present in the first four fractions extracted with CO_2 only. Figure 3-24 depicts the heteroatom distribution for the fractions from asphalt AAA-1, which is typical for the asphalts analyzed. The Sol-ext entry refers to the materials remaining on the aggregate after THF modified SFC treatment.

Attempts were made to correlate the amount of material extracted by supercritical CO_2 with chemical and/or physical properties of the asphalts. Trying to correlate the total amount of asphalt extracted by supercritical CO_2 with asphalt elemental analyses or number-average molecular weights resulted in R^2 values of nearly 0.5. However, the total amounts of 300 atm (30.45 MPa) fractions produced linear correlations with R^2's between 0.90 and 0.99 with different combinations of elemental analyses and molecular weight. Combinations of carbon and hydrogen elemental analyses produced a correlation coefficient of 0.90. Combining the molecular weight with the carbon and hydrogen values produced an R^2 of 0.94. However, the only positive contribution is from hydrogen. This correlation indicates that those materials being extracted by CO_2 at 300 atm (30.45 MPa) are mostly aliphatic and naphthenic hydrocarbons of moderate carbon number. These kinds of molecules are characterized by relatively high hydrogen to carbon atomic ratios, so that the correlation is positive with hydrogen and negative with carbon. Because the correlation with molecular weight is negative, carbon numbers of the extracts must not be high.

Correlating the 300 atm (30.45 MPa) fraction data with the heteroatom content of the asphalts resulted in a correlation coefficient of 0.99, and the contribution from each of the elements is positive. A summation of the percentage extracted for the 200, 300, and 400 atm fractions has about the same correlation with the heteroatoms as the 300 fraction by itself. The observed percentage extracted correlates well with the calculated percentage extracted, based on equation 3-24.

$$\text{Calculated percentage extracted} = 5.96\,(\%\ \text{Nitrogen}) + 12.22\,(\%\ \text{Oxygen}) + 4.09\,(\%\ \text{Sulfur}) - 7.5 \qquad (3\text{-}24)$$

This correlation is depicted in figure 3-25 and has an R^2 of 0.95. The coefficients for nitrogen, oxygen, and sulfur all have positive contributions similar to that seen for the 300 atm fraction. The fact that all of the coefficients are positive is interesting in that the extracted fractions are non-polar in nature and one would not expect that there would be large amounts of polar, heteroatom-containing molecules associated with these materials. Some heteroatom-containing molecules, such as thiophenes, sulfides, and carbazoles are non-polar and would probably be present in some of the fractions. The correlation indicates that as the heteroatom content of the asphalt increases, the low molecular weight neutral, non-polar material also increases. This would suggest that in order to meet specifications an asphalt with higher heteroatom content would probably have to have more of the lower molecular weight neutral material to counteract the effects of the heteroatom containing materials.

Table 3-7. Preparative SEC separation of SEC Fraction-I of SHRP asphalts, 4.0 g/160 mL.

Asphalt	Number of runs	Avg. yield of subfraction, mass %			
		I-1	I-2	I-3	I-4
AAA-1	9	25.4 ± 2.01	50.5 ± 1.96	18.2 ± 2.43	6.1 ± 1.47
AAB-1	8	26.5 ± 2.15	50.1 ± 2.05	16.4 ± 1.13	6.7 ± 0.83
AAC-1	3	34.2 ± 4.11	46.2 ± 4.75	13.0 ± 0.78	6.7 ± 0.78
AAD-1	25	23.5 ± 2.47	47.4 ± 2.29	22.2 ± 3.26	6.6 ± 1.55
AAF-1	3	27.3 ± 3.44	50.8 ± 3.44	15.3 ± 0.63	7.4 ± 0.73
AAG-1	3	36.3 ± 2.03	44.2 ± 3.16	11.0 ± 0.94	8.1 ± 0.33
AAK-1	5	23.9 ± 3.11	47.8 ± 1.45	21.4 ± 2.87	6.8 ± 1.35
AAM-1	3	14.2 ± 1.28	36.9 ± 2.11	36.9 ± 1.97	12.2 ± 1.18

Table 3-8. Elemental [1] composition of SEC Fraction-I subfractions.

Asphalt and SEC Fraction-I subfraction		Element, mass %				Total, mass %	H/C [2]
		C	H	N	S		
AAA-1	I-1	81.3	8.2	1.1	8.7	99.3	1.20
	I-2	81.5	8.4	1.3	8.4	99.6	1.23
	I-3	81.1	9.1	1.0	8.1	99.3	1.34
	I-4	81.4	9.3	0.9	-	-	1.36
AAB-1	I-1	83.4	7.6	1.3	5.8	98.1	1.09
	I-2	81.6	7.9	1.5	5.8	96.8	1.15
	I-3	85.3	9.0	1.3	5.4	101.0	1.26
	I-4	83.2	9.2	1.2	4.9	98.4	1.31
AAC-1	I-1	84.9, 86.4	7.7, 7.6	1.4, 1.4	3.6	97.6	1.08, 1.05
	I-2	81.9	8.1	1.6	3.3	94.9	1.18
	I-3	89.3	9.9	1.2	2.7	103.1	1.38
	I-4	85.4	9.8	1.3	-	-	1.36
AAD-1	I-1	79.9	8.4	1.8	8.8	98.7	1.26
	I-2	79.8	8.5	1.9	8.5	98.7	1.27
	I-3	80.5	8.9	1.8	8.7	99.9	1.32
	I-4	79.8	9.3	1.6	-	-	1.39
AAF-1	I-1	81.3	7.5	1.0	6.6, 6.7	96.4,	1.10
	I-2	83.9	8.0	1.2	6.0	96.5	1.14
	I-3	84.2	9.2	1.0	4.9	99.1	1.30
	I-4	83.3	8.9	1.1	-	99.4	1.27
						-	
AAG-1	I-1	83.4	8.6	1.8	1.2	95.0	1.23
	I-2	82.8	8.8	2.0	1.4	94.6	1.27
	I-3	84.2	9.6	1.9	1.4	97.1	1.36
	I-4	83.3	9.5	2.0	-	-	1.36
AAK-1	I-1	81.3	8.2	1.7	7.4	98.6	1.20
	I-2	81.4	8.3	2.0	7.4	99.1	1.21
	I-3	81.6	8.8	1.7	7.2	99.3	1.29
	I-4	81.2	9.1	1.6	6.8	98.7	1.34
AAM-1	I-1	86.9	9.7	0.7	1.4	98.7	1.33
	I-2	87.0	10.3	1.0	1.2	99.5	1.41
	I-3	85.5	11.4	0.8	1.0	99.6	1.59
	I-4	86.1	11.5	1.0	1.0	98.7	1.59

[1] Analyses for elements were performed using standard methods. Based on experience with a large number of fossil fuel samples, standard deviations are: carbon, 0.36; hydrogen, 0.20; nitrogen, 0.09; sulfur, 0.36.

[2] Lower values of H/C correspond to higher aromaticities, and vice versa.

Table 3-9. Relative amounts of aliphatic and aromatic carbon atoms in SEC Fraction-I subfractions of SHRP core asphalts by ^{13}C NMR.

Asphalt	Subfraction	% aliphatic carbon [1]	% aromatic carbon [1]
AAA-1	I-1	62.0	38.0
	I-2	61.0	39.0
	I-3	66.8	33.2
AAB-1	I-1	50.8; 51.8	49.2; 48.2
	I-1	50.8	49.2
	I-2	56.0	44.0
	I-2	52.5	47.5
	I-3	63.2	36.8
AAC-1	I-1	50.3	49.7
	I-1	47.6	52.4
	I-2	51.5	48.5
	I-3	62.9	37.1
AAD-1	I-1	65.9	34.1
	I-1	65.2	34.8
	I-2	65.4	34.6
	I-3	70.0	30.0
AAF-1	I-2	51.1	48.9
	I-2	53.5	46.5
	I-3	64.4	35.6
AAG-1	I-1	61.1	38.9
	I-2	64.4	35.6
	I-3	66.8	33.2
AAK-1	I-1	61.0	39.0
	I-2	59.3	40.7
	I-3	66.1	33.9

[1] Replicate measurements were performed on subfraction I-1 of AAB-1 only. Based on experience with a large number of fossil fuel samples, replicate determinations of aliphatic and aromatic carbon by NMR have standard deviations of 2.0.

Table 3-10. Molecular weights of SEC Fraction-I-1 subfractions by membrane osmometry.[1]

Asphalt	Run no.	Molecular weight, daltons	Mean ($\bar{x}$) and standard deviation (σ)
AAA-1	1 2 3	33,000 33,000 30,000	$\bar{x}$ = 32,000 σ = 1,414
AAB-1	1 2 3	35,000 36,000 30,000	$\bar{x}$ = 33,667 σ = 2,625
AAC-1	1 2 3	34,000 35,000 29,000	$\bar{x}$ = 32,667 σ = 2,625
AAD-1	1 2 3 4 5 6	40,000 42,000 36,000 41,000 40,000 36,000	$\bar{x}$ = 39,167 σ = 2,339
AAF-1	1 2 3	31,000 31,000 27,000	$\bar{x}$ = 29,667 σ = 1,886
AAG-1	1 2 3	26,000 27,000 23,000	$\bar{x}$ = 25,333 σ = 1,700
AAK-1	1 2 3	42,000 41,000 34,000	$\bar{x}$ = 39,000 σ = 3,560
AAM-1	1 2 3	18,000 18,000 15,000	$\bar{x}$ = 17,000 σ = 1,414

[1] Values are single readings with baseline corrections.

Table 3-11. Molecular weights of SEC Fraction-I-2 subfractions by membrane osmometry and vapor phase osmometry, both at 39°C.

Parent asphalt of subfraction	Run no.	Molecular weight, daltons	
		Membrane osmometry [1]	Vapor phase osmometry
AAA-1	1	21,000	12,000
	2	21,000	15,000
	3		13,000
	4		16,000
	5		16,000
	6		14,000
			$\bar{x}$ 14,333
			σ 1,491
AAB-1	1	22,000	16,000
	2	21,000	15,000
	3	23,000	13,000
		$\bar{x}$ 22,000	$\bar{x}$ 14,667
		σ 816	σ 1,247
AAC-1	1	20,000	11,000
	2		14,000
	3		10,000
			$\bar{x}$ 11,667
			σ 1,700
AAD-1	1	26,000	16,000
	2		18,000
	3		19,000
			$\bar{x}$ 17,667
			σ 1,247
AAF-1	1	19,000	14,000
	2		21,000
	3		17,000
			$\bar{x}$ 17,333
			σ 2,867
AAG-1	1	17,000	15,000
	2		18,000
	3		14,000
			$\bar{x}$ 15,667
			σ 1,700
AAK-1	1		20,000
	2		18,000
	3		15,000
			$\bar{x}$ 17,667
			σ 2,035

Table 3-11. Molecular weights of SEC Fraction-I-2 subfractions by membrane osmometry and vapor phase osmometry, both at 39°C (continued).

Parent asphalt of subfraction	Run no.	Molecular weight, daltons	
		Membrane osmometry [1]	Vapor phase osmometry
AAM-1	1	12,000	6,300
	2		6,000
	3		5,600
			$\bar{x}$ 5,967
			σ 287

[1] Values are single readings with baseline corrections.

Table 3-12. Molecular weights by vapor phase osmometry at 39°C of SEC Fraction-I-3 and I-4 subfractions of eight asphalts.

Asphalt	Subfraction	Run no.	Molecular weight, daltons
AAA-1	I-3	1	5,500
		2	5,300
		3	4,900
		$\bar{x}$	5,233
		σ	249
	I-4	1	3,200
		2	2,800
		3	2,600
		$\bar{x}$	2,867
		σ	249
AAB-1	I-3	1	4,700
		2	4,700
		3	3,900
		$\bar{x}$	4,433
		σ	377
	I-4	1	2,700
		2	2,300
		3	2,200
		$\bar{x}$	2,400
		σ	216
AAC-1	I-4	1	2,800
		2	2,500
		3	2,300
		$\bar{x}$	2,533
		σ	205
AAD-1	I-3	1	8,200
		2	8,400
		3	7,200
		$\bar{x}$	7,933
		σ	525
	I-4	1	2,700
		2	3,100
		3	3,000
		$\bar{x}$	2,933
		σ	170
AAF-1	I-4	1	2,600
		2	2,800
		3	2,900
		$\bar{x}$	2,767
		σ	125

Table 3-12. Molecular weights by vapor phase osmometry at 39°C of SEC Fraction-I-3 and I-4 subfractions of eight asphalts (continued).

Asphalt	Subfraction	Run no.	Molecular weight, daltons
AAG-1	I-4	1	2,300
		2	2,200
		3	2,200
			$\bar{x}$ 2,233
			σ 47
AAK-1	I-4	1	2,800
		2	2,700
			$\bar{x}$ 2,750
AAM-1	I-4	1	2,500
		2	2,300
		3	2,200
			$\bar{x}$ 2,333
			σ 125

Table 3-13. Molecular weights by VPO of AAD-1 SEC Fraction-I subfractions.

Run no.	Subfraction no.	Molecular weight, daltons
1	I-1	29,000
	I-2	17,000
	I-3	9,200
	I-4	2,900
2	I-1	29,000
	I-2	17,000
	I-3	8,600
	I-4	4,200
3	I-1	25,000
	I-2	18,000
	I-3	9,700
	I-4	3,000

Table 3-14. Rheological properties of mixtures of AAD-1 SEC Fraction-II (95%) [1] with AAD-1 SEC Fraction-I subfractions (5%) at 25°C.

AAD-1 SEC Fraction-I subfraction in mixture	ω, rad/s	G′, Pa	G″, Pa	η*, Pa·s [2]	Tan δ
I-1	0.1	-	83	826	-
	1.0	38	735	736	19
	10.0	363	6,675	667	18
I-2	0.1	13	88	888	7
	1.0	42	691	692	16
	10.0	316	6,280	629	20
I-3	0.1	8	95	955	12
	1.0	35	790	791	23
	10.0	353	7,322	733	21
I-4	0.1	6	65	655	10
	1.0	24	483	484	20
	10.0	97	4,513	452	46

[1] Viscosity of AAD-1 SEC Fraction-II is 336 Pa·s at 25°C and 1.0 rad/s.

[2] Rheological measurements were performed after argon annealing. Data obtained on the Rheometrics Mechanical Spectrometer are estimated to be accurate to ± 5%.

Table 3-15. Rheological properties of mixtures of AAD-1 SEC Fraction-II (90%) with AAD-1 SEC Fraction-I subfractions (10%) at 25°C.

AAD-1 SEC Fraction-I subfraction in mixture	ω, rad/s	G′, Pa	G″, Pa	η*, Pa·s [1]	Tan δ
I-1	0.1	82	793	7,970	9.7
	1.0	1,028	6,367	6,450	6.2
	10.0	9,951	46,670	4,773	4.7
I-2	0.1	38	474	4,759	12.5
	1.0	489	4,006	4,036	8.2
	10.0	5,447	31,381	3,186	5.8
I-3	0.1	24	281	2,816	11.7
	1.0	165	2,419	2,425	14.6
	10.0	1,961	20,983	2,108	10.7

[1] Rheological measurements were performed after argon annealing. Data obtained on the Rheometrics Mechanical Spectrometer are estimated to be accurate to ± 5%.

Table 3-16. Rheological properties of mixtures of AAD-1 SEC Fraction-II (85%) with AAD-1 SEC Fraction-I subfractions (15%) at 25°C.

AAD-1 SEC Fraction-I subfraction in mixture	ω, rad/s	G′, Pa	G″, Pa	η*, Pa·s [1]	Tan δ
I-1	0.1	361	1,957	19,900	5.4
	1.0	3,677	13,550	14,040	3.7
	10.0	27,690	85,090	8,950	3.1
I-2	0.1	187	1,396	14,080	7.5
	1.0	2,141	10,710	10,920	5.0
	10.0	19,760	74,590	7,719	3.8
I-3	0.1	131	1,315	13,210	10.1
	1.0	1,598	10,480	10,600	6.6
	10.0	17,020	78,120	7,997	4.6
I-4	0.1	66	429	4,345	6.5
	1.0	172	3,587	3,591	20.9
	10.0	3,017	31,931	3,208	10.6

[1] Rheological measurements were performed after argon annealing. Data obtained on the Rheometrics Mechanical Spectrometer are estimated to be accurate to ± 5%.

Table 3-17. Rheological properties of mixtures of AAD-1 SEC Fraction-II (80%) with AAD-1 SEC Fraction-I subfractions (20%) at 25°C.

AAD-1 SEC Fraction-I subfraction in mixture	ω, rad/s	G′, Pa	G″, Pa	η*, Pa·s [1]	Tan δ
I-1	0.1	2,532	7,218	76,490	2.85
	1.0	17,339	40,105	43,697	2.31
	10.0	98,377	208,500	23,060	2.12
I-2	0.1	1,635	5,529	57,654	3.38
	1.0	12,635	34,868	37,090	2.81
	10.0	81,235	192,100	20,861	2.36
I-3	0.1	446	2,590	26,281	5.80
	1.0	4,053	19,624	20,040	4.84
	10.0	37,638	137,600	14,269	3.66

[1] Rheological measurements were performed after argon annealing. Data obtained on the Rheometrics Mechanical Spectrometer are estimated to be accurate to ± 5%.

Table 3-18. Yields of SEC fractions of eight SHRP asphalts and viscosities of SEC Fraction-II.

Asphalt	Natural abundance of SEC Fraction, mass %		Viscosity (25°C; 1.0 rad/s) [1] of SEC Fraction-II, Pa·s
	SEC Fraction-I	SEC Fraction-II	
AAA-1	21.7	78.3	506
AAB-1	20.8	79.2	1,367
AAC-1	13.6	86.4	8,602
AAD-1	21.2	78.8	336
AAF-1	13.3	86.7	53,350
AAG-1	11.2	88.8	62,380
AAK-1	24.8	75.2	1,124
AAM-1	31.8	68.2	26,350

[1] Rheological measurements were performed after argon annealing. Data obtained on the Rheometrics Mechanical Spectrometer are estimated to be accurate to ± 5%.

Table 3-19. Viscosities (Pa·s) of crossblended mixtures of SEC fractions of asphalts, 25°C, 1.0 rad/s. [1]

Parent asphalt of SEC Fraction-I component of mixture	Parent asphalt of SEC Fraction-II component of mixture						
	AAA-1	AAB-1	AAC-1	AAD-1	AAF-1	AAG-1	AAK-1
AAA-1	65,200	179,600	230,100	36,100	642,400	204,400	155,100
AAB-1	90,500	148,400	220,800	36,800	384,900	403,600	198,600
AAC-1	95,900	148,000	156,100	43,300	571,900	362,950	251,300
AAD-1	177,300	223,100	225,400	59,200	884,300	764,800	240,700
AAF-1	101,400	185,400	225,900	50,000	507,000	466,300	217,400
AAG-1	36,700	97,300	138,600	26,600	502,400	405,500	164,750
AAK-1	95,800	145,100	185,700	31,300	344,600	332,250	165,450
AAM-1	3,500	10,200	26,500	3,000	114,900	125,900	10,600

[1] Rheological measurements were performed after argon annealing. Data obtained on the Rheometrics Mechanical Spectrometer are estimated to be accurate to ± 5%.

Table 3-20. Reduced specific viscosity values of crossblended mixtures of SEC fractions of asphalts, 25°C, 1.0 rad/s.

Parent asphalt of SEC Fraction-I component of mixture	Parent asphalt of SEC Fraction-II component of mixture						
	AAA-1	AAB-1	AAC-1	AAD-1	AAF-1	AAG-1	AAK-1
AAA-1	590	630	190	500	80	20	550
AAB-1	820	520	180	510	50	50	710
AAC-1	870	520	130	600	70	40	900
AAD-1	1,610	780	185	830	120	100	860
AAF-1	920	650	185	700	60	60	770
AAG-1	330	340	110	370	60	50	590
AAK-1	870	510	150	430	40	40	590
AAM-1	30	30	15	40	10	10	30

Table 3-21. Solubility parameters of 10 solvents [Barton 1975].

Solvent	Solubility parameter δ, $cal^{1/2}/cm^{3/2}$, of solvent
iso-octane	6.8 [1]
n-hexane	7.3
toluene	8.9
ethyl acetate	9.1
acetone	9.9
dioxane	10.0
propionic acid	10.3 [2]
pyridine	10.7
2-propanol	11.5
acetonitrile	11.9

[1] Assumed to be equal to n-butane. Not a measured value.

[2] Assumed to be intermediate between acetic and n-butanoic acids. Not a measured value.

Table 3-22. Solubilities of IEC neutral fractions in acetone and in ethyl acetate.

Parent asphalt of IEC neutral fraction	Mass % IEC neutral fraction soluble in ethyl acetate [1]	Mass % IEC neutral fraction insoluble in ethyl acetate [1]	Mass % IEC neutral fraction soluble in acetone [1]	Mass % IEC neutral fraction insoluble in acetone [1]
AAA-1	> 99	< 1.0	64.1	36.2
AAB-1	94.2	6.6	27.7	73.4
AAC-1	94.4	7.0	15.4	84.5
AAD-1	97.3	2.9	75.6	24.1
AAF-1	94.8	6.1	23.2	78.3
AAG-1	> 99	< 1.0	62.6	36.7
AAK-1	99.0	2.4	51.7	48.3
AAM-1	21.3	81.2	4.5	96.1

[1] Data are averages of three determinations and are not normalized to 100%.

Table 3-23. Surface tensions, densities, molecular weights, and solubility parameters of eight IEC neutral fractions at 60°C.

Parent asphalt of IEC neutral fraction	Surface tension, dynes/cm	Density, g/mL	Molecular weight, g/mol	Solubility parameter, δ
AAA-1	27.33	0.83	620	6.58
AAB-1	22.56	0.87	680	6.03
AAC-1	29.48	0.70	770	6.44
AAD-1	22.29	0.74	580	6.00
AAF-1	29.47	0.90	710	6.75
AAG-1	25.33	0.85	650	6.35
AAK-1	28.62	0.87	610	6.78
AAM-1	30.36	0.85	1,200	6.29

Table 3-24. Solubility parameters of SHRP core asphalts at 60°C calculated from surface tensions, densities, and molecular weights.

Asphalt	Surface tension, γ, dyne/cm	Density, ρ, g/mL	Molecular weight, g/mol	Solubility parameter, δ
AAA-1	33.9	1.03	790	7.27
AAB-1	31.9	1.03	840	7.02
AAC-1	32.2	1.01	870	6.99
AAD-1	31.5	1.02	700	7.15
AAF-1	33.9	1.03	840	7.21
AAG-1	33.2	1.02	710	7.31
AAK-1	34.9	1.02	860	7.27
AAM-1	32.9	0.99	1,300	6.64

Table 3-25. Activation energies of viscous flow and solubility parameters (δ) of SHRP core asphalts.

Asphalt	Weight-average molecular weight	Activation energy of viscous flow (E_a), Kcal/mol	Solubility parameter (δ)
AAA-1	3,078	32.8	6.2
AAB-1	2,537	37.2	7.3
AAC-1	1,781	37.8	8.6
AAD-1	2,341	34.3	7.2
AAF-1	2,017	41.9	8.7
AAG-1	1,611	39.1	9.3
AAK-1	3,169	36.1	6.4
AAM-1	2,281	40.9	7.9

Table 3-26. Masses of waxes in IEC neutral fractions of asphalts.

Asphalt	Mass % IEC neutrals	Mass % waxes in IEC neutrals	Mass % waxes in whole asphalt
AAA-1	66.6	2.1	1.4
AAA-1	66.6	2.2	1.4
Avg. AAA-1		2.2	1.4
AAB-1	64.5	7.4	4.8
AAB-1	64.5	7.1	4.6
Avg. AAB-1		7.2	4.7
AAC-1	72.1	10.6	7.6
AAC-1	70.5	11.2	7.9
AAC-1	66.8	10.9	7.3
AAC-1	67.3	10.0	6.7
AAC-1	67.3	8.8	5.9
AAC-1	67.3	19.4	6.3
Avg. AAC-1		11.8	7.0
Std. Dev. AAC-1		$\sigma = \pm 3.5$	$\sigma = 0.7$
AAD-1	56.3	3.3	1.9
AAD-1	52.2	3.6	1.9
AAD-1	60.4	3.3	2.0
AAD-1	59.1	3.2	1.9
Avg. AAD-1		3.4	1.9
Std. Dev. AAD-1		$\sigma = \pm 0.2$	$\sigma = \pm 0.04$
AAF-1	66.1	8.5	5.6
AAF-1	66.1	8.7	5.8
Avg. AAF-1		8.6	5.7
AAG-1	69.8	1.8	1.2
AAK-1	69.3	4.8	3.3
AAK-1	69.3	5.1	3.5
Avg. AAK-1		5.0	3.4
AAM-1	67.9	42.0	28.5
AAM-1	67.9	37.1	25.2
AAM-1	61.7	40.6	25.0
AAM-1	61.7	47.3	29.2
AAM-1	63.1	39.0	24.6
AAM-1	63.1	40.3	25.4
Avg. AAM-1		41.0	26.3
Std. Dev. AAM-1		$\sigma = \pm 3.2$	$\sigma = \pm 1.8$

Table 3-27. Wax contents of IEC neutral fractions of TFO/PAV (60°C - 144 hr) aged asphalts.

Aged asphalt	Mass % IEC neutral of aged asphalt	Mass % waxes in IEC neutrals of aged asphalt	Mass % waxes in aged asphalt
AAC-1	59.0	11.6	6.8
AAD-1	49.7	2.7	1.3
AAD-1	49.7	2.4	1.2
AAF-1	37.4	7.4	4.2

Table 3-28. Effect of wax content on asphalt rheological properties.

Sample description	Dynamic viscosity, Pa·s (η^*), 25°C, 1.0 rad/s [1]	Tan δ, 25°C, 1.0 rad/s
AAA-1, solvent treated	41,114	3.95
AAA-1 + 4.25% AAA-1 waxes	41,389	3.88
AAA-1 + 4.84% AAD-1 waxes	57,888	2.89
AAA-1 + 5.08% AAM-1 waxes	33,311	4.10
AAD-1, solvent treated	85,021	2.60
AAD-1 + 5.34% AAA-1 waxes	139,800	2.24
AAD-1 + 5.21% AAD-1 waxes	211,370	1.90
AAD-1 + 4.46% AAM-1 waxes	82,611	2.58
AAM-1, solvent treated	390,300	2.10
AAM-1 + 4.11% AAA-1 waxes	442,390	1.79
AAM-1 + 6.09% AAD-1 waxes	835,080	1.36
AAM-1 + 4.84% AAM-1 waxes	89,988	2.51

[1] Rheological measurements were performed after argon annealing. Data obtained on the Rheometrics Mechanical Spectrometer are estimated to be accurate to ± 5%.

Table 3-29. Rheological properties of mixtures of AAD-1 maltenes and asphaltenes with AAF-1 maltenes and asphaltenes, 25°C and 60°C, 1.0 rad/s.

Mixture number	Components of mixtures	Viscosity of mixture, Pa·s [1]		Tan δ 25°C, 1.0 rad/s	Reduced specific viscosity [2]	
		25°C, 1.0 rad/s	60°C, 1.0 rad/s		25°C, 1.0 rad/s	60°C, 1.0 rad/s
I	AAF-1 maltenes (85.8%) AAF-1 asphaltenes (14.2%)	836,690	597	2.5	229	120
II	AAF-1 maltenes (78.9%) AAD-1 asphaltenes (21.1%)	2,164,000	3,953	1.4	405	563
III	AAF-1 maltenes (85.8%) AAD-1 asphaltenes (14.2%)	676,350	740	2.3	183	151
IV	AAF-1 maltenes (78.9%) AAF-1 asphaltenes (21.1%)	3,376,300	3,741	1.3	635	533
V	AAD-1 maltenes (78.9%) AAD-1 asphaltenes (21.1%)	93,448	328	2.4	1,341	384
VI	AAD-1 maltenes (85.8%) AAF-1 asphaltenes (14.2%)	14,807	34	8.4	310	53
VII	AAD-1 maltenes (78.9%) AAF-1 asphaltenes (21.1%)	106,750	195	3.3	1,533	226
VIII	AAD-1 maltenes (85.8%) AAD-1 asphaltenes (14.2%)	13,232	46	13.2	276	74

[1] Rheological measurements were performed after argon annealing. Data obtained on the Rheometrics Mechanical Spectrometer are estimated to be accurate to ± 5%.

[2] To calculate reduced specific viscosities of the mixtures, maltene viscosities are required. These are: AAD-1 maltenes; 329 Pa·s at 25°C and 4 Pa·s at 60°C; AAF-1 maltenes; 25,000 Pa·s at 25°C and 33 Pa·s at 60°C.

Table 3-30. Selected rheological properties of mixtures of AAD-1 maltenes and asphaltenes with AAF-1 maltenes and asphaltenes, 25°C and 60°C, 10.0 rad/s.

Mixture number [1]	G* (Pa) [2]		Phase angle (δ)		G* sin δ, Pa, 25°C	G*/sin δ, Pa, 60°C
	25°C	60°C	25°C	60°C		
I	4,019,500	5,711	58.35	86.44	3,421,700	5,722
II	7,755,300	28,478	47.82	74.78	5,746,800	29,513
III	3,256,400	6,488	59.13	82.66	2,795,000	6,541
IV	10,975,000	30,981	45.02	79.35	7,762,700	31,524
V	481,020	2,825	63.54	80.94	430,630	2,860
VI	111,450	343	78.33	89.39	109,150	343
VII	536,870	1,880	67.87	87.19	497,320	1,883
VIII	93,720	438	74.49	87.57	90,732	439

[1] Mixture compositions are listed in table 3-23, column 2.

[2] Rheological measurements were performed after argon annealing. Data obtained on the Rheometrics Mechanical Spectrometer are estimated to be accurate to ± 5%.

Table 3-31. Rheological properties of mixtures of AAD-1 maltenes and asphaltenes with AAF-1 maltenes and asphaltenes, TFO/PAV aged.

Mixture number [1]	Viscosity of mixture, Pa·s [2]		Tan δ, 25°C, 1.0 rad/s	Aging index, [3] 60°C, 1.0 rad/s
	25°C, 1.0 rad/s	60°C, 1.0 rad/s		
I	3,967,100	6,016	1.1	10.1
II	9,687,100	89,408	0.6	22.6
III	2,925,500	14,040	0.9	19.0
IV	11,031,000	47,529	0.7	12.7
V	518,080	2,338	1.5	12.9
VI	98,741	203	3.2	5.9
VII	743,060	2,465	1.6	12.6
VIII	103,080	422	2.2	9.3

[1] Mixture compositions are listed in table 3-23, column 2.

[2] Rheological measurements were performed after argon annealing. Data obtained on the Rheometrics Mechanical Spectrometer are estimated to be accurate to ± 5%.

[3] Calculated by dividing 60°C, 1.0 rad/s viscosities of aged mixtures by 60°C, 1.0 rad/s viscosities of unaged mixtures (table 3-23, column 4).

Table 3-32. Selected rheological properties of mixtures of AAD-1 maltenes and asphaltenes with AAF-1 maltenes and asphaltenes, TFO/PAV aged, 25°C and 60°C, 10.0 rad/s.

Mixture number[1]	G* (Pa)[2]		Phase angle (δ)		G* sin δ, Pa, 25°C	G*/sin δ, Pa, 60°C
	25°C	60°C	25°C	60°C		
I	12,248,000	46,488	40.84	76.37	8,004,900	47,835
II	20,691,000	301,780	28.66	58.22	9,925,500	354,990
III	7,783,500	61,079	38.78	66.91	4,875,300	66,397
IV	24,975,000	231,450	29.82	67.31	12,420,000	250,870
V	1,533,900	23,378	55.85	67.22	1,269,400	25,356
VI	462,200	1,972	67.72	87.12	427,690	1,974
VII	2,224,700	19,739	56.07	77.41	1,845,900	20,225
VIII	515,600	3,442	62.03	80.42	455,430	3,490

[1] Mixture compositions are listed in table 3-23, column 2.

[2] Rheological measurements were performed after argon annealing. Data obtained on the Rheometrics Mechanical Spectrometer are estimated to be accurate to ± 5%.

Table 3-33. Rheological properties of mixtures of AAD-1 maltenes and asphaltenes with AAG-1 maltenes and asphaltenes, 25°C and 60°C, 1.0 rad/s.

Mixture number	Components of mixtures	Viscosity of mixture, Pa·s [1]		Tan δ 25°C, 1.0 rad/s	Reduced specific viscosity [2]	
		25°C, 1.0 rad/s	60°C, 1.0 rad/s		25°C, 1.0 rad/s	60°C, 1.0 rad/s
I	AAD-1 maltenes (79.0%) AAD-1 asphaltenes (21.0%)	49,011	189	3.2	705	220
II	AAD-1 maltenes (94.0%) AAG-1 asphaltenes (6.0%)	1,023	8	>10.0	35	17
III	AAD-1 maltenes (79.0%) AAG-1 asphaltenes (21.0%)	62,908	181	3.7	906	211
IV	AAD-1 maltenes (94.0%) AAD-1 asphaltenes (6.0%)	1,206	9	>10.0	44	21
V	AAG-1 maltenes (79.0%) AAD-1 asphaltenes (21.0%)	4,907,900	8,619	1.5	287	393
VI	AAG-1 maltenes (94.0%) AAD-1 asphaltenes (6.0%)	337,190	361	6.0	54	41
VII	AAG-1 maltenes (94.0%) AAG-1 asphaltenes (6.0%)	389,100	395	6.3	64	47
VIII	AAG-1 maltenes (79.0%) AAG-1 asphaltenes (21.0%)	3,544,900	4,419	1.7	206	198

[1] Rheological measurements were performed after argon annealing. Data obtained on the Rheometrics Mechanical Spectrometer are estimated to be accurate to ± 5%.

[2] To calculate reduced specific viscosities, maltene viscosities are required. These are: AAD-1 maltenes; 329 Pa·s at 25°C and 4 Pa·s at 60°C; AAG-1 maltenes; 80,000 Pa·s at 25°C and 104 Pa·s at 60°C.

Table 3-34. Selected rheological properties of mixtures of AAD-1 maltenes and asphaltenes with AAG-1 maltenes and asphaltenes, 25°C and 60°C, 10.0 rad/s.

Mixture number [1]	G* (Pa) [2]		Phase angle (δ)		G* sin δ, Pa, 25°C	G*/sin δ, Pa, 60°C
	25°C	60°C	25°C	60°C		
I	278,320	1,723	69.19	84.47	260,160	1,731
II	9,751	77	87.72	89.93	9,743	77
III	390,050	1,775	68.56	87.82	363,480	1,776
IV	11,125	87	86.54	89.51	11,105	87
V	18,129,000	61,324	46.79	74.28	13,213,000	63,706
VI	2,374,000	3,530	73.09	88.31	2,271,300	3,532
VII	2,764,800	3,747	72.73	89.29	2,640,100	3,747
VIII	13,844,000	38,696	48.92	81.89	10,436,000	39,087

[1] Mixture compositions are listed in table 3-27, column 2.

[2] Rheological measurements were performed after argon annealing. Data obtained on the Rheometrics Mechanical Spectrometer are estimated to be accurate to ± 5%.

Table 3-35. Rheological properties of mixtures of AAD-1 maltenes and asphaltenes with AAG-1 maltenes and asphaltenes, TFO/PAV aged.

Mixture number[1]	Viscosity of mixture, Pa·s[2]		Tan δ, 25°C, 1.0 rad/s	Aging index,[3] 60°C, 1.0 rad/s
	25°C, 1.0 rad/s	60°C, 1.0 rad/s		
I	550,650	2,908	1.5	15.4
II	7,108	29	>10	3.7
III	552,310	1,631	1.8	9.0
IV	8,365	35	8.0	4.0
V	20,662,000	132,870	0.8	15.4
VI	2,125,400	1,927	2.3	5.3
VII	1,086,400	1,578	1.6	4.2
VIII	28,728,000	70,349	0.8	15.9

[1] Mixture compositions are listed in table 3-27, column 2.

[2] Rheological measurements were performed after argon annealing. Data obtained on the Rheometrics Mechanical Spectrometer are estimated to be accurate to ± 5%.

[3] Calculated by dividing 60°C, 1.0 rad/s viscosities of aged mixtures by 60°C, 1.0 rad/s viscosities of unaged mixtures (table 3-27, column 4).

Table 3-36. Selected rheological properties of mixtures of AAD-1 maltenes and asphaltenes with AAG-1 maltenes and asphaltenes, TFO/PAV aged, 25°C and 60°C, 10.0 rad/s.

Mixture number[1]	G* (Pa)[2]		Phase angle (δ)		G* sin δ, Pa, 25°C	G*/sin δ, Pa, 60°C
	25°C	60°C	25°C	60°C		
I	2,231,600	18,546	55.49	69.56	1,838,900	19,792
II	58,055	292	80.98	89.82	57,337	292
III	1,926,200	13,914	57.21	80.15	1,619,200	14,122
IV	63,809	348	78.26	89.16	62,475	349
V	49,057,000	575,570	31.08	59.99	25,326,000	664,710
VI	10,227,000	17,416	56.18	84.16	8,496,700	17,507
VII	10,861,000	15,258	57.79	86.93	9,190,000	15,280
VIII	71,856,000	444,040	32.31	69.57	38,406,000	473,830

[1] Mixture compositions are listed in table 3-27, column 2.

[2] Rheological measurements were performed after argon annealing. Data obtained on the Rheometrics Mechanical Spectrometer are estimated to be accurate to ± 5%.

Table 3-37. Rheological properties of mixtures of AAF-1 maltenes and asphaltenes with AAG-1 maltenes and asphaltenes, 25°C and 60°C, 1.0 rad/s.

Mixture number	Components of mixtures	Viscosity of mixture, Pa·s [1]		Tan δ 25°C, 1.0 rad/s	Reduced specific viscosity [2]	
		25°C, 1.0 rad/s	60°C, 1.0 rad/s		25°C, 1.0 rad/s	60°C, 1.0 rad/s
I	AAG-1 maltenes (94.0%) AAG-1 asphaltenes (6.0%)	465,170	475	6.5	80	59
II	AAG-1 maltenes (85.5%) AAF-1 asphaltenes (14.5%)	2,136,200	2,105	2.0	177	133
III	AAG-1 maltenes (94.0%) AAF-1 asphaltenes (6.0%)	249,800	387	8.1	35	45
IV	AAG-1 maltenes (85.5%) AAG-1 asphaltenes (14.5%)	2,423,100	2,538	2.4	202	161
V	AAF-1 maltenes (85.5%) AAF-1 asphaltenes (14.5%)	389,340	521	3.3	101	102
VI	AAF-1 maltenes (85.5%) AAG-1 asphaltenes (14.5%)	595,270	664	3.1	157	132
VII	AAF-1 maltenes (94.0%) AAG-1 asphaltenes (6.0%)	57,550	99	9.7	22	33
VIII	AAF-1 maltenes (94.0%) AAF-1 asphaltenes (6.0%)	90,410	109	6.9	44	38

[1] Rheological measurements were performed after argon annealing. Data obtained on the Rheometrics Mechanical Spectrometer are estimated to be accurate to ± 5%.

[2] To calculate reduced specific viscosities of the mixtures, maltene viscosities are required. These are: AAF-1 maltenes; 25,000 Pa·s at 25°C and 33 Pa·s at 60°C; AAG-1 maltenes; 80,000 Pa·s at 25°C and 104 Pa·s at 60°C.

Table 3-38. Selected rheological properties of mixtures of AAF-1 maltenes and asphaltenes with AAG-1 maltenes and asphaltenes, 25°C and 60°C, 10.0 rad/s.

Mixture number [1]	G* (Pa) [2]		Phase angle (δ)		G* sin δ, Pa, 25°C	G*/sin δ, Pa, 60°C
	25°C	60°C	25°C	60°C		
I	3,413,700	4,726	72.37	89.29	3,253,000	4,726
II	10,068,000	19,666	54.12	86.42	8,157,600	19,705
III	1,912,200	3,871	75.59	89.42	1,852,100	3,871
IV	10,803,000	23,704	57.75	85.90	9,136,800	23,765
V	2,131,100	5,010	64.14	87.29	1,917,700	5,016
VI	2,208,100	6,325	63.73	86.80	1,980,000	6,335
VII	446,140	990	78.38	89.69	437,000	990
VIII	651,940	1,093	75.53	89.66	631,250	1,093

[1] Mixture compositions are listed in table 3-31, column 2.

[2] Rheological measurements were performed after argon annealing. Data obtained on the Rheometrics Mechanical Spectrometer are estimated to be accurate to ± 5%.

Table 3-39. Rheological properties of mixtures of AAF-1 maltenes and asphaltenes with AAG-1 maltenes and asphaltenes, TFO/PAV aged.

Mixture number[1]	Viscosity of mixture, Pa·s[2]		Tan δ, 25°C, 1.0 rad/s	Aging index,[3] 60°C, 1.0 rad/s
	25°C, 1.0 rad/s	60°C, 1.0 rad/s		
I	1,770,400	1,422	2.7	3.0
II	7,421,800	8,822	1.0	4.2
III	1,504,600	1,183	3.0	3.1
IV	11,514,000	12,233	1.2	4.8
V	2,765,200	3,650	1.4	7.0
VI	2,841,600	3,778	1.4	5.7
VII	196,080	330	2.2	3.3
VIII	367,790	385	3.2	3.5

[1] Mixture compositions are listed in table 3-31, column 2.

[2] Rheological measurements were performed after argon annealing. Data obtained on the Rheometrics Mechanical Spectrometer are estimated to be accurate to ± 5%.

[3] Calculated by dividing 60°C, 1.0 rad/s viscosities of aged mixtures by 60°C, 1.0 rad/s viscosities of unaged mixtures (table 3-31, column 4).

Table 3-40. Selected rheological properties of mixtures of AAF-1 maltenes and asphaltenes with AAG-1 maltenes and asphaltenes, TFO/PAV aged, 25°C and 60°C, 10.0 rad/s.

Mixture number[1]	G* (Pa)[2]		Phase angle (δ)		G* sin δ, Pa, 25°C	G*/sin δ, Pa, 60°C
	25°C	60°C	25°C	60°C		
I	8,745,400	13,756	59.02	87.29	7,498,000	13,772
II	19,831,100	74,603	36.30	80.71	11,740,000	75,590
III	7,910,800	11,555	60.20	87.71	6,864,719	11,564
IV	34,865,000	100,870	41.59	79.23	23,143,000	102,680
V	8,935,800	29,987	47.24	79.59	6,560,900	30,488
VI	9,188,500	31,055	47.18	79.33	6,740,100	31,602
VII	1,960,400	3,234	65.01	88.31	1,776,900	3,235
VIII	2,022,500	3,766	63.04	88.10	1,802,700	3,768

[1] Mixture compositions are listed in table 3-31, column 2.

[2] Rheological measurements were performed after argon annealing. Data obtained on the Rheometrics Mechanical Spectrometer are estimated to be accurate to ± 5%.

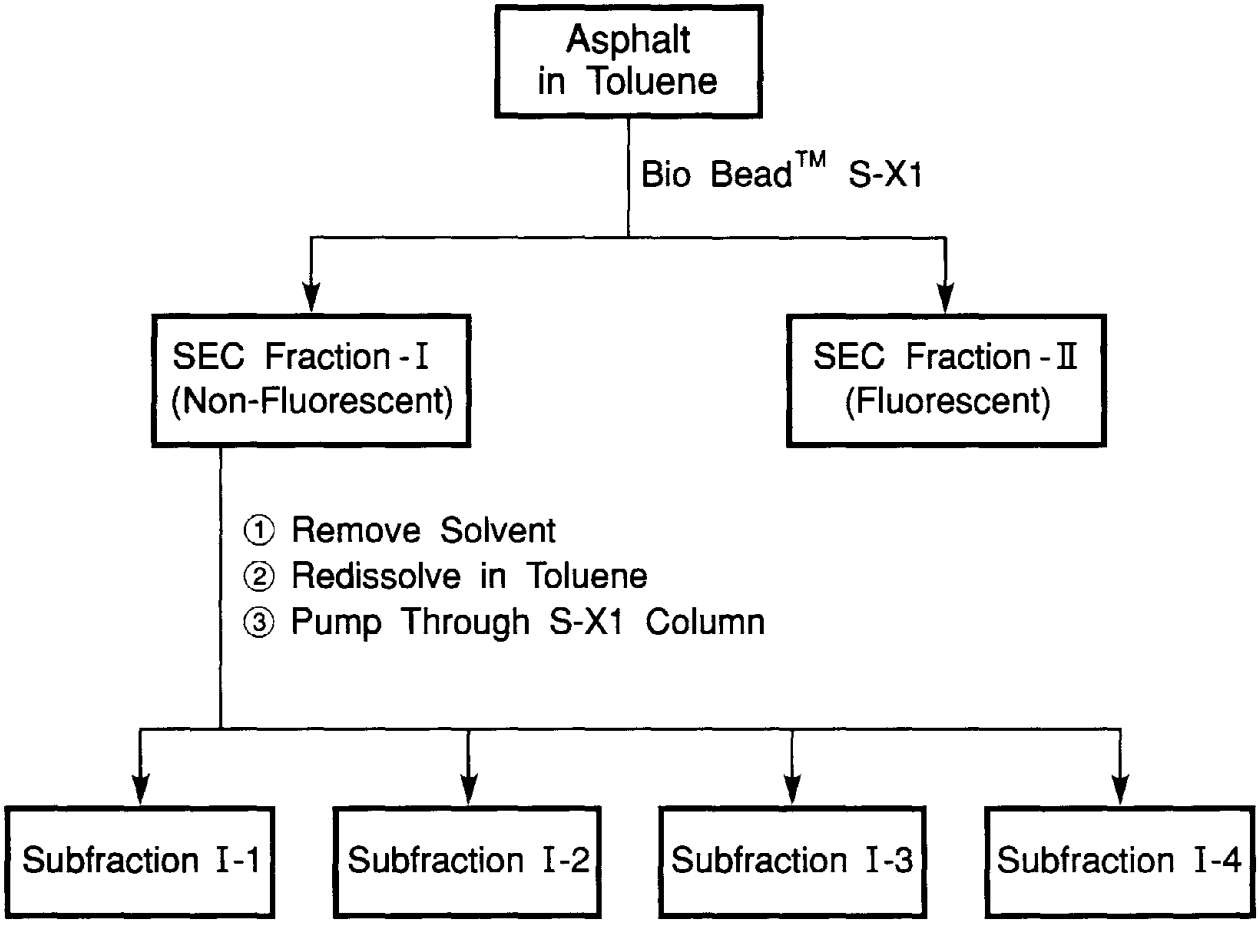

Figure 3-5. Flow sheet for size exclusion chromatography separation of asphalts.

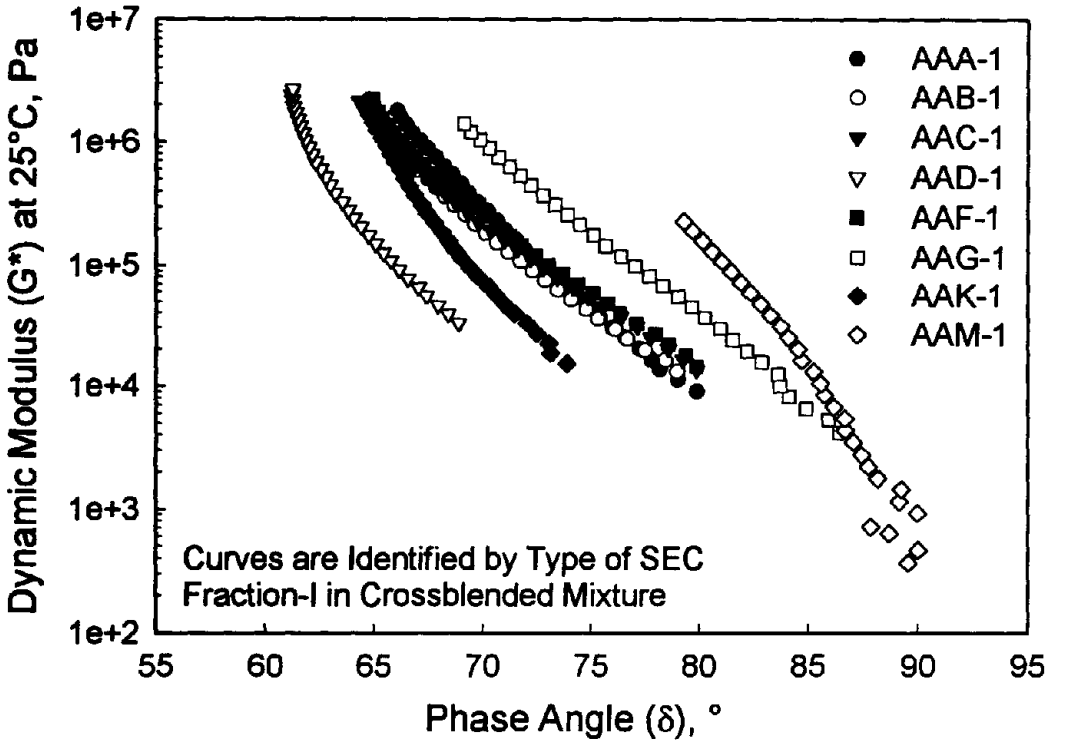

Figure 3-6. Black plot of G* vs. δ for mixtures of SEC Fraction-II of AAA-1 (78.3%) with SEC Fraction-I (21.7%) of eight SHRP core asphalts.

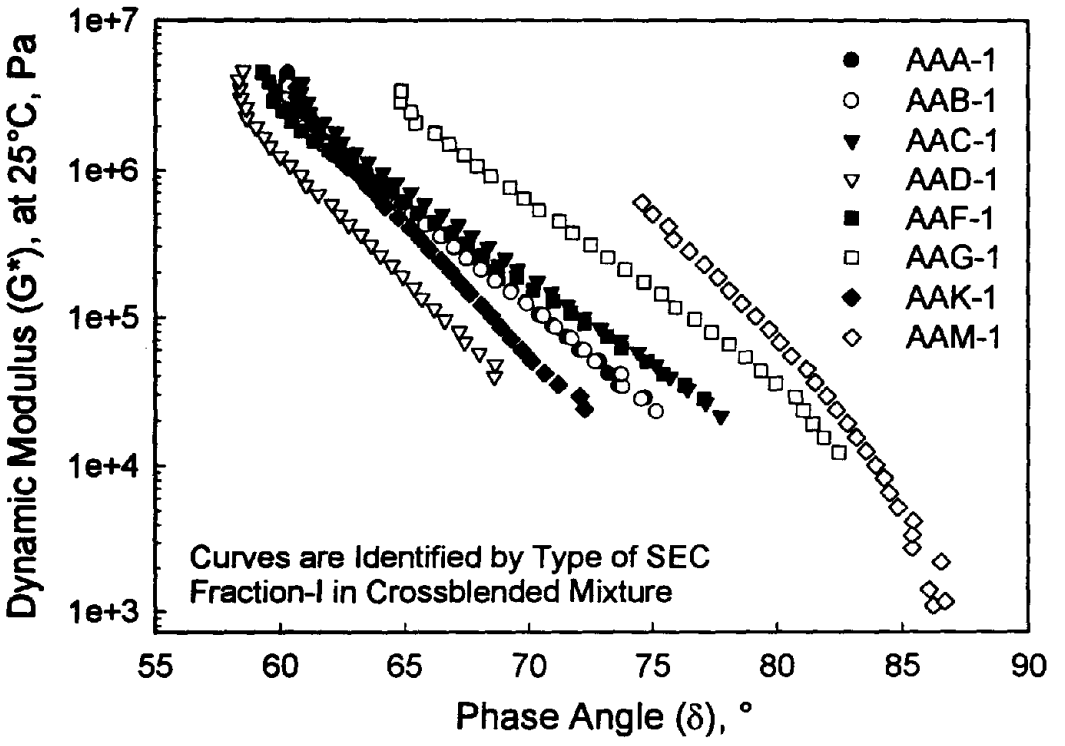

Figure 3-7. Black plot of G* vs. δ for mixtures of SEC Fraction-II of AAB-1 (79.2%) with SEC Fraction-I (20.8%) of eight SHRP core asphalts.

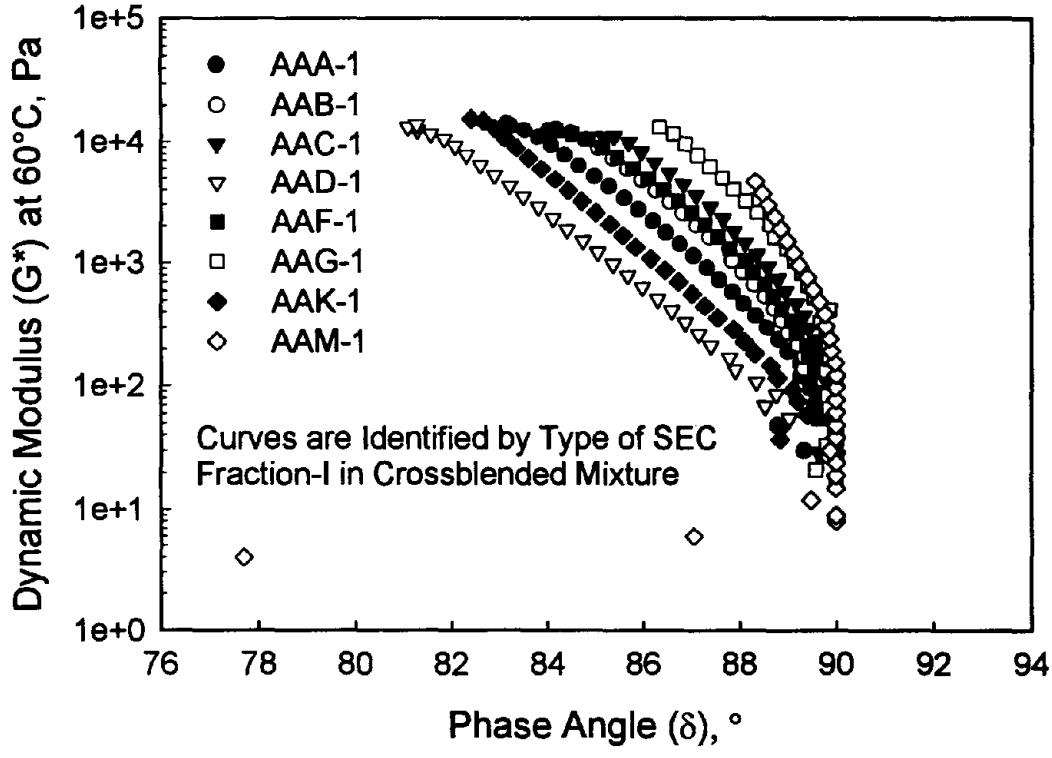

Figure 3-8. Black plot of G* vs. δ for mixtures of SEC Fraction-II of AAC-1 (86.4%) with SEC Fraction-I (13.6%) of eight SHRP core asphalts.

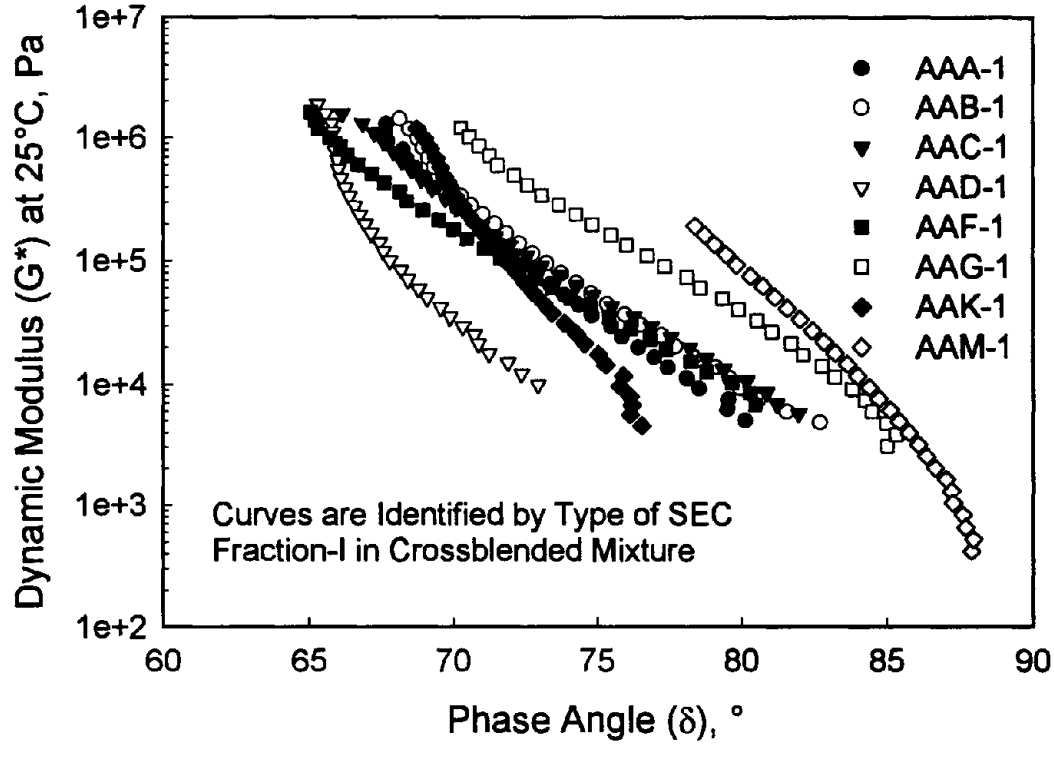

Figure 3-9. Black plot of G* vs. δ for mixtures of SEC Fraction-II of AAD-1 (78.8%) with SEC Fraction-I (21.2%) of eight SHRP core asphalts.

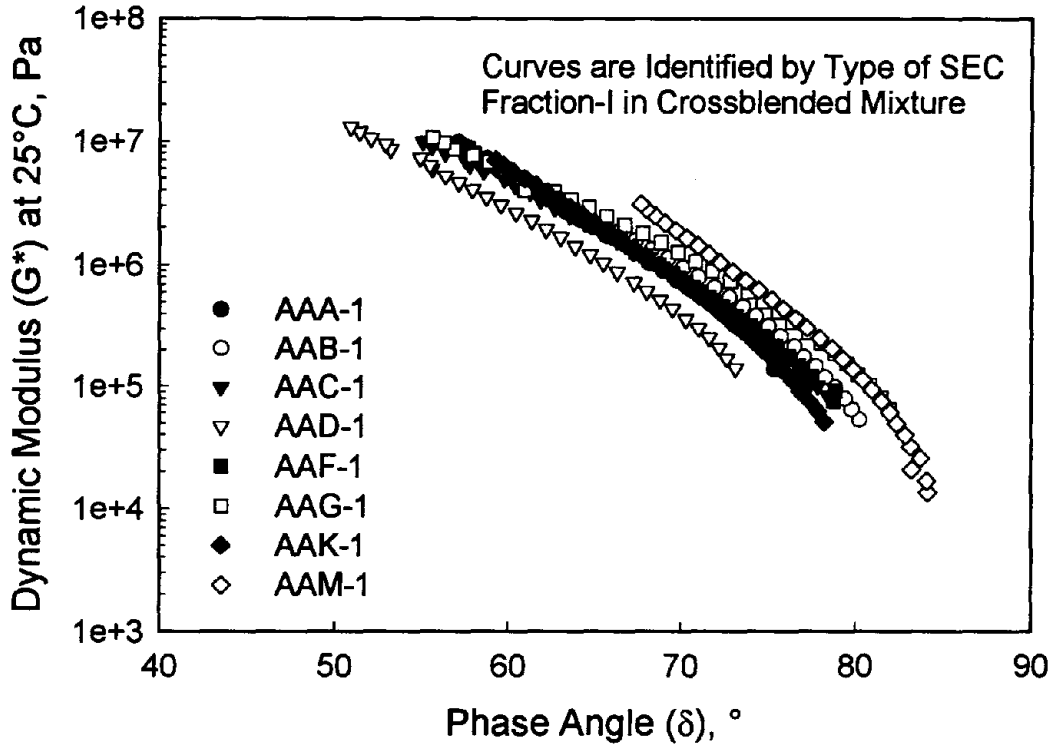

Figure 3-10. Black plot of G* vs. δ for mixtures of SEC Fraction-II of AAF-1 (86.7%) with SEC Fraction-I (13.3%) of eight SHRP core asphalts.

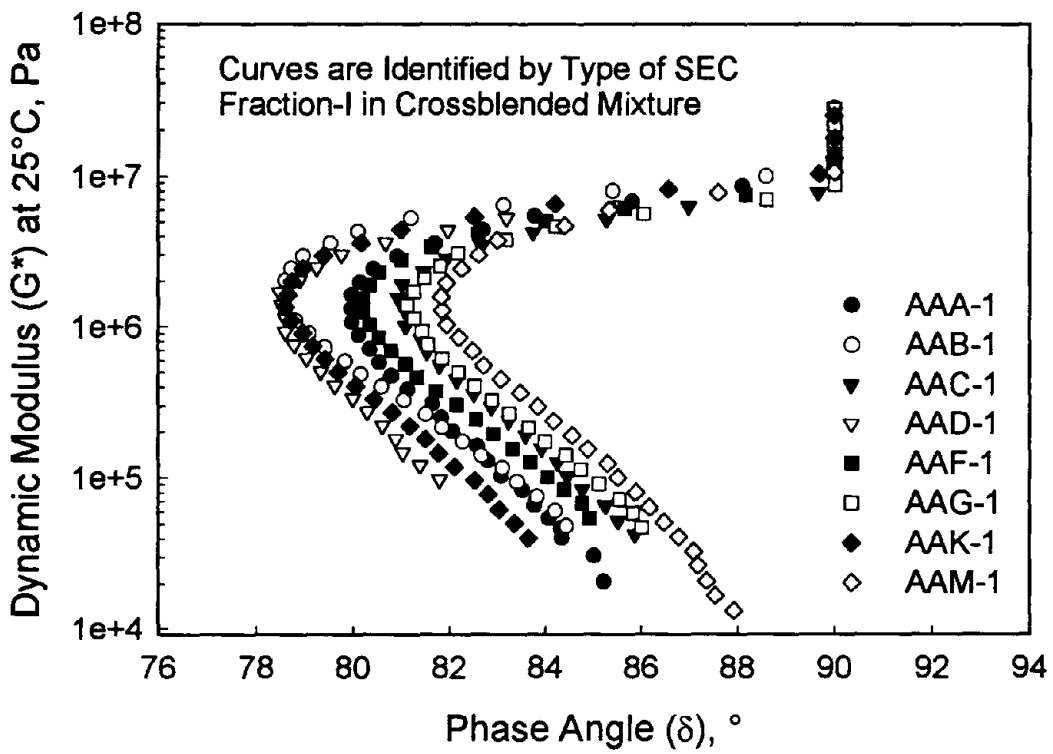

Figure 3-11. Black plot of G* vs. δ for mixtures of SEC Fraction-II of AAG-1 (88.8%) with SEC Fraction-I (11.2%) of eight SHRP core asphalts.

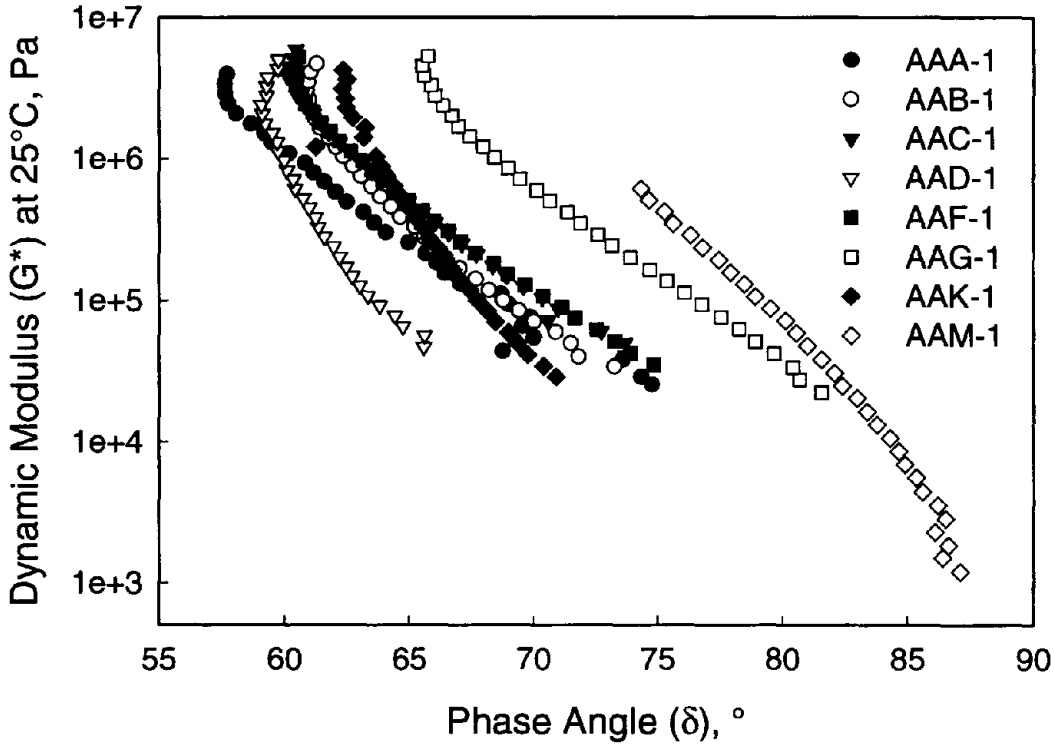

Figure 3-12. Black plot of G* vs. δ for mixtures of SEC Fraction-II of AAK-1 (75.2%) with SEC Fraction-I (24.8%) of eight SHRP core asphalts.

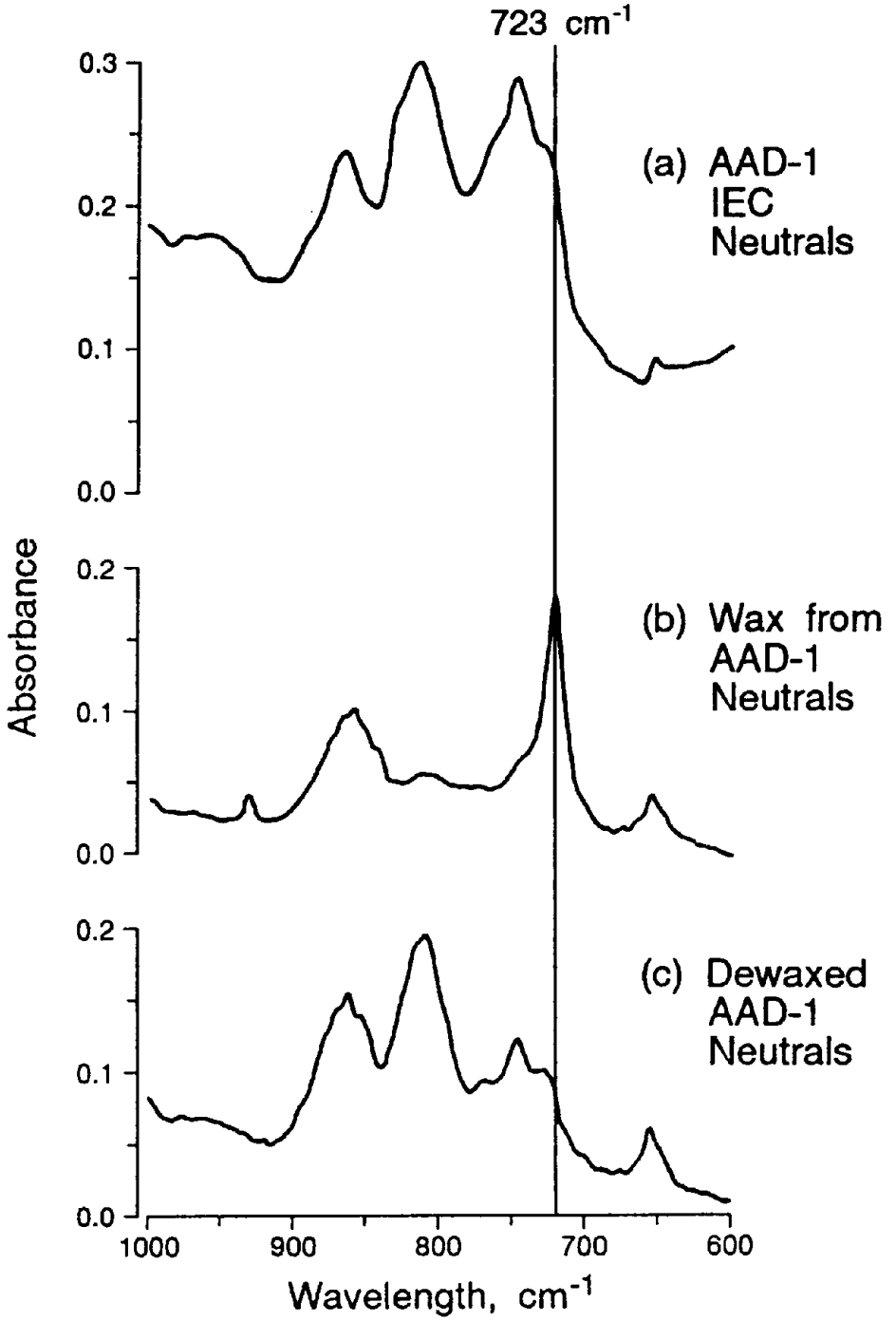

Figure 3-13. IR spectra of: (a) IEC neutrals of AAD-1; (b) wax from AAD-1 neutrals; and (c) dewaxed IEC neutrals of AAD-1.

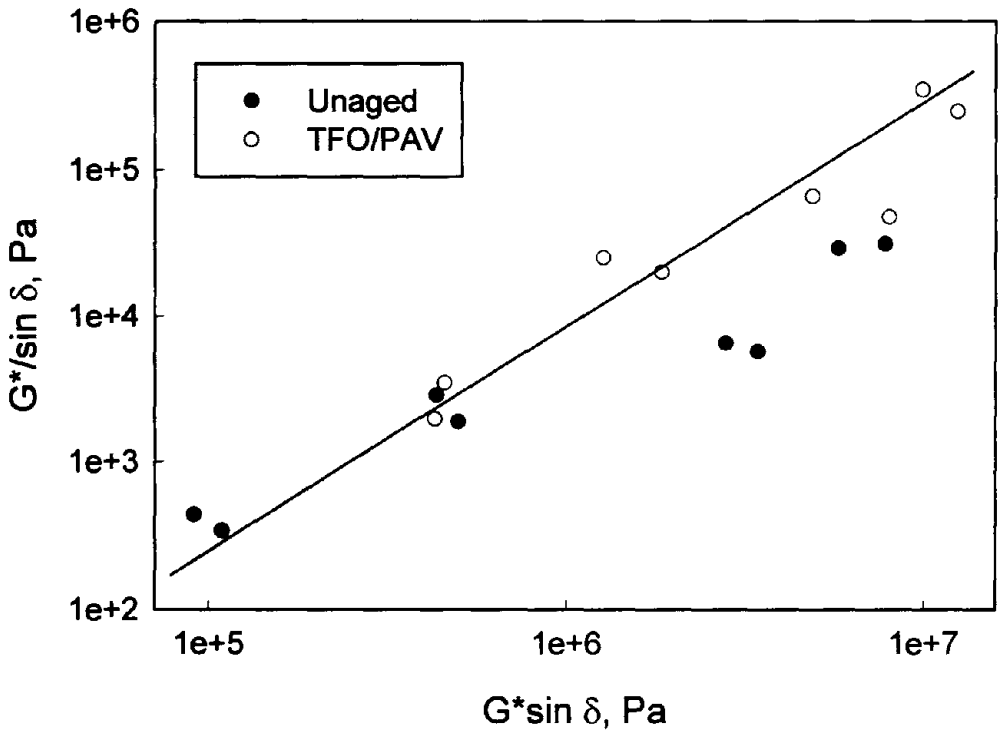

Figure 3-14. G*sin δ 25°C vs. G*/sin δ 60°C at 10.0 rad/s for unaged and aged crossblended mixtures of maltenes and asphaltenes of AAD-1 and AAF-1.

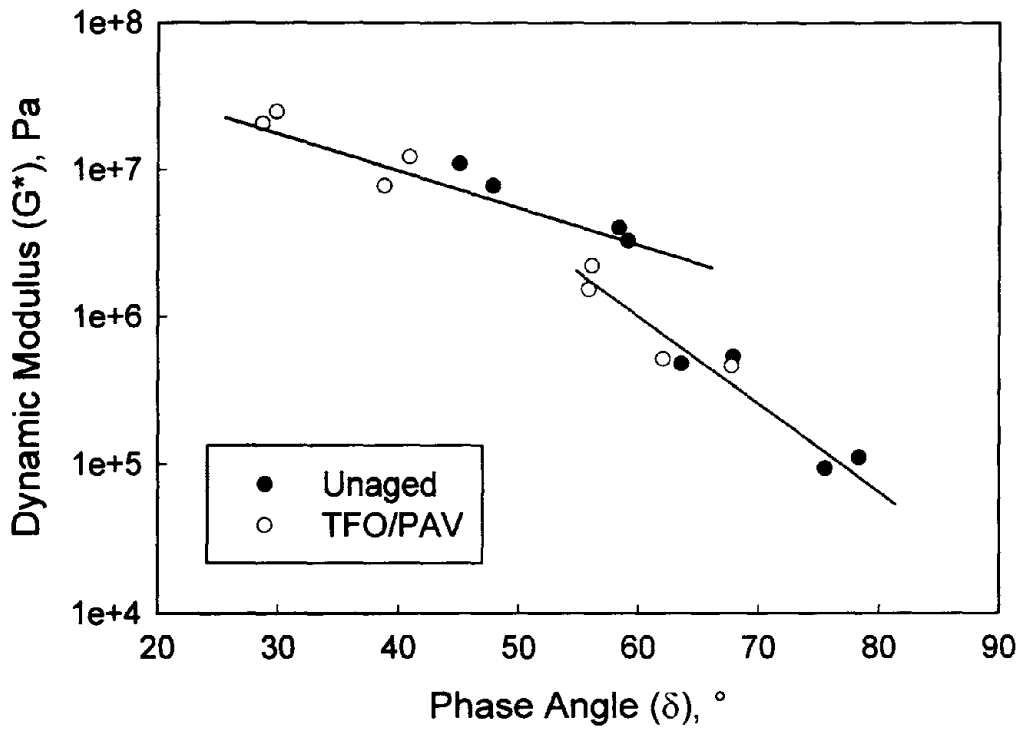

Figure 3-15. Black plot of G* vs. δ at 25°C and 10.0 rad/s for unaged and aged crossblended mixtures of maltenes and asphaltenes of AAD-1 and AAF-1.

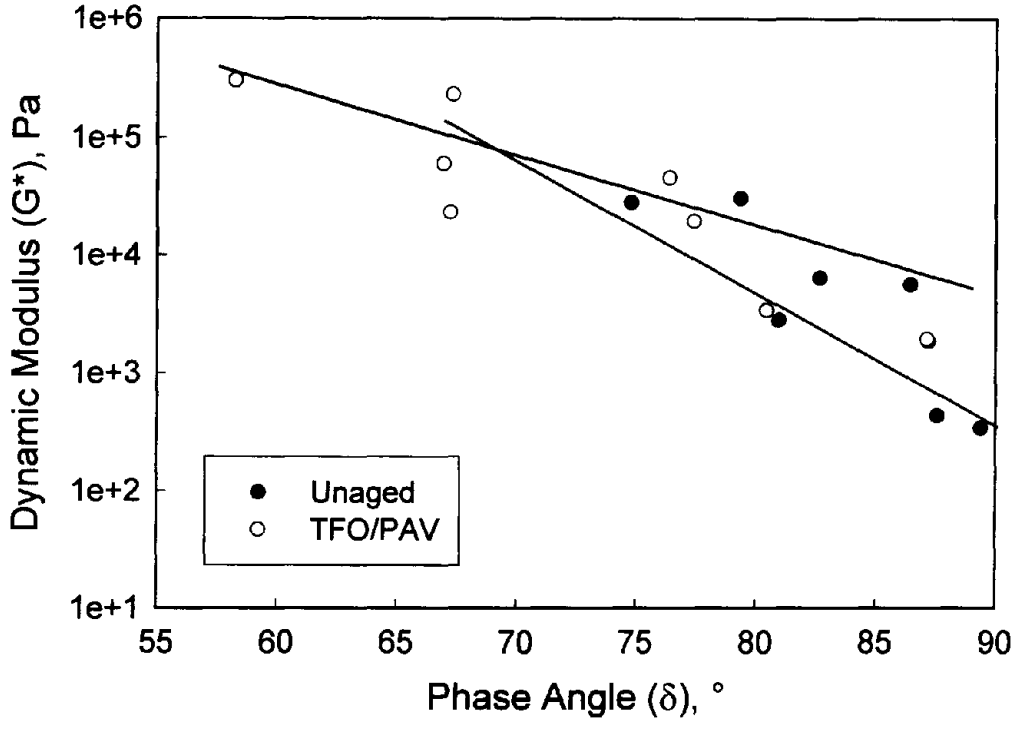

Figure 3-16. Black plot of G* vs. δ at 60°C and 10.0 rad/s for unaged and aged crossblended mixtures of maltenes and asphaltenes of AAD-1 and AAF-1.

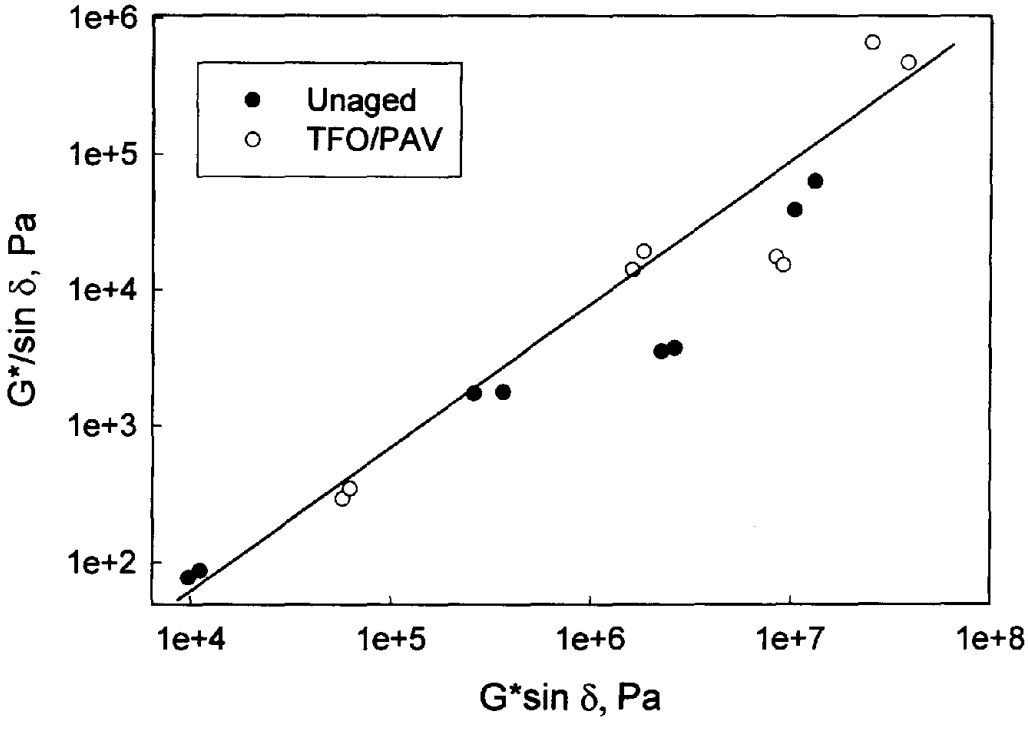

Figure 3-17. G*sin δ 25°C vs. G*/sin δ 60°C for unaged and aged crossblended mixtures of maltenes and asphaltenes of AAD-1 and AAG-1.

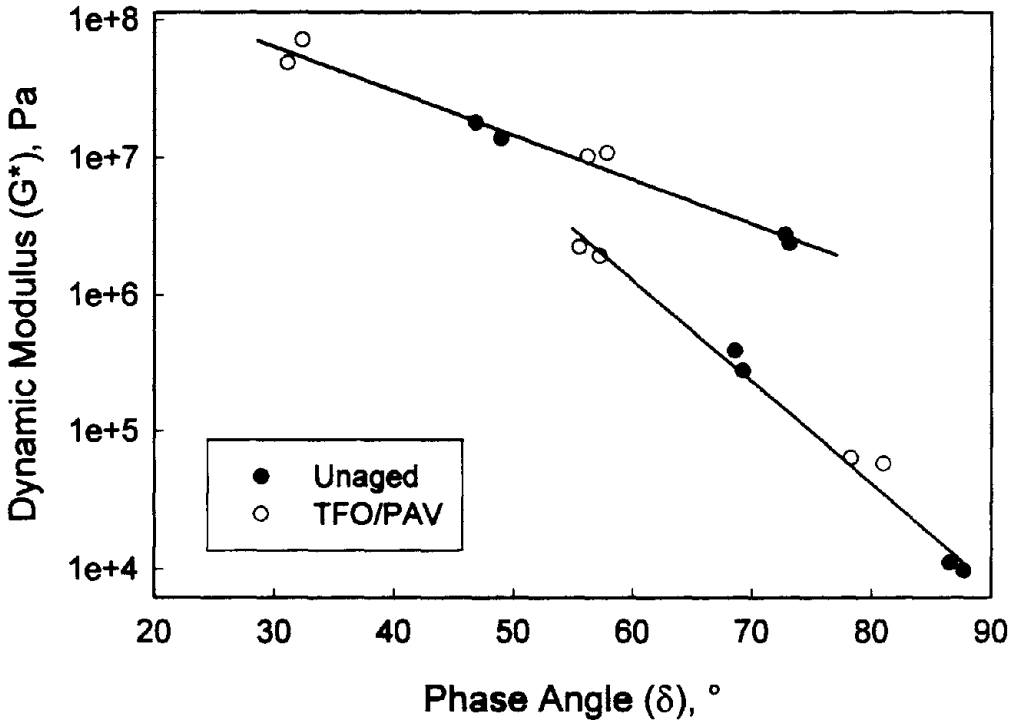

Figure 3-18. Black plot of G* vs. δ at 25°C and 10.0 rad/s for unaged and aged crossblended mixtures of maltenes and asphaltenes of AAD-1 and AAG-1.

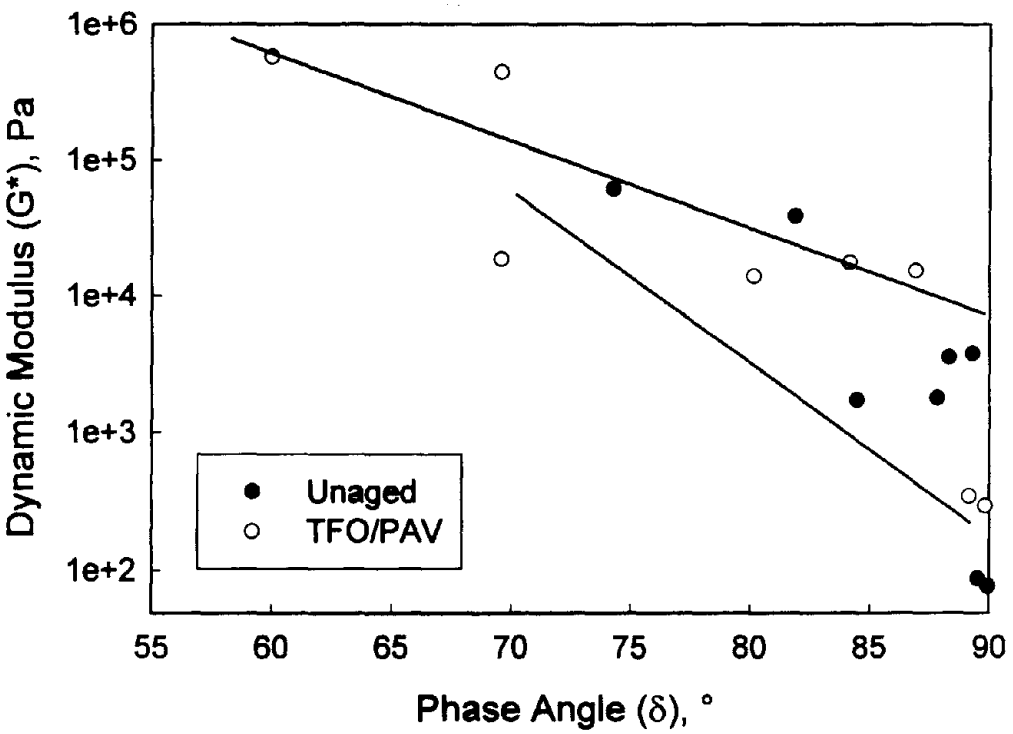

Figure 3-19. Black plot of G* vs. δ at 60°C and 10 rad/s for unaged and aged crossblended mixtures of maltenes and asphaltenes of AAD-1 and AAG-1.

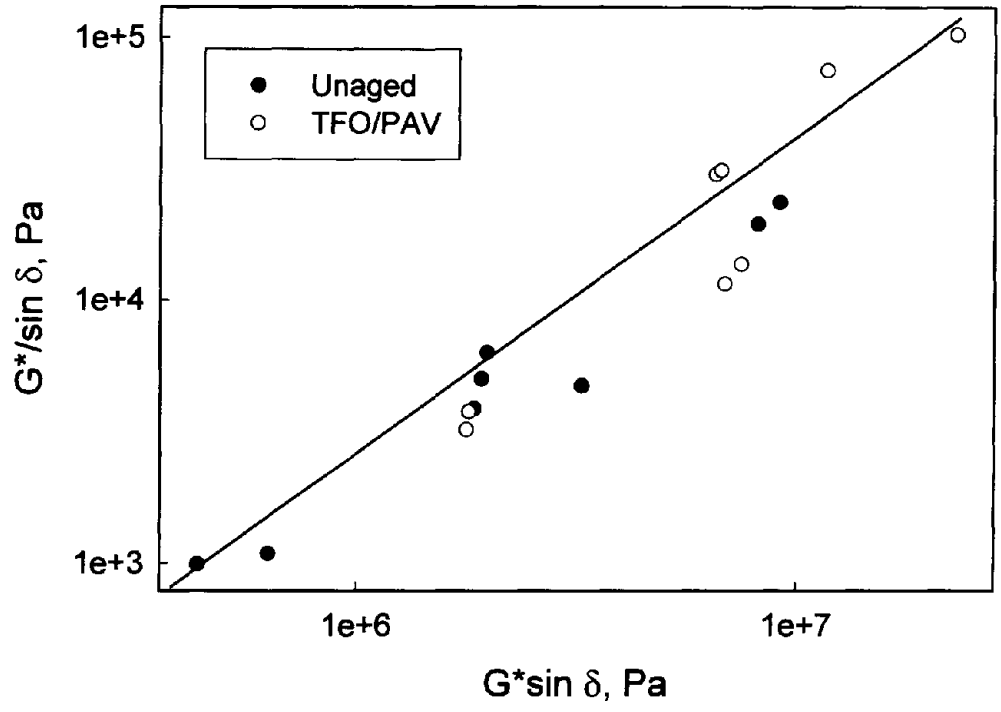

Figure 3-20. G*sin δ 25°C vs. G*sin δ 60°C for unaged and aged crossblended mixtures of maltenes and asphaltenes of AAF-1 and AAG-1.

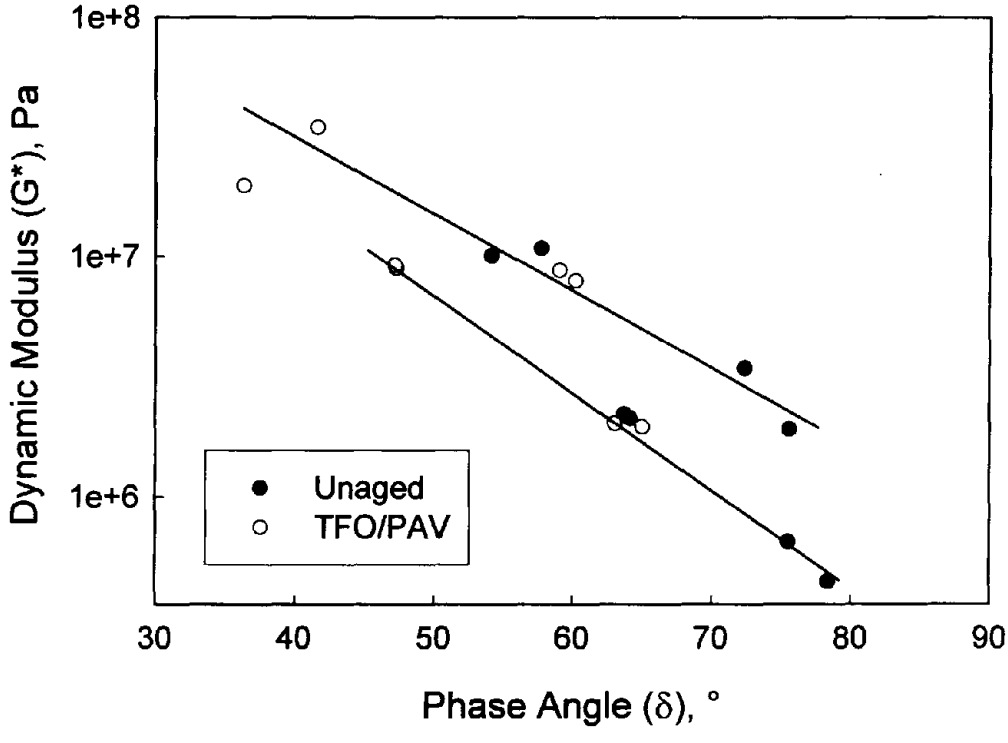

Figure 3-21. Black plot of G* vs. δ at 25°C and 10.0 rad/s for unaged and aged crossblended mixtures of maltenes and asphaltenes of AAF-1 and AAG-1.

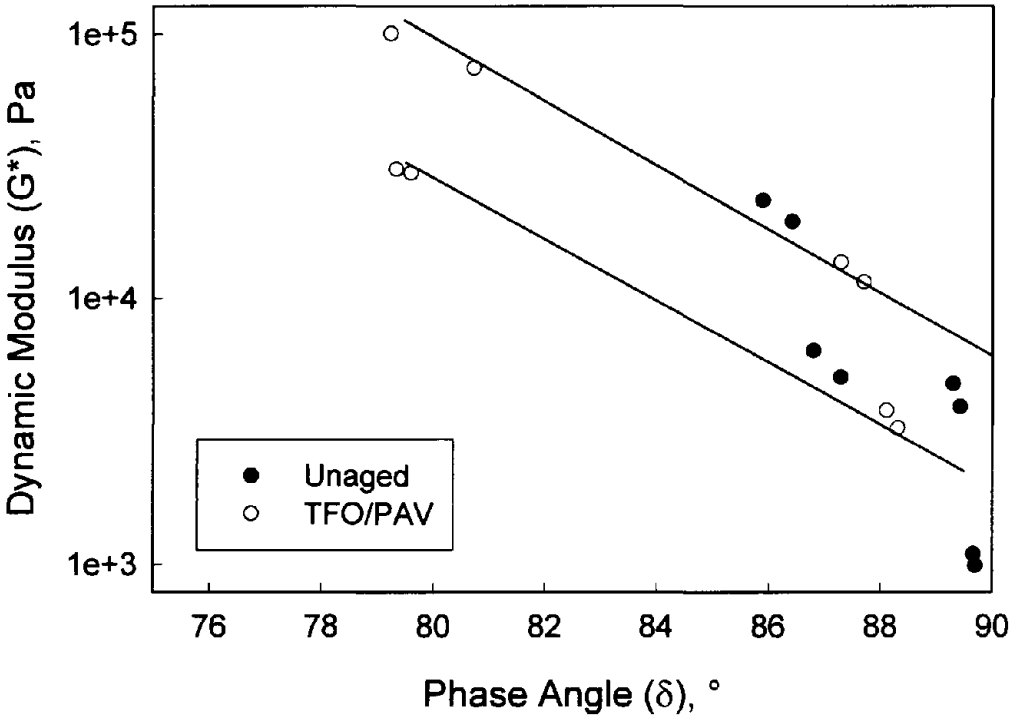

Figure 3-22. Black plot of G* vs. δ at 60°C and 10.0 rad/s for unaged and aged crossblended mixtures of maltenes and asphaltenes of AAF-1 and AAG-1.

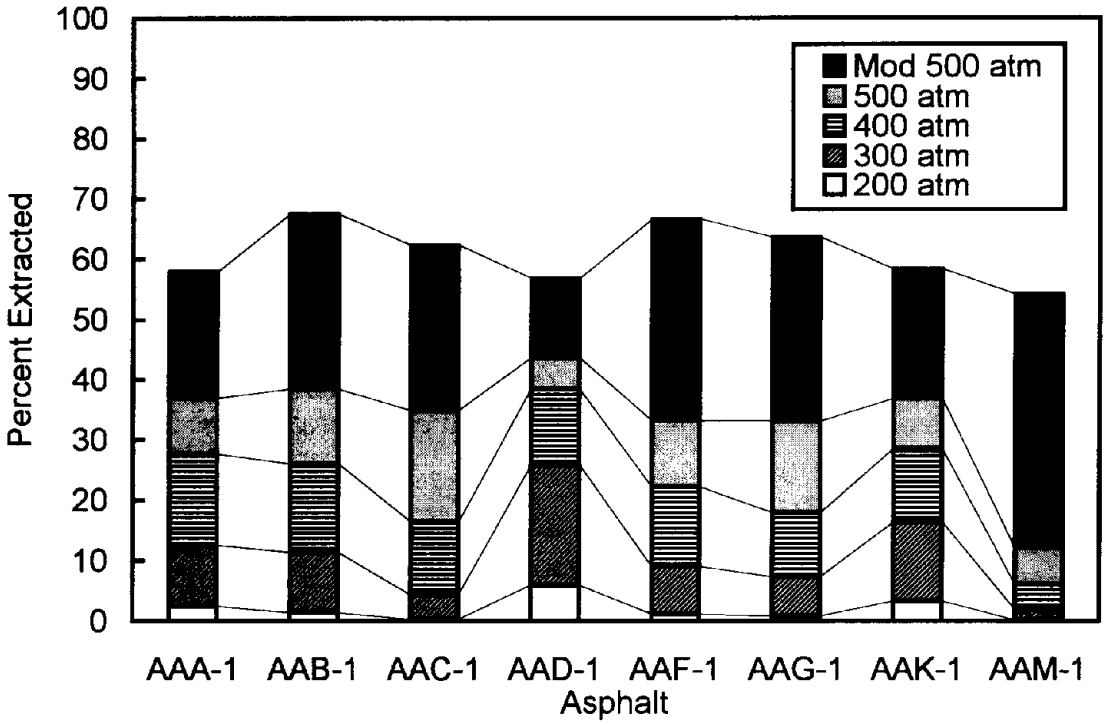

Figure 3-23. Percent of SFE fractions extracted from core asphalts by CO_2 and THF modified CO_2.

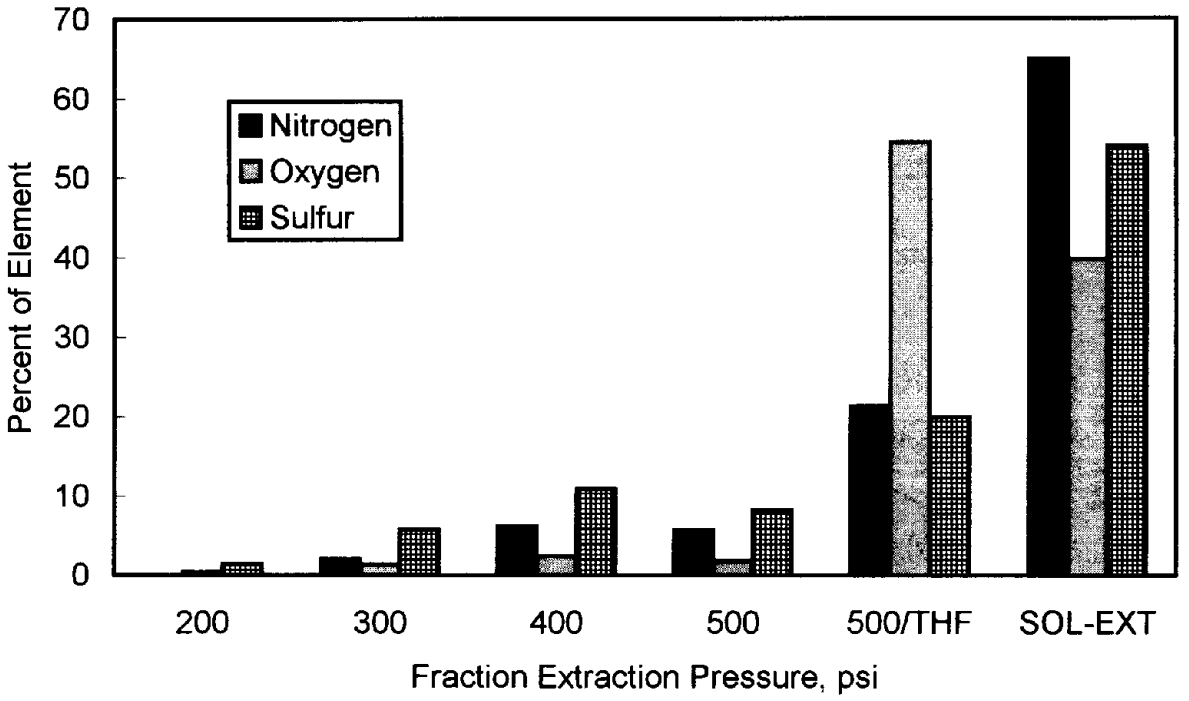

Figure 3-24. Heteroatom distribution in fractions obtained by SFE extraction of asphalt-aggregate mixtures and solvent extracts of asphalt-aggregate mixtures after SFE extraction.

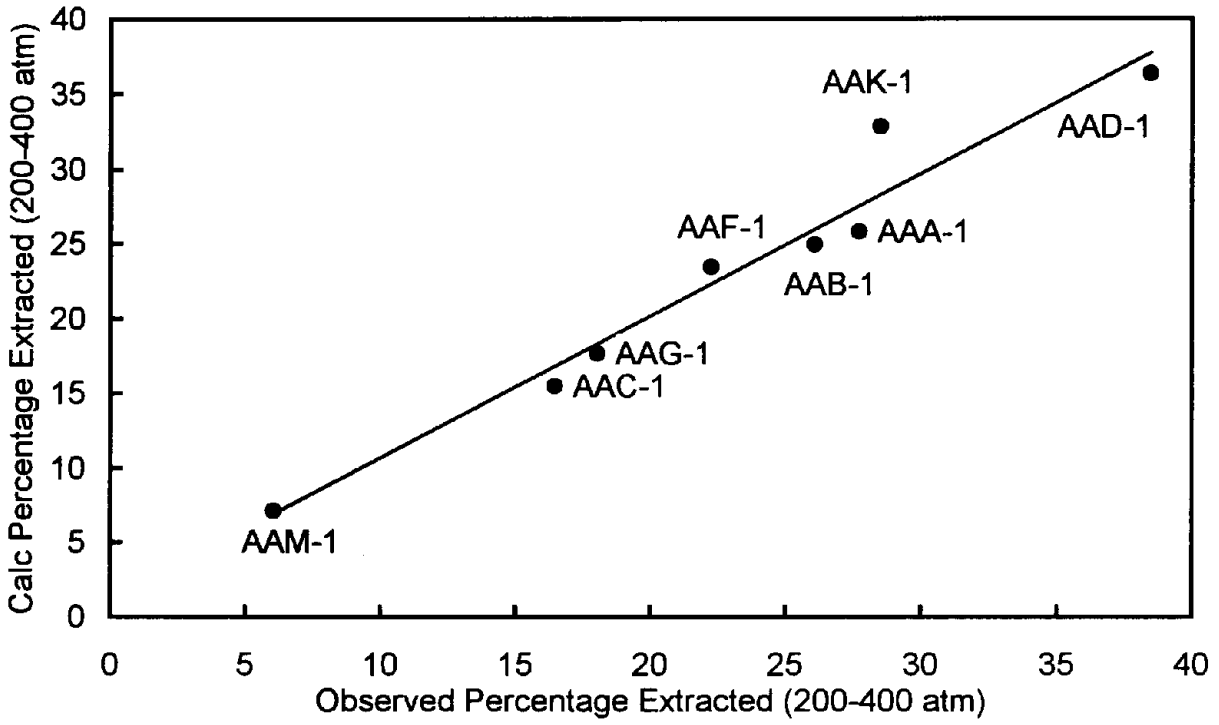

Figure 3-25. Comparison of experimental extraction yields with that of linear model based on heteroatom content.

SUMMARY OF SEPARATION RESULTS

Asphalts have been separated into various components by three different separation methods (IEC, SEC, and solvent precipitation), and the components have been characterized by various methods. The result of the experiments should provide support for or refute the model of asphalt structure advanced earlier.

It is known that petroleum residua are composed of a wide variety of compound types. This observation stands independently of any prediction by any model. Some of the compounds in asphalts are non-polar. Others are such highly polar organic compounds that they are not mutually soluble with the non-polar constituents, which comprise the bulk of the asphalts. There also exist compounds of intermediate polarity that solubilize, or peptize, the constituents that are by themselves incompatible.

Relatively non-polar compounds comprise 50-60 percent of asphalts based on separations by chemical compound type, e.g., IEC. The remaining compounds are fairly polar. They are present in such large amounts that there is certain to be interaction among them. If the solubility parameter values for IEC neutral fractions reported above are valid, i.e., that they are not at all polar, it is likely that there will exist in asphalts, at lower temperatures, distinct domains of polar, aromatic molecular associations. These molecular associations should consist of a variety of acidic, basic, and amphoteric compounds. All of the latter, and some of the acidic and basic components, are polyfunctional, and therefore are capable of engaging in extensive associations. The polyfunctional components are the major viscosity building components, and are responsible for the elastic properties of asphalts. The non-polar component is orders of magnitude less viscous than the parent asphalt. The viscosity of this component is a function of number-average molecular weight. The non-polar component greatly influences low temperature properties.

When asphalt molecular weight distributions are studied, it is found that there is a range over several tens of thousand daltons. These values are determined in toluene. Assuming that all of the entities larger than 2,500 daltons are really associations of many smaller components, then these associations persist in toluene. Effective molecular sizes of the associations in native asphalts probably are larger than in toluene. Even in toluene, the largest entities approach 40,000 daltons and comprise several percent of a given asphalt. This justifies the use of toluene as the SEC solvent. These large entities dominate rheological properties of asphalts and their existence rationalizes the resemblance of asphalts to polymers in rheological properties. The molecular size distributions of molecular associations in asphalts vary widely, accounting for unique properties of individual asphalts. Some asphalts contain large amounts of polar, associating molecules. These are the "incompatible" asphalts identified in the older literature, characterized by pronounced elastic properties and resistance to permanent deformation. Other asphalts contain smaller amounts of polar components or polar components that do not interact very strongly. These are the "compatible" asphalts of the older literature. As asphalt temperatures rise, or as shear is applied, polar associations tend to become smaller, and all asphalts probably become solution-like at high enough temperatures. At low temperatures, most of the low molecular weight solvent components of asphalts

probably are immobilized by the polar associations. If the wide variety of entities of differing molecular weights were not observed, then a different model of asphalt structure would be required than the one advanced previously. For all organic compounds and mixtures rheological properties are related to molecular weight values and molecular weight distributions. The low apparent molecular weight values of whole asphalts (compared with the molecular weights of polymers with similar rheological properties) cannot rationalize the rheological phenomena observed in asphalts. In the absence of true polymers, association phenomena must be postulated, and support for their existence has been found.

The validity of any model of asphalt structure is important when attempts to modify properties by use of additives are proposed. Of even more importance is the establishment of selection criteria for road asphalts. The criteria must be soundly based in the nature of the materials, which requires an accurate structural model of whole asphalts and knowledge of the way in which various components influence physical properties. In the next section of this chapter, the manner in which the various fractions discussed above affect low temperature properties is discussed. The necessity for separation of asphalts into generic fractions will be established.

LOW TEMPERATURE PROPERTIES

Introduction to Low Temperature Properties

The low temperature properties of asphalt binders are important because low temperature cracking is a primary asphalt pavement failure mode observed in cold climate roads. Low temperature cracking typically occurs during extreme low temperature weather, usually within the first year or two after pavement construction. This failure mode can be recognized by transverse cracks in the pavement caused by the inability of the asphalt binder to deform longitudinally at low temperatures to reduce stress. As the temperature of an asphalt binder decreases, its specific volume decreases. The glass transition is that temperature, T_g, at which large scale molecular motion is hindered on cooling or enabled by heating. As the temperature of an asphalt binder falls below T_g, the binder is transformed from a viscoelastic material to a brittle, amorphous solid. Since some reduction in specific volume occurs even below the glass transition temperature, internal stresses increase. In a roadbed, some shrinkage can occur laterally to relieve stress; however, longitudinally, the road length is effectively infinite, limiting shrinkage and stress relief. When the stresses exceed the asphalt binder's strength, the transverse cracks typical of low temperature cracking appear.

The glass transition temperature of an asphalt is dependent on the asphalt's chemical composition, which is determined by the petroleum source and subsequent refinery processing. The challenge for the asphalt producer is knowing what components and concentrations are important so that processing and blending of available petroleum stocks can reliably provide the needed asphalt properties.

One of the goals of this work is to identify those asphalt components that most strongly affect the glass transition and to quantify the extent of the effect. This goal could be achieved by measuring the glass transition by dilatometry, calorimetry, or rheology, or by methods that measure molecular motion such as NMR and IR [Lin et al. 1995]. The methods discussed in this chapter are based on differential scanning calorimetry (DSC), specifically, modulated differential scanning calorimetry (MDSC). The advantages of DSC and MDSC are speed, small sample size, and the capability of monitoring crystallization/association and melting phenomena as well as the glass transition. The details of the methods are described in Volume II, method 5.

Differential Scanning Calorimetry and Modulated Differential Scanning Calorimetry

DSC measures heat flow into and out of a sample (compared to a reference) as that sample is subjected to a temperature program [Wunderlich 1990]. The heat flow measured by a differential scanning calorimeter is a function of the heating rate, sample heat capacity, and any endothermic (e.g., melting) or exothermic (e.g., most crystallization) events occurring in the sample. This is summarized by:

$$dQ/dt = Cp\ dT/dt + f(t, T) \qquad (3\text{-}25)$$

where: dQ/dt = total heat flow, W/g
Cp = heat capacity, J/(g °K)
dT/dt = heating rate, °K/s
$f(t, T)$ = kinetic component, W/g

The first term on the right side of equation 3-25 is the heat-flow contribution due to heat capacity and heating the sample. Because there is a shift in heat capacity at the glass transition, this term contains the information about the glass transition. The second term on the right is the kinetic component, which comes from the time dependency of crystallization, melting, or chemical reactions. Difficulties arise with conventional DSC when searching for weak transitions and when analyzing systems with complex thermograms containing glass transitions and multiple overlapping exotherms and endotherms. The sensitivity of conventional DSC is proportional to the heating rate, as can be seen from equation 3-25. Unfortunately, the resolution is inversely proportional to heating rate.

MDSC is an adaptation in which the temperature (and, therefore, the heating rate) is modulated about an underlying heating or cooling program. The average temperature follows that of the conventional DSC; however, a periodic sinewave perturbation of the temperature is superimposed. This gives the advantage of providing a slow underlying heating rate for good resolution while still having short-duration high heating rates providing good sensitivity. Through signal processing of the resultant heat-flow signal, five thermograms (heat flow as a function of temperature) are produced: modulated heat flow, total heat flow, heat capacity, reversing heat flow, and non-reversing heat flow. The modulated heat flow signal is the measured heat flow to the sample. The total heat flow is calculated as the average of the modulated heat flow signal and is equivalent to the signal from a conventional differential

scanning calorimeter. The heat capacity is the ratio of the modulated heat flow amplitude divided by the modulated heating rate amplitude. It contains the sample heat capacity plus generally minor influences from changes in heat capacity caused by crystallization or other time-dependent phenomena. The reversing heat-flow signal is the product of the heat capacity and the average heating rate times minus one. The non-reversing signal is the difference between the total heat flow and the reversing heat flow. This signal contains time-dependent phenomena and any baseline irregularities that might have been in the total heat flow signal. With MDSC there is less uncertainty in selecting baselines and endpoints than in conventional DSC when analyzing where a change in Cp occurs, such as at the glass transition.

Glass Transition Properties

The glass transition is a fundamental property of amorphous materials, including asphalt binders. Below the glass transition temperature there is insufficient thermal energy in a material to allow large amplitude molecular motion. Without this motion viscous flow almost ceases, and the approach to a thermodynamic equilibrium state for a system such as asphalt is slow (this slow approach to equilibrium is called physical hardening). The glass transition, as described by Van Krevelen [1990],

> ". . . is a phase change *reminiscent* of a thermodynamic *second-order transition*. In the case of a second-order transition a plot of a primary quantity shows an abrupt change in slope, while a plot of a *secondary* quantity (such as expansion coefficient and specific heat) then shows a sudden jump.
>
> In fact T_g is *not* a thermodynamic second-order transition, but is kinetically controlled. The exact position of T_g is determined by the rate of cooling; the slower the cooling process, the lower T_g. Yet, for practical purposes one can say that every polymer is characterized by its own T_g."

The glass transition has been studied extensively in the polymer sciences because it marks a distinct change in polymer properties as a function of temperature and, thus, is important to tailoring product properties. Many excellent texts have been written containing large sections about the glass transition and its relation to physical and mechanical properties of polymeric materials [Wunderlich 1990; Van Krevelen 1990; Turi 1981; Turi 1997; Sperling 1992]. Three main theoretical developments have been applied to the glass transition: the free-volume theory, the kinetic theory, and the thermodynamic theory. Sperling [1992] discusses the development of these theories in detail. For the purposes of this discussion, it is only important to recognize that the glass transition depends on the thermal history of a sample and on the method used. Comparisons of glass transition temperatures should be made with this in mind.

Some of the early research on polymers is relevant to the study of behavior near the glass transition in asphalts and asphalt components. For example, it is generally recognized that the glass transition temperature increases with increasing molecular weight. This was formalized in an expression from Fox and Flory [1950] for weakly interacting molecules:

$$T_g = T_{g\infty} - K/M_n \quad (3\text{-}26)$$

where K is a constant, $T_{g\infty}$ is a limiting transition temperature at high molecular weight, and M_n is the number average molecular weight. The use of M_n rather than the mass-average molecular weight shows the importance of small molecules in controlling low temperature behavior. This can also be recognized as showing the importance of the concentration of molecular chain ends on low temperature behavior.

It has also been recognized that the glass transition temperature of a homogeneous blend of two polymers can be described by the Fox [1956] equation:

$$1/T_g = w_1/T_{g1} + w_2/T_{g2} \quad (3\text{-}27)$$

where T_g, T_{g1}, and T_{g2} are the glass transition temperatures of the whole blend, component 1 and component 2, and w_1 and w_2 are the mass fractions of the two components. Generalizing this relationship to multiple components gives

$$1/T_g = \Sigma\,(w_i/T_{gi}) \quad (3\text{-}28)$$

where, in this case, the summation is over all fractions, i [Gupta 1995]. With this relationship, one can calculate the relative influence of a single component on the T_g of a mixture. It may also allow us to identify fractions that do not blend homogeneously with others. This is common in polymer blend characterization where multiple T_g's indicate inhomogeneities due to incomplete mixing or immiscibility.

As stated previously, asphalts are extremely complex materials containing literally millions of different molecular species. Components of the asphalt can be crystalline, amorphous solids, or liquids, depending on temperature and thermal history. In addition, under typical usage, the asphalt is in contact with mineral aggregate and is exposed to oxygen and moisture for long periods over a potentially wide temperature range. These conditions cause continuing changes in the asphalt binder chemical composition and mechanical performance. This complexity has led to the simplification of this study by examining chemically distinct asphalt components using techniques adapted from polymer and petroleum sciences.

Measurements on Strategic Highway Research Program Core Asphalts

DSC/MDSC experiments were conducted on the SHRP asphalts to provide a base for evaluating the effects of dopants and asphalt components. Glass transition parameters were measured from the modulated heatup portion of each MDSC experiment after annealing at or above 150°C (302°F) and cooling at 10°C/min (18°F/min) to below -60°C (-76°F). Annealing is performed to ensure that each sample has a known thermal history. The annealing presumably breaks up most residual intermolecular associations (which are held together by weak bonds and are thermally labile) and resulting structuring (see section on steric hardening, chapter 5) due to the prior thermal history, which may be unknown. In any event, all samples are measured after this identical pretreatment. Glass transition measurements can also be made

on the cooling profile for simple experiments. However, to compare results from a variety of experiments where isothermal soaks may or may not be used during the cooling cycle, measurements must be performed during heating.

The results of DSC/MDSC analyses on SHRP asphalts are shown in table 3-41. The parameters were calculated both with the standard instrument software (T_g, Onset, End) and with a Gaussian curve-fit method (ΔCp). Onset- and end-temperatures are the low and high temperature limits of the glass-transition region as selected by the instrument software. T_g is selected at half the change in heat capacity, C_p, in the transition. ΔT is the width of the transition (end-temperature minus onset-temperature). The cumulative Gaussian line shape (with an underlying slope) fit to the thermogram provides the height of the transition at T_g, ΔC_p. Crystallizable fractions (CF) are calculated from melting or dissolution endotherms observed on heating. Measurements are continuing to provide more data than are listed in table 3-41.

One of the desired products of this work is the development of techniques and relationships that allow rapid estimations of pavement properties and specification measurements. The low-temperature Superpave® binder PG specification is based on bending beam rheometer (BBR) tests on PAV aged binders. The procedure takes a day to complete and requires approximately 12 grams of binder per beam. Recently, Memon and Chollar [1996] reported a correlation between the glass transition temperature measured by modulated DSC and the temperature at which the m-value (m is the rate of change of stiffness with respect to log of time) determined on the BBR equals 0.3 for unaged (and not modified), chemically modified, polymer modified, and crumb rubber modified asphalts (CRMA's). Our work with unaged asphalts (table 3-41) also indicates some correlation with low-temperature specifications but with some differences. Using data from Anderson et al. [1996], the temperatures at which stiffness (S) equals 300 MPa and m equals 0.3 are plotted in figure 3-26 against our measured glass transition temperatures. Clearly, there is a good correlation between the S-derived temperatures and the glass transition temperatures. The correlation with m-derived temperatures is not good ($R^2 = 0.40$), but the data distribution does not appear random. The SHRP low temperature specification is obtained from either S or m data, whichever gives the highest temperature. If the temperature at which m = 0.3 is higher than the temperature for S = 300 MPa, then m is controlling the specification. The correlation with the specification-controlling temperatures (S or m) results in $R^2 = 0.71$. The correlation in figure 3-26 ($R^2 = 0.95$) addresses the cases where S is controlling but not m.

The distribution of m-derived points in figure 3-26 is in some ways similar to that seen in plots of rheological defining temperature from dynamic shear rheometry versus the glass transition temperature of asphalts. The shapes of these plots were found to depend, in part, on the crystallizable fractions or wax contents of the asphalts. To pursue this idea, the wax contents of the asphalts have been plotted to highlight S- and m-controlling asphalts (figure 3-27). In general, low-wax asphalts are S controlled and high-wax asphalts are m controlled. This suggests that the differences between m-derived temperatures and S-derived temperatures in figure 3-26 might be proportional to wax content or crystallizable fraction. In figure 3-28, simple linear combinations of glass transition temperature and wax content and crystallizable

fraction are found to estimate the controlling temperature (the greater of S- and m-derived temperatures) very well. The crystallizable fraction gives a slightly better correlation and has the advantage of being obtainable from DSC thermograms.

Based on the discussion in the previous paragraph, it appears that the m-value "adjusts" the low temperature specification for the presence of crystallizing materials, which are probably mostly waxes. These materials, which melt and crystallize in the normal use range of pavements, must have effects on performance. If nothing else, crystals, when formed, might be centers of crack initiation.

Measurements on Asphalt Components

Asphalts were fractionated by several methods in the SHRP research and in this FHWA-supported work. Solvent precipitation methods generated heptane asphaltenes and maltenes, and iso-octane asphaltenes and maltenes. Several different fractions were obtained by SFE using carbon dioxide (CO_2). Molecular size separations, by SEC, provided fractions of varying degrees of molecular association and molecular weight. Separations by polarity or functionality were performed using IEC. These separation methods were discussed earlier in this chapter. The types of fractions prepared and their relative amounts are shown in figure 3-29 for asphalt AAA-1 (except for the SFE fractions, which are from AAD-1). The bars in figure 3-29 are configured so that the most polar or associated material is near the top (the relative placements of strong acids and strong bases are arbitrary, as are the placements of weak acids and weak bases relative to one another), while the solvent or least polar material is lower on the bar. There is a rough correspondence between the amount of maltenes separated by either of the two solvents and the amount of SEC Fraction-II material. Maltenes and SEC Fraction-II materials must contain IEC neutrals, weak acids and bases, and some strong acids and bases. Extracts from supercritical fluid extraction using CO_2 are not as easily related to the other fractionation methods, but are believed to be relatively non-polar and low molecular weight materials, except when a solvent modifier is used along with CO_2.

IEC Fractions

IEC produces defined chemical fractions (neutrals, strong acids, strong bases, weak acids, and weak bases), not solubility classes. The IEC neutral fractions comprise all non-polar asphalt components, which make up 50-60 percent of neat asphalts. The IEC neutral fractions used in this study were prepared in the SHRP program using the methods described in the *Binder Characterization and Evaluation* final report Volume 4 [SHRP 1994]. These materials are relatively volatile, losing weight at high annealing temperatures. The DSC/MDSC methods were modified to limit the high temperature to 100°C (212°F) to minimize sample weight loss.

DSC/MDSC results from analyses of neutrals show narrow glass transitions located 10°C (18°F) or more below the transitions for the whole asphalts. Individual thermograms are complex with substantial exo- and endothermic excursions caused by crystallization and melting. The glass transition temperatures are plotted as a function of reciprocal molecular weight by VPO [SHRP 1993] in figure 3-30. Also shown are data for two "weak neutrals"

samples. These more polar samples are composed of the neutrals plus the weak acid and weak base fractions. A linear least squares fit to the neutrals data produces an expression in the form of equation 3-26 where $T_{g\infty}$ = -17.5°C (0.5°F) and K = 12,728°C·g/mol. Presumably, this relationship fits the data because the IEC neutrals contain similar, relatively noninteracting, molecules. As expected, the addition of weak acid and weak base fractions increases the glass transition temperature because of increased intermolecular interactions. Since glass transitions only occur in amorphous structures and since substantial crystallization occurred during cooldown in these tests, the glass transition temperatures measured are properties of the portion of the IEC neutrals that did not crystallize.

SEC Fractions

In addition to separating asphalts into defined chemical fractions by IEC, asphalts have been separated into fractions of different molecular sizes by means of SEC. In an SEC separation of asphalts, the largest entities elute first, followed by those of moderate size, and the smallest molecules elute last. SEC fractions are isolated using a preparative SEC method described in detail in Volume II, method 15 and elsewhere [SHRP 1994]. Two collection schemes are applied to the SEC separations. In the first, eluate is collected in nine samples; in the second, two samples were collected. The SEC 1 (or I) fraction contains the largest molecular size materials. Fractions 2-9 have decreasing molecular sizes. Fractions 8 and 9 are combined with fraction 7 to provide enough material for analyses. The combined fractions 7 through 9 will hereafter be termed SEC 7. The second collection scheme produces two samples: SEC Fraction-I and SEC Fraction-II. SEC Fraction-I is equivalent to SEC 1, and SEC Fraction-II is equivalent to the combined samples SEC 2-9. The cut point between SEC 1 and 2, and SEC Fraction-I and II, is the onset of fluorescence in the eluate. The lack of fluorescence in the largest size material is believed to indicate quenching due to molecular association. It is important for the purposes of this discussion to also recognize that these separations are performed on solutions of asphalts in toluene, not in the condensed phase. DSC/MDSC experiments were conducted as described earlier with the maximum temperature limited to 100°C (212°F) to reduce weight loss during testing.

Glass transition temperatures for the SEC fractions are plotted against reciprocal molecular weights in figure 3-31. SEC Fraction 1 of each asphalt is on the left side of each plot with higher fractions following in order. Obviously, the Fox-Flory relationship expressed in equation 3-26 cannot describe the SEC data. The curves for each asphalt, however, follow a similar pattern. The T_g values of most of the high molecular weight SEC-1 fractions are relatively high. The T_g values of the SEC fractions of somewhat lower molecular weight are, except for AAM-1, considerably lower. As the molecular weights of the SEC fractions become even lower, a T_g minimum is observed. The lowest molecular weight SEC fractions have relatively high T_g values. This increase in glass transition temperature may be caused by the presence of low molecular weight, weakly polar materials in the asphalts. These fractions may contain some of the weak acid and weak base moieties responsible for the increased molecular interactions noted in the earlier discussion of the "weak neutrals." These materials are solvated in the toluene solution passing through the SEC column, but interact significantly in the condensed phase examined with the DSC. It was observed that SEC fraction 6 of asphalts

AAB-1 and AAM-1 has increased nitrogen, oxygen, and sulfur content compared with SEC fractions 2-5. Huynh et al. [1978] reported similar increases in glass transition temperatures in low molecular weight SEC fractions.

The glass transition temperature of the SEC Fraction-II materials of each asphalt can be compared with the result of applying equation 3-22 to the glass transition temperatures of SEC fractions 2-7. For asphalts AAA-1, AAC-1, and AAF-1, the difference is less than 3°C (5°F). Asphalt AAD-1 shows a difference of about 7°C (13°F), indicating less component compatibility than in the other three asphalts.

Experiments were conducted on mixtures of SEC Fraction-I and SEC Fraction-II materials to evaluate the relative influence of the SEC Fraction-I materials on the glass transition of the mixtures. The SEC Fraction-II moiety of a core asphalt was mixed with SEC Fraction-I moieties from all eight core asphalts at the natural abundance level of the asphalt from which the SEC Fraction-II was obtained.

DSC results for blends show that the SEC Fraction-I source asphalt has little influence on the glass transition except for SEC Fraction-I from asphalt AAM-1 (figure 3-32). Since asphalts AAM-1 and AAF-1 are solvent deasphaltened in the refining process, they might be expected to behave somewhat differently than the other core asphalts. The SEC Fraction-II moiety determines the base glass transition temperature. Addition of SEC Fraction-I shifts the transition temperature. The minor deviations from the like/like blends may be indicative of the relative solvent strengths of the SEC Fraction-II materials for the SEC Fraction-I materials. If the SEC Fraction-II component in a crossblend is a stronger solvent than the SEC Fraction-II from the same source asphalt as the SEC Fraction-I component, polar materials from the SEC Fraction-I will be added to the solvent phase of the blend. This raises the glass transition temperature of the crossblend above that of the like/like blends. The opposite would be true for weak solvent power SEC Fraction-II materials; the blend's glass transition should be lower because solvent polar materials move to the SEC Fraction-I, which is the dispersed phase discussed earlier. With one exception, the shift in glass transition temperature is only weakly dependent on the source of the SEC Fraction-I. For all blends of SEC Fraction-II materials containing SEC Fraction-I from asphalt AAM-1, the blend has a lower T_g than the whole SEC Fraction-II of the source asphalt.

Asphaltene/Maltene Mixtures

It is emphasized throughout this report that asphalts are complex mixtures of many different kinds of organic compounds. These individual compounds may differ from one another greatly in both polarity and molecular size or they may closely resemble each other in these properties. The more polar compounds will interact with one another by hydrogen bonding, π-π interactions, or other weak forces to form molecular associations (self assemblies) of varying strengths and sizes.

In the previous section it was shown that the source of the dispersed component, SEC Fraction-I, had only a minor effect on T_g. A difference between SEC Fraction-II T_g's and the

neat asphalt T_g's, however, does indicate that the amount of SEC Fraction-I influences low temperature properties. The effect of varying the concentration of the dispersed component is seen in asphaltene-maltene mixtures. Heptane asphaltenes, maltenes, and asphaltene-maltene mixtures of varying concentrations were prepared during SHRP. Descriptions of the preparation and properties of these samples are contained in the SHRP final report [SHRP 1993]. Six asphalt sets have been examined: AAA-1, AAD-1, AAF-1, AAK-1, and two sets of AAG-1 (two different ranges of asphaltene content).

DSC results for the five asphalts and mixtures of their maltenes and asphaltenes (prepared in the SHRP) are shown in figure 3-33. The addition of asphaltenes to the maltenes has little effect on the onset temperature (low temperature extreme) of the glass transition. There is no significant variation of onset temperatures except at very high asphaltene contents, as seen at the 40 percent level for asphalt AAK-1. The glass transition end temperature (high temperature extreme), however, is sensitive to asphaltene content. Increasing asphaltene concentration results in higher transition end temperatures and, as a result, wider glass transitions, ΔT_g (end to onset temperature), a sign of decreasing system compatibility and increasing homogeneity. Glass transition temperatures (selected at one-half the transition height), which are usually near the middle of the transition, follow the same trend. Transition end temperatures for all asphalts show rapid increases at asphaltene concentrations between 5 and 15 mass percent, indicating some change in structure or decrease in system compatibility. It is in this concentration range that Storm et al. [1995b] suggest the occurrence of the critical concentration for asphaltene association. Results for asphalt AAG-1 show a similar variation with asphaltene content. However, asphalt AAG-1 is the only asphalt examined with a natural asphaltene abundance below the level of the rapid increase. This may indicate that asphalt AAG-1 is more solution-like. The overall increase in T_g for asphalt AAG-1 is 0.41°C/mass percent (0.74°F/mass percent) of asphaltenes compared with 0.34, 0.47, 0.54, and 0.43°C/mass percent (0.61, 0.85, 0.97, and 0.77°F/mass percent) for asphalts AAA-1, AAD-1, AAF-1, and AAK-1, respectively. The peptizing power of the maltenes (p_0) and the state of peptization (P) of asphalt AAG-1 have been shown to be exceptionally high in Heithaus tests [Pauli 1995], which measures overall compatibility of maltene-asphaltene mixtures.

Another way of examining the asphaltene-maltene blend data is shown in figure 3-34 where all the data are plotted on the same scale. The increase in glass transition temperature with increasing asphaltene content is described well using a single average slope of 0.433°C/mass percent (0.779°F/mass percent)and a different zero intercept (maltene T_g) for each asphalt. As was shown in the SEC Fraction-I/SEC Fraction-II crossblending study, the dispersed phase materials, asphaltenes or SEC Fraction-I, have a common, approximately linear and mostly source-independent effect on glass transition temperatures. The largest contribution to neat asphalt glass transition temperature comes from the solvent-like materials such as SEC Fraction-II and maltene fractions. If maltene glass transition temperatures can be predicted, the neat asphalt temperatures can be calculated from the relationship discussed above.

Supercritical Fluid Extracts

Samples of the eight SHRP core asphalts were fractionated using SFE techniques. A more detailed discussion of this procedure was presented earlier in this chapter. The fractions were extracted sequentially from a 6 mass percent mixture of asphalt coated on an aggregate. The conditions selected were (1) 200 atm CO_2, (2) 300 atm CO_2, (3) 400 atm CO_2, (4) 500 atm CO_2, and (5) 500 atm CO_2 modified with 20 vol percent THF. All of the extractions were performed at a temperature of 115°C (239°F). The amounts of fractions generated using these conditions have been reported [Barbour et al. 1997].

DSC/MDSC experiments were run on the extracts from the SFE's, and the results exhibit some interesting trends. Increasing the extraction pressure results in the extraction of materials with higher glass transition temperatures (figure 3-35). With two exceptions, plots of the glass transition temperatures as a function of extraction pressure are parallel. The exceptions are the AAM-1 extracts, which have a much lower slope but still show a linear relationship with extraction pressure, and one set of AAD-1 extracts that have a higher slope. The extracts from AAG-1 are shifted to higher glass transition temperatures compared with the other asphalt extracts.

Supercritical CO_2, at pressures up to 500 atm, extracts relatively non-polar, low molecular weight materials. If the extracts have little intermolecular interaction, the glass transition temperatures of the extracts should exhibit a Fox-Flory dependence (equation 3-26) on the number-average molecular weights of the extracts. Molecular weights are not available, but the average carbon number of each extract has been estimated by SFC. A plot of the glass transition temperatures for the extracts versus the inverse average carbon numbers reveals limited Fox-Flory behavior (figure 3-36). For the extracts from each asphalt, there is a linear relationship between the glass transitions and the inverse carbon numbers. The line for each asphalt, however, has a different intercept and slope. The differences may be caused by variations in the concentrations of weakly polar molecules. This would be consistent with the data for IEC neutrals and weak neutrals discussed above.

Wax Effects

The wax content of asphalts concerns many in the asphalt industry. There is a tendency to distrust high wax asphalts, based primarily on anecdotal evidence. The precipitation or separation of waxes from petroleum is a familiar phenomenon. Unlike petroleum, the crystallization or association of waxes in asphalts may be hindered by the high viscosity of the asphalt. Most waxes found in asphalts are long chain n-alkanes or iso-alkanes that form semicrystalline associations at temperatures dependent on the source of the asphalt. Generally, wax association and dissolution occurs in a temperature range coinciding with pavement service temperatures and with asphalt binder low temperature specification measurement temperatures. In asphalt pavements, melting waxes might promote microfracture healing, but multiple temperature cycles may form larger crystals, which may contribute to fatigue damage. Certainly, the slow association or crystallization of waxes complicates the measurement of low temperature properties of asphalts, including low temperature specification measurements.

Many procedures can be used to separate waxes from petroleum and petroleum products, and each produces a wax unique to that procedure. In some crude oils, waxes are concentrated using a solvent precipitation method. When applied to asphalts, this simple, one-step method results in the precipitation of much polar material along with waxes. Thus, waxes concentrated from asphalts by this method are highly impure. A purer wax fraction may be isolated from asphalts by a two-step procedure. Polar and non-polar components first are separated by IEC. Then the non-polar components (neutrals) are dissolved in toluene, and methyl ethyl ketone is added to the chilled solution to precipitate waxes. Asphalts used in this study contain wax contents ranging from about 1 mass percent to about 29 mass percent [McKay et al. 1995] as measured by the two-step procedure. The waxes and asphalt-wax blends used in this work were prepared for the doping studies discussed earlier in this chapter. These were the samples available when the DSC work was performed.

Wax samples were examined using the DSC/MDSC techniques described above with minor modifications. Crystallization exotherms were integrated in both the unmodulated cooldown and the modulated heatup signals (the melting endotherm gives close to the same value). Crystallization during heating, termed cold crystallization, was commonly observed in these fractions. The total exotherm areas in Joules per gram of asphalt were converted to crystallized fractions using a value of 200 J/g of crystallized material [Claudy et al. 1991], which assumes the crystallized material is predominantly long chain, normal alkanes forming good crystals. The crystallization of waxes in asphalts is known to be time dependent [Claudy et al. 1991], meaning that cooling rates and profiles may significantly influence the DSC-measured crystallized fractions. For a given thermal history, as in this DSC study, the crystallized fraction is a function of both the wax content and the rate of formation of wax crystals for each asphalt.

Asphalts AAB-1, AAF-1, and AAG-1 were dewaxed in one step by solvent precipitation. This procedure yields a dewaxed asphalt and a wax concentrate, which contains polar impurities, as explained above. DSC/MDSC thermograms for the wax concentrates show little evidence of any glass transition, but have large crystallization exotherms during cooling. The dewaxed asphalts have smooth, well-defined glass transition profiles and only minor crystallization exotherms. Crystallized fractions of the whole asphalts range from 0.2 mass percent for AAG-1 to 2.5 mass percent for AAB-1. The ratio of crystallized fraction to wax content for the AAG-1 wax indicates that only 3 mass percent of the AAG-1 wax contributes to the crystallization exotherms compared with 8 mass percent and 13 mass percent for AAB-1 and AAF-1 waxes. In general, the same can be said for the contributions of the waxes in the whole asphalts. The crystallized fraction-to-wax content ratios for the whole asphalts are similar to those for the waxes. Compared with the glass transition temperatures of the neat asphalts, none of the three asphalts show any improvement (decreasing T_g) with increasing wax content, though asphalt AAF-1 shows almost no sensitivity to wax content at all. In asphalt AAG-1, each percent of wax added increases the glass transition temperature by 1°C (1.8°F).

Waxes isolated from asphalts using the two-step procedure do not contain polar impurities. These waxes have been added in small amounts as "dopants" to various asphalts. The effect of wax content on glass transition temperature is quantified using a dopant

efficiency term defined as the magnitude of the shift in glass transition in °C divided by the amount of dopant added in mass percent. A similar expression is used in the polymer industry to quantify plasticizer efficiency [Bair 1981]. To reinforce the concept that a shift of the glass transition to lower temperature improves pavement performance, the efficiency term in this work is defined to be negative when the glass transition temperature decreases with increasing dopant concentration. In general, adding up to 5 mass percent waxes to asphalts has little effect on the glass transition temperature. Exceptions are a 1.2°C/mass percent (2.2°F/mass percent) efficiency factor for AAD-1 waxes in asphalt AAM-1 and a -1.3°C/mass percent (-2.3°F/mass percent) efficiency factor for AAM-1 waxes in asphalt AAM-1.

The wax contents for asphalts AAA-1, AAD-1, and AAM-1 are calculated from the wax contents of the IEC neutral fractions and the weight percent of IEC neutrals in the whole asphalts. For doped asphalts, the total wax content is assumed to be the sum of the doped wax and the native wax contents. The relationships between crystallized fraction and wax content for the seven asphalts (now including the limited data for AAB-1, AAF-1, and AAG-1) are shown in figure 3-37. The plot for each asphalt used in the doping study contains the data for the whole asphalt, the IEC neutrals (except AAC-1), the wax, and the whole asphalt doped with its own wax. Although the evidence is not conclusive, it appears that the waxes from different asphalts have characteristic crystallized fractions that are not dependent on the concentration of the wax in the sample.

If the wax from each asphalt has a characteristic crystallizable fraction, it should be possible to predict the crystallized fractions of all the cross-doped asphalt mixtures in this study. This is accomplished for each mixture by multiplying the weight percent of each wax type in the mixture by its characteristic crystallized fraction and then adding those products. This simple procedure assumes the crystallizable fractions will add and that no interactions occur between the different waxes. The results of this exercise are shown in figure 3-38 where the calculated and measured crystallized fractions are compared. Outlying points above the 1:1 line in this figure are combinations that result in less measured crystallization than expected (crystallization is hindered). Those points below the line are combinations resulting in more crystallization than expected (crystallization is accelerated). All combinations that deviate substantially from the 1:1 line have asphalt AAM-1 involved either as the host asphalt or as the dopant wax source. Asphalt AAM-1 wax even appears to inhibit crystallization in asphalt AAM-1.

Miscellaneous Dopants

The effects of model compound dopants on the glass transitions of asphalts AAF-1, AAG-1, and AAM-1 have been measured. Dopant selection is based on molecular size, functional groups, and conformation (linear or branched). Linear hydrocarbon dopants include octadecane (n-$C_{18}H_{38}$), tetracosane (n-$C_{24}H_{50}$), and hexacontane (n-$C_{60}H_{122}$). Branched hydrocarbon dopants include pristane (2,6,10,14-tetramethylpentadecane, $C_{19}H_{40}$) and squalane (2,6,10,15,19,23-hexamethyltetracosane, $C_{30}H_{42}$). 1,3,5-triethylbenzene ($C_{12}H_{18}$) is an aromatic, but sterically hindered dopant. Two compounds with polar functional groups were

used, namely the diamine 1,12-diaminododecane ($C_{12}H_{28}N_2$) and the amphoteric compound 12-aminododecanoic acid ($C_{12}H_{25}NO_2$).

Dopant efficiencies have been calculated for the three asphalts. The most effective dopants for lowering the glass transition temperature are triethylbenzene, octadecane, and tetracosane. Dopants with polar functional groups are the least effective, although, in this small study, none of the dopants actually increases the glass transition temperature above that of the neat asphalt. Enough tests have been performed with asphalt AAG-1 to plot the resulting efficiencies versus the reciprocal carbon number of the dopants, as shown in figure 3-39. The similarity between this graph and the SEC fraction data shown in figure 3-31 is obvious and lends credence to the idea that low molecular weight polars are responsible for increasing glass transition temperatures at low molecular weights in the SEC fractions.

Effect of IEC Components on Maltene, SEC Fraction-II, and Weak Neutrals Glass Transition Temperatures

As discussed in prior sections, asphalt component analyses paint a relatively consistent qualitative picture of how the components contribute to the glass transition temperature and, therefore, the low temperature performance of an asphalt. The IEC neutral fractions contain only very weakly interacting molecules, and the glass transition temperature is dependent on their number-average molecular weight. The addition of weak acids and weak bases to the IEC neutrals (this combination of weak acids, weak bases, and neutrals is designated as the weak neutral fraction or weak neutrals) increases the intermolecular interaction, the viscosity, and the glass transition temperature, as is seen for weak neutrals. The SEC Fraction-II subfractions and maltenes are composed mainly of neutral materials and those polar molecules that are not part of the dispersed phase. Similar to the weak neutrals, they are mainly solvent-like fractions. In figure 3-40 where the logarithm of viscosity at 25°C (77°F) is plotted versus the glass transition temperature for asphalt components and neat asphalts, data for solvent-like components fall on the same line with only a couple of exceptions. For the neat asphalts, which obviously contain the dispersed phase, the data do not fall on the same line. The line through the solvent-like components data might then be considered indicative of solution behavior with relatively non-polar components at the low viscosity, low glass transition temperature end of the line and higher polarity materials being at the high viscosity, high glass transition temperature end of the line. When high polarity, strongly associating materials are added to the solvent, data for the resulting mix will be above the solution line. Position on the solution line is controlled by molecular weight and by polarity.

A quantitative model of asphalt component interactions must incorporate at its core the Fox-Flory behavior of the weakly interacting IEC neutrals and the limited Fox-Flory behavior seen for supercritical extracts and SEC fractions. In addition, the model must include contributions by polar materials to the glass transition temperature and to the viscosity. The best-defined polarity data come from quantitative IEC fractionations of SHRP core asphalts into weak acid (WA), weak base (WB), strong acid (SA), strong base (SB), and neutral fractions. In this IEC separation method, amphoterics are not isolated as a separate fraction, but are distributed among the four polar fractions. The concentrations (weight fractions) of

these fractions in, for example, heptane maltenes have been estimated by assuming that all the neutrals, weak acids, and weak bases are in the maltenes (see figure 3-29). The balance of the maltenes is then some mixture of strong acids and strong bases, which, for convenience, can be lumped into one term, SASB. The Fox-Flory equation (equation 3-26) has been modified by replacing the constant, K, with a linear combination of weak acid, weak base, and SASB concentrations (the neutrals contribute only implicitly to the correlation):

$$T_g = T_{g\infty} - (A + B \cdot WA + C \cdot WB + D \cdot SASB) / M_n \qquad (3\text{-}29)$$

WA, WB, and SASB are the weight fractions of weak acids (including those in amphoteric fractions), weak bases, and strong acid-strong base materials in the maltene, SEC Fraction-II, or weak neutral samples of interest. A, B, C, D, and $T_{g\infty}$ are adjustable parameters. For convenience it is assumed that the number-average molecular weight of the neutrals is approximately representative of the mixture of neutrals and polar materials.

The result of fitting heptane maltene, iso-octane maltene, SEC Fraction-II, and weak neutral data to equation 3-29 is shown in figure 3-41 for 22 samples. The quality of the fit to the data is a strong indication that the form of equation 3-29 addresses the most important factors controlling the glass transition temperature of the continuous or solvent phase of asphalts. An obvious test of equation 3-26 is to set the weight fractions WA, WB, and SASB to zero and compare the resulting equation with the equation for IEC neutrals. They do not match; they are not close except in form. Empirically, however, the IEC neutrals data can be incorporated by using equation 3-27 where w1 is the weight fraction of neutrals in the sample, T_{g1} is equation 3-26, w2 = 1- w1, and T_{g2} is equation 3-29. Optimizing all the adjustable parameters produces the fit shown in figure 3-42. It is thus possible to estimate the effects of non-polar and polar materials on the glass transition temperatures of heptane maltenes, iso-octane maltenes, and SEC Fraction-II subfractions. Finally, it is possible to estimate the effects of these materials on the low temperature SHRP specification through the simple incorporation of the dispersed phase contribution to the glass transition temperature (see figure 3-34) and the good correlation between the neat asphalt glass transition temperature (as corrected for CF or wax as in figure 3-25) and the low-temperature SHRP specification.

Low Temperature Molecular Dynamics of Asphalts as Determined by Solid State Nuclear Magnetic Resonance

It is known that the physical characteristics of any material are ruled by the chemical structural features of the material. This is true for steel, polymers, fabrics, glue, etc. To predict behavior of materials such as asphalts, which vary considerably in composition and properties according to source, the important structural features must be known.

At the beginning of this chapter, it was pointed out that asphalts are mixtures of many different organic compounds. Asphalts do not contain significant amounts of small molecules (below carbon number 20), however. As a result, asphalts become highly viscous and glassy at low temperatures. In the model of asphalt structure described earlier, most of the solvent moiety of an asphalt will be trapped, or immobilized, by asphaltene molecular associations at

low (room temperature and below) temperatures. The large number of different individual molecular species present discourage crystal formation and favor glassification. Nevertheless some of the components in the solvent moiety can form crystals (e.g., waxes), as is clear from the discussion in the preceding section.

The model of asphalt structure described in several sections of this report postulates that asphalts are not random mixtures of components. This fact becomes obvious from the observation of crystal formation at low (below T_g) temperatures. Some molecular species can form a separate phase from the rest of the material. Other changes also may occur over time, as the various components rearrange themselves into energetically more favorable associations that deviate from randomness. This is what is meant by changes in molecular structuring. Chemical reactivity, the changing of one molecular species into another, is not suggested to occur at low temperatures.

Specialized NMR spectroscopic methods, described below, have been applied to asphalts at low temperatures to elucidate significant changes in molecular structuring (e.g., molecular interactions affecting packing efficiencies) that occur at low service temperatures. This molecular structuring is a function of individual molecular mobilities, which can be detected by NMR in the frequency range of 1-100 kHz. When the structural features that control low temperature properties are better understood, cheaper analytical methods can be applied to select crudes and/or modify asphalts to desired low temperature performance properties.

The molecular motions of greatest interest for components of asphalts are methyl rotation, segmental motion (full and/or partial rotation of carbon-carbon segments of the long chain aliphatic hydrocarbons), cooperative aromatic ring motion, and phenyl twisting (torsional oscillation). Figure 3-43 illustrates the different kinds of motions in a complex "asphaltic" molecule. This molecule is an average structure. It is not suggested that such a species exists in asphalt, but that all structural features are found in at least some species. Molecular motion depends upon the thermal (kinetic) energy of the system. At high temperatures well above the glass transition point, translational motion of an entire molecule is possible and is responsible for the flow properties. Complete rotational motion of an entire molecule about any one of its axes is possible only for relatively small molecules. At moderate temperatures there is much internal motion within a molecule. Carbon atoms rotate freely about single bonds that connect them to each other. Rotation about double bonds does not occur. This internal rotation can result in segmental motion in long chain alkanes, which can be described as flexing (crankshaft type motion), coiling, and uncoiling. Twisting or torsional motion is possible for phenyl groups and other functional groups that are sterically hindered. At temperatures slightly above the glass transition temperature, segmental motion of a few carbon atoms as a unit (segments) along extended carbon chains may occur. Methyl group rotation also is observed. Below the glass transition temperature, carbon atoms are held in a rigid amorphous state, and vibrate about an equilibrium position much like vibrations of atoms in a crystal lattice, except that the positions of carbon atoms in an amorphous state are not in any regular arrangement relative to each other. The classification of motional types just described are in order of decreasing

energy of activation. That is, translational motion has the highest energy requirement, whereas segmental and vibrational motions require less energy and hence persist at low temperatures.

Many of the physical and rheological properties of asphalts are a direct consequence of the type of molecular motions occurring above and below the glass-transition temperature. Obviously, the more varied and energetic molecular motions that a molecule can undergo, the more free volume will be associated with it, and it will be less likely to engage in efficient packing configurations. Molecular associations restrict molecular motions at all temperatures as long as they persist. Below the glass transition temperature, translational and rapid rotational motions about many carbon-carbon bonds are stopped or "frozen out." An exception is the rapid rotation of methyl groups. Translational motion in some systems can, however, occur over extremely long periods of time. Segmental motion of small carbon-carbon segments of individual molecules is possible below the glass transition temperature. These motions permit conformational rearrangements to occur slowly, resulting in crystallization of paraffinic-like materials.

Temperature Profile of Molecular Mobility in Asphalts

A feature in the NMR spectrum of any material is the increase in the signal-to-noise ratio as the temperature is decreased. The increase in the signal is due to the difference in the population of nuclear spins in the ground state relative to a higher energy state. That is, as the temperature is lowered, the number of spins increases in the ground state, increasing the spin differences between the low and high energy states, resulting in an increase in the intensity of the NMR signal. A discussion of this phenomenon is presented in Netzel et al. [1998].

Figure 3-44 shows the molecular-mobility (as determined by NMR) versus temperature profile plots of the aliphatic and aromatic carbons for three asphalts. Also shown in each plot is the predicted signal enhancement as a function of temperature based upon the Boltzmann spin population distribution relative to that at 20°C (68°F). As the temperature decreases from 20° to -45°C (68° to -49°F), the signal enhancement for the aromatic and aliphatic carbons of the three asphalts deviates significantly from the predicted signal enhancement due to the Boltzmann factor alone. The deviations result from the "slowing down" of the molecular motions of the carbons in the asphalts. As the molecular motions decrease, more carbons (^{13}C only) are effectively cross-polarized by the isotopically more abundant ^{1}H protons, which have much stronger nuclear magnetic moments, and, thus, an increase in the signal intensity is observed with decreasing temperature. Therefore, the relative signal increase measures the relative extent of molecular motions of the components in asphalts above and beyond the signal increase due to changes in the Boltzman population distribution. That is, the greater the signal increase relative to the signal at 20°C (68°F), the greater number of mobile molecules that are "slowed-down" and become more rigid.

Asphalt AAA-1 shows greater enhancements of the aliphatic and aromatic carbon NMR signals over the temperature range from 20° to -45°C (68° to -49°F) than those of asphalt AAB-1 which, in turn, show greater enhancements than those of asphalt AAM-1. Thus, the relative extent of segmental and rotational motions of the aliphatic carbons and the low

frequency associated with a cluster of aromatic carbons in the asphalts can be ranked as follows: AAA-1 > AAB-1 > AAM-1. This ranking corresponds to the rheological properties and binder performance ranking of the asphalts that depend largely on molecular motion. Asphalt AAA-1 has the highest degree of molecular motion, which can be related to its low glass transition temperature and low viscosity. Asphalt AAM-1 having the lowest degree of molecular motion has the highest glass transition temperature and the highest viscosity.

The maximum signal enhancement at -45°C (-49°F) for the aliphatic carbons is greater than those of the aromatic carbons for each asphalt, as shown in figure 3-44. This suggests that, at any given temperature, the carbons in aliphatic molecular components have a greater degree of molecular motion than do the carbons in the aromatic components. Thus, the segmental motions of the long carbon chain hydrocarbons require a lower temperature to "slow-down" compared with the oscillatory motions of carbons in the more compact clusters of condensed aromatic rings.

The differences in signal enhancement between the carbons in the aliphatic and aromatic molecular components in asphalts AAA-1 and AAM-1 at -45°C (-49°F) are about equal. However, this difference in asphalt AAB-1 is about twice as large. This may indicate that the long carbon chain alkane hydrocarbons in asphalt AAB-1 have greater segmental motion relative to the overall molecular motion of the clusters of aromatic ring carbons than either asphalt AAA-1 or AAM-1.

As the temperature decreases from 20° to -45°C (68° to -45°F), the signal enhancement for the asphalts increases. Asphalts AAA-1 and AAB-1 show a discontinuity in the temperature range from -10° to -20°C (14° to -4°F), but for asphalt AAM-1 the discontinuity is barely discernable and occurs between 0° and -10°C (32° and 14°F). The discontinuities are in the region of the NMR-determined glass transition temperatures for the asphalts (see figures 3-45 to 3-47). NMR-determined glass transition temperatures are higher than those measured by DSC because the glass transition temperature depends on the frequency of the measurement [Komoroski 1986], which is different for each of the techniques. In the T_g region, the molecular free-volume of the asphalts apparently collapses rather abruptly as a result of the decrease in the thermal energy (molecular motion) of the system. Concurrently, much molecular motion decreases as a result of additional steric factors brought about by the closer packing of the molecules. Because large numbers of molecules are abruptly "frozen" in position in the glass transition region, the signal enhancement increases sharply. Asphalt AAA-1 shows the largest change in signal enhancement for the aliphatic and aromatic carbons in the NMR glass transition region (-10° to -20°C [14° to -4°F]). For asphalt AAM-1, the signal enhancements for the aliphatic and aromatic carbons show a fairly smooth transition through the NMR glass transition region (0° to -10°C [32° to 14°F]). This suggests that there is little abrupt free-volume change in asphalt AAM-1. It is speculated that the lack of an abrupt free-volume change in this asphalt might be due to the fact that it has a high number-average molecular weight with relatively little molecular motion. AAM-1 may already be closely packed at temperatures below ambient temperature but above the glass transition temperature.

To compare the NMR mobility data of the asphalts to their thermal and rheological data, which are obtained on the whole asphalts, the NMR signal intensity data for the aliphatic and aromatic carbons were summed together. Figures 3-45 to 3-47 give the NMR molecular-mobility/temperature profile plots of the sum of the aliphatic and aromatic carbons for the three asphalts. Superimposed on the NMR plots are the thermograms for the change in specific heat capacity with temperature as determined by DSC [Turner 1996].

The NMR molecular mobility-temperature profile plots of the asphalts follow qualitatively, but inversely, their DSC thermograms above and below the glass transition region. The NMR plots describe the change in molecular mobility (molecular dynamics) with changing temperature, whereas the DSC thermograms measure the changes in the thermal energy (molecular energetics) associated with molecular transitions with changing temperature. A reasonable agreement is obtained between the NMR inflection point temperature (T_{NMR}) and the rheological defining temperature (T_d). Only a rough correlation is obtained between the NMR inflection point temperature and the glass transition temperature (T_g) as measured using DSC. A one-to-one correlation is not to be expected because NMR measures the gross changes in molecular mobility while DSC measures the overall energy changes associated with phase changes of the different constituents in the asphalts.

The NMR onset temperatures (T_{os}^{NMR}) for the asphalts are several degrees higher than the DSC onset temperatures (T_{os}^{DSC}). Qualitatively, this is what would be expected if, at first, a specific amount of thermal energy needs to be absorbed before the onset of segmental motion. The energy needed to overcome the barrier to molecular motion is the activation energy.

Crystalline, Interfacial, and Amorphous Phases

Aliphatic carbon is the predominant type of carbon in all petroleum asphalts and is typically around 70 percent of total carbon. The aliphatic carbons are composed of linear, branched, and cyclic alkanes and alkyl groups that are substituents on other kinds of compounds. The normal and branched alkanes are the structural units of the waxes found in asphalts. At temperatures below their melting point, the waxes can crystallize. The first evidence of crystalline waxes in asphalts was reported in 1966 by Smith et al. [1966] using IR spectroscopy.

Giavarini and Pochetta [1973] reported that petroleum waxes have carbon numbers greater than C_{18}. The normal paraffinic waxes are characterized by a carbon chain length range of C_{18} - C_{40} (this range includes most of the waxes; higher carbon number constituents also may be present) and the microcrystalline waxes, which are composed of branched paraffins, have carbon numbers in the range of C_{25} - C_{65}. Noel and Corbett [1970], using DSC, studied the crystalline phases in a variety of asphalts and showed that asphalts are largely amorphous and contain poorly defined crystalline material. Recent DSC studies of the crystallinity of the waxes in asphalts have shown that crystalline components in asphalt exhibit distinct endothermic patterns, which depend on their chemical structure and the interactions with the amorphous phase [Daly et al. 1996]. Using the technique of co-crystallization (doping asphalts

with model compounds), Daly et al. [1996] found that the crystalline asphalt components have chain lengths comparable to eicosane ($C_{20}H_{42}$) and octacosane ($C_{28}H_{58}$).

NMR spectroscopy has not been used to study the crystalline structure of waxes in asphalts directly. To do so, ^{13}C solid-state NMR relaxation techniques must be used, and these techniques are not readily available in asphalt laboratories. However, NMR techniques have been used extensively in the study of semicrystalline polymers [Axelson 1986]. The crystalline phase in polymers has been shown to have an enormous influence on the rheological and performance properties of polymers. Some studies on the influence of crystalline waxes on the rheological and performance properties of asphalts have recently been reported [McKay et al. 1995; Bahia and Anderson 1992; Claudy et al. 1992]. Bahia and Anderson [1992] have shown that even though there is a direct statistical correlation between asphalt low temperature hardening and wax content, they proposed that the molecular weight of the entire non-polar component is also a factor in the correlation. The tendencies of asphalt pavement to crack in cold environments was attributed to its wax content [Claudy et al. 1992]. McKay et al. [1995] found that the paraffin waxes added to asphalts cause viscosity increases, whereas the microcrystalline waxes cause decreases in viscosity.

Figure 3-48 shows that the methylene carbons in the ^{13}C NMR spectrum of asphalt AAM-1 at 20°C (68°F) are split into two peaks. The peak at ~ 30 ppm is assigned to mobile-amorphous methylene carbons in a long chain and the peak at ~ 32 ppm to rigid-crystalline methylene carbons in a long carbon chain. These assignments are based on assignments made for polyethylene [VanderHart and Garroway 1979]. The chemical shift difference arises from chain conformational effects. The chemical shift of the crystalline phase is due to the all-trans conformation of the methylene carbons, whereas the chemical shift of the amorphous phase is the result of the methylene carbons in various gauche (random) conformations. The amount of crystalline and amorphous methylene carbons can be determined from intensity measurements resulting from curve-fitting (deconvolution) of the ^{13}C dipolar-dephasing NMR spectra.

The deconvolution of the ^{13}C dipolar-dephasing spectra for asphalts AAA-1, AAB-1, and AAM-1 at -45°C (-49°F) showed decreases in the NMR signal for the various carbon types as the dipolar-dephasing time increases [Netzel et al. 1998]. The differences in carbon type intensities observed in the spectra of one asphalt compared with another are due to differences in the quantity and the rate of relaxation of the carbon types. The changes in relaxation rate obtained from the dipolar-dephasing spectra are the result of the differences in the rigidity of the different carbon types. A plot of the deconvoluted area of the resonance peak of the terminal methyl carbons (14 ppm) as a function of the dipolar dephasing times for the three asphalts at -45°C (-49°F) is shown in figure 3-49a. The ^{13}C nuclear spin dephasing relaxation times, T_{2G}' [Netzel et al. 1998], calculated from the data shown in the figure, are given in table 3-42. The relaxation time for the terminal methyl carbons in asphalt AAA-1 is longer than that for asphalts AAB-1 and AAM-1. The longer time is the result of greater rotational motion. The T_{2G}' values of the methyl carbons are in complete agreement with the literature values for methyl carbons in rigid systems (50-121 μs) [Axelson 1986].

Figure 3-49b shows the dipolar-dephasing relaxation rates (slope of the lines) for the methylene carbons at 30 ppm for the three asphalts. The relaxation rates are composed of two components: the rigid-amorphous phase methylene (τ = 0 - 35 μs) and the mobile-amorphous phase methylene (τ = 40 - 80 μs) carbons. The relaxation times (T_{2G}' and T_{2L}', in which G is the Gaussian component and L is the Lorentzian component) for the two phase components are given in table 3-42. The rigid-amorphous phase methylene carbons (Gaussian component) have the same relaxation time (T_{2G}' ~ 20 μs) in each of the asphalts. There are considerable differences in the relaxation times (T_{2L}') for the mobile-amorphous methylene carbons (at 30 ppm - Lorentzian component) in the three asphalts (see table 3-42). Asphalt AAM-1 has the shortest relaxation time (48 μs) suggesting, therefore, that the segmental motion is much slower than the segmental motions of the methylene carbons in asphalts AAA-1 and AAB-1. In fact, it may be inferred that the segmental motion in asphalt AAA-1 is almost twice as fast as the motion in asphalt AAM-1 at -45°C (-49°F). The values reported here for asphalts are comparable to the literature values of amorphous polymers.

The dipolar-dephasing relaxation rate data for the methylene carbons at 32 ppm for asphalts AAA-1, AAB-1, and AAM-1 are shown in figure 3-49c. The dipolar-dephasing relaxation times are given in table 3-42. In general, the relaxation times T_{2G}' for the methylene carbons at 32 ppm are shorter (15-18 μs) than for the methylene carbons at 30 ppm (19-20 μs). Methylene carbons in a very rigid structure have relaxation times ranging from 12 to 29 μs [Axelson 1986]. Thus, it may be assumed that a fraction of the methylene carbons (the very rigid methylene carbons at 32 ppm) in the asphalts are part of a highly ordered crystalline structure.

The chemical shift difference between the terminal methyl carbons at ~14 ppm and the internal methylene carbons at ~32 ppm for asphalts AAA-1, AAB-1, and AAM-1 is ~ 17.8 ppm. This value lies between the chemical shift values reported for orthorhombic and monoclinic structures of n-alkanes given in table 3-43 [VanderHart 1981] suggesting, therefore, that the rigid methylene carbons in the three asphalts may be a mixture of paraffin wax crystals with orthorhombic and monoclinic lattice structures. The crystallization behavior of n-paraffins isolated from petroleum waxes has been studied by Srivastava et al. [1992] using x-ray diffractometry. These authors reported that the n-paraffins crystallized with a predominantly orthorhombic structure.

The relaxation and spectral data discussed above are in agreement with the known rheological properties for the three asphalts. The wax content [SHRP 1992] for asphalt AAA-1 (1.62 mass percent) is significantly less than for asphalts AAB-1 (3.85 mass percent) and AAM-1 (4.21 mass percent) and, thus, AAA-1 would be expected to have little, if any, crystalline phase. An extensive crystalline phase would impart significant rigidity to the asphalts. That is, the overall molecular motions of the asphalt components at low temperatures will decrease with increasing crystalline wax content of an asphalt. For asphalt AAM-1, which has the highest glass transition temperature of the three asphalts, the molecular motions at low temperatures are slower (smaller values of T_{2G}' and T_{2L}') relative to the other two asphalts. The slow molecular motions are probably due to the high average molecular weight for this

asphalt, which is nearly twice that of the other asphalts and to the high microcrystalline wax content.

It has been shown using solid-state NMR techniques that molecular structure and dynamics of asphalts can be described quite successfully in terms of crystalline, rigid amorphous, and non-rigid amorphous phases. This concept of different phases has been used extensively in polymer chemistry to relate molecular structure and dynamics to polymer rheological properties. Thus, the phase concept should also be applicable to describing many of the rheological properties and road performance behavior of asphalts. The fundamental structural and dynamic information obtained from NMR should be useful to adjust the overall molecular mobility (which determines flexibility) in an asphalt to achieve the desired low temperature performance by chemical modification of the asphalt, by the physical blending of two or more asphalts, or by the introduction of polymeric materials or other additives.

The fundamental structural features involved in the low temperature performance of an asphalt have been established using solid-state NMR techniques. Now other, less costly methods can be developed to select crudes for best low temperature performance.

Table 3-41. Summary of asphalt thermal properties.

Asphalt	T_g, °C	ΔT_g, °C [1]	ΔCp, J/g·°C	CF (%) [2] assuming 200 J/g [3]
AAA-1	-24.6	31.7	0.520	0.4
AAB-1	-22.5	35.0	0.347	2.3
AAC-1	-21.0	34.8	0.369	2.7
AAC-2	-23.3	34.6	0.322	3.5
AAD-1	-24.2	30.8	0.384	0.6
AAD-2	-26.5	27.5	0.302	0.7
AAE-1	-24.5	28.8	0.308	0.1
AAF-1	-16.8	39.5	0.355	1.7
AAG-1	-8.8	32.2	0.369	0.0
AAG-2	-6.8	37.2	0.356	0.0
AAH-1	-21.6	40.5	0.316	2.4
AAJ-1	-23.8	33.4	0.332	1.5
AAK-1	-21.5	30.3	0.347	0.4
AAK-2	-25.3	27.6	0.324	0.3
AAL-1	-24.0	29.5	0.328	0.2
AAM-1	-21.1	29.4	0.187	2.8
AAM-2	-21.0	29.9	0.307	3.5
AAN-1	-17.2	34.7	0.320	1.2
AAO	-20.8	37.9	0.335	2.0
AAP	-23.9	29.2	0.291	1.8
AAQ	-19.6	40.0	0.361	2.2
AAR	-17.5	35.0	0.234	1.7
AAS-1	-22.2	34.0	0.350	1.6
AAT-1	-18.6	45.1	0.337	1.3
AAU-1	-12.6	34.4	0.273	1.0
AAV	-18.9	35.7	0.340	1.6
AAW	-14.6	47.9	0.319	2.0
AAX	-16.7	38.1	0.307	1.7
AAY	-23.1	29.0	0.283	1.8
AAZ	-11.1	37.2	0.310	0.6
ABA	-27.1	31.3	0.314	3.7
ABC	-27.5	31.6	0.311	1.8
ABD	-2.9	33.6	0.337	0.0
ABF	-15.1	31.1	0.297	0.0
ABG	-18.4	32.2	0.310	0.0
ABH	-19.5	32.9	0.322	1.7
ABK	-	-	-	0.0
ABL-1	-21.3	27.4	0.299	1.0
ABM-1	-3.1	27.5	0.309	0.0

[1] ΔT_g is the width of the glass transition (T_{end} - T_{onset}).
[2] Crystallized fraction (CF).
[3] Estimated heat of fusion for waxes is 200 J/g from Brule et al. [1990].

Table 3-42. Dipolar dephasing relaxation times for methyl and methylene carbons in asphalts AAA-1, AAB-1, and AAM-1 at -45°C.

Carbon type	Spin dephasing relaxation times (μs)					
	AAA-1[1]		AAB-1[1]		AAM-1[1]	
	T_{2G}'	T_{2L}'	T_{2G}'	T_{2L}'	T_{2G}'	T_{2L}'
Terminal methyl carbons (14 ppm)	73 ± 3		66 ± 3		63 ± 1	
Methylene carbons (30 ppm)	19 ± 0.9	87 ± 42	20 ± 0.2	64 ± 12	20 ± 0.3	48 ± 5
Methylene carbons (32 ppm)	18 ± 0.7		16 ± 1		15 ± 0.2	

[1] T_{2G}' is Gaussian component (crystalline and rigid-amorphous phase); T_{2L}' is Lorentzian component (mobile-amorphous phase).

Table 3-43. Solid-state ^{13}C isotropic chemical shift values for selected *n*-alkanes [VanderHart 1981].

Crystal habit		^{13}C Chemical shifts (ppm)		
		CH_3	int-CH_2	Δ[(int-CH_2)-CH_3]
Alkane				
C-19	Pseudohexagonal	14.81	33.66	18.85
C-20	Triclinic	16.02	34.92	18.90
C-23	Orthorhombic	15.06	33.62	17.56
C-32	Monoclinic	15.25	33.66	18.41
Asphalt				
AAA-1		14.00	31.94	17.94
AAB-1		13.99	31.83	17.84
AAM-1		13.99	31.80	17.81

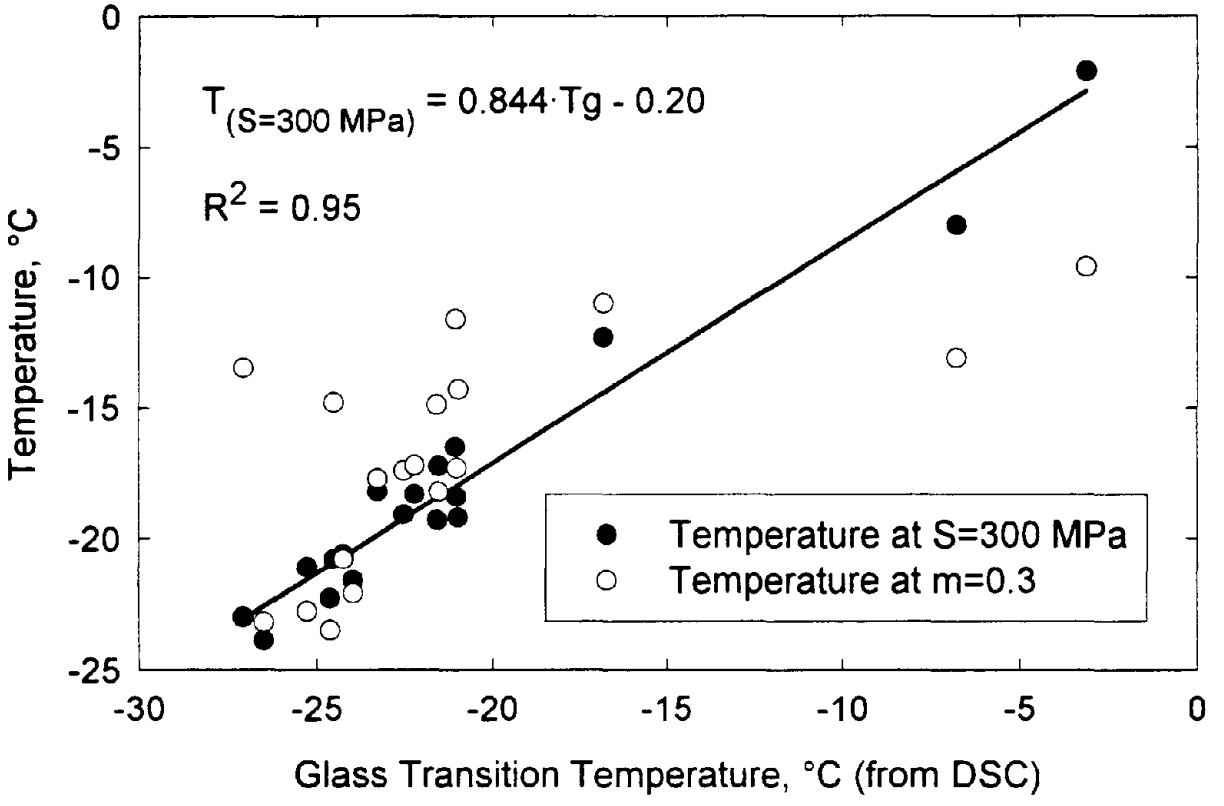

Figure 3-26. Temperatures at which S=300 MPa and m=0.3 as functions of DSC-derived glass transition temperatures.

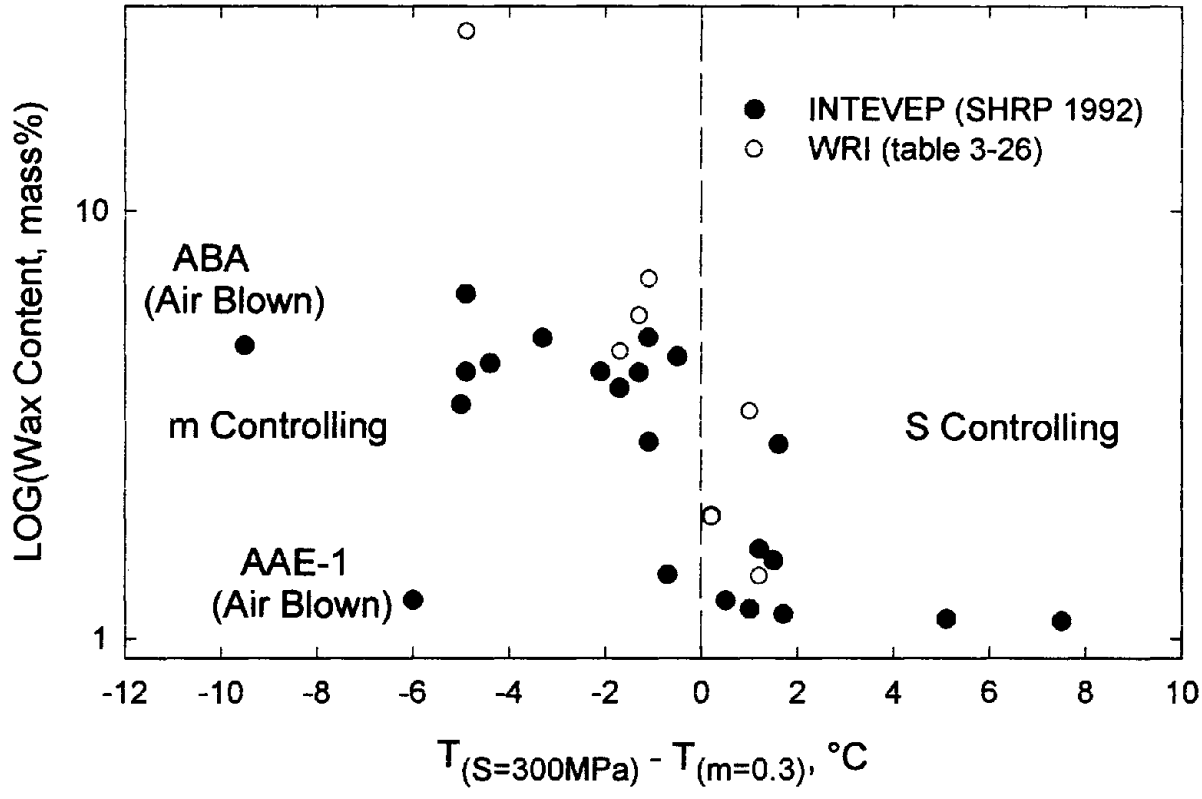

Figure 3-27. Relationship between wax content of asphalts and whether S or m controls the low-temperature SHRP specification.

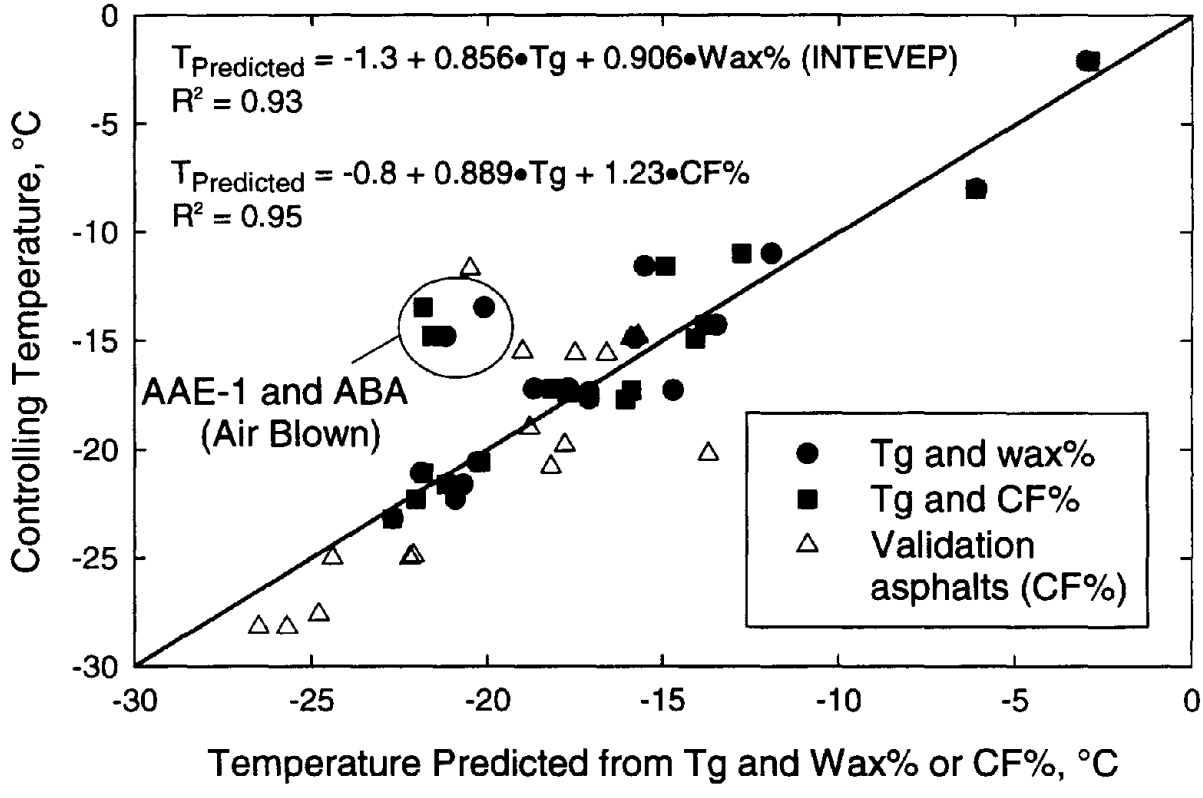

Figure 3-28. Correlation of specification controlling temperature to a linear combination of glass transition temperature and wax or crystallizable fraction.

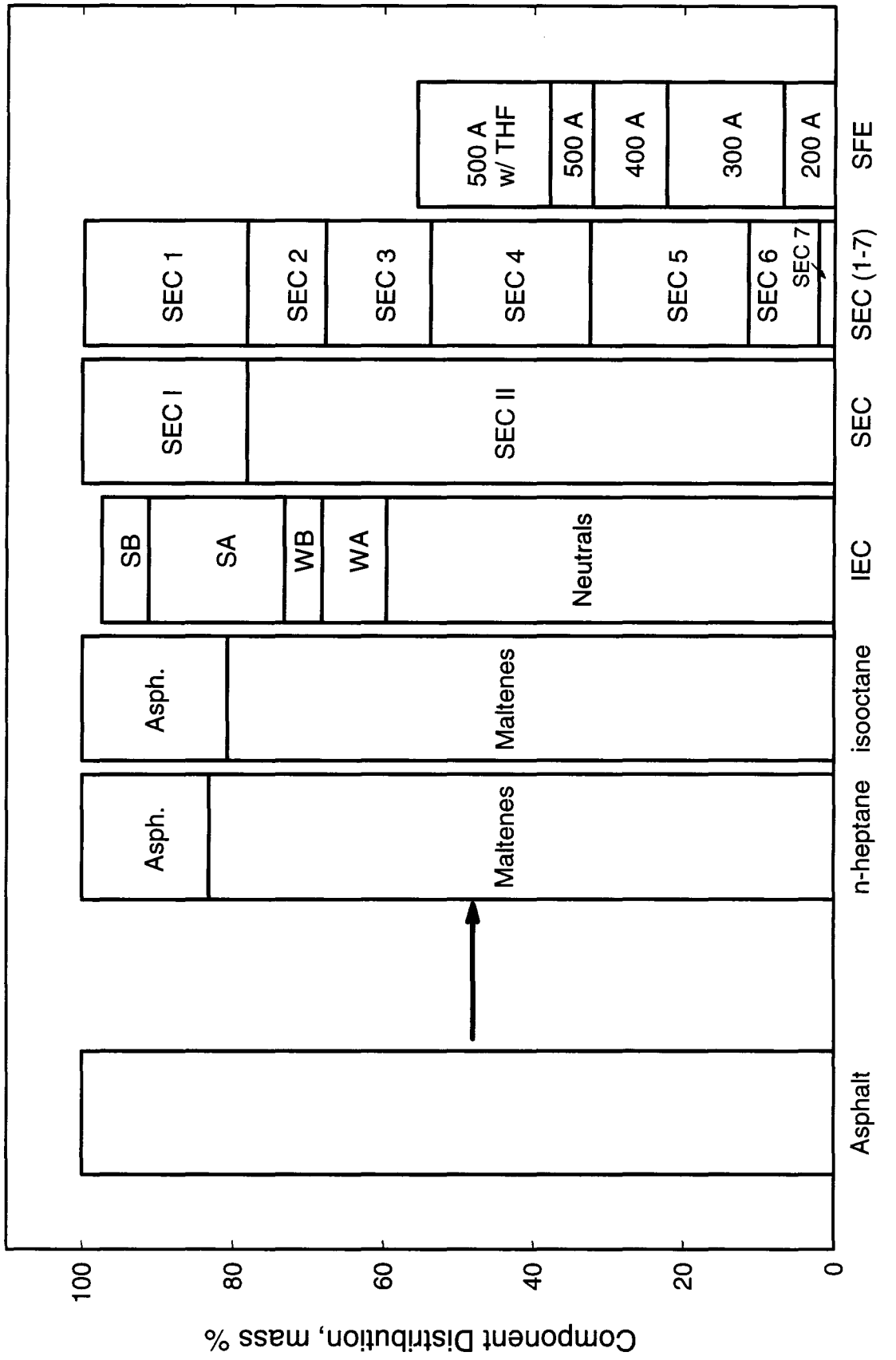

Figure 3-29. Asphalt fractionation by solvent, molecular size, and polarity.

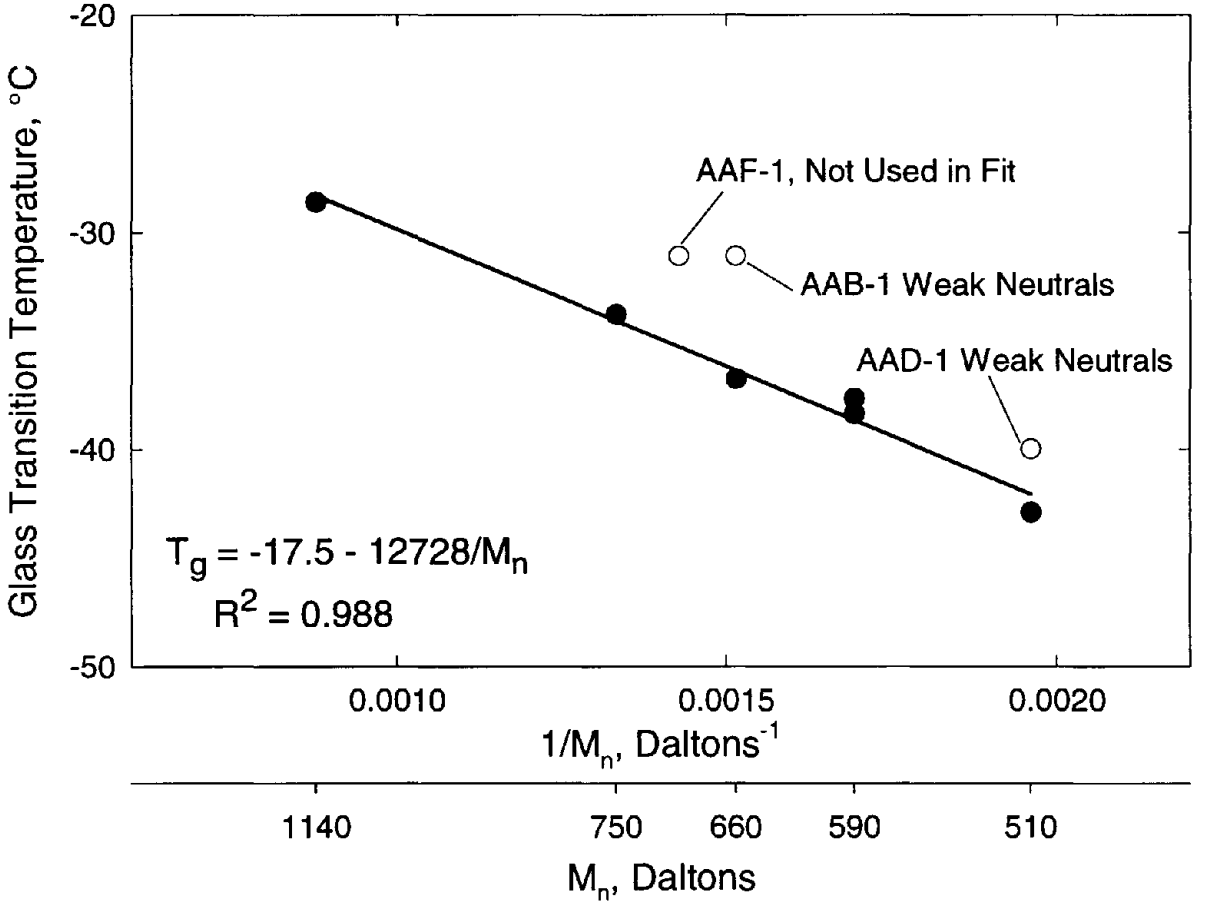

Figure 3-30. Fox-Flory behavior of IEC neutral fraction.

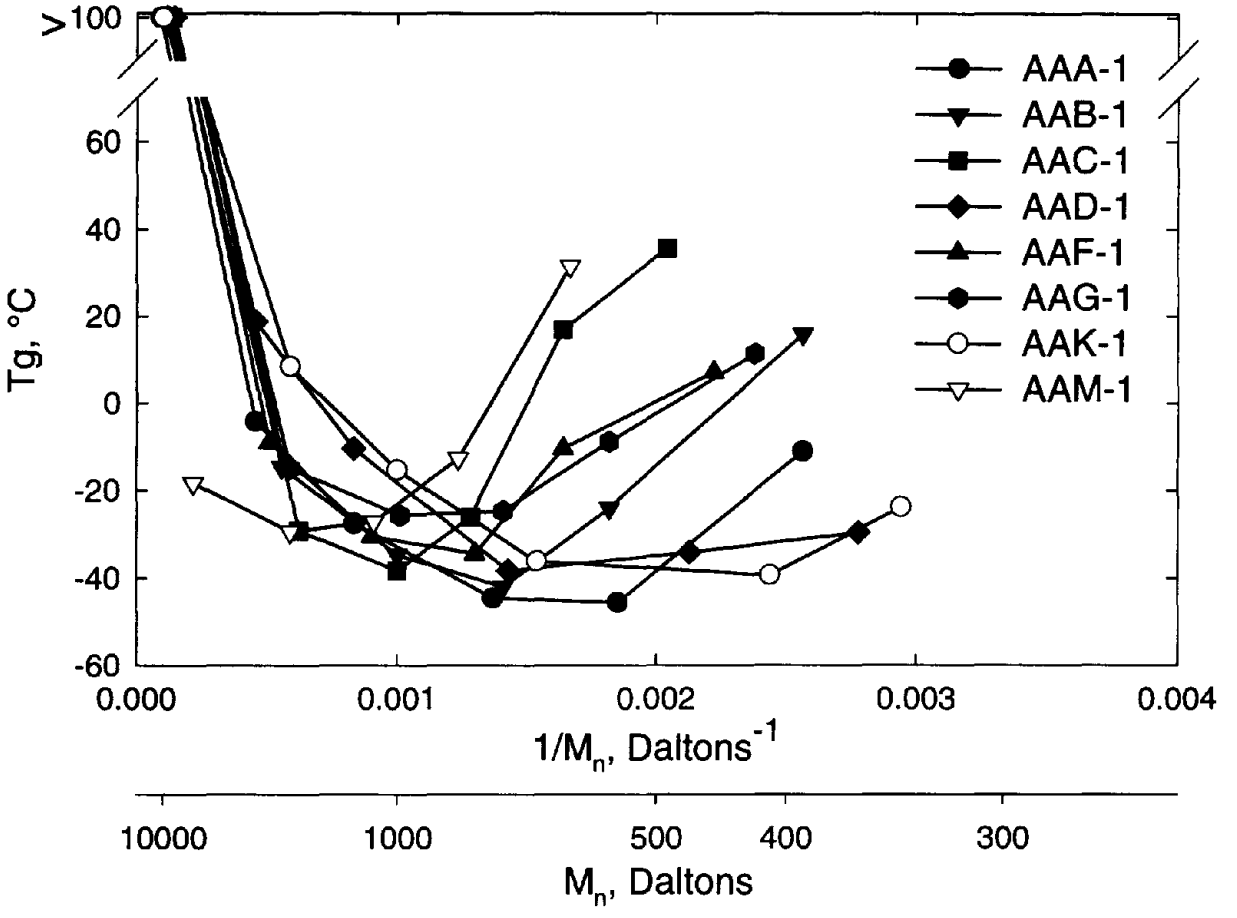

Figure 3-31. Variation of SEC fraction glass transition temperatures with molecular weight.

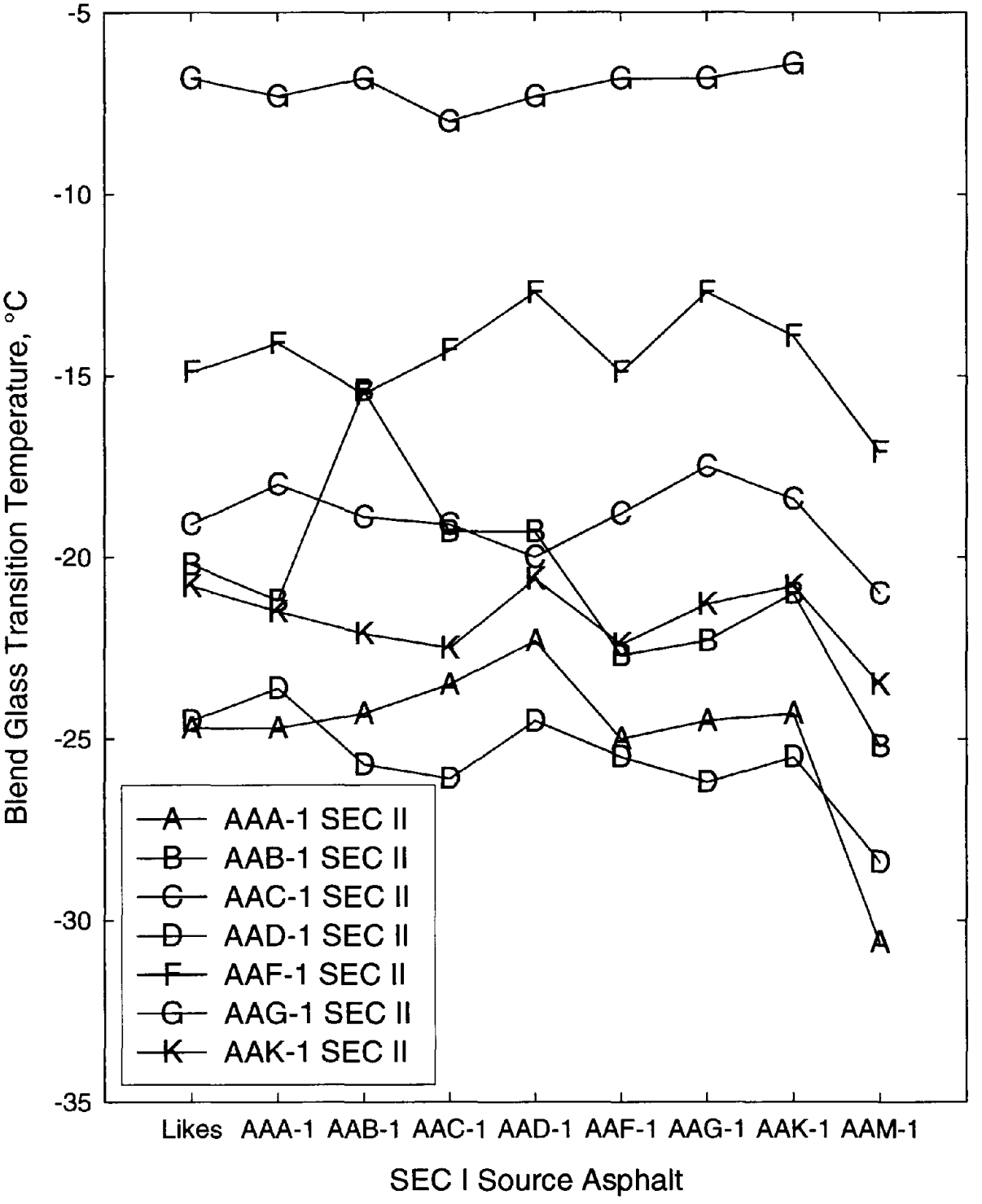

Figure 3-32. Glass transition temperatures of SEC Fraction-I/ SEC Fraction-II blends.

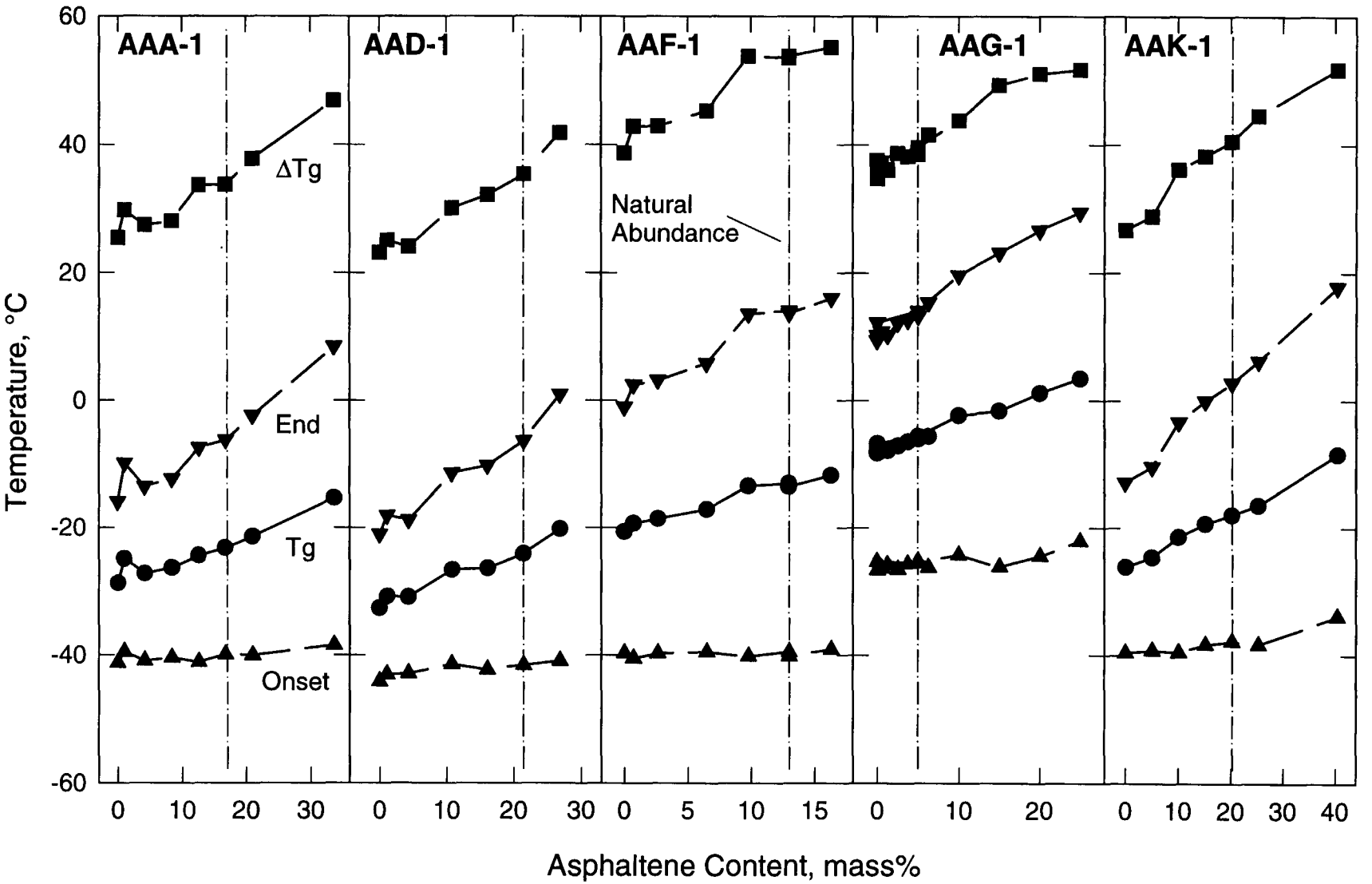

Figure 3-33. Glass transition parameter changes with asphaltene concentration for five SHRP asphalts.

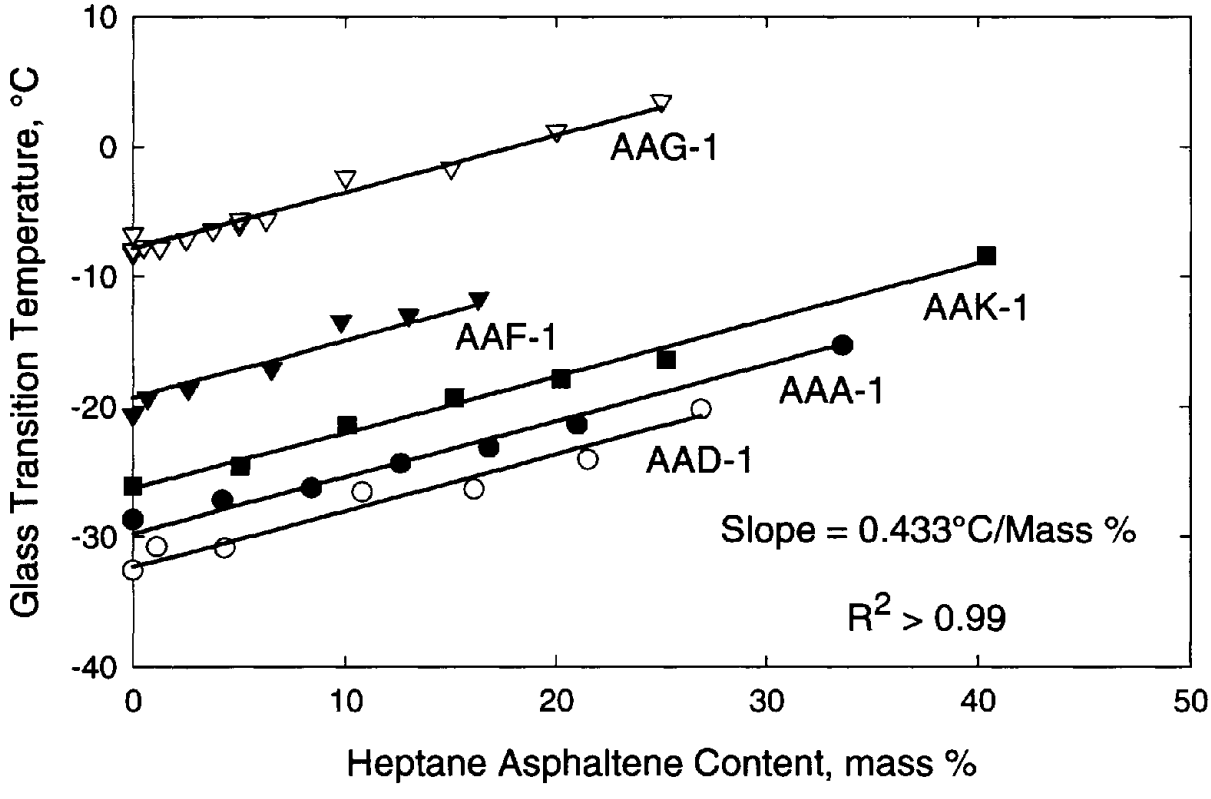

Figure 3-34. Glass transition temperatures in heptane asphaltene-maltene blends.

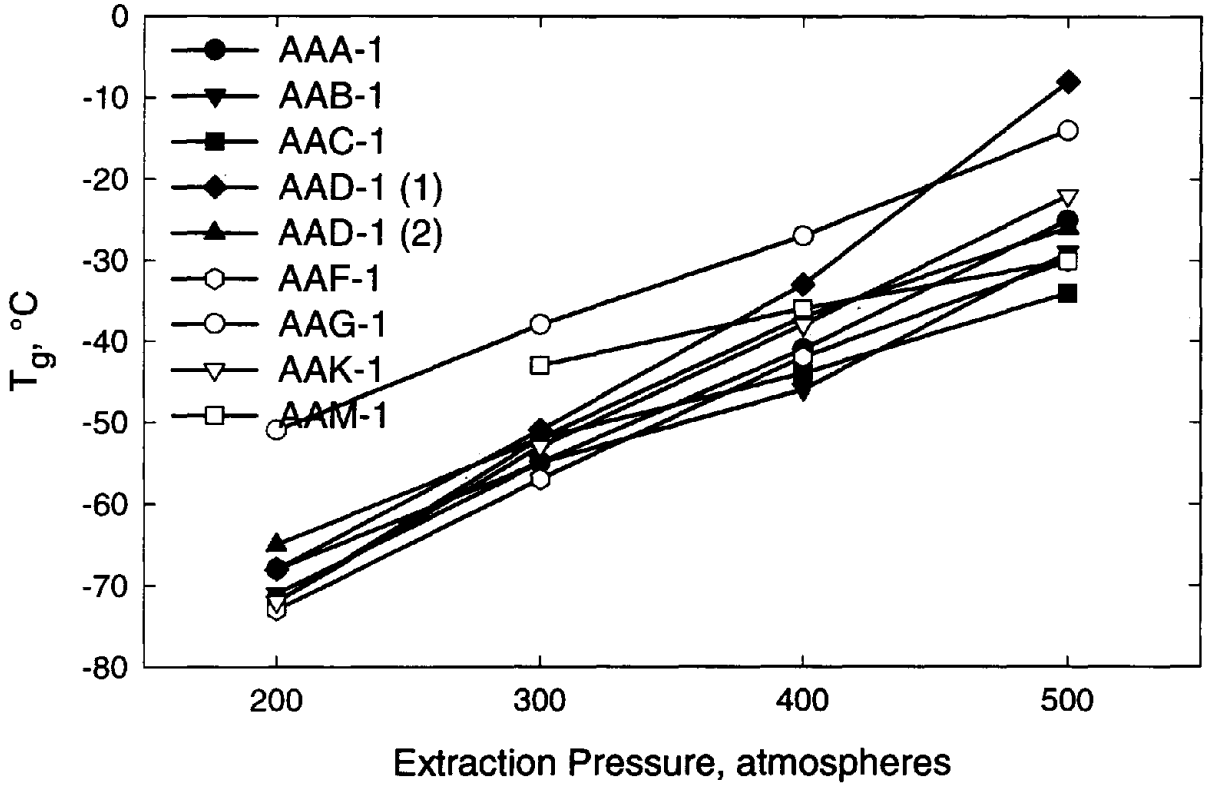

Figure 3-35. Glass transition temperature dependence on supercritical fluid extraction pressure.

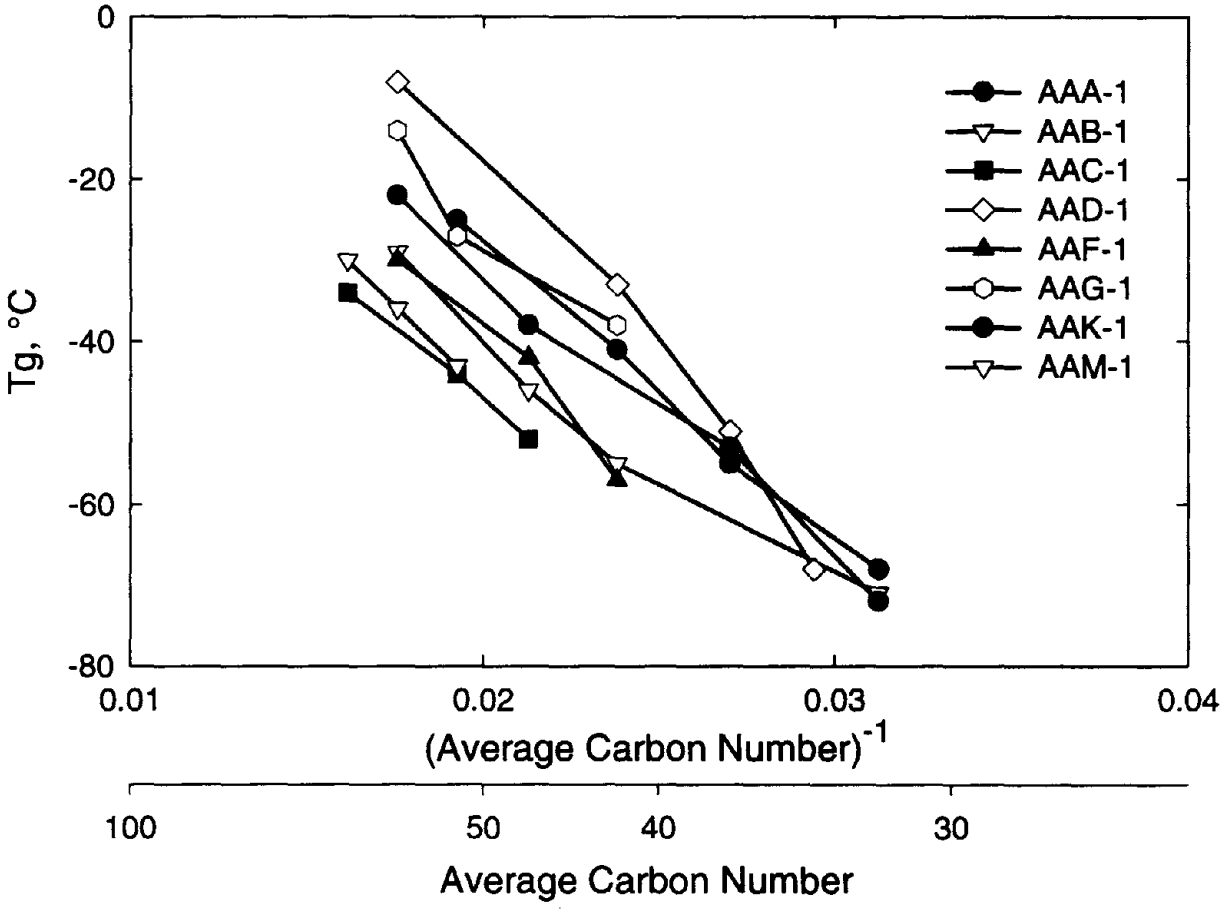

Figure 3-36. Variation of glass transition temperature of SFE fractions with molecular weight.

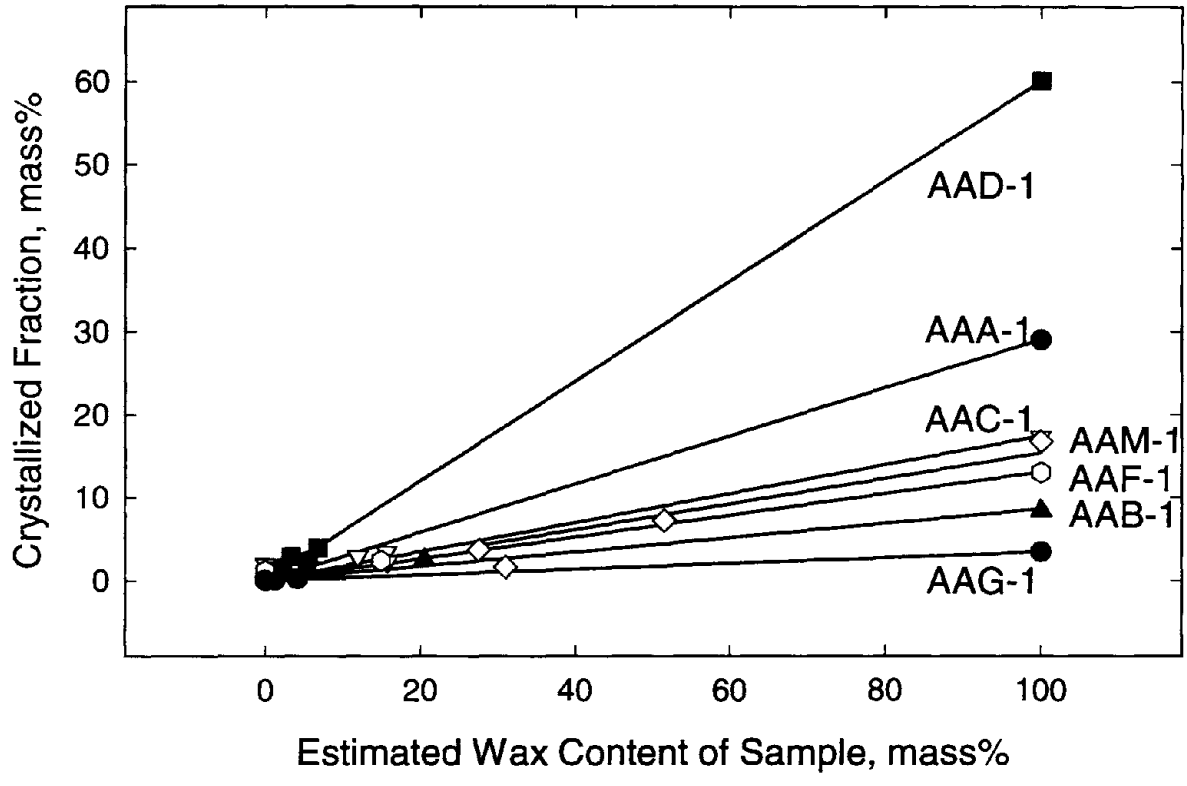

Figure 3-37. Crystallizable fractions of waxes, wax-doped asphalts, dewaxed asphalts, and asphalts compared with sample wax contents.

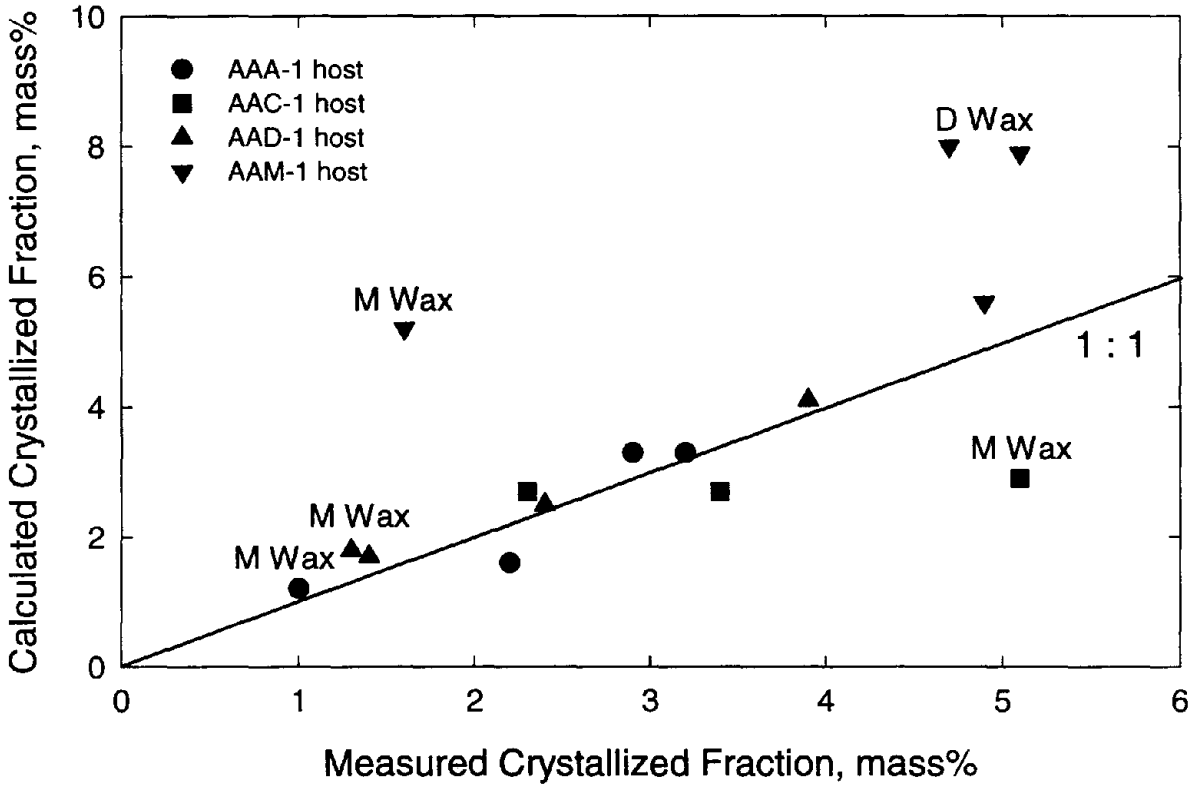

Figure 3-38. Additive behavior of waxes in asphalts.

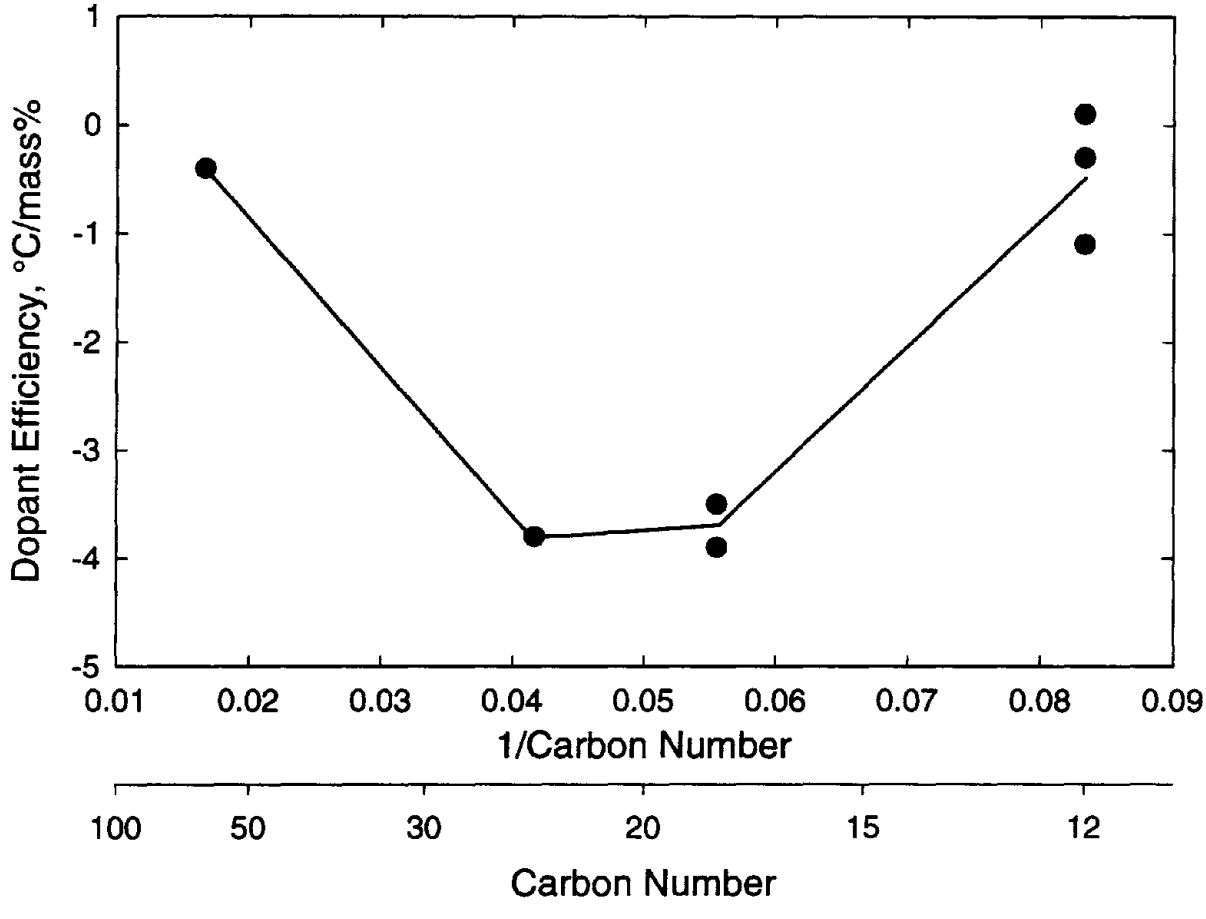

Figure 3-39. Variations of dopant efficiency as a function of dopant carbon number for asphalt AAG-1.

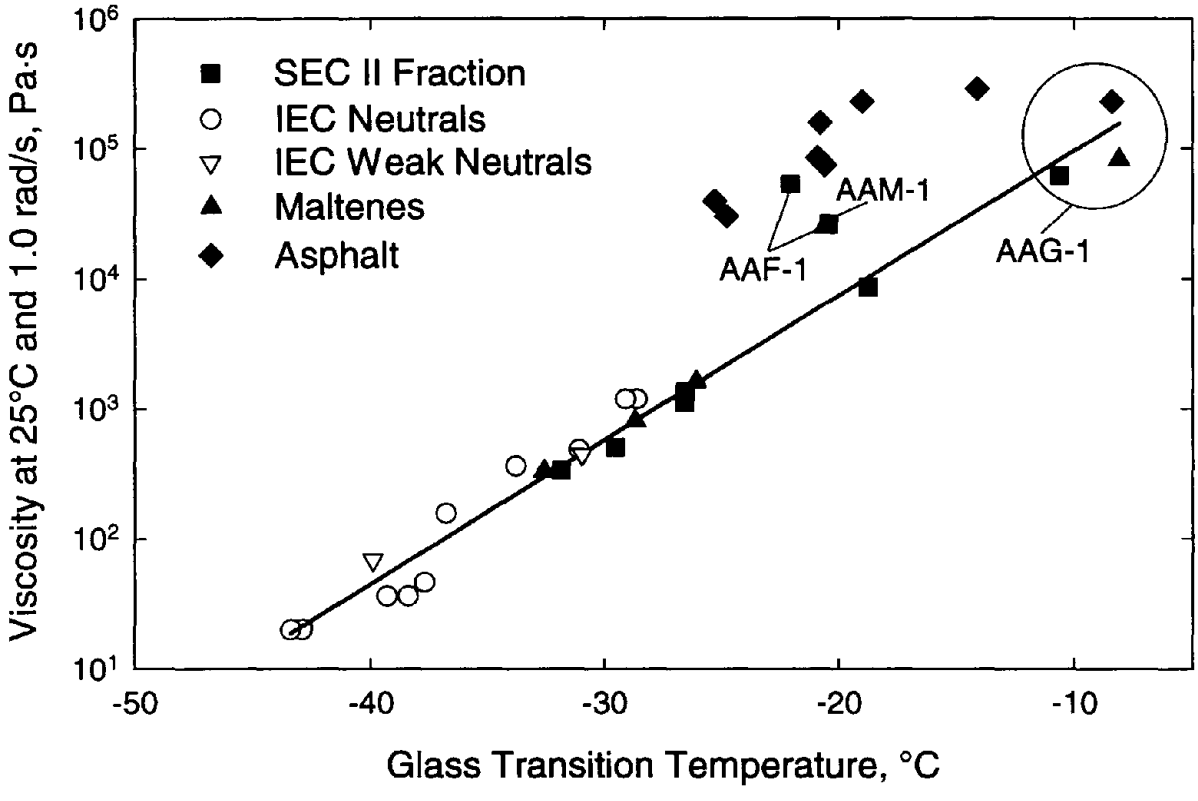

Figure 3-40. Relationship of asphalt and component glass transition temperatures to viscosity.

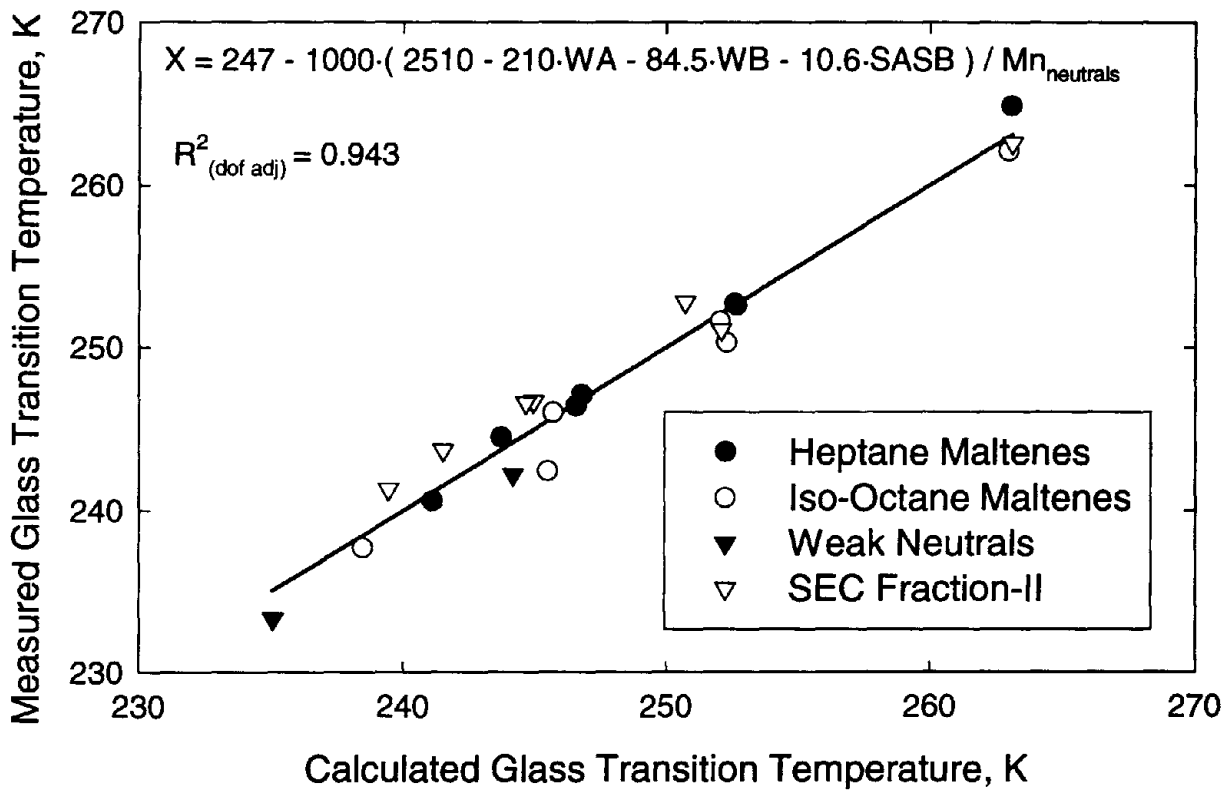

Figure 3-41. Glass transition temperature prediction for heptane maltenes, iso-octane maltenes, SEC Fraction-II, and two weak neutral fractions based on polar component concentrations.

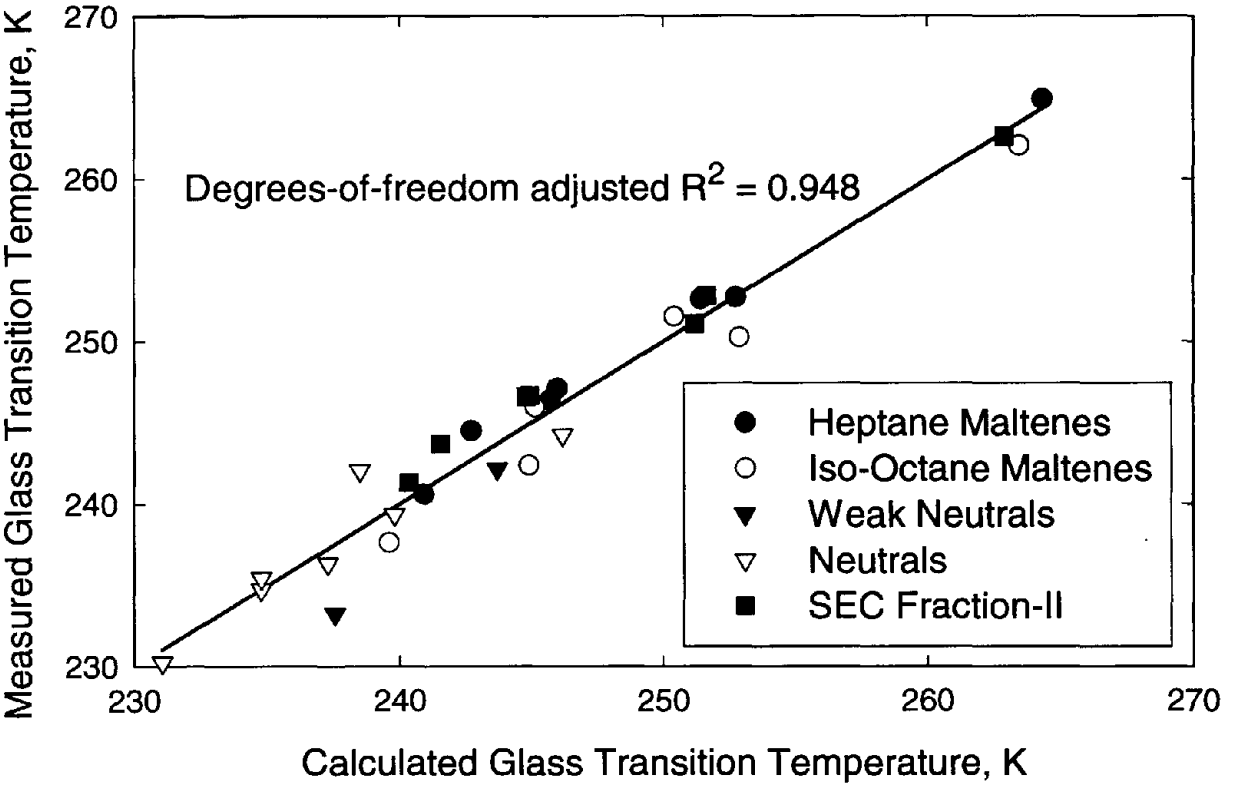

Figure 3-42. Correlation of glass transition temperatures of heptane maltenes, iso-octane maltenes, SEC Fraction-II, weak neutrals, and neutrals with IEC polar components.

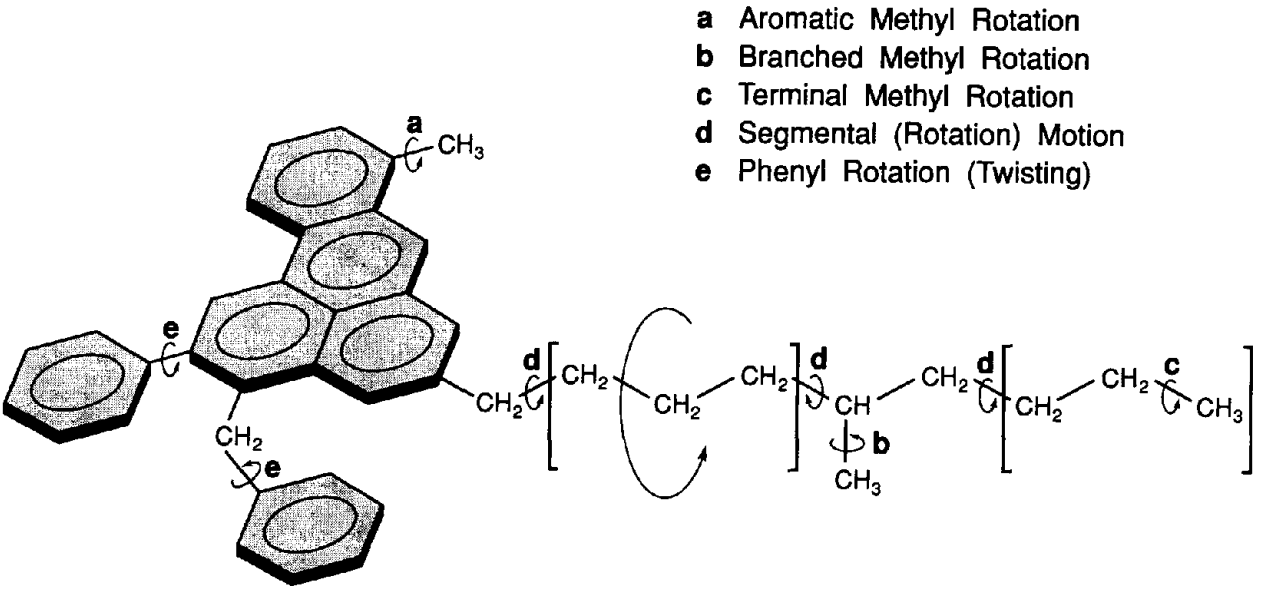

Figure 3-43. Schematic representation of the types of molecular motions in a complex "asphalt-like" molecule.

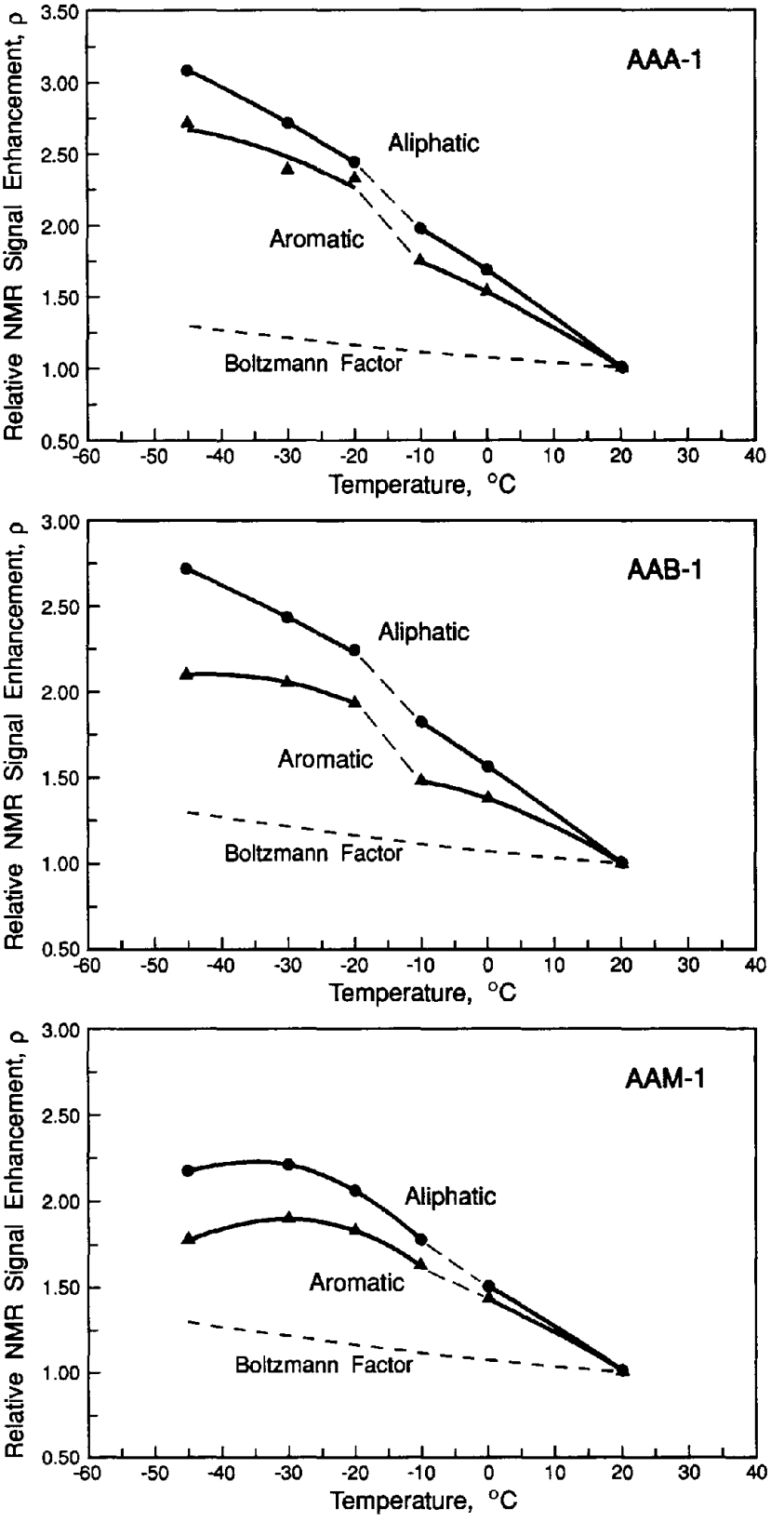

Figure 3-44. Carbon-13 CP/MAS NMR signal enhancement as a function of temperature for asphalts AAA-1, AAB-1, and AAM-1.

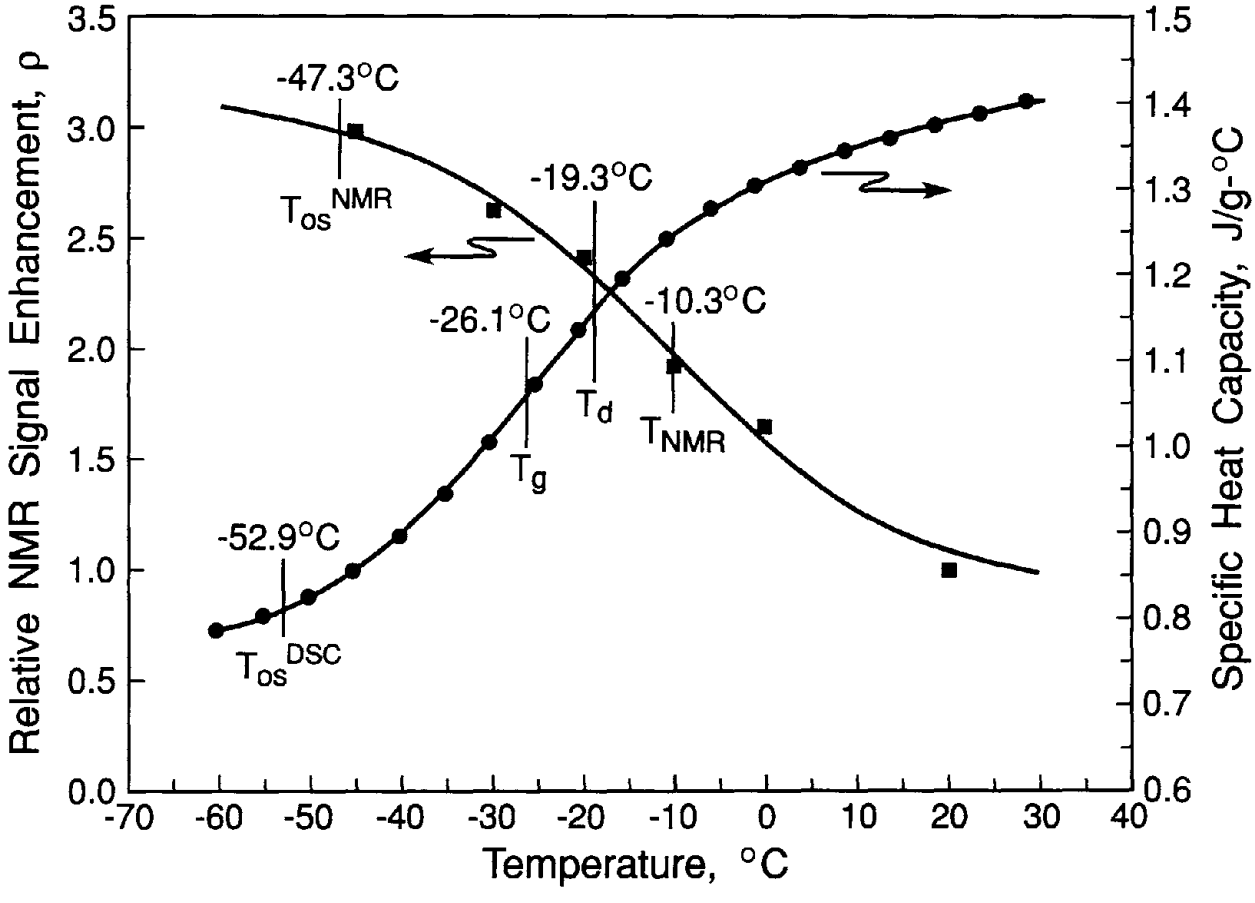

Figure 3-45. NMR molecular-mobility/temperature profile and DSC plots of the total carbons in asphalt AAA-1.

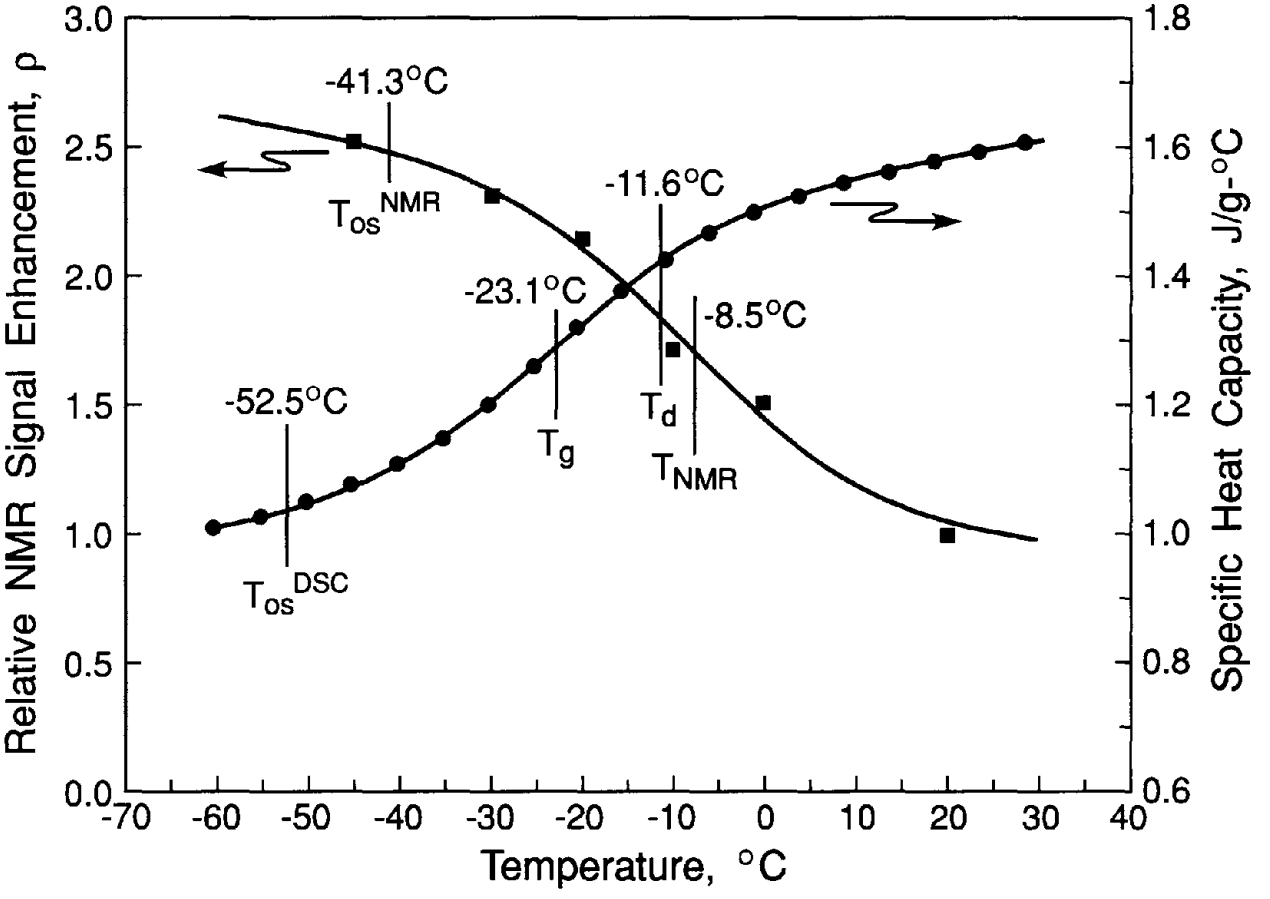

Figure 3-46. NMR molecular-mobility/temperature profile and DSC plots of the total carbons in asphalt AAB-1.

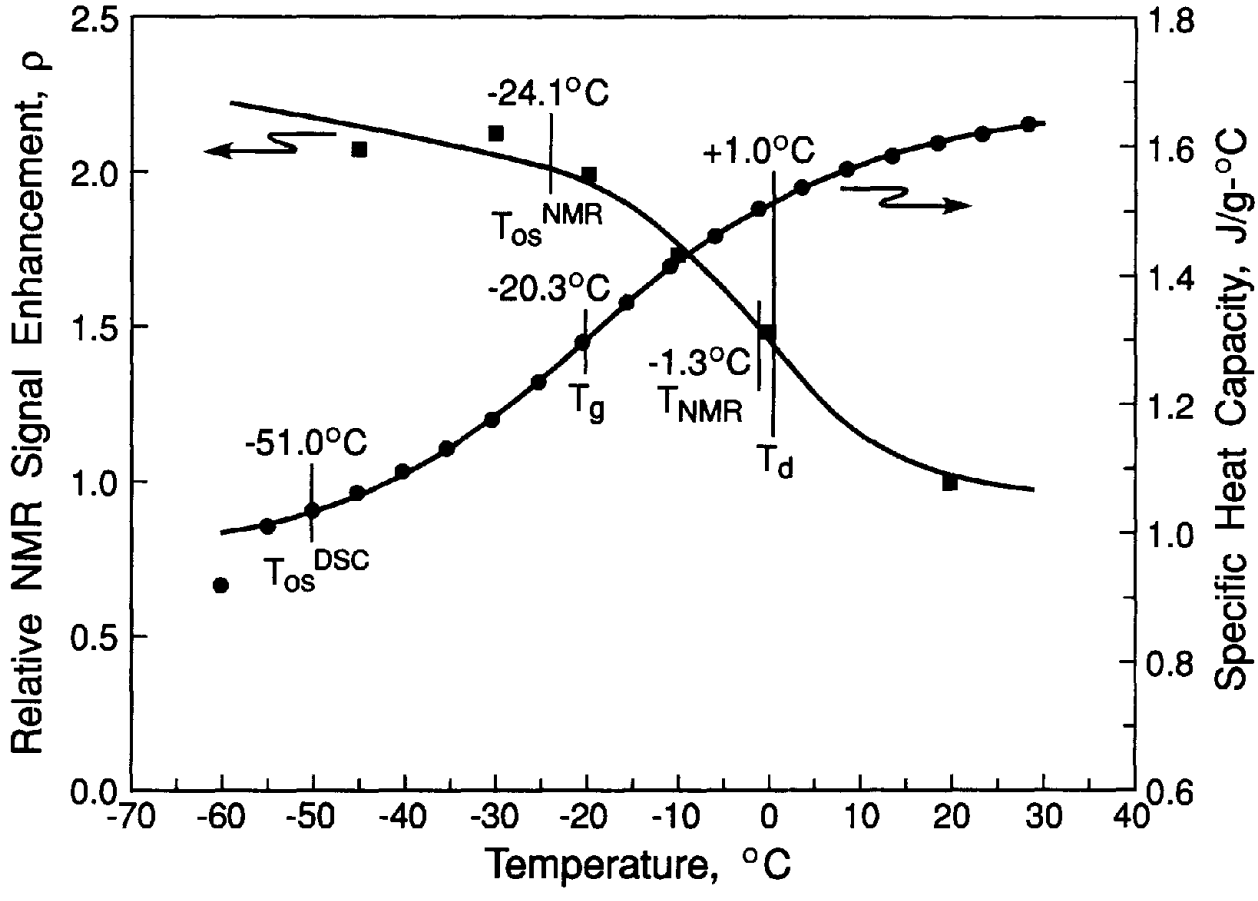

Figure 3-47. NMR molecular-mobility/temperature profile and DSC plots of the total carbons in asphalt AAM-1.

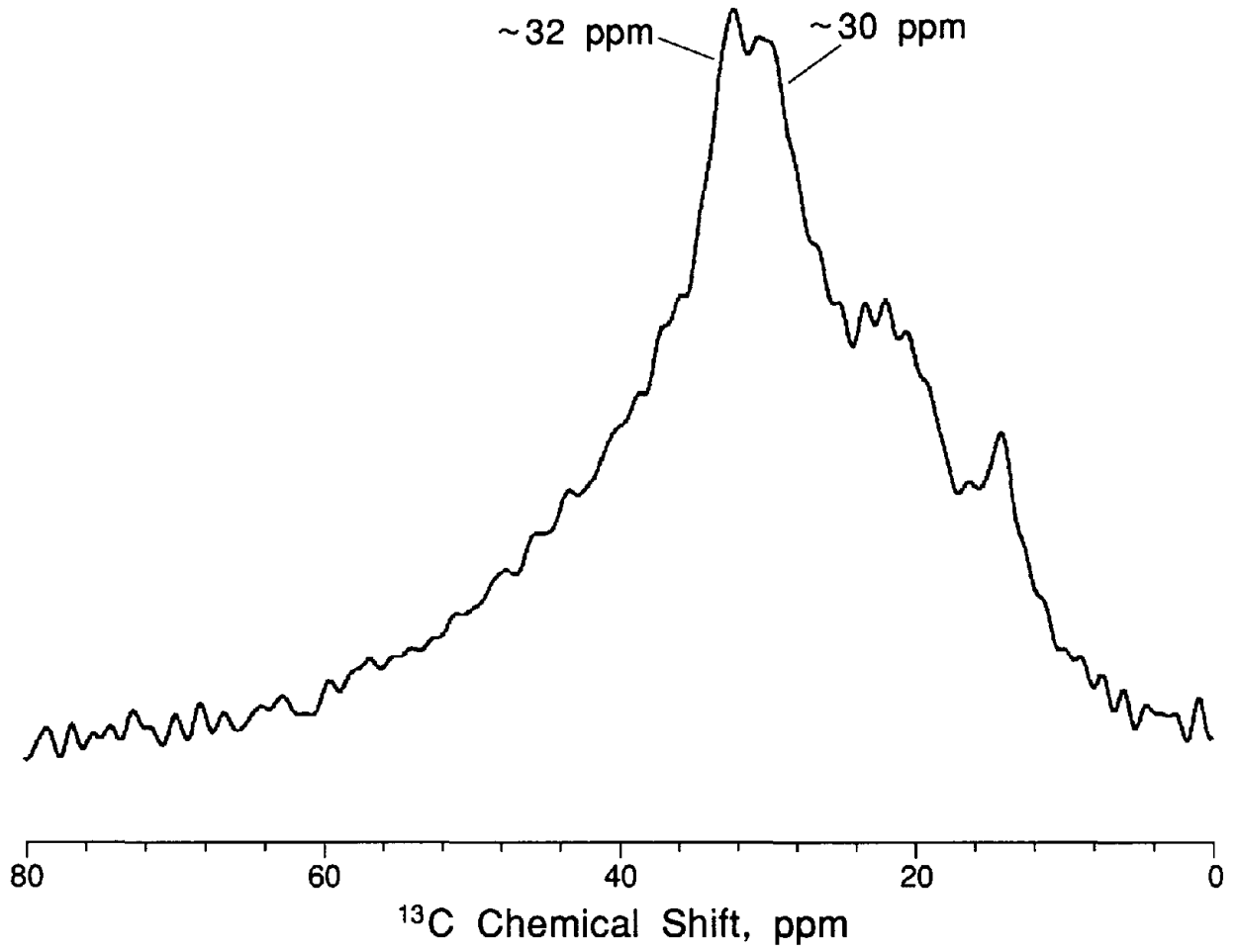

Figure 3-48. CP/MAS carbon-13 NMR spectrum of the aliphatic carbons in asphalt AAM-1 at 20°C.

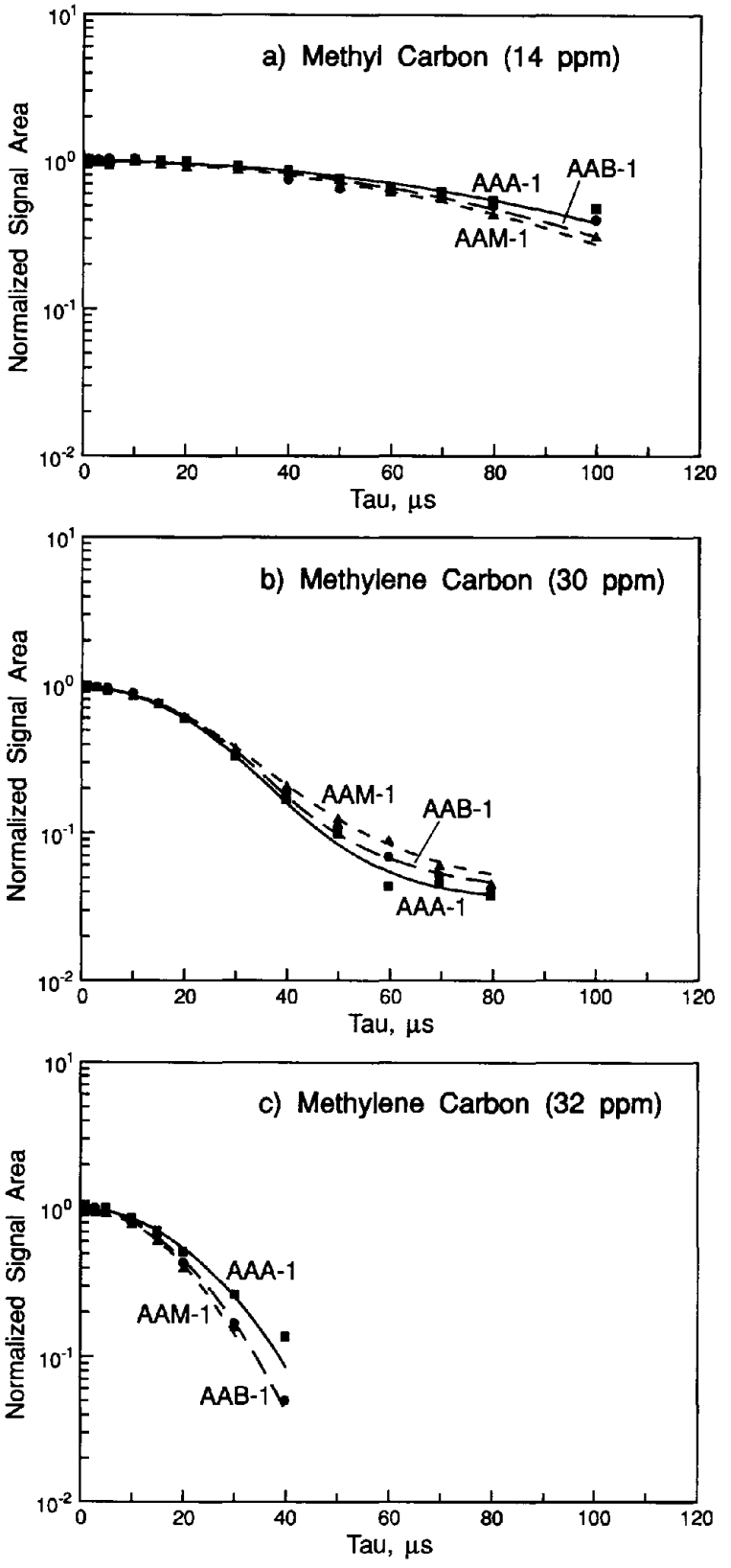

Figure 3-49. Carbon-13 dipolar-dephasing NMR relaxation rates in asphalts AAA-1, AAB-1, and AAM-1 at -45°C: (a) terminal methyl carbons (14 ppm), (b) methylene carbons (30 ppm) in the interfacial and amorphous phases, (c) methylene carbons (32 ppm) in the crystalline phase.

SUMMARY OF CHAPTER 3

In the introduction to this chapter, some important chemical and physical properties of paving asphalts were discussed. Because physical properties of any material are a function of its chemical composition, it is necessary to understand the relationships between chemical composition and physical properties if there is to be a satisfactory understanding of the engineering applications of a specific material.

It was emphasized that asphalts are petroleum residua. They consist of very many individual organic compounds. These compounds may be classified into a large number of chemical types having different chemical and physical properties. Hydrocarbons of various types predominate in asphalts, but compounds that contain one or more of the heteroatoms nitrogen, oxygen, and sulfur are abundant. Almost all compounds in asphalts contain 18 or more carbon atoms, which means that there are few volatile, low molecular weight compounds present. Nevertheless, the number-average molecular weight values measured for whole asphalts by various methods are not particularly high, ranging from several hundred to two thousand daltons. Yet asphalts behave rheologically as though they consist of molecules having molecular weight values an order of magnitude larger than were determined by such methods as VPO and mass spectrometry. It is known from research on a large number of organic materials (especially polymers) that the properties of molecular weight and molecular weight distribution largely determine rheological behavior. Asphalts exhibit viscoelastic behavior in the service temperature range. Also, asphalt viscosities are highly temperature and shear dependent. It is these properties that confer on asphalts their utility as paving materials. It is naturally of interest to determine why an apparently low molecular weight material could have properties more characteristic of a substance with much higher molecular weight.

Various models of asphalt structure have been proposed to account for these unique features of asphalts. By a model is meant a spatial representation of asphalt microstructure. A picture of asphalt as a random mixture of all constituent molecular species at asphalt service temperatures does not explain many of the important performance-related physical properties of asphalts.

The earliest researchers proposed that asphalts are colloidal dispersions of asphaltenes in a maltene solvent. Asphaltenes are the most polar, aromatic components of asphalts, and maltenes contain mostly non-polar molecules, along with some polar ones. It was assumed that the asphaltene particles are composed of associations of relatively small molecules and that these molecular associations can be broken up by heat and shear. The existence of heat and shear sensitive entities is essential to account for asphalt physical properties that vary markedly with changes in these variables. A variety of chemical and physical evidence was advanced in support of this model. In this chapter, it was shown that a somewhat similar model could be derived from rheological considerations, providing a more quantitative picture of asphalt structure. A comparison of this model with models of asphalt structure proposed by other researchers was provided. Some data that do not appear to support such a model were discussed.

The concept of asphalt compatibility has been further developed. Compatible asphalts differ from less compatible asphalts in rheological properties and in chemical composition. Additionally, pavements prepared from the more compatible asphalts may be more susceptible to rutting. A mathematical relationship was found to exist between certain compositional features of asphalts and asphalt relative viscosity. The fact that such a relationship exists lends credence to the model of asphalt structure proposed during SHRP and this program.

The amount of information that can be obtained from overall (global) chemical and physical properties of asphalts is somewhat limited. One important global property, and an obvious exception to the previous statement, is the glass transition temperature T_g. The technique of MDSC was used to accurately determine T_g values (or more accurately, ranges) of all SHRP asphalts. As observed by previous researchers for other asphalts, relationships between T_g, S, and m-values (these rheological parameters were discussed in a previous section) were noted for the SHRP asphalts. Crystallization phenomena in whole asphalts, which affect low temperature properties, also were verified.

Several NMR techniques were used to measure molecular motions of asphalt components at low temperatures in whole asphalts. Molecular motions of individual molecules determine flow properties. Evidence for immobilization of molecules having n-alkane-like structural features in crystalline and rigid amorphous phases was found. Differences in the relative amounts of immobilized molecular structures at a given temperature were measured for several asphalts, and were found to vary considerably.

To obtain more detailed information about the relationship of asphalt properties with composition, various fractionation methods were utilized. Among these methods are solvent precipitation and extraction, IEC, and SEC. One objective of some of these fractionations was the separation of the dispersed component from the solvent component of asphalts. Each method provides fractions that are highly polar and fractions that are relatively non-polar. The fractions may be further separated into subfractions of interest.

The non-polar fractions of asphalts isolated by all three methods were intensively studied by MDSC. It was found that T_g values are a function of the molecular weight values of the non-polar components. That is, these non-polar components exhibit what is termed Fox-Flory behavior. This very important low temperature property can be altered by addition of other materials. Adding polar molecules to non-polar asphalt components raises T_g of the mixture in proportion to the amount of polars added. In an experiment involving crossblended materials, it was found that the source of the polar materials has little effect on T_g. Adding lower molecular weight non-polar dopants lowers T_g values of asphalt non-polar components and of whole asphalts. An equation relating molecular weight values of non-polar components and mass fractions of polar components to T_g values of mixtures of asphalt components was proposed.

Solubility parameter values of non-polar components also were measured. This parameter must be an important consideration in the blending of different asphalts and when adding chemicals that alter asphalt properties. Solubility parameters of asphalt non-polar

components are surprisingly low. Therefore, these materials will not be good solvents for polar materials. The presence of materials of intermediate polarity is required for stable systems to exist.

Most work on oxidative aging of whole asphalts is reported in chapter 4. However, some work on oxidation of various mixtures of asphalt components was reported in this chapter. Based on results from oxidative aging of a series of crossblended mixtures of asphaltenes of one asphalt with maltenes of another, it appears that the solvent component of asphalts determines the course of oxidation. Relative amounts of the two components (solvent and dispersed component) also influence oxidative aging. The manner in which solvent and dispersed components interact affects rheological properties of aged and unaged materials and is not easily predicted from properties of whole asphalts.

When a specific solvent component from one asphalt (represented by SEC Fraction-II) is mixed with equal amounts of dispersed components (represented by SEC Fraction-I materials) from different asphalts, mixtures are obtained whose rheological properties are greatly influenced by the source of the dispersed component. Some dispersed components yield mixtures that have high elasticity and low shear susceptibility. Other dispersed components yield mixtures that are relatively more Newtonian or are highly shear susceptible. On the other hand, T_g values of the same mixtures are determined by the nature of the solvent component and relative amounts of solvent and dispersed components, but not the nature of the dispersed component. This series of experiments demonstrates that different asphalt components determine some properties but have little or no influence on others. These results follow from the model of asphalt structure proposed earlier. The results also allow for better prediction of the effects of blending asphalts and adding other materials to asphalts. It may be possible to alter some properties in a benign manner without adversely affecting other properties.

The solvent and dispersed components may be further subdivided into fractions. The dispersed component, as represented by an SEC fraction, was further fractionated by SEC into four subfractions. Molecular weights of these subfractions were measured. The subfractions assumed to be of highest molecular weight had molecular weight determinations performed using membrane osmometry. Values of up to 40,000 daltons, depending on source of material, were measured. Assuming that these subfractions are composed of highly associating polar units, then entities from asphalts are equivalent to some organic polymers in their apparent molecular weights. These materials comprise several mass percent of the asphalts studied and would be expected to dominate rheological properties. Their existence is not detected by measuring molecular weights of whole asphalts by techniques such as VPO, which yields average molecular weight values skewed toward the lowest molecular size components. Thus, the anomaly of asphalt rheology not correlating with global molecular weight values is resolved. Effective molecular weight values of some molecular associations in whole asphalts are probably much larger than 40,000 daltons. Other dispersed component subfractions are lower in molecular weight. When each dispersed component subfraction was mixed with an asphalt solvent component, mixtures were obtained whose rheological properties were a

function of the relative amounts and molecular weight values of the subfractions in each mixture. Thus rheological measurements were correlated with molecular weight values.

Naturally occurring waxes have attracted the attention of asphalt researchers in recent years. These compounds are the least polar constituents of asphalts and some (but not all) waxes are also among the lowest in molecular weight. They have a pronounced tendency to crystallize, i.e., form a separate phase. Waxes were isolated from neutral fractions of the eight SHRP core asphalts. Four of these asphalts contain small amounts of waxes. Three contain significant amounts of paraffin waxes. One asphalt contains large amounts of what appear to be microcrystalline waxes. Waxes isolated from certain asphalts were used as dopants in mixtures with their parent asphalts and in mixtures with other asphalts. Addition of paraffin waxes results in enhanced viscosities of mixtures, whereas addition of microcrystalline waxes caused decreases in viscosities of mixtures. The tendency of waxes to form crystals over time in asphalts influences low temperature properties and must influence pavement performance. It is known that as pavement temperatures are lowered, the influence of the binder on physical properties overtakes the influence of aggregates, so these results have practical significance. Also, formation of wax crystals in asphalts may result in centers of weakness, leading to cracking.

It was stated in chapter 1 that there is a need to reconcile perceptions of asphalts from engineers' and chemists' perspectives. In the work covered in this chapter, a chemical structural model of asphalt structure was developed from rheological theories based on engineering data. Using an equation derived from the theory, a rheological property was found to be predicted from compositional variables. Using NMR techniques, molecular motions were measured that were related to flow properties. Asphalts were separated into significant fractions, guided by considerations of the model of asphalt structure. These significant fractions were found to strongly influence certain asphalt physical properties, but not others. The effect on physical properties could be calculated from the nature and/or amounts of the particular fractions.

REFERENCES

Altgelt, K., and O. Harle, 1975, The Effect of Asphaltenes on Asphalt Viscosity. *Industrial Engineering Chemistry, Product Research Development*, 14: 240-246.

Anderson, D. A., M. Marasteanu, C. Antle, and T. Ruscitti, 1996, Relationship of SHRP Asphalt Binder Properties to Performance: Draft of Final Report, FHWA Contract DTFH-61-92-C-00170.

Andrade, E. N., 1934, A Theory of the Viscosity of Liquids. *Philosophical Magazine*, 17: 698-732.

Axelson, D. E., 1986, Carbon-13 Solid-State NMR of Semicrystalline Polymers, Chapter 5. In Komoroski, R. A., ed., *High Resolution NMR Spectroscopy of Synthetic Polymers in Bulk*, Methods in Stereochemical Analysis, Vol. 7. VCH Publishers, Deerfield Beach, FL.

Bahia, H. U., and D. A. Anderson, 1992, Physical Hardening of Paving Grade Asphalts as Related to Compositional Characteristics. *American Chemical Society Division Fuel Chemistry Preprints*, 37(3): 1397-1407.

Bair, H. E., 1981, Thermal Analysis of Additives in Polymers. In Turi, E. A., ed., *Thermal Characterization of Polymeric Materials*. Academic Press, New York, NY, p. 882.

Barbour, F. A., and J. F. Branthaver, 1992, Analysis of SHRP Asphalt Nonpolar Fractions by Supercritical Fluid Chromatography. *Fuel Science and Technology International*, 10(4-6): 979-1001.

Barbour, F. A., R. F. Blake, J. F. Branthaver, and R. E. Robertson, 1997, Evaluation of Supercritical Fluid Extraction of Asphalt Binders from Asphalt-Aggregate Mixes. FHWA Report in progress.

Barth, E. J., 1962, *Asphalt Science and Technology*, Gordon and Breach, New York, NY.

Barton, A. F. M., 1975, Solubility Parameters. *Chemical Reviews*, 75: 731-753.

Bharati, S., G. Rostum, and R. Loberg, 1994, Calibration and Standardization of Iatroscan (TLC-FID) Using Standards Derived From Crude Oils. Advances in Organic Geochemistry 1993. *Organic Geochemistry*, 22(3-5): 835-862.

Boduszynski, M. M., J. F. McKay, and D. R. Latham, 1980, Asphaltenes, Where Are You? *Proceedings, Association of Asphalt Paving Technologists*, 49: 123-143.

Branthaver, J. F., J. C. Petersen, J. J. Duvall, and P. M. Harnsberger, 1991, Compatibilities of Strategic Highway Research Program Asphalts. *Transportation Research Record* 1323, 22-31.

Branthaver, J. F., J. J. Duvall, J. C. Petersen, H. Plancher, and R. E. Robertson, 1992, Preparative Size-Exclusion Chromatography Separation of SHRP Asphalts: Correlation with Viscoelastic Properties. *Fuel Science and Technology International*, 10: 1003-1032.

Brule, B., J. P. Planche, G. King, P. Claudy, and J. M. Letoffe, 1990, Relationships Between Characterization of Asphalt Cements by Differential Scanning Calorimetry and Their Physical Properties. *American Chemical Society Division of Petroleum Chemistry Preprints*, 35(3): 330.

Burrell, H., 1955, Solubility Parameters. *Interchemical Review*, 14: 3-46.

Christensen, D., H. Bahia, and D. A. Anderson, 1996, Physical Properties of Asphalt Cement and Their Relation to Microstructural Model. *Proceedings, Association of Asphalt Paving Technologists*, 65: 385-407.

Claudy, P., J. M. Letoffe, G. N. King, J. P. Planche, and B. Brule, 1991, Characterization of Paving Asphalts by Differential Scanning Calorimetry. *Fuel Science and Technology International*, 9: 71.

Claudy, P., J. M. Letoffe, F. Rondelez, L. Germanaud, G. N. King, and J. P. Planche, 1992, A New Interpretation of Time-Dependent Physical Hardening in Asphalt Based on DSC and Optical Thermoanalysis. *American Chemical Society Division of Fuel Chemistry Preprints*, 37(3): 1408-1426.

Daly, W. H., Z. Qiu, and I. Negulescu, 1996, Differential Scanning Calorimetry Study of Crystallinity of Asphalts. *Transportation Research Record* 1535, 54-60.

Eilers, H., 1941, Die Viskositat von Emulsionen Hochviskoser Stoffe als Funktion der Konzentration. *Kolloid-Zeitschrift*, 97: 313-321.

Einstein, A., 1906, Eine Neve Bestimmung der Moleküldimensionen. *Annalen der Physik*, 19: 289-307.

Ewell, R. H., and H. Eyring, 1937, Theory of the Viscosity of Liquids as a Function of Temperature and Pressure. *Journal of Chemical Physics*, 5: 726-736.

Eyring, H., 1936, Viscosity, Plasticity, and Diffusion as Examples of Absolute Reaction Rates. *Journal of Chemical Physics*, 4: 283-293.

Fox, T. G., 1956, Influence of Diluent and of Copolymer Composition on the Glass Temperature of a Polymer System. *Bulletin of the American Physical Society*, [2] 1: 123.

Fox, T. G., and P. J. Flory, 1950, Second-Order Transition Temperatures and Related Properties of Polystyrene. I. Influence of Molecular Weight. *Journal of Applied Physics*, 21: 581.

Giavarini, C., and F. Pochetti, 1973, Characterization of Petroleum Products by DSC Analysis. *Journal of Thermal Analysis*, 5: 83-94.

Girdler, R. B., 1965, Constitution of Asphaltenes and Related Studies. *Proceedings, Association of Asphalt Paving Technologists*, 34: 45-79.

Gupta, M. K., 1995, Estimation of the Glass Transition Temperature of Acrylic Copolymers. *Journal of Coatings Technology*, 67(846): 53.

Heithaus, J., 1962, Measurement and Significance of Asphaltene Peptization. *Journal of the Institute of Petroleum*, 48: 45-53.

Huang, S. C., J. F. Branthaver, R. E. Robertson, and S. S. Kim, 1998, Effect of Film Thickness on the Rheological Properties of Asphalts in Contact with Aggregate Surface. To be submitted to *Transportation Research Record.*

Huynh, H. K., T. D. Khong, S. L. Malhotra, and L-P. Blanchard, 1978, Effect of Molecular Weight and Composition on the Glass Transition Temperatures of Asphalts. *Analytical Chemistry*, 50(7): 976.

Jennings, P. W., J. A. Pribanic, B. Fanconi, and D. L. VanderHart, 1991, SHRP A002C, Binder Characterization and Evaluation by NMR Spectroscopy, Final Report, Part III.

Kim, S. S., and J. F. Branthaver, 1996, Polarities of SHRP Asphalts Calculated from Ion Exchange Chromatography Separation Data. *Fuel Science and Technology International*, 14: 365-393.

Komoroski, R. A., ed., 1986, *High Resolution NMR Spectroscopy of Synthetic Polymers in Bulk*, Methods in Stereochemical Analysis, Vol. 7. VCH Publishers, Deerfield Beach, FL.

Lin, S.-Y., C.-M. Liao, and R.-C. Liang, 1995, Use of Microscopic FT-IR/DSC Combined System for the Study of Glass Transition Temperatures of Polymers. *Polymer Journal*, 27(2): 201-204.

Manson, J. A.,1982, *McGraw-Hill Encyclopedia of Science and Technology*, Vol. 10, pp 630-635, McGraw-Hill Book Co., New York.

Maron, S. H., and S. Fok, 1953, Effect of Concentration on Flow Behavior of Glass Sphere Suspensions. *Journal of Colloid Science*, 8: 540-542.

McKay, J. F., J. F. Branthaver, and R. E. Robertson, 1995, Isolation of Waxes from Asphalts and the Influence of Waxes on Asphalt Rheological Properties. *American Chemical Society Division of Petroleum Chemistry Preprints*, 40(4): 794.

Mehrotra, A. K., and W. Y. Svrcek, 1986, Viscosity of Compressed Athabasca Bitumen. *Canadian Journal of Chemical Engineering*, 64: 844-847.

Memon, G. M., and B. H. Chollar, 1996, Glass Transition Measurements of Virgin, Chemically Modified, Polymer Modified, and Crumb Rubber Modified Asphalts. The 11th Congress on Thermal Analysis and Calorimetry Proceedings, Philadelphia, PA.

Mooney, M., 1951, The Viscosity of a Concentrated Suspension of Spherical Particles. *Journal of Colloid Science*, 6: 162-170.

Mysels, K. J., 1967, *Introduction to Colloid Chemistry*. Interscience Publishers, Inc., New York.

Netzel, D. A., F. P. Miknis, J. L. Soule, A. E. Taylor, and M. L. Serres, 1998, Solid-State ^{13}C NMR Studies of the Structure and Dynamics of Asphalts, chapter.In Youtcheff, J., ed., Paving Asphalt Technology Handbook, in preparation.

Noel, F., and L. W. Corbett, 1970, A Study of the Crystalline Phases in Asphalts. *Journal of the Institute of Petroleum*, 56(551): 261.

Pal, R., and E. Rhodes, 1989, Viscosity/Concentration Relationships for Emulsions. *Journal of Rheology*, 33: 1021-1045.

Pauli, A. T., WRI/FHWA Annual Technical Report, Contract No. DTFH61-92-C-00170, November 1 - May 15, 1995, p. 251.

Reid, R. C., J. M. Prausnitz, and T. K. Sherwood, 1977, *The Properties of Gases and Liquids*, Third Edition. McGraw-Hill, New York, NY.

Roscoe, R., 1952, The Viscosity of Suspensions of Rigid Spheres. *British Journal of Applied Physics*, 3: 267-269.

Schmidt, R., and E. Barrall, 1965, Asphalt Transitions. *Journal of the Institute of Petroleum*, 51: 162-168.

Severs, E., 1962, *Rheology of Polymers*. Reinhold, New York, NY.

Shaw, D. J., 1980, *Introduction to Colloid and Surface Chemistry*, Third Edition. Butterworths, London.

Sheu, E., and D. Storm, 1995, Colloidal Properties of Asphaltenes in Organic Solvents. In Sheu, E. Y., and O. C. Mullins, eds., *Asphaltenes: Fundamentals and Applications*. Plenum Press, New York, NY, p. 1-52.

Sheu, E., M. DeTar, and D. Storm, 1991, Rheological Properties of Vacuum Residue Fractions in Organic Solvents. *Fuel*, 70: 1151-1156.

SHRP, 1992, *Materials Reference Library Asphalt Properties*. Strategic Highway Research Program National Research Council, Washington, D. C., May 1992.

SHRP, 1993, *SHRP-A-368, Binder Characterization and Evaluation, Volume 2: Chemistry*. Strategic Highway Research Program, National Research Council, Washington, D. C.

SHRP, 1994, *SHRP-A-370, Binder Characterization and Evaluation, Volume 4: Test Methods*. Strategic Highway Research Program, National Research Council, Washington, D.C.

Smith, C. D., C. C. Scheutz, and R. S. Hodgson, 1966, Relationship Between Chemical Structures and Weatherability of Coating Asphalts as Shown by Infrared Adsorption Spectroscopy. *Industrial Engineering Chemistry, Product Research Development*, 5: 153.

Sperling, L. H., 1992, *Introduction to Physical Polymer Science*, 2nd Edition. John Wiley & Sons, New York, NY.

Srivastava, S. P., R. S. Tandon, P. S. Verma, A. K. Saxena, G. C. Joshi, and S. D. Phatak, 1992, Crystallization behavior of n-paraffins in Bombay-High middle-distillate wax/gel. *Fuel*, 71: 533.

Storm, D., and E. Sheu, 1993, Rheological Studies of Ratawi Vacuum Residue at 366 K. *Fuel*, 72: 233-237.

Storm, D. A., E. Y. Sheu, R. J. Barresi, and M. M. DeTar, 1991, Colloidal Properties of Asphaltenes in Vacuum Residue. Proceedings, International Symposium Chemistry of Bitumens, Rome, June 5-8, 1991, 2: 813-841.

Storm, D., E. Sheu, and M. DeTar, 1993, Macrostructure of Asphaltenes in Vacuum Residue by Small-Angle X-ray Scattering. *Fuel*, 72: 977-981.

Storm, D., E. Sheu, M. DeTar, and R. Barresi, 1994, A Comparison of the Macrostructure of Ratawi Asphaltenes in Toluene and Vacuum Residue. *Energy & Fuels*, 8: 567-569.

Storm, D., R. Barresi, and E. Sheu, 1995a, Rheological Study of Ratawi Vacuum Residue in the 298-673 K Temperature Range. *Energy & Fuels*, 9: 168-176.

Storm, D. A., R. J. Baressi, and E. Y. Sheu, 1995b, Evidence for the Micellization of Asphaltenic Molecules in Vacuum Resid. *American Chemical Society Division of Petroleum Chemistry Preprints*, 40(4): 776-779.

Storm, D., R. Barresi, and E. Sheu, 1996, Flocculation of Asphaltenes in Heavy Oil at Elevated Temperatures. *Fuel Science and Technology International*, 14: 243-260.

Stroup-Gardiner, M., 1996, The Significance of Phase Angle Measurements for Asphalt Cements. *Journal of the Association of Asphalt Paving Technologists*, 65: 321-356.

Traxler, R. N., 1961, *Asphalt*. Reinhold, New York, NY.

Turi, E. A., ed., 1981, *Thermal Characterization of Polymeric Materials*. Academic Press, New York, NY, 972 p.

Turi, E. A., ed., 1997, *Thermal Characterization of Polymeric Materials*, 2nd Edition. Academic Press, New York, NY, 2420 p.

Turner, T. F., WRI/FHWA Annual Technical Report, November 1, 1995-May 15, 1996, Western Research Institute, Laramie, WY, p. 235.

Van Krevelen, D. W., 1990, *Properties of Polymers*, 3rd Edition. Elsevier, Amsterdam, The Netherlands, 875 p.

VanderHart, D. L., 1981, Influence of Molecular Packing on Solid-State ^{13}C Chemical Shifts: The *n*-Alkanes. *Journal of Magnetic Resonance*, 44: 117.

VanderHart, D. L., and A. N. Garroway, 1979, ^{13}C NMR Rotating Frame Relaxation in a solid with Strongly Coupled Protons: Polyethylene. *Journal of Chemical Physics*, 71(7): 2773.

Wunderlich, B., 1990, *Thermal Analysis*. Academic Press, San Diego, CA, 450 p.

CHAPTER 4: OXIDATION AND OXIDATIVE AGING

SYNOPSIS

Asphalt oxidative aging in pavements, accompanied by a major increase in asphalt stiffness, is the primary cause of pavement embrittlement leading to raveling, cracking, and premature pavement failure. To understand the progressive deterioration of performance-related physical properties resulting from oxidative aging, the kinetics of asphalt oxidation (rates of oxidation and age hardening) were studied as a function of oxidation time, temperature, oxygen concentration (pressure), and asphalt composition. The rates of oxidation and the corresponding increase in asphalt stiffness were found to be highly dependent on variations in the microstructure (molecular association) of asphalts, which varies widely with differences in asphalt composition. Because the level of microstructure in asphalts is highly temperature dependent, the maximum temperature that asphalt experiences in pavement service is a major determinant of pavement embrittlement. Increasing the oxidation temperature increases the viscosity sensitivity of asphalt to the oxidation products formed. A significant difference was found in the rates of age hardening between high pressure 100°C (212°F) PAV aging and diffusion-controlled, lower temperature aging as it occurs in pavements. Oxidation products formed during the 100°C (212°F) PAV test had a much greater relative effect on viscosity increase than did similar oxidation products formed during diffusion-controlled, atmospheric oxidation in the pavement temperature range. These findings emphasize the need for additional research to improve and validate an aging test so that it is more useful for asphalt specification and for predicting asphalt durability and useful service life in pavements.

Evaluation of the kinetic data and chemistry of asphalt oxidation led to the proposal of a dual, sequential oxidation mechanism for asphalt oxidation. In summary, an initial rapid oxidation and viscosity increase results from the reaction of a limited amount of highly reactive asphalt hydrocarbons. This reaction reaches completion in the early stages of oxidation. The initial rapid reaction forms predominantly sulfoxides and probably causes aromatization of dihydroaromatics. During the progress of this initial reaction, the major and much slower oxidation reaction of the benzylic carbon components in asphalt is initiated with the formation of ketones. This dual oxidation mechanism resolves conflicts among results of previous investigators regarding the mechanism(s) of asphalt oxidation. Ketones are the oxidation products primarily responsible for the increase in asphalt stiffness because they cause strong associations among molecular agglomerates in asphalts, leading to significant increases in apparent molecular weight.

The viscosity sensitivity of asphalts to ketone oxidation products decreases as the oxidation temperature is decreased; thus, in the low temperature range in which pavement transverse cracking becomes a problem, the ketone oxidation products probably play only a minor role on low temperature physical properties. The higher temperature PAV oxidation produced less change in bending beam rheological properties than did PAV oxidation in the maximum pavement temperature range. This difference may affect correlations between laboratory grading and actual field performance of asphalts. Aggregates in pavement mixtures

were found to have little or no effect on asphalt oxidative age hardening at pavement use temperatures; however, at 100°C (212°F) some aggregates significantly increased the rate of oxidative age hardening.

NMR imaging (NMRI) was explored as a non-invasive technique to visually follow the coagulation and precipitation of asphaltenes from solution throughout the cross section of the otherwise optically opaque sample. Results of the application of this technique, which is still in its infancy, to oxidatively aged asphalts suggest that NMR imaging might be used to assess the compatibility of aged asphalts.

IGLC was applied to the SHRP asphalts to further understand the role of asphalt oxidation products on asphalt molecular association and age hardening. Results of the technique, developed a number of years ago, had been shown to correlate with pavement resistance to cracking from oxidation in the California Zaca-Wigmore road test of the late 1950s. In the present investigation, the interactions of IGLC test compounds with oxidized asphalts were found to correlate with known oxidation products formed. Preliminary work has begun on modifying the IGLC technique to use capillary columns rather than packed columns so that asphalts can be evaluated much more rapidly.

SEC was found to be extremely useful during the SHRP to separate asphalts into fractions of different apparent molecular sizes, and these fractions also are chemically distinct from one another, thus enabling relationships to be established between asphalt composition and performance-related physical properties. The SEC procedure used in SHRP was preparative in nature and very labor and materials intensive. During the present project, a rapid high pressure liquid chromatography (HPLC) method operating in the SEC mode was developed and experimental conditions established so that the results of the preparative SEC method could be simulated. The technique thus should be useful as a rapid test for screening asphalts with regard to the key parameters that correlate with physical properties as established by preparative SEC.

INTRODUCTION

It is well accepted by the pavement engineering community that good performing asphalts must possess the correct balance of physical properties to produce a high quality, durable asphalt pavement. Deterioration of these optimum physical properties during pavement service inevitably produces a loss in pavement performance leading to such problems as increased pavement cracking and raveling, inferior rideability, increased maintenance costs, and shortened pavement life. The primary contributor to the deterioration of these properties is the reaction of the asphalt binder with atmospheric oxygen, causing asphalt hardening and embrittlement. The major strategy of the design engineer to combat oxidative age hardening is to reduce the pavement permeability to air (related to void content). Extensive past field studies [Goode and Lufsey 1965; Vallegra et al. 1970] have shown that void content correlated strongly with asphalt hardening, pavement embrittlement, and cracking. However, there is a lower limit on void-content below which the mixture becomes unstable and sensitive to rutting and shoving. Thus, optimum void content of pavement mixtures is a compromise. In addition to oxidation, loss of

volatile, oily components of the asphalt during pavement service could cause asphalt hardening. However, a study by Corbett and Merz [1975] showed that volatile loss could be discounted as a significant contributor to pavement embrittlement; they found that the saturates fraction, which contains the potentially volatile components, was virtually unchanged after 18 years of service in the well-known Michigan Road Test [Serafin et al. 1967].

Historically, the optimum void content necessary to achieve a good balance of pavement performance properties and reduced sensitivity to asphalt oxidation has been about 4 percent. However, even at this void level, pavements still have sufficient permeability to make oxidation the primary contributor to deterioration of the asphalt binder. Thus, to better design pavements and predict their service life, it is important to understand asphalt oxidation and its effect on physical properties.

A major barrier to understanding asphalt oxidation has been the wide variability in the susceptibility of asphalts to oxidative age hardening as a function of asphalt composition (crude source of the asphalt). It has been well established, particularly during the SHRP research [Branthaver et al. 1993], that wide variations in key performance properties can result from variations in initial asphalt chemical composition, even in asphalts of the same stiffness. As a result, because oxidation alters chemical composition, wide variations in physical properties among asphalts can result from the same level of chemical oxidation; therefore, predicting changes in physical properties on oxidation of a given asphalt becomes a highly complex problem.

The understanding of asphalt oxidation and its effects on properties involves two general, though highly interrelated areas. One is an understanding of the chemistry and mechanisms of asphalt oxidation reactions. The other is an understanding of how the products formed on oxidation influence the asphalt physical properties, and how this response varies as a function of asphalt composition. Asphalt is a dispersion of highly polar, associated molecular agglomerates (sometimes called micelles or dispersed phase, and often equated to the asphaltenes fraction) that are peptized by the more loosely associated resinous components of the asphalt in the oily, solvent phase sometimes equated to the neutrals fraction obtained by IEC. These IEC neutrals comprise 50-60 percent of most neat asphalts. The physicochemical state of this dispersion (component compatibility) determines the rheological response of the asphalt. Asphalts having a low concentration of dispersed components have high component compatibility and exhibit more Newtonian flow properties with less elastic response than less compatible asphalts, which are characterized by higher concentrations of dispersed components. In less compatible asphalts, the dispersed components interact to produce non-Newtonian flow properties and the elastic component of flow is increased. Work during SHRP showed that differences in the state of dispersion of asphalts alter the kinetics (rates) of asphalt oxidation. In addition, differences in the state of dispersion also greatly alter the response of an asphalt to the oxidation products [Petersen et al. 1993]. Thus, understanding the chemical mechanisms of oxidation and the effects of oxidation on performance-related physicochemical properties has been a major focus of the current research. This understanding is necessary not only to improve accelerated aging tests, usually performed under time-temperature conditions quite unlike pavement oxidative aging, but

also to provide the fundamental information necessary to improve specifications and to more accurately predict the useful life of pavements.

OXIDATION AND ITS EFFECTS ON PERFORMANCE-RELATED PHYSICAL PROPERTIES

Microstructural Model of Asphalt Composition as Related to Asphalt Oxidation

The physicochemical aspects of the microstructural model of asphalt composition provide the fundamental basis for the interpretation of the changes that occur in asphalt physical properties as its reactive components are oxidized. Also, the chemistry and kinetic data on asphalt oxidation should provide further validation of the asphalt microstructural model. Thus, to assist in the discussion, those aspects of the model particularly relevant to asphalt oxidation are reviewed.

The classical model of asphalt first proposed by Nellensteyn [1924; 1928] as a dispersion of associated submicroscopic components that are peptized by the resinous fraction in the asphalt solvating medium still provides the fundamental premise for the current model of asphalt microstructure. Past theoreticians have often equated the associated, dispersed components with the asphaltene fraction and the dispersing and solvating components to the maltenes fraction. Based on this model, the asphaltenes are kept dispersed (peptized) in the rather non-polar solvent components of the maltenes by the adsorption of the more polar, resinous components of the maltenes.

A pictorial representation of the microstructural model of asphalt is presented in figure 4-1. In the generally accepted model, the dispersed components are highly associated molecular agglomerates that appear to take on a particulate nature. They are composed of the most polar and aromatic molecules of the asphalt. Molecules containing heteroatoms such as oxygen, nitrogen, sulfur, and metals are concentrated in this fraction. Current research suggests that these molecular agglomerates are typically about 30 to 100 molecules in size and are relatively resistant to thermal dissociation below about 93°C [Storm et al. 1996]. It is believed that these "hard core" molecular agglomerates are the major components that coagulate to form the asphaltene fraction when asphalt is diluted in a hydrocarbon such as n-heptane (which strips away the stabilizing resinous components). It is also generally believed that there are no sharp boundaries between the so-called phases, but rather there exists a polarity gradient within the adsorbed resinous components consisting of the more strongly associated molecules near the interior of the micellar structure and the more weakly associated molecules near its extremities. In typical paving asphalts, as the concentration of micellar structures increases (higher asphaltene content or high levels of oxidation), or the solvent power of the continuous dispersing phase becomes poor, the extremities of the resinous solvation shells [Storm et al. 1996] surrounding the "hard core" of the microstructure begin to overlap and interact. Such interaction tends to inhibit free flow of the dispersed agglomerates past one another during shear, thus imparting non-Newtonian flow properties to the asphalt.

Of particular relevance to asphalt oxidation is the sensitivity of the microstructure to change with temperature and the location within the microstructure of the molecular components that are potentially reactive toward oxygen. As temperature is increased, the more weakly associated molecules in the extremities of the resinous solvation shell become more mobile, thus becoming more identified with the solvent phase of the asphalt. Of key importance to asphalt oxidation is that the oxidation reactions and oxygen diffusion proceed more rapidly as the molecules become more mobile. Molecular mobility greatly facilitates bimolecular reactions because the two molecules must find each other to react. A good example of this phenomenon is found in the oxidation of asphaltenes. Asphaltenes, when separated from asphalt as a dry powdery solid, are resistant to air oxidation; however, when their molecular mobility is increased by dissolving them in a solvent, or by heating them until they became fluid, they are the most reactive asphalt components toward air oxidation [Knotnerus 1971; Petersen 1984].

Ketones and sulfoxides are the major oxygen-incorporating products of asphalt oxidation [Petersen 1986]. Therefore, the location of their precursors in the asphalt microstructure is critical to their molecular mobility and, thus, their reactivity toward oxidation. This is illustrated in figure 4-2, which shows the probable distribution of reactive precursors among the classical asphalt generic fractions. These fractions are generated by the well-known Corbett procedure and often are referred to as Corbett fractions. After separation of an asphalt into asphaltenes and maltenes, the maltene fraction is separated by column chromatography into saturates, naphthene aromatics, and polar aromatics. As illustrated in the first bar of the figure, the saturates fraction is composed of the most non-polar, weakly associating, and mobile components of the asphalt. At the other extreme, the polar aromatics fraction contains the more strongly associated, less mobile components of the resinous dispersing phase. The effect of association on effective molecular weight of the generic fractions is illustrated in the second bar of the figure. The distribution among the fractions of the reactive precursors of oxidation products is shown in the third and fourth bars. The sulfides, precursors to sulfoxides, are concentrated in the more weakly associating asphalt solvent components; the benzylic carbons, precursors to the ketones, are concentrated in the more strongly associating, more immobilized resinous components. Benzylic carbons are concentrated in the most strongly associating components because they are located on aromatic ring compounds, which have the inherent tendency to associate because of the polarizable pi electrons and planar geometry. Also, the more polar heteroatoms in asphalt (nitrogen, oxygen, metals, etc.) are often associated with the aromatic molecules and, thus, increase the intensity of the association. As a result, the reactivity of the ketone precursors becomes highly sensitive to the state of dispersion of the asphalt microstructure and the effects of temperature on the microstructure. It logically follows that ketone formation, with its attendant viscosity increase, is highly sensitive to oxidation temperature.

Effects of Temperature and Oxygen Pressure on Oxidation Kinetics

Upon oxidation, all asphalts exhibit a parabolic-like kinetic curve when log viscosity is plotted versus oxidation time, showing a rapid initial increase in viscosity followed by a slower, nearly linear rate of viscosity increase [Petersen et al. 1993]. The initial period of rapid oxidation and increase in viscosity at the front end of the kinetic plot is referred to in this report as the oxidation spurt. Viscosity increase for a given asphalt has been found to correlate with ketone

formation during laboratory oxidation and oxidative aging in pavements [Petersen et al. 1993; Lau et al. 1992; Liu et al. 1996; Martin et al. 1990]. Each asphalt has its own unique ketone-viscosity relationship. The formation of polar asphaltene components on oxidation also correlates with viscosity increase [Plancher et al. 1976]; thus, it follows that the rate of asphaltene formation should correlate with the rate of ketone formation, a relationship that has been demonstrated [Plancher et al. 1976; Branthaver et al. 1993].

The chemical oxidation and attendant viscosity increase of asphalts is influenced by asphalt composition, oxidation products formed, temperature, oxygen partial pressure (concentration), and/or diffusion rate. These effects on the oxidation kinetics are directly related to, or interrelated with, the physicochemical state (microstructure) of the asphalt. Four SHRP core study asphalts, AAM-1 (1.2 percent sulfur), AAG-1 (1.3 percent sulfur), AAF-1 (3.4 percent sulfur), and AAA-1 (5.5 percent sulfur), have been selected to demonstrate the effects of temperature and oxygen concentration on oxidation kinetics. These asphalts represent a wide range of variations in asphalt composition and component compatibility. It has been shown [Branthaver et al. 1991] that asphalt component compatibility correlates inversely with sulfur content for the eight SHRP core asphalts (although the correlation is probably fortuitous), with the more compatible asphalts having the lower sulfur content. Oxidations were conducted using both the PAV [Branthaver et al. 1993] and the thin film accelerated aging test (TFAAT) [Petersen 1989] procedures. The PAV procedure oxidizes a 3.125-mm- (1/8-in-) thick asphalt sample at an air pressure of 2.07 MPa (20 atm). It has been shown [Branthaver et al. 1993] that at this pressure the asphalt is completely saturated with oxygen (no diffusion effects); this is evidenced by uniform oxidation throughout the sample thickness. In the TFAAT oxidation procedure, a thin film (0.16 mm) of asphalt is oxidized at ambient air pressure using a modified RTFOT bottle in which the opening of the sample bottle is restricted to prevent significant volatile loss, yet provide near normal oxygen concentrations in the air. Because ambient air pressure is used, the TFAAT oxidation is oxygen diffusion controlled as is pavement oxidation. In figures 4-3 through 4-6, PAV data are shown for 60°C (140°F) and 100°C (212°F) oxidations and TFAAT data for 85°C (185°F) and 113°C (235°F) oxidations. Although PAV and TFAAT data were also obtained at 80°C (176°F) and 130°C (266°F), respectively, the data are not reported here because the kinetics were nearly the same at the two higher oxidation temperatures by either method. This similarity undoubtedly results because, at both of the higher temperatures, the molecular association or microstructure of the resinous components surrounding the highly associated nucleus of the associated components is thermally dissociated, making the effective concentrations of the immobilized reactive components similar at the two higher temperatures.

Kinetic data for the four asphalts selected are also shown in figures 4-3 through 4-6. The time scales of the plots at the higher temperatures have been time-temperature shifted to offset the effect of an increase in temperature on the increase in chemical reaction rate. This procedure permits the effects of changes in kinetics between the two temperatures to be visually compared. This convention is used throughout the report. Data for the oxidation of the highly compatible asphalt AAG-1 oxidized by both the PAV and TFAAT methods at two temperatures are shown in figure 4-3. Note that the kinetics of viscosity increase with PAV aging at 60°C (140°F) and 100°C (212°F) are not significantly different, with only a slightly greater relative oxidation rate at

60°C (140°F). This slight difference between the 60°C (140°F) and 100°C (212°F) data could, at least in part, result from assumptions made for time-temperature shifting.

However, the relative (time-temperature shifted) differences in the rates of ketone formation at 60°C (140°F) and 100°C (212°F) are greater than can be accounted for by the small differences in the viscosities. Since ketones correlate with viscosity increase, this result shows that the collective influence of the ketones formed at 60°C (140°F) had less effect on viscosity increase than did the ketones formed at 100°C (212°F). This can be explained based on the model presented earlier by ketones being formed on more highly associated ketone precursors in the more dissociated state at 100°C (212°F), thus their greater effect on viscosity. The effects of oxidation products on viscosity increase will be discussed in more detail in the next section. Unlike ketone formation, sulfoxide concentrations reach a maximum in the early stages of oxidation, very likely from exhaustion of sulfoxide precursors in this low sulfur asphalt. The lower maximum amount of sulfoxides formed at 100°C (212°F) could result from a relatively high rate of thermal decomposition of sulfoxides at the higher temperature. Typically in asphalts, once sulfoxide concentration reaches a maximum, it levels off at a constant value for the duration of the oxidation period.

The oxidation kinetics of ambient pressure oxidation at AAG-1 using the TFAAT procedure (figure 4-3) are in stark contrast to the PAV kinetics. Unlike the PAV oxidation, the kinetics of viscosity increase at 85°C (185°F) show a significantly lower relative rate than at the higher 113°C (235.4°F) temperature, particularly following the rapid oxidation spurt, during which the rates appear nearly the same. The reason for the much lower relative rate at 85°C (185°F) becomes apparent from examination of the relative amounts of ketones and sulfoxides formed at the two temperatures. Following the spurt, the rate of ketone formation becomes much slower during 85°C (185°F) oxidation than at 113°C (235.4°F). Ketones appear to be formed to some extent at the expense of sulfoxides at the higher temperatures. Based on observations made in our laboratory over the years, the relatively lower amount of sulfoxides at 113°C (235.4°F) than at 85°C (185°F) most probably results from a much more rapid rate of sulfoxide thermal decomposition at the higher temperature as suggested for PAV oxidation at 100°C (212°F). It is believed that the large increase in the relative amounts of ketones formed at 113°C (235.4°F) results from greater dissociation of the microstructure at the higher temperature, thus mobilizing additional reactive ketone precursors and significantly increasing their effective concentration.

The effect of increasing temperature on the increase in the relative rate of ketone formation and viscosity increase has significant ramifications that affect oxidation. Oxidative aging in pavements is diffusion controlled, as is TFAAT oxidation, and usually takes place at a lower temperature than 85°C (185°F); thus, the dramatic effect of temperature on oxidation kinetics as evidenced by the decreased ketones and increased sulfoxide concentrations and the much slower rate of formation in the 85°C (185°F) versus the 113°C (235.4°F) TFAAT oxidations is probably further amplified at normal pavement temperatures. The high temperature sensitivity of diffusion controlled oxidation and the differences in results between TFAAT and PAV oxidation methods emphasize conclusions arrived at earlier [Branthaver et al. 1993; Petersen et al. 1993] that, when evaluating asphalts for pavement use, it is important to know the maximum expected pavement temperature and the validity of the results of the accelerated aging

test used. Or, in the case of the accelerated aging test, one must know how to properly interpret and use the aging test results. The importance of temperature on pavement aging was confirmed by the California Department of Transportation study of Kemp and Predoehl [1981], which showed that the maximum pavement temperature was the most important variable influencing oxidative age hardening of paving mixtures aged under field conditions — even more important than pavement void content. The California study also showed that the maximum pavement temperature reached during hot days was more critical to eventual age hardening than was average temperature. The effects of temperature on age-hardening kinetics just described for asphalt AAG-1 becomes even greater for less compatible asphalts, as will be demonstrated in the next three figures.

Oxidation kinetic data for asphalt AAM-1, another compatible asphalt, are shown in figure 4-4. Unlike most of the other SHRP asphalts, asphalt AAM-1 has virtually no asphaltenes and yet exhibits non-Newtonian flow properties. Also, AAM-1 is unique in that its number-average molecular weight is the largest of the SHRP core asphalts. As a result of the higher inherent molecular weight, the non-Newtonian flow properties of this asphalt are influenced more by actual molecular weight and less by molecular association. Therefore, the oxidation kinetics of AAM-1, though its component compatibility is good, should be influenced more by physicochemical effects than AAG-1. Viscosity data for PAV oxidation of AAM-1 at 60°C (140°F) and 100°C (212°F) show a lower time-temperature shifted rate of viscosity increase at 60°C (140°F) than at 100°C (212°F), just opposite that found for AAG-1. Also, unlike the spread in the data for ketone and sulfoxide formation in AAG-1, their relative rates of formation in AAM-1 are not largely different at the two temperatures. Considering both the ketone and viscosity data, it is proposed that ketone formation in AAM-1 is less influenced by the association of polar molecules than in AAG-1. Thus, ketones formed at both temperatures have a similar effect on viscosity. It should be kept in mind that during PAV oxidation, unlike diffusion controlled TFAAT oxidation, the asphalt is saturated with oxygen throughout the microstructure.

Unlike the kinetic data for PAV oxidation of AAM-1, kinetic data for TFAAT oxidation in figure 4-4 show a significant physicochemical effect related to changes in the molecular microstructure on ketone formation and viscosity increase. The kinetics of ketone formation and subsequent viscosity increase were significantly inhibited during 85°C (185°F) oxidation compared with 113°C (235.4°F) oxidation. Thus, in actual pavement application, it is predicted that oxidative age hardening of asphalt AAM-1 might be much more sensitive to environmental temperature changes than asphalt AAG-1.

The significant effect of molecular association and immobilization in less compatible asphalts becomes readily apparent from the PAV oxidation kinetics for asphalt AAF-1 shown in figure 4-5. Note the lower relative rate of ketone formation and viscosity increase for 60°C (140°F) versus 100°C (212°F) oxidation. This is a particularly useful set of kinetic data for confirmation of the proposed mechanisms because the relative change in slopes of the ketone and viscosity plots have almost the same temperature sensitivity at both low and high temperature. Because ketone formation has been shown to correlate directly with log viscosity increase for a given asphalt, this correspondence between ketone and viscosity data strongly supports the

proposal that during PAV oxidation the associated structure is saturated with oxygen, and that molecular mobility (of asphalt molecules) and reactivity control the rate of formation of ketones throughout the microstructure. Putting it another way, the relative amounts of ketones being formed throughout the depth of the microstructure follow a similar pattern at both temperatures. Greater total amounts are formed at 100°C (212°F) because more mobility is achieved in the microstructure at higher temperatures. This interpretation is in contrast to that for diffusion-controlled TFAAT oxidation where oxygen does not significantly penetrate the micellar structure at the lower temperatures. As a result, the slope of the viscosity plot for the TFAAT oxidation is more sensitive to increase with oxidation temperature than the slope for ketone formation (figure 4-5).

The much greater relative rate of viscosity increase for 113°C (235.4°F) than for 85°C (185°F) TFAAT oxidation shows that many of the ketones formed at 113°C (235.4°F) have a greater effect on viscosity than those formed at 85°C (235.4°F). This again is strong circumstantial evidence that ketones are being formed on molecules inherently deeper in the micellar structure at 113°C (235.4°F) than at 85°C (185°F).

The final example of the effects of temperature and pressure on oxidation kinetics is illustrated by kinetic data in figure 4-6 for the high sulfur (5.5 mass percent), less compatible asphalt AAA-1. The significantly reduced sensitivity to viscosity increase of the 60°C (140°F) PAV oxidation compared with the 100°C (212°F) PAV oxidation suggests that for this more strongly associated asphalt, even at high oxygen concentrations, precursors buried more deeply in the microstructure at 60°C (140°F) have their reactivity reduced by molecular immobilization than at 100°C (212°F).

The consistent and progressive change in the kinetic data and their interpretation not only provides important information on how chemistry, particularly oxidation, affects asphalt properties as the chemistry changes from one asphalt to another, but also provides strong confirmation that the hypothesis developed for asphalt microstructure is correct. The application of such information should be of significant importance in developing models to predict changes in asphalt physical properties on pavement oxidative aging and ,thus, more accurate predictions of useful pavement life. The kinetic data should also aid in significantly improving accelerated asphalt aging tests and/or in better using the data being obtained from present tests to more accurately predict asphalt aging characteristics at realistic pavement temperatures.

Effects of Oxidation Products on Physical Properties

Relative Effects of Ketones and Sulfoxides on Physical Properties

Data from the four kinetic plots presented in the previous section have been reformatted by plotting the concentration of ketones and sulfoxides formed versus log viscosity increase. Such plots, while not kinetic plots, are usually linear for ketone formation and better illustrate the effects of the oxidation products formed on viscosity increase as influenced by asphalt composition and temperature. Dynamic viscosity measured at 1 rad/s (which is equivalent to the asphalt stiffness, G*) was chosen as the parameter to represent asphalt hardening on oxidation in

developing these correlations. It was chosen rather than parameters involving the phase angle to simplify the interpretation of the data when comparing asphalts. Correlations involving the fundamental rheological parameters G' and G'' might be a future exercise to fine tune the interpretations with regard to specific rheological parameters on specific performance-related properties; however, at this point we consider this a variable of secondary importance in establishing correlations between oxidative age hardening (stiffness increase) and asphalt oxidation.

Prior to discussing the next four figures, a diagrammatic model is presented in figure 4-7 to illustrate the effects of the association of polar components on effective molecular weight. It is not intended to illustrate the true physical aspects of the asphalt microstructure in neat asphalts. The diagram is based on the premise that viscosity increase on oxidation is primarily the result of an increase in effective molecular weight brought about by association of polar asphalt components. The precursors to these components prior to oxidation may have been either in the dispersed or dispersing phase of the asphalt. In the first bar at the top of the figure is illustrated the association of two small polar bodies. This could represent a molecule containing a sulfoxide group interacting with another sulfoxide or some other well dispersed component in the dispersing phase. The increase in effective molecular weight from such association is relatively small. Because sulfoxides are formed primarily from alkyl or alkylaryl sulfides, which are rather non-polar and probably do not contain any additional associating polar functionality, the associated species should remain solvated in the dispersing phase and have only a relatively small effect on viscosity change.

In the second bar in figure 4-7, the association of a dispersed polar species, such as a sulfoxide, with an associated polar molecular agglomerate is illustrated. Typical asphalt molecules likely to comprise the associated polar agglomerate are aromatic molecules, which may or may not contain heteroatoms. As illustrated in the diagram, were the dispersed polar component a sulfoxide, effective molecular weight from association would again be increased by only a small increment.

Illustrated in the third bar is the association of an associated polar agglomerate with another associated polar agglomerate. Benzylic carbons, which are the known precursors of ketones, are present as part of the aromatic molecules in the associated agglomerates. Thus, if ketones were formed on associated agglomerates and caused additional agglomerate association, a significant increase in effective molecular weight would result, as illustrated in the figure. Based on the interpretation of this model, it becomes apparent why log viscosity increase correlates with ketone and not sulfoxide formation.

The slopes of the ketone plots for compatible asphalt AAG-1 are shown in figure 4-8 for both PAV and TFAAT oxidation. The slopes are almost the same for both oxidation methods and are nearly insensitive to temperature. (Keep in mind these are not kinetic plots and do not represent the rate of formation of functionality, which was shown in figure 4-3 to be highly temperature sensitive for TFAAT oxidation.) Note that sulfoxides, which form very rapidly and reach their maximum value in this asphalt near the end of the spurt, show no significant effect on the linear ketone-viscosity relationship. This suggests that the sulfoxide contribution to viscosity

increase in AAG-1 is minor, if not insignificant. The similar sensitivities of viscosity increase to ketone formation from oxidation by both methods at each temperature can be explained by the effectiveness of solvation of any new molecular agglomerates formed by oxidation. Polar species generated may become part of the solvent to some extent, assisting in the dispersion any additional associated materials. The sensitivity to viscosity change for ketone formation for AAG-1 is about 4.5 log Pa·s/mol·L^{-1}.

Next consider the viscosity-functional group relationships for asphalt AAM-1 in figure 4-9. Although the molecular components of AAM-1 are quite compatible, the increased effects of their larger inherent molecular weight when molecules associate from ketone formation is apparent when the plots in figure 4-9 are compared with those of compatible AAG-1 in figure 4-8. The sensitivity of viscosity to ketone formation for AAM-1 was 9.1 and 8.7 Pa·s/mol·L^{-1} for 60°C (140°F) PAV and 85°C (185°F) TFAAT oxidations, respectively, values much higher than those for AAG-1. The similarity of the sensitivities obtained using both diffusion- and non-diffusion-controlled oxidation further confirms that the larger true molecular weight rather than apparent molecular weight dominates in influencing oxidation kinetics. That is, ketone precursors oxidized by both PAV and TFAAT oxidations are molecules with nearly the same potential for association. Viscosity sensitivities for ketone formation in asphalt AAM-1 were 12.5 and 13.3 Pa·s/mol·L^{-1} for 100°C (212°F) PAV and 113°C (235.4°F) TFAAT oxidations, respectively. Again, sensitivity values were similar for both oxidation methods, which is consistent with high component compatibility.

Viscosity sensitivities to ketone formation calculated for asphalt AAF-1 from figure 4-10 were 8.7 and 10 Pa·s/mol·L for 60°C (140°F) PAV and 85°C (185°F) TFAAT oxidations, respectively. At the higher temperatures, they were 10 and 20 Pa·s/mol·L^{-1} for 100°C (212°F) PAV and 113°C (235.4°F) TFAAT oxidations, respectively. In contrast to the results for the less polar asphalt AAM-1, the effects of increased polarity in the higher sulfur asphalt AAF-1 become readily apparent. Instead of small differences between viscosity sensitivity to ketone formation by both oxidation methods, much larger differences exist between methods, with ketones formed during TFAAT oxidation showing significantly different effects on viscosity at low and high temperatures. The effects of temperature on the dissociation of the micellar structure are greater for the more associated asphalt AAF-1. As increasing temperature breaks up the associated resinous microstructure, oxidation to form ketones occurs on the more polar, highly associated components, whose oxidation has a much greater effect on viscosity increase than ketones formed less deeply in the microstructure.

The similar viscosity sensitivities (to ketone concentration) for both 60°C (140°F) PAV and 85°C (185°F) TFAAT oxidations of AAF-1 suggest that the increased oxygen concentration deep in the microstructure offsets the effects of lower molecular mobility in the 60°C (140°F) PAV oxidation relative to the 85°C (185°F) TFAAT oxidation, leading to about the same kinds of ketone precursors being oxidized in the 60°C (140°F) PAV oxidation as in the diffusion-controlled 85°C (185°F) TFAAT oxidation. The effects of immobilization of highly associating ketone precursors and their dissociation as temperature is increased is again illustrated by comparing the 100°C (212°F) PAV and 113°C (235.4°F) TFAAT oxidations; the viscosity

sensitivity to ketone formation is twice as large (20 compared with 10 Pa·s/mol·L^{-1} ketones) for the TFAAT oxidation.

At the risk of being repetitive, the large effect of temperature on the viscosity sensitivity to ketones in diffusion-controlled oxidation (as in pavements), and further, the unusually large effect of temperature in increased reaction rates in highly associated asphalts, again underscores the importance of pavement temperature on pavement oxidative age hardening.

With regard to the effects of the sulfoxides on viscosity, it is difficult to obtain quantitative data on their effects from the data plots. Their changing rate of formation during oxidation, as suggested by the changing slope of the plots, and apparent from the kinetic plots in the previous section, does not show them to have major effects on viscosity change compared with ketones. One experiment, however, was conducted at WRI during the SHRP asphalt research that did yield definitive results for the high (6.4 mass percent) sulfur, highly associated asphalt AAK-1. To determine the effects that sulfoxide thermal decomposition (in which the sulfoxide oxygen is lost with the formation of no new oxygen-containing functionality in the asphalt) might have on viscosity change while thermally conditioning asphalt samples for rheological measurements, asphalt AAK-1 was subjected to thermal treatment in an inert atmosphere for one hour at different temperatures followed by measurement of viscosity and sulfoxide changes. Ketone concentration did not change. From these data we calculated a viscosity sensitivity to sulfoxides of 1.3 Pa·s/mol·L^{-1} for asphalt AAK-1. Because the more polar and highly associated asphalts should show the greatest sensitivity to sulfoxides, and AAK-1 is typical of a polar, associated high sulfur asphalt used in pavement construction, its viscosity sensitivity to sulfoxides should be near the top of the sensitivity range for most asphalts. The viscosity sensitivity to ketones of AAK-1 is 14.7 and 15.1 Pa·s/mol·L^{-1} for 60°C (140°F) PAV and 85°C (185°F) TFAAT oxidation, respectively, compared with the calculated sulfoxide sensitivity of 1.3 Pa·s/mol·L^{-1}. Thus, for diffusion-controlled 85°C (185°F) TFAAT oxidation, ketones have about 12 times the effect on viscosity increase as sulfoxides in AAK-1. Based on considerations discussed thus far, it would be expected that the effect of sulfoxides relative to ketones on viscosity increase should usually be less than those observed for asphalt AAK-1.

The final set of viscosity sensitivity data to be discussed is contained in figure 4-11 for asphalt AAA-1. Of the asphalts considered thus far, this asphalt has the most highly associated microstructure and, thus, is most sensitive to viscosity increase on oxidation with increasing temperature, both during PAV and TFAAT oxidation. Viscosity sensitivities to ketone formation are 10.5 and 10.0 Pa·s/mol·L^{-1} for 60°C (140°F) PAV and 85°C (185°F) TFAAT oxidation, respectively. For 100°C (212°F) PAV and 113°C (235.4°F) TFAAT oxidations, the values are 21 and 28.5 Pa·s/mol·L^{-1}, respectively. The significantly large difference between sensitivities for 100°C (212°F) and 60°C (140°F) PAV oxidations are particularly striking compared with only small differences for the other asphalts. From this it is concluded that, even at high oxygen concentrations within the asphalt, at 60°C (140°F) the associations among many of the ketone precursors are so strong and the molecules so immobilized that they become relatively unreactive to oxidation. Thus, at lower temperatures, even though asphalts such as AAA-1 contain large amounts of reactive ketone precursors, only a limited amount have significant reactivity; and

further, those that do react are at the peripheries of the microstructure and have minimum effect on viscosity increase. Thus, given a maximum environmental temperature, hardening of these asphalts becomes somewhat self-quenching with time.

In table 4-1, the viscosity sensitivity to ketone formation of the five SHRP asphalts just discussed are summarized for 60°C (140°F) and 100°C (212°F) PAV oxidations and 85°C (185°F) and 113°C (235.4°F) TFAAT oxidations. A significant observation can be made from the data in this table regarding the reliability of the PAV test run at 100°C (212°F) to rank asphalts according to their aging characteristics in the field. Note the similarities between the viscosity sensitivities to ketone formation for PAV oxidation at 60°C (140°F) and TFAAT oxidation at 85°C (185°F). This similarity strongly suggests that during non-diffusion controlled 60°C (140°F) PAV oxidation and diffusion controlled 85°C (185°F) TFAAT oxidation that, by and large, the same population of ketone precursors are being oxidized by both methods or, if not, the ketones formed in both methods have similar effects on oxidative age hardening. The disparity between the 100°C (212°F) PAV data and these two sets of lower temperature data is significant. Two conclusions seem apparent. Even though both TFAAT and pavement oxidative aging are diffusion controlled, these results suggest strongly that aging of the type that occurs in pavements may be mimicked rather well by PAV aging at 60°C (140°F). Also the unusually high sensitivity to ketone formation of some asphalts, particularly AAA-1, to ketone formation at 100°C (212°F) suggests that a significant amount of ketone precursors, which lead to unusually high viscosities when oxidation occurs at 100°C (212°F), may never be oxidized in pavements at normal pavement temperatures. These data do not reflect the rate of ketone formation, only sensitivity to their presence; however, the kinetic data discussed in the previous section show that ketones are also formed at relatively increased rates at high (compared with low) temperatures in asphalts such as AAA-1. Thus, the problems are compounded.

For those familiar with the SHRP binder research, it will be recalled that 60°C (140°F) was the temperature initially selected for the PAV test and that this temperature was initially used routinely as the principal temperature to prepare asphalts for rheological studies. The PAV test was initially selected for the SHRP program to decrease testing time by increasing oxygen concentration in the asphalt, which would allow oxidation to take place at temperatures much closer to pavement temperatures. Prior SHRP work at WRI on asphalt component compatibility had clearly shown that results of a high temperature accelerated test, such as the TFAAT test at 113°C (235.4°F), could not be reliably extrapolated to pavement temperatures. (Note the discrepancy of 113°C (235.4°F) TFAAT data in table 4-1 with low temperature data.) This potential problem has been a concern for many years and was the reason that Lee [1968] pioneered the use of low temperature pressure vessel aging nearly 30 years ago.

SHRP research personnel were aware that the 60°C (140°F) PAV oxidation took about six days to complete, but on the other hand had the promise of giving more reliable data for predicting pavement aging. The concern of the 6-day test time was expressed to the project advisory committee early in the project, but industry concerns about the length of the test did not become serious until the last year or two of the project. A compromise between time and temperature was finally made by selecting a higher temperature so that the test could be completed in one day.

This discussion is not made to criticize the SHRP program, but to renew awareness of the fact that within the short time constraints of the original SHRP research, there was not time to properly complete the research on oxidative aging and to develop a properly understood and validated aging test. It is only now that we have acquired the kinetic data and an understanding of the physicochemical effects of microstructure on oxidative aging necessary for design and/or calibration of an acceptable accelerated aging test. This is another example, all too common in the asphalt industry, of a feasible technical solution being compromised because of the unwillingness or inability of the industry to find ways to work with the physical constraints. This said, the fact remains that we still do not have a reliable test to predict field oxidative aging, which is the primary factor causing asphalt embrittlement and leading to premature pavement failure.

The need for a reliable test to predict the age-hardening rates of asphalt in pavements was well recognized as a need and a major objective of the original SHRP binder research program. However, this objective was not realized and the need is still there. Further, the undesirable effects of asphalt oxidation are as yet not even being considered in the SHRP design procedures for important pavement performance properties known to be affected by asphalt oxidation. Thus, this area should be considered a major objective of the original SHRP binder research program that still needs completion before implementation can even be considered.

Effects of Temperature on Viscosity-Sensitivity of Asphalt to Oxidative Products

From research results in the current project and prior SHRP binder research, it has become increasingly clear that the rheological properties of asphalts in the upper pavement temperature range are largely controlled by the associating polar components of the asphalt. The associations of these polar components impart the non-Newtonian flow properties and elastic response in asphalt that is so important in preventing pavement rutting, shoving, and other forms of permanent deformation. At the low temperature range of pavement performance, several tasks in the current project have demonstrated that the non-polar components (chemically defined as the neutrals fraction by IEC) dominate in controlling the low temperature properties primarily related to such pavement performance problems as transverse cracking. Results in these tasks have further indicated that the effects of the polar, associating components on physical properties are diminished as temperature decreases. The following data provide fundamental information regarding the mechanism of the diminishing effect of polar components on physical properties as temperature decreases.

The effect of temperature on the viscosity sensitivity of PAV-oxidized asphalt AAD-1 to ketone oxidation products is illustrated in figure 4-12. The strong relationship between ketones in asphalt and asphalt microstructure has been discussed in detail in earlier sections of this chapter. Asphalt AAD-1 was chosen to demonstrate the proposed effects because its concentration of polar, associating microstructure is large. At the left in the figure is plotted the effects of ketone concentration on dynamic viscosity measured at 60°C (140°F) for asphalt AAD-1 previously oxidized at both 60°C (140°F) and 100°C (212°F). As explained in the previous section, at higher temperatures, the more strongly associating components are dissociated, allowing a greater relative amount of the ketones to be formed from precursors in the

more strongly associating components. Thus, ketones formed on these components result in the association of larger (or a higher population of) associated agglomerates, resulting in a higher effective molecular weight and a greater viscosity increase. As a result, the viscosity sensitivity to ketones, measured at 60°C (140°F), is greater in the asphalt oxidized at 100°C (212°F) than that oxidized at 60°C (140°F), as can be seen in the figure.

However, as can be seen in the plot on the right side of figure 4-12, if the slope of the viscosity/ketone plot for the 60°C (140°F) oxidized asphalt, whose viscosity was measured at 60°C (140°F), is compared with the slope of the 100°C (212°F) oxidized asphalt, whose viscosity was measured at 25°C (78°F), the slopes are identical. By measuring the viscosity of the 100°C (212°F) oxidized asphalt at 25°C (78°F) rather than at 60°C (140°F), the effect of the ketones on viscosity was reduced to that of the ketones formed during 60°C (140°F) oxidation.

An interpretation of this result, based on the microstructural model, is that, during 100°C (212°F) oxidation, ketones formed from precursors normally buried more deeply in the microstructure are being buried again in the microstructure as the temperature is lowered to 25°C (78°F) for the viscosity measurement. As a result, these deeply buried ketones have a greatly reduced effect on the rheological measurement, and only those formed from precursors inherently from the more weakly associated, outer regions of the microstructure, as in the 60°C (140°F) oxidation, are now playing a major role on viscosity at 25°C (78°F). Thus, the effect of ketones on viscosity measured at 25°C (78°F) for the 100°C (212°F) oxidized sample appears similar to the effect of ketones in the 60°C (140°F) oxidized sample on viscosity measured at 60°C (140°F).

If this line of reasoning is extended to temperatures approaching the brittle region of asphalt, a large percentage of the viscosity-influencing ketones should be buried in immobilized polar associations. The other components of these associations have sufficient inherent polarity to interact at these low temperatures whether or not the ketones produced by oxidation are present. Thus, thus the effect of ketones on physical properties at low temperatures becomes relatively insignificant. Pragmatically, what is observed is that the physical properties of oxidized and unoxidized asphalts are much more nearly the same in the low temperature pavement temperature range than they are in the higher pavement temperature range.

Consideration of the potential effects of the other major oxidation product, sulfoxides, on asphalt properties in both the high and low temperature ranges is germane at this point. As discussed in previous sections, sulfoxides are formed primarily from components in the non-polar phase of asphalt, probably aliphatic and alicyclic sulfides. These sulfides probably have no other chemical functionality that should cause them to associate strongly. As a result, at higher temperatures, their effect on viscosity increase is minimal. However, at low temperatures, sulfoxides should be the oxidation product found more highly concentrated in the asphalt "solvent" phase, the phase that becomes dominant in controlling low temperature properties. As a consequence, sulfoxides in the more non-polar components near the brittle point may modify low temperature properties. It is speculated that the presence of sulfoxides might interfere with wax crystallization and also lower the temperature at which the non-polar components take on the properties of a solid and become brittle.

Comparisons of the change in bending beam properties of asphalts AAG-1, AAM-1, AAF-1, and AAA-1 with the change in PAV oxidation temperature are shown in figures 4-13 to 4-20. The change in stiffness for each asphalt is shown in figures 4-13, 4-15, 4-17, and 4-19, respectively, whereas the change in m-value is shown in figures 4-14, 4-16, 4-18, and 4-20, respectively. The low temperature properties of these asphalts show the opposite trend than that shown based upon higher temperature rheological measurements, but are still consistent with the microstructural model proposed. The higher temperature PAV oxidation results in less change in the low temperature rheological measurements than does the lower temperature (60°C [140°F]) PAV oxidation. The possible exception to this is asphalt AAM-1, which shows essentially no change in low temperature stiffness and only a small change in m-value (figures 4-15 and 4-16) regardless of the oxidation temperature. As stated earlier, the 100°C (212°F) oxidation forms ketones from precursors that are buried more deeply in the microstructure than does the 60°C (140°F) oxidation. When the temperature of the oxidized asphalt is lowered, these ketones have less effect on the rheological properties because they become completely buried in the associated phase. On the other hand, the 60°C (140°F) oxidation tends to form ketones from precursors that are in the more weakly associated regions of the microstructure, such as the resins, and are more exposed when the temperature is lowered, resulting in a higher stiffness in the asphalt.

A similar argument can be made for the sulfoxides; however, the effect of the sulfoxides on the low temperature physical properties may be more complex. A higher temperature oxidation may oxidize asphalt sulfides that are buried further in the microstructure and may produce a lower equilibrium concentration of sulfoxides because of thermal decomposition, compared with a lower temperature oxidation. If the sulfoxides formed on oxidation become buried deep enough in the microstructure when the temperature is lowered, then the sulfoxides will have a minimal effect on the low temperature stiffness. On the other hand, if the sulfoxides remain in or near the solvent phase, then there could be a significant effect on the low temperature stiffness. The complicating factor is how the sulfoxides in the solvent phase interact with the solvent phase. If the sulfoxides increase the weakly polar association, then the low temperature stiffness will increase. If the sulfoxides interact to disrupt association and packing of the hydrocarbon molecules, then the result will be less of an increase in low temperature stiffness.

All asphalts also show a decrease in the amount of the IEC neutral fraction after oxidation. Therefore, the increase in low temperature stiffness of asphalts is a function of the ketone and sulfoxide oxidation products in the solvent phase, the interaction of the oxidation products with components in the solvent phase, and the volatile loss of the solvent phase. The m-values of asphalts are also affected by oxidation in a related manner. The 60°C (140°F) PAV oxidation temperature is more comparable to pavement temperature than is the 100°C (212°F) PAV oxidation. In the four asphalts shown in the figures and also in asphalts AAB-1, AAC-1, AAD-1, and AAK-1, the 60°C (140°F) PAV oxidation results in a higher stiffness and a lower m-value than the 100°C (212°F) PAV oxidation. If the effects of the lower temperature PAV oxidation on bending beam rheological properties are more representative of pavement aging than the 100°C (212°F) PAV oxidation, then the PG grading and actual field performance of asphalts may be different. It is obvious that there remains a considerable amount of work necessary to understand these effects on low temperature properties.

Effects of Aggregate on Asphalt Oxidation

Over the years, there has been much discussion and debate about the effects of aggregates on the oxidative aging of asphalts. This controversy continued during the SHRP asphalt research activities. Different studies by various researchers have shown conflicting results. Studies by Petersen et al. [1974] showed that aggregates have a catalytic effect on the oxidation of some asphalt fractions and, to a lesser extent, on some whole asphalts. However, these studies were conducted at temperatures higher than pavement temperatures and physical property measurements were not performed. In the asphalt fraction studies, the least polar fraction (saturates) showed the greatest catalytic oxidation when they alone were in contact with the aggregate surface. The polar asphaltene fraction was not catalytically oxidized by the aggregate when it alone was in contact with the aggregate. It was proposed that the polar functionality (probably nitrogen) in the asphaltenes poisoned catalytic sites on the aggregate surface. Studies performed by Bell et al. [1992] on laboratory-prepared pavement mixtures showed that aggregates may have differing effects on various asphalts, and in some cases the age-hardening was reduced. Different test conditions used by different investigators have probably contributed to the widely varying results. One condition that may have biased results is that past investigations have used temperatures significantly higher than maximum pavement temperatures. During the last year of the SHRP A-002A project at WRI, an asphalt-aggregate aging study was begun to measure both the oxidative changes (i.e., chemical changes) and the physical property changes (viscoelastic properties) that occur in asphalts when they are aged at lower temperatures on aggregate surfaces. Samples were prepared, using a 5 mass percent coating of asphalt on 20-35 mesh aggregate particles, and then were PAV-aged for 144 hours at 60°C (140°F). A portion of each asphalt-aggregate mixture was extracted almost immediately after mixing to provide the zero-hour data point for subsequent comparisons. The advantages of this study over some others is that the mixtures prepared had realistic ratios (5 mass percent asphalt - 95 mass percent aggregate) and the oxidative aging step was performed in the pavement temperature range (60°C [140°F]). Criticism of this method mainly focused on the fact that a 5 mass percent coating on 20-35 mesh aggregate particles may result in a film thickness thicker than in actual paving mixtures. The matrix consisted of the eight SHRP core asphalts, five aggregates, and Teflon® as an "inert" aggregate.

Dynamic rheological measurements at 60°C (140°F) and 25°C (78°F) were obtained on the zero-hour samples and the samples were aged for 144 hours at 60°C (140°F). The results from these measurements are shown in tables 4-2 and 4-3. The poor precision noted in the data in tables 4-2 and 4-3 is because all data obtained are shown in the tables and the results obtained early on while the procedure was being developed tended to be less precise than the data obtained in the later experiments. Also, as with many mixture experiments, the extraction of asphalt from aggregate introduces more variability than does aging asphalt alone. The results are compared using an AI calculated from the dynamic viscosities of the samples after aging divided by the viscosity before aging but after mixing. AI values could also be calculated using the complex modulus, G*, the specification values G*sin delta and G* divided by sin delta, or others and used to compare the effects of aging. The 60°C (140°F) AI values shown in table 4-2 suggest that there was not a large effect of the aggregate on asphalt oxidative aging when the aging occurred at temperatures approximating maximum pavement temperature (60°C [140°F]). In general, it

appears that aggregate RA caused all eight asphalts to age more than the other aggregates, Teflon®, and the neat asphalt alone based upon the 60°C (140°F) AI; however, this trend does not hold for the 25°C (78°F) AI values. TFO was not included in the neat asphalt AI's because the asphalts were not TFO aged prior to coating on the aggregates. It must be noted that the goal of these experiments was to determine if there were aggregates that would cause large differences in asphalt aging.

IR analysis was conducted on the zero-hour and the 144-hour aged asphalts to determine the carbonyl and sulfoxide contents. The results from these analyses are shown in table 4-4. The amount of oxidation products formed in the asphalts coated on the aggregates was very similar to the amounts of oxidation products formed in the neat asphalts. Again, there are cases where the amounts of oxidation products in the asphalts aged on aggregate are substantially different from those of the neat asphalt; the largest differences are in asphalts AAG-1 and AAM-1, both compatible asphalts that have low sensitivity of viscosity increase to carbonyl formation. It was shown in the previous section that carbonyl formation (ketones) has much more effect on viscosity increase than does sulfoxide formation.

A small number of experiments were conducted using a smaller 2.5 mass percent asphalt coating. These experiments were conducted using asphalts AAG-1 and AAK-1 on aggregate RB. The results are shown in tables 4-2, 4-3, and 4-4 and are identified using the (2.5 percent) notation. These experiments produced the same results as the 5 mass percent experiments. It is possible that the 2.5 mass percent coating still did not produce a film thickness thin enough to observe a possible catalytic effect of the aggregate; however, if significant differences were not seen between 2.5 and 5 mass percent coatings, it is unlikely that significant aggregate effects would be seen in pavements.

Additional experiments were conducted with asphalts AAG-1 and AAK-1 at a 5 mass percent coating on aggregate RB, but the PAV aging temperature was elevated to 100°C (212°F) and the time was shortened to 20 hours. The results from these experiments are shown in table 4-5. Both asphalts AAG-1 and AAK-1 show large increases in AI's and also carbonyl formation compared with their respective neat asphalts aged at 100°C (212°F) for 20 hours. This limited number of experiments indicates that it may not be appropriate to laboratory age loose mixes at significantly elevated temperatures. It is not known at this time at what point between the temperatures of 60°C (140°F) and 100°C (212°F) the asphalt aging on aggregate becomes substantially higher than the aging of the neat asphalt alone.

Table 4-1. Viscosity sensitivity to ketones for selected SHRP asphalts oxidized by both PAV and TFAAT methods.

Asphalt	Viscosity sensitivity to ketones, $Pa \cdot s/mol \cdot L^{-1}$			
	PAV oxidation		TFAAT oxidation	
	60°C	100°C	85°C	113°C
AAG-1	4.5	4.5	5.4	5.4
AAM-1	9.1	12.5	8.7	13.3
AAF-1	8.7	10.0	10.0	20.0
AAA-1	10.5	21.0	10.0	28.5
AAK-1	14.7	9.1	15.1	19.2

Table 4-2. Results from 5 mass % asphalt coated on aggregate aging experiments using the PAV method at 60°C for 144 hours. Asphalts extracted from aggregates. 60°C aging indices.

Asphalt	Asphalt aging index (η^* after aging/η^* after mixing), 60°C						Neat asphalt aging index excluding TFO[1]
	Aggregate						
	RA	RB	RC	RD	RK	Teflon	
AAA-1	4.24 3.70	3.60 4.28	4.29 4.37	3.43	3.15	2.94 3.27	4.60
AAB-1	8.03 3.53 3.90	0.84 3.48	4.37 5.01	4.01	3.48	4.55 4.36	4.64
AAC-1	4.77 3.82 3.83	4.40 3.33	2.78 4.66	4.53	3.46	4.08	5.68
AAD-1	6.38 6.06	5.05 3.94	3.87 7.00	4.46	5.30	3.96	6.82
AAF-1	8.42 9.97 9.75	7.77 8.74	4.00	3.21	6.66	5.62	7.76
AAG-1	5.81 6.05	4.83 3.56 (2.5%)[2] 3.72 (2.5%)[2]	4.06	4.90	7.43	3.98	3.62
AAK-1	4.99 4.72	4.89 6.05 14.69 (2.5%)[2] 3.90 (2.5%)[2] 4.71 (2.5%)[2]	3.55	2.54	5.65	4.46	7.34
AAM-1	7.97 10.26 4.87	5.65 4.33	4.50	4.89	7.80	5.29	7.00

[1] TFO not included in aging index because the asphalts used in the mixtures were not TFO aged.

[2] These results were obtained using a 2.5 mass % coating instead of 5 mass %.

Table 4-3. Results from 5 mass % asphalt coated on aggregate aging experiments using the PAV method at 60°C for 144 hours. Asphalts extracted from aggregates. 25°C aging indices.

Asphalt	Asphalt aging index (η^* after aging/η^* after mixing), 25°C						Neat asphalt aging index excluding TFO [1]
	Aggregate						
	RA	RB	RC	RD	RK	Teflon	
AAA-1	44.37 11.06	5.50 5.97	8.01 7.29	5.12	4.56	3.91 4.70	6.91
AAB-1	16.23 4.77 5.63	3.67 3.50	5.07 6.69	5.56	3.85	5.42 5.69	6.30
AAC-1	10.43 10.18 4.78	6.96 4.85	5.38 7.67	7.75	5.26	6.31	10.75
AAD-1	8.78 7.35	5.43 4.47	4.32 5.65	5.14	5.55	4.12	7.88
AAF-1	11.12 11.96 10.17	10.61 9.86	6.54	4.10	8.04	7.85	10.45
AAG-1	10.80 9.93	8.05 6.06 (2.5%) [2] 5.55 (2.5%) [2]	6.37	7.95	17.23	6.35	5.51
AAK-1	4.53 3.98	4.29 3.26 14.24 (2.5%) [2] 3.95 (2.5%) [2] 3.92 (2.5%) [2]	3.94	2.58	5.51	4.33	6.87
AAM-1	6.31 7.25 4.30	4.82 3.15	10.15	4.71	5.97	5.31	6.38

[1] TFO not included in aging index because the asphalts used in the mixtures were not TFO aged.

[2] These results were obtained using a 2.5 mass % coating instead of 5 mass %.

Table 4-4. Infrared analysis of aged asphalts recovered from 5 mass % asphalt coated on aggregate aging experiments using the PAV method at 60°C for 144 hours. Asphalts extracted from aggregates.

Asphalt	Functional group	Aggregate						Neat asphalt excluding TFO [1]
		RA	RB	RC	RD	RK	Teflon	
AAA-1	Carbonyl	.065	.06	0.06	0.06	0.07	0.065	0.07
	Sulfoxide	0.29	0.29	.275	0.20	0.21	0.285	0.22
AAB-1	Carbonyl	.063	0.06	0.06	0.07	0.07	0.055	0.05
	Sulfoxide	0.27	0.29	0.285	0.25	0.26	0.275	0.25
AAC-1	Carbonyl	0.12	0.12	0.125	0.13	0.14	0.12	0.12
	Sulfoxide	0.23	0.215	0.17	0.15	0.16	0.19	0.16
AAD-1	Carbonyl	0.075	0.08	0.085	0.08	0.09	0.08	0.09
	Sulfoxide	0.32	0.35	0.28	0.24	0.27	0.30	0.27
AAF-1	Carbonyl	0.093	0.085	0.08	0.09	0.10	0.08	0.09
	Sulfoxide	0.305	0.30	0.22	0.21	0.23	0.23	0.24
AAG-1	Carbonyl	0.215	0.23	0.18	0.22	0.23	0.20	0.17
	Sulfoxide	0.225	0.22	0.17	0.17	0.18	0.17	0.18
	Carbonyl		0.23 (2.5%) [2]					
	Sulfoxide		0.21 (2.5%) [2]					
AAK-1	Carbonyl	0.07	0.075	0.07	0.06	0.08	0.06	0.06
	Sulfoxide	0.305	0.305	0.24	0.23	0.39	0.23	0.22
	Carbonyl		0.06 (2.5%) [2]					
	Sulfoxide		0.30 (2.5%) [2]					
AAM-1	Carbonyl	0.147	0.145	0.15	0.14	0.17	0.14	0.12
	Sulfoxide	0.113	0.105	0.07	0.06	0.07	0.07	0.07

[1] TFO not included in the neat asphalts because the asphalts used in the mixture were not TFO aged.

[2] These results were obtained using a 2.5 mass % coating instead of 5 mass %.

Table 4-5. Results from 5 mass % asphalt coated on aggregate aging experiments using the PAV method at 100°C for 20 hours. Asphalts extracted from aggregate.

Asphalt	Aggregate	Aging time, hr	Dynamic viscosity, 60°C, Pa·s	Aging index	Dynamic viscosity, 25°C, Pa·s	Aging index	Carbonyl absorbance units	Sulfoxide, mol/L
AAG-1	none	0	3.22E+02		4.64E+05		0.02	0.05
AAG-1	none	20	1.44E+03	4.47	2.62E+06	5.65	0.18	0.19
AAG-1	RB	0	2.26E+02		2.62E+05		0.02	0.05
AAG-1	RB	20	2.61E+03	11.55	4.95E+06	18.89	0.31	0.17
AAG-1	RB	0	2.48E+02		3.00E+05		0.02	0.07
AAG-1	RB	20	3.87E+03	15.60	8.42E+06	28.07	0.31	0.22
AAK-1	none	0	1.04E+03		5.27E+05		0.03	0.02
AAK-1	none	20	1.15E+04	11.06	3.75E+06	7.12	0.07	0.29
AAK-1	RB	0	8.64E+02		4.07E+05		0.03	0.10
AAK-1	RB	20	1.50E+05	173.61	9.75E+06	23.96	0.23	0.53
AAK-1	RB	0	6.97E+02		2.97E+05		0.03	0.05
AAK-1	RB	20	2.98E+05	427.55	2.28E+07	76.77	0.24	0.56

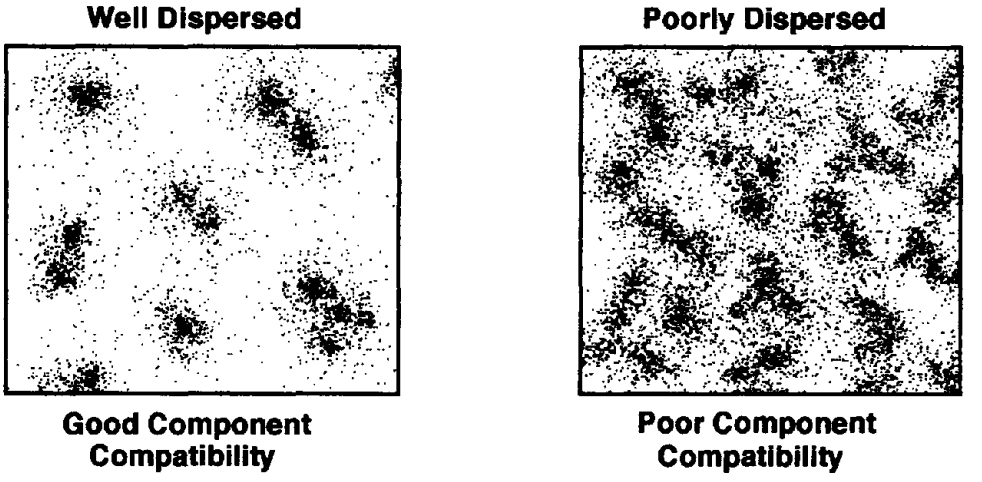

Figure 4-1. Pictorial diagrams of the microstructural model of asphalt.

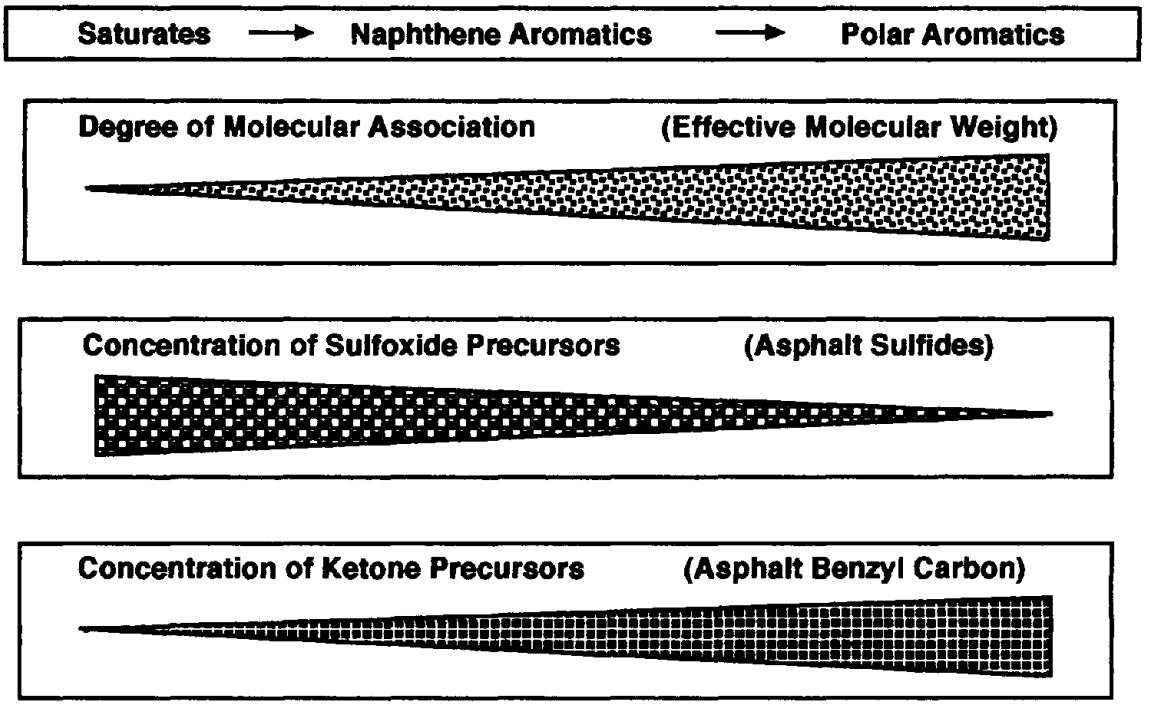

Figure 4-2. Diagrammatic representation of the effects of composition on the physical properties of asphalts.

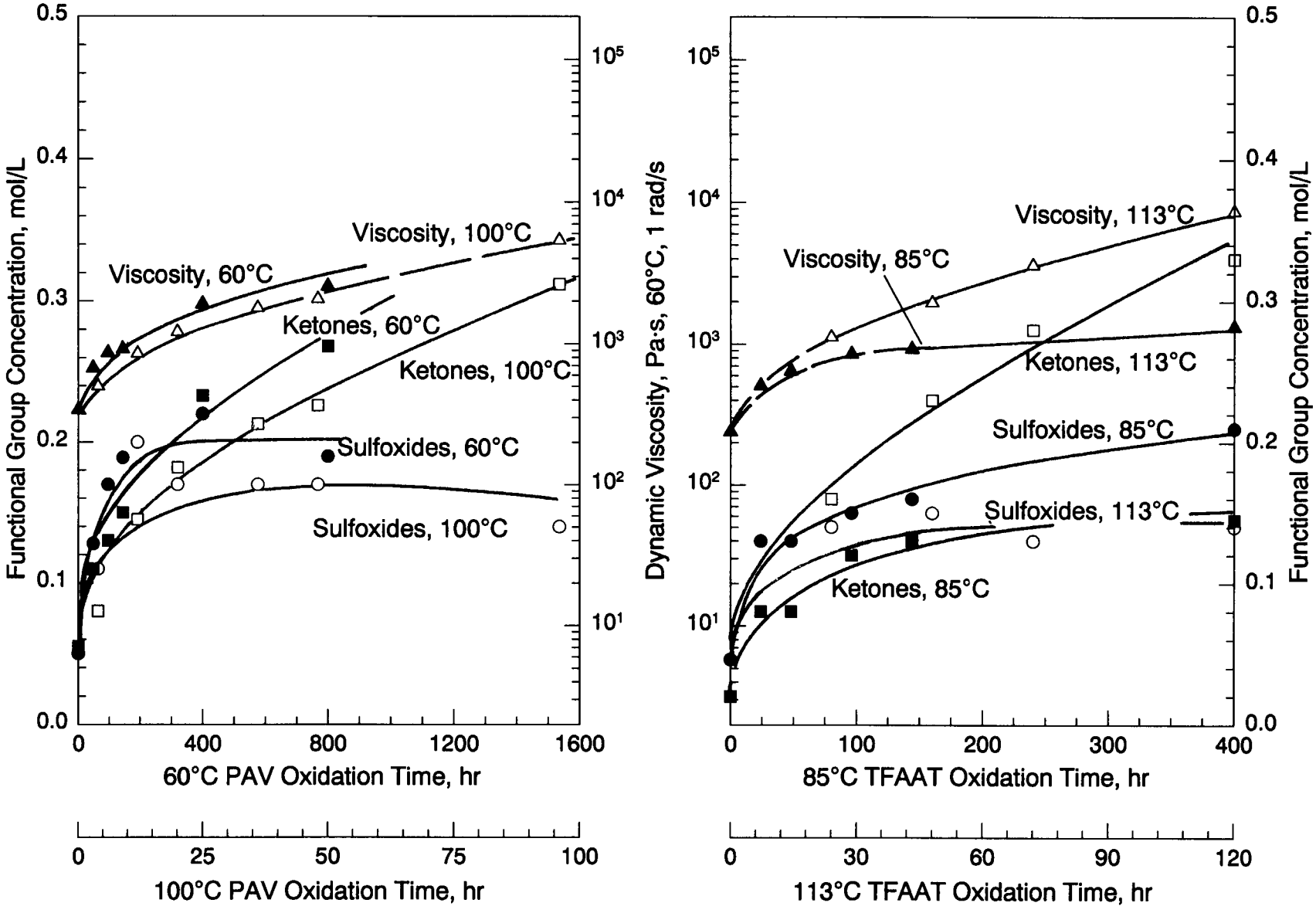

Figure 4-3. Comparison of TFO/PAV and TFAAT aging of asphalt AAG-1.

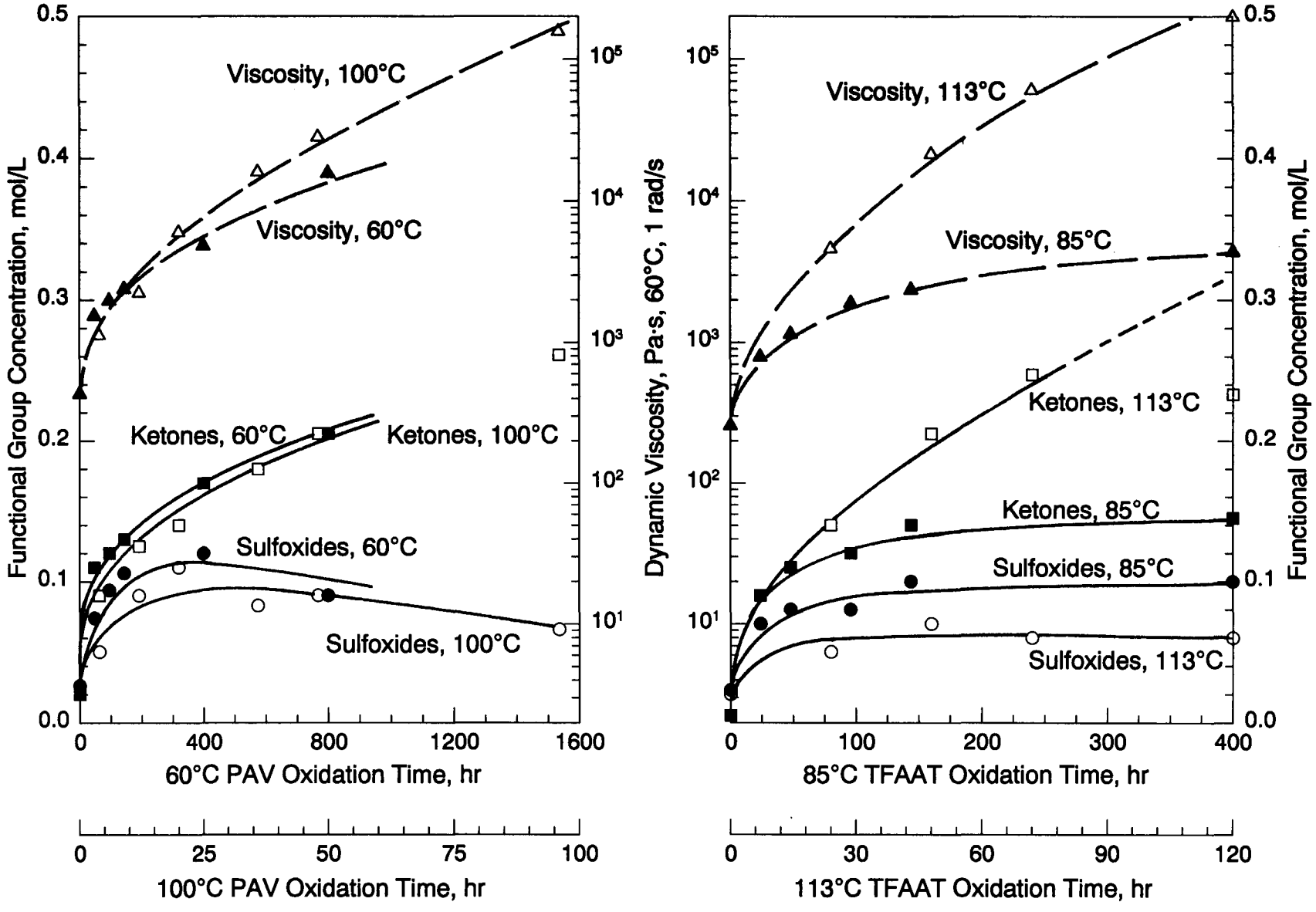

Figure 4-4. Comparison of TFO/PAV and TFAAT aging of asphalt AAM-1.

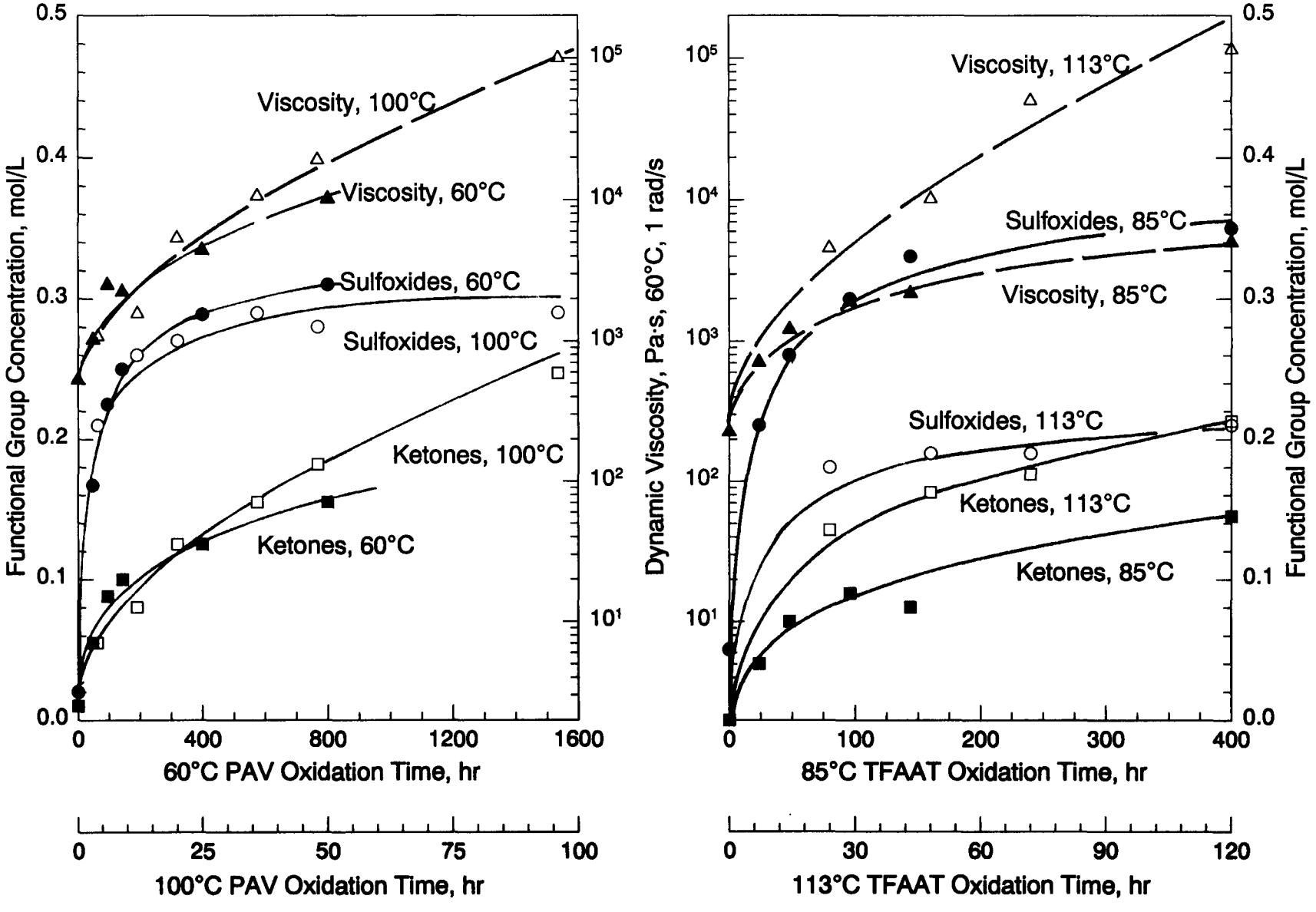

Figure 4-5. Comparison of TFO/PAV and TFAAT aging of asphalt AAF-1.

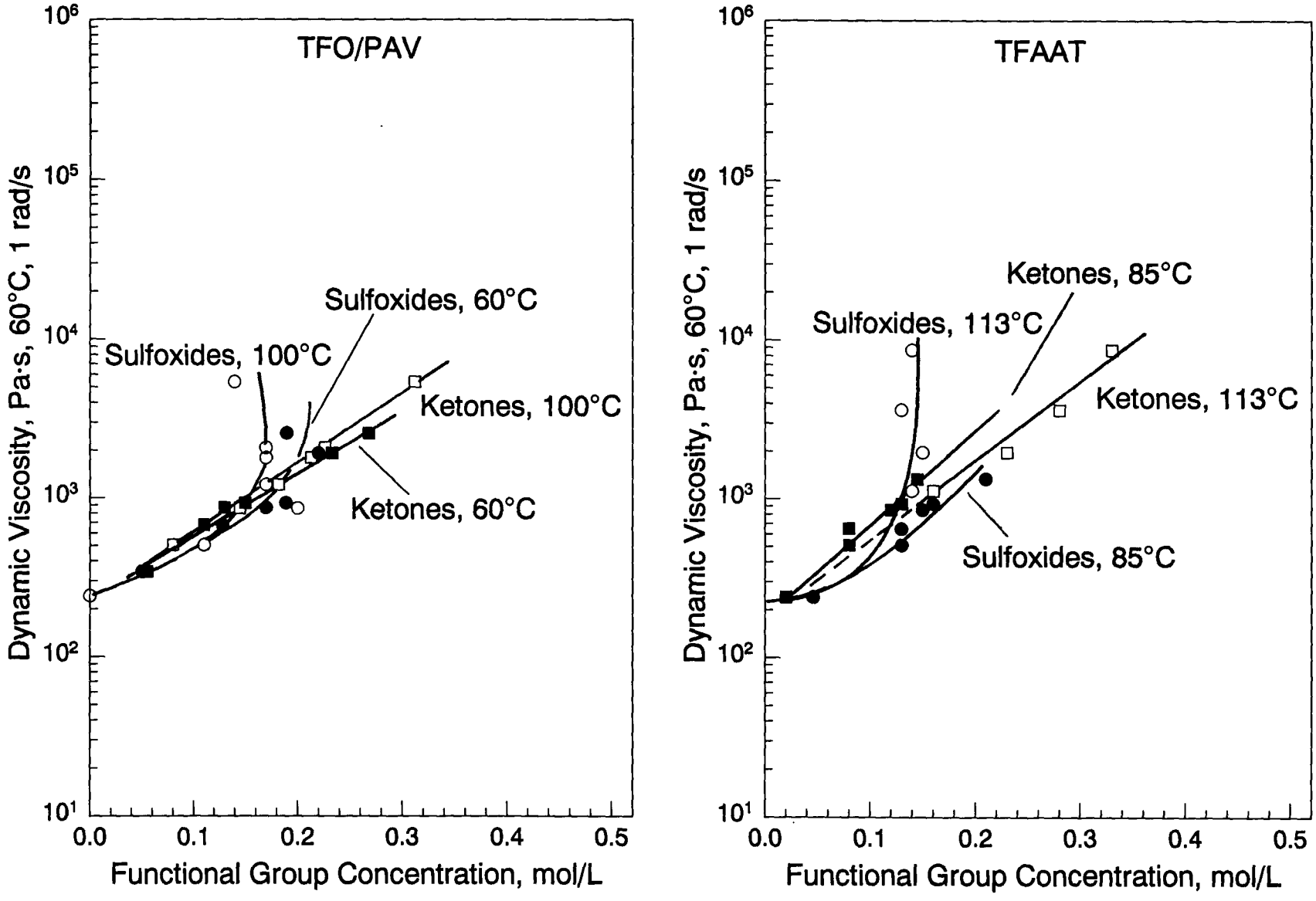

Figure 4-8. Comparison of TFO/PAV and TFAAT aging of asphalt AAG-1.

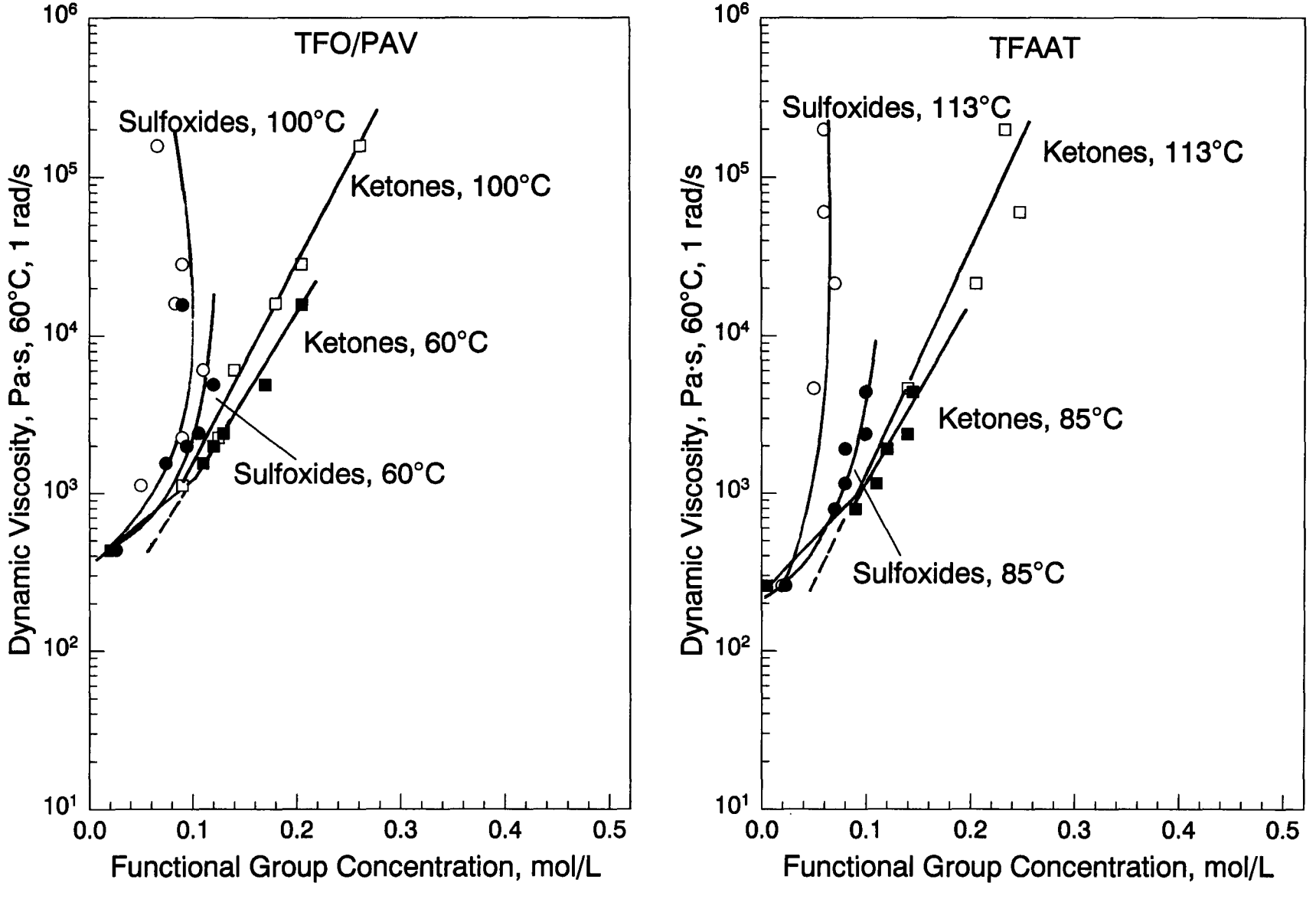

Figure 4-9. Comparison of TFO/PAV and TFAAT aging of asphalt AAM-1.

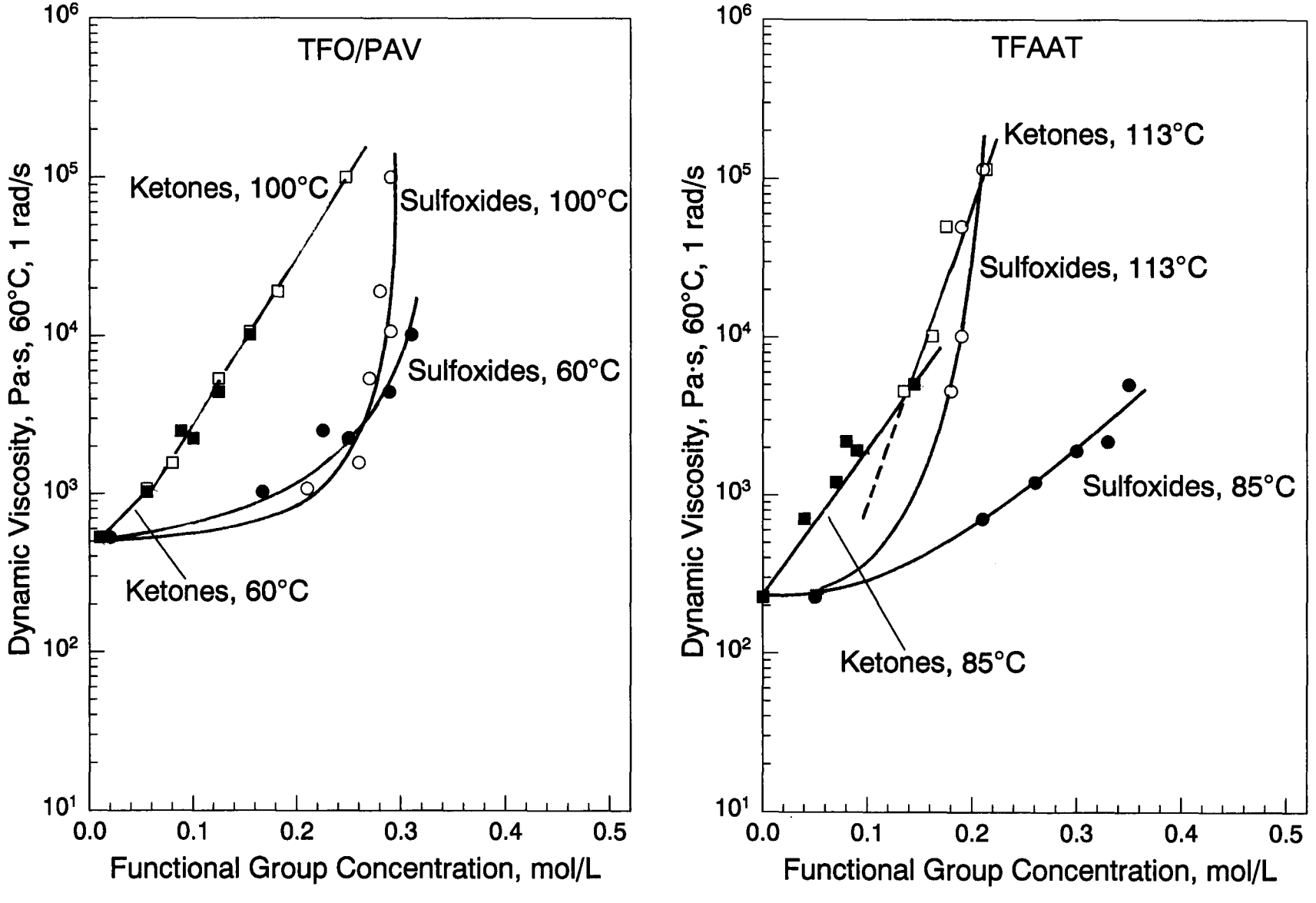

Figure 4-10. Comparison of TFO/PAV and TFAAT aging of asphalt AAF-1.

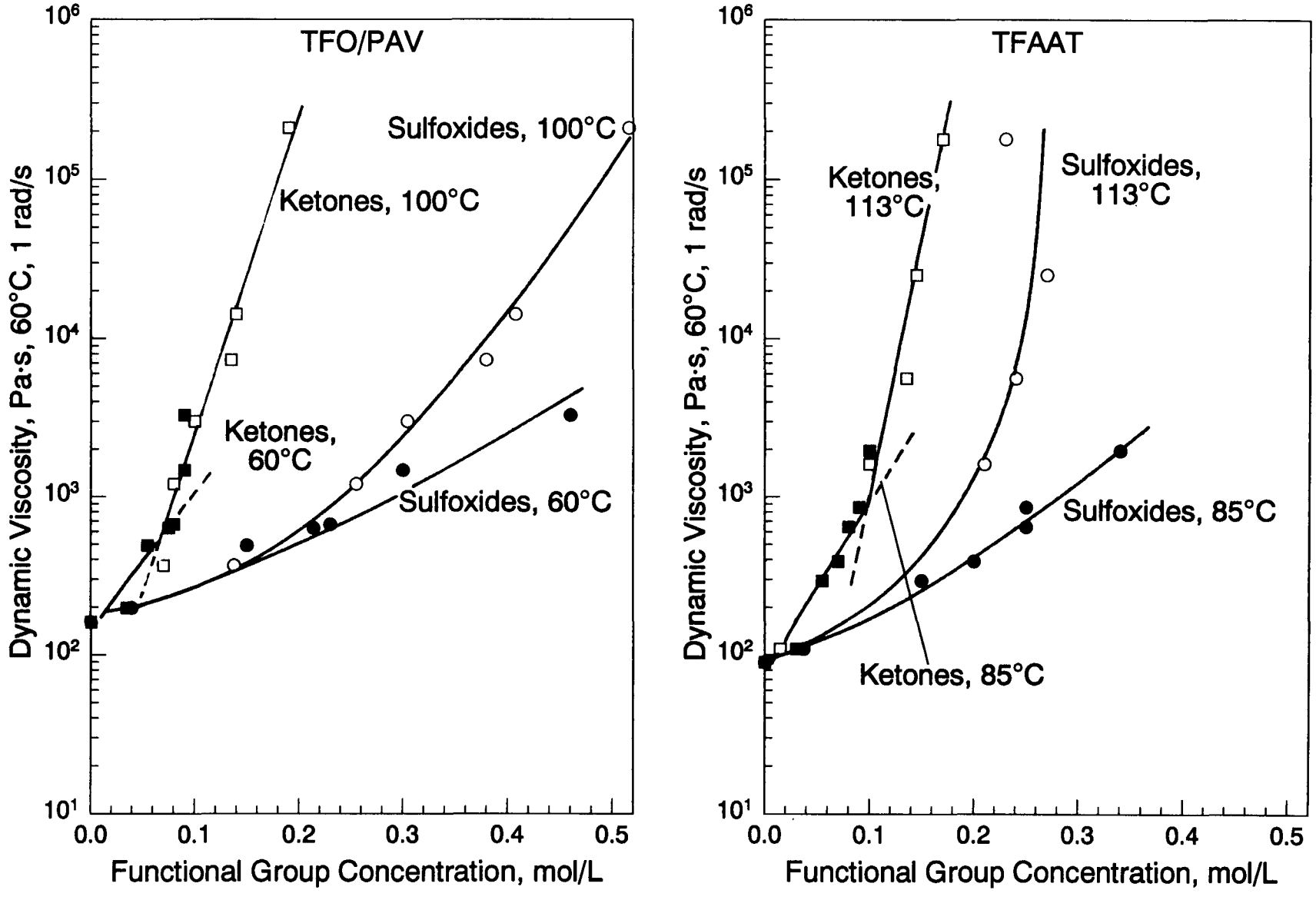

Figure 4-11. Comparison of TFO/PAV and TFAAT aging of asphalt AAA-1.

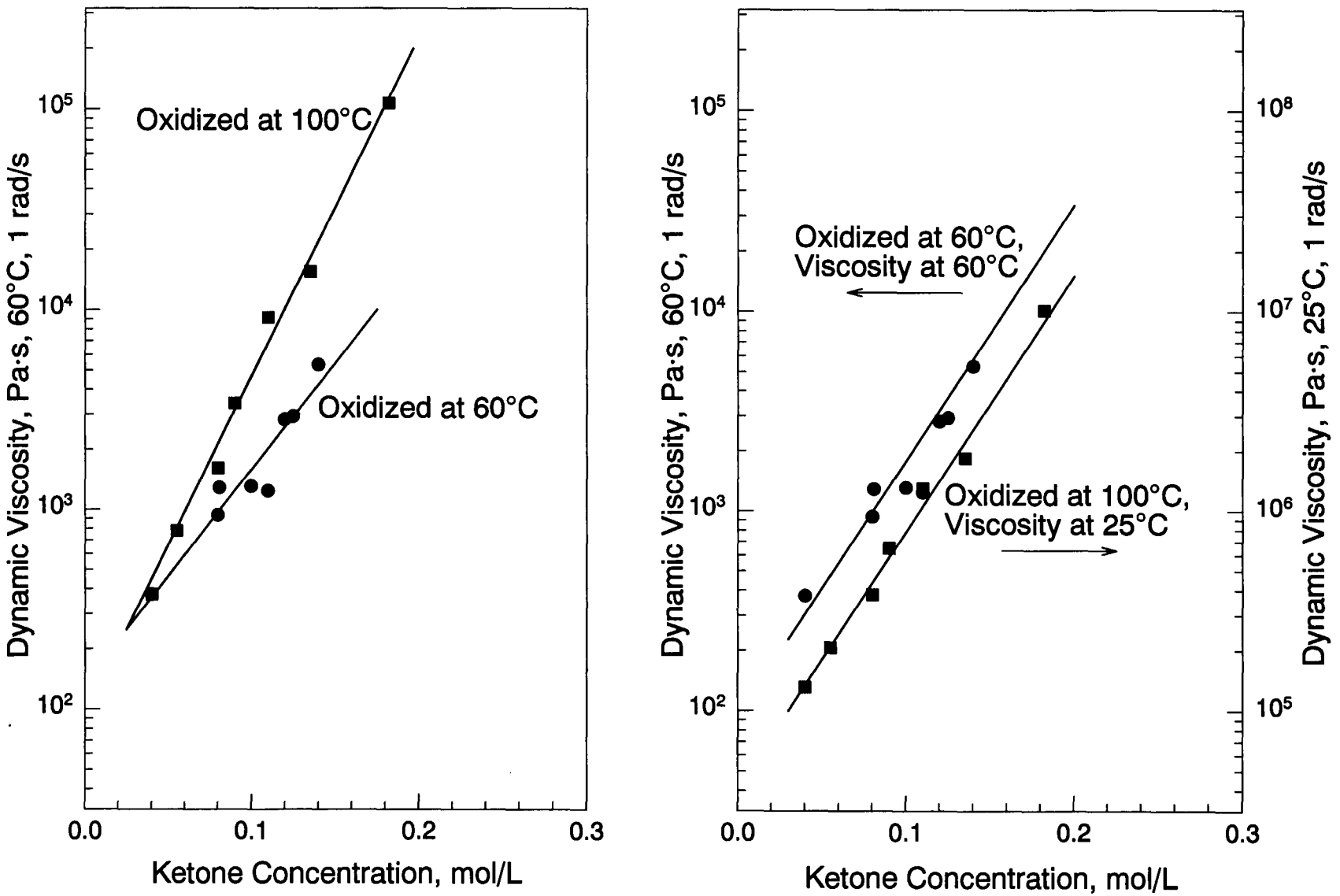

Figure 4-12. Effect of temperature on the viscosity sensitivity of PAV oxidized asphalt AAD-1 to ketone oxidation products.

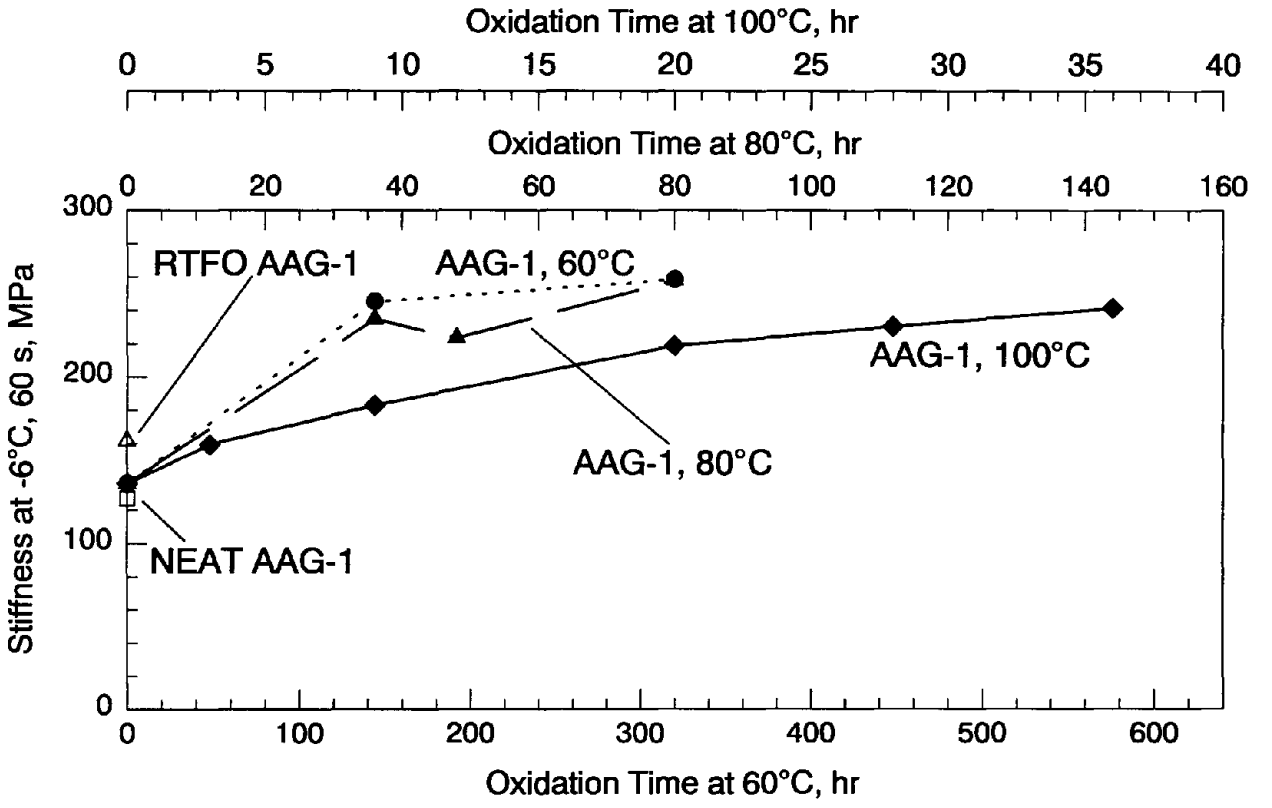

Figure 4-13. Bending beam stiffness values of 60, 80, and 100°C TFO/PAV-aged asphalt AAG-1.

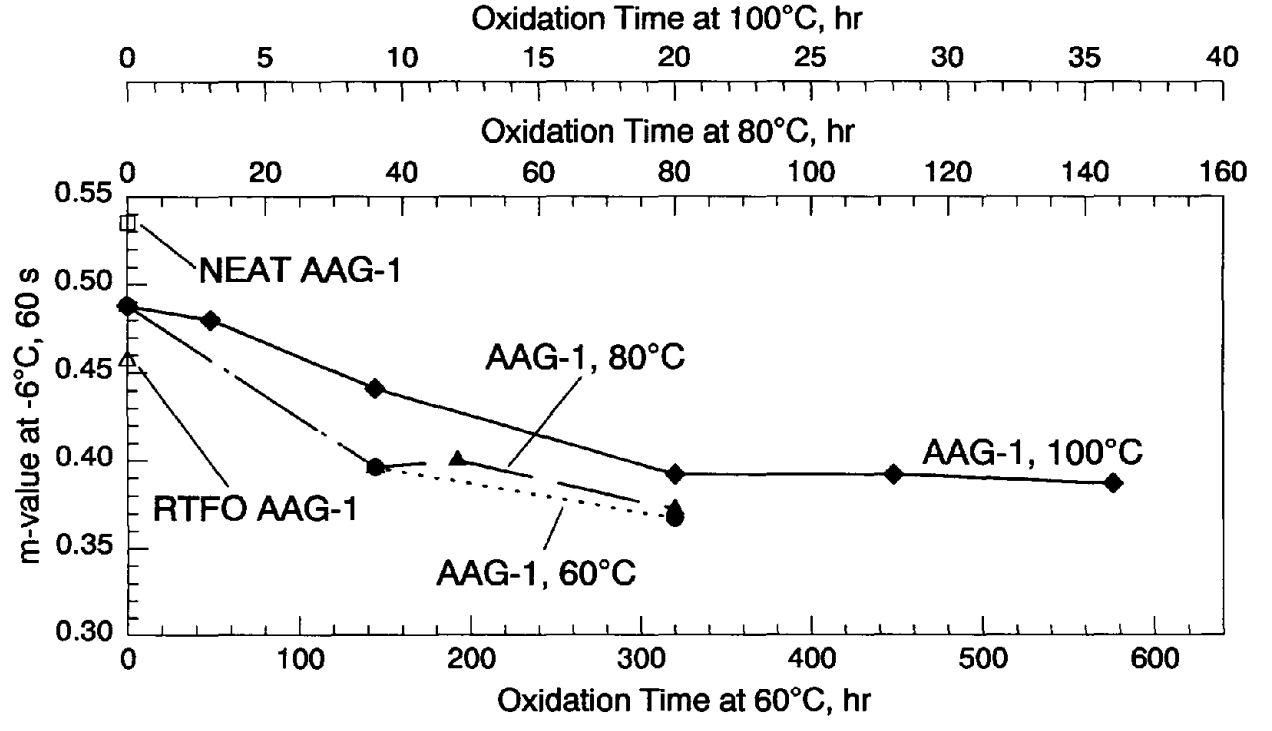

Figure 4-14. Bending beam m-values of 60, 80, and 100°C TFO/PAV-aged asphalt AAG-1.

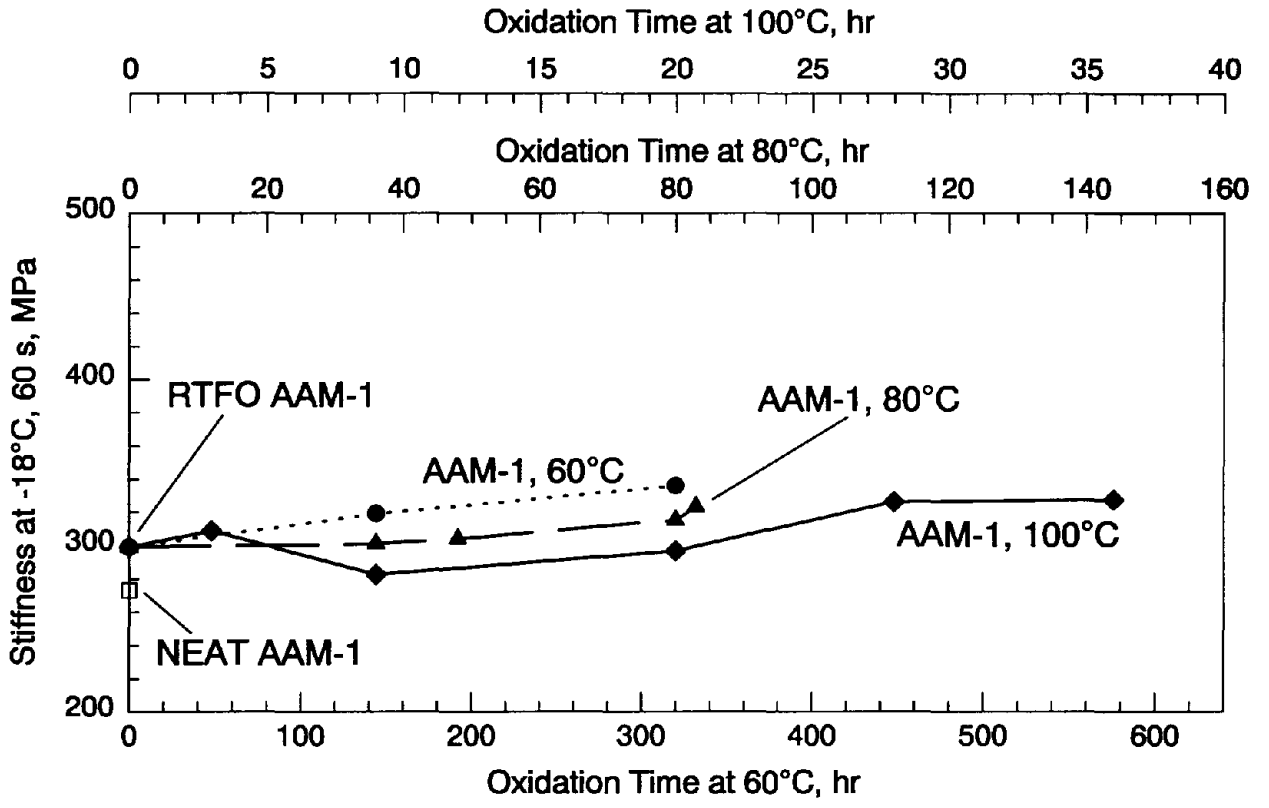

Figure 4-15. Bending beam stiffness values of 60, 80, and 100°C TFO/PAV-aged asphalt AAM-1.

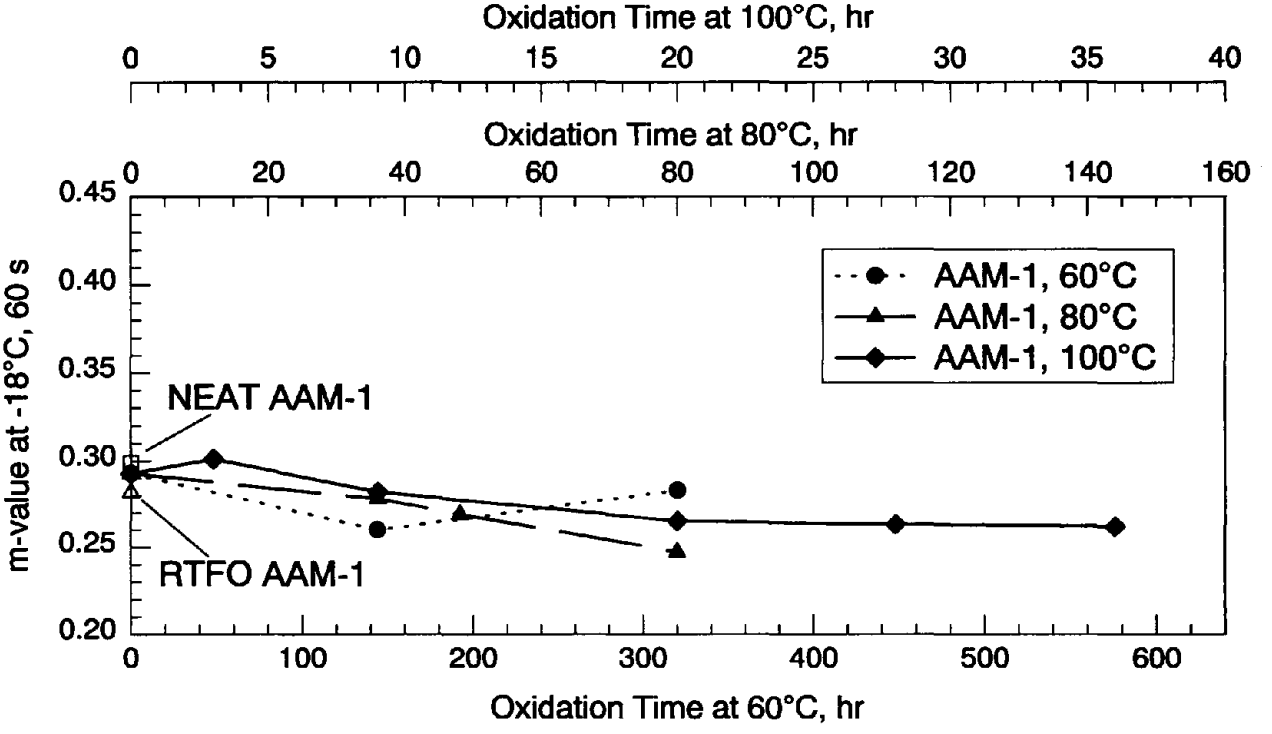

Figure 4-16. Bending beam m-values of 60, 80, and 100°C TFO/PAV-aged asphalt AAM-1.

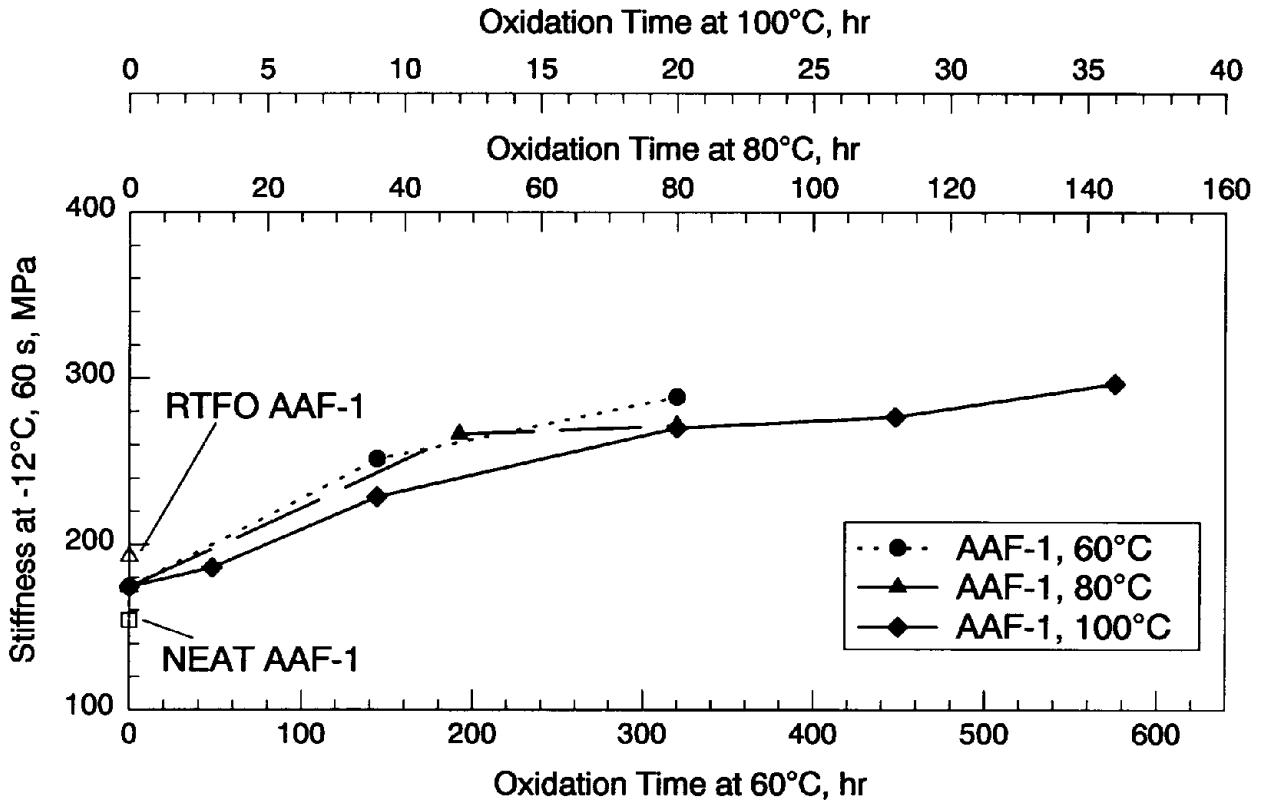

Figure 4-17. Bending beam stiffness values of 60, 80, and 100°C TFO/PAV-aged asphalt AAF-1.

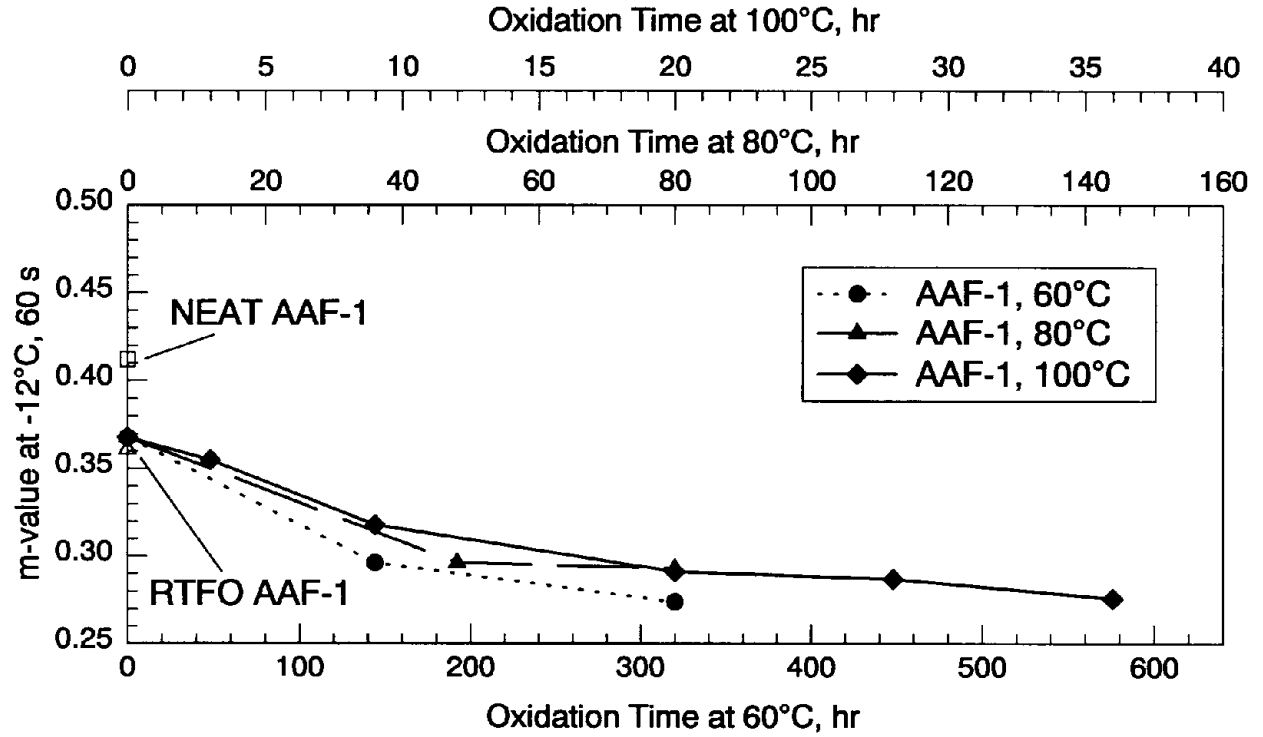

Figure 4-18. Bending beam m-values of 60, 80, and 100°C TFO/PAV-aged asphalt AAF-1.

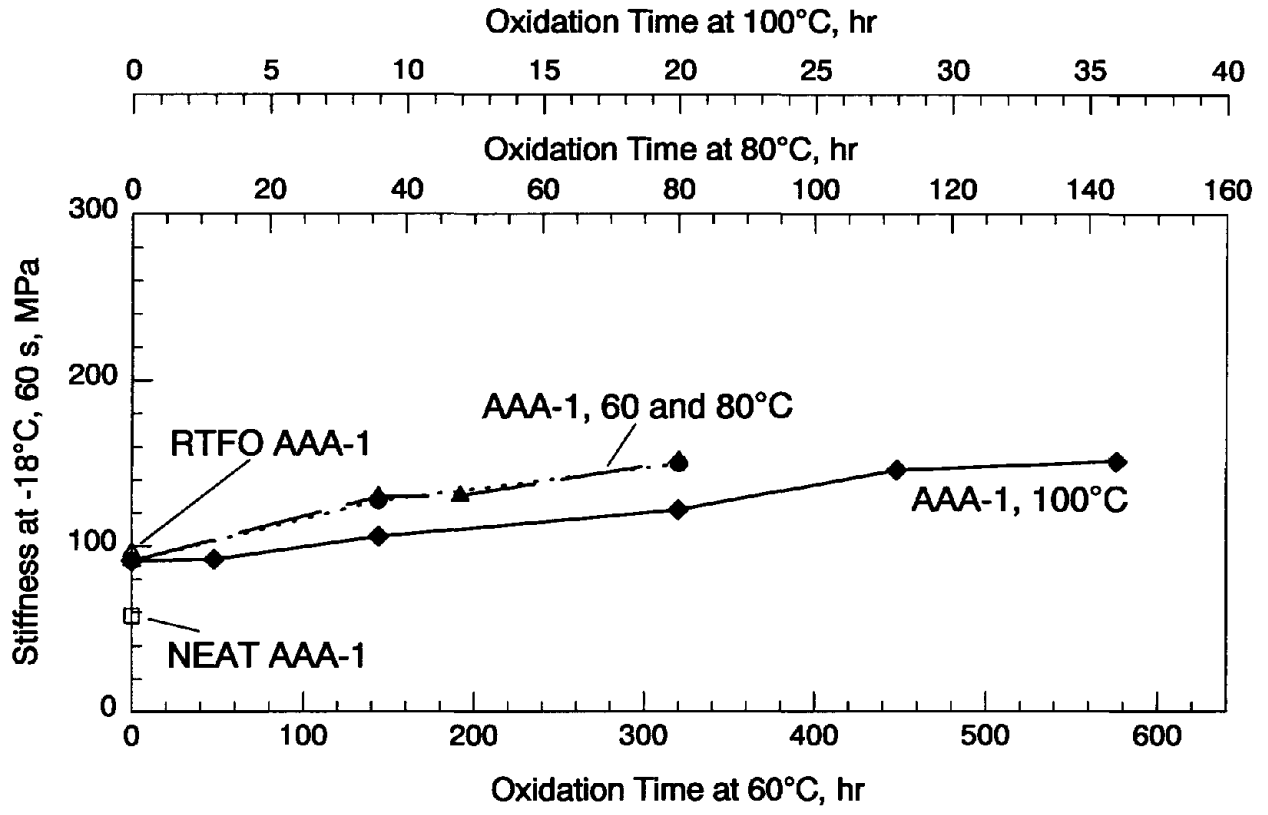

Figure 4-19. Bending beam stiffness values of 60, 80, and 100°C TFO/PAV-aged asphalt AAA-1.

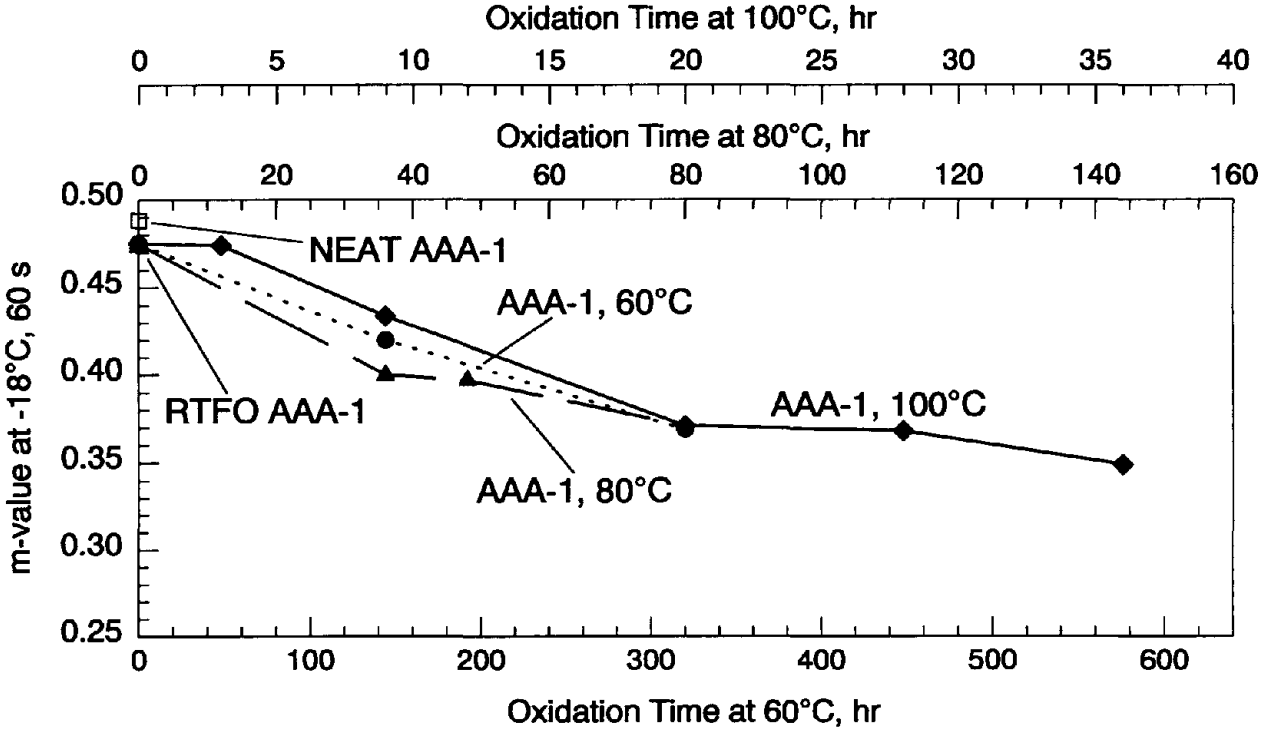

Figure 4-20. Bending beam m-values of 60, 80, and 100°C TFO/PAV-aged asphalt AAA-1.

ASPHALT OXIDATION MECHANISMS

Historical Background

Although individual oxidized asphalt molecules have not been isolated and characterized, the major functional groups formed on oxidation have been identified. These include ketones [Dorrence et al. 1974] and sulfoxides [Petersen et al. 1981] as the major products with lesser amounts of dicarboxylic anhydrides [Petersen et al. 1975] and carboxylic acids [Petersen and Plancher 1981]. Anhydrides and carboxylic acids do not begin to form in significant amounts until the latter stages of oxidation. The kinetics of the formation of functional groups on oxidation and their effects on asphalt physical properties have also been studied [Lau et al. 1992; Petersen et al. 1993; Petersen et al. 1996; Liu et al. 1996]. Asphalt can be considered as a dispersion of polar, strongly associated molecular species in a solvating medium consisting of the less polar asphalt molecules. Therefore, because polar molecules associate, the formation of polar oxidation products greatly alters the state of dispersion of asphalt. The state of dispersion not only affects the physical properties of asphalt, but also the mobility, and thus the chemical reactivity, of asphalt molecules susceptible to oxidation [Petersen et al. 1996]. Because asphalts from different sources have different states of dispersion and different relative amounts of reactive species, the mechanism(s) of asphalt oxidation has (have) been elusive.

Early fundamental kinetic studies of the oxidation of asphalt by Knotnerus [1971] showed that the initial reaction of asphalt with oxygen proceeded rapidly at a low activation energy; then, after a time, proceeded at a much slower rate. He proposed that asphalt contained a collection of highly reactive hydrocarbons whose oxidation might be initiated by stable free radicals already present in the bitumen. Following initiation, he proposed that hydroperoxides are formed that may then further react. He suggested, based on model compound oxidation studies, that the initial rapid oxidation could result from oxidation of asphalt components containing highly reactive polycyclic hydrocarbons. In his model studies, 9,10-dihydroanthracene and 5,12-dihydronaphthacene had relative rates of reaction with oxygen of 800 and 1,400, respectively, compared with relative rates of 17 and 16 for 1,2,3,4-tetrahydrophenanthrene and 1-methyl-7-isopropylphenanthrene, respectively. The latter model compound contains a benzylic carbon of the type proposed by Dorrence et al. [1974] to be precursors to ketone formation in asphalts. Dodecylbenzene (containing no alkyl substituted benzyl carbon) was unreactive under Knotnerus's experimental conditions (1.25 g in 50 mL of toluene, 30°C [86°F], light). Knotnerus concluded that the straight line plot of oxygen absorbed versus the log concentration for the oxidation of both 9,10-dihydroanthracene and bitumens (oxidized in the dark) suggested that the same type of reaction occurred in both. He also showed that the oxidation reaction had no induction period. He further concluded that asphalt oxidation in the dark was primarily related to the presence of high molecular weight compounds with highly condensed aromatic ring systems, some of which are known to contain traces of metals and some of which form fairly stable free radicals.

In related studies, Martin [1966; 1968] evaluated the effects of a wide variety of classical antioxidants on asphalt oxidation. He found that antioxidants that functioned as free radical

traps were generally effective in stabilizing bitumens against photo oxidation. He concluded that the additives, however, were not highly efficient in this situation because they did not appear to confer an induction period on the oxidation reaction. Under conditions of dark oxidation, the free radical trap antioxidants had little effect, but certain peroxide decomposers stabilized the bitumens to a considerable extent. Of the antioxidants evaluated, N-phenyl-N-isopropyl-p-phenylenediamine (a free radical trap) and zinc diethyldithiocarbamate (a hydroperoxide decomposer) were generally the most effective models used in his studies. Martin's results [1966] were consistent with oxidation involving free radical reactions, but results were severely modified by, and highly variable with, asphalt source. The effectiveness of the hydroperoxide decomposing dialkyldithiocarbamates as asphalt antioxidants has been confirmed [Haxo and White 1979; Oliver 1995].

Examination of asphalt oxidation mechanisms by van Gooswilligen and coworkers [1985] led to their conclusion that asphalt oxidation did not proceed via a free radical chain reaction. This conclusion was apparently based primarily on their observation that there was no oxidation induction period and that the addition of an initiator did not increase the rate of oxygen uptake as is typical of hydrocarbon oxidation. They attributed the apparent absence of a typical free radical oxidation chain reaction to the presence in asphalts of a high concentration of natural inhibitors of free radical chain oxidation. Based on solution oxidations at different concentrations as a function of time and temperature, van Gooswilligen concluded that bitumens contain a low concentration of highly reactive components that are preferentially depleted in the initial stages of oxidation. The addition of known oxidation catalyst poisons (KCN and NaN_3) to a bitumen solution greatly reduced the rate of oxidation, which van Gooswilligen said indicated that the oxidation could proceed mainly via metal catalysis, probably metal porphyrin structures. He proposed, based on his studies, an oxidation mechanism in which a metal catalyst, a reactive asphalt molecule, and an oxygen molecule form a transitory complex that then decomposes into an oxidized molecule, i.e., bitumens containing carbonyl and sulfoxide functional groups.

King [1993] has proposed the concept of an oxycyclic reaction mechanism in an attempt to pull together many ideas into one simple, unified oxidation theory. This theory views the net chemical oxidation reaction, not looking at each individual mechanistic step, as a series of two or more cyclic steps that follow reasonable pathways based on the current knowledge of chemistry. Individual steps in this pathway may be heterolytic, homolytic, or perhaps combinations of the two. King notes that while it may still be appropriate to speak of electron transfer, free radicals, electron pairs, back-bonding, and a myriad of other individual mechanistic events, a model involving an intermediate oxycyclic complex can explain such unexpected events as epoxide ring formation, intermolecular oxygen transfer, anhydride formation, metal oxidation and reduction, and even the destruction of carbon-carbon sigma (primary) bonds at relatively low temperatures. Thus, King's proposed oxycyclic mechanism could include the formation of a molecular complex between oxygen, an asphalt molecule, and a metal as proposed by van Gooswilligen, but is much broader and includes many molecular types with potentially mobile electrons as facilitators to lower the overall or net energy barrier to the oxygen transfer during oxidation.

Effects of Asphalt Composition on Oxidation Kinetics

Kinetic data for the ketones and sulfoxides formed during asphalt oxidation of the type shown in figures 4-3 through 4-6 provided important clues and insight about the mechanisms of asphalt oxidation. Because variations in asphalt composition influence the kinetics of the formation of oxidation products, it was deemed desirable to consider key kinetic data on all eight of the SHRP core study asphalts. As will be shown later, the dominating oxidation mechanisms during the initial rapid oxidation spurt and during most of the slower oxidation following this spurt involve the oxidation of two different types of reactive hydrocarbons in asphalt. The discovery and understanding of this fact has been a major breakthrough in understanding the mechanisms of asphalt oxidation, and has resolved much of the conflict and confusion regarding asphalt oxidation that persisted in the past.

Because of the two proposed mechanisms involved and their sequential appearance on the oxidation time line (i.e., during and after the oxidation spurt), two significant points on the time line of the kinetic plots were selected for subsequent charting. The selection of single data points on the kinetic time line also greatly simplified the comparison of the effects of composition on the oxidation mechanisms, as represented by the eight different SHRP asphalts; all eight could be compared on a single data plot. The first set of data points was taken from near the end of the rapid oxidation spurt in the inflection point region of the parabolic-like curve (e.g., figure 4-5). These data points were at 200, 50, and 12.5 hr at 60°C (140°F), 80°C (176°F), and 100°C (212°F) for PAV oxidation, and at 60, 18, and 6 hr for TFAAT oxidation at 85°C (185°F), 113°C (235.4°F), and 130°C (266°F), respectively. The second set of data points was taken from the kinetic plots after a significant amount of oxidation had occurred following the spurt. These points were taken at 800, 200, and 50 hr for PAV oxidation, and 250, 75, and 25 hr for TFAAT oxidation, respectively, and at the same respective temperatures. Oxidation occurring between the two sets of data points is primarily the oxidation that occurs following the spurt. The total oxidation times selected produced approximately the same level of oxidation in the asphalts using either oxidation procedure.

Although kinetic data were obtained at three temperatures for each oxidation procedure, only one of the two higher temperatures was used in most of the figures because the kinetic data (except for effects of sulfoxide thermal decomposition at high temperatures) were similar for the two higher temperatures. The data points were plotted as a function of asphalt sulfur content because sulfur content is the asphalt composition parameter that has been shown to correlate well with asphalt component compatibility [Branthaver et al. 1991]. Further, component compatibility is fundamentally related to important performance-related chemical and physical properties, including oxidative hardening characteristics of asphalts [Petersen 1984; Petersen et al. 1993; Branthaver et al. 1993].

The concentrations of ketones and sulfoxides formed in the eight SHRP asphalts during the initial rapid oxidation spurt, and the net increase following the oxidation spurt, are plotted versus asphalt sulfur content in figure 4-21 for TFO/PAV oxidation at 60°C (140°F) and 100°C (212°F). During the oxidation spurt (figure 4-21, top display), the concentrations of ketones formed decreased and the concentrations of sulfoxides formed increased in a somewhat regular

manner with increasing asphalt sulfur content. At about 3-4 mass percent sulfur content, sulfoxide formation during the spurt was generally insensitive to increasing asphalt sulfur content. Following the spurt (figure 4-21, bottom display), the rate of ketone formation, except for variations resulting from differences in asphalt composition, decreased slightly with increasing sulfur content. On the other hand, unlike sulfoxide formation during the spurt, the rate of sulfoxide formation following the spurt increased only slightly with sulfur content until the asphalt sulfur content reached about 3-4 mass percent, after which sulfoxide formation increased substantially with increasing asphalt sulfur content. It is noteworthy that the rate of sulfoxide formation after the spurt decreased significantly in the high sulfur asphalts at the higher temperature. The reason for the unusual deviation in the sulfoxide and ketone data for asphalt AAD-1 at 100°C (212°F) compared with the 100°C (212°F) data for the other asphalts is not known. Data for 80°C (176°F) oxidation of AAD-1, inserted into figure 4-22, show "normal" behavior at this temperature.

Because the inflection point at the end of the spurt for the formation of ketones and sulfoxides may not be at exactly the same point on the time line for all asphalts, choosing the same fixed time to define the end of the oxidation spurt may cause some variation in the data among the asphalts relative to the proportions of ketones and sulfoxides assigned as occurring during and after the spurt. To offset this potential bias, the concentrations of ketones and sulfoxides and their sums for the total oxidation period, as a function of sulfur content, are shown in figure 4-22 for TFO/PAV oxidation. Because ketones and sulfoxides are the major identifiable oxidation products, their sums indicate the relative sensitivity of the asphalts to reaction with oxygen. As seen in figure 4-22, sensitivity to oxidation increased with sulfur content; however, the rate of ketone formation decreased and sulfoxides increased with increasing sulfur content. This is fortunate because ketone formation correlates strongly and sulfoxides weakly, if at all, with viscosity increase on oxidative aging [Petersen et al. 1993].

Data for atmospheric pressure TFAAT oxidation of the eight SHRP asphalts, presented in the same manner as for the PAV oxidations, are shown in figures 4-23 and 4-24. The most significant difference between the kinetic data for TFO/PAV and TFAAT oxidations is the much greater sensitivity of the asphalts to the relative amounts of ketones and sulfoxides formed as a function of temperature for TFAAT oxidation. In general, both during and after the oxidation spurt, greater amounts of ketones appear to be formed at the expense of sulfoxides at the higher temperature (figure 4-23). Also, as seen in figure 4-24, and unlike the TFO/PAV oxidation data (figure 4-22), the total amounts of ketones and sulfoxides formed were nearly the same as a function of sulfur content except for slightly lower total amounts being formed in the three asphalts of lowest sulfur content.

Oxidation Kinetics in the Pavement Temperature Range

Unpublished data obtained a number of years ago by J. C. Petersen, H. Plancher, G. M. Miyake, and P. M. Harnsberger provide important information on lower temperature oxidation that are relevant to the present work. In the past work, several non-SHRP asphalts were oxidatively aged in the pavement temperature range of 45°C (113°F) as thin films on Ottawa sand in briquettes (5 mass percent asphalt). Asphalt was extracted from the briquettes as a

function of oxidation time, the asphalt was recovered, and determinations were made of dynamic viscosity, and ketone and sulfoxide contents. At this low oxidation temperature, oxidation rates were relatively slow, thus yielding a number of data points during the oxidation spurt, but data were not obtained at the higher oxidation temperatures used for the SHRP asphalts. Low temperature data for one of the asphalts (Shell Wood River) are shown in figure 4-25.

It is apparent from the kinetic data in figure 4-25 that, during the initial part of the oxidation spurt, sulfoxides were formed at the virtual exclusion of ketone formation. Ketones did not begin to form in significant amounts until the formation of sulfoxides had leveled off. The significance of these data will be considered during the following discussion of the oxidation mechanisms.

Proposed Oxidation Mechanisms

As pointed out in the Historical Background, both Knotnerus [1971] and van Gooswilligen et al. [1985] recognized that asphalts contain a limited amount of highly reactive hydrocarbon components that are depleted on oxidation. Neither investigator, however, studied the oxidation reaction beyond the exhaustion of these reactive components (near the end of the oxidation spurt as defined in this report). The possibility of more than one distinctly different type of hydrocarbon reaction, as proposed in the present paper, apparently was not considered by previous investigators. In the present report, it is proposed that oxidation reactions involving two different types of hydrocarbons dominate asphalt oxidation, one type on either side of the inflection point of the kinetic plot. It is believed that the lack of recognition of this phenomenon has contributed significantly to the confusion that has existed regarding the mechanisms of asphalt oxidation.

Oxidation during the spurt will first be considered. Both Knotnerus [1971] and Mill [1996] have proposed reactive polycyclic hydroaromatic hydrocarbons as reactants during asphalt oxidation. The reaction of model hydroaromatics with oxygen is very rapid [Knotnerus 1971] and occurs without an apparent induction period [Mill 1996]. Thus, such a reaction could account for the apparent absence of an induction period during asphalt oxidation. The major chemical reactions occurring during the oxidation spurt proposed in this paper are illustrated in figure 4-26, using dihydroanthracene as the model hydrocarbon. Oxidation of polycyclic hydroaromatics could produce either hydrogen peroxide (H_2O_2) or a hydroaromatic hydroperoxide (structure III). In the model studies of the oxidation of dihydroanthracene by Mill et al. [1997] during the present project, dihydroanthracenyl hydroperoxide accounted for about 90 percent of the air- or oxygen-oxidized dihydroanthracene, with only about 10 percent reacting to form hydrogen peroxide. Either product could then react with reactive asphalt sulfides to produce sulfoxides [reaction (2), figure 4-26] by well known mechanisms (e.g., Bateman and Hargrave [1954a,b]). The relative ease with which oxygen reacts with potential hydroaromatics in asphalt is not known, but has been discussed by Mill [1996]. Mill et al. [1997] further report that, in oxygen uptake measurements in air, oxidation of dihydroanthracene accounted for 95 percent of the oxygen. Replacement of air with oxygen led to only a 2.3 fold increase in rate, indicating the presence of a free radical chain component in

the reaction [Mill and Hendry 1980]. Additional evidence for a chain process is found by the inhibition of oxidation by addition of the free radical scavenger butylmethyl phenol [Walling 1964].

During the oxidation spurt it is reasonable to suppose that small amounts of hydroperoxides might decompose, the rate being dependent on temperature, to form free radicals as shown in reaction (3), figure 4-26. These free radicals could contribute to the initiation of the subsequent chain reactions involving benzylic carbons in asphalts. It is proposed that the major oxidation reaction following the oxidation spurt is the oxidation of asphalt benzylic carbons to form ketones and sulfoxides. Possible oxidation sequences for this reaction are outlined in the schemes shown in figure 4-27. These schemes are not intended to represent all possible intermediate pathways nor are all of the pathways shown expected to be significant contributors to the formation of the known oxidation products. Initiation of the oxidation of benzylic carbon requires the abstraction of a relatively active hydrogen to form the benzyl radical (structure II). It has been reported by Mushrush [1992 and papers cited therein] that the peroxy radical (structure III) is the most stable of the free radicals formed during typical hydrocarbon chain transfer oxidation reactions and is probably the primary precursor of ketone formation. This reaction is illustrated by reaction (c), figure 4-27. Hiatt et al. [1968] reported that secondary peroxy radicals undergo non-radical self reaction to form ketones. Once the chain reaction has begun, it has been reported that formation of alkyl free radicals (e.g., structures II and VI) is usually rate-controlling; however, at very low oxygen concentrations (ca 1 ppm), reaction of oxygen with the alkyl free radicals [reaction (b)] can be rate-controlling [Mushrush et al. 1996].

The most probable route for sulfoxide formation is via reaction of a benzylic alkylarylhydroperoxide (structure VII, figure 4-27) with sulfides in the asphalt [reaction (g)]. This reaction apparently occurs with relative ease as illustrated by the data in figure 4-25 for low temperature asphalt oxidation. Bateman and Hargrave [1954a,b] showed that the rate of the reaction of hydroperoxides with sulfides to form sulfoxides in alcohol solutions increases with increasing acidity of the alcoholic OH, and that the reaction rate is greatly accelerated by stronger acids such as acetic acid. They concluded that the actual oxidant is a cyclic complex between the hydroperoxide, the hydrogen-donating molecule (alcohol or acid), and sulfide. An oxygen transfer then occurs with the sulfide being promoted to a sulfoxide by a synchronous hydrogen atom exchange process within the complex. Such a catalytic reaction also takes place in hydrocarbon solvents as well as alcohols when acidic molecules are present. It is not unlikely that asphalts contain catalysts that promote sulfoxide formation from sulfides. The ease with which sulfides in asphalts, present in relative abundance, react with hydroperoxides may account for difficulties encountered in past efforts to find hydroperoxides in detectable concentrations in oxidized asphalts.

Although it was suggested that the dominant precursor to ketone formation might be the peroxy radical (structure III, figure 4-27), formation of ketones from the decomposition of hydroperoxides [structure VII, reaction (f)] could be an alternate route for their formation. In Mushrush's [1992] review of the literature, it is reported that decomposition of hydroperoxides can be induced by catalytic amounts of metal ions; and in a basic medium, alkyl hydroperoxides

can give carbonyl compounds. Catalytic amounts of metals are present in many asphalts. Asphalts have also been shown to have hydrogen bonding basicity with phenol [Barbour and Petersen 1974], with an enthalpy of formation of the hydrogen bond of 6-8 kcal/mol in carbon tetrachloride solution.

It is instructive at this point to examine the kinetic data in the plots shown in the previous section with regard to the reaction mechanisms just proposed. The time frame, within which the proposed dual, sequential oxidation of the proposed polycyclic hydroaromatics and the benzylic carbons occurs in asphalts, will first be considered. The kinetic data for ketone and sulfoxide formation reveal that considerable amounts of sulfoxides are formed prior to the formation of significant amounts of ketones, particularly in asphalts oxidized in an oxygen-poor, diffusion controlled environment. Examination of kinetic data for oxidation at the rather low temperature of 45°C (113°F) shows (figure 4-25) that sulfoxides are initially formed with the virtual exclusion of ketone formation. These results strongly support the proposal that asphalt oxidation begins with the reaction of highly reactive hydrocarbons that does not produce ketones in the process, but rather sulfoxides, as proposed by the scheme in figure 4-26. Mill [1996] showed that dibutyl sulfide, which does not react significantly by itself in air, oxidized rapidly to sulfoxide in a dihydroanthracene solution, consistent with reaction (2) in figure 4-26.

The question arises as to whether or not any ketones are formed from dihydroanthracene oxidation intermediates. If ketones are formed, they should form at a bridgehead carbon containing an active hydrogen, thus resulting in the formation of carbonyls of the quinone type. Examination of the IR carbonyl frequencies of a series of model quinone-type compounds showed absorption frequencies ranging from 1,681 cm^{-1} for anthraquinone down to 1,653 cm^{-1} for anthrone. Further, IR spectra from an unpublished pre-SHRP kinetic study, which included a number of spectra taken during the oxidation spurt on through to a rather high oxidation level of about 0.5 mol/L ketones, were examined. No evidence of carbonyl frequencies other than that of the benzylic carbon ketone at about 1,695 cm^{-1} was found. This peak maximum is typical and constant for all asphalts and is consistent with the frequency of 1,696 cm^{-1} for the carbonyl of acetophenone (a ketone formed on a benzylic carbon) and the ketones identified in asphalt by Dorrence et al. [1974].

Further confirmation that ketones are formed in asphalt only from benzylic carbons, and that the mechanism (not rate) of their formation is independent of temperature and oxygen concentration, is found in the data presented in figures 4-28 and 4-29 for the oxidations of the highly compatible asphalt AAG-1 and the less compatible asphalt AAD-1. Compared in each figure are the kinetics of ketone formation for both high temperature (130°C [266°F]) TFAAT and low temperature (60°C [140°F]) PAV oxidations. To make the kinetic data comparable, the time scales for ketone formation at 130°C (266°F) were shifted so that the point on the two temperature scales that produced the same level of ketones after 400 hours of 60°C (140°F) PAV oxidation overlapped. This time-temperature shift produced identical kinetic plots for ketone formation by both oxidation methods and for both asphalts, thus confirming that ketones are formed during and after the oxidation spurt by one mechanism only. As might be expected, variations in asphalt composition (AAG-1 versus AAD-1), while not altering the oxidation mechanism, altered the rates of ketone formation as shown by the different values for the

time-temperature shift for the two asphalts. Viscosity data shown in the figures will be discussed later.

Based on data discussed thus far, it is apparent that the benzylic carbon chain reaction illustrated in figure 4-27 begins sometime during the course of the rapid oxidation spurt. It is also apparent that, at atmospheric pressure and at 45°C (113°F) (figure 4-25), this reaction does not become significant until near the end of the oxidation spurt when the reaction of the hydroaromatics is near completion. Thus, there is evidence for an induction period typical of hydrocarbon chain reactions prior to the oxidation of the asphalt benzylic carbons. Natural phenolics in asphalt may in part be responsible for this apparent induction period. Numerous past functional group analyses of asphalts before and after oxidation have shown that most of the phenolics in asphalt are not consumed during the oxidation of neat asphalt, even at 130°C (266°F). It is believed that most of these potential free radical scavengers are locked up in the strongly associated, immobilized aromatic components of the microstructure and, thus, they are physically unavailable for reaction with the free radicals formed. This hypothesis is supported by an asphalt oxidation experiment conducted in benzene solution during the SHRP asphalt research by Dr. T. Mill [Branthaver et al. 1993]. Mill found that the asphalt phenolics were consumed during the solution oxidation. This indicates that the associated micellar structures containing the phenolic functionalities were dissociated in the solvent, thus making the phenolics available to react with free radicals produced.

Data in figures 4-21a and 4-23a, showing ketone and sulfoxide formation during PAV and TFAAT oxidations, respectively, at different temperatures, show that above ambient temperature ketones begin forming sometime during the oxidation spurt, and that during atmospheric oxidation the ratio of ketones to sulfoxides is highly temperature dependent (figure 4-24). A possible explanation for this behavior is as follows. At low temperatures (e.g., 45°C [113°F]), the decomposition of hydroperoxides to form free-radicals [figure 4-26, reaction (3)] is slow, thus favoring sulfoxide formation [reaction (2)] rather than free radical formation. At higher temperatures, the probability of free radical production is increased. Also at higher temperatures, free radical initiation reactions proposed by others (see Introduction) involving trace metal catalysis, oxycyclics and other concerted reactions, naturally occurring electron-rich centers (highly condensed aromatics), complexes involving asphalt heteroatom moieties such as pyrrolics, etc., may increase the rate of free radical production. Such entities would shorten the induction period and, thus, cause the benzylic carbon oxidation reaction shown in figure 4-27 to become significant during the oxidation spurt prior to the exhaustive oxidation of the polycyclic hydroaromatics.

Evidence that the majority of the sulfoxides formed during the oxidation spurt are not formed by the same reaction as the sulfoxides and ketones formed following the spurt is shown by data in figure 4-30. These data are from previously unpublished work by H. Plancher and J. C. Petersen. A Boscan asphalt was oxidized as a thin film at 130°C (266°F) as a function of temperature, with and without the addition of the antioxidant triphenyltin hydroxide (TPTH). Note that during the oxidation spurt the rapid sulfoxide formation was not affected significantly by the presence of the TPTH; however, the production of ketones was significantly inhibited. These data provide further confirmation of the simultaneous and independent operation of the

two different oxidation mechanisms proposed in figures 4-26 and 4-27, with the bulk of the sulfoxides being formed during the spurt from oxidation of the hydroaromatics. Near the end of the spurt, when the supply of the proposed hydroaromatics becomes exhausted, the rate of sulfoxide production decreased significantly. It is proposed that at this point the major source of hydroperoxides for sulfoxide formation are the benzylic carbon hydroperoxides [figure 4-27, reaction (g)]. Because the production of these hydroperoxides depends on the concentration of free radicals, which is reduced by the TPTH, both the rate of production of ketones and hydroperoxides are reduced by the TPTH following the oxidation spurt.

Because most of the sulfoxides produced during the spurt result from oxidation of hydroaromatics, it is proposed that the amount of sulfoxides formed during the spurt is a relative indicator of the hydroaromatics content of asphalts. To test this hypothesis, unpublished data collected over a number of years, by various WRI researchers, of the amounts of sulfoxides formed near the surface of asphalt stored in sample cans at ambient temperatures, and as thin films on chromatographic supports that were allowed to stand exposed to air for extended periods of time at ambient temperatures, were examined. Only those asphalts were considered in which sulfoxides, but no significant amounts of ketones, had formed. Three viable candidates from different asphalt sources were found. These showed sulfoxide contents of 0.10, 0.11 and 0.12 mol/L, in good agreement with data in figure 4-25. Since two equivalents of reactive hydrogen are consumed to form one equivalent of sulfoxide (figure 4-26), the sulfoxide data indicate that the concentration of the proposed hydroaromatic hydrogen ranged from 0.20 to 0.24 mol/L. These values are consistent with high temperature oxidation data in figure 4-30 and figure 4-21a if one subtracts the estimated sulfoxides formed during the spurt period from benzylic carbon oxidation.

The effects of molecular association (physicochemical effects) and asphalt composition on the oxidation kinetics, as rationalized by the proposed mechanisms and the microstructural model of asphalt, will next be considered. Comparison of PAV and TFAAT oxidations during the spurt show a low temperature sensitivity for the ratio of sulfoxides to ketones formed during PAV oxidation (figure 4-21, top display), and a high temperature sensitivity of the ratio during TFAAT oxidation (figure 4-23, top display). As previously mentioned, asphalt has sufficient dissolved oxygen during PAV oxidation so that oxygen concentration is not rate limiting; however, during TFAAT oxidation, particularly at lower temperatures, oxygen diffusion effects limit asphalt oxygen concentration and thus reduce reaction rate. It is proposed that, during PAV oxidation, there is a higher concentration of oxygen in the more highly associated, more aromatic components that contain the hydroaromatics than during TFAAT oxidation. Also, a higher concentration of the benzylic carbons responsible for ketone formation should be present in the more highly associated components. Further, during TFAAT oxidation, since the asphalt solvent phase is the continuous phase, oxygen diffusing into the asphalt must first move through the continuous phase before it can enter the more associated phase where the hydroaromatic and ketone precursors are likely concentrated. This migration of oxygen into the associated structure is greatly reduced at lower temperatures when the microstructure increases in size. As a result, greater amounts of hydroaromatics should react during the spurt to produce sulfoxides, for example, during the non-diffusion controlled 60°C (140°F) PAV oxidation than during the diffusion controlled 85°C (185°F) TFAAT oxidation. That this occurs appears evident by

comparing sulfoxide production shown in figure 4-21 (top display) with that shown in figure 4-23 (top display). The effect is intensified for the more highly associated, high sulfur asphalts, as would be predicted by the asphalt microstructural model. In fact, based on the above interpretation, part of the hydroaromatics appear not to oxidize in the high sulfur asphalts during the spurt for TFAAT oxidation (asphalts AAK-1 and AAD-1, figure 4-23, top display). Further, for asphalts AAK-1 and AAD-1, the amounts of sulfoxides formed during the TFAAT oxidation become nearly temperature insensitive. One might argue that the decrease in sulfoxide content during the 113°C (235.4°F) TFAAT oxidation may result from sulfoxide decomposition; however, it is unlikely that decomposition could contribute significantly during the short time of the spurt. Also, the similar amounts of ketones formed during the spurt for both PAV and TFAAT oxidations of the high sulfur asphalts, and the larger amounts of sulfoxides formed for PAV oxidations, provide further evidence that more sulfoxides are formed from hydroaromatics.

Another factor that could contribute to the sensitivity of the TFAAT oxidation to temperature might be that at lower temperatures, oxygen concentration leading to free radical formation and formation of peroxy radicals (structure III, figure 4-27), which are the precursors of ketones, may be rate controlling. Because the peroxy radical is relatively stable compared with the other radicals formed, at lower temperatures ketone formation via reaction (c) should be reduced; and because of the lower activation energy for sulfoxide formation than for ketone formation [Huh and Robertson 1996], sulfoxide formation via reactions (d) and (g) should be favored. However, at high temperatures, reactions of the peroxy radical (structure III, figure 4-27) should become more favored. Possible mechanisms and/or rate limiting steps for the higher pressure PAV oxidation are less obvious. The rate limiting step(s) are most likely with or beyond those reactions involving the peroxy radical.

Oxidation following the oxidation spurt, as previously discussed, is believed largely the result of free radical oxidation typified in figure 4-27. Ketone and sulfoxide data in figures 4-21 (lower display) and 4-23 (lower display) for PAV and TFAAT oxidation, respectively, show a much greater sensitivity of the ratio of ketone to sulfoxide formation for TFAAT than for PAV oxidation. Note that, during the 85°C (185°F) TFAAT oxidation, the rate of ketone formation generally decreased with increasing sulfur concentration. This is believed to result largely from the reduced mobility, and thus reactivity, of the ketone precursors in the higher sulfur asphalts because of increased molecular association. Also, because the reaction of the peroxy radical to form ketones [reaction (c), figure 4-27] is bimolecular [Correa et al. 1988], such immobilization should greatly reduce ketone formation. This reaction should be much more sensitive to molecular structuring than the reaction of the peroxy radical with benzylic hydrogen [reaction (d)] to form sulfoxide precursors because benzylic hydrogens would be available in much greater concentrations than the peroxy radical.

One might also suggest that more sulfoxides than ketones are formed in the higher sulfur asphalts because of the greater concentration of asphalt sulfides. However, the mechanisms just presented and other experimental data suggest that this possibility is not significant. It has been shown [Petersen et al. 1981] that the addition of a large excess of dibenzyl sulfide to two different asphalts did not lead to an increase in the total amount of sulfoxide formed on oxidation. Sulfoxides were formed from the dibenzyl sulfide at the expense of asphalt sulfides.

These results strongly support the reaction scheme proposed in figure 4-27, suggesting that the concentration of free radicals (related to oxygen concentration) is rate-limiting and that ketones and sulfoxides are formed by different routes. Thus, sulfoxide formation is probably limited by the amount of benzyl hydroperoxide (structure VII, figure 4-27) available.

The physicochemical effect apparently limiting the relative amounts of ketones formed in high sulfur asphalts is indeed fortunate, because the sensitivity of asphalts to viscosity increase from ketone formation is greater in the less compatible, higher sulfur asphalts. This is most likely because the ketones produced in less compatible and more highly associated asphalts result in the formation of larger or more structured molecular agglomerates than ketones produced in more compatible asphalts with highly dispersed microstructure [Petersen et al. 1993]. However, as oxidation temperature increases, the relative amounts of ketones to sulfoxides produced during diffusion controlled oxidation (pavement oxidation) increase, unlike PAV oxidation, thus producing much greater sensitivity to viscosity increase in the high sulfur asphalts.

The differences in oxidation kinetics between 100°C (212°F) PAV oxidation and low temperature atmospheric pressure oxidation, such as in asphalt pavements, demonstrate the potential unsuitability of the PAV data, without taking into account the physicochemical effects induced by asphalt microstructure, for use in predicting the age hardening characteristics of a large percentage of the asphalts now being used in pavement service. More work is needed in this area to resolve this problem.

The effects of physicochemical factors on viscosity increase from oxidation are illustrated in figures 4-28 and 4-29 for the oxidation of both a highly compatible asphalt (AAG-1) and a highly associated asphalt (AAD-1) by both low temperature (60°C [140°F]) PAV and high temperature (130°C [266°F]) TFAAT oxidations. Time scales have been time-temperature shifted to superimpose the kinetic plots for ketone formation, as previously described, so that the relative effects of ketones on viscosity under the different oxidation conditions could be evaluated. Note that, for the compatible asphalt (AAG-1, figure 4-28), the effect of ketones on viscosity increase is nearly the same for both low and high temperature oxidation. However, comparable data for the less compatible asphalt (AAD-1, figure 4-29) show a much greater sensitivity to ketone formation during high temperature TFAAT oxidation than during low temperature PAV oxidation. It is proposed that a greater percentage of the ketones formed during low temperature oxidation are formed on benzyl carbons contained in the more weakly associating aromatic molecules in the peripheral regions of the microstructure. Thus, because they are formed on smaller, more weakly associated molecular components, their effect on association leading to an increase in apparent molecular weight, and thus viscosity, is minimized. On the other hand, at high temperatures during the TFAAT oxidation in which the associated solvation shell [Storm et al. 1996] is mobilized and becomes part of the solvent phase of the asphalt, benzylic carbons that were immobilized in the microstructure at lower temperatures are now mobilized and can readily react to form ketones. Thus, when the asphalt is returned to 60°C (140°F) for viscosity measurement after oxidation, the ketones formed on the inherently more highly aromatic and more strongly associating molecules cause the formation of much larger agglomerates and apparent molecular weight, thus, the greater

viscosity sensitivity of the asphalt to ketone formation when oxidized at high temperatures. That the microstructure of asphalt AAG-1 is also sensitive to dissociation at higher temperatures, resulting in increased reaction of benzylic carbon buried deeper in the micellar structure, is evidenced by data for ketone formation shown in figure 4-24; however, it is believed that the effect on viscosity evidenced for asphalt AAD-1 from oxidation of the more deeply buried benzylic carbon does not show up in the viscosity data for AAG-1 because the concentration of micellar structures is too low, even after oxidation, to permit significant interaction between them.

The results in figures 4-28 and 4-29 underscore the pragmatic importance of the conclusion reached earlier during the SHRP research [Branthaver et al. 1993] that the maximum temperature that a pavement experiences in service is the major determinant of the level of oxidative hardening that pavements will experience in service. The data also vividly demonstrate the inappropriateness of making judgments regarding the oxidative hardening of asphalts in pavements from the results of accelerated aging tests performed at temperatures significantly higher than the maximum temperature that a pavement will routinely experience.

To conclude the discussion, a few additional observations and comments are made. During oxidation following the oxidation spurt, the amounts of sulfoxides formed are nearly the same for all asphalts with sulfur contents less than 3-4 percent (figures 4-21 and 4-23). This is undoubtedly because the excess supply of asphalt sulfides has been exhausted during lower temperature oxidation, or at higher temperatures the rate of sulfoxide thermal decomposition and the rate of indicated sulfide regeneration have reached a steady-state concentration. After the oxidation spurt, significant amounts of sulfoxides are formed in the asphalts with higher sulfur contents, particularly for PAV oxidized asphalts. Most of the sulfoxides formed in the lower sulfur asphalts have been formed by the time defined as the end of the spurt, near the point at which sulfoxides reach a steady-state concentration. Figure 4-24 shows that the total ketones plus sulfoxides formed during the total ambient pressure oxidation is essentially constant for all asphalts containing 3-4 percent sulfur or higher. These latter results support the previous conclusion that oxidation at atmospheric pressure is oxygen diffusion controlled, which controls the rate of formation of free radicals. Data in figure 4-24 also show that, as oxidation temperature is increased, ketones are formed at the expense of sulfoxides, while the total amount of oxidation products remains nearly the same at both low and high temperatures. On the other hand, during PAV oxidation (figure 4-22), sulfoxide plus ketone content continues to increase as a function of sulfur content where it is above the 3-4 percent threshold seen for atmospheric pressure (TFAAT) oxidation. These results strongly suggest that part of the sulfoxides formed at higher pressures may result from a different mechanism than those formed at atmospheric pressure.

A likely possible route for the production of additional sulfoxides during PAV oxidation is via the reported reaction [Bridgewater and Sexton 1978; Mushrush 1992] illustrated by reaction (e), figure 4-27. Under high oxygen concentrations during PAV oxidation, the concentration of the peroxy radical (structure III, figure 4-27) should be much higher than at atmospheric pressure. Under such circumstances, asphalt sulfides in abundance may be able to compete successfully for the peroxy radical to form additional sulfoxides via reaction (e). It has

also been reported [Correa et al. 1988] that electron rich substrates such as olefins can be oxidized to produce a relatively stable radical cation that can be trapped, by normal and relatively unreactive triplet ground state oxygen, to yield an oxygenated radical cation that is a potent oxidant. If such were to happen, a net reaction could occur directly between oxygen and asphalt sulfides to produce sulfoxides. This reaction is reported to be promoted by increased oxygen concentration (pressure). Because the highly condensed aromatic, asphaltene-like, components of asphalt are rich in mobile or polarizable pi electrons, and even contain stable free radicals [Knotnerus 1971], the possibility of such a reaction as discussed by Correa should not be overlooked as a possible contributor to sulfoxide formation during PAV oxidation.

With regard to the initiation of the oxidation reaction in asphalts, many possibilities exist. Knotnerus reported that dark oxidation in solution of a n-hexane asphaltene fraction from a Middle East bitumen, whose stable free radical content as measured by electron spin resonance was 34 spins/g $\times 10^{-17}$, reacted with 1.43 mg/g of oxygen compared with no measurable reaction of oxygen with the maltene fraction, whose free radical count was 2 spins/g $\times 10^{-17}$. Active catalysts in asphalt such as metals [Branthaver et al. 1984], nitrogen-containing molecules, and concerted reactions such as proposed by King [1993] should also be considered as contributors to the oxidation of such a complex material as asphalt.

The evidence presented appears to establish that asphalt oxidation proceeds sequentially by dual hydrocarbon oxidation mechanisms. Asphalts apparently contain a limited amount of highly reactive hydrocarbons, probably of the polycyclic hydroaromatic type, which react rapidly with atmospheric oxygen to produce the rapid initial increase in viscosity at the onset of asphalt aging. This rapid reaction is followed by the much slower reaction of oxygen with benzylic carbons to produce ketones whose formation causes association of polar components and the viscosity increase associated with long-term age hardening. The recognition of the dual mechanism for asphalt oxidation has rationalized apparent conflicts among the results and interpretations of previous researchers on mechanisms of oxidation. The current interpretation of the oxidation kinetic data further confirms the correctness of the current microstructural model.

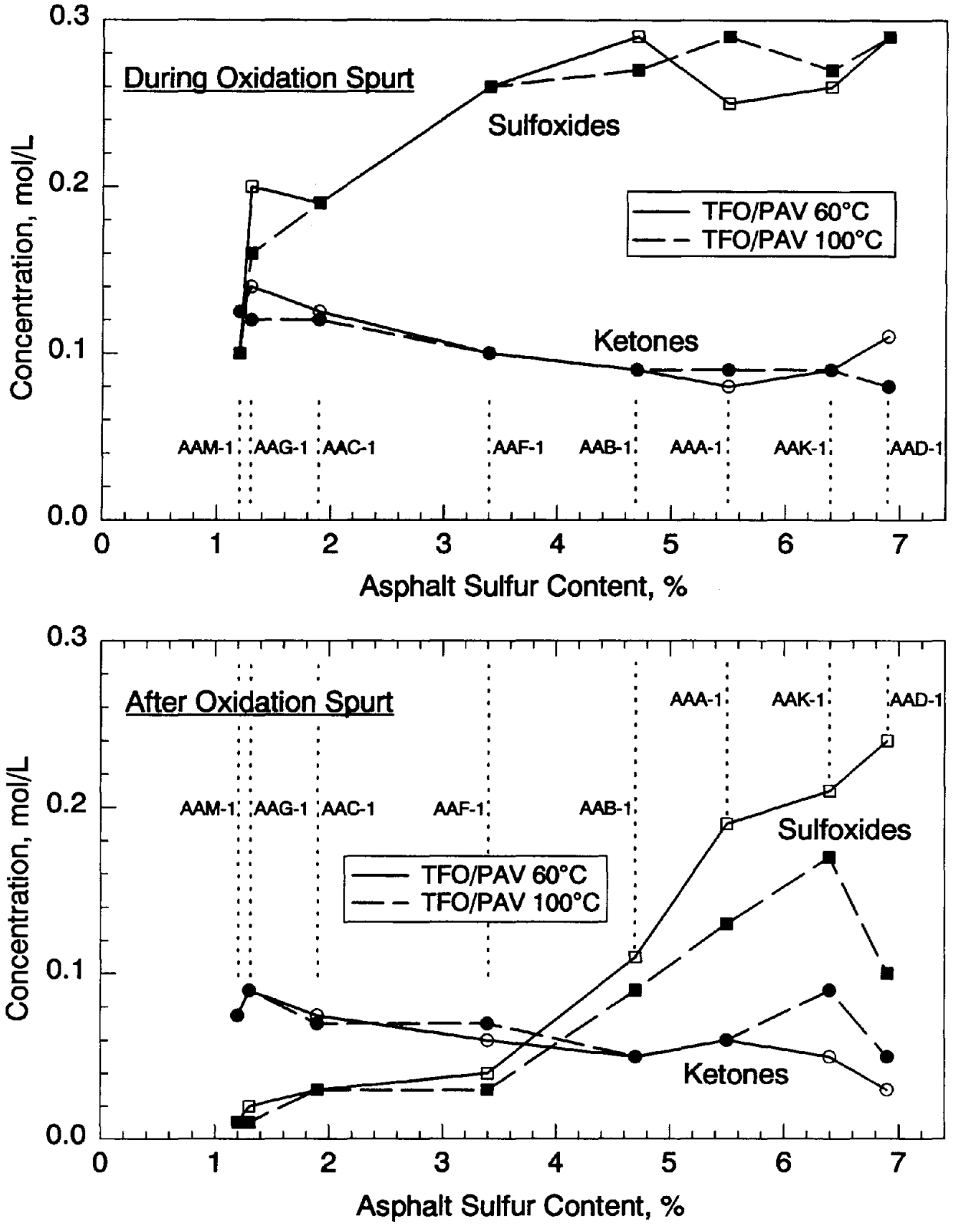

Figure 4-21. Ketones and sulfoxides formed during and after oxidation spurt on TFO/PAV oxidation at 2.07 MPa (20 atmospheres) pressure.

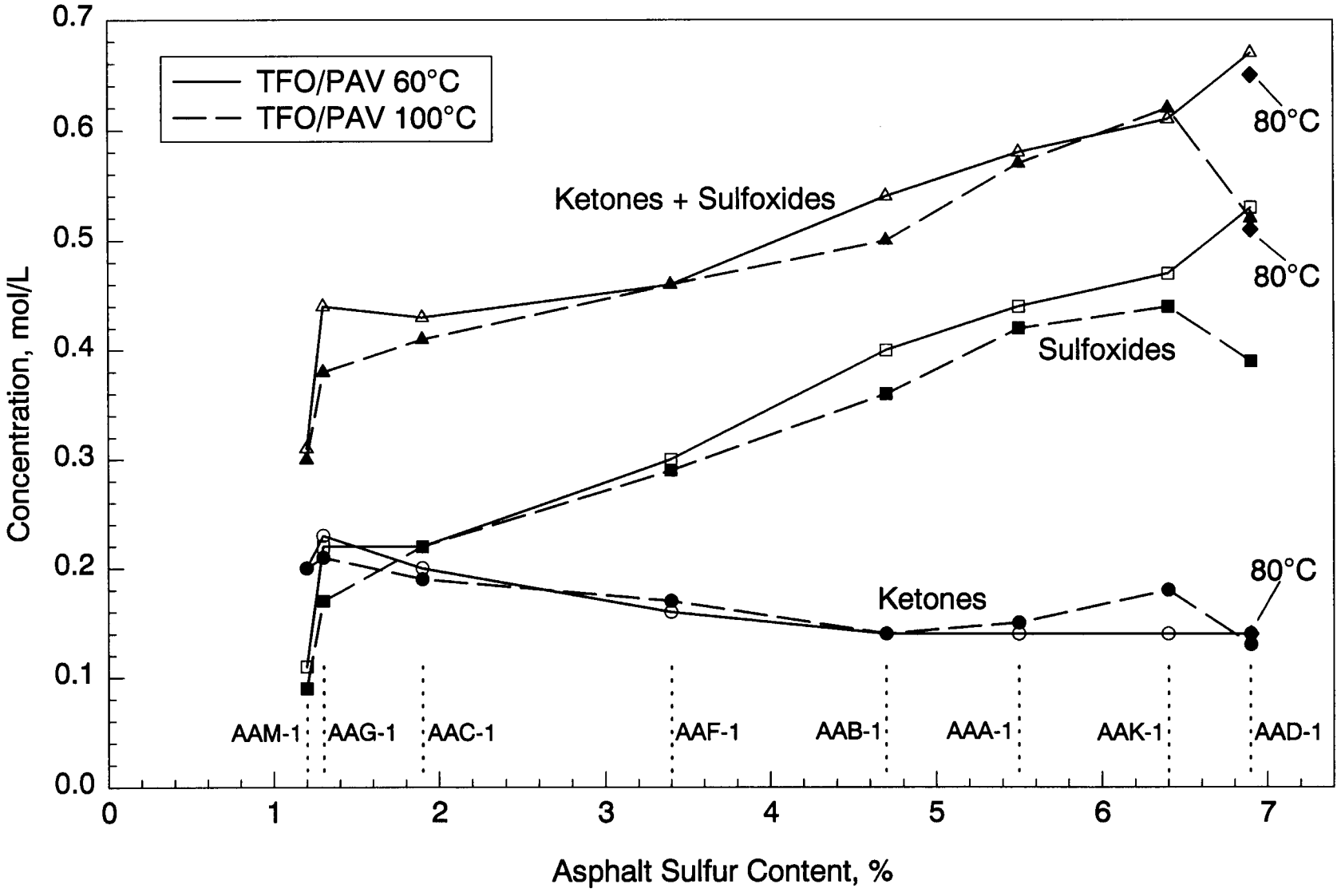

Figure 4-22. Ketones and sulfoxides formed during TFO/PAV oxidation at 60°C and 100°C at 2.07 MPa (20 atmospheres) pressure.

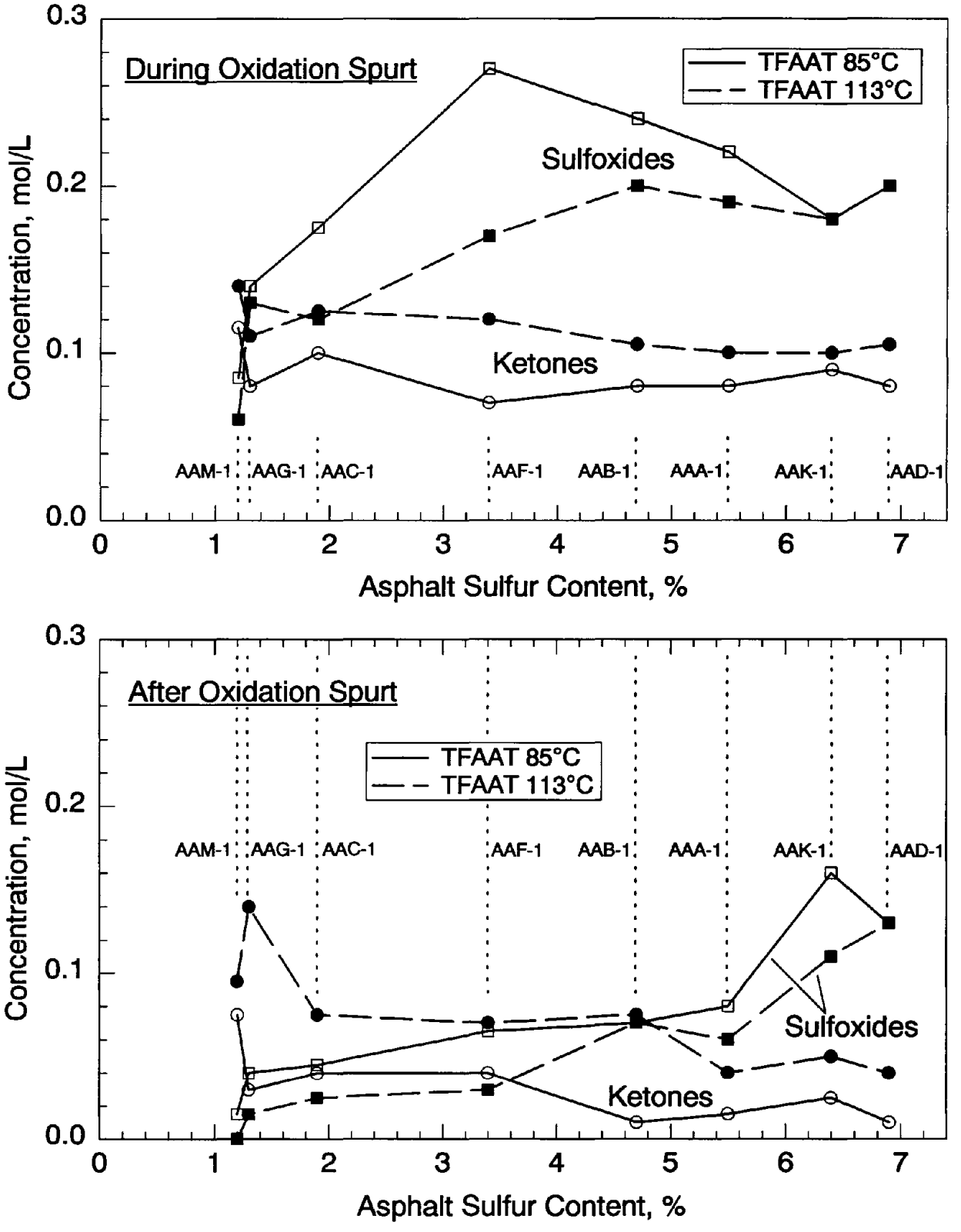

Figure 4-23. Ketones and sulfoxides formed during and after oxidation spurt on TFAAT oxidation at atmospheric pressure.

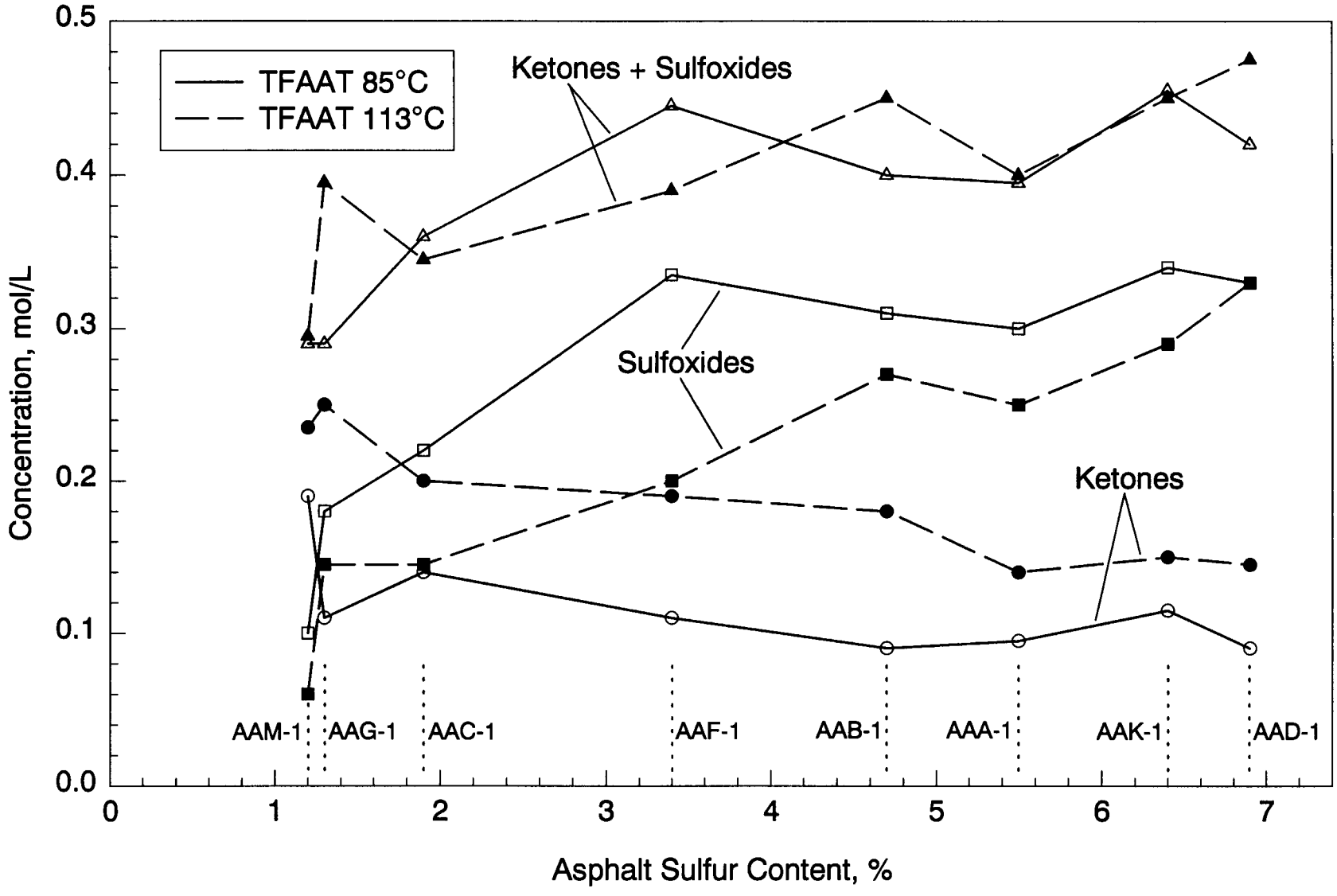

Figure 4-24. Ketones and sulfoxides formed during TFAAT oxidation at 85°C and 113°C at atmospheric pressure.

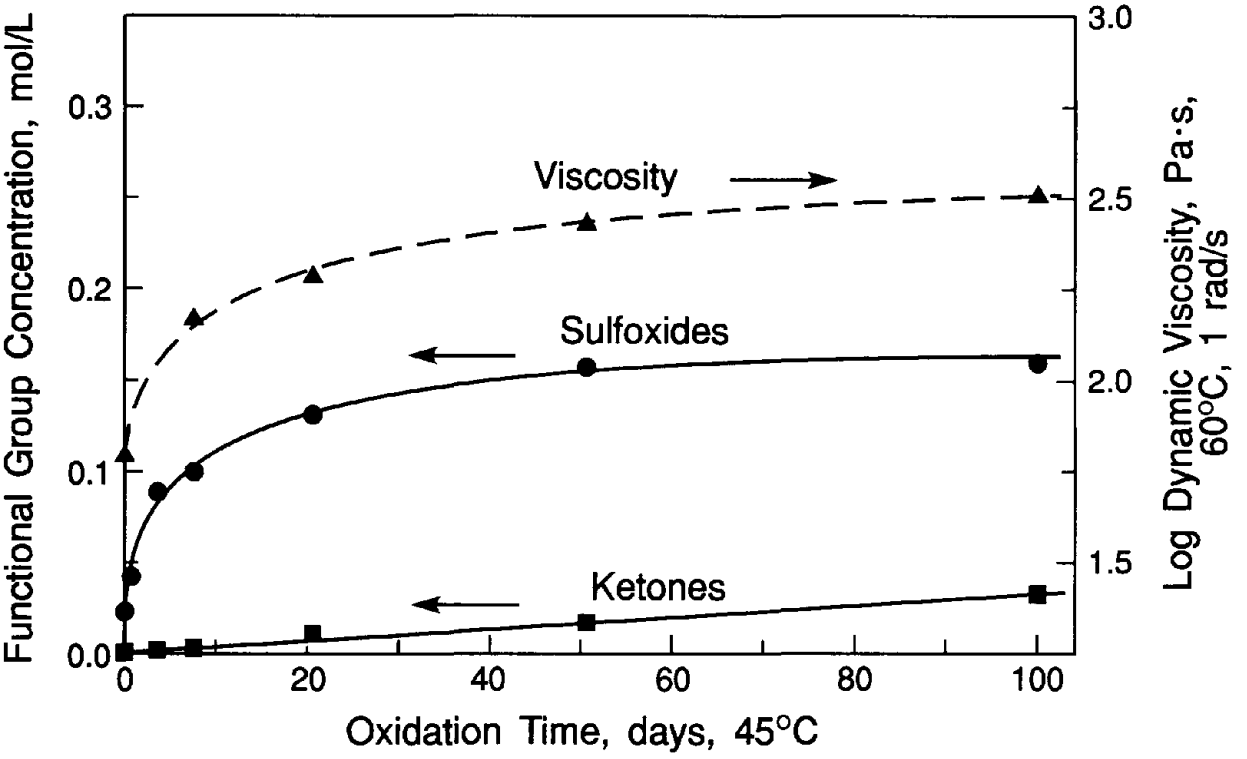

Figure 4-25. Kinetic data for the formation of ketones and sulfoxides in Shell Wood River Asphalt during thin film ambient pressure oxidation at 45°C.

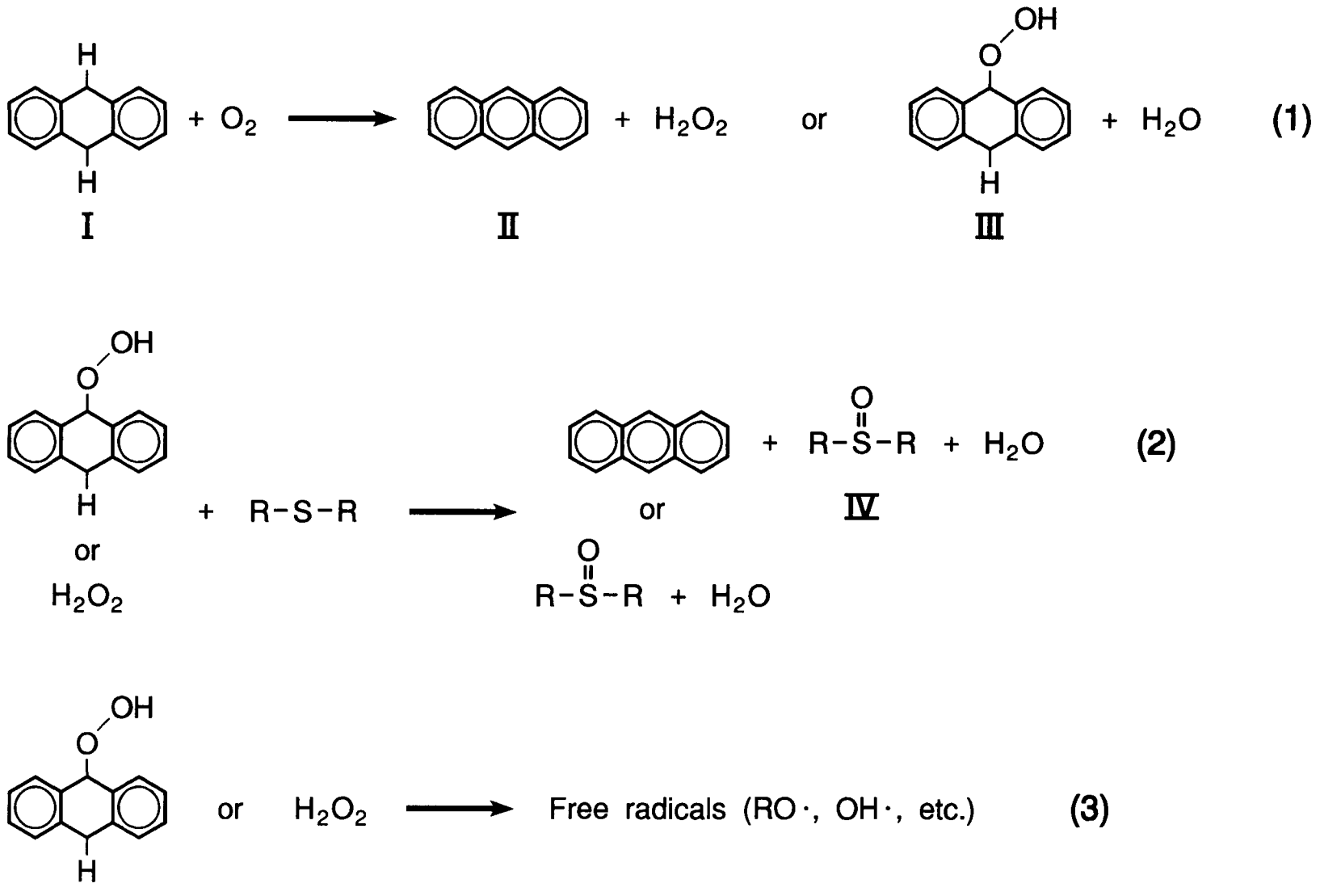

Figure 4-26. Reaction sequences for oxidation of proposed polycyclic hydroaromatics in asphalt during oxidation spurt, illustrated for dihydroanthracene.

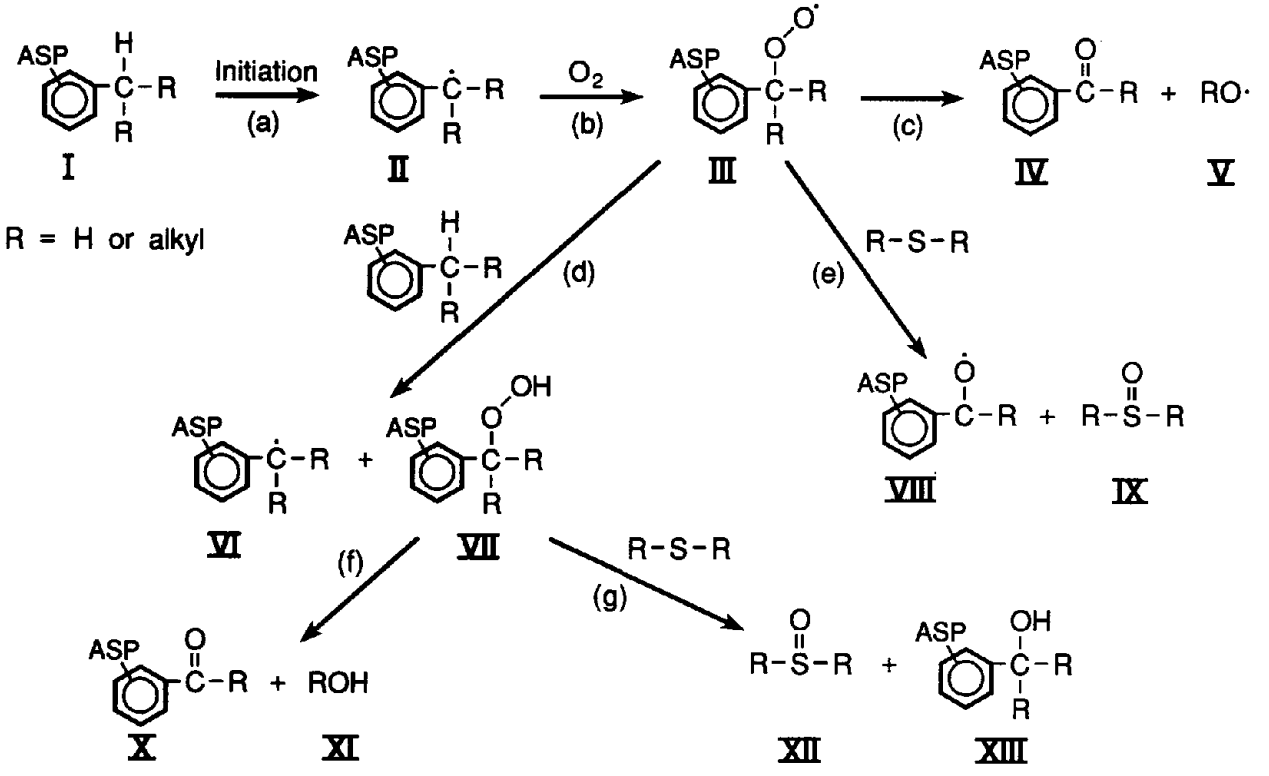

Figure 4-27. Possible reaction sequences for ketone and sulfoxide formation during oxidation of asphalt benzylic carbon.

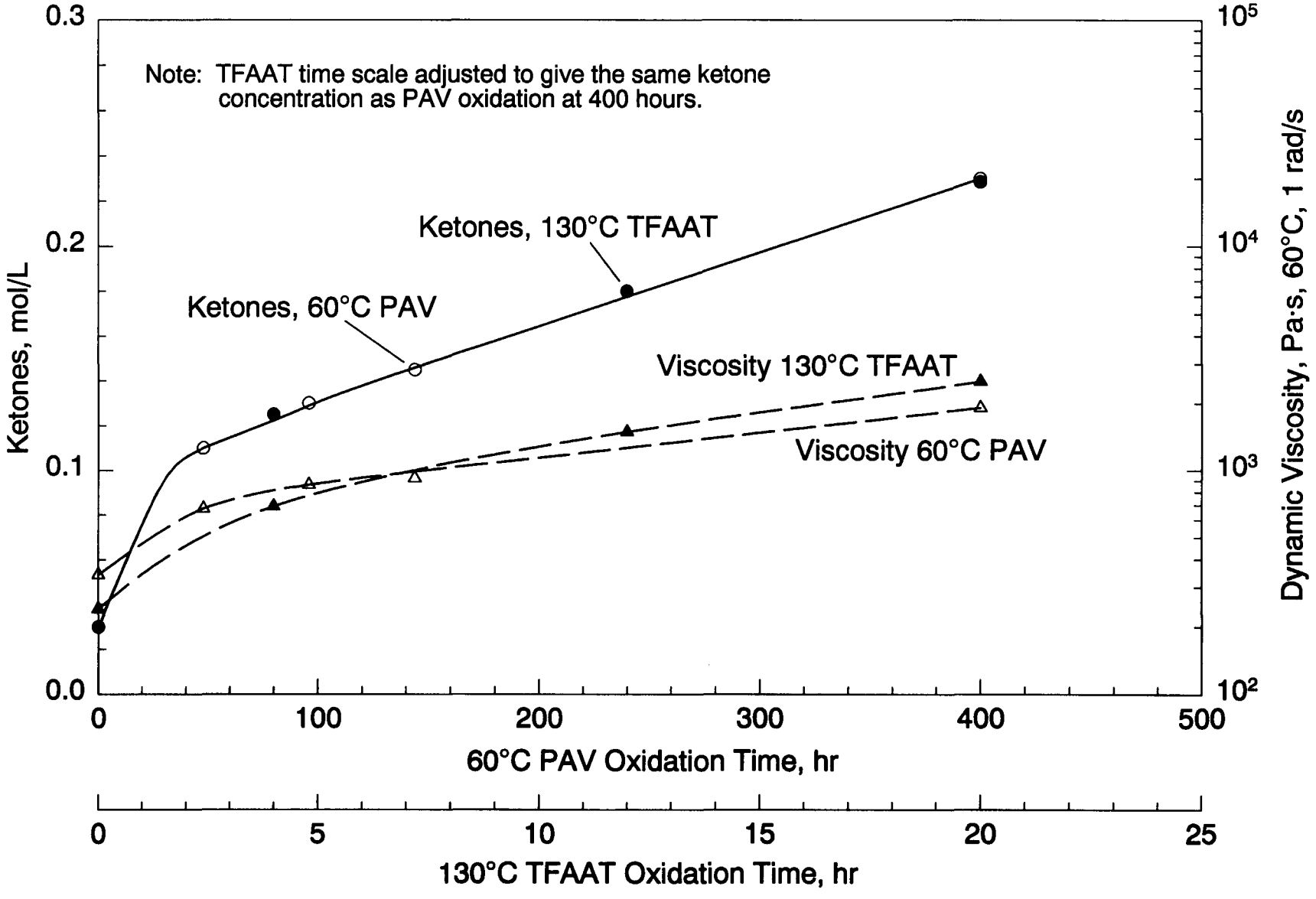

Figure 4-28. Comparison of kinetics of ketone formation in asphalt AAG-1 from PAV oxidation at 60°C with TFAAT oxidation at 130°C.

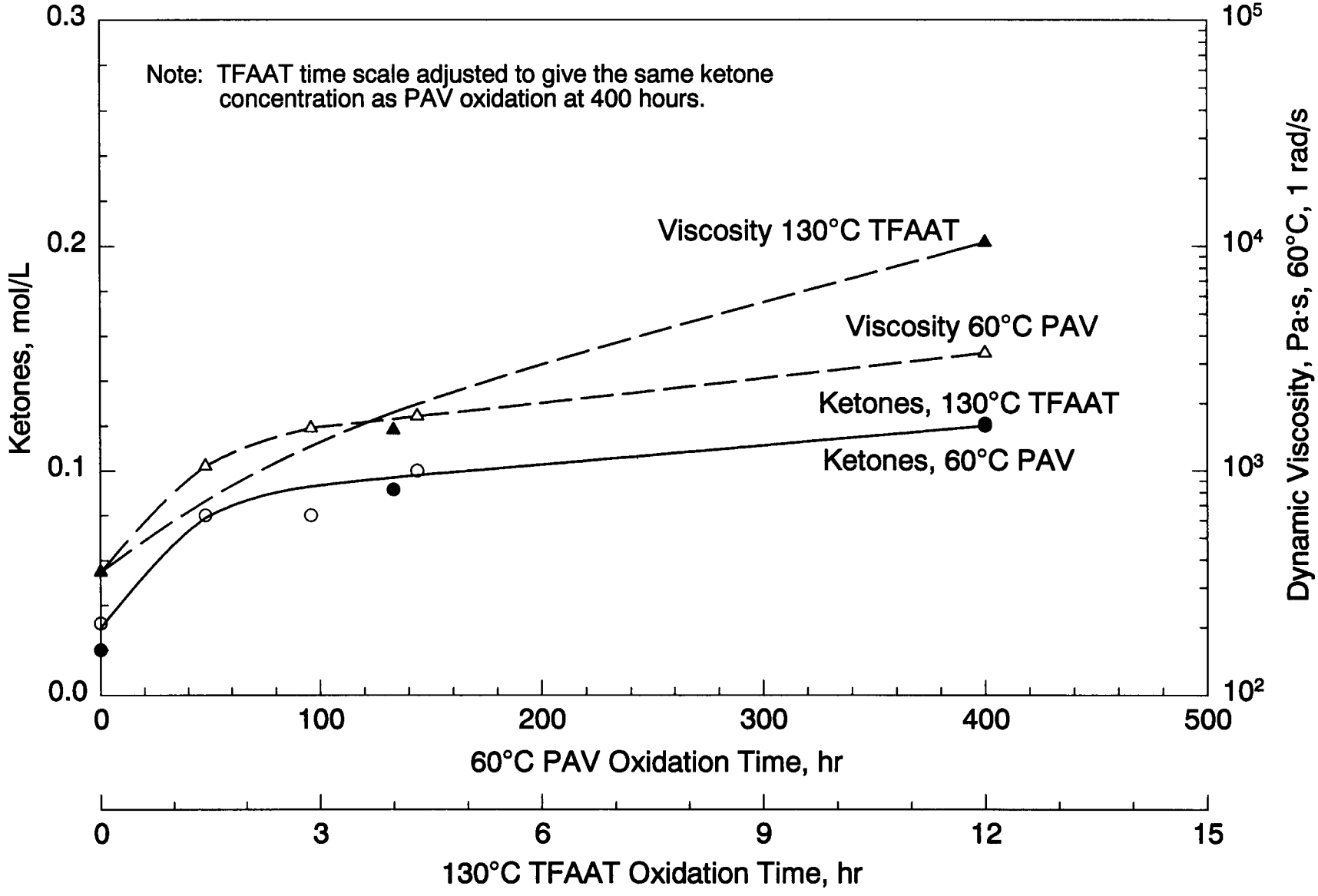

Figure 4-29. Comparison of kinetics of ketone formation in asphalt AAD-1 from PAV oxidation at 60°C with TFAAT oxidation at 130°C.

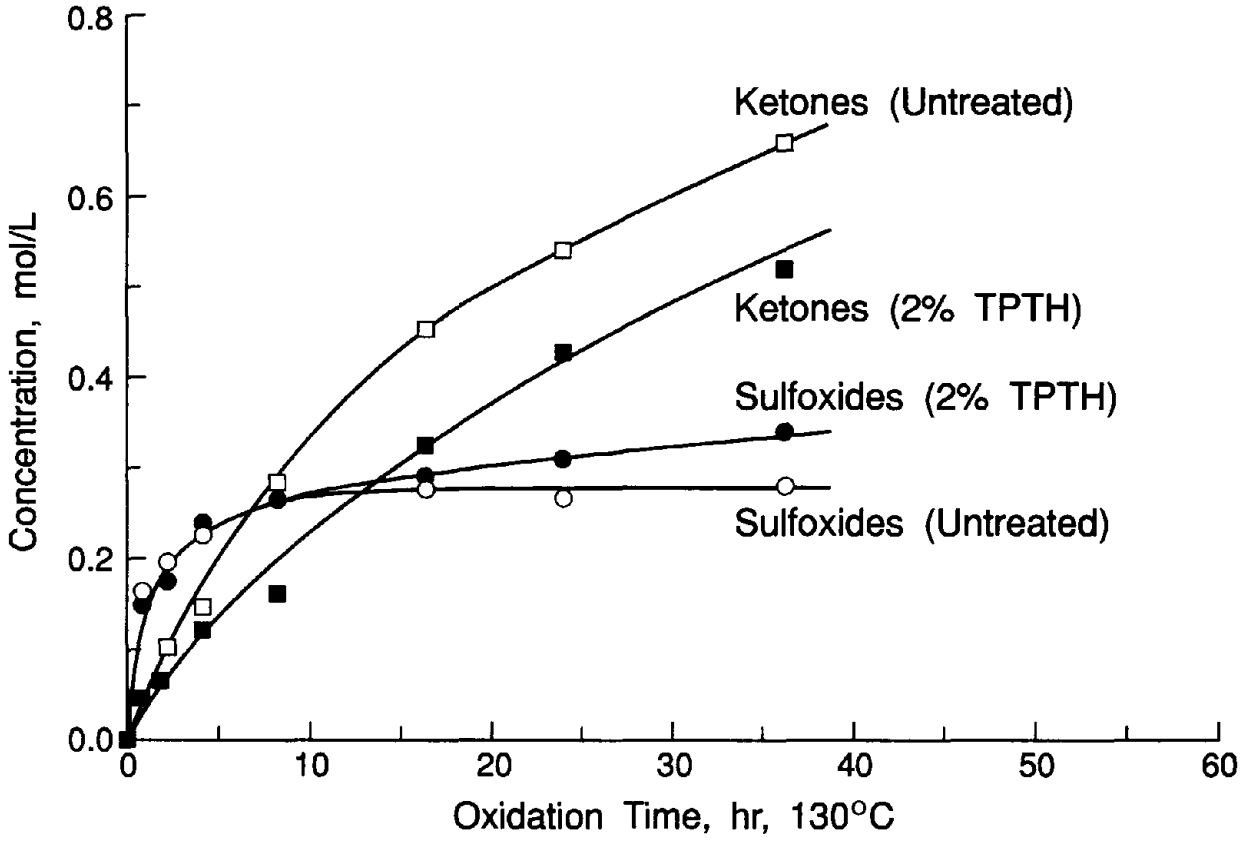

Figure 4-30. Thin film GC column oxidation of Boscan asphalt with and without triphenyltin hydroxide.

NUCLEAR MAGNETIC RESONANCE IMAGING INVESTIGATION OF ASPHALTENE PRECIPITATION IN AGED AND UNAGED ASPHALTS

The compatibility of an asphalt is important for practical reasons because the degree of asphalt compatibility affects *inter alia* rutting propensities and asphalt age hardening. Asphalt age hardening contributes to pavement embrittlement and excessive pavement cracking [Petersen et al. 1996]. Oxidation is the major cause of asphalt hardening. Oxidation of an asphalt will decrease compatibility by formation of polar molecules, which cause increased association and formation of more asphaltenes. The effects of asphalt composition on asphalt compatibility have been investigated in this project. As part of that study, NMR imaging methods were explored to study asphaltene dispersion and association behavior, and compatibility in oxidatively aged asphalts.

The NMR imaging method is a powerful, relatively new technique that can be used for noninvasive chemical, physical, and morphological characterization of local regions in the interior of intact samples [Komoroski 1993]. In addition, NMR imaging is able to characterize chemical and physical processes noninvasively over time. Because of these abilities and the fact that asphalt systems are usually optically opaque, NMR imaging has the potential to provide information about asphalt systems not obtainable by other methods. The work reported here is an exploratory application of NMR imaging to study asphaltene precipitation in oxidatively aged asphalts.

The asphalts studied are part of the SHRP study asphalts [Cominsky et al. 1989]. Their chemical properties have been characterized [Branthaver et al. 1993], and selected data are listed in table 4-6. The asphalts were aged using a combination of TFO treatment followed by PAV oxidation [Petersen et al. 1994]. These aging tests were designed to simulate a level of oxidative aging in the field. The TFO procedure is a standard one and has been described previously. Reaction times and temperatures in the PAV method may vary, and so these parameters are listed in descriptions of the combined methods. Some NMR imaging measurements were made on asphalts AAB-1, AAD-1, AAK-1, AAM-1, and ABM-1 that were TFO/PAV aged for 12 hr at 100°C (212°F). Additional NMR imaging measurements were made on asphalts AAE-1 and AAS-1 that were both TFO/PAV aged for 144 and 400 hr at 60°C (140°F). In one set of experiments, asphalt AAD-1 was aged by TFO only, as well as TFO aging followed by PAV aging. This produced a set of 4 samples consisting of unaged, TFO aged, and TFO followed by PAV aging for 4 and 12 hr at 100°C (212°F).

Samples were prepared for NMR imaging experiments in the following manner. Aged and unaged asphalt samples were dissolved in toluene. To this solution, isooctane was added to cause flocculation and asphaltene precipitation. The amount of isooctane needed to cause maximum flocculation was calculated from previous work on the development of an automated Heithaus method [Pauli 1996]. Two samples were prepared for each asphalt. In one case, the samples were stirred after the addition of the isooctane; and in the other case, the isooctane was added slowly to the asphalt-toluene solution to minimize mixing at the solvent interface. Images were acquired after the addition of the isooctane and for different times afterwards to observe settling of the asphaltenes.

The NMR imaging experiments were carried out at a nominal proton resonance frequency of 200 MHz using a Chemagnetics/Otsuka Electronics microimaging probe. Samples for NMR imaging experiments were placed in 23-mm outer diameter (OD) glass vials, which were then placed in 25-mm (OD) glass tubes. The glass tubes are much more valuable than the vials, so routine laboratory manipulations were performed using the vials, which fit snugly in the tubes. The tubes were inserted into the NMR probe and were positioned in the probe using O-rings such that the cross sections to be imaged were contained in the experimental field of view (FOV). Image slices could be obtained in the XY, XZ, or YZ planes, as depicted in figure 4-31. The number of slices could vary from 1 to 16. The thickness of the slices and the distance between slices could also be varied.

The NMR images of asphaltene precipitation were made using the spin echo method. The spin echo method is designed to provide sharp images. The responses (relaxation times) of protons in a magnetic field are measured. Molecules in asphalts that do not exhibit association behavior have high hydrogen to carbon atomic ratios (and, therefore, relatively more protons) and tend to be highly mobile. These molecules are characterized by long relaxation times. They will be detected by the spin echo method. Regions in which such molecules predominate will be seen as bright in the images. On the contrary, molecules involved in molecular associations tend to have relatively low hydrogen content. The protons in these molecules, because they are part of more rigid structures, will have very short relaxation times. Regions in which molecular associations predominate will be dark in images. Images were acquired using a pulse delay of 1 s, a free induction decay size of 256 data points, 128 phase encodes, and a gradient strength of 34 G/cm. The echo time was varied from 40 to 80 ms. Eight slices, 1-mm thick and separated by 1 mm, were obtained for each set of images. The time required to obtain a set of images was about 35 minutes using these parameters.

The effects of aging (oxidation) and stirring on asphaltene precipitation, as viewed with NMR imaging, are illustrated in figure 4-32. In these images, and in the images in subsequent figures, only the fourth slice of an image set of eight slices is shown unless otherwise noted. The fourth slice corresponds closely to the longitudinal cross section across the center of the sample vial. The times in figure 4-32 are settling times and refer to the time elapsed between addition of isooctane and the time when the image was recorded. Also, in figure 4-32 and in all other figures, the different contrasts represent regions of different molecular mobility. The lightest areas of contrast are due to the hydrogens in molecules that have a high degree of molecular mobility such as those in dissolved asphalt, toluene, and isooctane. The darker regions in the images are due to hydrogens in molecules having a greater degree of molecular association and aggregation (hence less molecular mobility), such as the asphaltenes.

When isooctane was added to the unaged AAD-1 asphalt and the mixture stirred, the asphaltenes precipitated and settled to the bottom of the vial in a normal fashion (figure 4-32a). When isooctane was added to a sample of AAD-1 asphalt that was aged for 12 hr at 100°C (212°F) and the mixture stirred, the asphaltenes settled to the bottom of the vial also in a normal fashion (figure 4-31b). However, when isooctane was added to the top of the aged AAD-1 asphalt/toluene solution without stirring, an additional layer of material formed at the isooctane-toluene/asphalt interface that appeared to have experienced different solvent interactions than

did the asphaltenes. This is illustrated by the dark band in figure 4-32c that formed at about the level of the original isooctane-toluene/asphalt interface and that appeared to be quite stable toward settling for some period of time. As these are cross-sectional images, the dark band is actually a layer at the interface.

The time evolution of the interface layer is shown in figure 4-33 (a-d) by the images taken at different settling times after addition of the isooctane. The first image (figure 4-33a) shows the asphalt dissolved in toluene before addition of the isooctane. Figure 4-33b was taken after isooctane was added unstirred to the sample vial, and before the asphaltenes could settle to the bottom. In this image a thin layer of additional material, which also contains spherical globules, can already be seen forming at the solvent interface. After 1 day of undisturbed settling (figure 4-33c), the layer became more prominent and additional globules can be seen forming near the interface layer. The precipitation of some asphaltenes is also noted by the darker diffuse band developing below the interface (figure 4-33b). After 1 week (168 hr) of settling, the interface layer is still apparent and the asphaltenes can be seen settling to the bottom of the vial (figure 4-33d). On other samples, the layer has been imaged for settling times of up to 648 hr. A set of radial images, 1-mm thick and separated by 1 mm, through the interface layer of figure 4-33d is shown in figure 4-34 (a-d). This set of images shows the inhomogeneity of the asphalt solution. The distribution of spherical globules near the interface is shown in figure 4-34c.

The formation of the dark layer appears to be related to the degree of aging. In figure 4-35 (a-d), the asphaltene layer is seen at the bottom of the vial in all images for a settling time of 1 week, and no dark layer is visible in the unaged and mildly (TFO) aged samples (figure 4-35 a and b). However, the dark layer is present at the interface for the TFO/PAV-aged samples (figure 4-35 c and d) and is most pronounced for the asphalt sample that was aged the longest.

The formation of the interface layer appears to depend also on the concentration of asphaltenes in the unaged asphalt. In addition to asphalt AAD-1, the layering was observed in asphalts AAB-1, AAK-1 and AAE-1. These asphalts have asphaltene concentrations of about 20 percent or greater (table 4-6). The layering was not observed in asphalts AAM-1 and ABM-1, which have low asphaltene concentrations, nor was it observed in asphalt AAS-1, which has a high asphaltene concentration. The reasons for the anomalous behavior of asphalt AAS-1 are not obvious at present. Asphalts AAS-1 and AAE-1 were both PAV aged at a lower temperature (60°C [140°F]), but for longer periods of time (144 and 400 hr). Both have high concentrations of asphaltenes, but only AAE-1 demonstrated the effect. The effects of time and temperature on asphaltene precipitation are currently under study.

The dark layer at the interface, formed by the slow addition of isooctane, appears to act as a barrier toward asphaltene flocculation. This is illustrated by the images in figure 4-36 a-f for asphalts AAK-1 (top row) and AAE-1 (bottom row). In figure 4-36 a is shown the image of asphalt AAK-1 that had been settling undisturbed for 2,500 hr after addition of isooctane. In figure 4-36 d is shown the image of asphalt AAE-1 that had been settling 1,488 hr after addition of isooctane. The images in figures 4-36 b and e were taken immediately after the surfaces of these long undisturbed samples were disrupted by stirring with a spatula. The images in figures

4-36 c and f were taken 24 hr after the samples were stirred. For both asphalts, stirring increased the bulk amount of asphaltenes (figures 4-36 b, e). In addition, a third layer, as noted by its different brightness and of different apparent solubility, formed at the interface between the maltenes and the asphaltenes. Pieces of the original dark layer can be seen as the dark spots in the asphaltene layer.

The chemical nature of the material near the isooctane-toluene/asphalt interface is not known. This layer could be composed of freshly formed asphaltenes that are becoming more rigid with time at the isooctane-toluene/asphalt interface. A more rigid system would have shorter relaxation times and would appear darker in the NMR images. The layer could also be due to oxidation of the maltenes, which are then attracted to the highly polar surface of the asphaltenes and form a distinct layer at the interface. Compositional factors such as the amounts of strong and weak acids, bases, and neutrals probably also contribute to the extent of oxidation and the associated interactions. Other possibilities exist. Nevertheless, the layer of material at the interface appears to have properties that are different from the asphaltenes and the maltenes. For example, the dark layer appears to be a more rigid material than the asphaltene layer. If the sample is stirred with a spatula, the dark layer breaks into pieces. An example is shown in figure 4-37. The top two images show the breakup of the interface layer longitudinally across the solvent-asphaltene boundary. The bottom two images show the breakup of the interface layer radially across the solvent-asphaltene boundary. In both types of images, the rigid nature of the interface layer is apparent. This material will need to be characterized in the future to determine how it might affect and/or predict asphalt compatibility.

In summary, application of magnetic resonance imaging (MRI) to study various aspects of asphalts is in its infancy. Consequently, a number of imaging methods and instrumental parameters need to be investigated to determine the feasibility of MRI to study asphalts. In this study, exploratory MRI measurements were made on the effects of aging on the flocculation and precipitation of asphaltenes from asphalt. NMR images were obtained of asphalts that were dissolved in toluene and titrated with isooctane to the point of maximum flocculation. When the titrant was added slowly to minimize mixing at the isooctane-asphalt/toluene interface, the images showed that a layer of material formed at the solvent interface that was different from the asphaltenes or the maltenes. The formation of this layer appeared to be dependent on asphaltene concentration and degree of aging, i.e., the greater the asphaltene content (except for AAS-1) and the degree of aging, the more prominent the layer. These observations suggest that NMR imaging might be used to assess the compatibility of aged asphalts and work is in progress along these lines.

Table 4-6. Summary of chemical properties of selected asphalts.

Property	AAB-1	AAD-1	AAE-1	AAK-1	AAM-1	ABM-1	AAS-1
Crude Source	Wy Sour	Calif.	Lloydminster air blown	Boscan	West Texas Intermed.	Calif. Valley	Arab Heavy
Component by Corbett Analysis, %							
Asphaltenes	19.3	23.9	24.8	22.9	9.4	8.3	21.3
Polar aromatics	38.3	41.3	30.5	41.8	50.3	52.4	34.1
Naphthene aromatics	33.4	25.1	31.6	30.0	41.9	29.6	39.7
Saturates	8.6	8.6	12.7	5.1	1.9	9.0	5.9
Other Properties							
Carbon aromaticities (NMR)	0.32	0.24	0.33	0.32	0.25	--	--
Hydrogen aromaticities (NMR)	0.071	0.068	0.087	0.068	0.065	--	--
H/C atomic ratio	1.55	1.59	1.45	1.46	1.55	1.43	1.43
Molecular weight (VPO in toluene)	840	700	--	860	1,300	--	960

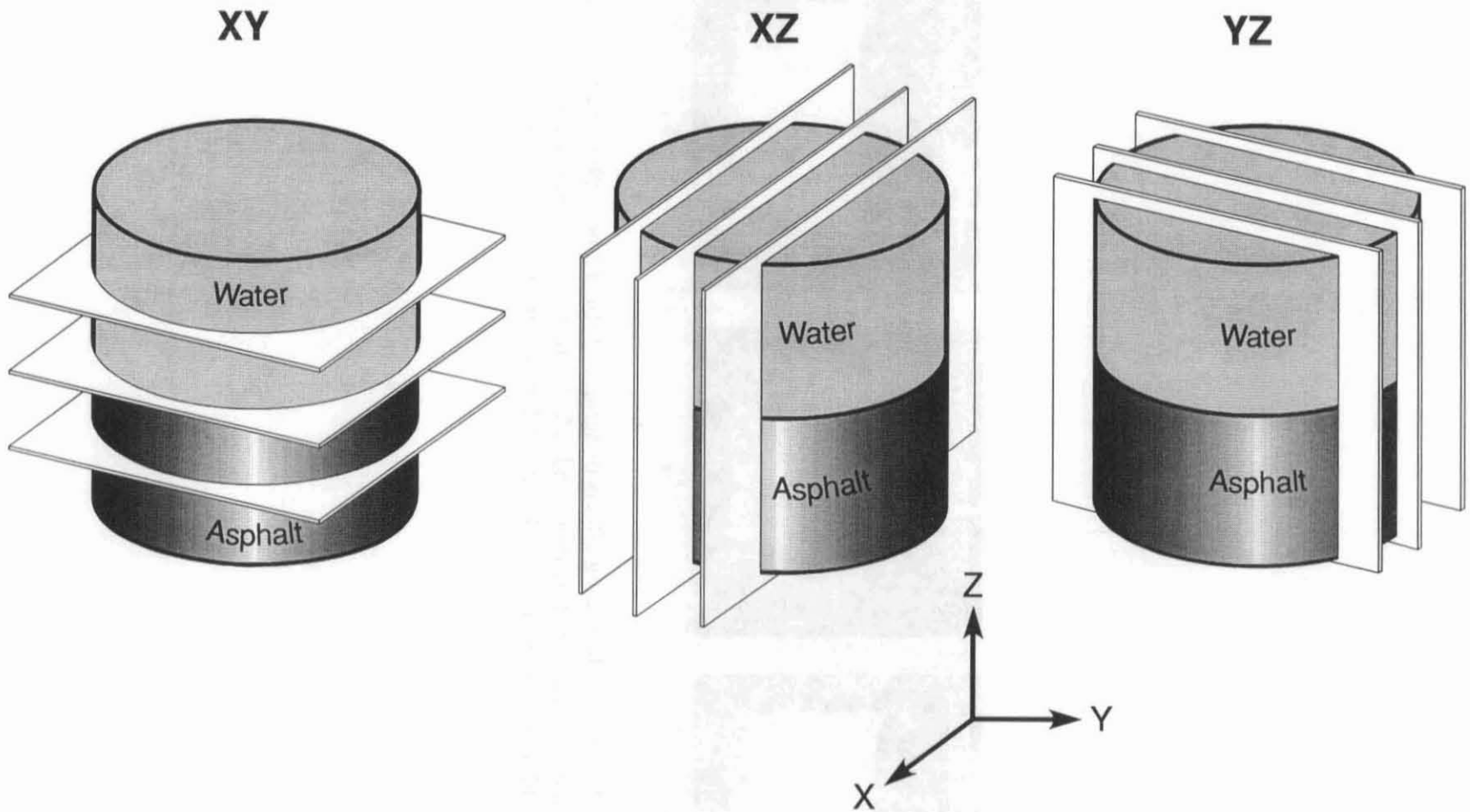

Figure 4-31. Illustration of slice geometry used in magnetic resonance imaging experiments.

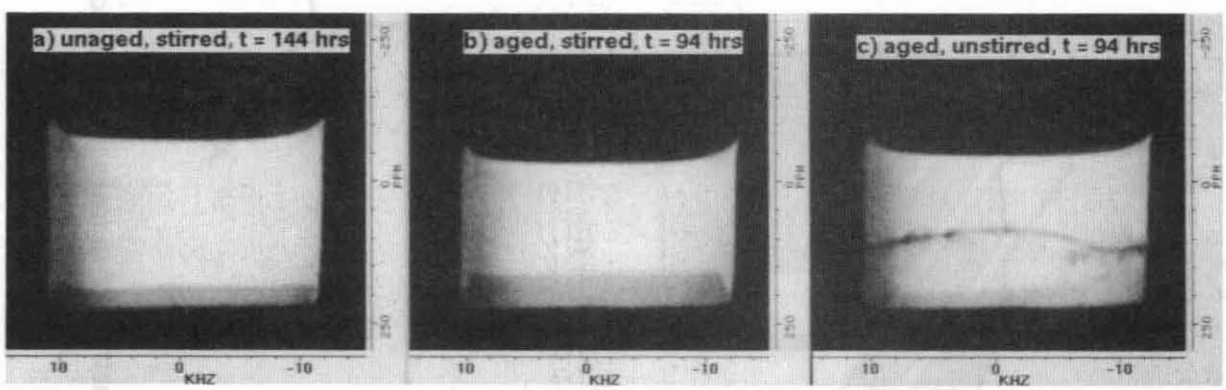

Figure 4-32. NMR images illustrating effects of aging and stirring on asphaltene precipitation. Times listed are settling times and refer to the time elapsed between addition of isooctane and the time when the image was recorded.

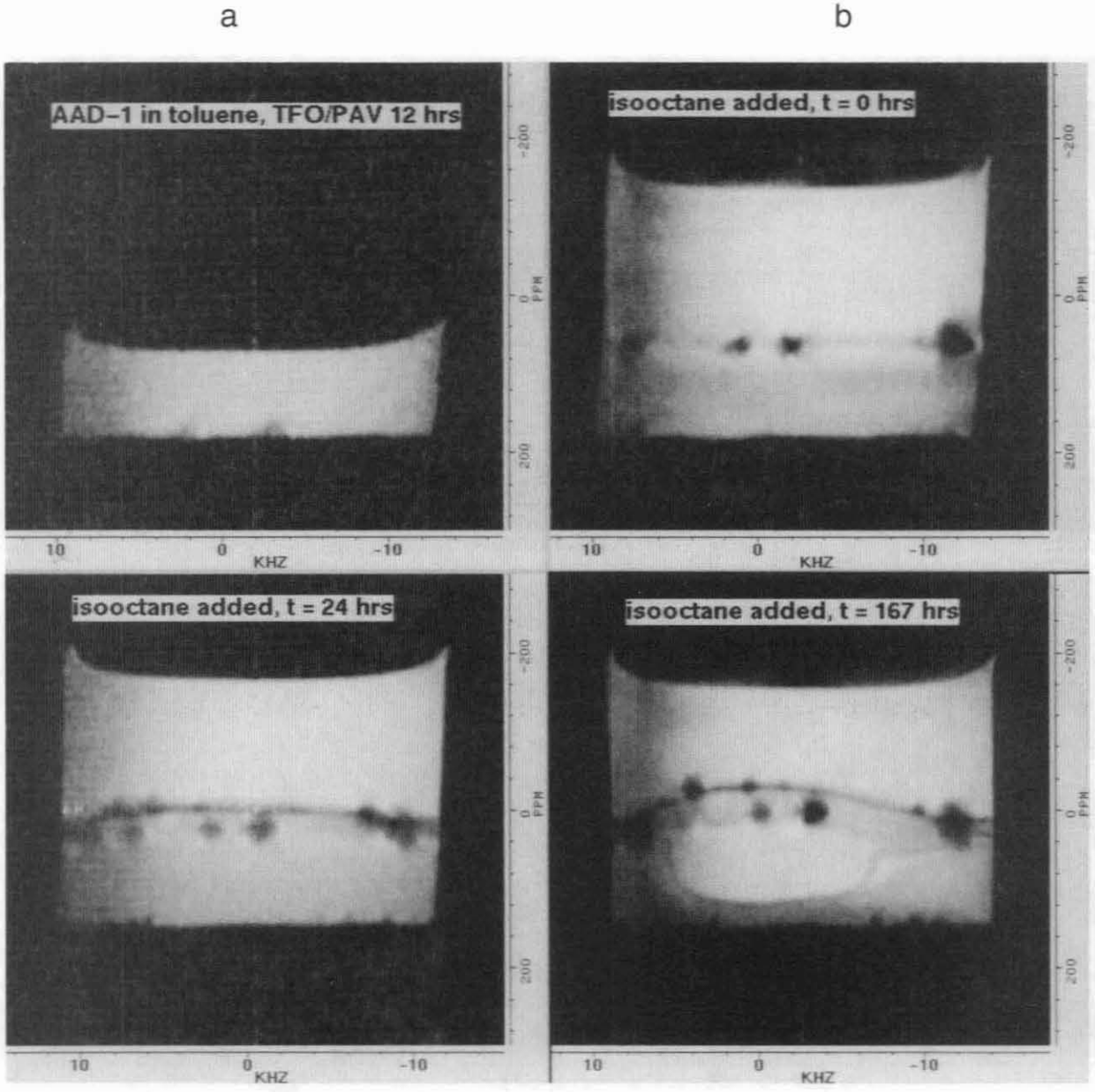

Figure 4-33. NMR images illustrating time evolution of interface layer in aged asphalt. Times listed are settling times.

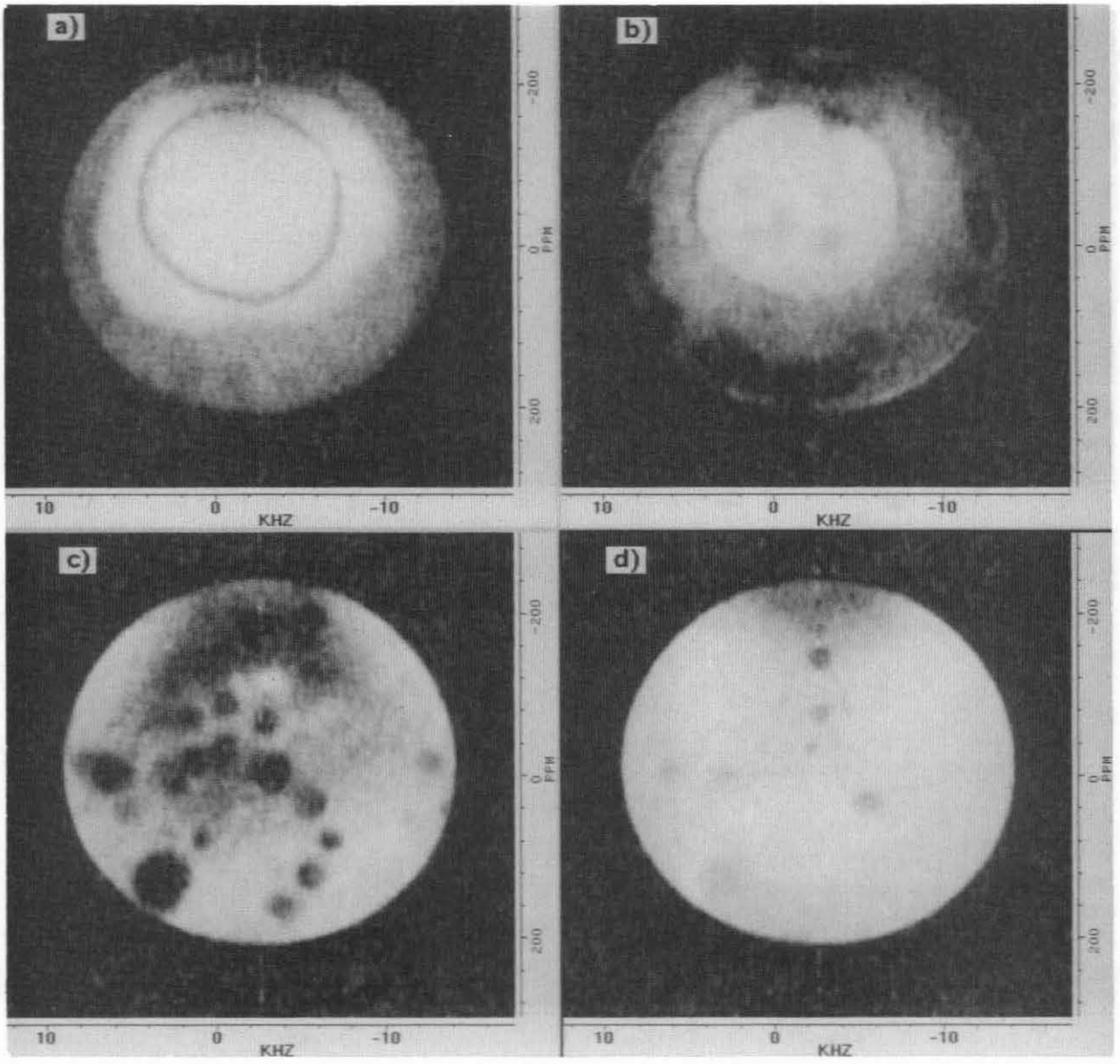

Figure 4-34. Radial NMR images at different depths illustrating spherical globules in the solvent interface layer.

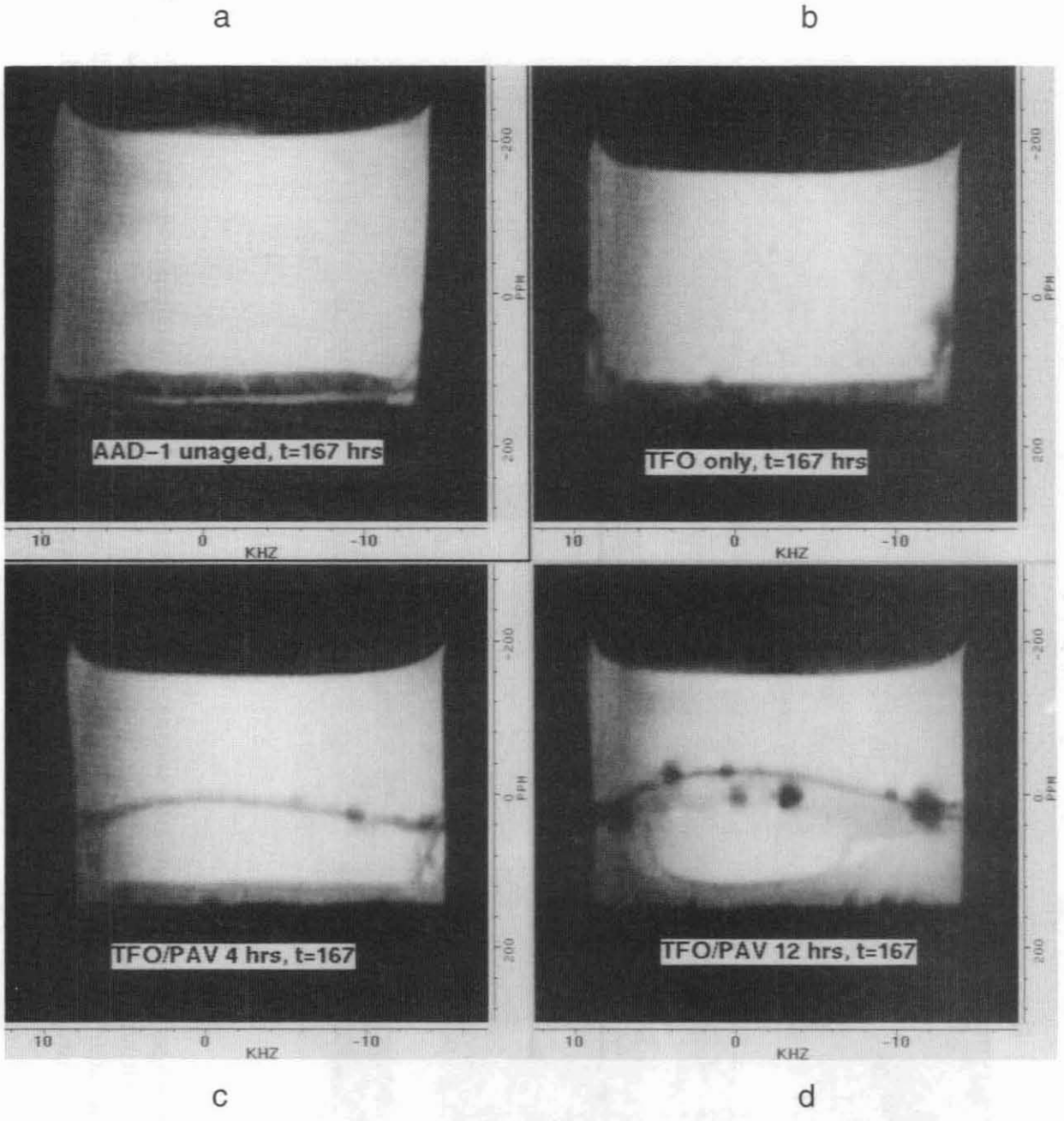

Figure 4-35. NMR images illustrating the effect of aging on asphaltene settling.

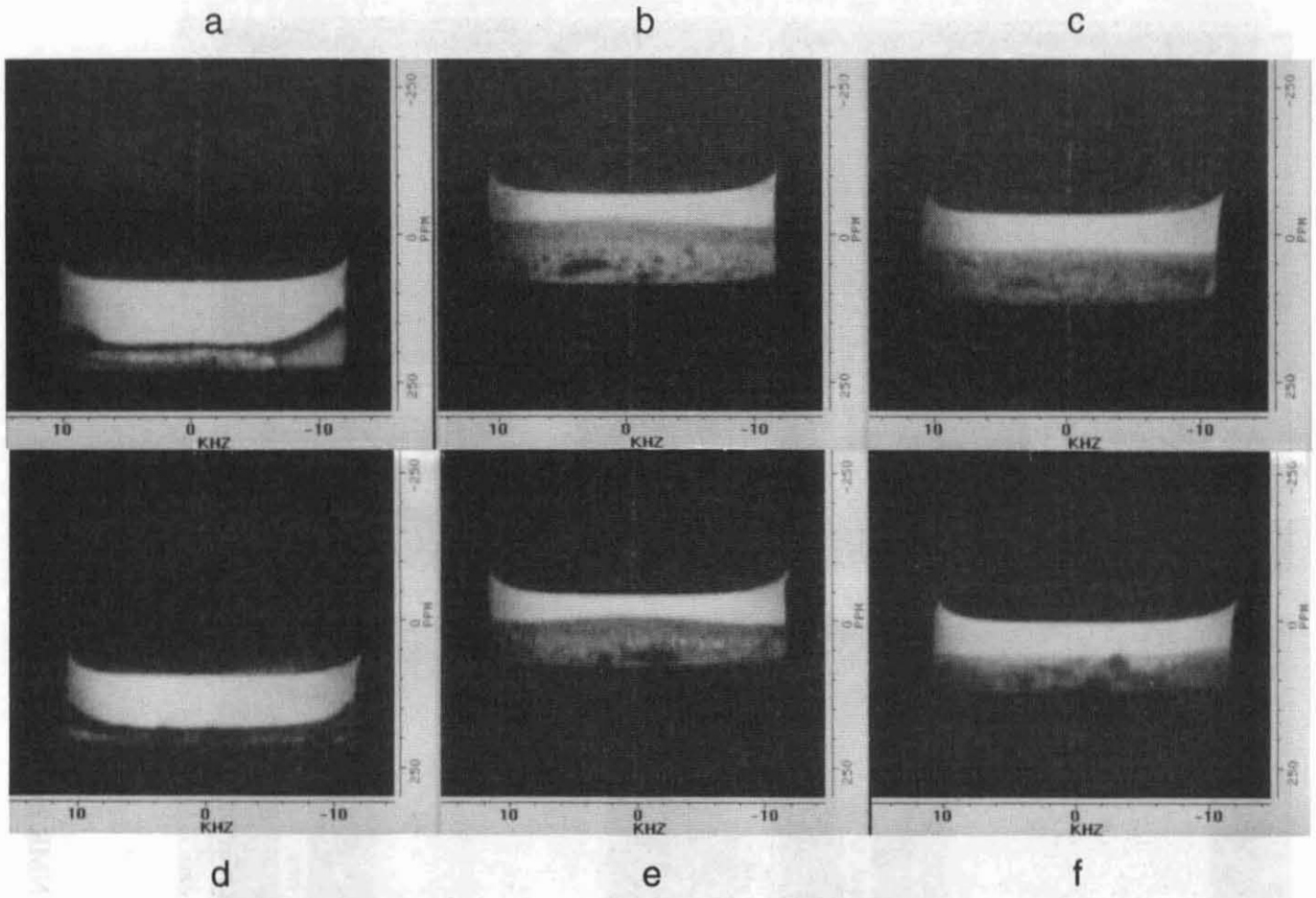

Figure 4-36. NMR images of aged asphalts after stirring. AAK-1 (top row) and AAE-1 (bottom row). In (a) asphalt AAK-1 had been setting undisturbed for 2,500 hr after addition of isooctane. In (d) asphalt AAE-1 had been setting undisturbed for 1,488 hr after addition of isooctane. The images in (b) and (e) were taken immediately after the surfaces of these samples were disrupted by stirring. The images in (c) and (f) were taken 24 hr after the samples were stirred.

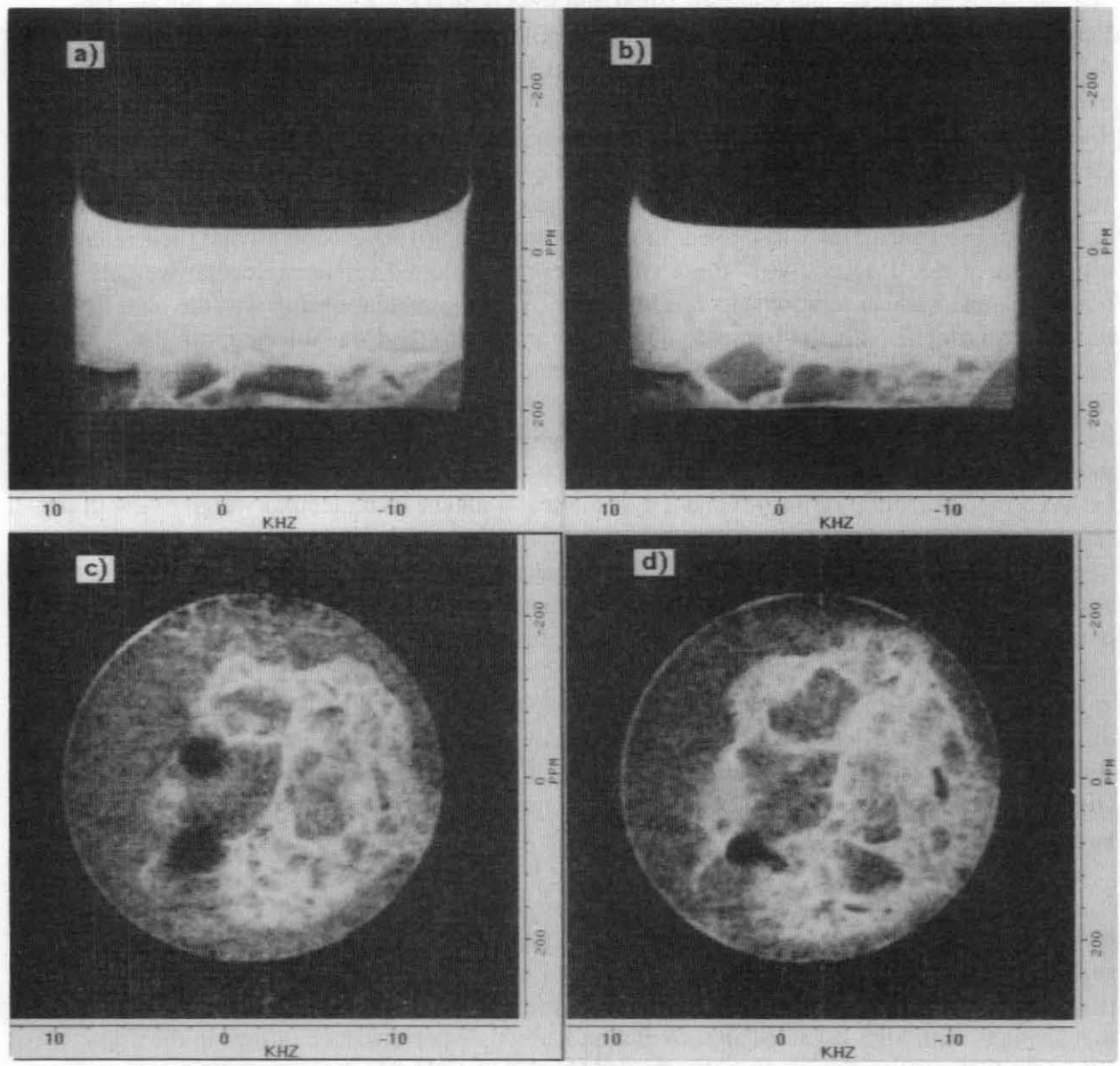

Figure 4-37. NMR images illustrating breakup of interface layer with stirring.
a), b) Longitudinal cross-section images at different positions,
c), d) Radial cross-section images at different positions.

USE OF INVERSE GAS LIQUID CHROMATOGRAPHY TO STUDY ASPHALT OXIDATIVE AGING

Previous IGLC work with petroleum asphalts demonstrated a good correlation between IGLC data (after IGLC column oxidation) with the tendency of an asphalt to form cracks in both Weather-Ometer [Davis and Petersen 1966] and road tests [Davis and Petersen 1967]. The IGLC data used in these studies consisted of phenol interaction coefficients (I_p), obtained as follows. Samples of asphalts to be tested were coated on a granular inert solid supporting material (Fluoropak 80 - a Teflon® based material). The asphalt coated grains then were used to fill a gas-liquid chromatography (GLC) column. The asphalt is thus the stationary phase in GLC experiments, hence the designation as inverse-GLC. The column was placed in an oven and was conditioned at 130°C (266°F) while He gas was passed through the column for 6 hours. A series of n-alkanes then was passed through the column at 130°C (266°F) and their retention times were noted. Logarithms of these values were then plotted versus molecular weights of the n-alkanes, and a linear relationship was observed. This linear relationship was the base line for further experiments. Phenol (or some other test compound) then was injected into the column. Because phenol is polar, its retention time is much longer than that of any of the n-alkanes. The logarithm of the phenol retention time was then plotted versus the molecular weight of phenol, 94. A vertical line then was drawn from this point to the base line. The length of this line multiplied by 100 is defined as the phenol interaction coefficient, I_p. It represents the difference between the interaction of phenol and a hypothetical n-alkane of molecular weight 94 with the test asphalt. There is no real n-alkane having a molecular weight of 94, the closest being n-hexane (molecular weight 86) and n-heptane (molecular weight 100). The I_p value will vary according to the asphalt used in the test. If the column is oxidized by replacing He with air (the oxidation is usually performed at 130°C [266°F] for several hours), the oxidatively aged asphalt will have a higher I_p value compared with the neat asphalt. The difference between the two values is a measure of the propensity of a given asphalt to undergo oxidative aging, a large difference indicating that an asphalt will age rapidly under service conditions. In Weatherometer tests, which measure durability as a function of days to failure, oxidized asphalts characterized by high I_p values failed much more rapidly than oxidized asphalts with low I_p values [Davis and Petersen 1966].

Davis and Petersen [1967] also oxidized several of the original Zaca Wigmore asphalts by IGLC. After oxidation, I_p values were determined. These values were compared with road surface performance ratings of the asphalts in the Zaca Wigmore test. The pavement performance ratings were obtained from visual observations and crack densities. It was noted that asphalts with high I_p values after oxidation had worse performance ratings in the Zaca Wigmore test compared with asphalts characterized by low I_p values after oxidation.

Different oxidation conditions and use of test compounds other than phenol were studied to determine the best conditions for oxidative aging of SHRP asphalts in IGLC columns. The initial IGLC oxidation studies used air at 121 kPa (17.5 psi) and 130°C (266°F) for 24 hr [Davis and Petersen 1966]. In the present work, using the same pressure and temperature and studying oxidation times of 6 and 12 hours, results indicated that a 6-hr oxidation period approximated the same amount of oxidation as samples prepared by PAV aging at 80°C (176°F), 144 hr and

2,068 kPa (300 psi) pressure. Comparison of 6-hr IGLC oxidation with that of the PAV aging resulted in similar IGLC interaction coefficients for all test compounds used.

Good correlations between 1-butanol and phenol interaction coefficients and the results of NAPT of bases were observed. As shown in figure 4-38, the interaction coefficient of 1-butanol determined on 6-hr column-aged asphalts correlates with the total titratable base in TFOT/POV aged samples. This procedure differs from the PAV method in the replacement of air with oxygen gas. Conditions used in these experiments were 60°C (140°F), 300 psi O_2, and 1,000 hr reaction time. Figure 4-39 shows a relationship between the phenol interaction coefficient for 6-hr column-aged asphalt and the increase in the amount of titratable weak base from TFOT/POV aging.

The phenol interaction coefficient of 6-hr aged asphalts also was found to be strongly correlated with the concentration of sulfoxides in the TFOT/PAV (300 psi at 80°C [176°F], 144 hr) aged asphalts (figure 4-40). It is well known that sulfur exists in asphalt in the thiophenic and sulfide forms and that sulfide is the predominant oxidizable sulfur. Upon oxidation, the neutral sulfide is converted into weakly basic sulfoxide. The formation of sulfoxide is believed to be the cause of the increase in the weak base fraction upon aging. Therefore, the amount of sulfide sulfur that is oxidized in an asphalt sample will determine the amount of change in titratable weak base upon aging. This is clearly shown in figure 4-41.

The IGLC method is responsive to chemical changes that occur in paving asphalts during oxidative aging [Kim et al. 1997]. For the polar compounds phenol and 1-methylpyrrolidine, interaction coefficients become larger as a function of aging, particularly for the latter compound. This behavior parallels oxygen incorporation in asphalts to form more polar molecules, both acidic and basic. It is possible that sulfoxides might be oxidatively cleaved to sulfinic and sulfonic acids, which are strong acids, as shown below:

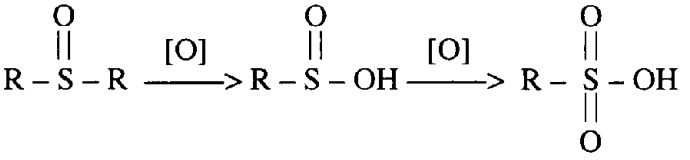

Interaction coefficients for toluene do not change with oxidation, suggesting that interactions of aromatic centers are not changed significantly. For unaged asphalts the interaction coefficient of 1-methylpyrrolidine (I_{1MPD}) increases as the concentration of carboxylic acid functionality increases. The strongly basic 1-methylpyrrolidine appears to interact with this strong acidic functionality. The I_{1MPD} is positively related to the amount of IEC strong acid fraction in asphalt. The IEC strong acid fraction is believed to contain most of the carboxylic acid functionality and would have a similar relationship with I_{1MPD} as carboxylic acid. The amount of change in I_{1MPD} due to 6-hr column aging is negatively related to the amount of IEC strong base. A high concentration of strong basic functionality would reduce the degree of acidification of asphalt due to oxidation and result in low I_{1MPD} after 6-hr column aging. The same mechanism may be invoked to explain the extraordinary IGLC behavior that was observed

in the AAG-1 asphalt sample. Lime treatment neutralized acids and made asphalt AAG-1 basic, resulting in a very high propionic acid interaction coefficient on an unaged sample and small increases in the interaction coefficients of triethylamine (I_{TEA}) and 1-methylpyrrolidine after oxidation. The interaction coefficient of triethylamine on unaged and aged asphalt samples also shows similar relationships. It is generally known that the concentration of carboxylic acids in asphalts does not change very much upon oxidation. Therefore, it may be reasonable to postulate that a strong acidic functionality, at least as strong as the carboxylic acids but different from the carboxylic acids, forms during oxidation and sharply increases I_{1MPD} and I_{TEA} of most aged asphalts. The buildup of a strong acid, possibly a sulfonic or sulfinic acid, is supported by NAPT measurements on aged paving asphalts and extraction of the acid from aged asphalts by water. Strong acids in extensively aged asphalts could increase moisture damage in pavements constructed using acidic aggregates. Presumably basic aggregates would neutralize strong acids, as does added lime.

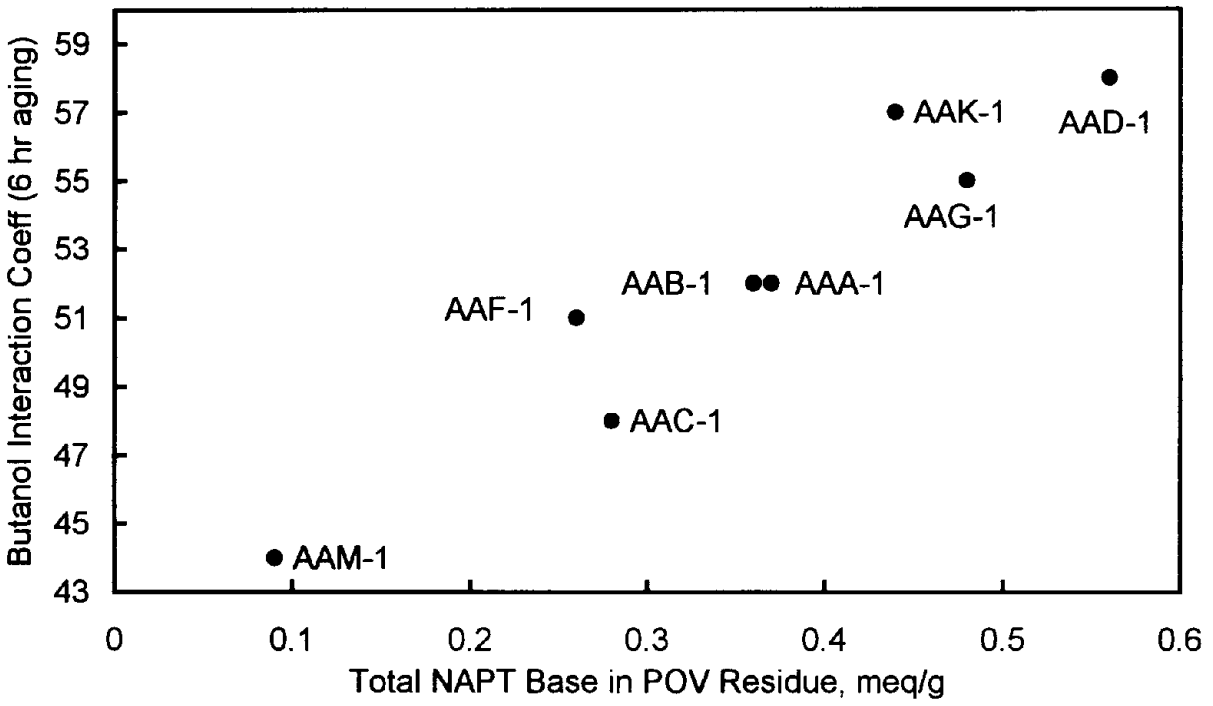

Figure 4-38. Butanol interaction coefficient of 6 hour column aged asphalts vs. titratable total base in TFOT/POV (60°C, 1,000 hour, 300 psi oxygen) residue.

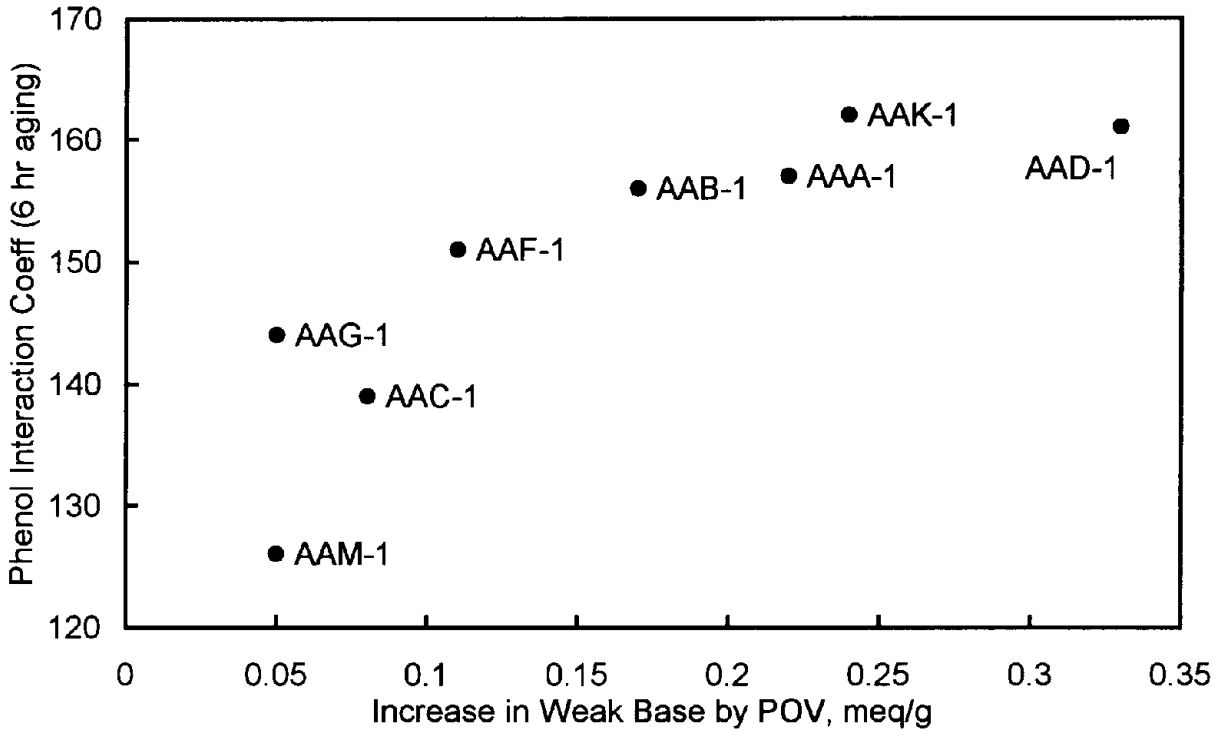

Figure 4-39. Phenol interaction coefficient of 6 hour column aged asphalts vs. the amount of titratable weak base increase due to TFOT/POV (60°C, 1,000 hour, 300 psi oxygen).

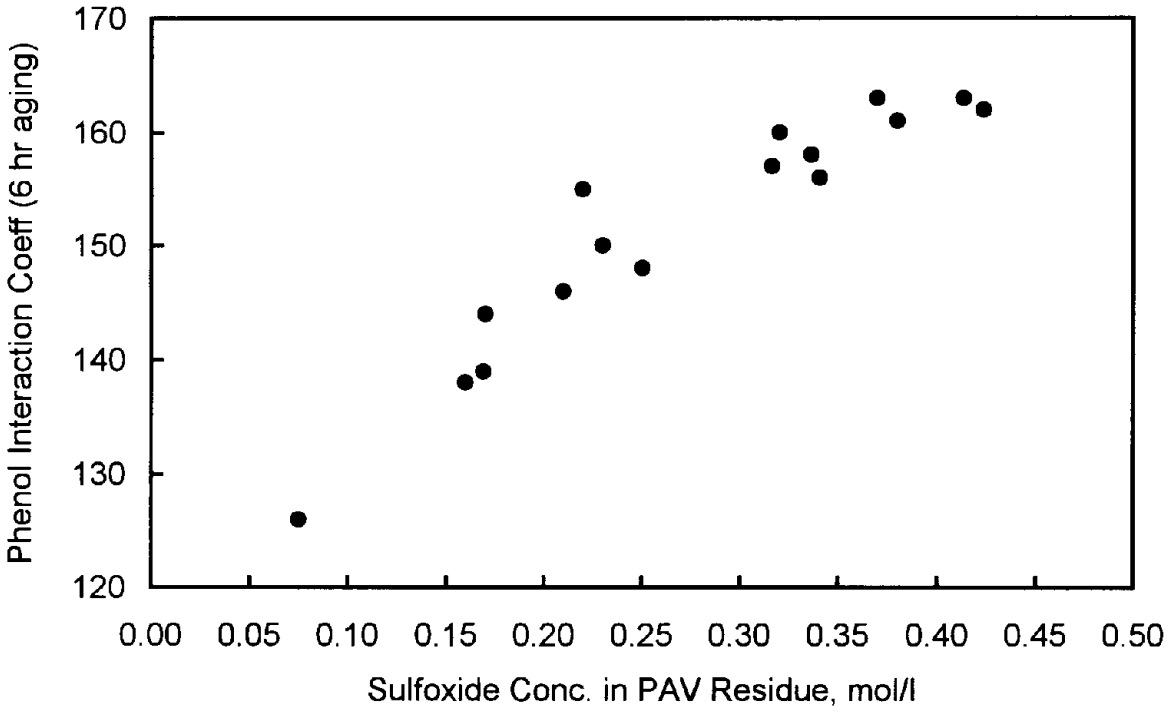

Figure 4-40. Phenol interaction coefficient of 6 hour column aged asphalt vs. sulfoxide concentration in TFOT/POV (80°C, 144 hour, 300 psi oxygen) residue.

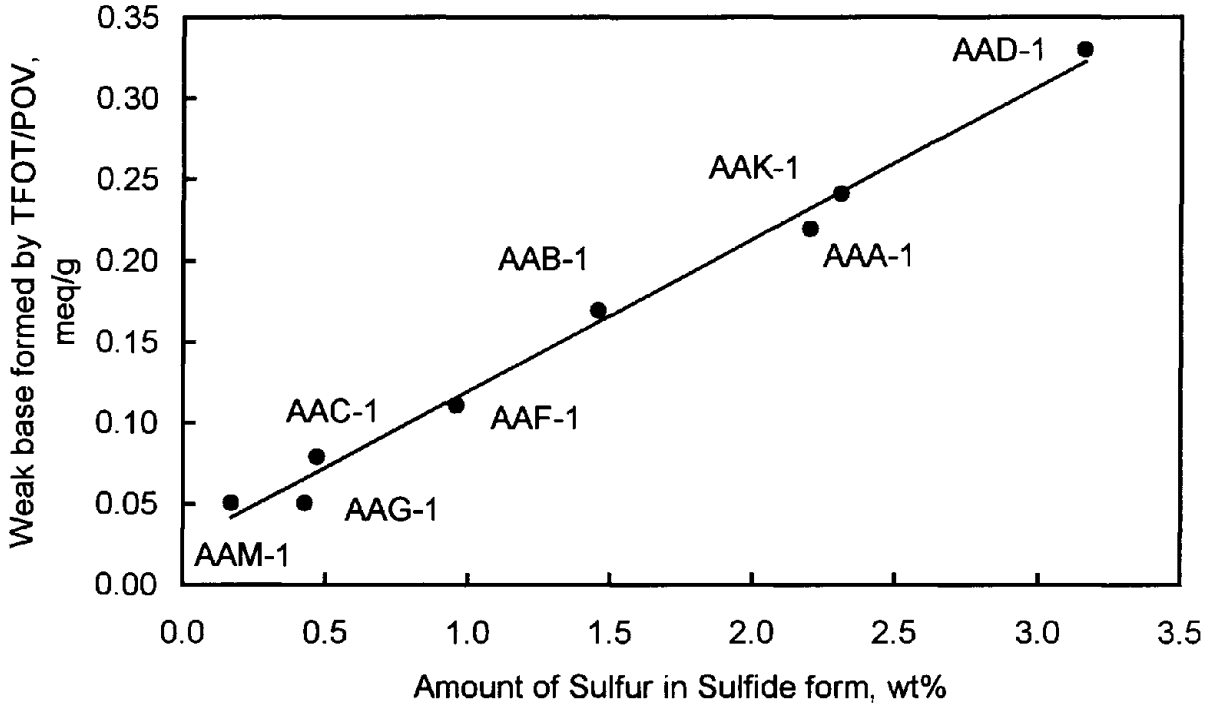

Figure 4-41. Amount of titratable weak base formed by TFOT/POV (60°C, 1,000 hour, 300 psi oxygen) vs. the amount of sulfur in the unaged asphalt in sulfide form.

HIGH PRESSURE LIQUID CHROMATOGRAPHY USING SIZE EXCLUSION RESINS TO ANALYZE OXIDIZED ASPHALTS

A preparative SEC procedure was developed during SHRP that showed how SEC can be usefully applied to the investigation of asphalts. This labor and material intensive procedure yielded two or several fractions, depending on the objectives of the separation. A description of the procedure is provided in chapter 3, and in Volume II, method 15. It was found that the mass percent yields from the two fraction separations could be related to physical properties of asphalts. Based on these promising results, it was decided to develop an instrumentally based analytical SEC procedure that would essentially replicate the results obtained from the preparative procedure, but would be fast, reproducible, efficient, and utilize small amounts of sample.

A detailed description of the analytical SEC procedure is provided in Volume II, method 2. The analytical SEC method is fully automated, unlike the preparative method, and thus conserves operator time. Separations of small (24 mg) amounts of samples in toluene solution are performed using standard HPLC columns and equipment. As solutions of separated fractions exit from the HPLC column, they pass through various detectors and may be collected in fraction collectors. The detectors measure refractive indices or ultraviolet absorbances of the solutions. From the information obtained by the detectors, chromatograms are traced out by a computer. The materials in the fraction collectors are divested of solvent and may be used to provide a gravimetric finish (mass percentages of original sample in each fraction). The operational variables of the HPLC system were adjusted so that the separations correspond as closely as possible to results obtained using preparative SEC for SHRP asphalts.

All SHRP core asphalts, unaged and TFO/PAV aged for 12, 20, and 36 hours at 100°C (212°F), were analyzed using analytical HPLC/SEC to evaluate the effects of oxidation on molecular association of polar components. Chromatograms and data are reported in this chapter for three of the core asphalts (AAF-1, AAK-1, and AAM-1) as examples. Chromatograms for the remainder of the SHRP asphalts are reported in Volume II, method 2. Figure 4-42 shows the overlaid chromatograms from the differential refraction index detection (DRID) of unaged and aged asphalt AAF-1. This is an example of the type of results obtained on aged asphalts using the analytical SEC technique developed during this contract. Figure 4-43 shows a similar set of chromatograms for asphalt AAK-1. This asphalt has a much different molecular size distribution than AAF-1, as can be seen by comparison of the figures. The chromatograms are drawn so that the major broad peaks, which represent the unassociated (or least associated), later-eluting molecules for all four chromatograms in each set, are at the same intensity level, so that the changes in the first part of the chromatograms, which represent the more highly associated species, are readily apparent. The figures also show the gravimetrically determined F-I cutpoint. This is the cutpoint time for the analytical SEC run, which gives the same mass percent yield of SEC Fraction-I as the preparative SEC run, for each asphalt. Later eluates are designated F-II. The figures show that the amount of nonfluorescing, associated material of high apparent molecular weight (F-I material eluting at the front end of the chromatogram) increases with increased oxidative aging. The increase of materials of high apparent molecular weight with aging was observed previously [Branthaver et al. 1993;

Jennings et al. 1991; Bishara et al. 1991]. Also shown in these two figures are the results of estimating molecular weights of materials eluting at the peaks and shoulders present in the chromatograms. These estimates are arrived at by comparison with elution times of model compounds. It is noteworthy, considering that these molecular weights are estimates only, that the molecular weight for materials eluting at peak 1 of asphalt AAF-1 is approximately three times the molecular weight of those materials eluting at peak 2, which in turn are approximately 10 times larger than the materials eluting at peak 3. For asphalt AAK-1, the molecular weight of materials eluting at peak 1 is double that of peak 2 materials, which in turn is double that of peak 3 materials. The fact that higher molecular weight peaks tend to be integral multiples of lower molecular weight peaks suggests that the materials responsible for some larger molecular agglomerates are the result of further association of materials responsible for smaller molecular agglomerates, and suggests that associations may aggregate two at a time. In other cases, numerous smaller molecules or associations may combine to make much larger aggregations. The fact that the molecular associations represented by the peaks are distinct and different for different asphalts may also indicate something of the origin or geochemistry of the asphalt.

Another way to portray data for unaged and aged asphalts is shown in figures 4-44 and 4-45 where normalized integrals for HPLC/SEC fractions for asphalts AAF-1 and AAM-1 are plotted versus aging time. The percents of HPLC/SEC fraction F-I were determined by making the DRID area percent for F-I equal to the weight percent of F-1 from preparative SEC. The line for F-II is for the sum of the F-II subfractions (designated IIa-IIe) and is complementary to F-I. The sum of F-I and F-II represents the whole asphalt. For AAM-1, F-I is the sum of two subfractions, F-Ia and F-Ib. Subfractions where the integrals are very small are not presented in these figures. It can be seen from these figures that the integrands for F-I increase and the integrands for F-II decrease on aging, indicating that components present in F-II in unoxidized asphalts are associating on oxidation, and thus becoming part of F-I.

For asphalt AAF-1, fractions F-IIb and F-IIc decrease with increased aging while other F-II subfractions remain more or less constant. The elution time frames for F-IIb and F-IIc are 22.45 to 25.89 minutes and 25.89 to 29.32 minutes, respectively, and cover estimated molecular weight ranges from the calibration curve of 1,000 to 300 and 300 to 200 daltons, respectively. This time span encompasses the highest peak in the DRID chromatogram (see figure 4-42) and, therefore, subfractions F-IIb and c seem to be a logical source of materials that undergo oxidation. It should be pointed out, however, that it would take a number of units in this molecular weight range to combine in order to be transferred to F-I, where the elution time span is 14.8 to 19.02 minutes and the molecular weight range is estimated to be ca. 90,000 (onset or breakthrough of largest materials) to 4,400 daltons. For example, it would take about sixty 500 dalton units to make one 30,000 unit or ten 800 dalton units to make one 8,000 dalton unit.

A similar analysis of figure 4-45 shows that F-I for AAM-1, which includes both an initial spike (Fraction F-Ia; see figure 2-22, Volume II) and the rest of F-I (Fraction F-Ib), also grows at the expense of F-II. However, unlike AAF-1, fractions F-IIa, F-IIb, and F-IIc of AAM-1 all decrease with increasing aging. The elution time range for these three fractions extends from 19.65 to 23.01 to 26.36 to 29.72 minutes with an estimated molecular weight range from 3,600 to 900 to 300 to 200 daltons. Again, a number of these units would be needed to transfer

significant amounts of these materials to F-I, which has an estimated molecular weight range of from ca. 100,000 to 3,600 daltons. For example, it would take approximately twenty 3,000 dalton units to reach a molecular weight of 59,000 daltons, which is the estimated molecular weight of the initial spike for asphalt AAM-1.

In summary, an HPLC/SEC method has been developed that yields results similar to those obtained by the preparative SEC method developed during SHRP. This HPLC method uses a column combination of two 500 Å columns followed by one 100 Å column with toluene as the separation solvent. The method uses a differential refractive index detector and/or a fraction collector (to yield a gravimetric finish) to provide chromatograms (molecular weight distributions). A computer is used to control the instrumentation and to manipulate the data obtained. This procedure has been used to analyze the SHRP core asphalts both unaged and TFO/PAV aged to three levels. Further work describing the use of analytical SEC with asphalts mixed with crumb rubber or recycling agents is reported below in chapter 6 and also in Volume II, method 2.

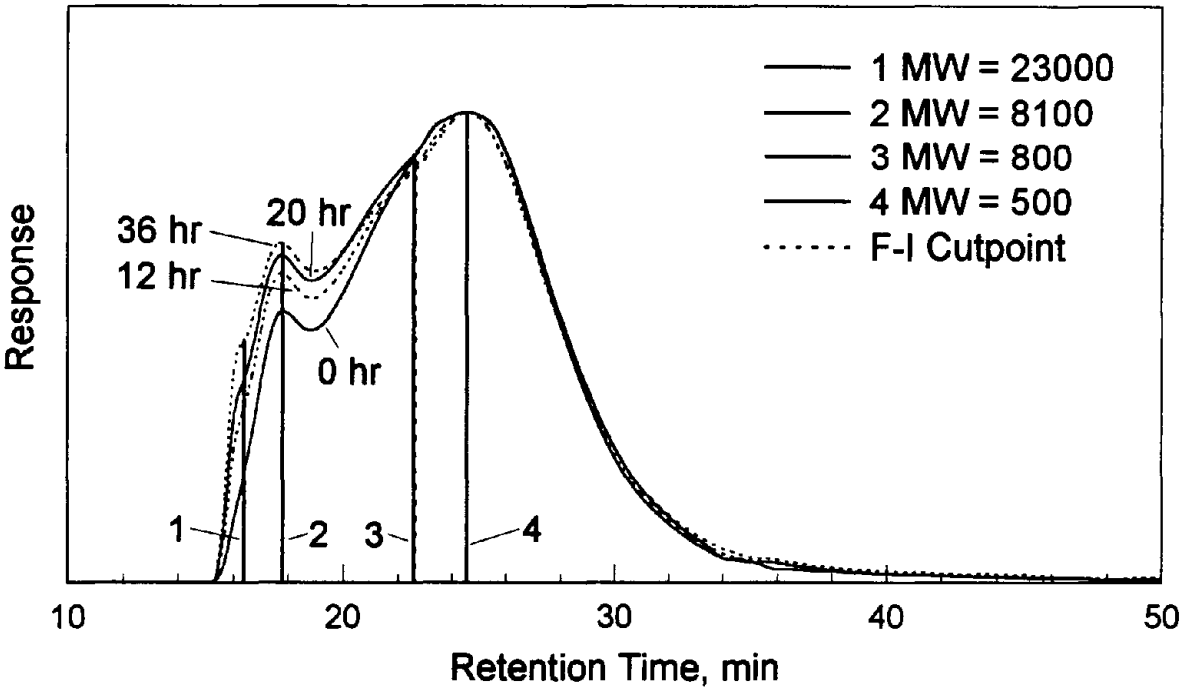

Figure 4-42. HPLC/SEC DRID chromatograms of asphalt AAF-1 TFO/PAV aged for 0, 12, 20, or 36 hours with molecular weights estimated from the calibration curve; gravimetrically determined F-I cutpoint = 22.59 min.

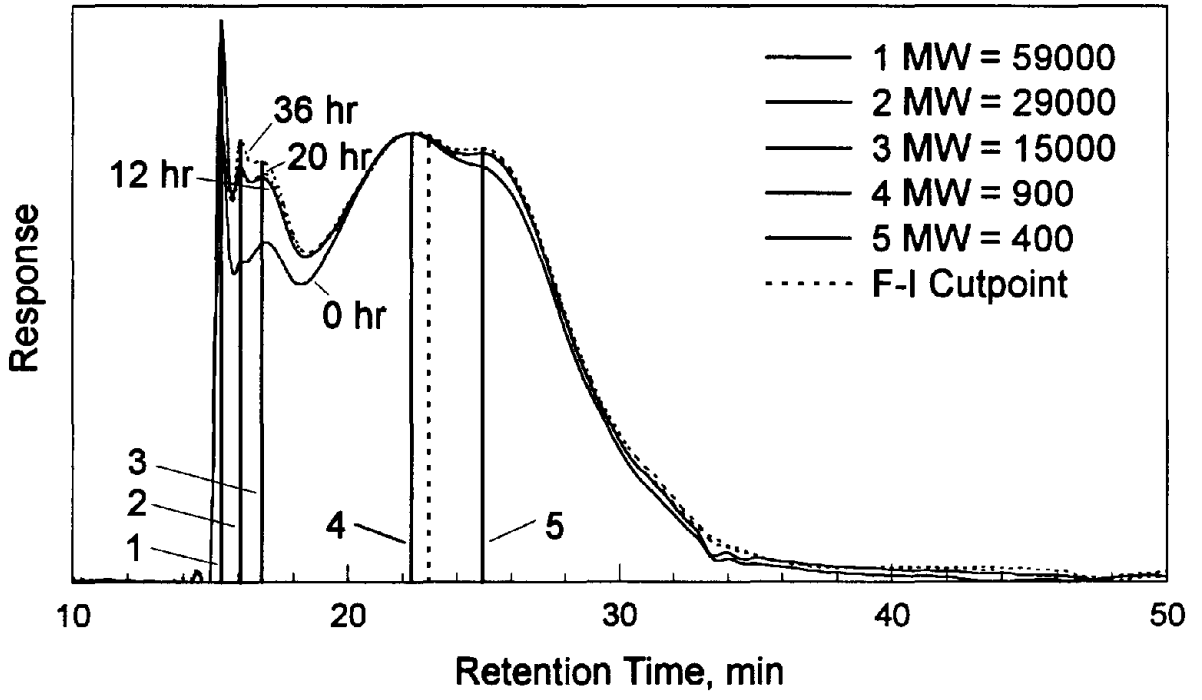

Figure 4-43. HPLC/SEC DRID chromatograms of asphalt AAK-1 TFO/PAV aged for 0, 12, 20, or 36 hours with molecular weights estimated from the calibration curve; gravimetrically determined F-I cutpoint = 22.95 min.

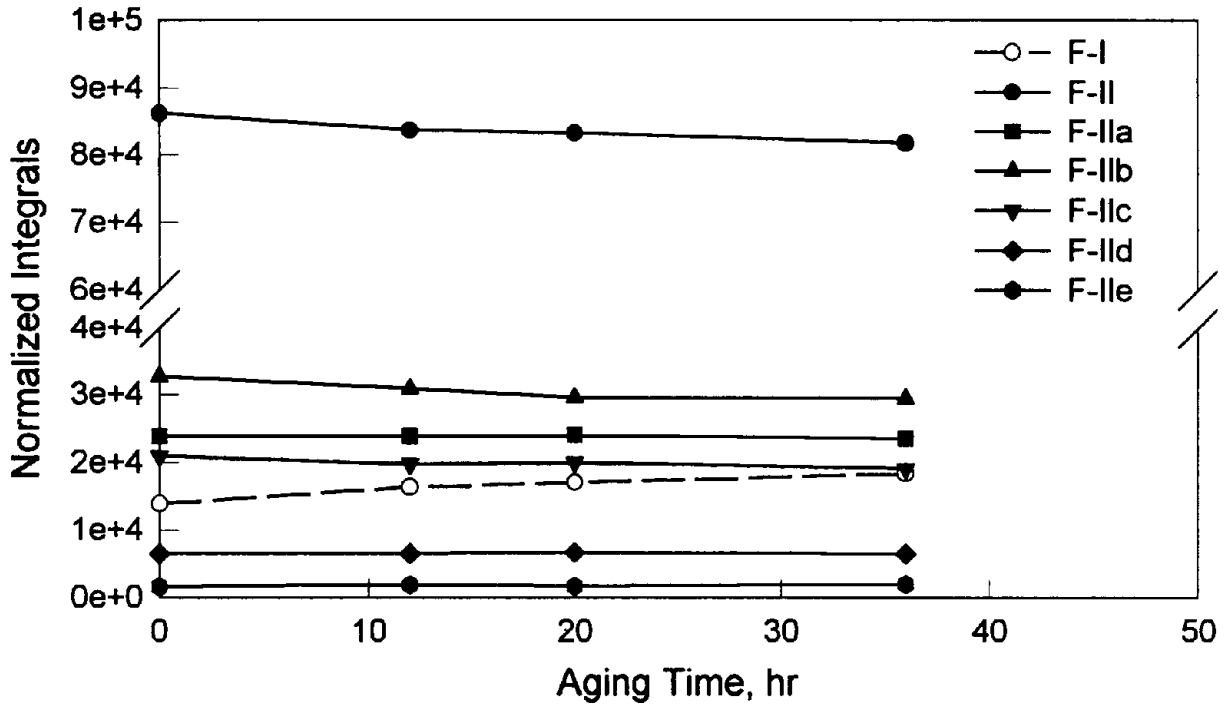

Figure 4-44. Integrals, normalized to a total integral of 100,000, versus aging time for asphalt AAF-1 HPLC/SEC fractions; F-I cutpoint used is from DRID area % equal to preparative SEC weight % F-I.

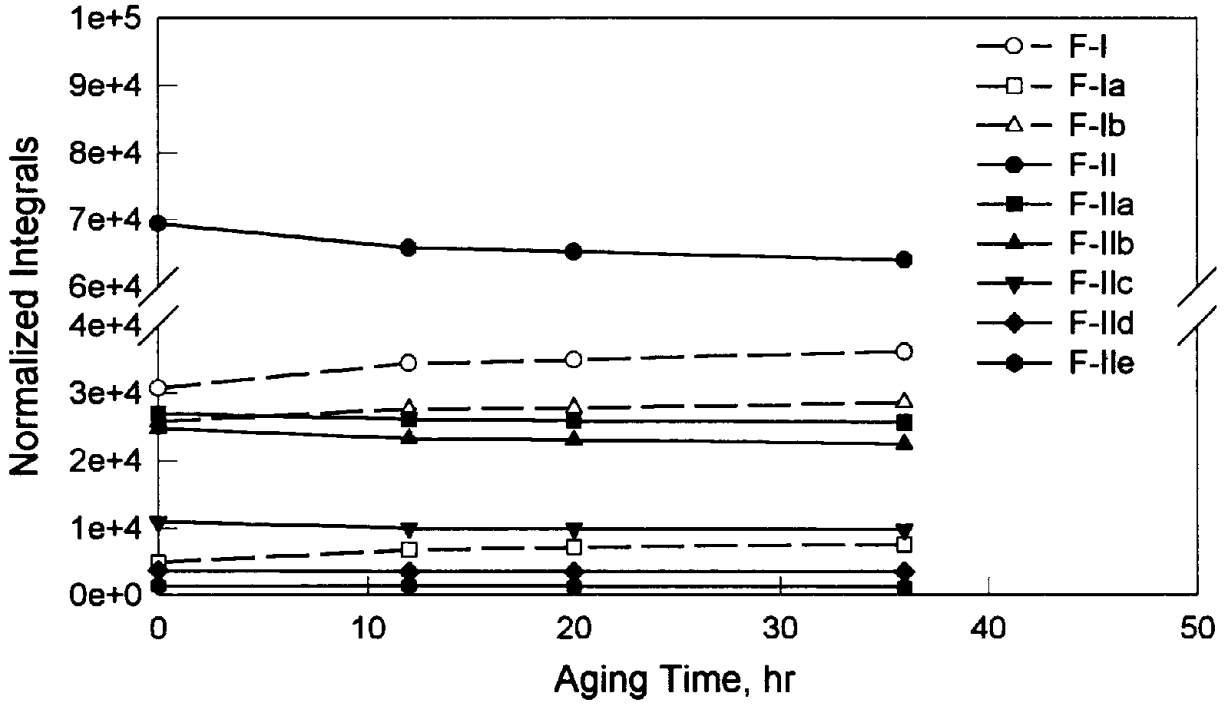

Figure 4-45. Integrals, normalized to a total integral of 100,000, versus aging time for asphalt AAM-1 HPLC/SEC fractions; F-I cutpoint used is from DRID area % equal to preparative SEC weight % F-I.

REFERENCES

Barbour, R. V., and J. C. Petersen, 1974, Molecular Interactions of Asphalts. An Infrared Study of Hydrogen-Bonding Basicity of Asphalts. *Analytical Chemistry*, 46: 273-277.

Bateman, L., and K. R. Hargrave, 1954a, Oxidation of Organic Sulfides. I. Interaction of Cyclohexylmethyl Sulfide with Hydroperoxides in Alcohols. *Proceedings of the Royal Society*, A224 (part 1), 389-398.

Bateman, L., and K. R. Hargrave, 1954b, Oxidation of Organic Sulfides. II. Interaction of Cyclohexylmethyl Sulfide with Hydroperoxides in Hydrocarbons. *Proceedings of the Royal Society*, A224 (part 1), 399-411.

Bell, C. A., Y. AbWahab, J. E. Kliewer, D. Sosnovske, and A. Wieder, 1992, Aging of Asphalt-Aggregate Mixtures. 7th International Conference on Structural Design of Asphalt Pavements, Vol. 2, Nottingham, UK.

Bishara, S. W., R. L. McReynolds, and E. R. Lewis, 1991, Interrelationship between Performance-Related Properties of Asphalt Cement and Their Correlation with Molecular Size Distribution. *Transportation Research Record* 1323, 1-9.

Branthaver, J. F., M. Nazir, J. C. Petersen, S. M. Dorrence, and M. J. Ryan, 1984, The Effect of Metalloporphyrins in Asphalt Oxidation. II. The Effect of Vanadyl Chelates Found in Petroleum. *Liquid Fuels Technology*, 2(1): 67-89.

Branthaver, J. F., J. C. Petersen, J. J. Duvall, and P. M. Harnsberger, 1991, Compatibilities of Strategic Highway Research Program Asphalts. *Transportation Research Record* 1323, 22-31.

Branthaver, J. F., J. C. Petersen, R. E. Robertson, J. J. Duvall, S. S. Kim, P. M. Harnsberger, T. Mill, F. A. Barbour, and J. F. Schabron, 1993, *SHRP-A-368, Binder Characterization and Evaluation, Volume 2: Chemistry*. Strategic Highway Research Program, National Research Council, Washington, D. C., 479 p.

Bridgewater, A. J., and M. D. Sexton, 1978, *Journal of the Chemical Society Perkins Transactions,* 530-536.

Cominsky, R. J., J. S. Moulthrop, W. E. Elmore, and T. W. Kennedy, 1989, *SHRP Materials Reference Library Asphalt Selection Process*. Strategic Highway Research Program, National Research Council, Washington, D. C., 31 p.

Corbett, L. W., and R. E. Merz, 1975, Asphalt Binder Hardening in the Michigan Test Road after 18 Years of Service. *Transportation Research Record* 544, 27-34.

Correa, P. A., G. Hardy, and D. P. Riley, 1988, Selective Autoxidation of Electron-Rich Substrates under Elevated Oxygen Pressures. *Journal of Organic Chemistry*, 53: 1695-1702.

Davis, T. C., and J. C. Petersen, 1966, An Adaptation of Inverse Gas-Liquid Chromatography to Asphalt Oxidation Studies. *Analytical Chemistry*, 38: 1938-1940.

Davis, T. C., and J. C. Petersen, 1967, An Inverse GLC Study of Asphalts used in the Zaca-Wigmore Experimental Road Test. *Proceedings, Association of Asphalt Paving Technologists*, 36: 1-15.

Dorrence, S. M., F. A. Barbour, and J. C. Petersen, 1974, Direct Evidence for Ketones in Oxidized Asphalts. *Analytical Chemistry*, 46: 2242-2244.

Goode, J. F., and L. A. Lufsey, 1965, Voids, Permeability, Film Thickness vs. Asphalt Hardening. *Proceedings, Association of Asphalt Paving Technologists*, 34: 430-463.

Haxo, H. E., and R. M. White, 1979, Reducing the Hardening of Paving Asphalts through the Use of Lead Antioxidants. *Proceedings, Association of Asphalt Paving Technologists*, 48: 611-645.

Hiatt, R., T. Mill, K. C. Irwin, and J. K. Castleman, 1968, Homolytic Decompositions of Hydroperoxides. III. Radical-Induced Decompositions of Primary and Secondary Hydroperoxides. *Journal of Organic Chemistry*, 33: 1428-1430.

Huh, J. D., and R. E. Robertson, 1996, Modeling of Oxidative Aging Behavior of Asphalts from Short Term, High Temperature Data As a Step Toward Prediction of Pavement Aging. *Transportation Research Record,* (in press).

Jennings, P. W., J. A. Pribanic, M. F. Raub, J. A. Smith, and T. M. Mendes, 1991, Advanced High Performance Gel Permeation Chromatography Methodology. SHRP AIIR-14 Final Report.

Kemp, G. R., and N. H. Predoehl, 1981, A Comparison of Field and Laboratory Environments on Asphalt Durability. *Proceedings, Association of Asphalt Paving Technologists*, 50: 492-531.

Kim, S. S., G. W. Gardner, J. F. McKay, R. E. Robertson, and J. F. Branthaver, 1997, Detection of Strongly Acidic Compounds in Extensively Aged Asphalts. In Usmani, A. M., ed., *Handbook of Asphalt Science and Technology*. Marcel Dekker, New York.

King, G. N., 1993, Oxycyclics: Understanding Catalyzed Oxidation Mechanisms on Bitumen and Other Petroleum Products. *Fuel Science and Technology International*, 11(1): 201-238.

Knotnerus, J., 1971, Oxygen Uptake by Bitumen Solutions As a Potential Measure of Bitumen Durability. *American Chemical Society Division of Petroleum Chemistry Preprints*, 16(1): D37-D59.

Komoroski, R. A., 1993, Nonmedical Applications of NMR Imaging. *Analytical Chemistry*, 65: 1068A-1077A.

Lau, C. K., K. M. Lundsford, C. J. Glover, R. R. Davidson, and J. A. Bullin, 1992, Reaction Rates and Hardening Susceptibilities as Determined for Pressure Oxygen Vessel Aging of Asphalts. *Transportation Research Record* 1342, 50-57.

Lee, D. Y., 1968, Development of a Laboratory Durability Test for Asphalts. *Highway Research Record* 231: 34-49.

Liu, M., K. M. Lundsford, R. R. Davidson, C. J. Glover, and J. A. Bullin, 1996, Kinetics of Carbonyl Formation in Asphalts. *AIChE Journal*, 42(4): 1069-1076.

Martin, K. G., 1966, Influence of Stabilizers on Bitumen Durability. *Journal of Applied Chemistry*, 16: 197-202.

Martin, K. G., 1968, Laboratory Evaluation of Antioxidants for Bitumens. Fourth Conference, Australian Road Research Board, 1-14.

Martin, K. L., R. R. Davidson, C. J. Glover, and J. A. Bullin, 1990, Asphalt Aging in Texas Roads and Test Sections. *Transportation Research Record* 1269, 9-19.

Mill, T., 1996, The Role of Hydroaromatics in Oxidative Aging in Asphalt. *American Chemical Society Division of Fuel Chemistry Preprints*, 41(4): 1245-1249.

Mill, T., and D. G. Hendry, 1980, Kinetics and Mechanisms of Free Radical Oxidation of Alkenes and Olefins in Liquid Phase. In Bamford, C. H., and C. F. H. Tipper, eds., *Comprehensive Chemical Kinetics*, vol. 16. Elsevier, Amsterdam, p. 1-83.

Mill, T., C. C. D. Yao, and M. Su, 1997, Asphalt Oxidation Pathway Studies. Final Report, SRI Project No. 1271, prepared for Western Research Institute.

Mushrush, G. W., 1992, Fuel Instability 1: Organo-Sulfur Hydroperoxide Reactions. *Fuel Science and Technology International*, 10(9): 1523-1560.

Mushrush, G. W., E. J. Beal, E. Slone, and D. R. Hardy, 1996, Reaction of Organosulfur Compounds with Naturally Occurring Peroxides in Jet Fuel. *Energy & Fuels*, 10: 504-508.

Nellensteyn, F. J., 1924, The Constitution of Asphalt. *Institute of Petroleum Technology*, 10: 311-325.

Nellensteyn, F. J., 1928, Relation of the Micelle to the Medium of Asphalt. *Institute of Petroleum Technology*, 14: 134-138.

Oliver, J. W. H., 1995, Results of Road Trials of Two Asphalt Antioxidants. *Transportation Research Record 1488*, 96-102.

Pauli, A. T., 1996, Asphalt Compatibility Testing Using the Automated Heithaus Titration Test. *American Chemical Society Division of Fuel Chemistry Preprints*, 41(4): 1276-1281.

Petersen, J. C., 1984, Chemical Composition of Asphalt as Related to Asphalt Durability: State of the Art. *Transportation Research Record* 999, 13-30.

Petersen, J. C., 1986, Quantitative Functional Group Analysis of Asphalts Using Differential Infrared Spectrometry and Selective Chemical Reactions — Theory and Practice. *Transportation Research Record* 1091, 1-11.

Petersen, J. C., 1989, A Thin Film Accelerated Aging Test for Evaluating Asphalt Oxidative Aging. *Proceedings, Association of Asphalt Paving Technologists*, 58: 220-237.

Petersen, J. C., and H. Plancher, 1981, Quantitative Determination of Carboxylic Acids and Their Salts and Anhydrides in Asphalts by Selective Chemical Reaction and Differential Infrared Spectroscopy. *Analytical Chemistry*, 53: 786-789.

Petersen, J. C., F. A. Barbour, and S. M. Dorrence, 1974, Catalysis of Asphalt Oxidation By Mineral Aggregate Surfaces and Asphalt Components. *Proceedings, Association of Asphalt Paving Technologists*, 43: 162-177.

Petersen, J. C., F. A. Barbour, and S. M. Dorrence, 1975, Identification of Dicarboxylic Anhydrides in Oxidized Asphalts. *Analytical Chemistry*, 47: 107-111.

Petersen, J. C., S. M. Dorrence, M. Nazir, H. Plancher, and F. A. Barbour, 1981, Oxidation of Sulfur Compounds in Petroleum Residues: Reactivity-Structural Relationships. *American Chemical Society Division of Petroleum Chemistry Preprints*, 26(4): 898-906.

Petersen, J. C., J. F. Branthaver, R. E. Robertson, P. M. Harnsberger, J. J. Duvall, and E. K. Ensley, 1993, Effects of Physicochemical Factors on Asphalt Oxidation Kinetics. *Transportation Research Record* 1391, 1-10.

Petersen, J. C., R. E. Robertson, J. F. Branthaver, P. M. Harnsberger, J. J. Duvall, S. S. Kim, D. A. Anderson, D. W. Christensen, H. U. Bahia, R. Dongre, C. E. Antle, M. G. Sharma, J. W. Button, and C. J. Glover, 1994, *SHRP-A-370, Binder Characterization and Evaluation, Volume 4: Test Methods*. Strategic Highway Research Program, National Research Council, Washington, D. C., 193 p.

Petersen, J. C., P. M. Harnsberger, and R. E. Robertson, 1996, Factors Affecting the Kinetics and Mechanisms of Asphalt Oxidation and the Relative Effects of Oxidation Products on Age Hardening. *American Chemical Society Division of Fuel Chemistry Preprints*, 41(4): 1232-1244.

Plancher, H., E. L. Green, and J. C. Petersen, 1976, Reduction of Oxidative Hardening of Asphalts by Treatment with Hydrated Lime — A Mechanistic Study. *Proceedings, Association of Asphalt Paving Technologists*, 45: 1-24.

Serafin, P. J., L. L. Kole, and A. P. Chritz, 1967, Michigan Bituminous Experimental Road: Final Report. *Proceedings, Association of Asphalt Paving Technologists*, 36: 582-614.

Storm, D. A., R. J. Barresi, and E. Y. Sheu, 1996, Development of Solid Properties and Thermochemistry of Asphalt Binders in the 25-65°C Temperature Range. *Energy & Fuels*, 10: 855-864.

Vallegra, B. A., R. M. White, and F. S. Rostler, 1970, Changes in Fundamental Properties of Asphalts During Service in Pavements. Final Report, Contract No. FH-11-6149 for Office of Research and Development, U. S. Bureau of Public Roads, January 1970.

van Gooswilligen, E. H., H. Berger, and F. Th. de Bats, 1985, Oxidations of Bitumens in Various Tests. Proceedings, European Bitumen Conference, 95-101.

Walling, C., 1964, *Free Radicals in Solution*. John Wiley and Sons, New York.

CHAPTER 5: ASPHALT IN CONTACT WITH AGGREGATE AND WATER

SYNOPSIS

Chapter 5 includes eight studies designed to show how aggregates and water affect the physical properties of mixes. Several of the studies were conducted to determine whether simple, fast tests could be developed to predict performance properties such as water-stripping and long-term hardening. Other studies used new instrumental techniques to elucidate the effects of aggregates and/or water on the physical properties of asphalts. Additional studies show that the physical properties of asphalts (even asphalts of the same PG and mastics depend on the compositions of the asphalts and aggregates and that performance properties cannot always be predicted from current PG specifications.

Occasional and unpredictable extreme embrittlement of asphalt concrete pavements has been reported (but generally not well documented) by several State highway departments. It was hypothesized that this may result from some specific asphalt compositional features and/or specific combinations of asphalt (likely oxidized material) and aggregate. This work was undertaken to determine the expected level of involvement of materials composition on rapid, extreme embrittlement. Steric hardening (isothermal reversible hardening) studies of oxidized and unoxidized asphalts, with and without aggregate, showed that the degree of hardening (increase in stiffness) in 3 months at 25°C (77°F) depends upon the composition of the asphalt and ranges between about 10 and 130 percent for 18 different asphalts. Most hardening occurs within 72 hours and then continues at a much slower rate. The development of a fast rheological method to predict the magnitude of long-term hardening will be difficult because the rate of hardening changes with time.

The results of an asphalt-aggregate interaction study suggest that substantial aggregate surface-induced molecular structuring can occur at the asphalt-aggregate interface. Thin films of asphalt on an aggregate surfaces, compared with bulk asphalt, have substantially changed rheological properties, and asphalts that are graded alike as bulk materials do not exhibit the same rheological properties as thin films.

Penetration measurements on mastics have shown that mineral filler will "scatter" the rheological properties of asphalts having different chemical compositions despite the fact that the asphalts are all the same PG. Penetration measurements have shown that classification of binders by PG do not correlate well with the mechanical performance properties of asphalts in road service conditions.

The effect of water on the steric hardening of unaged and aged asphalts was studied by monitoring changes in rheology over time. Preliminary data indicate that water is incorporated into asphalt, and the amount increases with time and the level of aging of the asphalt. It is proposed that water mitigates steric hardening by interfering with the formation of hydrogen bonds between polar compounds in the asphalt. IR reflectance spectroscopy studies demonstrated that carbonyl-containing compounds such as ketones and carboxylic acids that

occur naturally in asphalts can migrate to a solid surface, zinc selenide (ZnSe), suggesting that polar compounds in asphalt can migrate to an aggregate surface in a similar manner.

The ESEM was used to investigate water penetration into asphalt surfaces and the effects of freeze-thaw cycling on asphalt-aggregate bonds. The results showed clearly that there are differences in water penetration rates due to asphalt type and degree of oxidative aging, and that asphalt-aggregate bonds are more susceptible to disruption when water is present during the freeze cycle. Further, some asphalt-aggregate combinations produce more stable interfaces than others.

The feasibility of using NMR imaging methods to study asphalt-water-aggregate interactions during freeze-thaw cycling was investigated. NMR imaging showed evidence of water displacement at the asphalt-aggregate interface for an intermediate stripping aggregate, suggesting that NMR imaging may have applicability in the study of moisture susceptibility of asphalts.

Time-dependent molecular structuring of the n-alkane (paraffins) in asphalts at ambient temperature (22°C [71.6°F]) was investigated using carbon-13 solid-state NMR techniques. This study showed that microcrystalline components form in asphalts and continue to increase in amount over long time periods (1 year or more). The formation of a separate phase of microcrystalline components is the result of slow molecular realignment in the amorphous (solvent) phase of asphalts to form more organized structures. The slow molecular restructuring can cause gradual changes in the physical properties of asphalts.

A pyrolytic nitrogen analyzer was employed to measure the thermal desorption of pyridine from 18 different aggregates as a possible test method for predicting moisture susceptibility (stripping) of the aggregates. Thermal desorption of pyridine does not correlate well with the propensity of an aggregate to water-strip. However, the research demonstrated that water-stripping propensity is better predicted when compositional features of both asphalt and aggregate are considered together. Efforts to develop a simple test to predict water-stripping based on the composition of both aggregate and asphalt using 88 different asphalt-aggregate mix combinations have been encouraging.

STERIC HARDENING OF ASPHALTS AND MASTICS

Catastrophic, or extreme, embrittlement in asphalt concrete pavements, which typically leads to severe cracking, has been reported by State highway departments, but only on an occasional basis. Further, such an event is viewed as a failed roadway to be replaced and documentation is usually sketchy to non-existent. This study of asphalts and mastics was undertaken with asphalts and aggregates having widely varied compositions to determine whether extreme embrittlement is likely to be a simple materials problem. The question is: are specific asphalt composition(s) or specific combinations of asphalt and aggregate the culprit in these occasional extreme embrittlement events? The objective of this work was to measure the possible contribution of the phenomenon known as steric hardening to embrittlement of asphalt-

aggregate mixtures. It is already known that oxidative hardening (chapter 4) contributes strongly to embrittlement.

Steric hardening (isothermal reversible hardening) is defined as the reversible, non-oxidative hardening of asphalt with time. It has long been known that when an asphalt is heated to mix-plant temperatures and is then allowed to cool and stand at ambient temperature, the viscosity of the asphalt will increase, even if maintained at the same temperature and protected from oxidation. This isothermal increase in viscosity can be reversed when the asphalt is reheated. One of the original goals of the project was to determine whether or not it would be possible to develop a rapid rheological test, using a specially designed cup and cylinder sample container for dynamic shear measurements, to measure and predict the hardening and softening characteristics of an asphalt over time. This information would be useful for mix design when asphalts to be used for construction show significant amounts of steric hardening. Further, it was hoped that some specific chemical property (or property set) could be used to predict the magnitude of steric hardening for any given asphalt. Another goal was to determine whether exceptionally high steric hardening can or cannot be identified in neat asphalts and/or in mastics. In this project steric hardening information was obtained on six core asphalts in experiments conducted at 25°C (77°F). Each asphalt was studied in three different stages of oxidation: (1) unoxidized, (2) RTFO-oxidized, and (3) RTFO-PAV-oxidized, to deconvolute the effects of irreversible oxidative hardening from reversible molecular structuring. The unoxidized asphalts studied were found to harden from 45-130 percent over a 3-month period. Heavily oxidized asphalts showed less steric hardening over 3 months than the unoxidized asphalts based on percentage increases in properties such as G* and viscosity. The hardening range for the highly oxidized asphalts was about 10-40 percent at 25°C (77°F). Steric hardening of both unoxidized and heavily oxidized asphalts can be completely reversed by heat treatment at 150°C (302°F). Thus, steric hardening at 25°C (77°F) of asphalts alone results in relatively small but significant changes in physical properties such as hardness and stiffness. Increases in hardening of orders of magnitude due to steric hardening were never observed in these studies. In general, the degrees of steric hardening observed in this project are similar to the degrees of hardening observed earlier by Traxler, Brown, and other workers (see references below). Based on a time limit of 3 months, some asphalts were found to harden by as much as 130 percent, depending on the composition of the asphalt, but extreme embrittlement resulting from steric hardening was not observed within that period of time. A 130 percent increase in viscosity equates to a Superpave® grade decrease of about 8°C (14.4°F).

The major goal of the final phase of the project was to define the effect of aggregates on the isothermal, reversible hardening process in experiments conducted at 30°C (86°F), based on the fact that large amounts of steric hardening were not observed in neat asphalts, either oxidized or unoxidized. Mastic samples were prepared using 18 different combinations of three different aggregates and three different unoxidized and heavily oxidized asphalts. Compression strengths and modulus measurements of the briquettes were measured over a 4-month period to determine whether or not aggregates induced steric hardening. The data showed that neither limestone aggregates nor a granite aggregate induced steric hardening or extreme embrittlement in the specimens studied over the 8-month period. The degree of steric hardening of the mastic samples was similar to the degree of steric hardening observed earlier in the same neat

unoxidized and oxidized asphalts. Overall, the research results of this task support the model describing asphalt as being a highly associated and complex mixture of compounds having hardening and softening properties that result from the inherent chemical composition of the asphalt, the changes in chemical composition of the asphalt resulting from oxidative aging, and the thermal history of the asphalt.

Hardening of asphalts over time has both reversible and irreversible components [Traxler and Coombs 1936; Brown et al. 1957; Coombs and Traxler 1937; Traxler and Schweyer 1936; Traxler and Coombs 1937; Traxler et al. 1944]. Traxler and Coombs [1936] used the term "age hardening" to describe the reversible hardening of asphalts over time while Brown et al. [1957] used the term "steric hardening" to describe the same phenomenon. In 1936, Traxler and Coombs, using a falling coaxial cylinder viscometer at 25°C (77°F), demonstrated that age hardening could be reversed by a heat treatment. Air-blown asphalts also showed an increase of viscosity with time. At the end of 1,850 hours after an initial annealing, a sample was reheated, and the viscosity reverted to approximately the original value. Coombs and Traxler, in additional experiments, showed that the amount of permanent hardening due to volatilization or chemical reaction is small in comparison with the reversible increase in viscosity over the time of the experiments [Coombs and Traxler 1937]. Brown also demonstrated the heat induced reversibility of steric hardening by measuring shear slip as a function of curing time [Brown et al. 1957]. Both cut-back and hard (highly viscous) asphalts were cured for a specified amount of time, heated to pouring temperatures, cooled, and retested. Both kinds of asphalts, within experimental error, returned to their original degrees of hardness. Brown attributed the hardening and its reversible nature to the formation of loose three dimensional networks held together by low energy bonds among molecules. These low energy bonds are, by definition, weak and could be easily broken by heat and shear. Heating would destroy the networks, which would re-form slowly upon cooling. The three dimensional networks increase resistance to flow, which results in the observed viscosity increases. The formation of the networks is often referred to as molecular structuring. Alternatively steric hardening may be the result of changes in packing of polar molecular associations, or of the extent of solvation of the molecular associations. In any case, asphalts heated to relatively high temperatures attain a certain stable thermodynamic state. Upon rapid cooling to ambient temperatures, the high temperature thermodynamic state apparently is partly preserved. A new thermodynamic state is slowly attained at ambient temperatures. Because no chemical changes occur during these temperature increases and decreases, the isothermal viscosity increases must be caused by some changes in the microstructure of asphalts.

The work on steric hardening discussed herein had been started during the SHRP, but was suspended because of higher priorities and hence completed in this project. Neat asphalts used in this study were obtained from the SHRP Materials Reference Library located in Sparks, Nevada. Special cells were designed and fabricated to contain neat asphalt for the rheological studies [Plancher et al. 1993]. The cells are based on a cylinder and cup design and allow dynamic (oscillatory) rheological measurements to be made over a wide time and temperature range without physically disturbing the asphalt sample. A Rheometrics model RMS-605 mechanical spectrometer was used for this study. Parameters such as dynamic viscosity (η^*), storage modulus (G'), loss modulus (G''), complex modulus (G^*), and tan delta ($\tan G''/G'$)

were measured or calculated for all neat asphalts described above. To find the percent hardening that occurred over time in neat asphalts, parameters such as dynamic viscosity, G*, or G*sin delta were plotted versus time.

Steric hardening experiments on mastics were conducted by measuring the compression strength (axial mode) at the point of failure of 50 gram, Marshall-like specimens having a composition of 15 mass percent asphalt and 85 mass percent -200 mesh aggregate. Modulus data were also recorded. Five identical samples were prepared for each asphalt-aggregate combination and the specimens were tested periodically over a time span of 4 months. In these experiments, the load required to break the specimen was plotted versus hardening time to measure the steric hardening that occurred over time. The details of these measurement procedures are described in Volume II of this report, Additional Test Results, Section C.

Steric hardening and softening experiments were conducted on both unoxidized and RTFO-oxidized neat asphalts AAA-1, AAB-1, AAD-1, AAG-1, AAK-1, and AAM-1. An example of steric hardening is shown in figure 5-1 for unoxidized asphalt AAD-1, where the percent of hardening, as measured by G* data, is plotted versus time. All asphalts showed the same general hardening and softening (after heat treatment for 2 hours at 150°C [302°F]) characteristics, but the magnitude of hardening depended on the chemical composition of each asphalt. Most unoxidized or RTFO-aged asphalts, as shown in the example, harden by about 15-20 percent during the first 72 hours after an initial heat treatment and then continue to harden at a slower rate up to the final measurement time of 3 months. The unoxidized asphalts hardened by 45 percent (AAG-1) to 130 percent (AAM-1), as molecular structuring occurred with time. The inherently less viscous, or softer asphalts, usually show a higher degree (percent increase) of steric hardening with time than stiffer asphalts, possibly because of the increased mobility of molecules in the less viscous systems. However, asphalt AAM-1, which is highly viscous, is an exception to this generalization. Heat treatment at 150°C (302°F) largely reverses the steric hardening of all samples, regardless of the degree of oxidation, as molecular structuring causing steric hardening is broken up. The molecules tending to engage in molecular structuring become randomized by dissolution and the system assumes an initial degree of structural organization (or lack thereof). The ability of the heat treatment to return an asphalt to an initial state of hardening was, as shown in earlier studies, not dependent on the composition of the asphalt. The degree to which hardening reverses at 70°C (158°F), to mimic the temperature of a pavement on a hot summer day, was shown in preliminary experiments with some asphalts to be about 100 percent, but more experiments are necessary to show that complete reversibility at 70°C (158°F) takes place in all asphalts. The question is important as it is related to the problem of crack healing in the field. Experiments at temperatures lower than 70°C (158°F) to measure the reversibility of steric hardening were not performed.

Additional experiments were designed to define the reversible hardening characteristics of highly oxidized (aged) asphalts. In these experiments the hardening and softening properties at 25°C (77°F) of RTFO/PAV-oxidized asphalts were measured. The results were similar for those of unoxidized and RTFO-oxidized asphalts. Figure 5-2 shows an example of hardening for highly oxidized asphalt AAM-1, where G*sin delta is used as the measurement of hardening. For any given asphalt, the degree of isothermal hardening was found to depend on the

composition of the original asphalt and the degree of oxidation of the asphalt. The degree of steric hardening of a highly oxidized asphalt was found generally to be less than the degree of hardening of the corresponding neat or RTFO-oxidized asphalt. Again, the initial high viscosity of highly oxidized asphalts probably inhibits molecular mobility and, therefore, retards the structural reorganization of the system. In no case was hardening of the SHRP RTFO-oxidized asphalts at 25°C (77°F) (only 25°C was studied) found to increase with time by more than 40 percent in 3 months. These observations show how chemical composition, the kinds and amounts of polar and non-polar compounds, determine the ability of the asphalt to structure (harden) over time. After hardening, the asphalts were heat treated at 150°C (302°F) to determine whether or not the highly oxidized asphalts could be reversed to the original state of hardness. The results showed that with the application of heat the hardening of RTFO/PAV-oxidized asphalts is reversed to the original degree of hardening in the same manner as unoxidized and RTFO-oxidized asphalts. Oxidation produces more polar molecules in the asphalt but these molecules associate and disassociate with change in temperature and time in the same manner as the polar molecules initially present in the virgin asphalt.

Figures 5-3 to 5-6 show how various stages of oxidation affect the hardening of four different asphalts. Reversible hardening data for three different oxidation levels can be seen in each of the figures, data for the unoxidized asphalt, data for the RTFO-oxidized asphalt, and data for the RTFO/PAV-oxidized asphalt. The examples show hardening data (based on G* values) for asphalts AAG-1, AAD-1, AAK-1, and AAM-1 and the associated levels of hardness to which the asphalts were reduced by heat treatment at 150°C (302°F). The data indicate that, as expected, the degree of oxidation of the asphalts has a large effect on overall age hardening. The figures illustrate the relative magnitude of overall age hardening at each level of oxidation and the comparison of that hardening with the magnitude of steric hardening induced by time. These data indicate that, for the purpose of predicting pavement performance, the prediction of the amount of steric hardening that occurs over time can be significant for certain asphalts, but it is not as significant as knowing or predicting the initial hardness of the oxidized asphalt. The accumulated data indicate that, in most cases, steric hardening of neat asphalt alone, even in highly oxidized asphalts, is not enough to cause catastrophic embrittlement. If failure resulting from binder embrittlement is ever observed, it is likely to be caused by factors other than steric hardening of the binder alone. Obviously, a highly oxidatively aged binder exhibiting strong tendencies to sterically harden will fail earlier than an oxidatively aged binder with lesser steric hardening tendencies, but such failure will have been caused mostly by the process of oxidation. Catastrophic embrittlement also may result from asphalt concrete that was overheated in the mix plant, from non-uniform compaction (allowing rapid oxidative aging of lesser compacted areas), or unusually warm weather; none of which are materials related and none of which would likely be well documented. The rheological tests conducted in this phase of the research also showed that development of a predictive test for steric hardening of neat asphalts using dynamic rheological measurements would be difficult. Such a test must be conducted for at least 72 hours, and probably a matter of months, to identify accurately asphalts susceptible to a high degree of steric hardening.

Experiments to determine whether aggregates can induce steric hardening in a mix were also conducted. The experiments, by design, maximized the probability of observing aggregate-

induced steric hardening by (1) using mastic mixes having large amounts (85 mass percent) of high-surface-area aggregates and by (2) using mastics made from aggregates of dramatically different chemical composition in contact with asphalts of different chemical compositions. Mastic specimens were prepared using nine combinations of aggregates of different chemical composition (RD, RC, and RB) together with unoxidized asphalts of different chemical composition (AAD-1, AAG-1, and AAM-1). A second complete set of the Marshall-like briquette specimens also was prepared using highly oxidized asphalts, resulting in a total of 18 different asphalt/aggregate combinations being studied. Ten identical briquette specimens of each mastic combination were prepared and the compression strength and moduli of these specimens were measured as a function of time (up to 4 months). These hardening experiments, conducted at 30°C (86°F), measured the amounts of steric hardening induced in the mastics by the aggregates as compared with the steric hardening of the asphalts alone. The experiments also were designed to identify any unusually high embrittlement induced by the chemically different aggregates.

The compression strength and moduli measurements made over a 4-month period showed that, in the 18 mastics studied, aggregates did not induce significant amounts of steric hardening in mastics. In general, the amount of steric hardening of the mastics was similar to the amount of steric hardening of the asphalts alone and the rate of steric hardening of the mastics was similar to the rate of steric hardening of the asphalts alone. None of the 18 different mastic combinations of asphalts and aggregates (having different chemical compositions) showed an unusually high degree of embrittlement over a 3-month period of storage at 30°C (86°F). It should be noted that replicate compression strength measurements showed a standard deviation as high as 25 percent for some samples, a standard deviation that is of a similar magnitude as the steric hardening being observed. Thus in some cases, due to the scattering of data, the relatively small amounts of steric hardening could not be measured accurately. Figure 5-7 shows an example of how briquettes made from unoxidized and heavily oxidized asphalts hardened over time using compression strength (at the point of failure) as the measurement of steric hardening. The mastic made from highly-oxidized asphalt AAM-1 had about double the initial compression strength compared with the mastic made with unoxidized asphalt. Over a 4-month period the unoxidized sample hardened by only 23 percent. The steric hardening shown by the mastic having highly oxidized asphalt was small, less than 50 percent, but could not be measured accurately because the amount of hardening was within the range of data scattering. Again, the general observation made from these experiments was that aggregate-induced steric hardening was marginal in spite of the fact that experimental conditions were designed to maximize and detect the phenomenon, if it occurred. Modulus data likewise showed that aggregate-induced steric hardening and aggregate-induced embrittlement during the 8-month test period was marginal. An example of typical modulus data plotted versus time is shown in figure 5-8 for the two mastics prepared from unoxidized and highly oxidized asphalt AAD-1 and aggregate RC. Figures 5-9 and 5-10 are examples of plots showing that, in the 18 combinations of aggregates and asphalts studied, the chemical nature of the aggregate had very little influence on the steric hardening of a mix over time. In each figure the steric hardening of a mastic prepared from a single asphalt and three different aggregates is plotted versus time. Within experimental variation, the chemical nature of the aggregate does not appear to have a major influence on the rate or amount of steric hardening of the mix.

Overall, the steric hardening experiments on neat asphalts and the steric hardening experiments on mastics demonstrate that, when all other factors are equal, the chemical composition of the asphalt is the main factor determining the initial hardness of a sample and the amount of steric hardening developed by the sample over time. Polar components of asphalts that may be immobilized on aggregate surfaces evidently are not involved in the phenomenon of steric hardening in bulk asphalts, based on the data presented here.

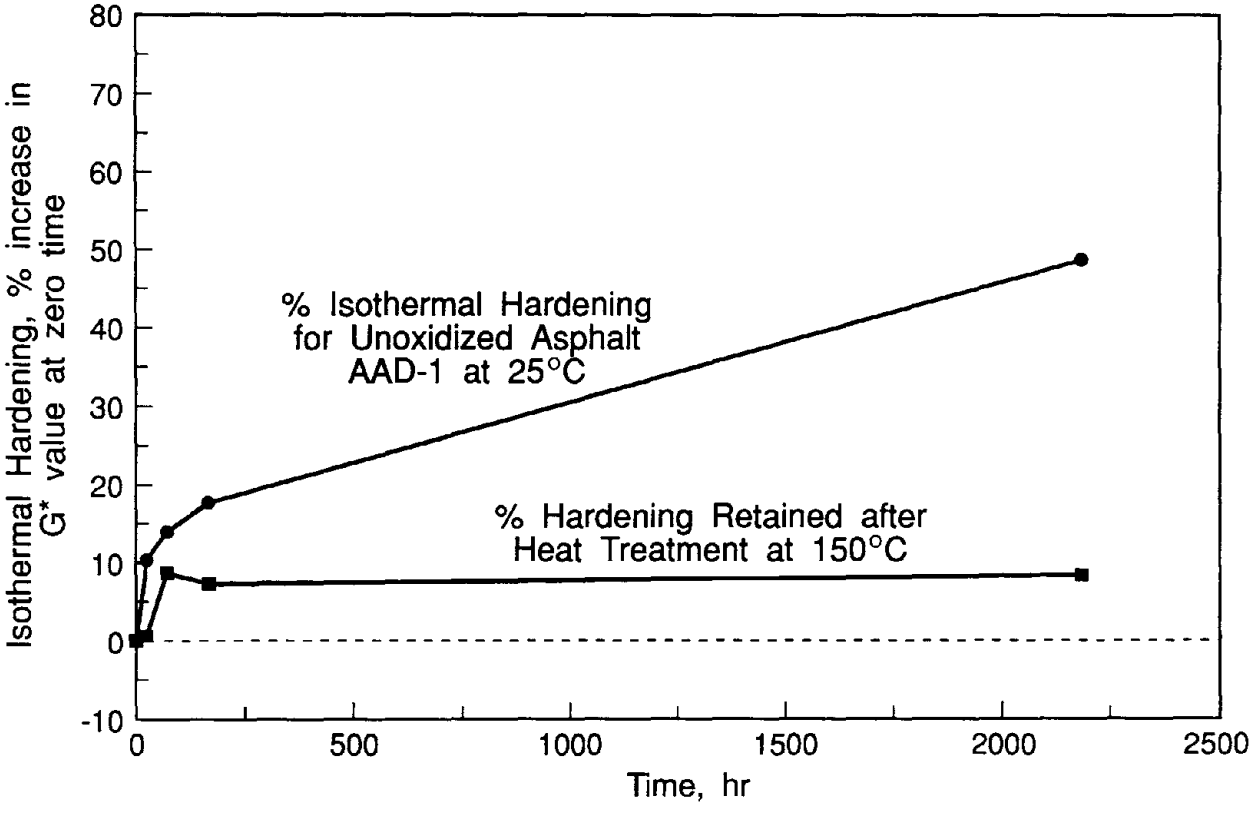

Figure 5-1. Normalized G* data at 0.50 rad/s for unoxidized asphalt AAD-1 at 25°C.

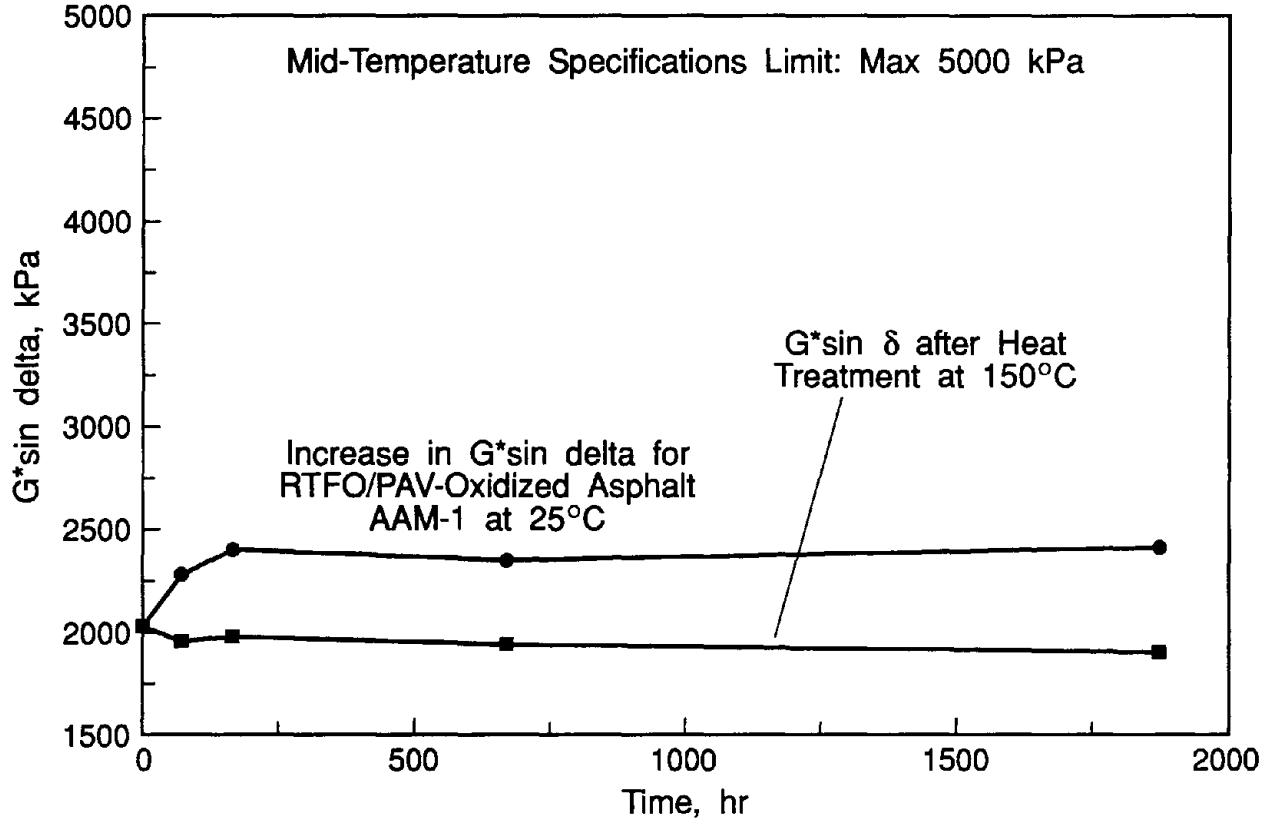

Figure 5-2. Normalized G*sin delta data at 10 rad/s for RTFO/PAV-oxidized asphalt AAM-1 at 25°C.

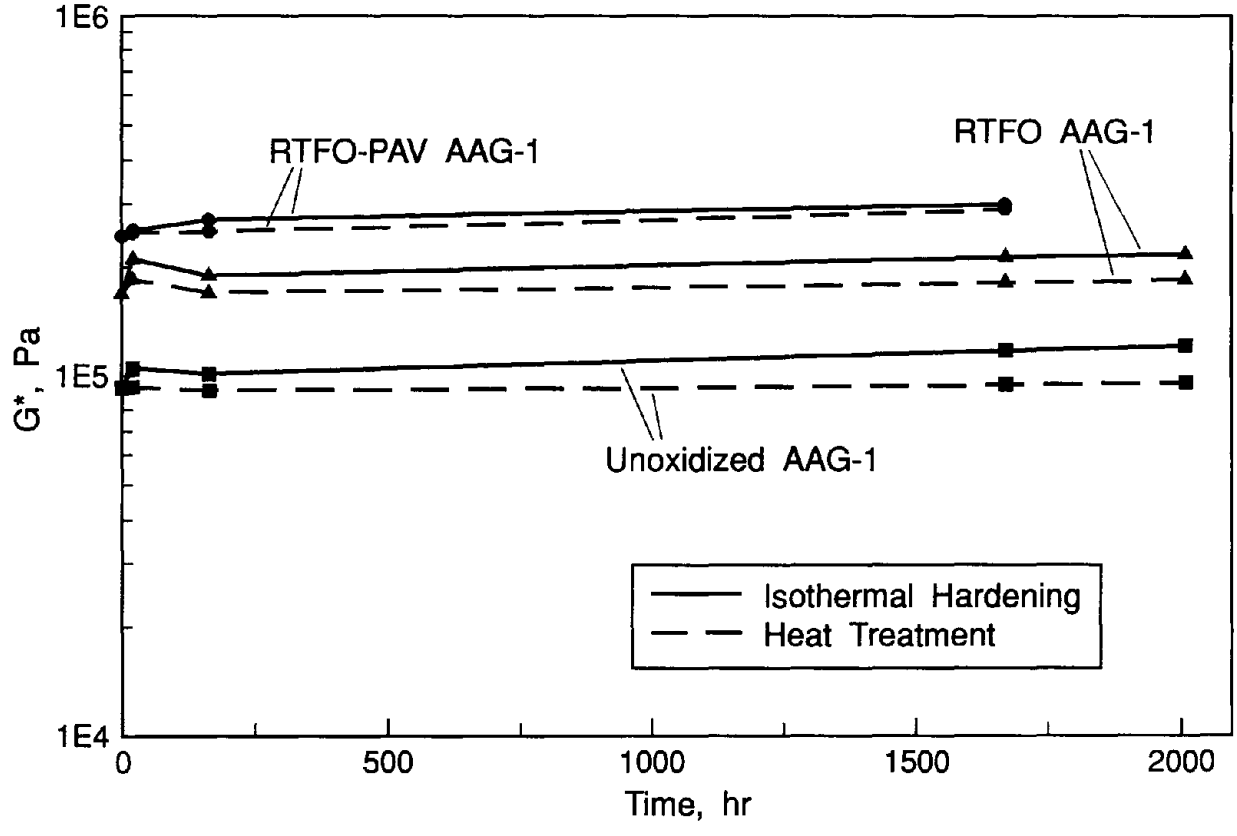

Figure 5-3. G* data at 0.50 rad/s for asphalt AAG-1 at three levels of oxidation for isothermal hardening and heat treatment.

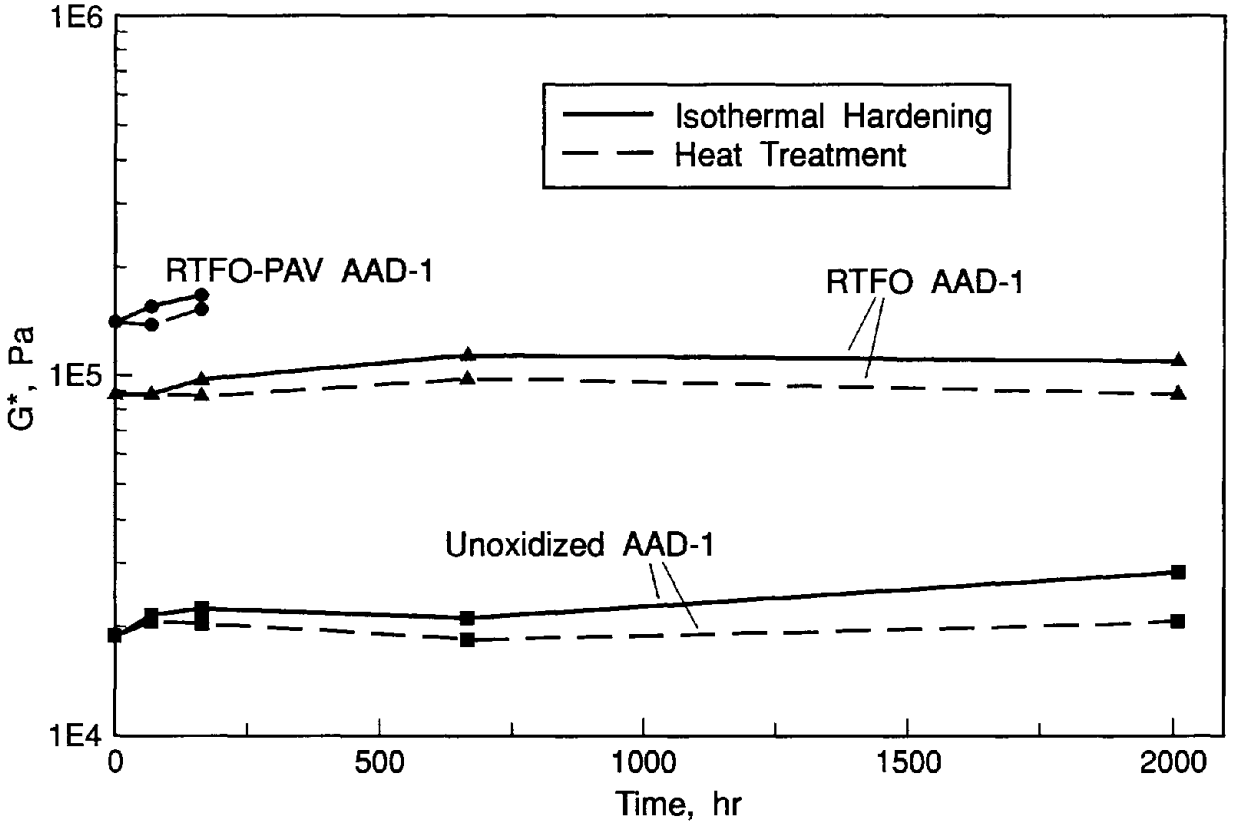

Figure 5-4. G* data at 0.50 rad/s for asphalt AAD-1 at three levels of oxidation for isothermal hardening and heat treatment.

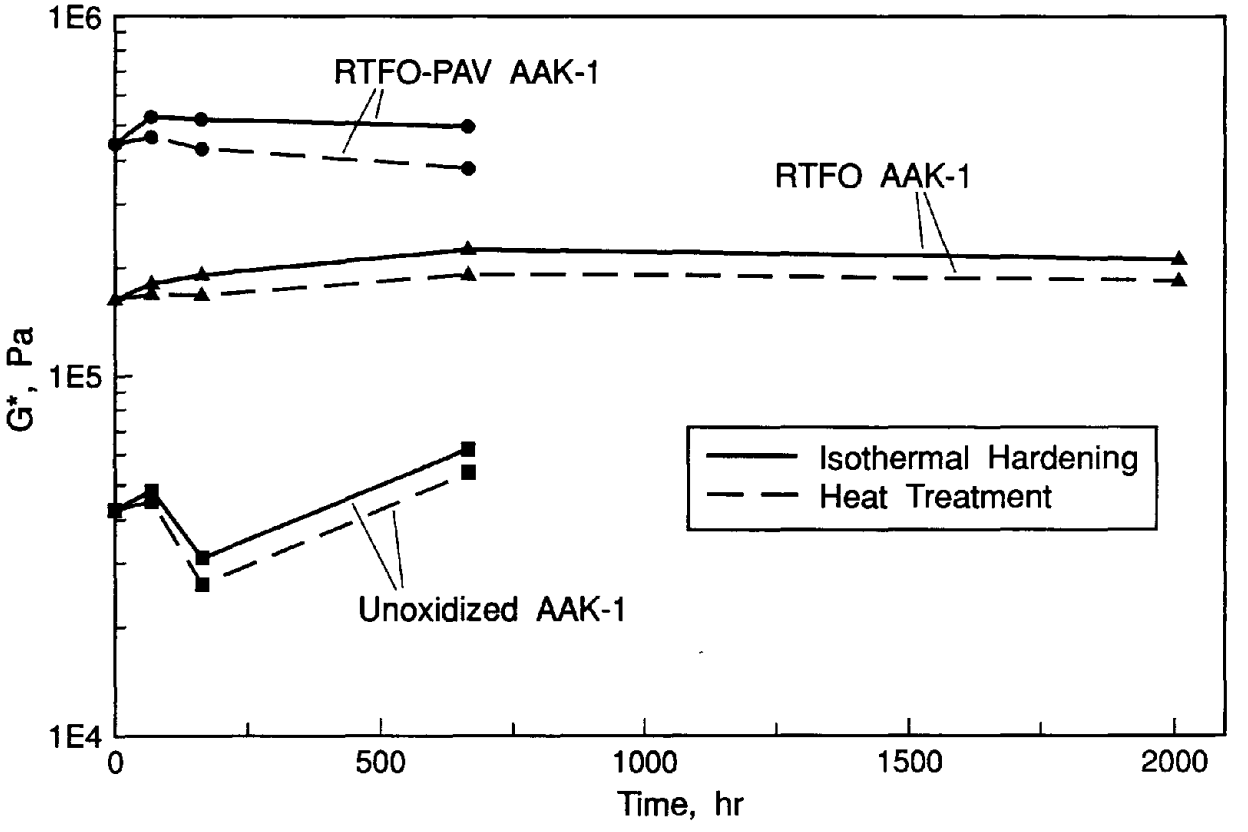

Figure 5-5. G* data at 0.50 rad/s for asphalt AAK-1 at three levels of oxidation for isothermal hardening and heat treatment.

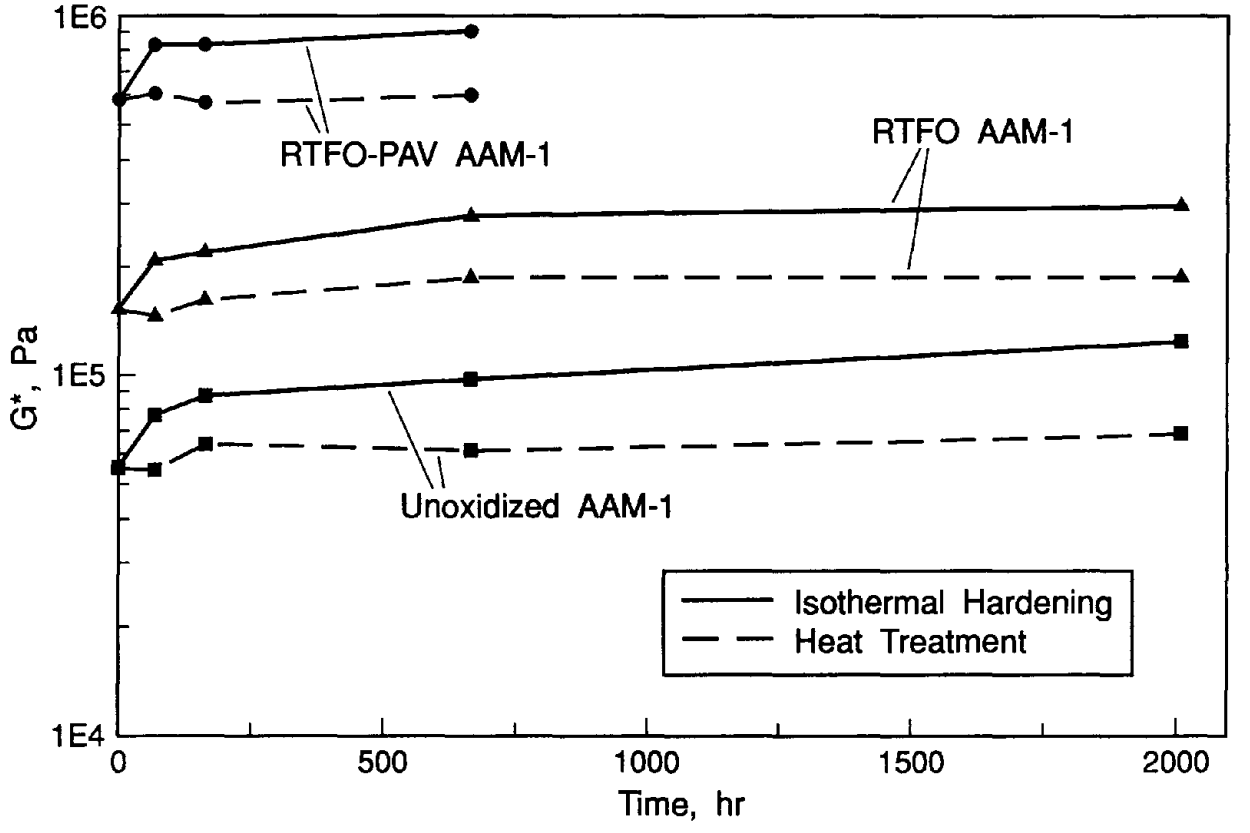

Figure 5-6. G* data at 0.50 rad/s for asphalt AAM-1 at three levels of oxidation for isothermal hardening and heat treatment.

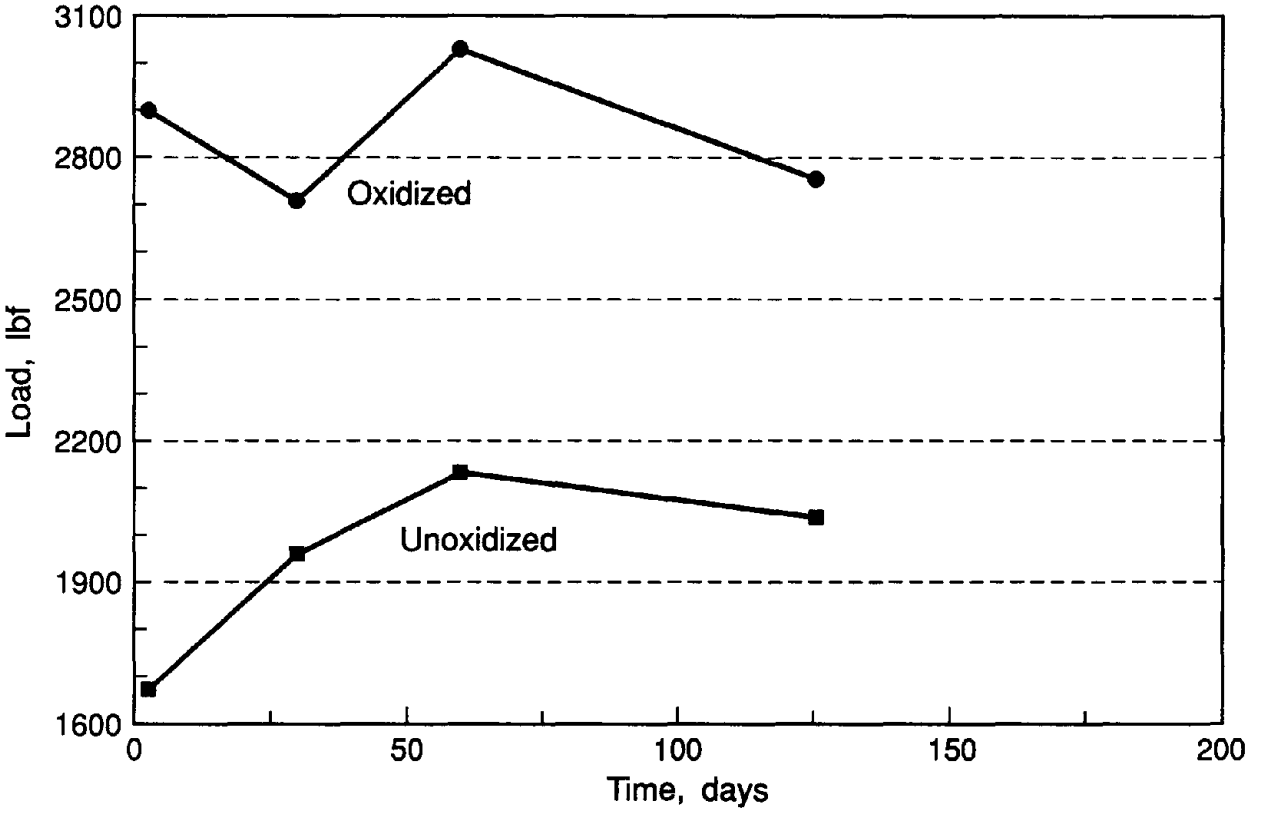

Figure 5-7. Compression strength of unoxidized and oxidized mastics RD-AAM-1 as a function of time.

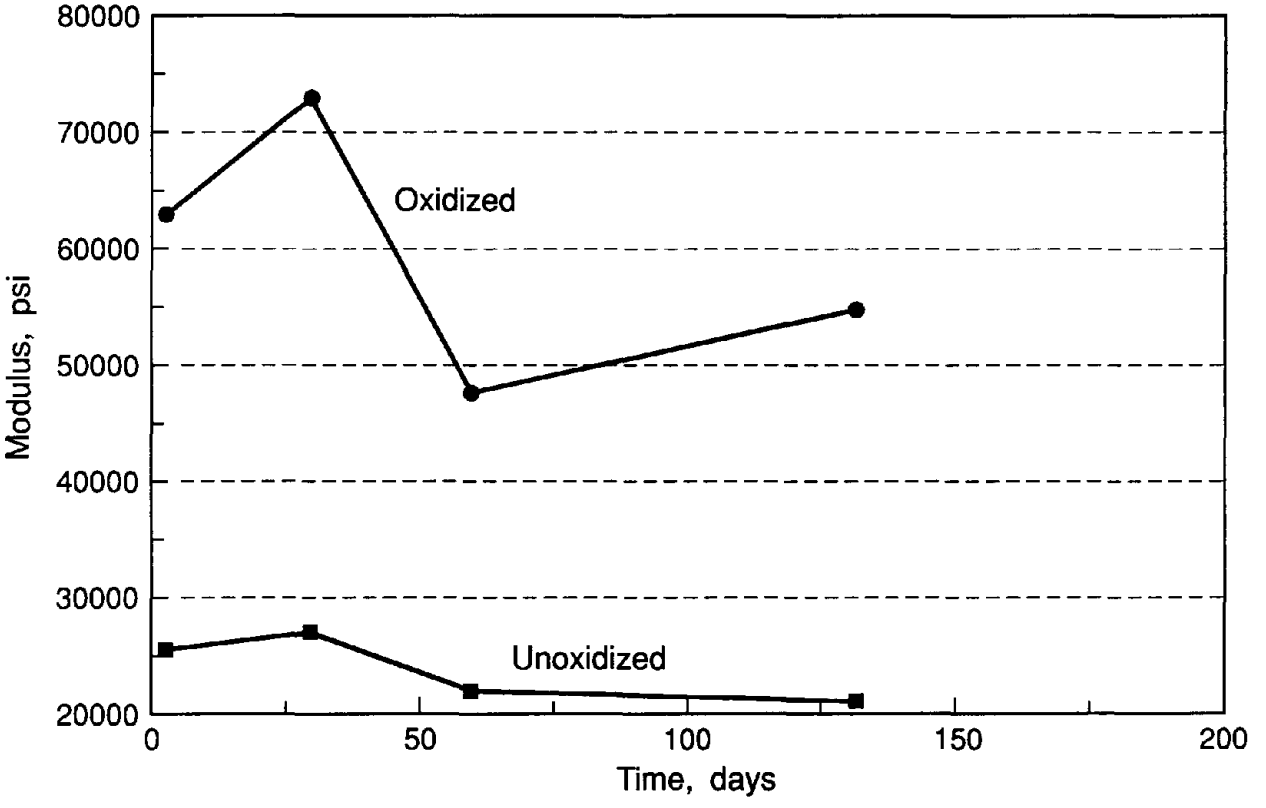

Figure 5-8. Modulus of unoxidized and oxidized mastics RC-AAD-1 as a function of time.

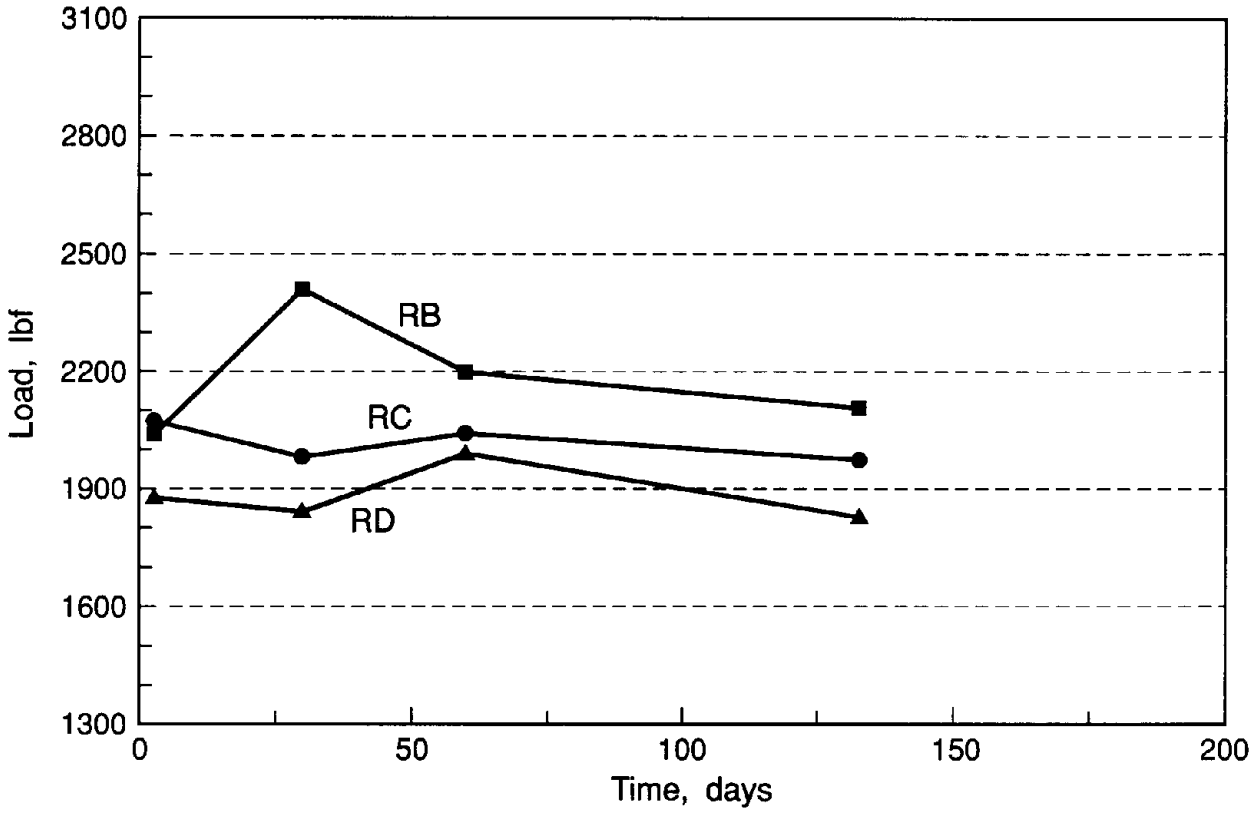

Figure 5-9. Compression strength at failure of mastic briquettes prepared from aggregates RB, RC, RD and unoxidized asphalt AAD-1 as a function of time.

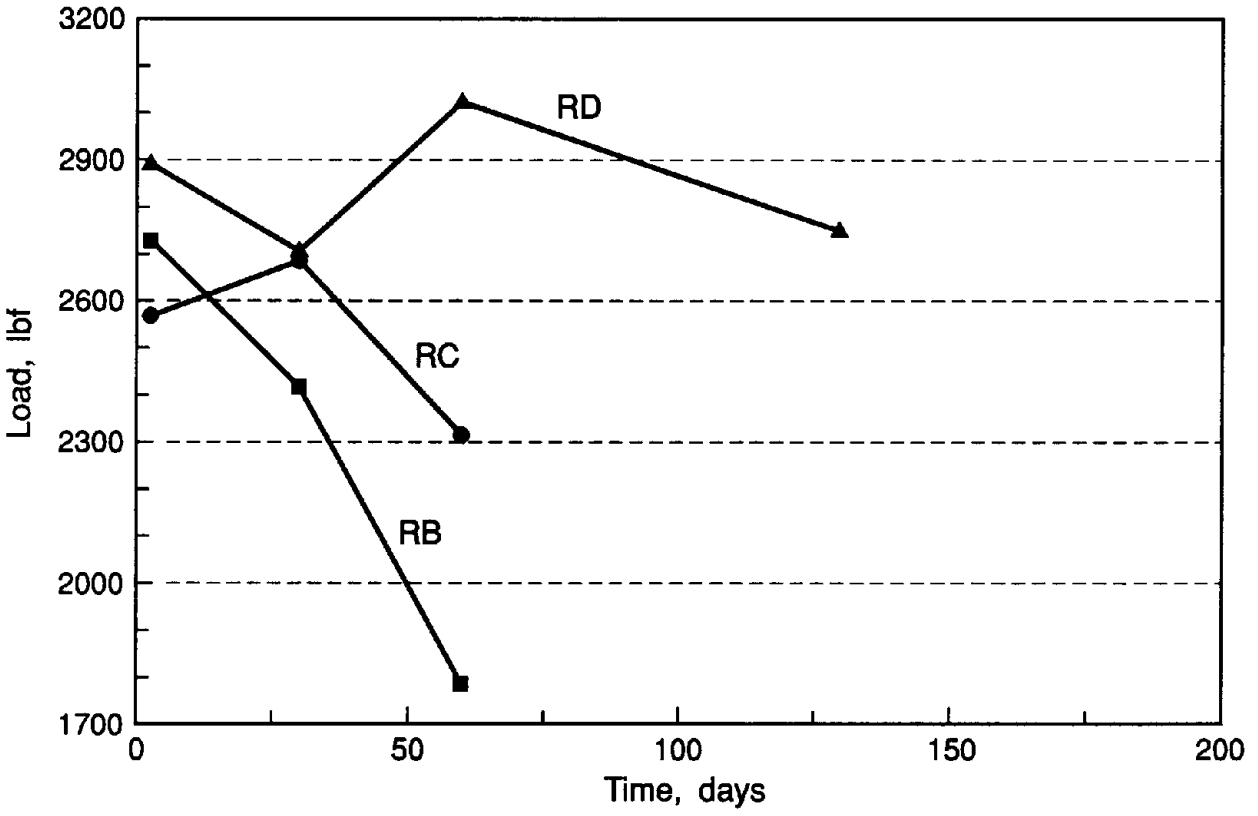

Figure 5-10. Compression strength at failure of mastic briquettes prepared from aggregates RB, RC, RD and oxidized asphalt AAM-1 as a function of time.

SLIDING PLATE MICROVISCOMETER STUDIES OF ASPHALT-AGGREGATE INTERACTIONS

The effect of the interaction between aggregate and asphalt on asphalt mix physical properties has been a subject of many studies. However, studies using compacted mixtures cannot isolate the pure effects of the asphalt-aggregate interactions. This is because the sizes of individual aggregate pieces are non-uniform, surface roughness varies among the aggregate pieces, and asphalt film thickness also varies. These variables can be controlled by experimentation with machined aggregate plates of uniform dimensions to eliminate roughness and size variations. Mixtures of asphalts and fines have limited utility as surrogates for asphalt-aggregate mixes because there is no practical method for measuring rheological properties at the surface of small particles. In this study, direct measurement of asphalt rheology at the interface is being investigated using the sliding plate geometry with machined aggregate plates. A detailed description of this method is presented in Volume II, method 16. Glass or aggregate plates 30 mm x 20 mm x 6 mm were prepared, and one surface of the aggregate plates was polished. A sample of asphalt then was applied to the glass plate or polished surface of the aggregate plate so that the plate was uniformly coated. A second plate of the same kind then was placed in contact with the asphalt surface. In pavements, asphalt film thickness varies between 5 and 15 μ. In these experiments, film thickness varied between 5 and 120 μ. The thick asphalt layers were studied to determine at what thickness changes in film properties become detectable. A force then was applied to one of the plates in the direction of the longest (30 mm) dimension, and the deformation caused by the force was measured.

Although the nature of intermolecular forces involved in asphalt-aggregate mixtures has long interested scientists, rigorous treatments of the subject have tended to concentrate on the bulk mechanics of asphalt-aggregate mixtures [Curtis et al. 1993] and with very little done on the chemistry and physics of the asphalt-aggregate interfaces, especially at the very thin film levels that are common in pavements. There is considerable experimental evidence to show that when a liquid is confined in a narrow gap (thin films), new dynamic behavior emerges [Henniker 1949; Kumler 1940; Granick 1991; Marek and Herrin 1968]. The principal effects are a considerably increased viscosity and a greater elastic strength of the liquid near the surface of a solid compared with the same material in bulk form. This effect has been observed in asphalts [Mack 1957; Scholz and Brown 1996], and has been designated surface-induced structuring. It is possible that asphalts that are graded alike as bulk materials may not have the same rheological properties in thin films, which are the real service environment. Thus, it is important to ascertain how the physical properties of such microscopic structures differ from those of the bulk materials.

The objectives of this study are (1) to evaluate asphalt-aggregate interactions for different combinations of asphalts and aggregates, (2) to identify the factors affecting the interactions, (3) to establish how certain fundamental physical properties vary during the transition from very thin films to thick films where properties are practically indistinguishable from the bulk, (4) to determine the effects of the aggregate surface on asphalt aging, and (5) to determine the effects of the aggregate surface on molecular structuring. Meeting all of these objectives should contribute to an understanding of a more realistic environment for asphalt in

road service than asphalt in bulk. The sliding plate microviscometer (SPM) method is relatively fast and inexpensive and suited to measuring asphalt rheological properties in thin films. Therefore, this method could prove to be useful for distinction among asphalts that are classified as being alike by the Superpave® binder specification, but in fact behave differently in service because the asphalts have different compositions and thus react differently with aggregate.

In this investigation, the apparent viscosity of asphalts was measured at a temperature of 25°C (77°F) at varied film thicknesses, and the apparent viscosity was obtained at a shear rate of 0.05 s^{-1} by interpolation from the apparent viscosity-shear rate relationship derived from the applied load, displacement velocity, and dimensions of the asphalt film. Figure 5-11 shows the relationship between apparent viscosity and shear rate for SHRP core asphalt AAD-1 using machined limestone aggregate plates and glass plates at film thicknesses of 20 μm and 10 μm. As shown in figure 5-11, the rheological behavior of asphalt AAD-1 with glass plates is almost Newtonian. The apparent viscosity was only marginally affected by very low shear rate. However, asphalt AAD-1 with limestone plates clearly exhibits non-Newtonian behavior, the asphalt viscosity substantially increasing as the shear rate decreases. This implies that there are strong interaction forces at the asphalt-aggregate interface when limestone plates are used, but not with the glass plates. As seen from figure 5-11, the interaction forces at the asphalt-aggregate interface on limestone become more dominant as the shear rate decreases. As shear rate increases, the asphalt-aggregate interaction becomes less and less significant in influencing rheological properties, and presumably raising the temperature would have the same effect. This indicates that the molecular interactions at the asphalt-aggregate interface may be more important at moderate to low pavement service temperatures compared with higher service temperatures. The intermolecular forces (the control of viscosity) in the bulk asphalt itself become more important than the asphalt-aggregate molecular interactions at high shear rate or high temperatures. Most likely this is due to disruptions of specific interactions between asphalt components and limestone by heat and shear.

On the other hand, the interaction of asphalt AAG-1 with both glass plates and limestone plates, as shown in figure 5-12, illustrates the important effect of asphalt source on the properties of the asphalt aggregate interface. It can be seen that the apparent viscosity is lower for asphalt AAG-1 with limestone plates as compared with the glass plates. This lower viscosity of AAG-1 between limestone plates than between glass plates may be the result of lime treatment of AAG-1.

Generally speaking, it can be speculated that the interaction at the asphalt-aggregate interface plays a major role in influencing asphalt rheological properties at moderate pavement service temperatures or low speed traffic. However, it is speculated that the viscosity of an asphalt binder should be less influenced by the asphalt-aggregate interface interaction at high pavement service temperature. The above results also indicate some inadequacy in the current Superpave® binder specification. Asphalts AAD-1 and AAG-1 originally were graded as PG58- in the performance-grading system, although more recently AAG-1 was upgraded to PG64-. In spite of their similar grades, they behave quite differently in contact with limestone aggregate.

To aid in the comparison, viscosities obtained using the dynamic shear rheometer (DSR) were plotted versus viscosities obtained using the SPM, and a least-square linear regression was performed. These results are shown in figure 5-13. The viscosities measured using the sliding plate viscometer show a general offset of approximately 18,000 Pa·s with a factor of 0.9 as compared with the viscosity obtained using the DSR. However, the relationship between the SPM and the DSR is still a reasonably good correlation (R^2=0.904). This indicates that the use of SPM to measure binder properties at various film thicknesses could be a cost-effective way to measure physical properties of asphalts under service conditions. The reasons for the differences in viscosity determinations measured by the two methods are that non-Newtonian viscosities depend on the nature of the apparatus used. The DSR operates in the linear regime. The SPM is not always in the linear regime.

Several different film thicknesses (ranging from 10 μm to 150 μm) between both glass plates and limestone plates were investigated to see how physical properties of asphalts vary in the presence of aggregate with the change of film thickness. Figure 5-14 shows the viscosity at shear rate of 0.05 s^{-1} versus different film thicknesses for SHRP asphalt AAD-1 with both glass plates and machined limestone plates at 25°C (77°F). It can be seen that the viscosity of asphalt AAD-1 with limestone substantially increased as the film thickness decreased to very thin films. However, the asphalt with glass plates shows the opposite effect. The viscosity measured using glass plates shows a decreasing trend as the film thickness decreases. It is possible that bulk asphalt molecular associations are broken down due to the shear-induced friction at the asphalt-glass interface in very thin films. Presumably there is little molecular interaction at the asphalt-glass interface, so it is possible that shear-induced friction, generating heat energy, disrupts the internal molecular associations in thin films of asphalts and results in a lowering of viscosity. This phenomenon would occur with limestone plates but would be outweighed by the effects of interactions between asphalt components and the interface.

Figure 5-15 shows the same type of plot as in figure 5-14 for asphalt AAK-1. It can be seen that asphalt AAK-1, with both glass plates and limestones plates, exhibits the same trend as that of AAD-1, increased viscosity as film thickness decreases for the limestone plates, but decreasing viscosity at low film thicknesses on the glass plates. This result for asphalt AAK-1 is not surprising since asphalts AAD-1 and AAK-1 are basically alike in many chemical respects [Branthaver et al. 1993a]. However, asphalt AAK-1 appears to experience the influence of the limestone aggregate surface at greater film thicknesses than asphalt AAD-1, in which there is little effect above 50 μm (figure 5-14). The longer range asphalt-aggregate surface interaction of asphalt AAK-1 results in the lower viscosity enhancement at the lowest film thicknesses for asphalt AAK-1 as compared with AAD-1.

On the other hand, the interaction of asphalt AAG-1 with limestone aggregate is totally different from that of limestone with AAD-1 and AAK-1, as shown in figure 5-16. It is well known that asphalt AAG-1 is different from the other SHRP asphalts in terms of chemical composition. This asphalt is unique in having been lime treated [Branthaver et al. 1993a]. More important, it is a highly compatible material, i.e., a good "solvent" for its own polars, as shown both by Heithaus compatibility analyses and by SEC fractionation. It is speculated that some of weakly interacting polar molecules in asphalt AAG-1 may be absorbed into the

aggregate pores and the remaining enhanced oil components account for the lower viscosity on asphalt AAG-1 with limestone plates. Such absorption (as opposed to adsorption, a surface phenomenon) would not occur with glass. Alternatively, the fact that AAG-1 has been lime treated may in some way be responsible for the difference in its behavior.

It is speculated that reorganization, or enhanced "self-assembly," of polar molecules in thin films of asphalts is responsible for viscosity enhancements on limestone plates. Asphalts contain significant amounts of molecules with functional groups that impart significant dipole moments to those molecules [Siffert et al. 1996]. Many of these molecules contain more than one such functional group. Of these polyfunctional molecules, a large proportion is amphoteric, containing both acidic and basic functional groups [Branthaver et al. 1993a]. These amphoteric molecules play an important role in the formation of molecular associations in asphalt matrices. Additionally, it has been suggested that a small proportion of the polar, organic components of asphalts may be capable of forming charged ions under certain conditions [Folland and Anfindsen 1996]. Organic carboxylic acids and strongly basic amines might lose or gain protons to form negatively charged anions and cations, respectively. Chemical equilibrium theory states that small populations of these species would exist under any circumstances. IR spectra of materials extracted from aggregates that had been in contact with asphalts demonstrate that carboxylic acids, 2-quinolones, and condensed nuclear aromatic hydrocarbons are strongly adsorbed on limestone. Hence, it has been shown that highly polar molecules such as these do migrate to aggregate surfaces from the bulk asphalt.

According to the model of asphalt structure described in chapters 1, 3, and 4, most of these polar components are involved in molecular associations of varying sizes. There is an equilibrium between the solvent component, or the continuous phase of an asphalt, and the polar molecular associations. That is, the solvent will contain small amounts of these molecules at any time, depending on such factors as temperature and shear. Because of this equilibrium, some highly polar molecules will irreversibly adsorb on rock surfaces when asphalt is coated onto aggregate. If the quantity of the asphalt is large compared with the surface layer, there will be little change in bulk asphalt physical properties. Compared with the amount of polar molecules involved in bulk asphalt molecular associations, the fraction of polar molecules adsorbed on aggregate surfaces would be small. However, as the total thickness of the asphalt layer decreases, the relative influence of adsorbed polars increases.

In thin films of asphalt, the dimensions of an immobilized surface layer are substantial compared with the dimensions of the total asphalt film. The immobilized surface layer should consist of the more polar components of an asphalt, particularly those capable of forming ions. Limestone consists of calcium (Ca^{++}) and carbonate ($CO_3^{=}$) ions in an insoluble crystal matrix together with varying amounts of clay particles (clay particles in particular bond strongly with polar organic molecules). Thus, limestone presents a highly polar surface at the ion or molecular size level. Adsorption of polar organic molecules on the aggregate surface together with a high level or organization of polars in a thin film of asphalt between aggregate surfaces causes a significant rise in the stiffness of the asphalt. Highly organized molecular associations are always stiffer than more randomized groupings of the same molecules. For example, water frozen into the organized crystal structure of ice is much stiffer than the more random

organization of liquid water. In the case of asphalt, the influence of the polar aggregate appears to "freeze" the polar organics into an organized, stiff material, although certainly not to the same extent as freezing a pure liquid into a crystalline solid.

In a lime-treated asphalt such as AAG-1, carboxylic acids and phenols are converted to calcium salts. These salts are particularly stable. There would be no particular driving force to cause a carboxylic acid anion to bond to a Ca^{++} cation on an aggregate surface in preference to a Ca^{++} cation in the bulk asphalt. Thus, an immobilized surface layer is far less likely to form in the case of an asphalt such as AAG-1.

The interactions of asphalt and aggregate at an interface are characterized by means of the interaction index, which is defined as the ratio of viscosity of asphalt with limestone plates to the viscosity of asphalt with glass plates. It is assumed that glass, which is an amorphous silica, will not interact as strongly with asphalt polar components as will materials such as limestone, granite, etc. Thus, the glass plates serve as controls. Figure 5-17 shows the interaction indices versus various film thicknesses for three SHRP core asphalts, AAD-1, AAG-1, and AAK-1. As seen from this figure, asphalt AAD-1 shows a stronger interaction as the films between limestone plates become very thin. Asphalt AAK-1 shows an interaction that is measurable in thicker films compared with AAD-1. On the other hand, asphalt AAG-1 shows essentially no interaction at the asphalt-aggregate interface in the thinner films. This indicates that the rheological properties of asphalt binders in the presence of aggregate are sharply dependent upon asphalt composition. The rheology of asphalt under pavement conditions, therefore, is asphalt (i.e., crude oil) source and film thickness dependent. Hence, the PG system does not predict the physical properties of asphalt correctly when asphalt is in a service environment.

After the initial rheological measurements using the glass and aggregate plates were performed, the sheared glass and aggregate plates were sheared back immediately in a direction opposite to the original shearing force. The back-sheared viscosities were compared with original viscosities. Statistical analysis based on a 95 percent confidence interval indicated that there is no significant difference between original and back-sheared viscosities at 25°C (77°F) with glass or aggregate plates. Within the time frame of the experiment (30 minutes), there are not changes in rheological properties such that the SPM method is invalid.

Following this, the sheared plates were stored at 25°C (77°F) for a longer period of time to study the setting and molecular structuring phenomena for asphalt in contact with machined limestone aggregate plates at various film thicknesses. Figure 5-18 shows the viscosity versus film thickness relationship for both original and stored (at 25°C [77°F] for 46 hours) asphalts on glass plates and on limestone plates. As can be seen, asphalt AAD-1 in contact with limestone plates increases in stiffness at small (~ 10 μm) film thickness during this short period of storage. The increase is not very large. Asphalt AAD-1 in contact with glass and stored is slightly stiffer than AAD-1 in contact with glass at the start of the storage period. It is concluded, as seen from the figure, that the initial rate of molecular structuring is fast compared with time of asphalt concrete construction. Asphalt AAG-1 shows no significant hardening (if anything, the stored materials are less stiff) after 46 hours storage at 25°C (77°F) with different film thicknesses, as

seen from figure 5-19. What is clear here is that the "in pavement" physical properties of asphalt cannot be predicted from thick film (bulk) rheological measurements!

The effect of steric hardening in very thin asphalt films in the presence of aggregate under long-term storage was investigated next. In these experiments, one film thickness was chosen instead of a wide range of film thicknesses. Twenty-micron films of asphalts AAD-1 and AAG-1 with limestone plates were sheared first to establish a base viscosity, and then were stored at 25°C (77°F) over extended time periods (1, 2, 4, 8 weeks) to investigate the phenomenon of molecular reorganization in thin films. The rates of molecular structuring of asphalt in contact with limestone plates during storage are characterized by means of the ratio of viscosity after and before storage. Figure 5-20 shows the hardening index (viscosity after storage divided by viscosity before storage) versus time periods for SHRP core asphalts AAD-1 and AAG-1. It can be seen clearly that asphalt AAD-1 with limestone plates showed large gains in viscosity with time. This is much larger than steric hardening effects on the bulk asphalt. It is possible that some of the increase is due to oxidative aging, and this point requires validation. Normally, steric hardening effects level off after 8 weeks. However, asphalt AAG-1 showed much less of a tendency for change in viscosity with time than asphalt AAD-1. It is possible that the high levels of highly polar asphaltene components in asphalt AAD-1 may account for the increase in viscosity over extended periods of time at a temperature of 25°C (77°F). This further decreases the predictability of the physical properties of asphalt in pavement.

It is important to understand that the properties of asphalt thin films in the presence of aggregate can be different from the properties of bulk asphalts. They depend upon (1) the nature of the asphalt binder, (2) the structure and uniformity of the aggregate surfaces, (3) the asphalt-aggregate interaction effects, (4) the distance between the surfaces, (5) the direction of shear, and (6) the shear rate.

The results presented here suggest that equating the properties of asphalts in bulk to those in thin films as in pavements may lead to erroneous conclusions with respect to predicted performance. These results show that the viscosity of asphalts in very thin films is remarkably different from the bulk values and that other in-service physical properties may vary significantly for materials of the same PG.

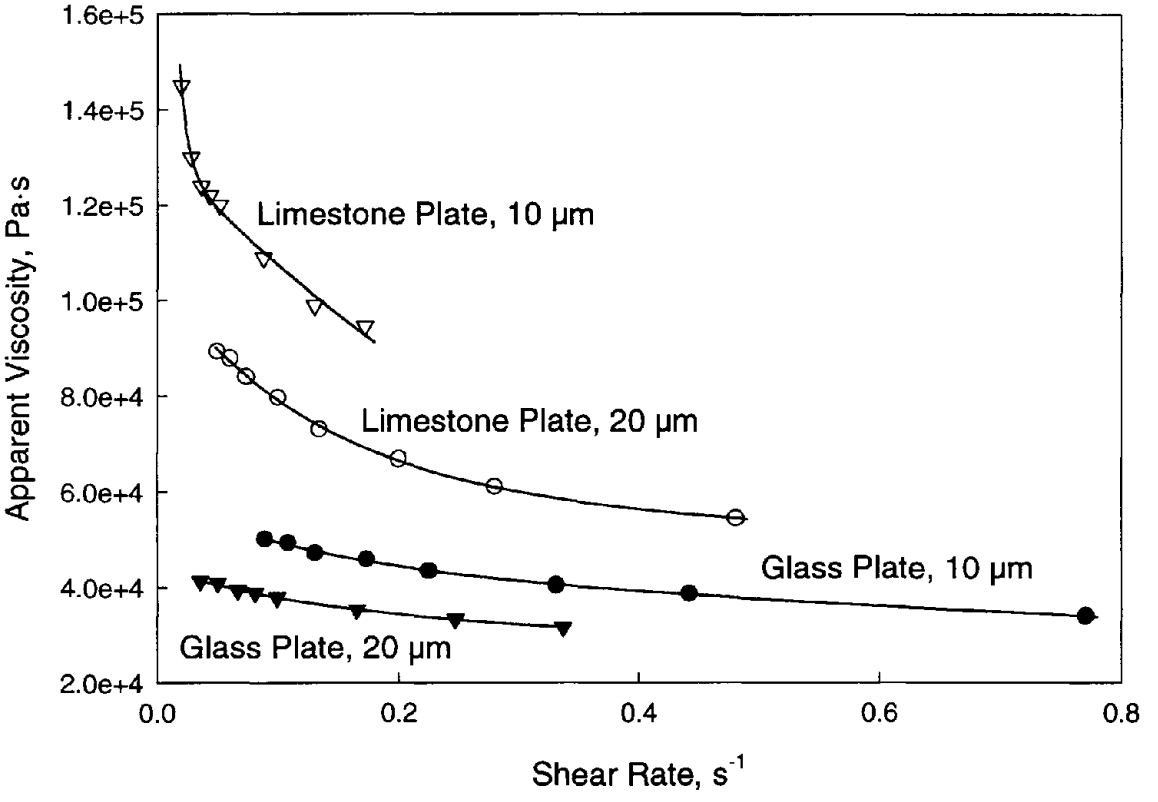

Figure 5-11. Viscosity versus shear rate relationship for AAD-1 at 25°C using glass plates and limestone plates at different film thicknesses.

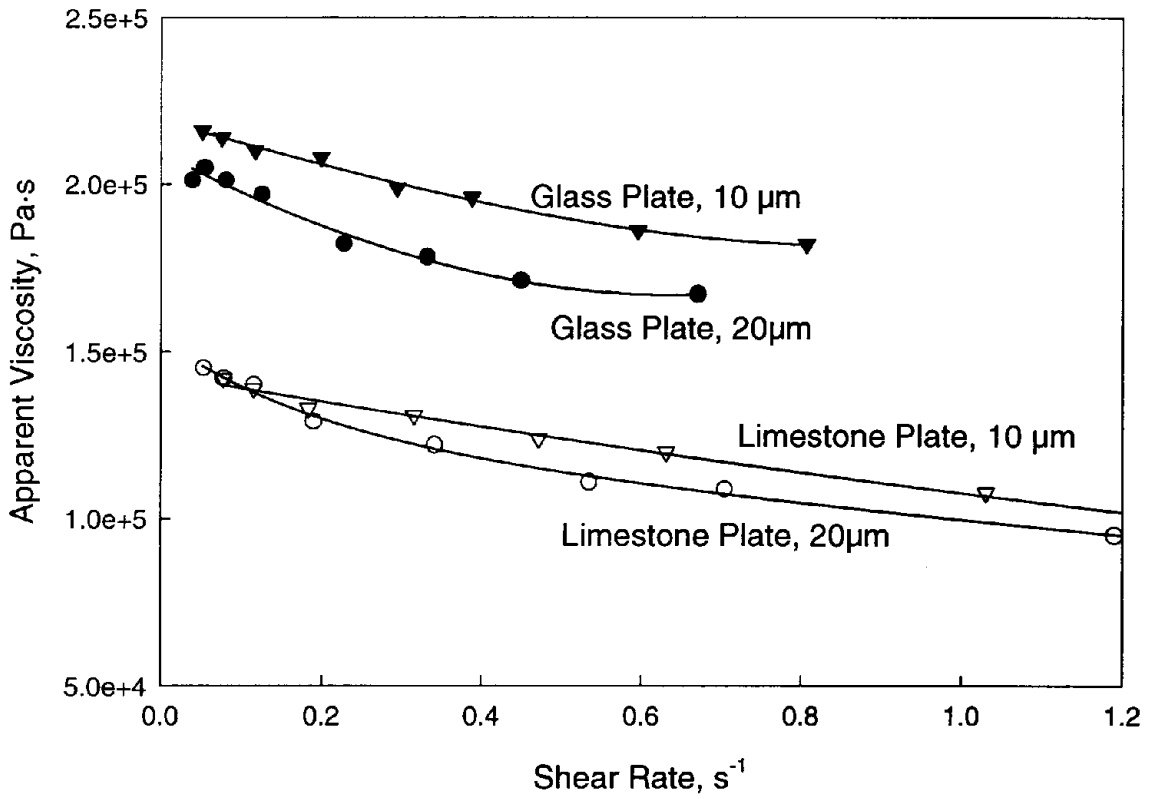

Figure 5-12. Viscosity versus shear rate relationship for AAG-1 at 25°C using glass plates and limestone plates at different film thicknesses.

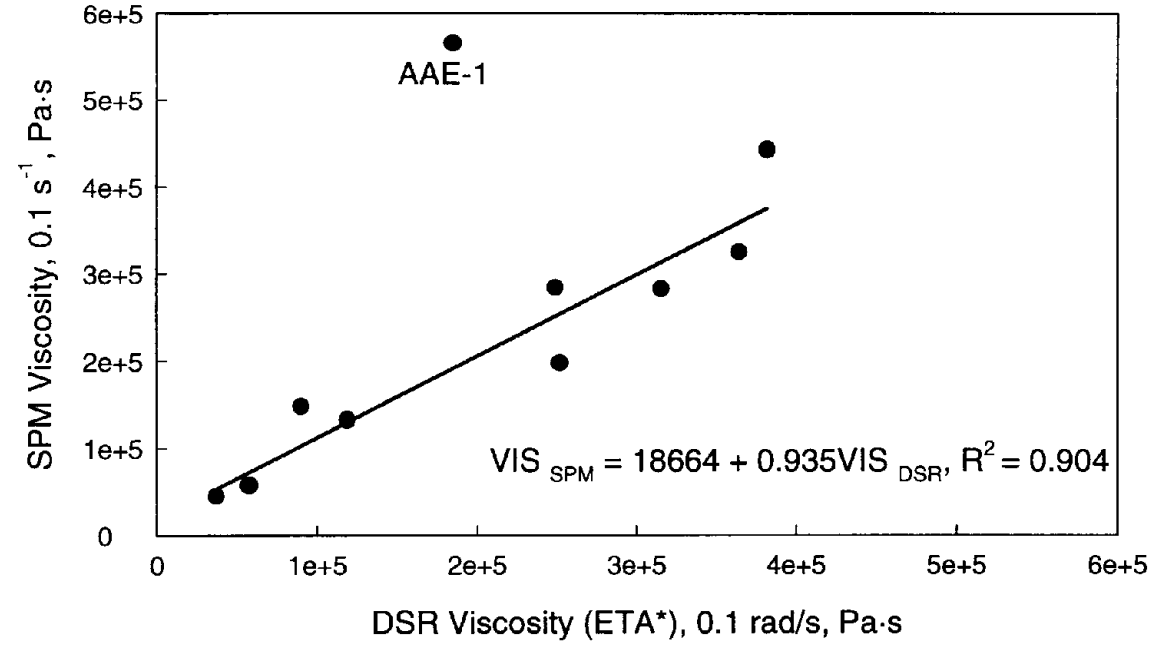

Figure 5-13. Comparison of viscosity measurements by glass sliding plate (SPM) and dynamic shear rheometer (DSR) using 10 SHRP asphalts at 25°C.

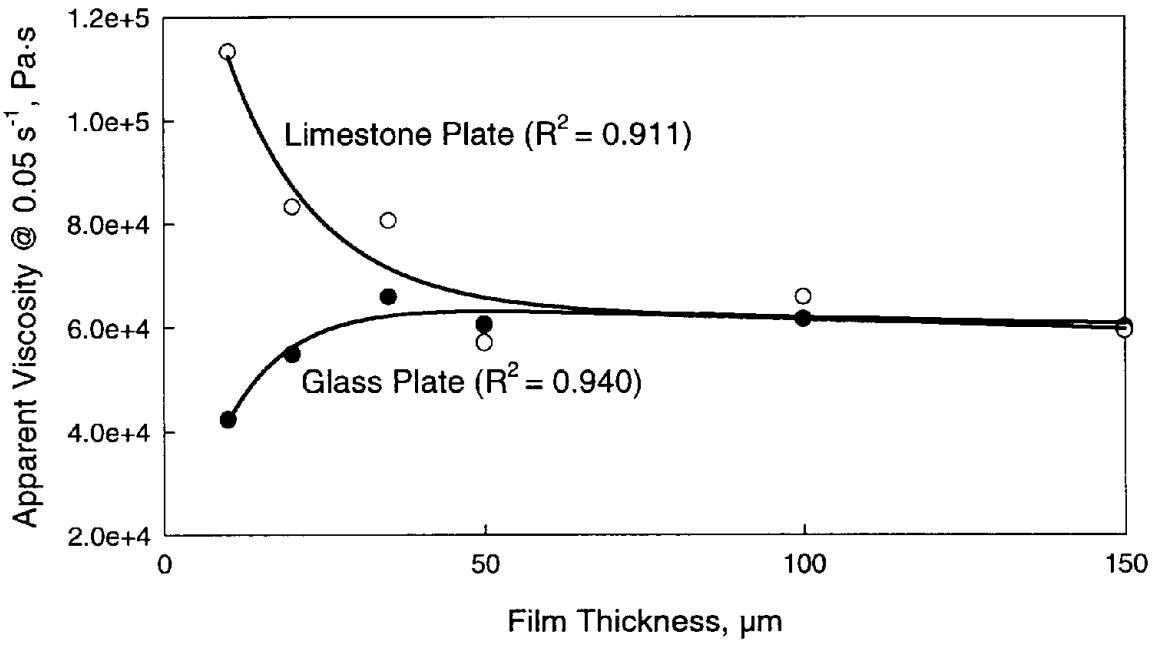

Figure 5-14. Viscosity versus film thickness for asphalt AAD-1 with both glass plates and limestone plates at 25°C.

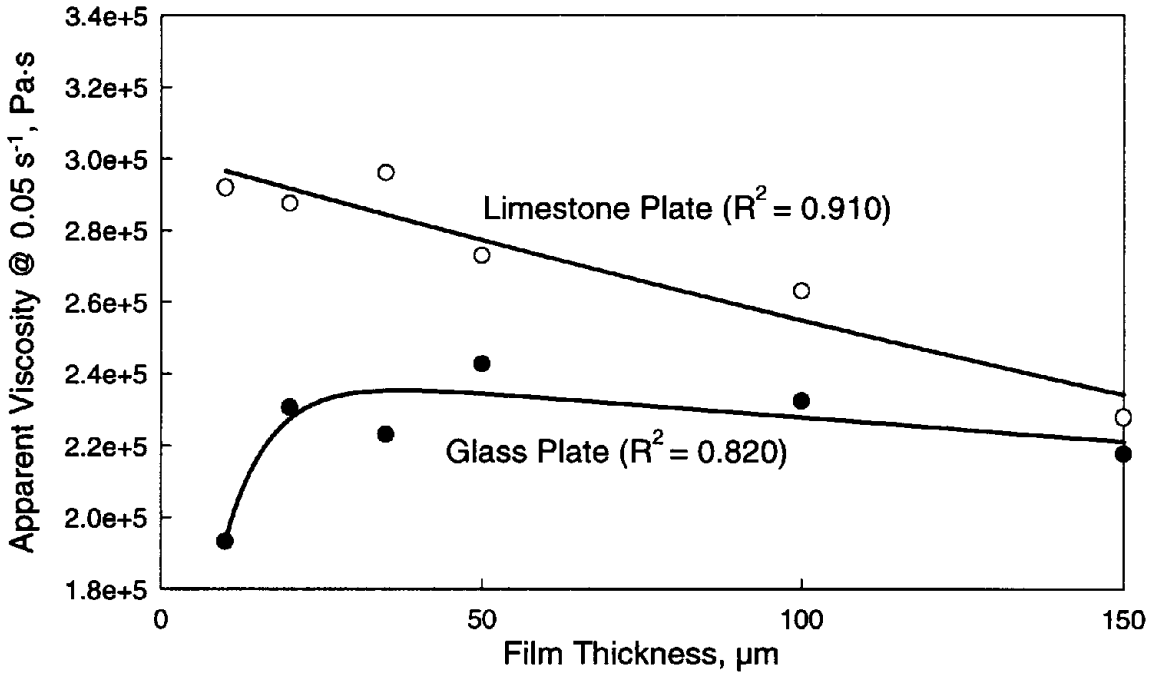

Figure 5-15. Viscosity versus film thickness for asphalt AAK-1 with both glass plates and limestone plates at 25°C.

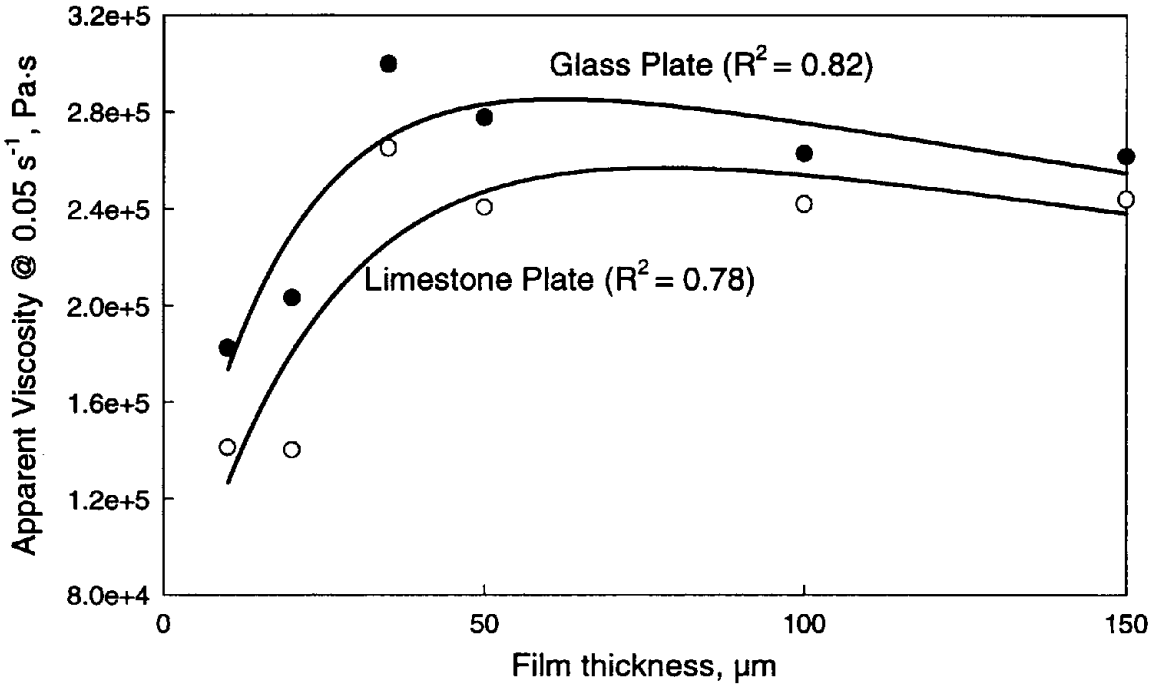

Figure 5-16. Viscosity versus film thickness for asphalt AAG-1 with both glass plates and limestone plates at 25°C.

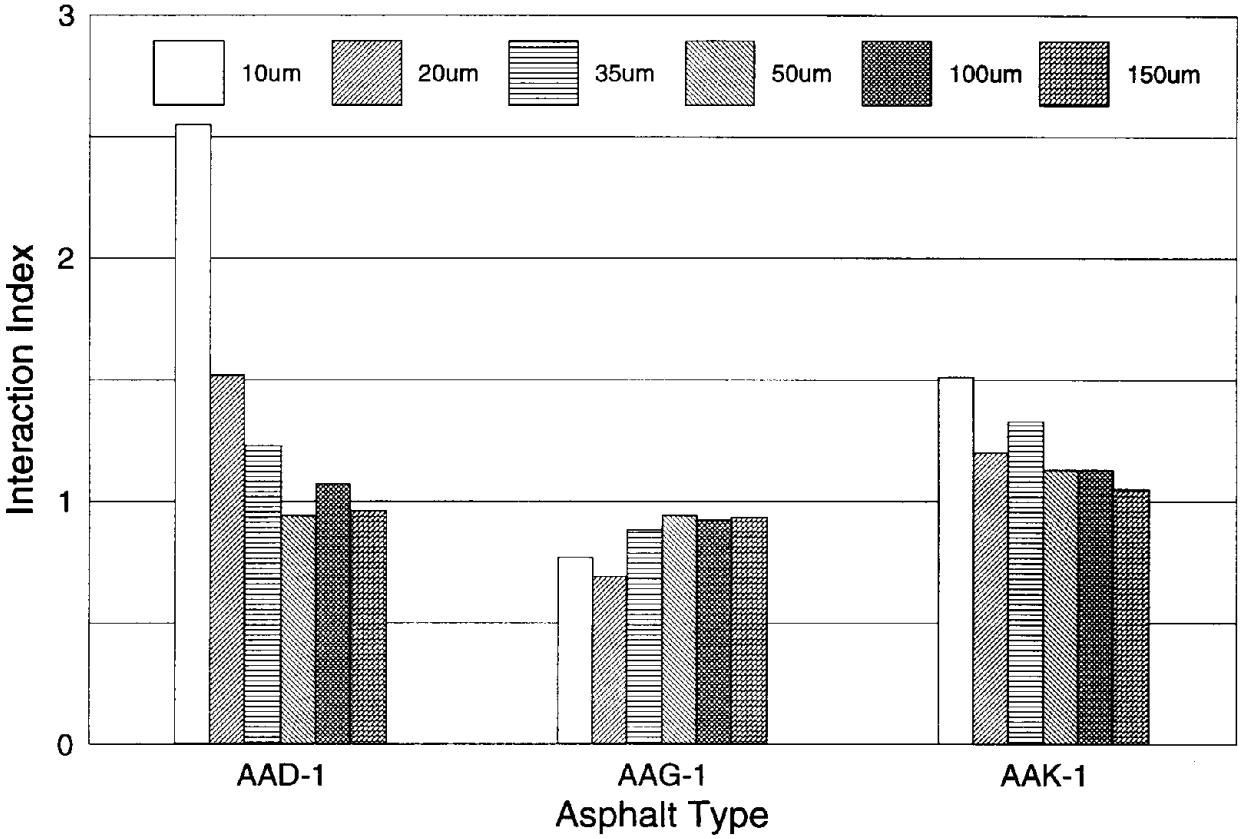

Figure 5-17. Interaction index at different film thicknesses for SHRP core asphalts AAD-1, AAG-1, and AAK-1.

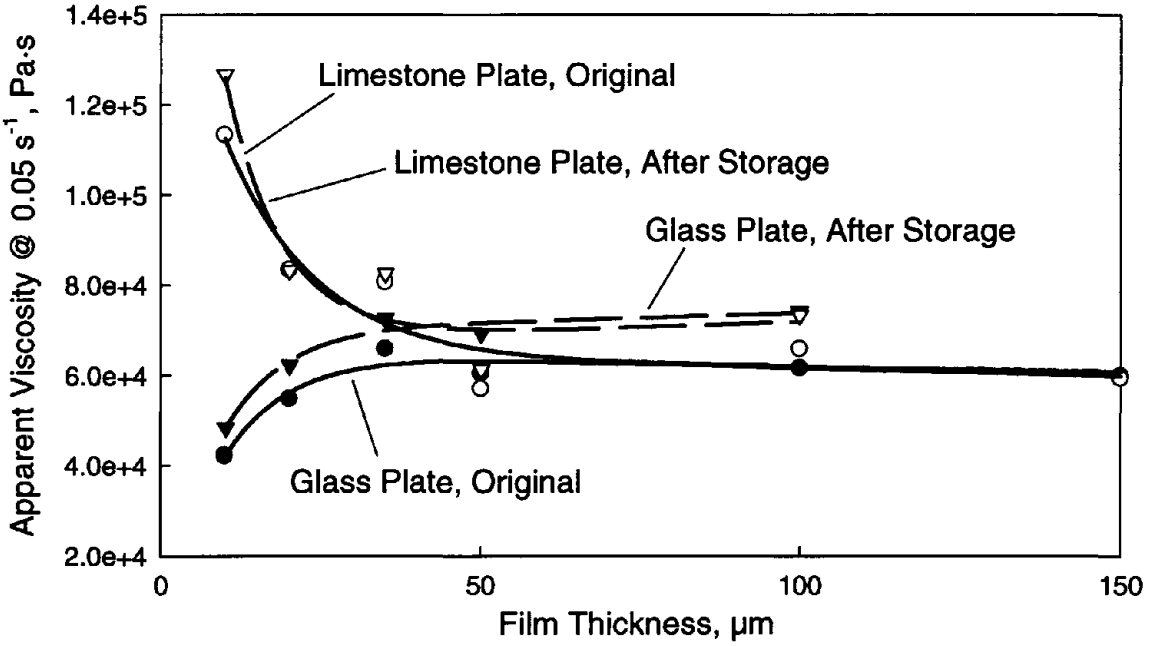

Figure 5-18. Viscosity versus film thickness for asphalt AAD-1 with both glass plates and limestone plates before and after storage at 25°C.

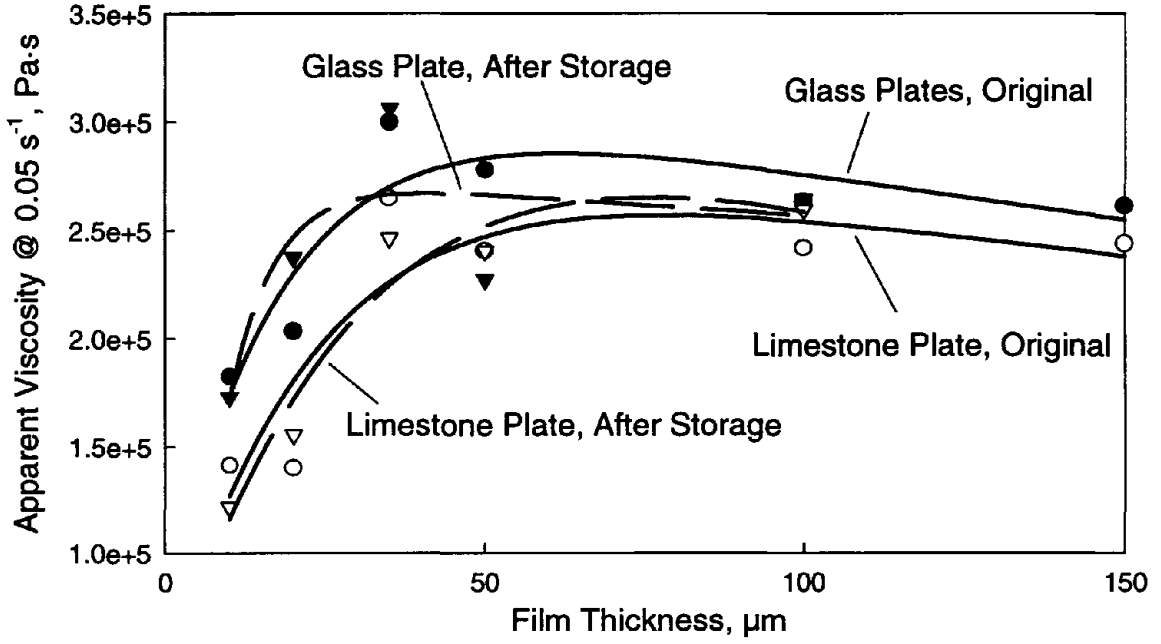

Figure 5-19. Viscosity versus film thickness for asphalt AAG-1 with both glass plates and limestone plates before and after storage at 25°C.

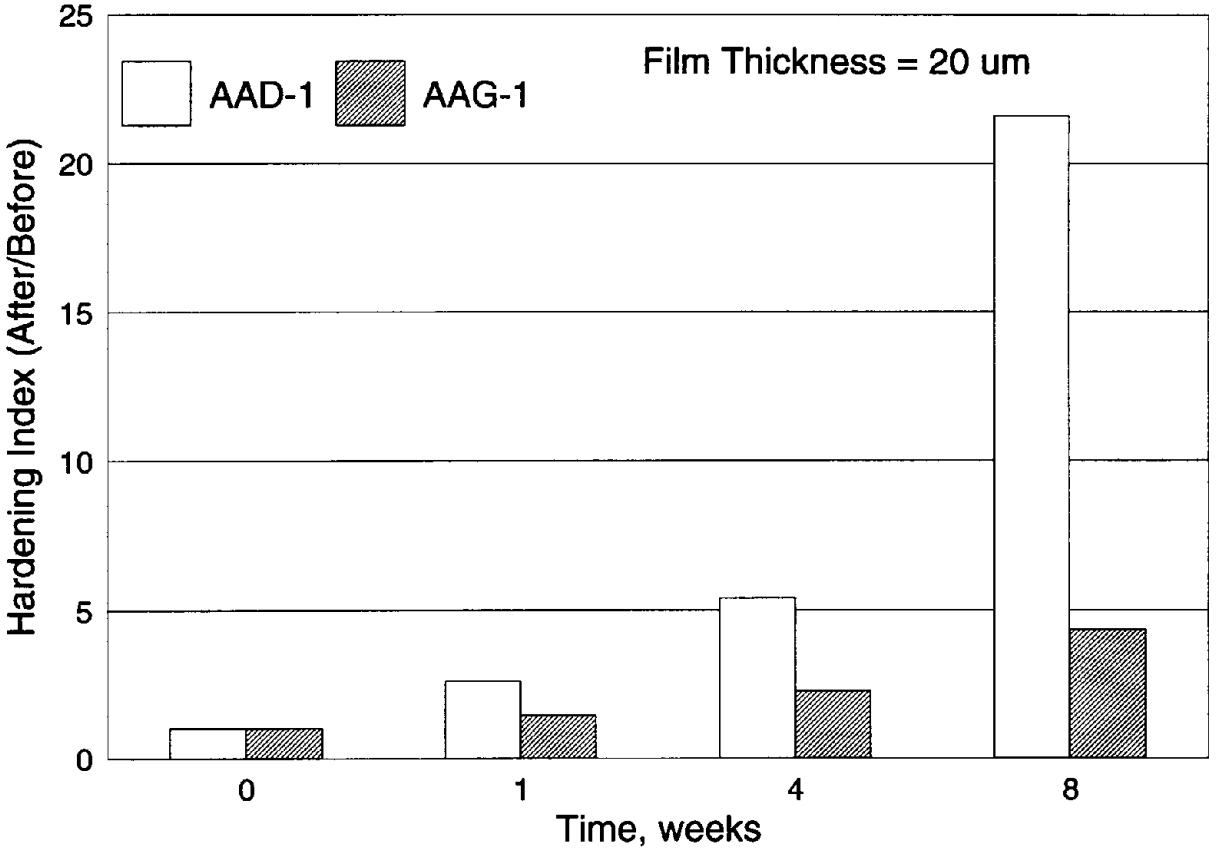

Figure 5-20. Hardening index for SHRP core asphalts AAD-1 and AAG-1 over extended time period of storage at 25°C.

INTERFACIAL ADHESION STRENGTH OF MASTICS MEASURED BY PENETRATION

The phenomenon of physical properties of asphalts becoming altered in the presence of aggregate has been reported previously by Marek and Herrin [1968], Scholz and Brown [1996], and has been observed in sliding plate experiments described elsewhere in this report. It is predictable that the polar surface of an aggregate should induce polarization of polar molecular species in an asphalt that in turn will affect its physical properties. Considering that the distributions of the types and amounts of polars in asphalt vary widely with crude oil source, it is obvious that any change in the physical properties of a tank asphalt being made into a mix will be crude oil composition dependent. Even tank asphalts that are graded alike can be expected to have physical properties that differ from each other when they exist as thin films on aggregate. The associated molecular structures that exist in tank asphalts, that might confer on two different asphalts some similar bulk properties, might be altered differentially in the presence of aggregate. This is obvious from a host of chromatographic separation data. Chromatographic separation sorbants have polar surfaces much like aggregate. Separation of asphalts from different crude oil sources show distinctly different patterns of adsorption (polarization of polar molecules). The classical Corbett analysis is one example of sorption chromatographic separation. It follows that the physical properties of asphalts in a mix will also be changed differentially. This experimental sequence was undertaken to evaluate the magnitude of the differences in binder properties in the presence of aggregate.

Mastics were prepared using SHRP core asphalts and mineral filler prepared from SHRP core aggregates. An Instron 8511 instrument was used to penetrate each sample where sample geometry, penetration tool geometry, and penetration rate were kept constant. Test temperature, the ratio of asphalt to filler, composition of asphalt, and composition of aggregate were varied. The observed stress to achieve a constant rate of penetration was recorded.

Figure 5-21 shows the rather typical response observed for all mastics. There is a relatively constant increase in stress up to a penetration depth of about 0.1 cm in this case, then the rate at which the stress increases diminishes with additional penetration. Possibly this decrease is due to formation of microfractures as the penetration depth increases. However, attention should be focused on the low levels of penetration that are more characteristic of the small strains that asphalt experiences in pavement. Figure 5-22 shows that mastics made of asphalts AAD-1, AAG-1, and AAM-1 exhibit different penetration stresses at 25°C (77°F) when all other variables were held constant. Asphalts AAD-1 and AAM-1, which are different PG of 58-28 and 64-10, respectively, show very similar behavior at low penetration values. The striking feature is that asphalt AAG-1 is quite different from the other two. Originally AAG-1 was graded as a PG58-10, but quite recently Anderson et al. [1995] have shown AAG-1 to be a PG64-10. Regardless of which is the correct high temperature grade, the stress response for asphalt AAG-1 should be more similar to one of the others if all asphalts had very similar physical properties over the entire temperature range of a given PG and responded to aggregate uniformly. Asphalt AAG-1 is the same high temperature grade as one of the others, but shows a different stress response. The other two asphalts, which respond alike, have different high temperature grades. Further, the high and low temperature grades of AAD-1 (PG58-28) and

AAM-1 (PG64-10) are different, yet AAG-1, with the same low temperature grade of -10 as AAM-1, shows a totally different stress response from that of AAM-1. The data in figure 5-22 were collected at 25°C (77°F), a temperature intermediate to the high and low PG classification. Again, it is commonly known that asphalts graded alike have different physical properties at intermediate temperatures. In this experiment, the only alteration to the bulk asphalts was the addition of an aggregate filler. Aggregate may have been expected to enhance or mitigate the differences in physical properties at intermediate temperatures. However, it is concluded from the data, for which figure 5-22 is representative, that this is further evidence that aggregate does not mitigate differential molecular structural arrangements in thin films of asphalt. That is, the differential, or unpredictable, physical properties of an asphalt in a mix are quite significant in the presence of an aggregate. Note in figure 5-22, at a low penetration value of around 0.05 cm, that the difference between two asphalts that are graded alike is about 2 to 1 in penetration value. This is a major difference in physical properties and constitutes an area of unpredictability, or a "hole" in the PG system.

Figure 5-23 shows the data for the same asphalts, aggregates, and all other conditions except for temperature. Here, the data were collected at 40°C (104°F). The stress responses are all more similar to each other than at 25°C (77°F), as shown in figure 5-22. It is concluded from these representative data that the combined effects of the differences among native asphalts together with aggregate diminish sharply from 25°C (77°F) to 40°C (104°F).

This experimental sequence is not intended to predict pavement performance per se, but rather to show that the physical properties of asphalts as thin films on aggregate, which dictate performance, are not readily predictable from bulk asphalt properties. The experimental details for this method are given in Volume II of this report, method 13.

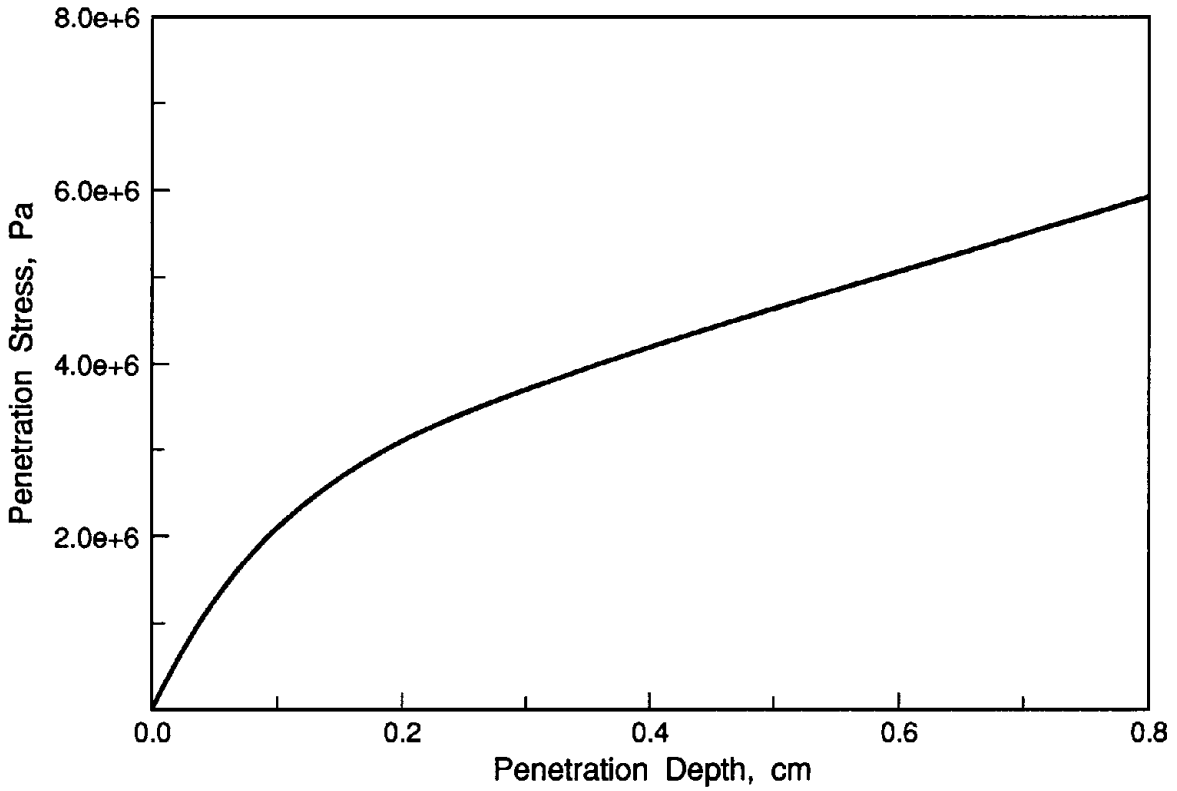

Figure 5-21. Penetration test data for mastic made of 17 mass percent AAA-1 (PG 58-28) and 83 mass percent, -#200 RD filler at 40°C.

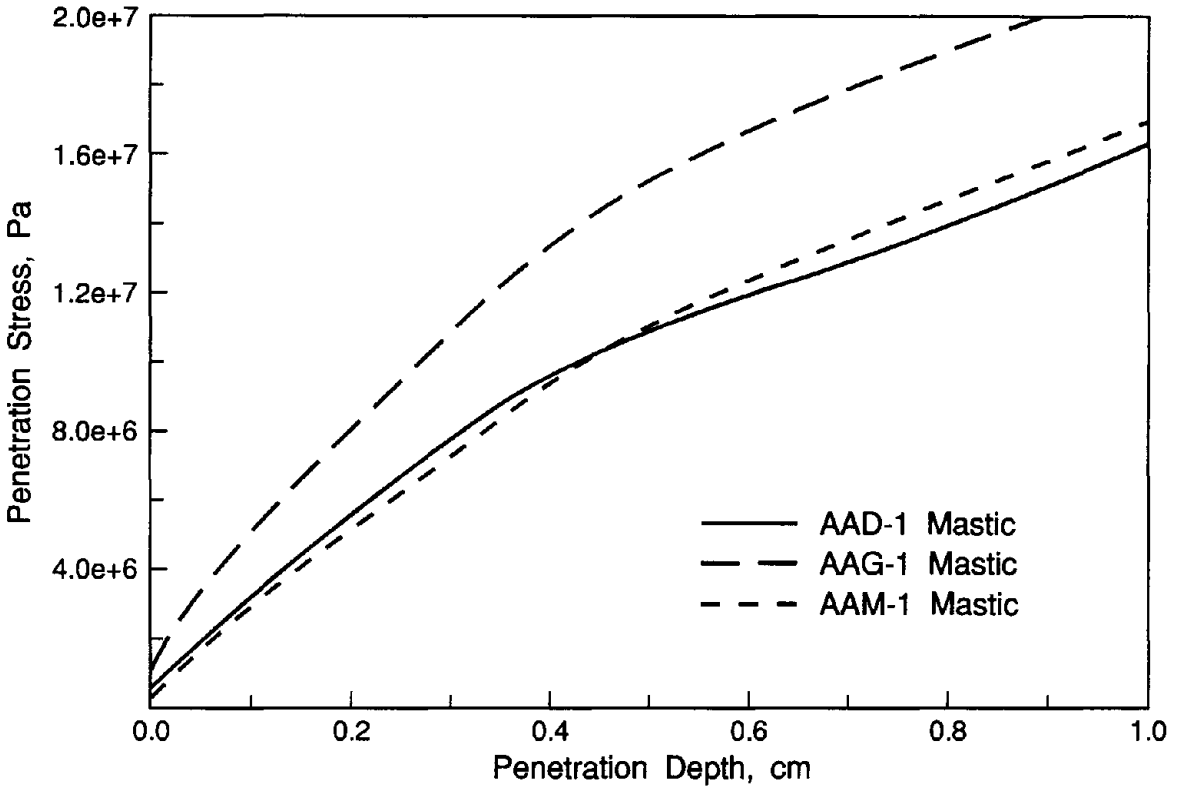

Figure 5-22. Comparison of the penetration test data at 25°C for unaged AAD-1 (PG 58-28), AAG-1 (originally graded as PG 58-10, now graded PG 64-10) and AAM-1 (PG 64-10) mastics made of 85 mass percent, -#200 RD filler.

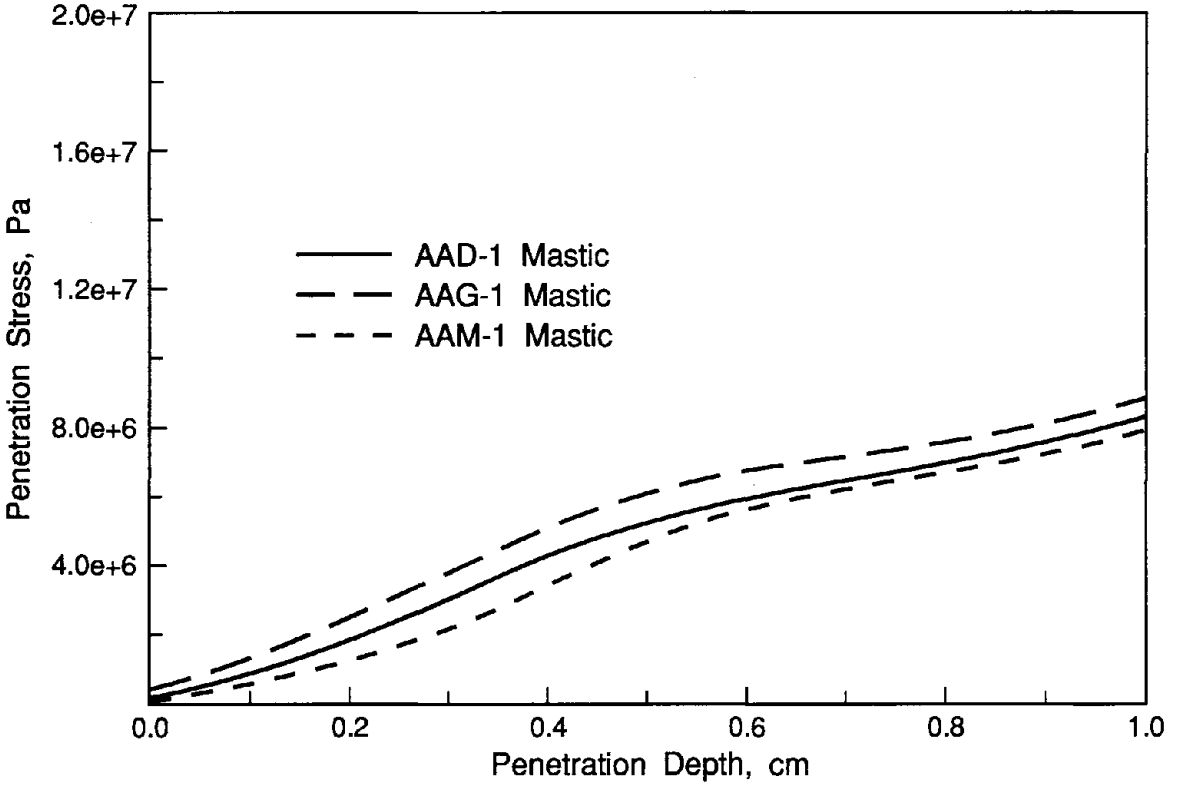

Figure 5-23. Comparison of the penetration test data at 40°C for unaged AAD-1 (PG 58-28), AAG-1 (originally graded as PG 58-10, now graded PG 64-10) and AAM-1 (PG 64-10) mastics made of 85 mass percent, -#200 RD filler.

THE IMPACT OF MOISTURE ON ASPHALT RHEOLOGY AND AGING

The loss of strength in asphalt pavements as a result of the invasion of water, including, in the extreme case, stripping of the asphalt from the aggregate, is one of the principal events that leads to the failure of asphalt pavements. Oxidative aging, which is a chemical change in the condition of the pavement, may also contribute to increased rates of failure and, quite likely, compounds the ill effects of water in pavements. Typically, the Lottman test, the modified Lottman test (AASHTO T-283), or other water immersion tests are used to evaluate moisture damage in cores obtained from pavements [Terrel and Shute 1989]. Another test, which was developed at WRI, that evaluates the propensity of briquets (constructed with a binder and an aggregate) to moisture damage is the water susceptibility test [Plancher et al. 1980]. An additional test method, that is currently under evaluation, is the Pyridine Test, which is described later in this chapter. The limitations of the WRI methods are (1) that the water susceptibility test can be very time consuming and, in some cases, may not be very reliable and (2) both tests do not specifically address the fundamental problem that results in moisture damage of asphalt pavements. However, none of the tests currently used are perfect in predicting the impact of water on asphalt pavements.

The rationale for this task is based upon interesting results of unrelated experiments carried out over the past several years. In 1962 Campbell et al. [1962] determined that temperatures from 43 to 66°C (110 to 150°F) and humidities from 17 to 70 percent have a positive effect on the air oxidation of air-blown asphalts. The effect was measured by monitoring the carbonyl absorbance and the appearance of cracking in thin films of asphalt. Petersen [1967] demonstrated, by soaking (in water) a thin film of Wilmington maltenes spread on a glass plate, that some water was incorporated into the structure of the maltenes through hydrogen bonding. The fact that water was incorporated into the structure of the maltenes was substantiated by IR analysis of a thin film of the maltenes that was spread on a sodium chloride plate. IR spectroscopic analysis of the maltenes dissolved in carbon tetrachloride showed that the water content of the maltenes was 0.3 mass percent. This represents a very significant amount of water incorporated into the asphalt structure. For example, if it is assumed that the molecular weight of an asphalt is 1,500 daltons, then 0.3 mass percent water is 20 mole percent in the asphalt, or there is one water molecule for every four "asphalt" molecules.

A more recent study by Green et al. [1993] showed that, in four of the eight SHRP core asphalts, there exists a variety of sulfur compound types, and the distribution of these sulfur types is very different for the four asphalts. The two major sulfur compound types are thiophenes and aliphatic sulfides. It was concluded by the authors that the oxidation of aliphatic sulfides to sulfoxides would increase asphalt viscosity, but it could also increase the potential for water stripping. Green et al. [1993] concluded that the data indicate that a negative correlation exists between asphalt performance and the amounts of oxidizable sulfur present in asphalt. Mill, in a recent SHRP report [Branthaver et al. 1993b], also concluded that aliphatic sulfides in asphalts are oxidized to sulfoxides but that aryl sulfides and thiophenic sulfur are not affected by thermal oxidation. He went on to state that, due to the growing body of data, this conclusion can probably now be applied to all asphalts.

Of course, not only is the composition of an asphalt important regarding its potential for moisture damage, but so too is the interaction between the asphalt and the aggregate and the composition of the aggregate. In regard to these considerations, the oxygen-containing functional groups present in asphaltenes were shown by Scott [1978] to be the principal components that are involved in the interaction of asphalt with the aggregate surface. The important oxygen-containing functional groups in asphalts are ketones, anhydrides, carboxylic acids, sulfoxides, and phenols. Carboxylic acids and phenols may form strong bonds with aggregate surfaces by means of hydrogen bonding. Unfortunately, the presence of water can disrupt the hydrogen bond between carboxylic acids and the aggregate surface, thus weakening the interaction between the asphalt and the aggregate [Plancher et al. 1977]. In addition, the strength of this interaction is adversely affected by the presence of sodium and potassium ions in the aggregate because their salts are usually quite soluble in water. It was proposed by Scott that a simple method of evaluating the susceptibility of aggregates to water stripping might be the determination of the amounts of these ions in aqueous solution. As suggested by Scott [1978], a recent study by Podoll et al. [1991] showed that aggregate RC, a limestone that was the most soluble in water of the aggregates tested, was also the aggregate that was most prone to water stripping when used in mixes with asphalts. However, this type of limestone is not usually used in asphalt pavement applications.

Based upon the results reported in the literature cited above, it is apparent that water can be incorporated into the structure of an asphalt, thus affecting its hydrogen bonding characteristics. Water can also attack the aggregate surface, thereby disrupting the asphalt-aggregate bond. Therefore, asphalts that are classified as being equivalent by, for example, PG, may perform differently in asphalt concretes as a result of their interaction with water. The reader is reminded that there is no current specification that addresses the effects of water on the performance of asphalt concrete that can be related to the properties of the binder. Thus, the object of this study is to answer the following fundamental question. Does the incorporation of water into asphalt binders disproportionately produce different building materials from binders that were originally graded alike?

The obvious advantage of knowing the deleterious effects of water on asphalt is to be able to exclude from consideration unsuitable binders at the earliest point in the purchase process. Further, and maybe more important, in the current road construction industry equivalent PG's can be used interchangeably, and there is no differentiation between asphalts based on the effects of the water that will eventually be part of every asphalt pavement.

Treatment of Asphalts with Water

The initial experiments addressed determination of the most appropriate method for incorporating water into the asphalt. The proposed methods included soaking asphalt samples in a closed container of water at room temperature, soaking asphalt samples in a closed container of water at an elevated temperature, and exposing asphalt samples to controlled humidity and temperature (ASTM method D 1412 [ASTM 1992]). These three methods were evaluated using unaged AAD-1, an asphalt that is reported to be susceptible to moisture damage. The results of this testing are shown in figure 5-24. For this preliminary work, the

asphalt was not thermally aged because the goal of this first part of the task was to determine what method results in the incorporation of water into the asphalt structure. Shown in the figure is the value of G* at 58°C (136°F) and 10 rad/s for samples of AAD-1 that were soaked in deionized water for different lengths of time and at different temperatures. For comparison, G* versus time for AAD-1 at 20°C (68°F) in a static, dry nitrogen atmosphere is also shown in the figure. These latter data represent the base case or the control for the data set. The values determined for the samples exposed to water (or to 96 percent relative humidity) are the average of the analysis of two different samples, while the data for the samples exposed to dry nitrogen are the results of the analysis of single samples. The duplicate values obtained for the samples exposed to water were well within the experimental error as stated by the manufacturer of the rheometer, that is, less than 10 percent, and typically the variation was less than 5 percent. Consequently, it was concluded that in the future the analysis of single samples was warranted. As a point of reference for the reader, there are 168 hours in 1 week and about 720 hours in 1 month (30 days).

From the results of these short-duration, scouting experiments, the following conclusions are drawn. First, at a constant temperature, there appears to be a direct correlation between G* and time. Second, at a constant time and independent of water treatment, there is a direct correlation between G* and temperature. Third, the increase in G* with time could simply be the result of steric hardening.

In light of these results, the investigation was expanded by including AAM-1 and AAG-1, in addition to AAD-1, in the experimental matrix and conducting the experiments at 60°C (140°F). Asphalt AAM-1 was included because it is reported to be not susceptible to moisture damage, while AAG-1 was included because it is a lime-treated asphalt, thus mitigating its susceptibility to moisture damage. The rheological results of these experiments are shown in figure 5-25 and will be discussed later. In Volume II (figures 10-2 through 10-7) are shown additional rheological and IR data that demonstrate that the level of oxidation for each pair of samples, a control sample (in an inert atmosphere) and a test sample (in deionized water), is comparable. It is important that comparisons made between pairs of samples be made at the same level of oxidation. Thus, the impact of oxidation on the sample pair, as regards to its influence on G*, is negated. Notice in paired figures 10-2 and 3 and 10-6 and 7 of Volume II, two sets of data are shown that demonstrate the impact of oxidation on the rheological properties of AAD-1 and AAM-1.

For the work described in this section, the level of oxidation of the asphalts was monitored by obtaining their IR spectra and by measuring the total area under the carbonyl peak centering at 1,700 cm^{-1} and the sulfoxide peak centering at 1,030 cm^{-1}. It is realized that small amounts of other compounds may be generated during the oxidation of asphalt, for example carboxylic acids, sulfones, sulfonic acids, etc. However, to simplify the analysis procedure, the amounts of these types of compounds were not determined.

In figure 5-25 are shown plots of G* versus time for samples of unaged AAD-1, AAG-1, and AAM-1 stored in either an inert atmosphere (nitrogen or argon) or in water at 60°C (140°F). From these data, the following conclusions are drawn. First, it appears that, apparently, for

AAD-1 and, more emphatically, for AAM-1 the rate of change in G* with time is unaffected by water relative to the control experiment. Second, for AAG-1 it appears that the rate of increase in G* with time is mitigated by water relative to the control. Third, it is proposed that the increase in G* for AAD-1 and AAG-1 is the result of steric hardening and that steric hardening can occur in the presence of water. Thus, it appears that for AAG-1 the water molecules are interfering with the structuring that this asphalt undergoes with time. Shown in Volume II, figures 10-8 and 10-9, are G′ (the storage or elastic modulus) and G″ (the viscous flow or loss modulus), respectively, for the three unaged asphalts. Increasing values of G′ are primarily the result of structuring or aggregation of the polar compounds in the asphalt, while G″ is associated with the non-polar, neutral components in the asphalt [Branthaver et al. 1993c]. These materials may be separated from asphalts by IEC. The variation in G′, as shown in figure 10-8 of Volume II, appears to be minimal except for possibly AAD-1. However, in this case the changes are judged to be inconclusive. On the other hand, the variation in G″, as shown in figure 10-9 of Volume II, is much more significant and parallels the trends shown in figure 5-25 of this volume. Thus, under these conditions of sample aging and temperature, G″ dominates the rheological properties of the three asphalts. (The scale for these two figures is the same as that for G* to demonstrate that G″ is the significant parameter.) As mentioned above, changes in G″ are associated with the IEC neutral fraction. Elemental analysis of the IEC neutral fraction from AAG-1 shows that of the eight SHRP core asphalts, it contains the highest percentage of nitrogen (0.2 mass percent) and has the lowest H/C atomic ratio (1.47), indicating greater aromaticity and some polarity, and therefore the possibility of weak intermolecular interactions. Thus, it is possible that the increase in G″ with time may be the result of increases in the effective molecular size of the IEC neutral fraction as a result of polar interactions and/or pi-pi interactions between aromatic structures.

To assess the effect of oxidative aging on the impact of water on G*, AAD-1, AAG-1, and AAM-1 were artificially aged using the standard Superpave® RTFO and PAV procedures. As described above for the unaged samples, these aged samples were stored at 60°C (140°F) in an inert atmosphere or in deionized water. The rheological results, G*, for these three asphalts after treatment are shown in figure 5-26 of this volume. In Volume II, figures 10-10 through 10-15, are shown additional rheological and IR data that demonstrate that the level of oxidation for each pair of samples (control sample in an inert atmosphere and test sample in deionized water) is equivalent. From these data, the following conclusions are drawn. First, it appears that for aged AAM-1 the rate of increase in G* with time is unaffected by water relative to the control experiment conducted in an inert atmosphere. Second, for aged AAD-1, and possibly for aged AAG-1, it appears that the rate of increase in G* with time is mitigated by water relative to the control. These results are different from those observed for the unaged asphalts, see figure 5-25 (this volume). Third, it is again proposed that the increase in G* for the three asphalts studied in this experiment is the result of steric hardening and that steric hardening occurs in the presence of water. Thus, it appears in this case that for RTFO/PAV-aged AAD-1, and possibly for AAG-1, water does influence the molecular structuring in asphalts that leads to steric hardening. Shown in Volume II, figures 10-16 and 17, are G′ and G″, respectively, for the three RTFO/PAV-aged asphalts. The variation in G′, as shown in Volume II, figure 10-16, appears to be minimal except for AAD-1. As mentioned above, changes in G′ are attributed to structuring of the polar compounds in the asphalt. Oxidative aging of these three asphalts has resulted in

products that contain significantly increased levels of oxygen-containing compounds. Compare the IR data shown in figures 10-3, 5, and 7 of Volume II with that shown in figures 10-11, 13, and 15 of Volume II. During oxidation the formation of additional mono-functional and multi-functional compounds occurs. However, from the model compound studies described by Branthaver et al. [1993d], mono-functional compounds can form dimers that have less of an impact on viscosity than di-functional and multi-functional compounds, which can have a significant impact on the viscosity of the asphalt. Consequently, consideration of only the increase in the oxygen content or the amount of carbonyl and sulfoxide compounds does not necessarily correlate with increases in the rheological properties of asphalts. Apparently, the oxidation of AAD-1 has resulted in the formation of multi-functional compounds that are involved in hydrogen bonding to a greater extent than the products of oxidation found in RTFO/PAV-aged AAG-1 and AAM-1. Consequently, the incorporation of water into this developing structure in AAD-1 results in mitigation of hydrogen bonding, and thus, has an effect on the elastic (storage) modulus (G'). The variation in G'', as shown in figure 10-17 of Volume II, is comparable to that shown in figure 10-16 of Volume II and, of course, figure 5-26 (this volume). This implies that as a result of oxidation the production of the appropriate mono-functional compounds is more prevalent in AAD-1 than in AAG-1 and AAM-1. As mentioned above, the dimerization of mono-functional compounds such as carboxylic acids can also result in increases in the rheological properties of asphalt through the production of complexes that have an increased apparent molecular weight. As discussed above for G', the incorporation of water into this developing structure in AAD-1 results in mitigation of hydrogen bonding, and thus, also has an affect on, in this case, the viscous flow modulus (G'').

An interesting observation was made regarding the rheological data collected for the aged asphalt samples. Shown in figure 5-27 is a plot of the normalized percent change in G* for the RTFO/PAV-aged asphalts versus time of treatment. The normalized percent change in G* for each time is calculated by subtracting G* for the control (dry) from the G* for the test (wet) sample, dividing the result by the G* for the control, and then multiplying by 100. The relative position and shape of the curves for the three asphalts are comparable to data collected for the same three asphalts studied by Nguyen et al. [1994]. In their work the authors were studying the rate of migration of water through thin films (60 μm) of unaged asphalt and the consequent loss of adhesion of 200-μm-thick asphalt films to a granite substrate. In figure 5-28 is shown their plot of water thickness versus time. From their data Nguyen et al. conclude that the migration rate of water through the three asphalts is of the order AAD>AAG>AAM and that the loss of adhesion follows the same order. These results parallel what has been observed during this project regarding the rheological properties of the RTFO/PAV-aged asphalts soaked in water. The correlation between these two different sets of data seems to imply that the concentration of compounds containing functional groups not only has an impact on the rheological properties of asphalts but, apparently, aids in the transport of water through the asphalt to the aggregate surface.

The determination of the amount of water that is incorporated into the asphalt structure was accomplished using a procedure that was developed for the measurement of water in organic solvents and inorganic hydrates [Critchfield and Bishop 1961] and, subsequently, applied to coals [Netzel et al. 1996]. The procedure is described in Volume II, method 10.

Briefly, the procedure relies upon the catalytic reaction of 2,2-dimethoxypropane with water to produce acetone. Subsequently, the IR carbonyl absorption of acetone is quantified. Shown in figures 5-29 and 5-30 (this volume) are plots of the amount of water incorporated with time into the structure of unaged and RTFO/PAV-aged asphalts, respectively. The data that are shown are the results of only single determinations, thus, they are considered to be preliminary at this time. However, based on these preliminary results the following tentative conclusions are drawn. As one would expect, the percentage of water increases with time, and the more polar RTFO/PAV-aged asphalts tend to absorb more water than the unaged asphalts. Of course, the procedure that is being used here to measure the incorporation of water does not distinguish between hydrogen-bonded water and free water existing as an emulsion. Thus, it is assumed that the water in these samples is involved in both hydrogen bonding with polar compounds (dissolved water) and may also exist as micro droplets of free water (an emulsion).

To evaluate the impact of water on aging, three RTFO-aged SHRP asphalts were subjected to PAV aging while in the presence of water. The water was contained in a pan in the aging vessel while aging of the three asphalts was being conducted. The three asphalts aged were AAD-1, AAG-1, and AAM-1. The variables studied during aging were time (0 to 480 hours) and temperature (60 and 80°C [140 and 176°F]). A control experiment was also conducted in which the pan of water was eliminated from the aging vessel. The results of the IR analysis of the samples is contained in Volume II, figures 10-18 and 10-19. Rheological analysis of the samples of PAV aged at 80°C (176°F) was conducted, and a plot of G* versus time is presented in figure 5-31 (this volume). These results show that the effect of the presence of water, during PAV aging on G* of the three asphalts, is varied. The order of impact of the presence of water during aging on G* is AAD>AAM>AAG. Based on these results it is concluded that the presence of water during aging can promote the oxidation of asphalts (see figures 10-18 and 10-19 in Volume II) and affect the resultant rheological properties of asphalts. In the asphalts studied, the effect is most pronounced on AAD-1 and is least pronounced on AAG-1. This order is different from what was observed above when oxygen was not included in the experimental environment. Thus, it has been demonstrated that, for two asphalts originally similar based on PG, the results of oxidative aging in the presence of water are different from the results in the absence of water.

Infrared Reflectance Spectroscopic Study

The investigation of the premise that asphalt molecules slowly migrate to and possibly orient themselves with respect to the aggregate surface [Henniker 1949; Ensley 1975] was investigated using IR reflectance spectroscopy (IRRS). IRRS is an extremely useful technique for dealing with materials, such as asphalt, that are difficult to analyze by transmission IR spectroscopy [Jemison et al. 1992]. IRRS measurements are made by using an attenuated total reflectance (ATR) element in contact with the sample surface. The ATR element used in this experiment is a zinc selenide (ZnSe) crystal. The ZnSe crystal has a 45° face angle, which results in a depth of penetration into the sample of about 10μm. A liquid vessel cell was used to hold the ZnSe crystal and the asphalt sample. This accessory allows the ATR crystal and the sample to remain undisturbed for extended periods of time.

In essence, the liquid vessel cell is a rectangular metal box that holds the ZnSe crystal locked into a fixed central position. Asphalt is then poured into the remaining space on either side of the crystal. The crystal is oriented in the cell such that the two reflecting surfaces of the crystal are adjacent to the asphalt. During the spectroscopic measurement, the IR (light) beam impinges onto the face of the crystal, traverses the face, and travels the length of the interior of the crystal, rebounding off the two crystal faces that are adjacent to the sample. In this case, the crystal was a parallelogram 6 x 6 x 60 mm long. The attenuated beam is then detected by a photomultiplier tube and electronically converted into an absorbance signal that is stored in the memory of the computer of the instrument.

The initial experiment was conducted using unaged asphalt AAD-1. The sample contained in the liquid vessel cell was stored under a blanket of argon at 60°C (140°F) for an extended period of time. Periodically, the cell was removed from the oven, and an IR spectrum was obtained. In spite of the exclusion of added oxygen to the cell, an increase in the carbonyl region of the spectrum with time was noted. No increase in the sulfoxide region of the spectra was noted during the course of the experiment. Consequently, the experimental matrix was expanded to include AAG-1. However, in this case the samples of AAD-1 and AAG-1 were stored under argon at 100°C (212°F) and at 30°C (86°F). It was anticipated that changes in temperature would result in changes in the rate of increase in the carbonyl region due to the change in the viscosity of the asphalts. Asphalts AAD-1 and AAG-1 were chosen because of their high polarity. Asphalt AAD-1 has a high percentage of carboxylic acids when compared with asphalt AAG-1. Conversely, AAG-1 has a high percentage of carboxylic acid salts when compared with AAD-1. Asphalts AAD-1 and AAG-1 have comparable amounts of sulfoxides [Branthaver et al. 1993e].

The spectra that have been collected throughout the experiments were converted to absorbance spectra and analyzed using QuantBasic®. The relative amounts of carbonyls and sulfoxides were obtained and plotted with respect to time. The results are shown in figures 5-32 and 5-33. It appears that the concentration of compounds containing a carbonyl functional group is increasing at the crystal surface. In addition, the rate of migration is apparently the same for AAD-1 at both 60°C (140°F) and at 100°C (212°F). In hindsight, the increase in the temperature from 60 (140°F) to 100°C (212°F) may not have been sufficient to observe a change in the rate of migration. This increase is only about 12 percent when the temperatures are converted to a Kelvin basis, which is the basis normally used for kinetic calculations. In addition, the resulting volumetric expansion of the asphalt due to the increase in temperature is only about 2 percent [Anderson et al. 1994]. Thus, this increase in temperature and volume of the asphalt may not have been enough to affect the rate of migration of compounds through the bulk asphalt. The concentration of carbonyls at the crystal face for AAG-1 at 100°C (212°F) after 1,700 hours is four times greater than the concentration for AAD-1 at 100°C (212°F) after 1,700 hours. This happens to parallel the concentrations of carboxylic acids (0.015 moles/L) in AAD-1 and carboxylic acid salts (0.055 moles/L) in AAG-1 [Branthaver et al. 1993e]. As a result of the leakage of asphalt from the liquid vessel cell, it might be argued that oxidation may be a possible explanation for the increasing concentrations of carbonyl compounds at the crystal face. However, since the concentration of sulfoxides is not increasing in either sample at 60°C (140°F) or 100°C (212°F), oxidation of the asphalt is probably not occurring. No increase in the

carbonyl or sulfoxide content was observed for the two asphalts stored at 30°C (86°F) after more than 2,000 hours. This probably indicates that at 30°C (86°F) the rate of migration of the polar compounds is decreased such that the time frame of the experiment is too short to notice an increase in the relative amount of carbonyls. The identification of increasing relative amounts of carbonyl compounds at the crystal surface appears to support the view that with time the polar asphalt molecules migrate to the aggregate surface and are the basis for the asphalt-aggregate interaction [Scott 1978; Plancher et al. 1977].

A possible explanation for why this occurs is that an acid-base interaction may be occurring between the ZnSe crystal and the compounds in asphalt that contain carbonyl functional groups. The zinc ion (Zn^{+2}) is a borderline soft Lewis acid and the selenium ion (Se^{-2}) is a soft Lewis base. Lewis acids will accept an electron pair and Lewis bases will donate an electron pair. As a general rule of thumb, soft acids tend to bind to soft bases and hard acids tend to bind to hard bases [Shriver et al. 1990]. Knowing this, one can conclude that the Zn^{+2} is acting as a soft acid as it binds to the soft base, Se^{-2}, to form ZnSe. Although no specific information could be located on the acidic or basic nature of ZnSe, two similar compounds were identified. Zinc compounds formed with other Lewis bases in the same group of the periodic table as selenium, that is oxygen and sulfur, were considered. Zinc oxide is categorized as amphoteric, while zinc sulfide is a Lewis acid [Tanabe et al. 1989]. This would lead us to believe that ZnSe is probably also a Lewis acid. The carbonyl group consists of a carbon-oxygen double bond [Ege 1989]. The non-bonding electrons of the oxygen in the carbonyl group cause compounds containing this functional group to act as Lewis bases, electron donors [Luder and Zuffanti 1961]. If indeed ZnSe is a Lewis acid, the attraction of a Lewis base, such as the carbonyl group, could explain the mechanism, acid-base interaction, for the observed increase in concentration of carbonyl compounds at the surface of the crystal.

Steric hardening of asphalt with time is an accepted, but so far poorly quantified, phenomenon that occurs in pavements, and, apparently, this process also occurs even when the asphalt is submerged in water. However, in some cases the presence of water mitigates the steric hardening process. It is proposed that water mitigates steric hardening by interfering with the formation of hydrogen bonds between the appropriate polar compounds in asphalt. The mitigation of hydrogen bonding results in a decrease in the rate of the normal and gradual increasing stiffness of asphalt with time.

Very preliminary data indicate that water is incorporated into asphalt, and the amount increases with time and the level of aging of the asphalt. Since the procedure that was used to measure the amount of water does not discriminate between bound water and free water, it is assumed that the water in asphalt is involved in both hydrogen bonding with polar compounds and may also exist as micro droplets of free water.

Using the IRRS technique it was demonstrated that with time carbonyl-containing compounds, such as ketones and carboxylic acids, migrate to a crystal surface, such as ZnSe. This appears to substantiate what others have believed in that it is the polar compounds in asphalt that bind with the aggregate, resulting in the asphalt-aggregate interaction.

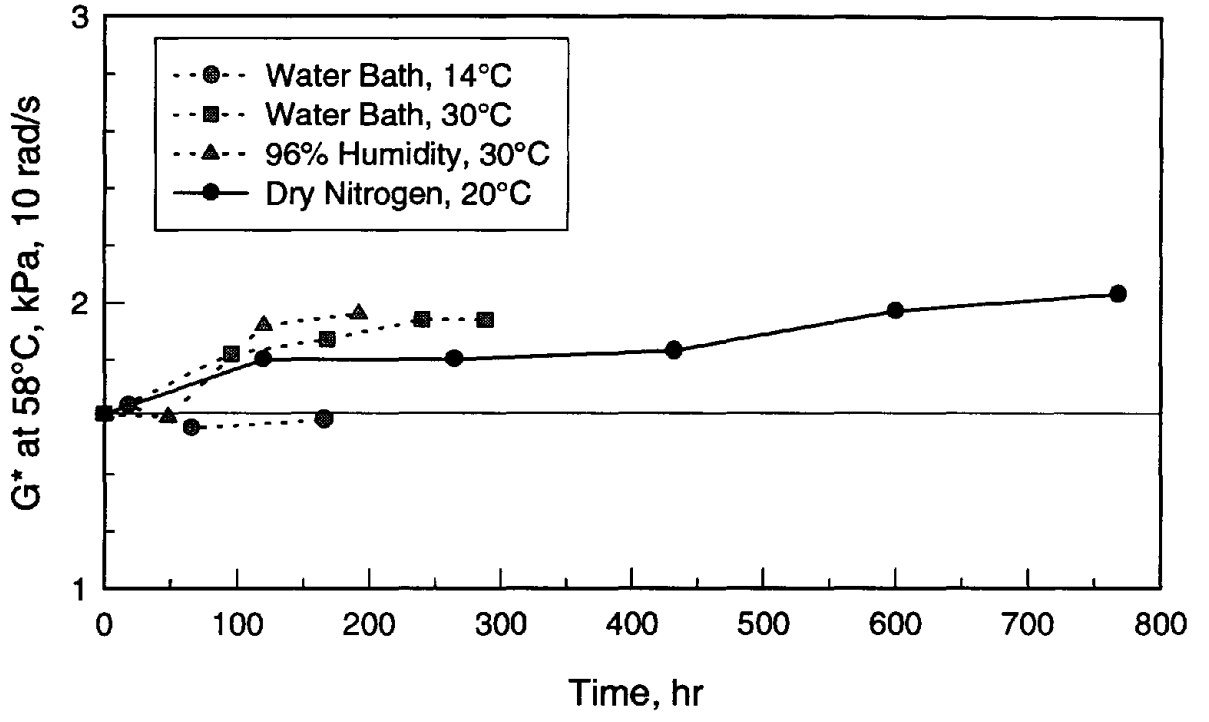

Figure 5-24. The change in G* with time for asphalt AAD-1 following various treatments.

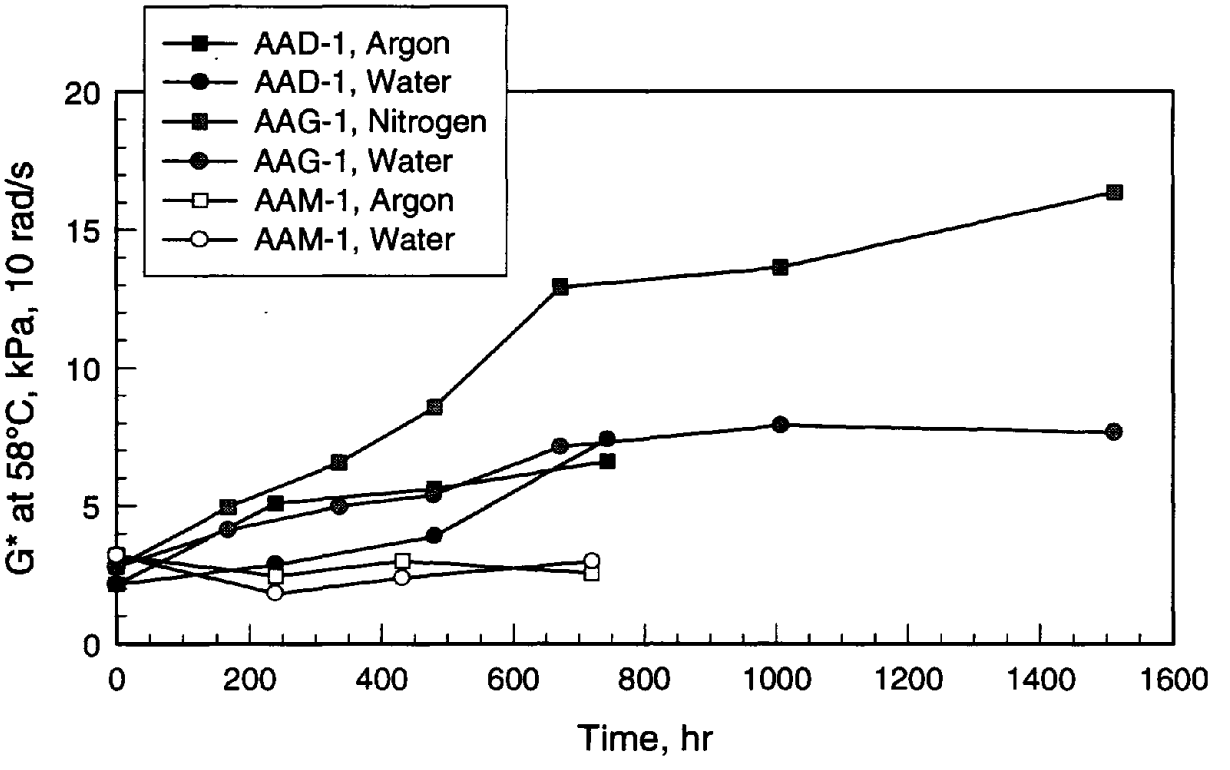

Figure 5-25. The impact of the environment at 60°C on G* of unaged AAD-1, AAG-1, and AAM-1.

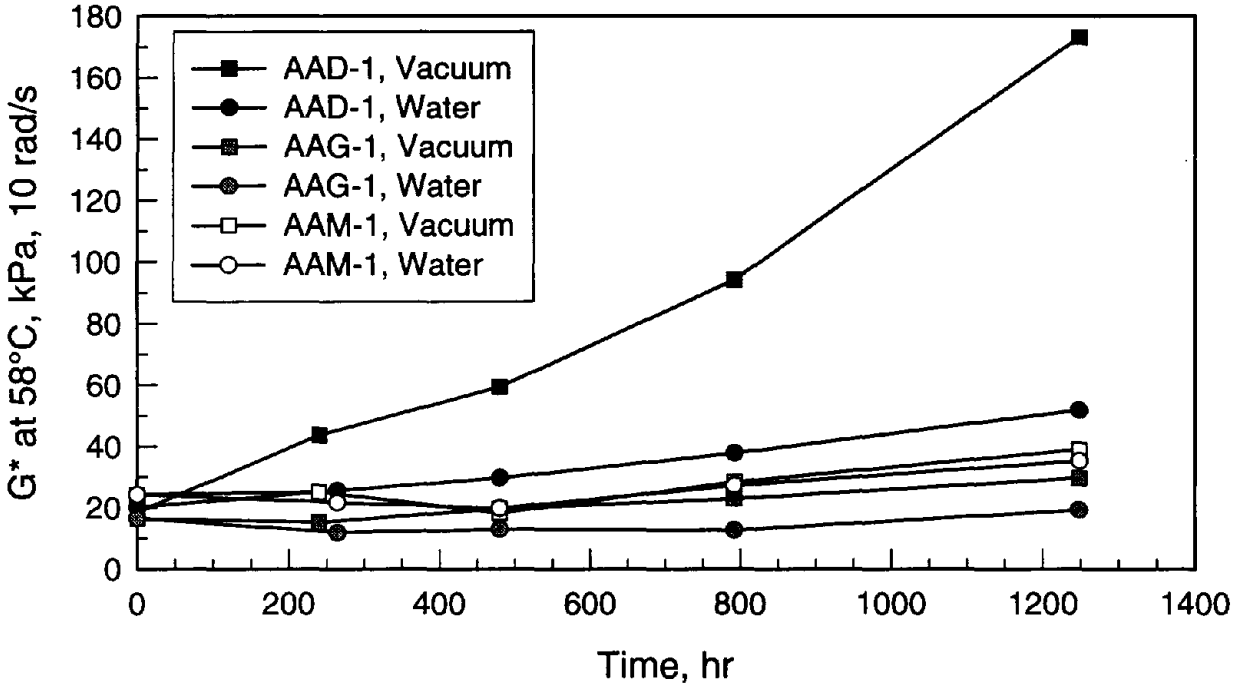

Figure 5-26. The impact of the environment at 60°C on G* of RTFO/PAV-aged AAD-1, AAG-1, and AAM-1.

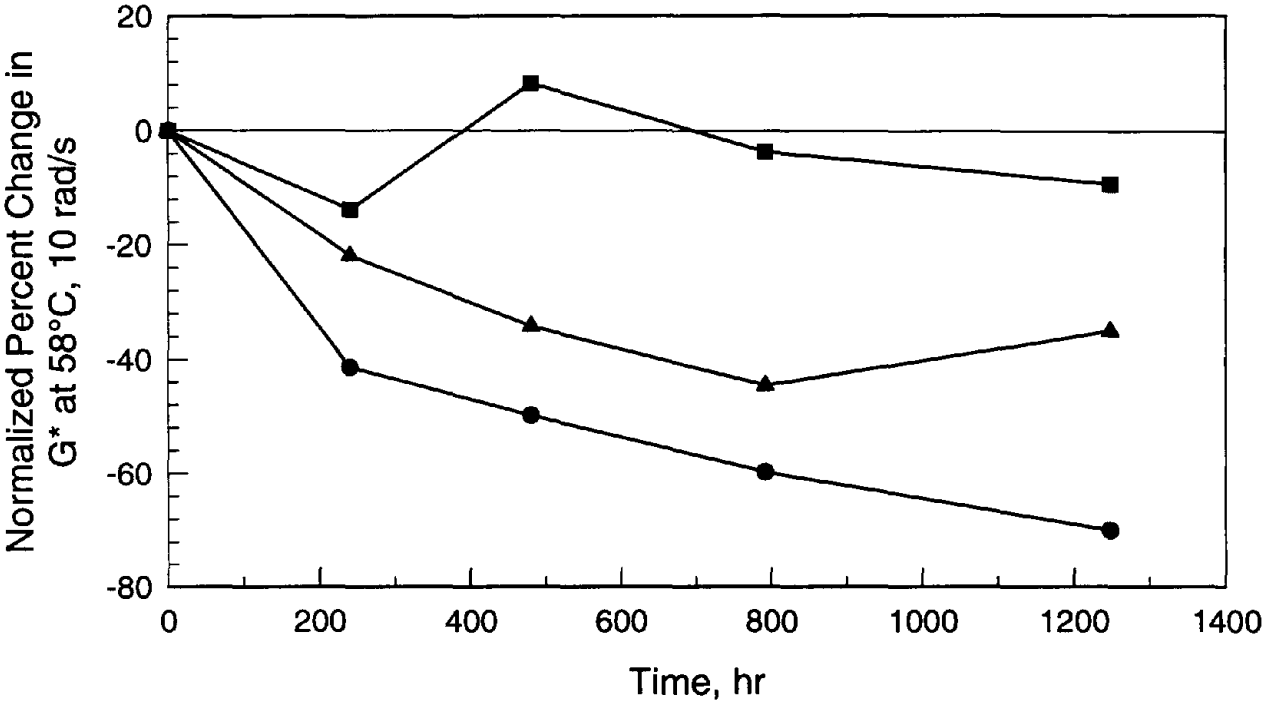

Figure 5-27. A comparison of the normalized percent change in G* with time for RTFO/PAV-aged samples. All samples stored at 60°C.

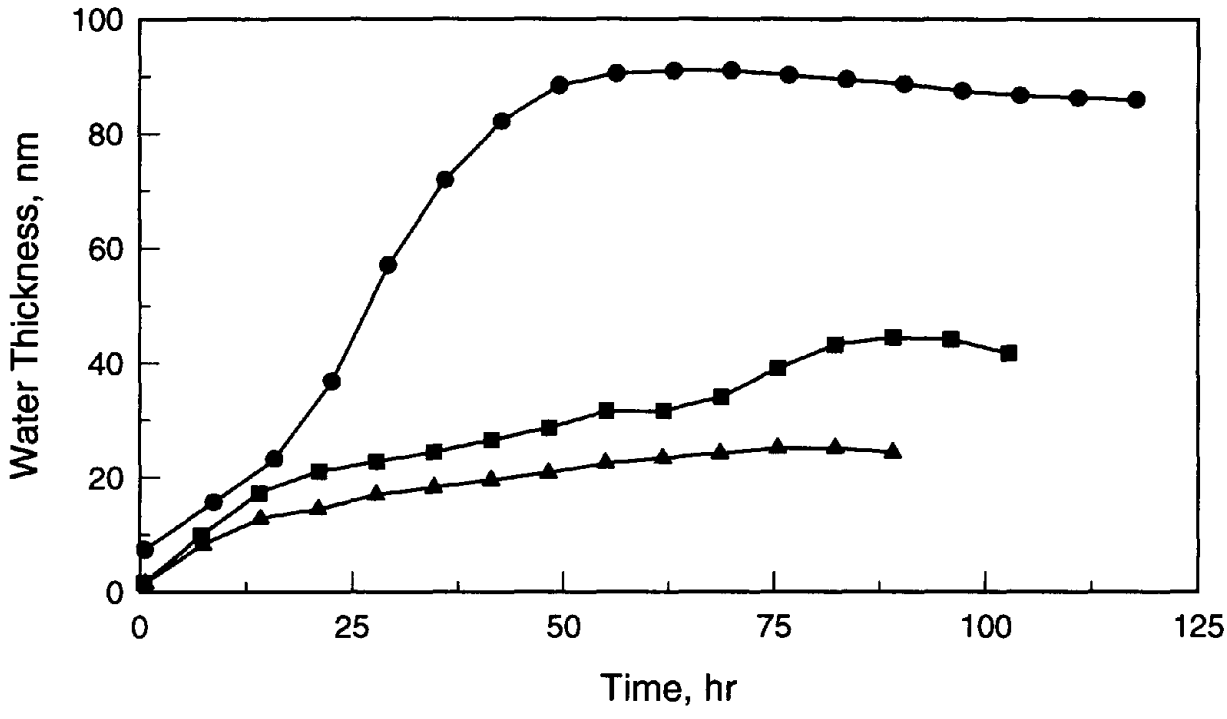

Figure 5-28. The thickness of the water layer at the asphalt/silicious substrate interface as a function of exposure time in water for unaged asphalts (from Nguyen et al. [1994]).

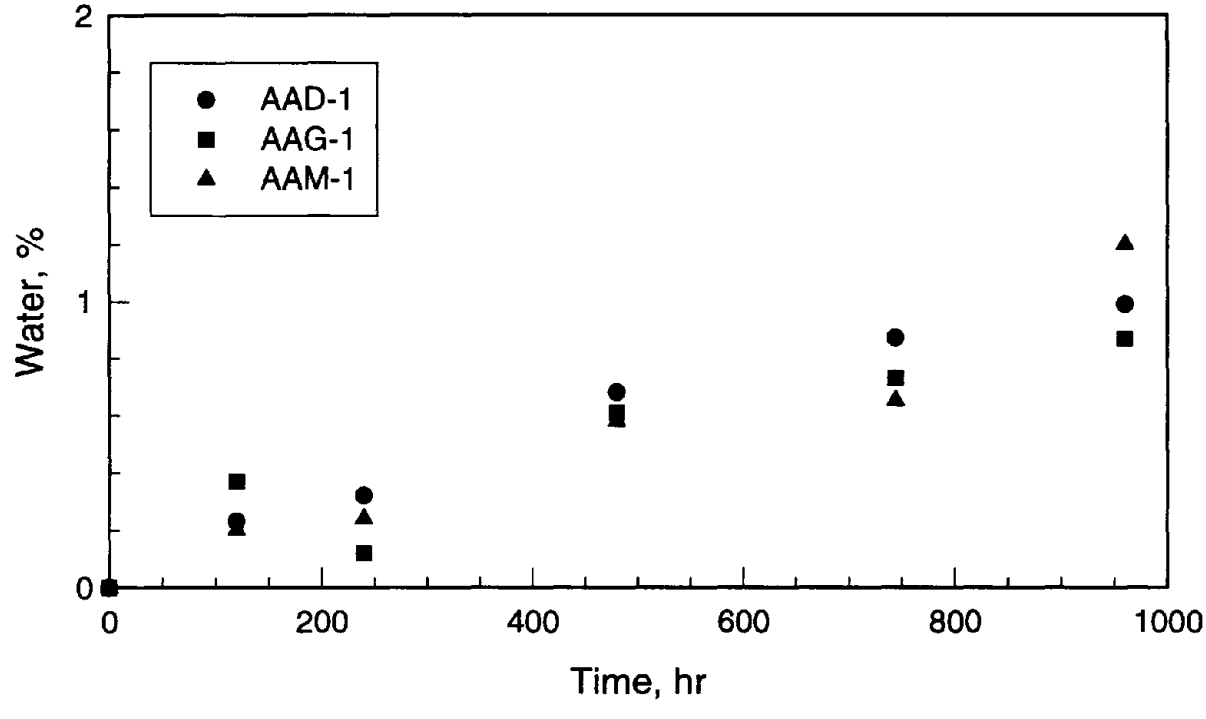

Figure 5-29. A plot showing the amount of water incorporated into various unaged asphalts stored at 60°C.

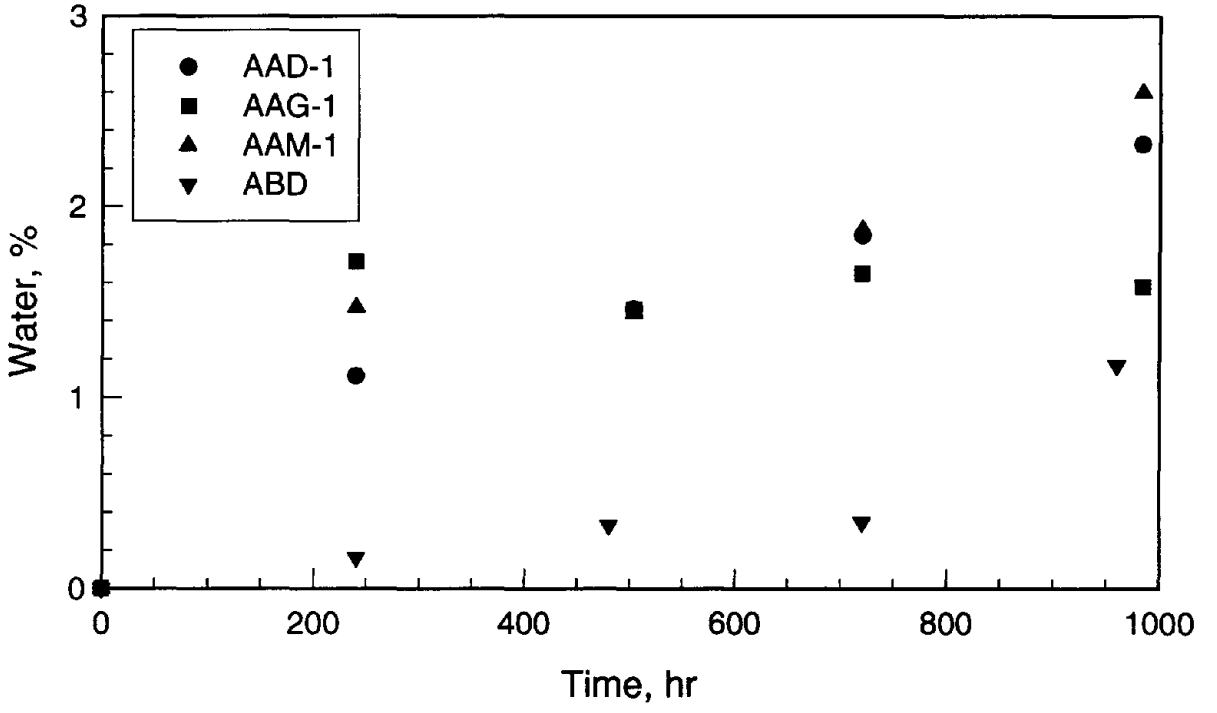

Figure 5-30. A plot showing the amount of water incorporated into several RTFO/PAV-aged asphalts stored at 60°C.

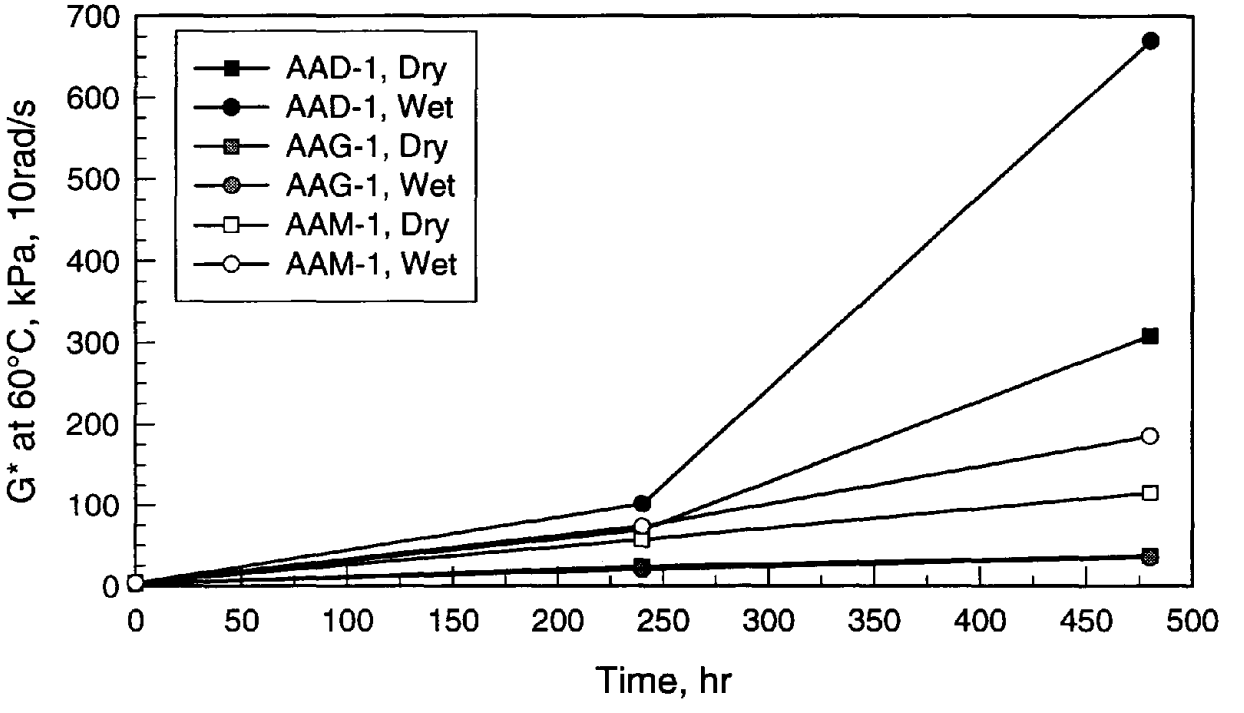

Figure 5-31. The impact of the presence of water during PAV aging at 80°C on G* of RTFO-aged SHRP asphalts.

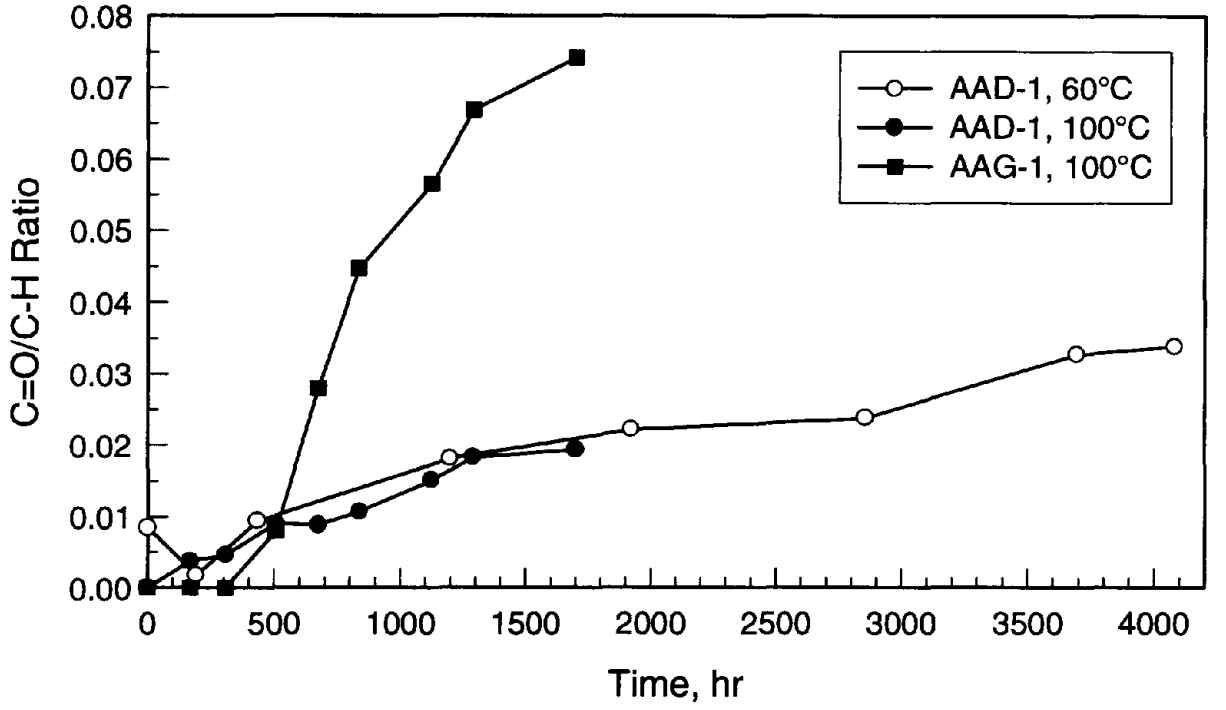

Figure 5-32. A plot of the ratios of the amounts of carbonyl versus alkanes with time for unaged asphalts AAD-1 and AAG-1. (The asphalts were stored in argon.)

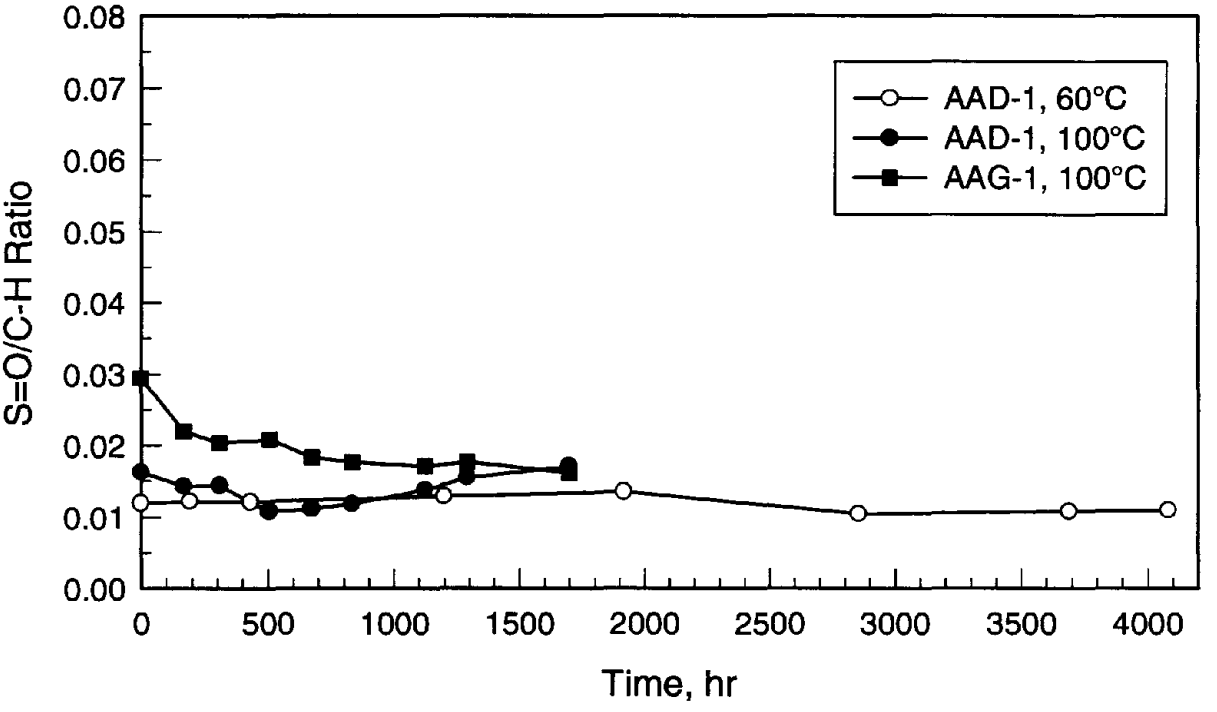

Figure 5-33. A plot of the ratios of the amounts of sulfoxide versus alkanes with time for unaged asphalts AAD-1 and AAG-1. (The asphalts were stored in argon.)

ENVIRONMENTAL SCANNING ELECTRON MICROSCOPE OBSERVATIONS OF ASPHALT-WATER AND ASPHALT-AGGREGATE-WATER INTERACTIONS

Use of the ESEM to Study Water Penetration into Neat and Aged Asphalt Surfaces

Although the ESEM provides only qualitative or semiquantitative measurements, it is a useful tool for studying asphalts because there is no other direct method that provides a visual image of moisture penetration into asphalts. The ESEM was used to image the morphological changes in the surfaces of neat and aged asphalts during contact with water. It is generally believed that asphalt and water are immiscible. Nevertheless, it was hypothesized that water would penetrate the surfaces of asphalts submerged under water for long periods of time, and that water would then diffuse into different asphalts at variable rates and depths, depending on their chemical and physical properties.

Asphalts AAA-1, AAB-1, AAG-1, and AAM-1 were selected from among the SHRP core asphalts [Cominsky et al. 1989], and their chemical properties have been published [Branthaver et al. 1993a]. Asphalt AAA-1 has at least twice the carboxylic acid content of asphalts AAB-1 and AAM-1. Asphalt AAG-1 is also high in carboxylates, but in the form of calcium salts. Carboxylic acid content is believed to be closely related to susceptibility to water damage.

Oxidative aging of the asphalts was performed using a combination of the RTFO test and the PAV test [Petersen et al. 1994]. The aged asphalts cover the extremes of oxidative aging that asphalts experience in pavements. Test samples of the aged and unaged asphalts were formed in molds the size of a one cent coin and maintained under water at 50°C (122°F) for periods of 1, 2, 4, 8, 16, and 32 weeks. One sample of each unaged and aged asphalt was examined under the ESEM before soaking in water to act as a control for the study (figure 5-34a). In figure 5-34a, the large dark area to the left is the bulk asphalt sample. The light vertical line is the asphalt-air interface. The area to the right is air. The white bar in the lower center is 50 μm in length.

After each soak period (1, 2, 4, 8, 16, and 32 weeks), one of each of the disc-shaped samples was placed on dry ice and a cross-section was exposed by fracturing the sample with a razor blade. The small samples were placed on edge in steel sample holders and kept cold on dry ice until placed into the ESEM. The ESEM stage was cooled to 2.5°C (36.5°F). The ESEM pressure and beam energy were set at 665 Pa (5 mm Hg) and 15 keV and the images were printed at 250x. The images of the samples were examined to determine depth of water penetration into the discs and differences in surface morphology among the samples. The depth of water penetration is correlated with the appearance of what appear to be spherical voids in the images.

Table 5-1 is a summary of the measurements of depth of penetration. Control samples of neat and oxidized asphalts were examined in the ESEM after cooling in the penny-size molds, but before soaking in water. The images of these samples had smooth cross-sections without any visible voids or flakes (figure 5-34a). There were very few voids observed in any of

the images of the samples after 1 week of soaking under distilled water at 50°C (122°F). The numbers in table 5-1 represent the depth of penetration, in μm, based on the depth of the concentrated area of voids for each sample image. Concentrated area of voids is a term used to describe the area of the most spherical voids near the surface of each cross-section and is semiquantitative in nature because there are no definite boundaries to this area. There was a great deal of variability in the depth of penetration for many of the samples and this is shown by the range of measurements listed in table 5-1. For example, after 8 weeks the depth of the concentrated area of voids for sample AAB-1 neat ranged from 93 μm in some areas to 179 μm in other areas.

The RTFO-PAV aged samples were all soaked in the same container. After 2 weeks of soaking, some asphalt-like material floated on the surface of the soak water. Samples AAA-1 and AAB-1 appeared thinner than the previous week, so it was assumed that most of this material came from the AAA-1 and AAB-1 samples. If so, this explains why the water penetration, as measured by thickness of the concentrated void area, was much less for these two samples at all measurement intervals than for any of the other samples.

Figure 5-34 shows cross-sections of neat AAM-1 before soaking (figure 5-34a), after 8 weeks under water (figure 5-34b), after 16 weeks under water (figure 5-34c), and RTFO-PAV aged AAM-1 after 16 weeks under water (figure 5-34d). In figures 5-34b and c, air is on the left. The spherical voids appear to be concentrated near the air-asphalt interfaces in these figures, but some voids are observed far into the asphalt layers on the right. In figure 5-34d, air is on the right, asphalt (with voids) on the left. The light area in the upper left of figure 5-34d is a dust particle. The areas penetrated by water in figures 5-34b, c, and d appear spongy, i.e., filled with spherical voids. The voids are thought to have been created by the evacuation of the water under the relatively low pressure conditions of the ESEM. The penetrated layer appears to be porous but not permeable as there do not appear to be any connections between the voids. The penetrated layer in the 8-week sample (figure 5-34b) is not as wide as that of the 16-week sample. This sequence (figure 5-34a, b, c) shows increased penetration over time and (figure 5-34d) that there is little difference in morphology between the RTFO-PAV aged and neat asphalt AAM-1 after 16 weeks. However, after 32 weeks, the voids in the aged sample are more distinct and larger than the voids in the neat sample. The numbers in table 5-1 show that the RTFO-PAV aged AAM-1 samples were penetrated by water at a faster rate and to a deeper level than the neat AAM-1 samples. Asphalt AAM-1 is emphasized here because no particles broke off from the disc of the aged sample after prolonged soaking.

Figures 5-35a-d (air is on the right and asphalt on the left in these images) illustrate the changes observed after soaking the AAA-1 samples. After 2 weeks of soaking, images of RTFO-PAV aged AAA-1 exhibit a few widely scattered voids (figure 5-35a). It is interesting that there is a channel running to the surface from many of the deeper voids. The origin of the apparent channeling is not clear. It could be either a connecting tunnel to the surface or microfractures in the asphalt that caused the asphalt to fracture along these lines when the sample was cross-sectioned. This corresponds to observations made by Lottman and Johnson [1970] when they were running freeze-thaw cycles on moisture-saturated asphalt-aggregate

samples. After many freeze-thaw cycles, they pulled the aggregate off of the asphalt and examined the asphalt surface with a light microscope. They described it as having pinholes and channels leading to voids in the asphalt from the asphalt-aggregate interface surface. Alternatively, water in aged AAA-1 may have migrated to the interface under vacuum.

After 8 and 16 weeks, the concentrated void area is 25 and 76 μm thick, respectively, in the aged AAA-1 samples (figures 5-35b, c). The neat AAA-1 sample has a layer of smooth asphalt above the concentrated void layer after 14 weeks (figure 5-35d). The variable thickness of the concentrated void area is depicted in photomicrograph d as the thickness is much greater near the bottom of the photomicrograph than near the top.

Water penetration into AAB-1 is illustrated in figures 5-36a-d. In these images, air is on the right and asphalt on the left. Asphalt AAB-1 behaved differently when the RTFO-PAV aged sample was compared with the neat sample. It is clear that the voids in the neat samples at 4 and 8 weeks (figures 5-36a, b) are much smaller and the concentrated void layer penetrates more deeply than in the RTFO-PAV aged samples at 8 and 16 weeks (figure 5-36c, d). The diminished water penetration could be due to the upper layer of the asphalt having floated off after 2 weeks of soaking. The more water penetrated layer could have floated off leaving a less penetrated layer, and these measurements might be more accurately compared with those of the neat samples measured 2 weeks previously. Even if RTFO-PAV aged samples are compared with neat asphalts soaked 2 weeks fewer, the large difference between the neat and RTFO-PAV aged sample results is not explained. Water penetration into asphalt AAB-1 is affected by either the change caused by the removal of the floating layers and/or the aging process. The voids in the aged sample are larger and more concentrated at the surface. The figures also show that the concentration of voids continues to increase over time in both the neat and aged AAB-1 samples.

The neat AAG-1 sample shows a great deal of variability in the penetration of the voids from 4 weeks (figure 5-37a - air at upper right) to 8 weeks to 16 weeks (figure 5-37b - air at left), but there is a general trend for penetration to increase over time in both the neat and RTFO-PAV aged samples. There appear to be more tiny voids penetrating more deeply into the 4-week neat sample than the 8-week RTFO-PAV aged sample (figures 5-37a, c); however, the concentrated void layer is thicker in the 8-week RTFO-PAV aged sample than in the 4-week neat sample. The RTFO-PAV aged AAG-1 sample appears to have many more small voids at deeper penetration after 16 weeks than the neat sample (figures 5-37b, d). However, close inspection of the images shows that this is not so. Data in table 5-1 show that there was little difference in water penetration depth between the neat and RTFO-PAV aged AAG-1 samples.

The objectives of this work were to determine the depth of water penetration into aged and unaged asphalts, to determine whether aging affects water penetration and to elucidate at least part of the mechanism of transport of water into asphalt. The ESEM photomicrographs clearly show the extent of water penetration into neat and aged asphalt in the form of spherical voids. The penetration depths of the concentrated void areas in the tested asphalts have been measured and are listed in table 5-1. These concentrated void areas did continue to extend

deeper into the asphalts with increased time under water. The water penetrated more deeply into the neat samples of AAA-1 and AAB-1 than the RTFO-PAV aged samples. This is probably due to the upper layers of aged AAA-1 and aged AAB-1 floating off at 2 weeks. These layers may have been severely penetrated by water, possibly due to the presence of products of oxidation that would have some affinity with water. There was little difference in penetration rates between neat and RTFO-PAV aged AAG-1 samples, and water penetrated more deeply into the aged AAM-1 samples than the neat AAM-1 samples. This table shows that there clearly are differences in water penetration rates due to asphalt type and aging. The reason for this is that oxidation causes buildup of sulfoxides, ketones, and other oxygen-containing molecules in asphalts. These molecules interact with water by hydrogen bonding, facilitating penetration by water molecules.

Use of the ESEM to Study Asphalt-Aggregate Interfaces before and after Freeze-Thaw Treatments

Moisture damage in asphalt pavements generally leads to stripping, raveling, and late rutting. Fatigue and thermal cracking also may be exacerbated by water penetration of asphalt pavements. One probable mechanism responsible for these failures is loss of adhesion of the asphalt at the aggregate interface. Water is suspected to play a major role in this damage mechanism. However, direct observation of this failure mode has been difficult because of the lack of suitable instrumentation. The ESEM is a relatively new advance in scanning electron microscopy (SEM) that offers an approach to study this failure mode. The foundations, principles, and applications of ESEM are detailed by Danilatos [1988] and Cameron [1994]. The primary advantage of the ESEM over conventional SEM is that the ESEM does not require the test sample to be under extremely high vacuum, but only about 5 mm Hg (665 Pa). Thus, wet, oily, dirty, or non-conductive samples can be examined in their natural state without modification or preparation. The sample environment can be varied through a range of pressures, temperatures, and gas compositions. These factors combine to make the ESEM a powerful tool to investigate moisture damage at the asphalt-aggregate interface.

The ESEM has been used to study corrosion, wet-dry cycles, solvent action, capillary action and infiltration, salt crystallization, melting and solidification cycles, freeze-thaw cycles, paint drying, crack formation and propagation, and topographical changes of polymers during curing [Doehne and Stulik 1990; Hwang et al. 1993]. The ESEM has also been used to study fluid/solid interactions in hydrocarbon reservoir rocks [Baker et al. 1992; Uwins et al. 1993] and recently, to study the morphology of polymer modified asphalt cements [Bhurke et al. 1997; Rozeveld et al. 1997]. However, the potential of ESEM for the study of the low temperature properties of asphalt-aggregate interactions has not yet been investigated.

Three asphalts, AAD-1, AAG-1 and AAM-1, were chosen from among the SHRP core asphalts [Cominsky et al. 1989]. Asphalts AAD-1 and AAG-1 are classified as asphalt grade AR-4000. Asphalt AAM-1 is classified as asphalt grade AC-20. The aggregates used in this study, RA and RD, were obtained from the Materials Reference Library (MRL). These are characterized as an intermediate stripping granite (RA) and a non-stripping limestone (RD) with regard to their ability to maintain asphalt adhesion during freeze-thaw cycling. The aggregates

were tested both wet and dry to determine whether moisture on the aggregate would affect the asphalt-aggregate bond.

Water wet and dry samples of aggregates RA and RD were partly immersed into hot (150°C; 302°F) asphalts AAD-1, AAG-1, and AAM-1. The asphalt-coated aggregate samples were allowed to cool and were then examined under the ESEM at the aggregate surface along the line of contact with the asphalt to identify positions of interest to observe after freeze-thaw cycling. Photomicrographs taken at a magnification of 250x were made at four locations on each sample. For these measurements, the ESEM pressure was 665 Pa (5 mm Hg) and the beam energy was 15 keV. Samples of each combination were subjected to 10 freeze-thaw cycles either in air or submerged in distilled water for 18 hours.

The samples frozen in air maintained a constant asphalt-aggregate interface throughout the 10 freeze-thaw cycles, whereas most samples frozen under water exhibited some change at the interface, including cracking and separation of the asphalt from the aggregate. There was no significant difference in separation at the asphalt-aggregate interface between samples prepared with wet aggregate and those prepared with dry aggregate. Evidently most of the moisture in wet aggregate is evaporated when the aggregate is dipped into the hot asphalt (150°C; 302°F).

Of all of the combinations tested, only aggregate RD coated with asphalt AAD-1 maintained a constant asphalt-aggregate interface after 10 freeze-thaw cycles when frozen under water (figures 5-38a-d. Aggregate is to left, asphalt to right). All other samples frozen under water had some significant changes at the interface.

Figure 5-38 shows the interface of dry (figures 5-38a, b) and wet (figures 5-38c, d) aggregate RD and asphalt AAD-1 before freeze-thaw cycling (figure 5-38a, c) and after 10 freeze-thaw cycles (figures 5-38b, d). There was no separation at the interface in either sample. Only one of the 32 locations monitored in the AAD-1 coated RD samples showed any separation — a crack in the asphalt (lower right corner of figure 5-38b, unfortunately not readily observable except in the original images). There was a textural change in the asphalt in both samples after 10 freeze-thaw cycles. This could be due to an effect of water on the asphalt as described above, or to the environment of the ESEM (i.e., beam damage or result of the vacuum).

For the samples prepared with aggregate RD and asphalt AAG-1 and frozen under water, many areas showed no separation after 10 freeze-thaw cycles; however, some locations had separation after only one freeze-thaw cycle. Figures 5-39a-d illustrate two cases of this failure. Photomicrographs of wet RD coated with AAG-1 before freeze-thaw cycling (figure 5-39a) and after one freeze-thaw cycle (figure 5-39b) show the asphalt folded away from the aggregate in the upper left of photomicrograph b and pulled away along the interface in the center of photo b. Photomicrographs of AAG-1 coated onto dry RD before (figure 5-39c) and after freeze-thaw (figure 5-39d) also show that the asphalt had pulled away from the aggregate after only one freeze-thaw cycle. In these figures, the darker areas are the asphalt layers.

The samples prepared with aggregate RD and asphalt AAM-1 and frozen under water also showed very little change after 10 freeze-thaw cycles in most locations, but some locations exhibited separation of asphalt from aggregate after only 1 freeze-thaw cycle. Figures 5-40a-d are a series of photomicrographs of AAM-1 coated onto RD before (figure 5-40a), after 1 (figure 5-40b), after 3 (figure 5-40c), and after 10 (figure 5-40d) freeze-thaw cycles. There was good contact between the asphalt and aggregate before freezing. After one freeze-thaw cycle (figure 5-40b), the asphalt began to separate from the aggregate, as seen on the right side and center left of the image. The asphalt continued to lift and fold on the left side and to separate from the aggregate on the right side after three freeze-thaw cycles (figure 5-40c) and a piece of the aggregate began cracking away from the main aggregate in the center of the photomicrograph. After 10 freeze-thaw cycles (figure 5-40d), the piece of aggregate in the center separated from the larger piece of aggregate. This is an example of aggregate failure, which can be a mechanism contributing to separation of asphalt and aggregate near the interface.

Figures 5-41a-d are a series of photomicrographs depicting the separation of asphalt AAD-1 from dry aggregate RA, including before freeze-thaw (figure 5-41a) and after 3 (figure 5-41b), 4 (figure 5-41c), and 10 (figure 5-41d) freeze-thaw cycles. The asphalt is on the left in all of the photomicrographs. Small "blobs" of asphalt can be seen adhering to the aggregate in figures 5-41b and c after the main body of the asphalt has pulled away. These could be areas where the asphalt is especially well bonded to the aggregate due to chemical or morphological differences at these locations. Separation at the interface was observed at many locations in all samples of RA coated with AAD-1 after being frozen in water once. A dramatic failure of the bond occurred at most locations after three freeze-thaw cycles (figure 5-41b). At this location (figure 5-41b) the asphalt continued to separate from the aggregate following each freeze-thaw cycle, but in some locations there was little change at the interface from after 3 freeze-thaw cycles to after 10 freeze-thaw cycles.

Samples prepared with aggregate RA and asphalt AAG-1 are illustrated in figures 5-42a-d. An area of dry RA coated with AAG-1 that was imaged before freeze-thaw (figure 5-42a) had a small gap between the aggregate and the asphalt (near the 50 μm bar). There is separation in this area and upward along the interface after only one freeze-thaw cycle (figure 5-42b). In wet RA coated with AAG-1, cracking in the asphalt appeared after four freeze-thaw cycles (figure 5-42c near center), but was mostly healed after five freeze-thaw cycles (figure 5-42d). This crack healing occurred either before the sample was refrozen or as the sample was warming after the fifth freeze-thaw cycle. This could be visual evidence of the microcracking and healing described by Williams et al. [1997]. The separation at the interface that was observed after 4 freeze-thaw cycles was more pronounced after 5 freeze-thaw cycles and only increased slightly after 10 freeze-thaw cycles.

Asphalt AAM-1 separated from wet aggregate RA after only one freeze-thaw cycle (figures 5-43a, b). The asphalt-aggregate interface moved over 100 μm to the left of the original interface. Continuous freeze-thaw cycles exposed more and more aggregate. All samples of RA coated with AAM-1 and frozen under water showed this dramatic failure. A location on a dry sample of RA coated with AAM-1 is illustrated in figure 5-43c before freeze-thaw and figure 5-43d after 10 freeze-thaw cycles. The increase in the separation between the asphalt and

aggregate with the increase in the number of freeze-thaw cycles is thought to be due to water that had seeped into the cracks and expanded when frozen, thus displacing the asphalt further from the aggregate with each cycle. This mechanism obviously might be applicable to other asphalt-aggregate combinations.

The extensive failure of the asphalt-aggregate bond in samples prepared with aggregate RA and frozen under water demonstrated that this aggregate bonds weakly with all of the asphalts tested. All three asphalts formed more water resistant coatings on aggregate RD than on aggregate RA. Results of these experiments showed that there was no difference in the performance of samples prepared with wet aggregate compared with those prepared with dry aggregate.

It was hypothesized that cracks in asphalt and asphalt-aggregate separation would heal over time when subjected to heat or pressure and that the extent of healing would be different in different asphalts. Healing of a crack in asphalt AAG-1 was observed during the course of these experiments and is illustrated in figures 5-42c and d. This healing probably occurred at room temperature after the image in figure 5-42c was made and before freezing the fifth time or while the sample was warming before the image in figure 5-42d was taken. Experiments subjecting the cracked asphalts to heat and pressure have not been performed yet.

The hypothesis guiding this work was that some asphalts would crack and separate from aggregate surfaces more than others during freeze-thaw cycling and that the presence of water during the freeze cycle would increase the amount of cracking and separation. The results clearly show that the presence of water during the freeze cycle increased the amount of cracking and separation in many asphalt-aggregate combinations. Lottman and Johnson [1970] also found that moisture was required to cause stripping under similar conditions as described for these experiments. All of the samples frozen without water maintained an intact asphalt-aggregate bond, as observed at the interface, throughout 10 freeze-thaw cycles. With the exception of RD coated with AAD-1, all of the samples frozen under water exhibited some degree of cracking and separation along the asphalt-aggregate interface. Furthermore, some asphalt-aggregate combinations exhibited more cracking and separation along the interface than others. By far the best adhesion at the asphalt-aggregate interface was exhibited by the RD aggregate-AAD-1 asphalt combination. The distant second was AAG-1 on RD followed by a close third, AAM-1 on RD. All of the asphalts showed better adherence to RD than to RA.

The ESEM can be used to determine which asphalt-aggregate combinations best resist freeze-thaw damage. A standard procedure to rapidly freeze-thaw samples under water for 10 cycles and then examine them in the ESEM for asphalt-aggregate compatibility should be developed.

Table 5-1a. Depth in microns of concentrated layer of voids resulting from soaking asphalt samples in distilled water at 50°C for different periods of time.

Asphalt	Treatment	1 week	2 weeks	4 weeks	8 weeks	16 weeks	32 weeks
AAA-1	RTFO-PAV	N/A [1]	2-16	11-114	26-41	60-80	100-110
AAB-1	Neat	N/A [1]	N/A [1]	34-79	93-179	180-230	30-50
AAB-1	RTFO-PAV	N/A [1]	N/A [1]	16	18-28	47-71	76-116
AAG-1	Neat	N/A [1]	11-56 [2]	68-160	34-79 [3]	79-287	70
AAG-1	RTFO-PAV	N/A [1]	22-34	126	90	80-295	82
AAM-1	Neat	N/A [1]	11-23 [2]	11-23	22-68	34-114	100-150
AAM-1	RTFO-PAV	N/A [1]	11-23 [2]	90-110 [2]	91-114	102-160	190

[1] Very few voids were present and there was no concentrated void layer.

[2] The voids were more loosely arranged in the void layer of these samples than in other samples.

[3] At the 8 week analysis, a layer of floating asphalt was present.

Table 5-1b. Depth in microns of concentrated layer of voids resulting from soaking asphalt samples in distilled water at 50°C for different periods of time.

Asphalt	Treatment	1 week	2 weeks	6 weeks [1]	14 weeks [1]	30 weeks [1]
AAA-1	Neat	N/A [2]	80	95	38/57-114 [3]	16

[1] The original sample was lost 2 weeks into the experiment and restarted, resulting in different soak times.

[2] Very few voids were present and there was no concentrated void layer.

[3] This sample had a layer of smooth asphalt above the concentrated void area; the numbers represent thickness of smooth area/range of thickness of the concentrated void area.

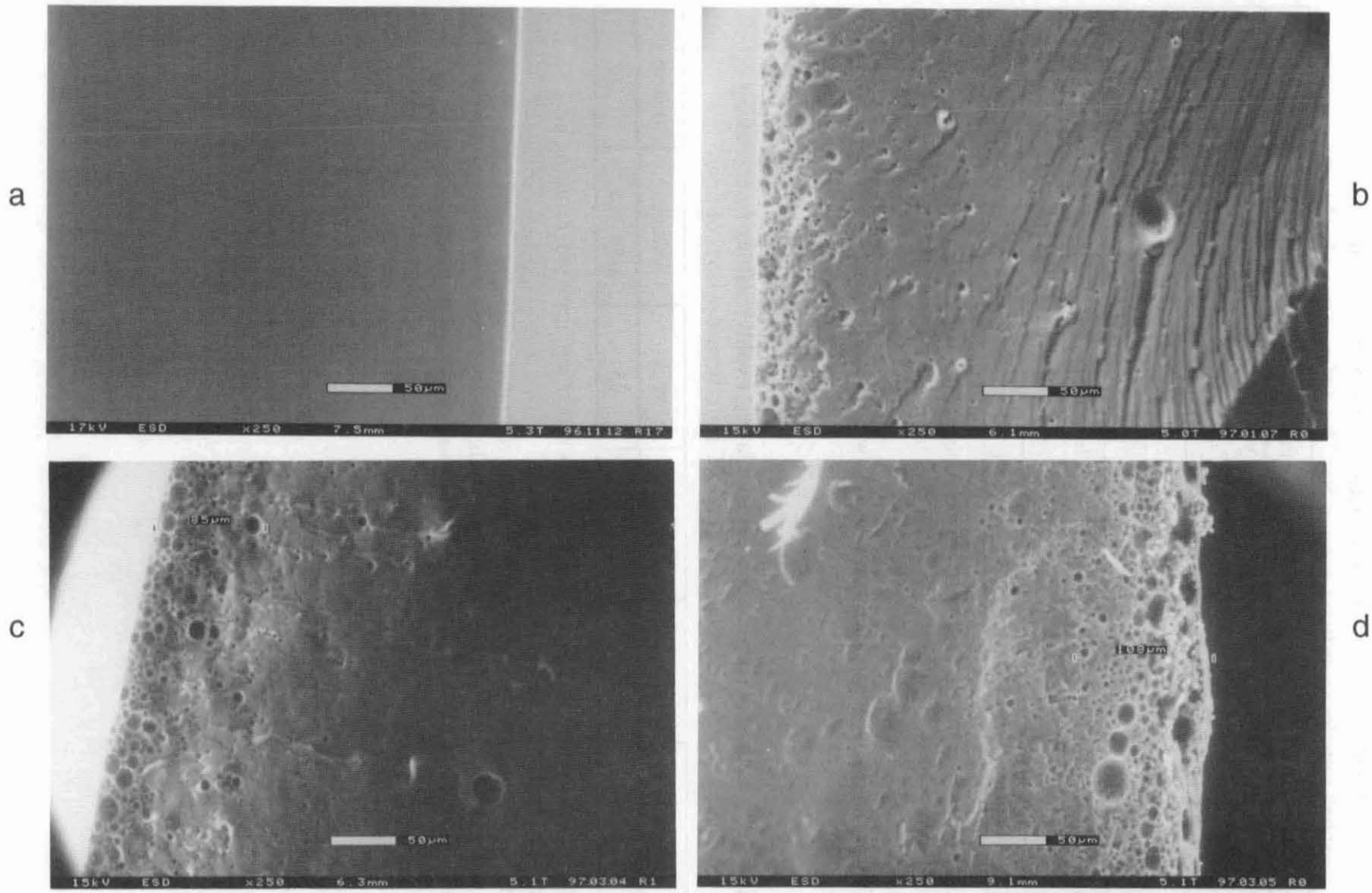

Figure 5-34. ESEM photomicrographs of cross-sections of asphalt AAM-1 showing water penetration into the neat sample: (a) before soaking in water at 50°C (122°F), (b) after 8 weeks, (c) after 16 weeks, and (d) RTFO PAV aged sample after 16 weeks.

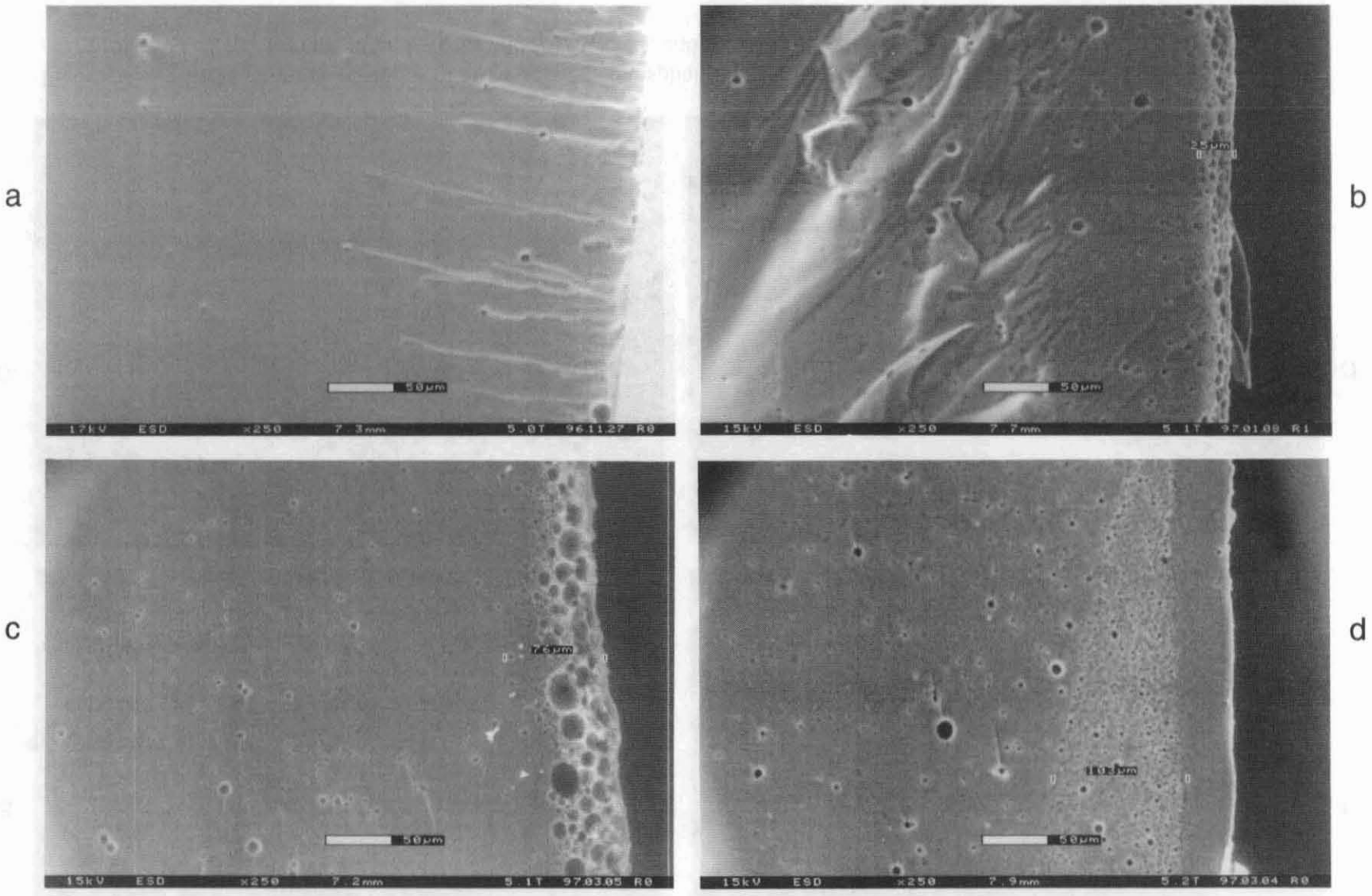

Figure 5-35. ESEM photomicrographs of cross-sections of asphalt AAA-1 showing water penetration into the RTFO PAV aged sample after soaking in water at 50°C (122°F) for (a) 2 weeks, (b) 8 weeks, and (c) 16 weeks, and (d) the neat sample after 14 weeks.

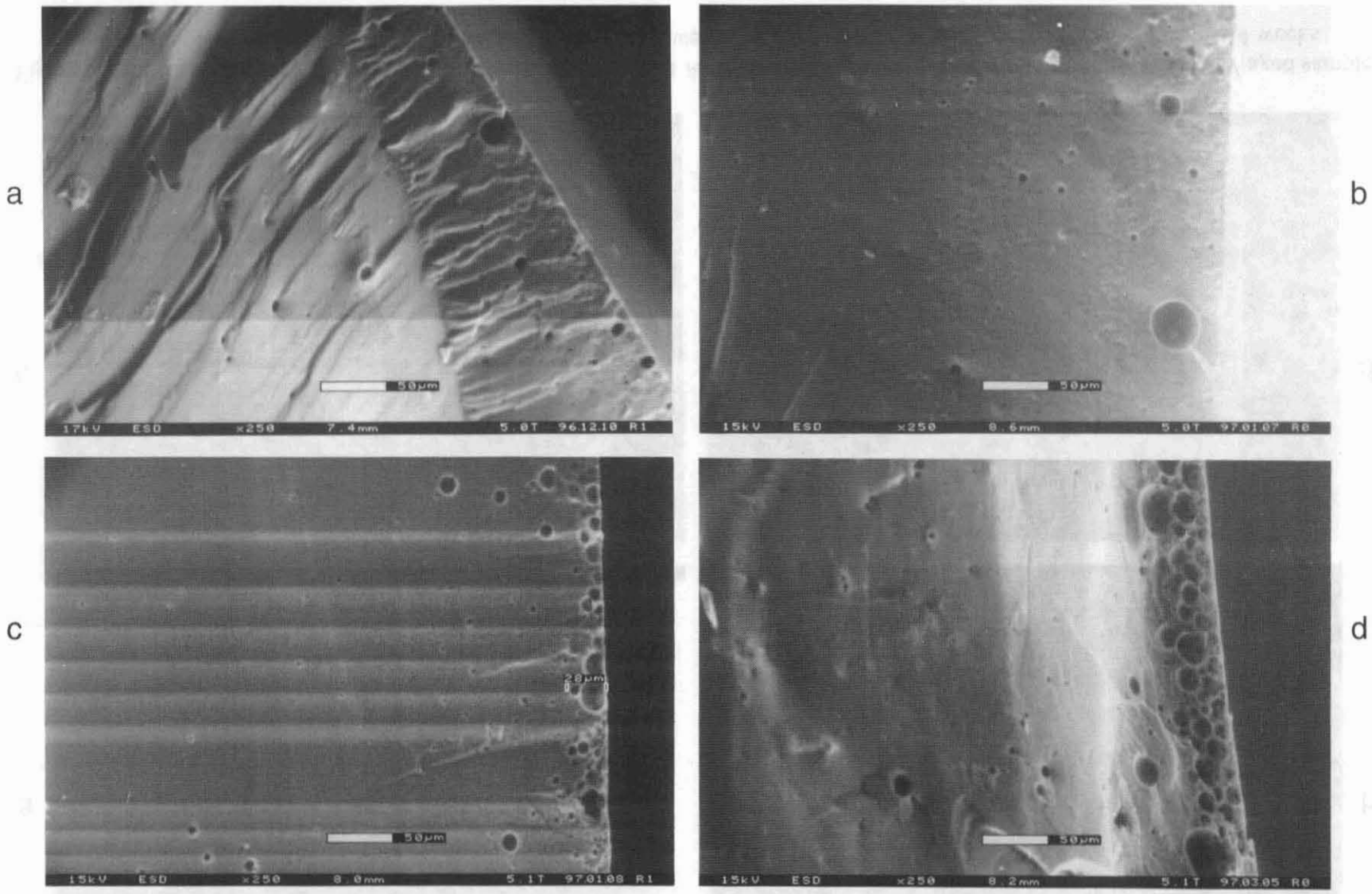

Figure 5-36. ESEM photomicrographs of cross-sections of asphalt AAB-1 showing water penetration after soaking in water at 50˚C (122˚F): (a) neat after 4 weeks and (b) 8 weeks, and (c) RTFO PAV aged after 8 weeks and (d) 16 weeks.

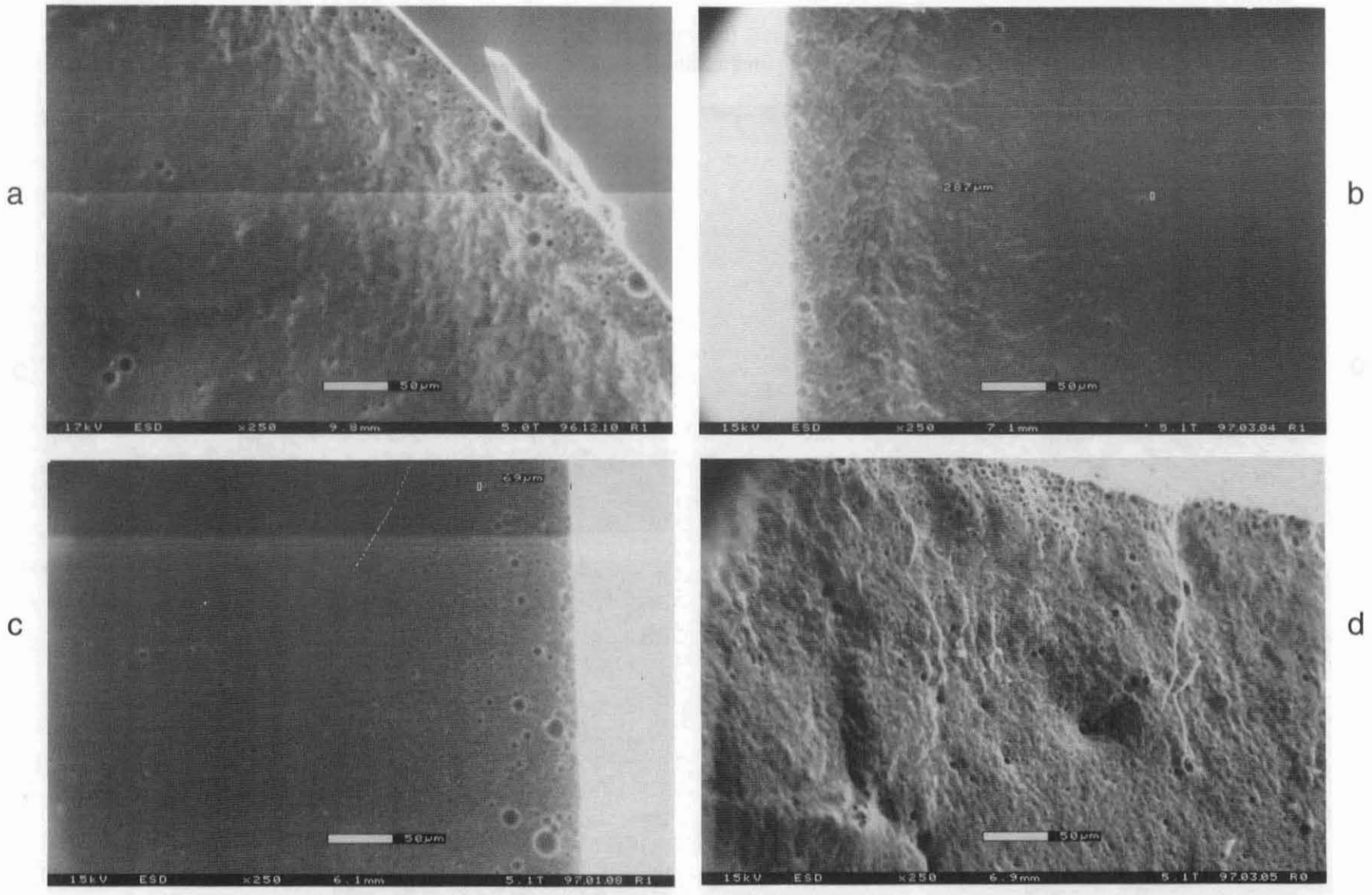

Figure 5-37. ESEM photomicrographs of cross-sections of asphalt AAG-1 showing water penetration after soaking in water at 50°C (122°F): neat for (a) 4 weeks and (b) 16 weeks, and RTFO PAV aged for (c) 8 weeks and (d) 16 weeks.

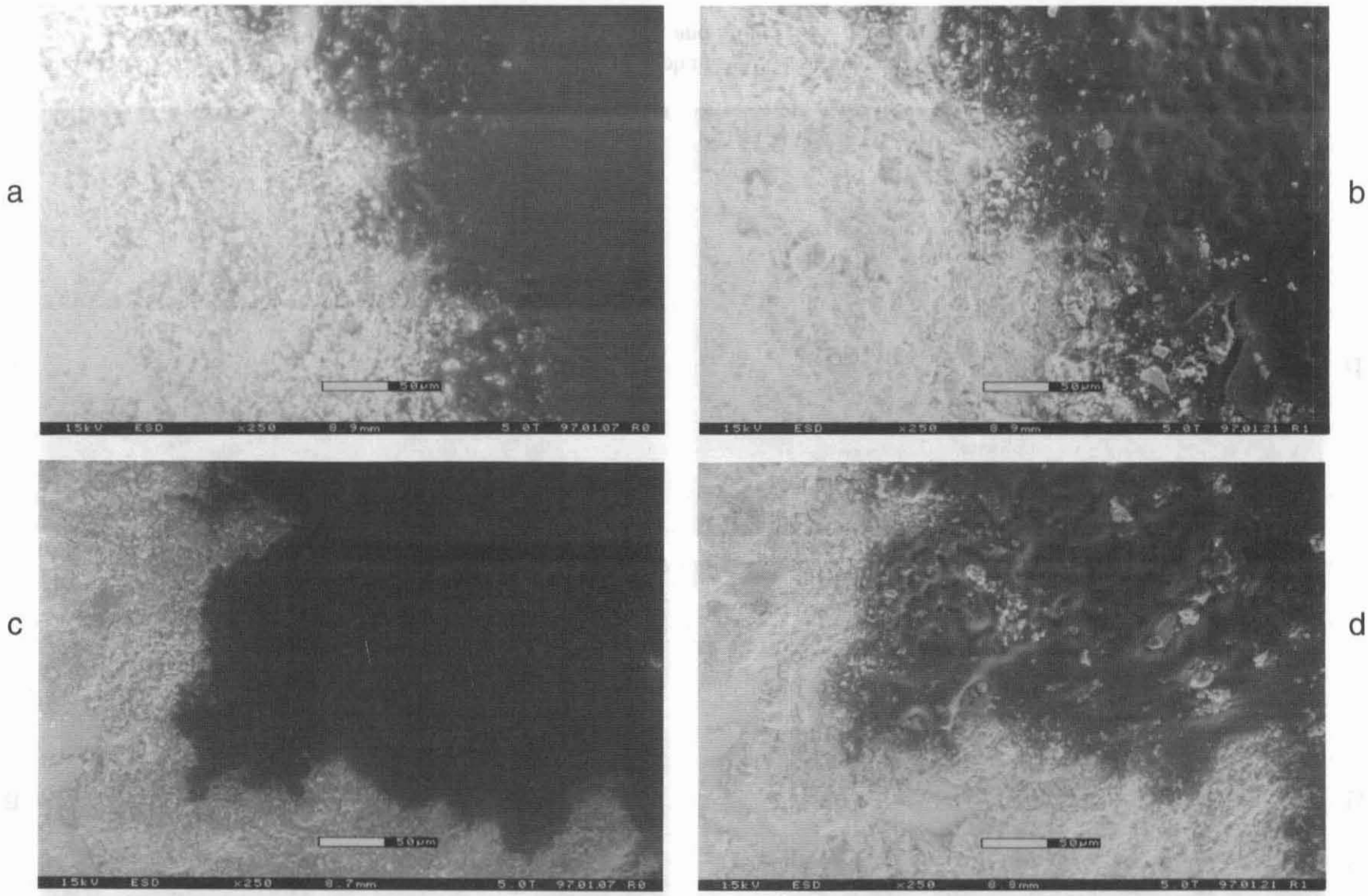

Figure 5-38. ESEM photomicrographs showing interface of aggregate RD and asphalt AAD-1 before and after freeze-thaw cycling: (a) dry RD before, (b) dry RD after 10 cycles, (c) wet RD before, and (d) wet RD after 10 cycles.

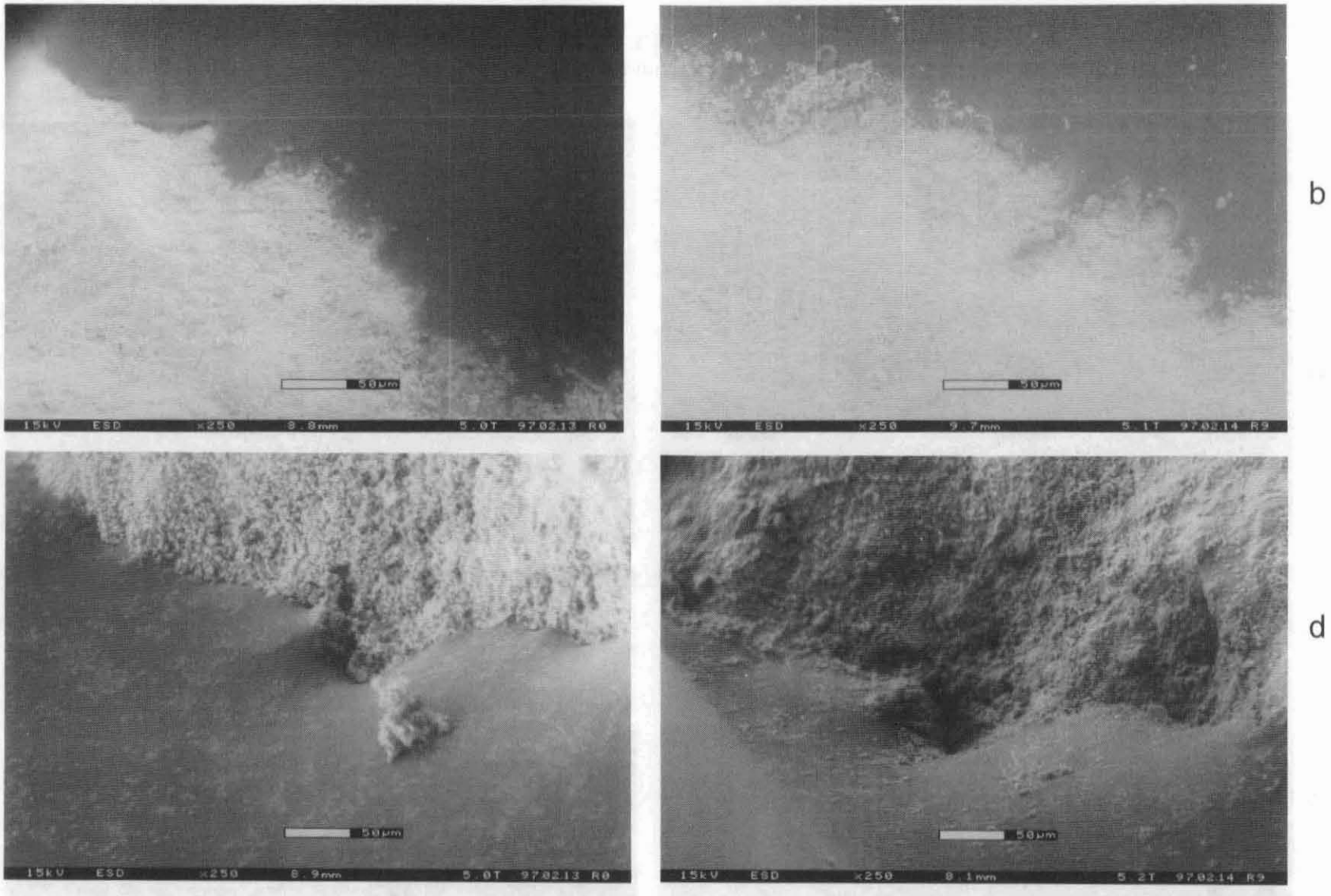

Figure 5-39. ESEM photomicrographs showing interface of aggregate RD and asphalt AAG-1 before and after freeze-thaw cycling: (a) wet RD before, (b) wet RD after one cycle, (c) dry RD before, and (d) dry RD after one cycle.

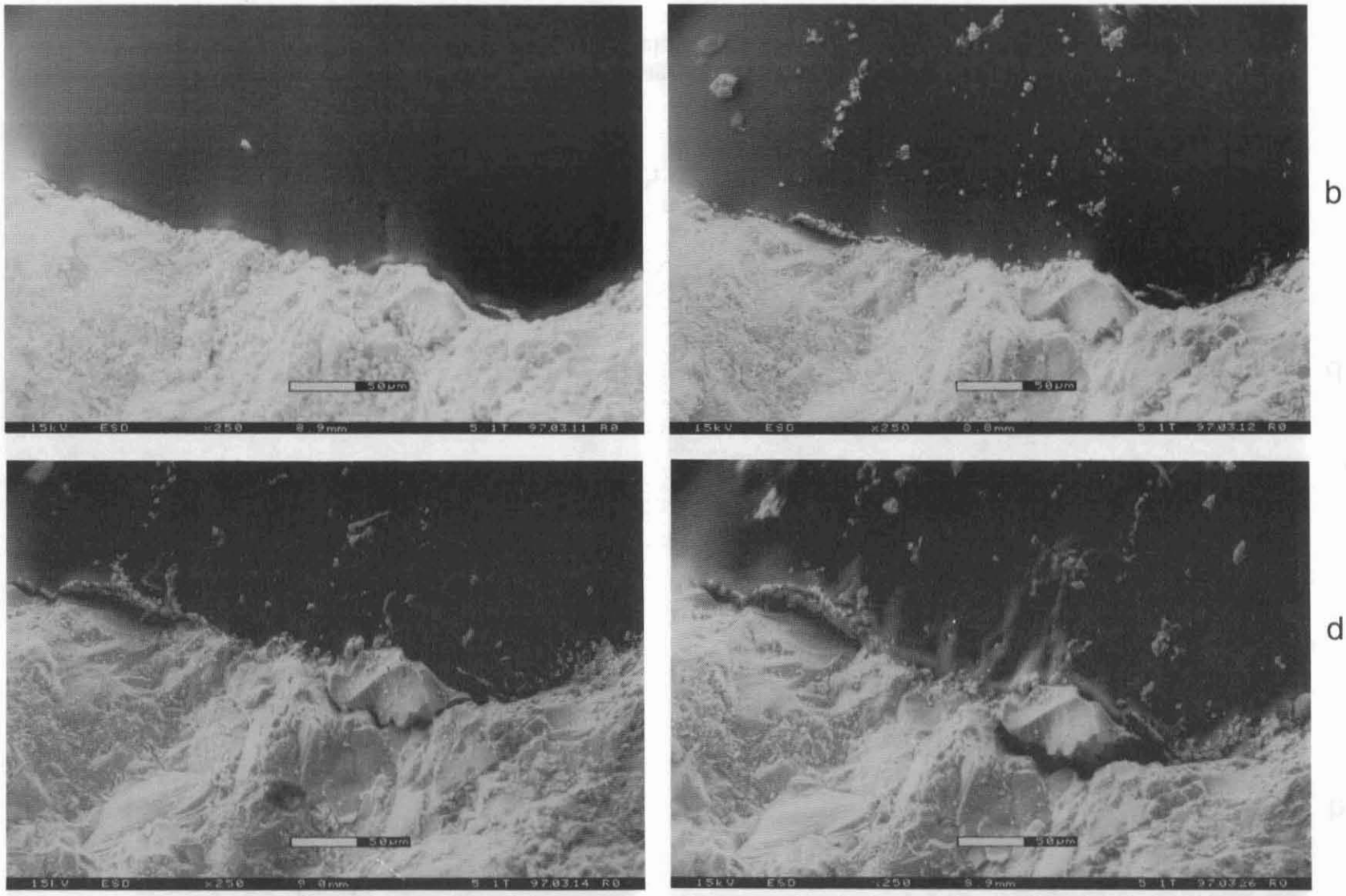

Figure 5-40. ESEM photomicrographs showing interface of wet aggregate RD and asphalt AAM-1 (a) before and after (b) 1, (c) 3, and (d) 10 freeze-thaw cycles.

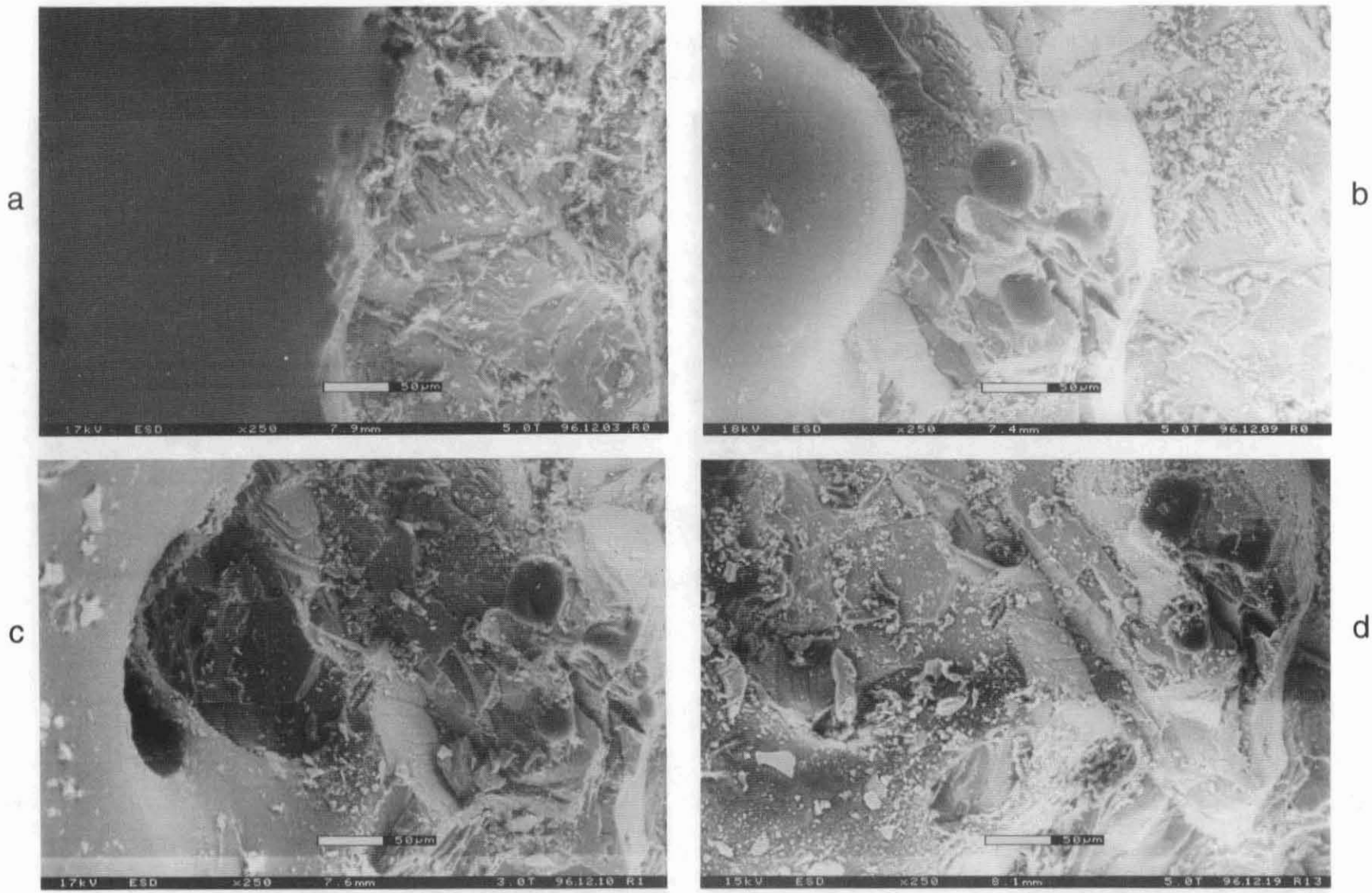

Figure 5-41. ESEM photomicrographs showing interface of dry aggregate RA and asphalt AAD-1 (a) before and after (b) 3, (c) 4, and (d) 10 freeze-thaw cycles.

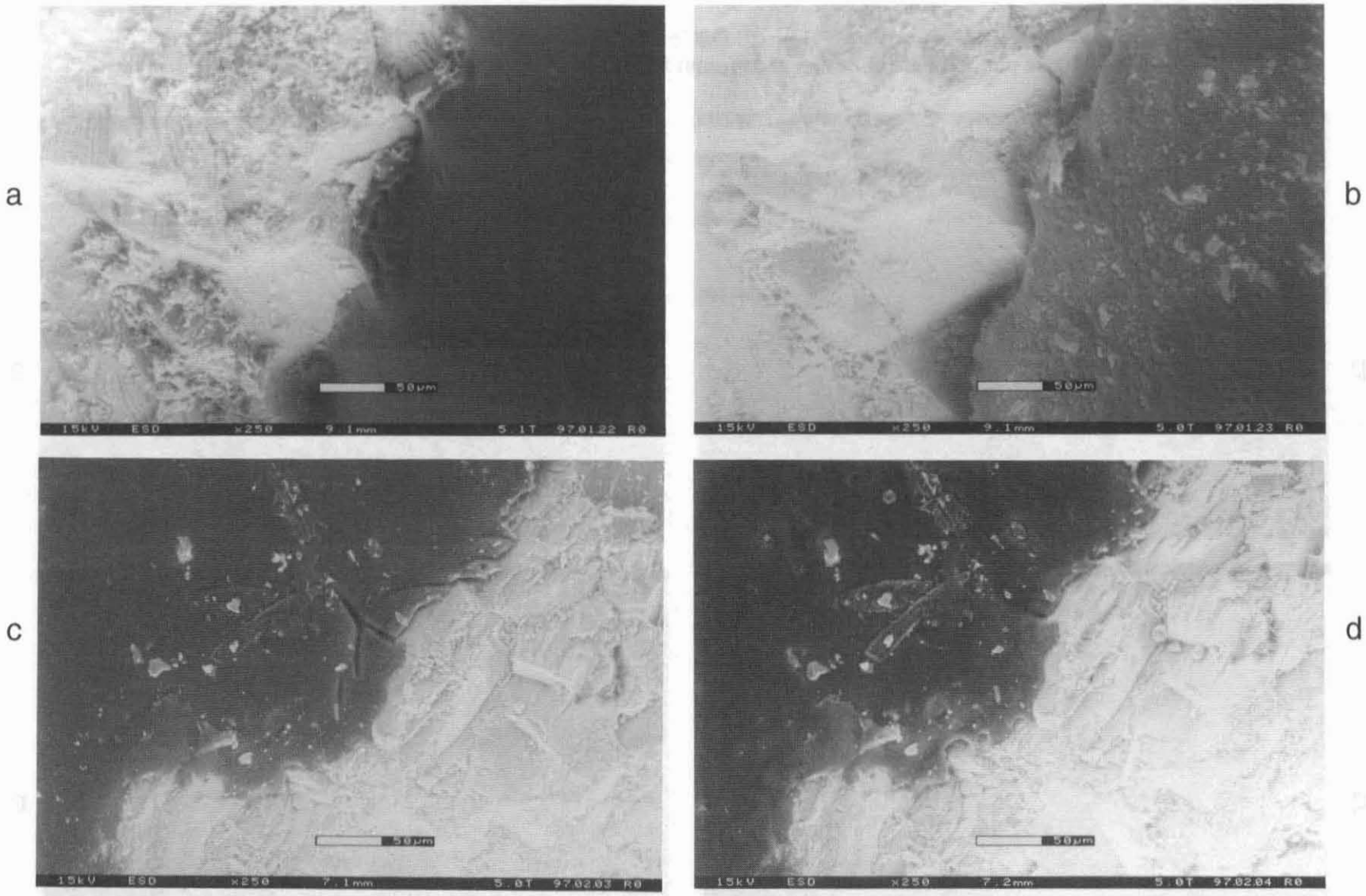

Figure 5-42. ESEM photomicrographs showing interface of aggregate RA and asphalt AAG-1 before and after freeze-thaw cycling: (a) dry RA before, (b) dry RA after one cycle, (c) wet RA after four cycles, and (d) wet RA after five cycles.

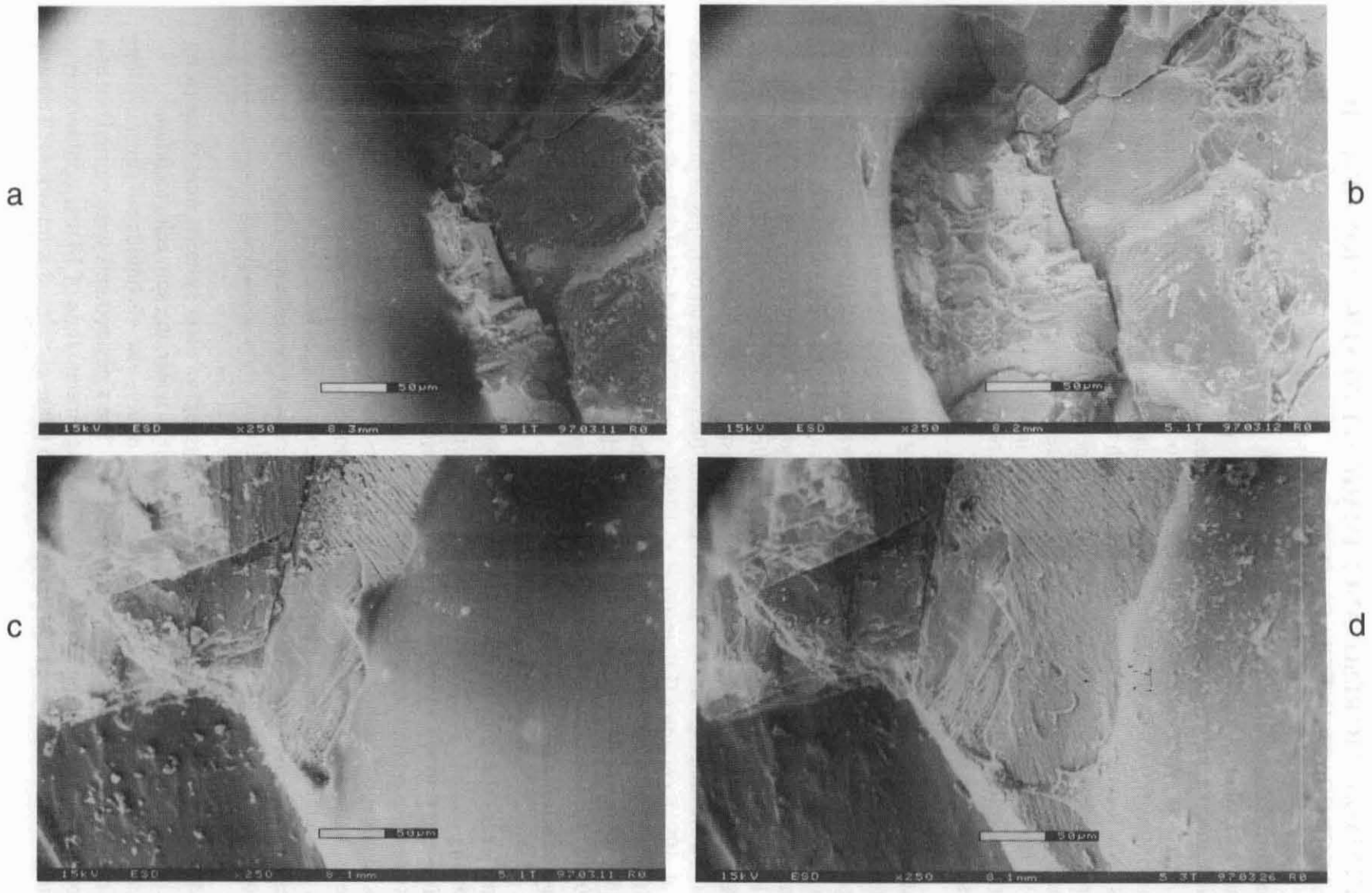

Figure 5-43. ESEM photomicrographs showing interface of aggregate RA and asphalt AAM-1 before and after freeze-thaw cycling: (a) wet RA before, (b) wet RA after 1 cycle, (c) dry RA before, and (d) dry RA after 10 cycles.

NUCLEAR MAGNETIC RESONANCE IMAGING INVESTIGATION OF ASPHALT-WATER-AGGREGATE INTERACTIONS

Moisture damage in pavements generally leads to stripping, raveling, and late rutting. Fatigue and thermal cracking also may be influenced by water penetration of asphalt pavements. One probable mechanism responsible for these failures is loss of adhesion of the asphalt at the aggregate interface. Water is suspected to play a major role in this damage mechanism. Direct observation of this failure mode has been difficult because of the lack of suitable instrumental techniques. NMR imaging methods offer an approach to study this mechanism because of the favorable response of water in NMR imaging experiments. However, little research has been done on the use of NMR imaging to study asphalt-water-aggregate interactions in order to validate whether NMR imaging methods can provide insight into moisture damage mechanisms. In this section, exploratory experiments on the use of NMR imaging to study asphalt-water-aggregate systems are described.

NMR imaging combines the basic principles of magnetic resonance with spatial encoding to obtain images of the distribution of fluids in samples. Because of the sensitivity of the hydrogen nucleus in NMR and because of its favorable relaxation times, water is the fluid most often imaged. This favorable aspect suggests that NMR imaging might be used to obtain valuable information about water susceptibility and moisture damage mechanisms in asphalt. However, it has only been fairly recently that nonmedical applications of NMR imaging have been increasing, partly because of improvements in instrumentation and speed of data acquisition. NMR imaging has been used to measure the distribution of fluids in porous rocks [Sarkar et al. 1991], ceramics [Ellingson et al. 1988], wood [Chang et al. 1989], other plant materials [Cofer et al. 1989], synthetic polymers [Rothwell et al. 1984], solvent diffusion in polymers [Weisenberger and Koenig 1991], coals [Webb et al. 1993], and bonding of adhesives [Koenig 1991]. Little work had been done on the use of NMR imaging in asphalt research until this program was initiated.

Samples for the imaging experiments on asphalt-water-aggregate systems were prepared in the following manner: asphalts were added to 23-mm OD glass vials to a depth of ~7 mm. The asphalts were warmed and pieces of aggregate were embedded in the asphalt to make good contact between the asphalt and aggregate surface. The aggregates extended an additional ~7 mm beyond the level of asphalt in the vial. Aggregates RE, RJ, and RH from the MRL and SHRP core asphalts AAA-1, AAB-1, and AAM-1 were selected for use in these experiments. Water was then added to cover the asphalt and aggregate. Images were acquired before freezing the samples and after the samples had undergone successive freeze-thaw cycles of 18 hours each to determine whether the freeze-thaw cycles had any effect on the asphalt-aggregate interface.

NMR imaging measurements on the asphalt-aggregate-water systems were made using the spin echo technique. For non-viscous liquids, such as water, the spin echo technique provides the best images because the relaxation times of non-viscous liquids are generally long and, therefore, more favorable for spin echo imaging. The measurements were carried out at a nominal proton resonance frequency of 200 MHz using an echo time of 10 ms, a pulse delay of 1 s, a free induction decay size of 256 data points, 256 phase encodes, 8 acquisitions, 2 dummy

pulses, and a gradient setting of 38 G/cm. Eight slices, 1 mm thick, and separated by 1 mm were obtained. Under these conditions, the measuring time was 3,584 s, although this time can be shortened considerably by choosing fewer phase encodes, number of acquisitions, and dummy pulses. For example, for 128 phase encodes, 4 slices, and 1 dummy pulse, the measuring time would be 1,152 s. To determine whether water had an effect at the asphalt-aggregate interface, images were acquired in the XZ plane (see figure 4-31, chapter 4).

Preliminary NMR imaging measurements on the asphalt-water-aggregate systems before the freeze-thaw cycles indicated that aggregate RE was best suited to observe changes that might result from the freeze-thaw cycling. The other aggregates (RJ and RH) had varying amounts of magnetic components (probably iron minerals) and, therefore, gave distorted images. This was particularly true for aggregate, RJ. NMR imaging measurements were limited to asphalts AAA-1, AAB-1 and AAM-1 with the RE aggregate.

For all three asphalt-aggregate-water systems there was evidence of water displacement of the asphalt at the walls of the glass vial after just a few (two to four) freeze-thaw cycles. An example is shown in figure 5-44. These images are for the fourth slice of an image set of eight slices and represent a cross-sectional area of the asphalt-aggregate-water system across the center of the vial. In these images, NMR signals are only observed from the hydrogens in the water. Thus, the light areas in figures 5-44a-d represent the water layer sitting on top of the asphalt. The dark area slanting through the water is the aggregate that is embedded in the asphalt and is covered with water. Signals are not observed from the aggregate because it does not contain any hydrogens. The asphalt is located below the water and extends across the vial. It does not show any NMR signal because, in this case, the relaxation times of the hydrogens in asphalt are too short to provide a spin echo for imaging. The air above the water gives no signal and appears dark also. Thus, areas affected by water during freeze thaws would show different areas of contrast. For example, the progressive displacement of the asphalt from the wall of the glass vial is seen at the right edge of figures 5-44c and d and at the left in figure 5-44d.

Of the three asphalts studied, AAM-1 was the only one that showed displacement of asphalt from the RE aggregate under the conditions of the freeze-thaw cycling. This is indicated in panels b-d in figures 5-45a-d and 5-46a-d. Comparison of the boundary at the water-aggregate-asphalt interface in the lower right center of each panel, with successive freeze-thaw cycles, shows an increase in the amount of water extending downward into the asphalt along the aggregate interface beginning after four freeze thaws. The amount of water increases slightly with successive freeze thaws, although there is not much difference between 6 and 13 freeze thaws (panels c and d in figures 5-45a-d and 5-46a-d). The displacement of the asphalt from the walls of the glass vial is also seen at the right edge in panels b-d in both figures.

In summary, the work described in this section was largely exploratory and was undertaken to determine the feasibility of using NMR imaging techniques to study moisture susceptibility of asphalt-aggregate systems. For aggregate RE coated with asphalt AAM-1, NMR images showed water penetration between the asphalt-aggregate interface as a result of freeze-thaw cycling. NMR imaging measurements of aggregate RE, coated with asphalts AAA-1 and AAB-1, did not show any displacement of asphalt from the aggregate during a

limited number of freeze-thaw cycles. Demands for the NMR spectrometer did not allow for a more thorough investigation in this area of research. Nevertheless, the results are sufficiently encouraging to suggest that NMR imaging methods can be used to provide better insight into moisture susceptibility of asphalt-aggregate systems. In any future work, more combinations of asphalts and aggregates would be studied.

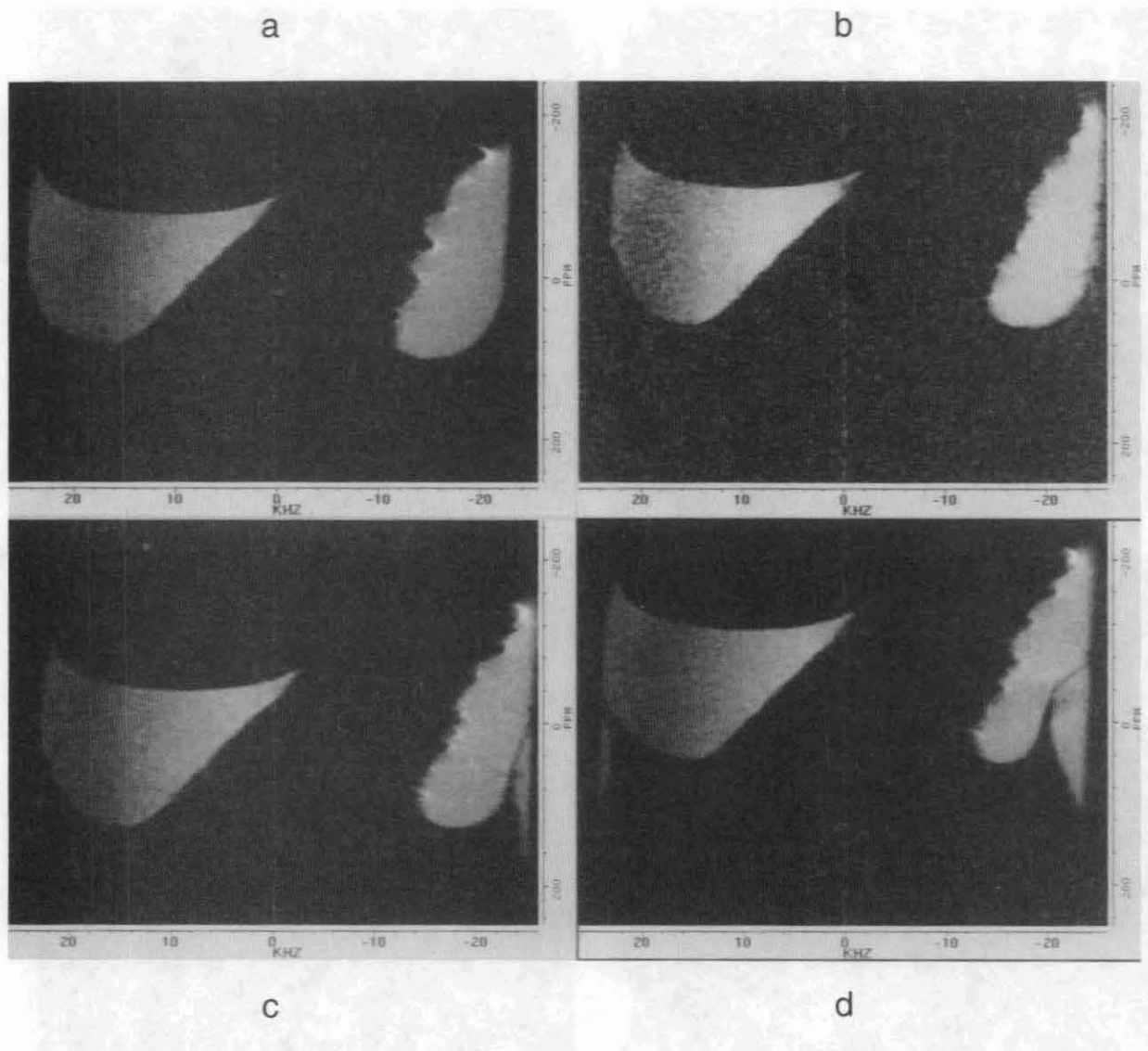

Figure 5-44. Spin echo XZ planar images of SHRP asphalt AAA-1 and MRL aggregate RE in water after successive freeze thaw cycles.
Images are for slice 4 after: (a) 0, (b) 3, (c) 4, and (d) 7 freeze thaws.

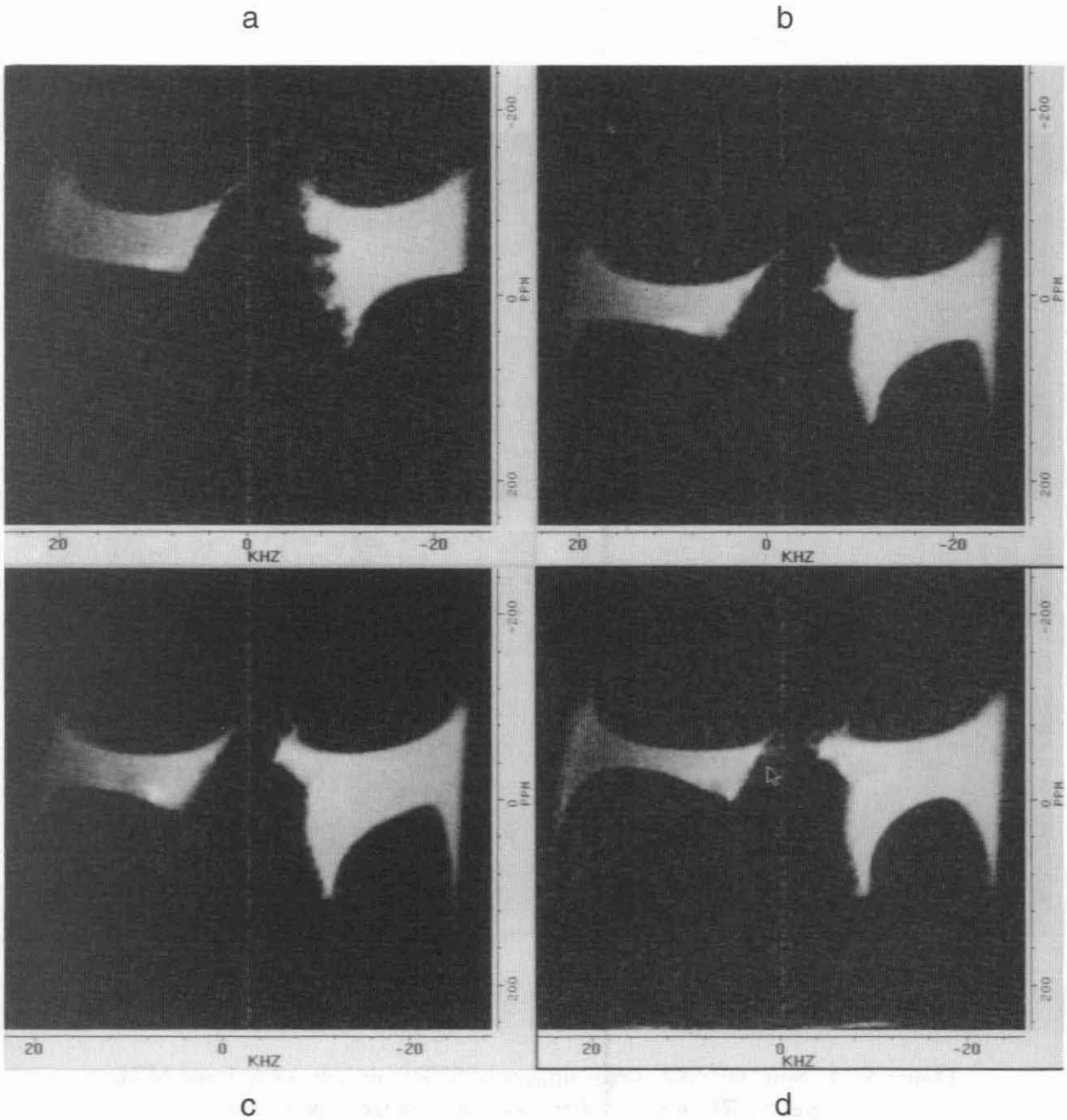

Figure 5-45. Spin echo XZ planar images of SHRP asphalt AAM-1 and MRL aggregate RE in water after successive freeze thaw cycles.
Images are of slice 5 after: (a) 0, (b) 4, (c) 6, and (d) 13 freeze thaws.

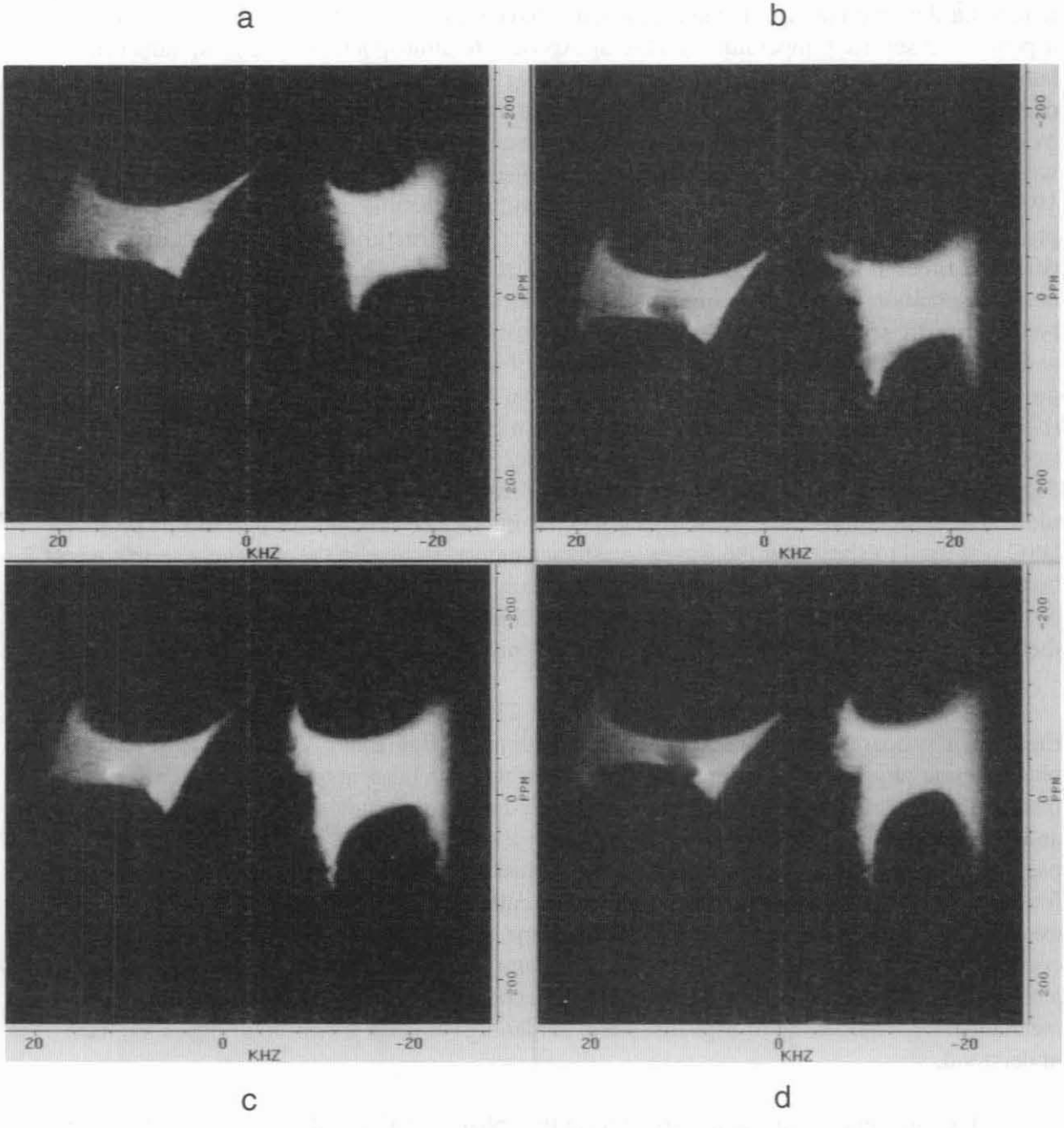

Figure 5-46. Spin echo XZ planar images of SHRP asphalt AAM-1 and MRL aggregate RE in water after successive freeze thaw cycles.
Images are of slice 6 after: (a) 0, (b) 4, (c) 6, and (d) 13 freeze thaws.

TIME-DEPENDENT MOLECULAR STRUCTURING

The rheological properties of asphalts are known to change with time. That is, asphalts tend to harden upon aging. Three mechanisms have been observed for the hardening of asphalts. At service temperatures and with exposure to atmospheric oxygen, asphalts can harden because of oxidative aging. This hardening mechanism is due to the formation of oxidation products and the mechanism is partially understood (refer to chapter 4). The oxidation process is non-reversible. Asphalts can also harden in this same temperature range without oxidative aging. This phenomenon is called steric hardening [Traxler and Coombs 1936, 1937; Brown et al. 1957; Petersen 1984], and is reversible upon heating the asphalt. A plausible mechanism for steric hardening is molecular restructuring of the asphalt over a long period of time. It has been speculated that the restructuring with time is related to: (1) changes in the association of the polar components (such as acids, bases, amphoterics, and other heteroaromatic species) in the asphalts, (2) the crystallization of the non-polar cyclic, branched, and long-chain alkanes, and (3) the combination of association and crystallization. In another part of this project (refer to the section on steric hardening earlier in this chapter), the changes in rheological properties of asphalts with time were measured, and it was observed that the isothermal steric hardening process in asphalt alone is mostly completed in 72 hours. Time-dependent hardening was attributed to the overall restructuring (or reorganization) of asphalt molecular associations rather than to any specific interaction. In another part of this project, DSC was used to show that the waxes in asphalts can crystallize in the relatively short time of 2 hours when asphalts are subjected to cooling. Thus, steric hardening may be caused by breakup of weak polar molecular associations formed by kinetic processes to form more thermodynamically favored associations and the conversion of amorphous materials to crystals.

At low service temperatures (below -5°C; 23°F) under isothermal conditions, the rheological properties of asphalts also change with time. Bahia and Anderson [1992] called this phenomenon physical hardening. It is also reversible upon heating the asphalts. The mechanism for this mode of hardening is not well understood. It has been suggested by Bahia and Anderson [1992] that the hardening is simply a collapse of free volume due to closer packing of molecules as an asphalt cools to the glass-transition region. This is the explanation for a similar phenomenon observed in polymers, called physical aging. However, another explanation for the observed change in free volume is the volume change due to the crystallization of the wax component in the asphalts [Claudy et al. 1992]. This mechanism may also be a manifestation of the steric hardening mechanism at higher temperatures. Of the three mechanisms for hardening of asphalts, steric hardening (molecular restructuring) is the least understood.

Time-dependent molecular structuring in asphalts AAB-1 and AAM-1 stored at room temperature (21-24°C; 69.8-75.2°F) was monitored by observing the methylene chemical shift region of the NMR spectra. Inspection of the cross polarization/magic angle spinning (CP/MAS) spectra at 20°C (68°F) taken approximately 1 month after NMR sample rotors were first loaded with asphalts showed only a broad signal resonance peak for the methylene carbons centered at 30 ppm. After 1 year, two resonance peaks for the methylene carbons were observed. The initial spectrum of asphalt AAM-1 and the spectrum taken 2 years later are

shown in figures 5-47a and 5-47b. The resonance peaks at 30 and 32 ppm have been identified as the methylene carbons in the amorphous and crystalline phases, respectively.

The appearance of the doublet of resonance peaks in the spectra of the asphalts was first noted after 1 year of storage at 20°C (68°F) and before the asphalt sample was cooled to -45°C (-49°F). Thus, physical hardening observed by Bahia and Anderson [1992] as a result of low-temperature treatment is not related to the appearance of the observed doublet simply because the sample was never subjected to any temperature below room temperature. Oxidative hardening can also be ruled out as a cause of the appearance of the doublet because the asphalt was loaded in the rotor, flushed with dry nitrogen, sealed, and stored at room temperature. The observed time-dependent conversion of methylene carbons in an amorphous phase to an ordered phase may be part of the steric hardening phenomenon, that part related to the crystallization of the waxes in the asphalts. However, the conversion of amorphous to crystalline materials is a long-term change, and would not likely be part of the initial, rapid steric hardening observed in asphalts.

To verify if the crystalline methylene carbons are definitely associated with the wax component in the asphalt, a sample of asphalt AAM-1 that had been stored for 2 years at 21-24°C (69.8-75.2°F) was heated in the rotor to 40°C (104°F) for 4 hours, cooled to 23°C (73.4°F), and the CP/MAS spectrum recorded. This spectrum is shown in figure 5-47c and clearly shows a decrease in the methylene carbons at 32 ppm relative to the methylene carbons at 30 ppm. Further heating of the sample on successive days at higher temperatures reduced even further the resonance peak at 32 ppm taken at ambient temperature, as shown in figures 5-47d and e. The final spectrum resembles that of the initial spectrum. It should be noted also that the overall intensity of the signal decreases with heating of the sample. This reduced intensity is due to inefficient cross-polarization as a result of increased molecular motion of all components in the asphalt. Also of interest, note that the loss of structuring is not instantaneous at 40°C (104°F). After 4 hours at 40°C (104°F), a major portion of the original crystalline wax still remains. It is reasonable then to believe that short periods of warming may not totally reverse crystallization of asphalt components in pavements.

The effects of time and temperature on the ^{13}C CP/MAS NMR spectra of the aromatic carbons were also recorded. Other than changes in signal intensity on heating as observed for the aliphatic carbons, no other changes are evident (figure 5-48). Thus, it may be concluded that molecular structuring is, in part, due to the formation of crystalline methylene carbons of the long chain alkane components. Asphalts contain several types of long carbon chain molecular species such as (1) alkyl-substituted aromatics, (2) long chain carboxylic acids, and (3) normal and branched alkanes. We speculate that it is possible that all long chain species can participate, to some extent, in the crystallization process. However, any components with branched substituents would impart a disorder in the crystal lattice structure.

For the crystallization process to occur, the long n-alkane (paraffinic) carbon chains must change from gauche (a random chain structure, high energy state) conformations into preferred all-trans conformations (an ordered chain structure, low energy state) [Koenig 1991; Mandelkern 1993; Bruch 1996]. The energy difference between the gauche and trans

conformers in polyethylene is reported to be 2 kJ/mol [Ando et al. 1984]. The all-trans conformation is a precursor to the formation of organized assemblies of long chain molecules, which eventually results in their crystallization. Thus, the time-dependent molecular structuring in asphalts may, in part, be due to the slow gauche to all-trans transformation resulting in formation of various crystalline species over a long period of time. The rate of crystallization in a given asphalt can be very slow, as reported by Daly et al. [1996].

In addition to a random to all-trans transformation process, crystal habit transitions can also occur for n-alkanes. That is, at higher temperatures (near the melting point), orthorhombic or monoclinic crystal structures can transform into a pseudohexagonal structure depending upon the chain length of the n-alkanes [Stewart et al. 1996; Filatov et al. 1985]. During the transformation at the higher temperatures, the cell volume increases, and the number of chains performing complete rotation increases. Whether or not this process occurs in asphalts is not known.

The practical implication of this work is to show that changes in physical properties due to crystallization at ambient temperature and below are complex, composition-dependent processes. This work showed that microcrystallites are formed in asphalts over long periods of time at ambient temperature and that the restructuring of the asphalt is not totally reversible, even at higher than ambient temperatures for short periods of time. This demonstrated slow equilibration between amorphous and crystalline forms of long hydrocarbon chains in asphalts strongly suggests that the rapid PG system probably does not predict the expected long-term performance of asphalts at intermediate and low temperatures. The various transformations of long chain hydrocarbons occur slowly and cause changes in physical properties slowly.

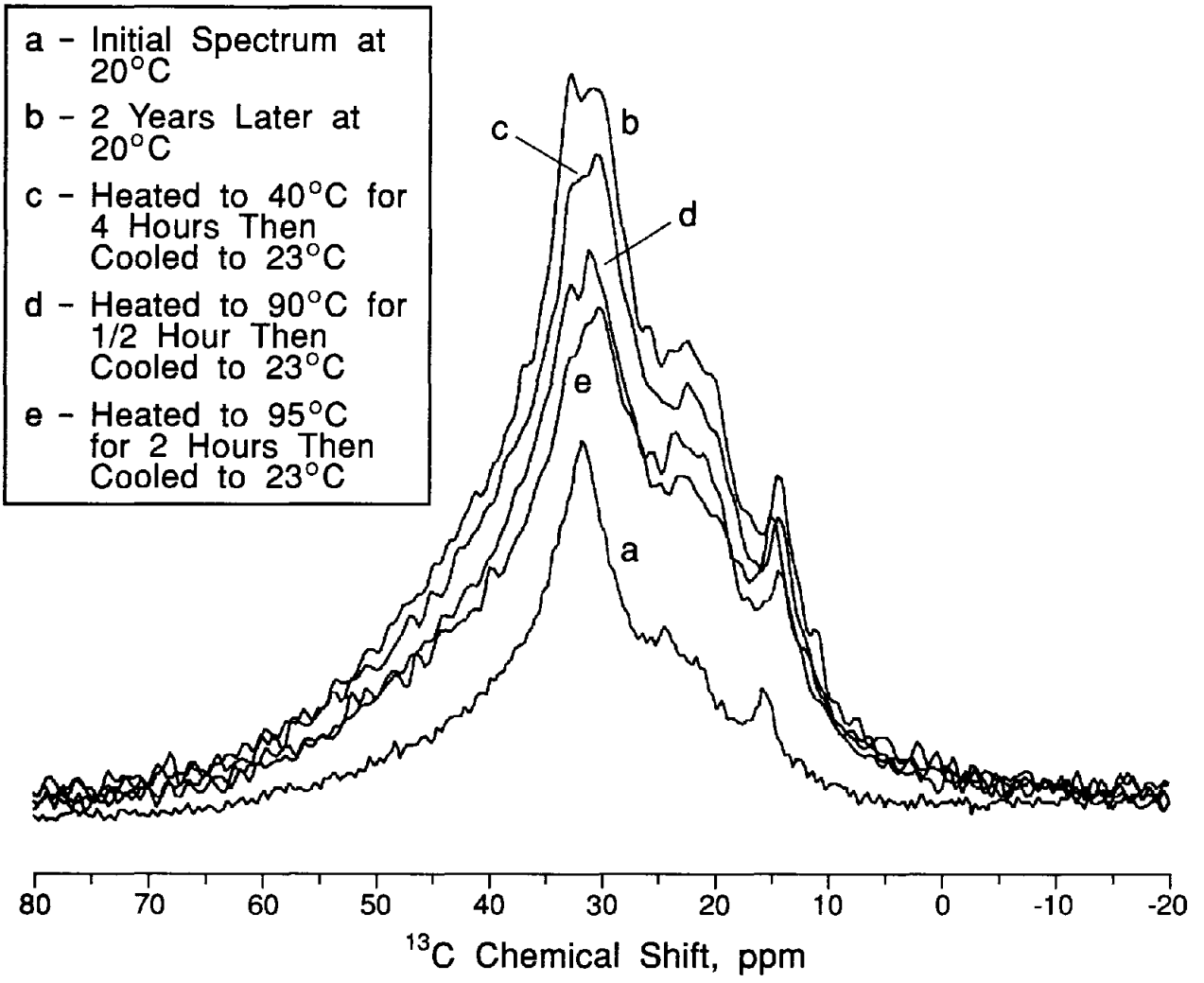

Figure 5-47. Carbon-13 CP/MAS NMR spectra of the aliphatic carbons in asphalt AAM-1: (a) initial spectrum at 20°C, (b) 2 years later at 20°C, (c) heated to 40°C for 4 hours then cooled to 23°C, (d) heated to 90°C for 1/2 hour then cooled to 23°C, and (e) heated to 95°C for 2 hours then cooled to 23°C.

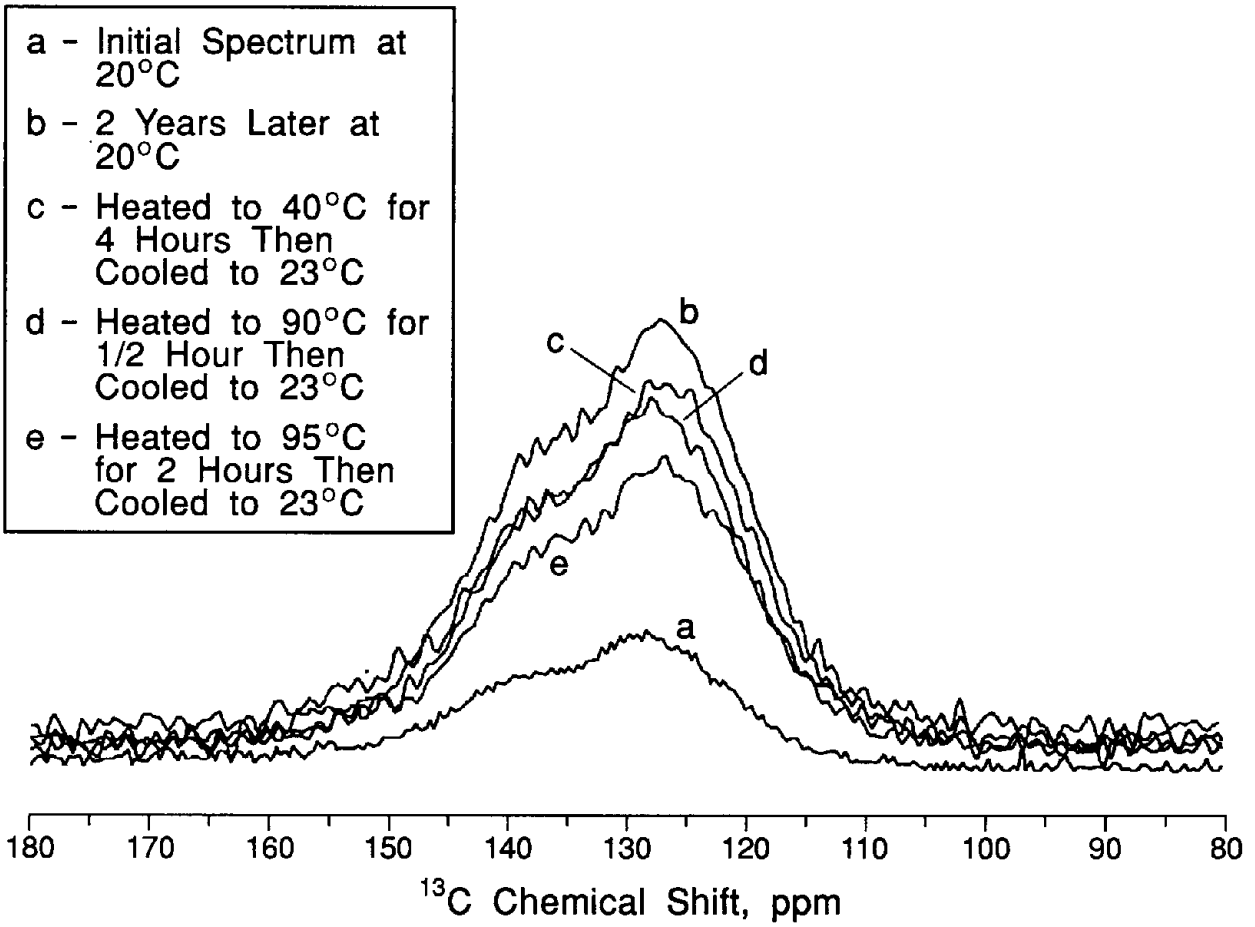

Figure 5-48. Carbon-13 CP/MAS NMR spectra of the aromatic carbons in asphalt AAM-1: (a) initial spectrum at 20°C, (b) 2 years later at 20°C, (c) heated to 40°C for 4 hours then cooled to 23°C, (d) heated to 90°C for 1/2 hour then cooled to 23°C, and (e) heated to 95°C for 2 hours then cooled to 23°C.

PYRIDINE DESORPTION TEST FOR MOISTURE SUSCEPTIBILITY (STRIPPING) OF AGGREGATES

Moisture damage (water stripping) is a significant contributor to fatigue failure and rutting in asphalt pavements. In many pavement mixtures, the properties of the aggregate dominate in determining the sensitivity of the mixture to moisture damage. Thus, a test that could indicate the relative contribution of the aggregate to the moisture sensitivity of the mixture should be of great value. Interest in the development of a fast, simple water sensitivity test grew out of efforts of Petersen et al. [1982] to correlate the thermal desorption of nitrogen from pyridine-treated aggregates and the observed moisture damage of the Lottman experimental pavements and moisture damage using the WRI laboratory freeze-thaw water susceptibility test (WST). In this work, the pyridine desorption test was employed to attempt to rank the thermal desorption of pyridine from aggregates in the same order as the moisture sensitivity of the mixtures as measured by (1) the tensile strength ratio as measured by Lottman's test and (2) their actual 5-year performance as determined in the Lottman field studies. The purpose of this task was to expand the database on the pyridine desorption test to include additional aggregates from asphalt-aggregate mixtures on which performance data were available (e.g., field studies, Lottman testing, WRI pedestal test data, etc.) to assess the value of the test in predicting the water stripping propensity of aggregates. Details of standard procedures for the pyridine desorption test are cited in Volume II, Additional Test Results, Part B.

Previous workers have observed that the basic nitrogen compounds found in petroleum and oil shale adsorb strongly on mineral surfaces. By bonding strongly to a mineral surface the basic nitrogen compounds retard the displacement of organic material by water. Behaving by the same chemical mechanism, basic compounds such as amines are used routinely as asphalt antistrip agents. Plancher et al. [1977] used pyridine as a surrogate model compound in the development of the pyridine thermal desorption test for aggregates. These studies were conducted to determine whether the thermal desorption of pyridine from aggregates at high temperatures correlated with the propensity to resist moisture damage as measured by the Lottman's tensile strength test. The recent pyridine thermal desorption and water-stripping studies were started in mid 1995, using SHRP aggregates as well as the earlier Lottman aggregates as a continuation of the earlier pyridine desorption studies. The immediate objective of the work was to reproduce, as closely as possible, the pyridine thermal desorption results using the original Lottman aggregates and, in addition, expand the pyridine thermal desorption studies and water stripping studies to the newly acquired SHRP aggregates. By plotting the moisture sensitivity test data of an aggregate (Lottman tensile strength values or WRI pedestal test values) versus pyridine thermal desorption test data for the same aggregate, it was possible to determine if pyridine desorption results could be used to predict water sensitivity. A good correlation between the two tests would demonstrate the possibility of replacing the slow Lottman or WRI pedestal test with a fast, predictive, pyridine thermal desorption test for the water sensitivity of aggregates. In addition, an understanding and explanation of any limitations of the pyridine desorption test were sought.

Pyridine thermal desorption tests were conducted using an Antek thermal analyzer fitted with a nitrogen detector to detect the evolution of nitrogen compounds as a function of temperature. Desorption profiles for the evolution of nitrogen-containing compounds from 60-80 mesh aggregates were obtained using temperature programming from 230°C to 800°C (446°F to 1472°F) in 30 minutes. Thus, for each sample information was obtained that described the temperature range of desorbing nitrogen compounds and the quantity of nitrogen desorbed, reported in parts-per-million (ppm). Thermal desorption data were obtained first on raw, washed aggregates in order to measure the amount of indigenous nitrogen in each aggregate and the temperature range over which the indigenous nitrogen evolved. Thermal data were also obtained on each aggregate that had been treated with pyridine to measure the amount of pyridine adsorbed by each aggregate and the temperature range over which the pyridine desorbed. Finally, thermal data were obtained on each aggregate, which had been coated with pyridine and then washed with water, to measure the amount of pyridine desorbed by the water wash and the temperature range over which the remaining pyridine was thermally desorbed. In summary, the three sets of thermal desorption data discussed above were produced for each aggregate, usually in duplicate or triplicate. The earlier pyridine desorption and water stripping studies were extended to include 6 Lottman aggregates, 11 SHRP core aggregates, and 2 clay-containing aggregates in more than 500 experiments. A summary of the thermal desorption data for each aggregate is shown in table 5-2 together with other pertinent composition and water stripping data for each aggregate.

Typical results are shown in figure 5-49 where thermal desorption profiles for the Idaho Lottman aggregate (indigenous nitrogen from raw aggregate, pyridine-coated aggregate, and pyridine remaining on the aggregate after a water wash) are plotted. These profiles are similar to the profiles for pyridine-coated aggregates produced in the earlier thermal desorption studies [Petersen et al. 1982], except in the earlier studies desorption thermograms were not produced to show the thermal desorption distribution of indigenous nitrogen compounds from virgin aggregates or from pyridine-coated aggregates that had been water-washed. The thermal desorption profile for indigenous nitrogen shows that the raw Idaho Lottman aggregate contains about 1.6 ppm of indigenous nitrogen that thermally desorbs in the 330-470°C (626-878°F) temperature range. The profile for adsorbed pyridine shows that the Idaho Lottman aggregate adsorbs 19 ppm of pyridine nitrogen that desorbs in the three different programmed temperature ranges. The profile for pyridine not stripped from the aggregate by a water wash shows that the Idaho Lottman aggregate retains 9.5 ppm of pyridine nitrogen that also desorbs in the three different programmed temperature ranges. Thus, for each aggregate, thermal desorption profiles were obtained from the raw aggregate, the pyridine-coated aggregate, and the pyridine-coated/water washed aggregate that describe the amount of nitrogen compounds desorbed and the temperature ranges in which the desorption occurred. The aggregates were thereby compared or ranked according to their ability to desorb pyridine in any particular temperature range. Figures 5-50 through 5-54 show pyridine thermal desorption characteristics of the Colorado, Arizona, Montana, Virginia, and Georgia Lottman aggregates.

In general, the pyridine desorption tests showed large variability among aggregates in their ability to adsorb pyridine, as had been observed in the earlier experiments. For example, the Lottman Georgia aggregate, a granite, adsorbed no detectable pyridine while the Idaho

Lottman aggregate, an uncharacterized river gravel, adsorbed 18 ppm pyridine. As in the earlier desorption experiments, pyridine desorbed from all aggregates over the same general temperature range with only minor variations from aggregate to aggregate. However, large differences were seen in the ability of water to strip pyridine from the various aggregates. For example, water stripped almost all of the adsorbed pyridine from the Montana Lottman aggregate but stripped less than half of the adsorbed pyridine from the Idaho Lottman aggregate. Large differences were also seen in the indigenous nitrogen content of the aggregates studied, a factor that had to be considered in all quantitative measurements of pyridine desorption. For example, SHRP aggregate RC, a limestone, contained 53 ppm indigenous nitrogen, while SHRP aggregate RD, also a limestone, contained only 1 ppm indigenous nitrogen. Unlike the thermal desorption of pyridine from various aggregates, the temperature range for thermal desorption of indigenous nitrogen was found to be unique for each aggregate. In some cases indigenous nitrogen was desorbed in the same temperature range usually observed for pyridine while in other aggregates indigenous nitrogen evolved from the aggregate at temperatures above 600°C (1,112°F). The two clay minerals studied, kaolinite and bentonite, showed the same general pyridine thermal desorption and water-stripping characteristics as the Lottman and SHRP aggregates, but the amounts of adsorbed pyridine were larger, in the 200-300 hundred ppm range, probably due to the high surface areas of the clays.

The successful development of a pyridine thermal desorption test for predicting moisture sensitivity depended on a good correlation of the laboratory-produced thermal desorption test data and the predictive moisture sensitivity data obtained by a currently accepted test method, such as the Lottman tensile strength ratio (TSR) test. The following text shows examples of the poor correlations that were observed in the attempted development of the pyridine test. The amount of pyridine that desorbed at high temperatures, that is, above 300°C (572°F), was plotted versus Lottman water sensitivity data to determine if a correlation existed between thermal desorption data and water sensitivity data. A typical plot is shown in figure 5-55 where data points falling on a straight line would indicate a good correlation. In the figure, the amount of pyridine desorbed in the temperature range of 470-650°C (878-1202°F) is plotted versus Lottman TSR data for the same aggregates. The statistical R-squared value is 0.50, showing a poor correlation between pyridine desorption data and Lottman moisture sensitivity data. Earlier studies on Lottman samples above 300°C (572°F) showed a statistical R-squared value of only 0.35. Figure 5-56 is concerned with the amount of pyridine retained on the aggregates after a water wash. The amount of retained pyridine desorbing in the temperature range of 470-650°C (878-1,202°F) is plotted versus Lottman TSR data for the same aggregates. The R-squared value is 0.01, showing no correlation between the amount of pyridine retained on the aggregates after a water wash and Lottman moisture sensitivity data. Correlations were also attempted using data from 11 SHRP aggregates. Pyridine thermal desorption data obtained on SHRP aggregates were plotted with WRI pedestal test water sensitivity data [Plancher 1993] and again, poor correlations were observed. All 18 aggregates studied showed a poor correlation of pyridine thermal desorption data with moisture sensitivity data.

In this project many correlations were attempted using many different temperature ranges for thermally desorbed pyridine, but in all cases the low R-square values of the correlations suggested that a simple, predictive thermal desorption test, based on pyridine,

probably was not feasible. The experimental results, shown in table 5-2, also suggest that indigenous nitrogen compounds found in the limestone aggregates RC, RD, and RF were not playing a role in determining the water-stripping properties of an aggregate. As shown in the studies of the Lottman aggregates, the total amounts of pyridine adsorbed by the SHRP aggregates were observed to be unrelated to the moisture sensitivity characteristics of the aggregates. Additionally, the amounts of pyridine tightly bound to the aggregates after a water wash (to mimic the water-stripping properties of nitrogen compounds in asphalt) could not be used to predict the moisture sensitivity of the aggregates. In summary, this phase of the work determined that the various pyridine thermal desorption properties shown by the different aggregates could not be correlated with the Lottman or the WRI moisture susceptibility test data. The development of a fast, predictive moisture sensitivity test based on thermal desorption of pyridine was determined to be unlikely. However, there is another obvious conclusion. In all cases the mixture performance (Lottman data) are plotted versus the desorption data for aggregate alone. The relatively poor correlation suggests strongly that the behavior of asphalt-aggregate mixtures depends upon the composition of asphalt *and* aggregate, i.e., not simply on one component of the mixture. In the Lottman study, both asphalt and aggregate sources varied. Clearly there is a need for control experiments of the type conducted by Lottman, but employing several aggregates with a single asphalt. To date there has been no opportunity to acquire this type of data. However, if there is a straight line relationship between Lottman failure data and pyridine desorption for several aggregates made into mixtures with a single asphalt, then the case would be made that moisture damage is controlled to a significant extent by both components of asphalt concrete. Data from other parts of this study suggest strongly that the composition of both asphalt and aggregate influence moisture sensitivity strongly.

A separate series of experiments was conducted to determine the thermal desorption behavior of model carboxylic acids from aggregate surfaces. The model carboxylic acids were tagged with non-basic nitrogen in order to determine the desorption profiles using the Antek nitrogen analyzer. Both carboxylic acids and pyridine, very polar compounds, mimic the compounds in asphalt most likely to be involved with adhesion of asphalts to aggregate. However, the two different compound types may interact with the aggregate surface by totally different mechanisms. An important step would be to identify the chemical mechanisms of water stripping. Literature from the SHRP program [Tarrer and Wagh 1992; Firth et al. 1993; Labib 1992] and previously unpublished information by Petersen and Plancher [1997] suggested that organic acids, such as the carboxylic acids found in asphalt, play a major role in determining the water sensitivity of a mix. Literature data concerning the adsorption-water desorption properties of various model compounds, including carboxylic acids, indicated that carboxylic acids react with and bind to the aggregate more than other compound types. Importantly, the data [Plancher et al. 1977] also demonstrated that carboxylic acids were not only the most strongly "adsorbing" compound type, but the compound type most easily stripped from the aggregate surface by water. A review of the experimental work conducted in this project and the literature cited above strongly suggested that the chemistry of water stripping of asphalts was directly dependent on the adsorption of carboxylic acids onto carbonate aggregates to form strong bonds at the asphalt-aggregate interface. These experiments suggest that the chemistry of both aggregates and asphalts, rather than the adsorption properties of the aggregate alone, is determining how susceptible any given asphalt-aggregate pair is to water stripping.

In the SHRP program, Tarrer and Wagh [1992] and Firth et al. [1993] developed a simple titration test to rank limestone aggregates according to chemical reactivity of the carbonate minerals with a model compound carboxylic acid (stearic acid) and correlated the results with Lottman TSR data. For the limestones studied, a good correlation was found between the chemical reactivity test and the Lottman water susceptibility test. Aggregates showing the largest amount of carbonate reactivity with stearic acid to form calcium salts were seen to be the aggregates most resistant to water stripping. Following these leads, WRI conducted thermal desorption experiments to test the thermal desorption properties of carboxylic acid model compounds after the acids had been adsorbed and/or reacted on an aggregate surface. Thermal desorption experimental results using non-basic, nitrogen-containing carboxylic acids suggest that carboxylic acid salts may be formed from the chemical reaction of carboxylic acid model compounds with SHRP and Lottman aggregates, especially limestones and limestone-containing gravels. The results support the idea that the chemical reaction of carboxylic acids in asphalts to form salts is playing a major role in determining the water stripping properties of a mixture. These experimental results suggest that the high molecular weight carboxylic acids found in most asphalts are reacting on the surface of carbonate aggregates to produce water-insoluble calcium salts, chemically bonded to the aggregate surface and forming a water insoluble interfacial layer that resists water stripping.

During the last year of the project (mid 1996-mid 1997), research continued to determine whether a fast, simple, water stripping test, based on key chemical characteristics of both the aggregate and the asphalt, could be developed to allow highway engineers to *predict* the water stripping susceptibility of any specific aggregate-asphalt combination to be used in a mix. The goal was to develop a simple, practical test that could be performed rapidly in any State highway laboratory. As designed, the water stripping test developed required one simple potentiometric titration test on the aggregate and one simple potentiometric titration test on the asphalt. This method employed SHRP aggregates, some of which were limestones, and SHRP asphalts. During the course of the work additional information was acquired to help identify the chemical mechanism(s) by which limestone and the pretreatment of aggregates with lime prevent water stripping. This research extended the work of Tarrer and Wagh [1992] by developing a fast, simple, potentiometric titration test to rank the aggregates according to chemical reactivity with a model carboxylic acid that mimics the carboxylic acids found in asphalt. Indole-3-acetic acid was used as the model compound. This method was expanded to include elemental analysis for metallic ions (Ca, Mg, Fe, Al, Na, and K), which identified the chemical nature of the water soluble or water insoluble salts formed during the reaction of the carboxylic acid with the aggregates. The identification of the metallic ions that form salts at the asphalt-aggregate interface appears to be one of the three key pieces of information for predicting the water stripping characteristics of any asphalt-aggregate pair. (The solubility of the salts in water is determined by the kind of metallic ion forming the salt. Calcium salts are insoluble while sodium salts are soluble.) Tarrer's original test was extended to measure the amounts of carboxylic acids in the asphalts because this predictive test is based on the carboxylic acid content of the asphalts as well as the carbonate and calcium content of the aggregates. The measurement of the amounts of carboxylic acids in an asphalt is made by a second potentiometric titration, a technique for the analysis of carboxylic acids that was developed in another part of this research program and is described elsewhere in this report.

Data collected in the present research indicated that at least three factors are involved in the chemistry of water stripping, the three most important being (1) the carbonate content (and reactivity) of the aggregate, (2) the calcium, magnesium and sodium content of the aggregate, and (3) the carboxylic acid content of the asphalt. The following tables show the three different kinds of compositional data that were collected. These data were then correlated with the WRI-WST water stripping (briquette) data produced in the SHRP program to determine the degree to which the water stripping characteristics of any asphalt-aggregate pair can be correctly predicted from the compositional data.

Data from the simple potentiometric titration test measuring the carbonate content and chemical reactivity of the aggregates are shown in table 5-3 and graphically displayed in figure 5-57. Figure 5-57 shows the wide differences in acid-base reactivity of the different aggregates, due primarily to different carbonate content of the different aggregates and the different morphology of the different aggregates. The data demonstrate how a simple titration test is used to rank aggregates according to carbonate reactivity with the model carboxylic acid.

Data showing the amounts of calcium, magnesium, sodium, and other metallic salts formed from the reaction of model carboxylic acid with aggregates are shown in tables 5-4 and 5-5. These data are a measure of the ability of various aggregates to form insoluble or soluble metal salts at the asphalt/aggregate interface. High molecular weight calcium and magnesium salts are presumed to be insoluble in water and should resist water stripping while sodium and potassium salts are often surface active materials (soaps) that likely promote water stripping at the interface.

Data showing the carboxylic acid content of the asphalts, as measured by a second simple potentiometric titration test developed in this project, are shown in table 5-6. The basic concept is that water stripping is retarded when carboxylic acids in the asphalt adsorb onto and/or react with carbonate minerals on the aggregate surface. Water stripping is thought to be *promoted* when carboxylic acids in the asphalt react with aggregate (such as high-surface-area sodium-containing clays) to form soluble sodium salts of the carboxylic acids that behave like soaps at the asphalt-aggregate interface. It is important to quantify carboxylic acids in asphalts because the amount of carboxylic acids determines the absolute maximum amount of all kinds of carboxylic acid salts that can be formed at the interface. The amounts of carboxylic acids shown in table 5-6 below were used to predict the water stripping characteristics of the asphalt-aggregate combinations.

The moisture sensitivity test results shown in table 5-7 below were not produced in the current program but were published in the SHRP project final report (SHRP-A-341) [Curtis et al. 1993] and were used in the current work to correlate water stripping data with compositional data quantitatively. The briquettes used for the previous SHRP freeze-thaw tests were made from the same asphalts and aggregates being used in the current water stripping test, thus the data from previous and current work can be correlated. The data represent the number of freeze-thaw cycles to failure for 88 *different* asphalt-aggregate combinations measured by the WRI-WST briquette test. These data were used as a representation of the water stripping characteristics of the 88 defined aggregate-asphalt combinations. This data set from the SHRP

program containing quantitative water stripping data was used to classify asphalt combinations as "nonstrippers, intermediate strippers, or strippers" and was valuable to the current experimentation to develop a fast, simple test to predict water stripping. The quantitative water stripping results of the freeze-thaw tests were correlated directly with the quantitative compositional data determined by the potentiometric titration tests. The data shown below in table 5-8 are the same WRI-WST briquette test data shown in table 5-7 but arranged to rank the asphalt-aggregate combinations clearly according to stripping characteristics as measured by freeze-thaw cycles-to-failure. Low numbered cycles-to-failure indicate a stripping asphalt-aggregate pair; high numbered cycles-to-failure indicate a non-stripping combination. These data were used for both discriminate and regression statistical analyses at the University of Wyoming Department of Statistics.

Compositional data from tables 5-3, 5-4, 5-5, and 5-6 above were correlated with WRI-WST briquette data shown in table 5-8 above to determine the degree to which freeze-thaw water stripping data could be predicted from compositional data. The briquette data, measuring freeze-thaw cycles-to-failure of briquettes, provided data from 88 different combinations of SHRP asphalts and aggregates. The compositional data from the above tables were produced by potentiometric titration of the asphalts, potentiometric titration of the solution resulting from the reaction of the aggregate with the model carboxylic acid, and from the analyses of metals in the reacted solution. Two kinds of statistical analyses were performed at the University of Wyoming: (1) discriminate analyses and (2) regression analyses. Discriminate analyses showed that, using simple compositional data from both asphalts and aggregates, any asphalt-aggregate pair could be successfully predicted to be a stripper, intermediate stripper, or non-stripper 85-90 percent of the time, depending on the number of cycles-to-failure used to define a stripping or non-stripping mix. The discriminate analyses also showed that, using the three stripping categories, asphalt-aggregate combinations were never identified as being non-strippers when in fact they were strippers, a mistake that could prove costly in pavement design. Regression analyses of the same simple compositional data showed R-square values ranging from 0.88 to 0.93, meaning that almost all of the variability in water stripping resulted from the compositional data obtained from the asphalts and the aggregates. The most important compositional factors influencing water stripping were found by regression analyses to be the calcium, magnesium, and carbonate content of the aggregates and the carboxylic acid content of the asphalts. The regression analyses showed that freeze-thaw cycles-to-failure were correctly predicted over 90 percent of the time. The experimental results suggest that the development of a simple, practical, water stripping test, based on easily obtained compositional data, is possible.

In general, the ability to predict WST-defined moisture susceptibility correctly suggests strongly that the most "active players" in moisture sensitivity have been identified. R-squared values of over 0.90 probably would not be observed if the wrong chemical parameters were used for the regression analyses. A speculative chemical model of water stripping may involve reactions of asphalt acids and aggregate to form salts at the surface of the aggregate, creating an interface layer. The reactions at the surface generate the layer forming the bond between the asphalt and the aggregate. Carboxylic acid salts, being both ionic in nature (at the carboxylate end) and non-polar in nature (the hydrocarbon end), are the transition film between the ionic aggregate and the much less polar asphalt. The second, critical, feature of this model is the

degree of water solubility of the salts formed at the interface. High molecular weight calcium and magnesium salts are generally insoluble in water and can, over time, maintain a strong water-insoluble bond at the surface and thus prevent water stripping. High molecular weight sodium and potassium salts are detergents that form weak bonds at the interface and would be expected to promote water stripping.

This experimental work, like that described in the pyridine desorption experiments, shows that the compositions of both aggregate and asphalt influence moisture sensitivity. Again, consider the data in table 5-8. Briquettes prepared with aggregate RK and asphalt AAM-1 survive >50 freeze-thaw cycles while those using aggregate RK and asphalts AAF-1, AAA-1, and AAG-1 survive only a few cycles. Conversely, briquettes prepared from asphalt AAM-1, when used with aggregates RJ, RL, RE, RB, and RH survive only a few freeze-thaw cycles. To reiterate, the composition of aggregate *and* asphalt must be considered in order to predict moisture susceptibility of asphalt concrete.

For the development of a fast, simple, and predictive water stripping test, several areas of experimentation should be followed. More briquette specimens produced from aggregates and asphalts of known chemical composition should be produced and tested for moisture sensitivity. This would expand the database of asphalt-aggregate pairs of known chemical composition and produce more examples correlating chemical data with briquette water stripping susceptibility data. A greater level of statistical significance would then be achieved. The set of 88 different combinations already studied has generated reasonably good statistical data, but more examples are needed to validate these observations. Two sets of WRI-WST briquettes, one prepared from lime-treated aggregates and one prepared from lime-treated asphalts, should be prepared and freeze-thaw tested. The results of these freeze-thaw tests would be compared with previous WRI-WST test results to determine the relative effectiveness of adding lime to aggregates or asphalts before mixing. Samples of asphalts and aggregates being used in current pavement construction should be acquired and analyzed by the simple titration tests being developed for the prediction of moisture susceptibility. The usefulness of the new test could then be validated. Finally, samples of both aggregates and asphalts used in Long Term Pavement Performance (LTPP) construction projects should be subjected to validation tests (titration tests) to determine if the new water stripping titration tests predict field performance accurately.

Table 5-2. Summary of aggregate test data, including pyridine sorption/thermal desorption data and pyridine water stripping data.

Sample	Mineral type	Major elements as oxides and loss on ignition (LOI), mass %	Indigenous nitrogen, ppm	Pyridine adsorbed, ppm	Pyridine removed by water, ppm	Water stripping classification by visual observation	Moisture sensitivity, WRI pedestal test freeze-thaw cycles	Moisture sensitivity, Lottman TSR, (cond./dry)	Surface area, m2/g
RA	Lithonia Granite, GA	Si 73.4 Al 13.4 K 4.9 Na 3.4 LOI 0.22	0	Trace	Trace	Stripping	3-12		0.19
RC	Limestone, KS	Ca 48.9 C 40.3 Si 6.5 Mg 2.5 LOI 40.3	53	7	7	Non-stripping	29-50		2.90
RD	Limestone, MD	Ca 39.1 C 35.0 Si 16.4 Mg 5.3 LOI 35.0	1	2	2	Non-stripping	26-50		0.72
RE	Piedmont Gravel, MD	Si 93.7 Al 1.86 Fe 1.46 Ca 0.42 LOI 0.43	0	Trace	Trace	Intermediate stripping	1-3		0.95
RF	Glacial Gravel, IL	Ca 25.9 Mg 16.7 Si 15.8 Al 1.89 LOI 37.4	1	1	1	Intermediate stripping	8-50		1.66
RG	Sandstone, PA	Si 52.8 Ca 23.8 Al 2.3 K 0.9 LOI 18.7	0	33	33	Intermediate stripping	4-44		1.99

Table 5-2. Summary of aggregate test data, including pyridine sorption/thermal desorption data and pyridine water stripping data (continued).

Sample	Mineral type	Major elements as oxides and loss on ignition (LOI), mass %	Indigenous nitrogen, ppm	Pyridine adsorbed, ppm	Pyridine removed by water, ppm	Water stripping classification by visual observation	Moisture sensitivity, WRI pedestal test freeze-thaw cycles	Moisture sensitivity, Lottman TSR, (cond./dry)	Surface area, m2/g
RH	Graywacke, CA	Si 66.0 Fe 12.9 Al 10.4 Na 2.57 LOI 0.96	41	62	62	Non-stripping?	1-5		2.74
RJ	Mtn Gravel Conglomerate, WY	Si 76.5 Al 12.2 K 4.3 Na 2.9 LOI 0.59	0	27	27	Stripping	1-2		1.32
RK	Basalt, OR	Si 50.1 Fe 15.7 Al 13.7 Ca 10.3 Mg 6.88 LOI -0.36	2	241	241	Non-stripping	2-50		15.73
RL	Gulf Coast Gravel, TX	Si 63.1 Ca 14.5 Al 4.7 K 1.72 LOI 11.2	30	2	-7 (loss of clays?)	Stripping	1-2		2.41
Idaho, Lottman	Salmon River Gravel	Ca high Fe high Si medium Al medium	2	37	32	Very slightly stripping	2	0.82	2.30
Montana, Lottman	Bench Gravel	K high S high Si medium Al medium	0	4	0	Intermediate stripping	5	0.62	0.47

Table 5-2. Summary of aggregate test data, including pyridine sorption/thermal desorption data and pyridine water stripping data (continued).

Sample	Mineral type	Major elements as oxides and loss on ignition (LOI), mass %	Indigenous nitrogen, ppm	Pyridine adsorbed, ppm	Pyridine removed by water, ppm	Water stripping classification by visual observation	Moisture sensitivity, WRI pedestal test freeze-thaw cycles	Moisture sensitivity, Lottman TSR, (cond./dry)	Surface area, m2/g
Virginia, Lottman	Coarse Granite	K high Ca medium Si medium Al medium	1	1	1	Stripping	3,4	0.35	2.61
Colorado, Lottman	Coarse Morrison crushed stone, fine Platte River material	K high S high Si medium Al medium	1	47	45	Stripping	3	0.22	1.95
Arizona, Lottman	Santa Cruz River Gravel	K high Ca medium Si medium Al medium	1	39	39	Stripping	2	0.21	3.00
Georgia, Lottman	Granite Gneiss	K high Ca medium Si medium Al medium	0	0	0	Very severe stripping	2	0.00	0.10
Bentonite Clay	Montmorillonite, volcanic origin	Na high Al high Si high	109	426	426				
Kaolinite Clay	Clay	Al high Si high	125	343	343				

Table 5-3. Potentiometric titration test results ranking the amount of model carboxylic acid (indole-3-acetic acid) consumed by SHRP aggregates.

Aggregate	Acid consumed meq/g, trial run 1	Avg. acid consumed meq/g, run 1 expts.	Avg. acid consumed meq/g, run 2 expts.
RA	0.001	0.1792	0.3057
RB	-0.001	0.1938	0.3393
RC	0.0205	1.1466	2.0699
RD	0.0216	1.2284	1.6348
RE	-0.001	-0.0773	0.5455
RF	0.0505	2.3699	2.1921
RG	0.0179	0.9955	1.2179
RH	0.0179	1.0091	1.7213
RJ	0.0044	0.2909	0.6943
RK	0.0129	0.7784	0.7232
RL	0.0134	0.7580	0.7586

Table 5-4. Elemental analyses of solutions resulting from the reaction of indole-3-acetic acid with SHRP aggregates, run 1.

Sample number	Sample	Mesh	Prep time, days	Ca, mg/L	Mg, mg/L	Fe, mg/L	Al, mg/L	Na, mg/L	K, mg/L
0889-53-15	Blank Sol.			3	0.14	<3	<10	5.50	<2
0889-57-13	RA	60-80	2	17	9.92	<3	<10	3.55	3
0889-66-13	RB	60-80	2	26	13.5	<3	53	14.3	<2
0889-57-18	RC	60-80	2	108	24.9	<3	<10	3.04	<2
0889-53-13	RD	60-80	2	90	19.2	<3	<10	19.9	<2
0889-66-18	RE	60-80	2	11	10.8	<3	<10	5.82	<2
0889-53-18	RF	60-80	2	50	40.7	<3	<10	10.7	<2
0889-70-13	RG	60-80	2	103	21.4	<3	25	5.57	<2
0889-63-13	RH	60-80	2	47	15.3	<3	22	6.19	<2
0889-63-18	RJ	60-80	2	34	10.6	<3	<10	10.8	<2
0889-60-13	RK	60-80	2	39	54.7	<3	<10	8.28	<2
0889-60-18	RL	60-80	2	58	17.2	<3	<10	17.5	<2

Table 5-5. Elemental analyses of solutions resulting from the reaction of indole-3-acetic acid with SHRP aggregates, run 2.

Sample number	Sample	Mesh	Prep time, days	Ca, mg/L	Mg, mg/L	Fe, mg/L	Al, mg/L	Na, mg/L	K, mg/L
E8787	Blank Sol.			<2	0.4	<2	<10	5.1	<1
0889-84-11	RA	80-100	2	<2	18.6	<2	20	14	<1
0889-84-13	RB	80-100	2	12	25.8	<2	<10	27.7	<1
0889-84-15	RC	80-100	2	38	41.7	<2	<10	14.5	<1
0889-86-11	RD	80-100	2	46	44.7	<2	<10	6.6	<1
0889-86-13	RE	80-100	2	3	18.9	<2	12	7.0	<1
0889-84-17	RF	80-100	2	23	160	<2	17	7.9	<1
0889-86-15	RG	80-100	2	43	36.8	<2	<10	6.8	<1
0889-86-17	RH	80-100	2	19	27.7	<2	11	11.8	<1
0889-84-19	RJ	80-100	2	12	21.3	<2	15	12.1	<1
0889-86-18	RK	80-100	2	58	115	<2	117	10.9	16
0889-86-20	RL	80-100	2	12	30.2	<2	15	22.1	<1

Table 5-6. Potentiometric titration of carboxylic acids in asphalts.

Asphalt	Carboxylic acid content, meq/g
AAD-1	0.042
AAK-1	0.035
AAA-1	0.03
AAF-1	0.025
AAG-1	0.02
AAB-1	0.015
AAM-1	0.013
AAC-1	0.011

Table 5-7. Moisture sensitivity test results[1] for SHRP asphalt-aggregate combinations.

SHRP asphalts	Aggregates (20-35 mesh size)																					
	RJ		RL		RC		RD		RH		RA		RE		RF		RB		RG		RK	
	A	B	A	B	A	B	A	B	A	B	A	B	A	B	A	B	A	B	A	B	A	B
AAA-1	1	1	1	1	29	36	48	49	4	4	7	7	2	2	49	49	3	3	6	6	4	4
AAB-1	1	1	1	1	40	44	47	50	3	3	3	4	2	3	40	44	2	2	7	8	12	11
AAC-1	2	2	2	2	>50	>50	>50	>50	4	5	36	36	3	3	42	>50	5	5	24	26	40	20
AAD-1	1	1	1	1	>50	>50	>50	>50	3	4	4	6	3	3	21	16	2	2	25	25	13	7
AAF-1	1	1	1	1	>50	>50	>50	>50	2	2	12	12	3	3	>50	41	3	3	9	9	4	4
AAG-1	1	1	1	1	42	43	26	31	1	1	6	7	1	1	8	9	1	1	4	5	2	2
AAK-1	1	1	2	2	>50	>50	>50	>50	2	3	9	10	2	2	10	15	2	3	11	11	5	4
AAM-1	2	2	2	2	>50	>50	>50	>50	5	5	>50	>50	2	2	40	30	6	5	41	44	>50	>50

[1] Number of repeated freeze-thaw cycles required to fracture test specimen
A and B = Test specimens containing 5 wt percent asphalt and 95 wt percent aggregate
>50 = Test terminated after 50 freeze-thaw cycles, no specimen failure

Table 5-8. Sorted WST data. Same data as in table 5-7 above, but sorted by freeze-thaw cycles-to-failure.[1]

SHRP asphalts	Aggregates (20-35 mesh size)																					
	RJ		RL		RE		RB		RH		RG		RA		RK		RF		RC		RD	
	A	B	A	B	A	B	A	B	A	B	A	B	A	B	A	B	A	B	A	B	A	B
AAM-1	2	2	2	2	2	2	6	5	5	5	41	44	>50	>50	>50	>50	40	30	>50	>50	>50	>50
AAC-1	2	2	2	2	3	3	5	5	4	5	24	26	36	36	40	20	42	>50	>50	>50	>50	>50
AAK-1	1	1	2	2	2	2	2	3	2	3	11	11	9	10	5	4	10	15	>50	>50	>50	>50
AAF-1	1	1	1	1	3	3	3	3	2	2	9	9	12	12	4	4	>50	41	>50	>50	>50	>50
AAD-1	1	1	1	1	3	3	2	2	3	4	25	25	4	6	13	7	21	16	>50	>50	>50	>50
AAB-1	1	1	1	1	2	3	2	2	3	3	7	8	3	4	12	11	40	44	40	44	47	50
AAA-1	1	1	1	1	2	2	3	3	4	4	6	6	7	7	4	4	49	49	29	36	48	49
AAG-1	1	1	1	1	1	1	1	1	1	1	4	5	6	7	2	2	8	9	42	43	26	31
	Stripper										Intermediate Stripper										Non-stripper	

[1] Number of repeated freeze-thaw cycles required to fracture test specimen
A and B = Test specimens containing 5 wt percent asphalt and 95 wt percent aggregate
>50 = Test terminated after 50 freeze-thaw cycles, no specimen failure

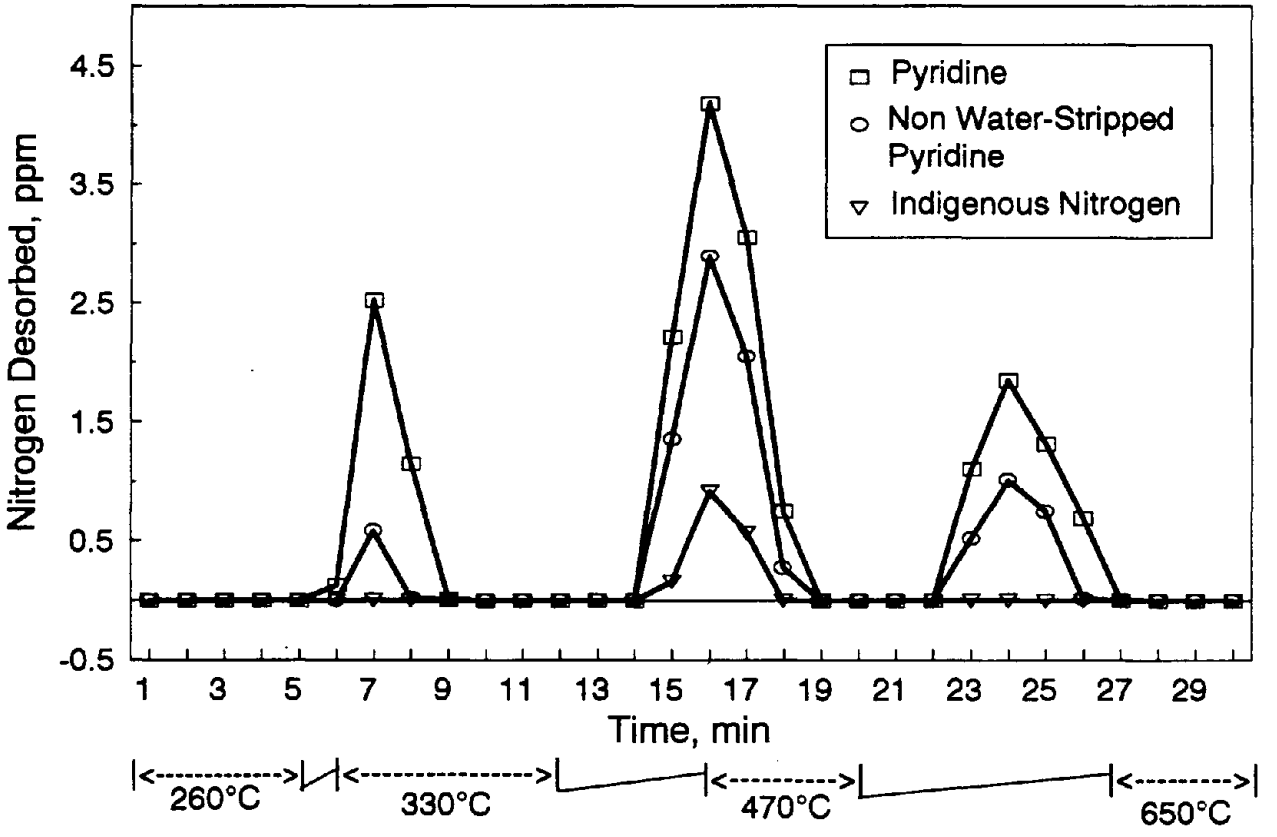

Figure 5-49. Thermal desorption characteristics of nitrogen-containing compounds from 70-80 mesh Idaho Lottman aggregate.

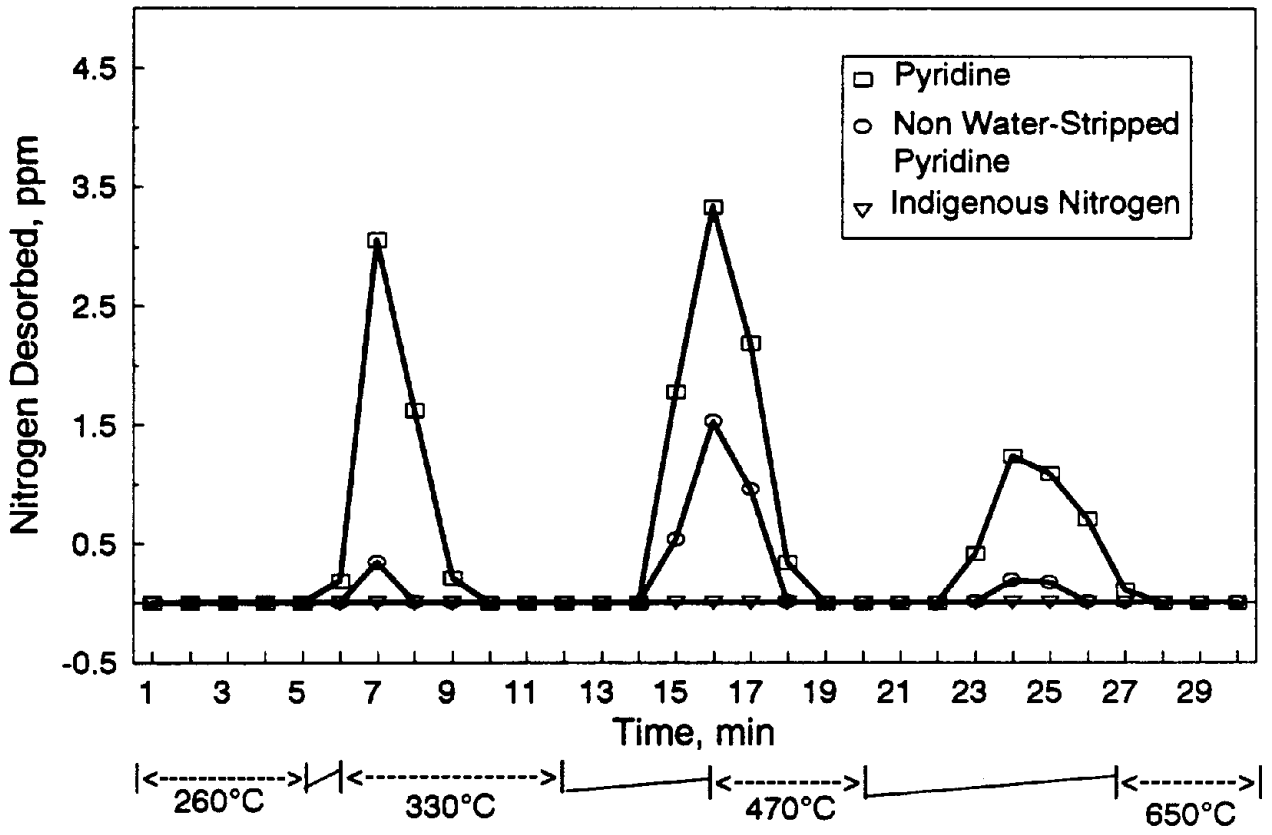

Figure 5-50. Thermal desorption characteristics of nitrogen-containing compounds from 70-80 mesh Colorado Lottman aggregate.

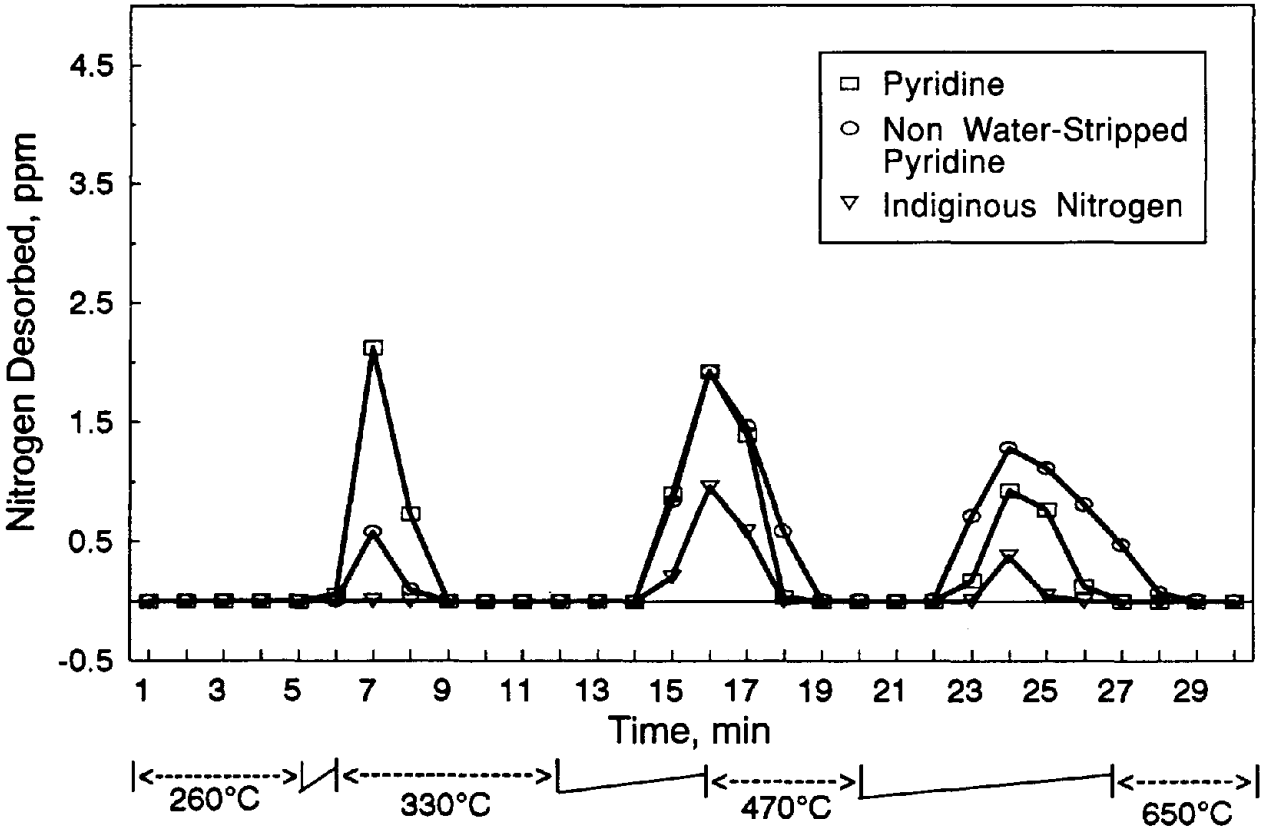

Figure 5-51. Thermal desorption characteristics of nitrogen-containing compounds from 70-80 mesh Arizona Lottman aggregate.

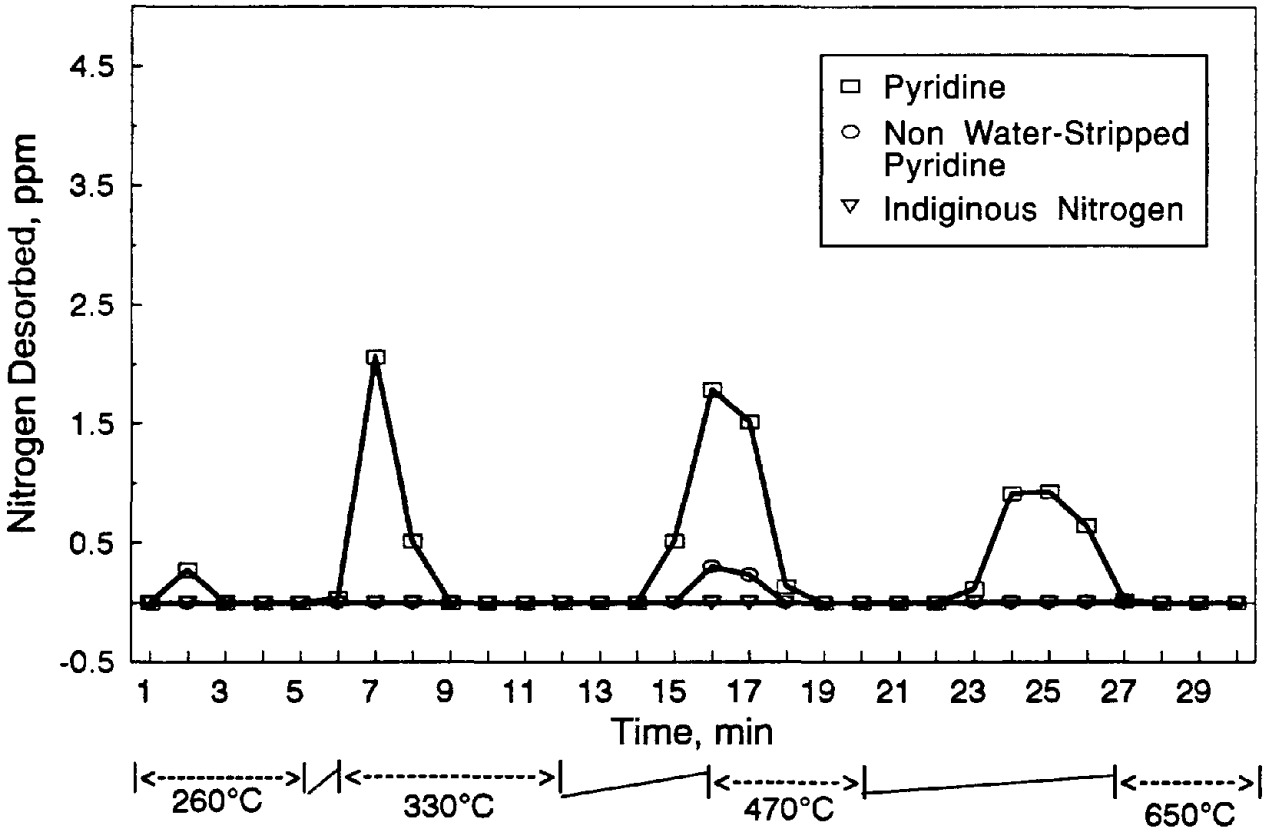

Figure 5-52. Thermal desorption characteristics of nitrogen-containing compounds from 70-80 mesh Montana Lottman aggregate.

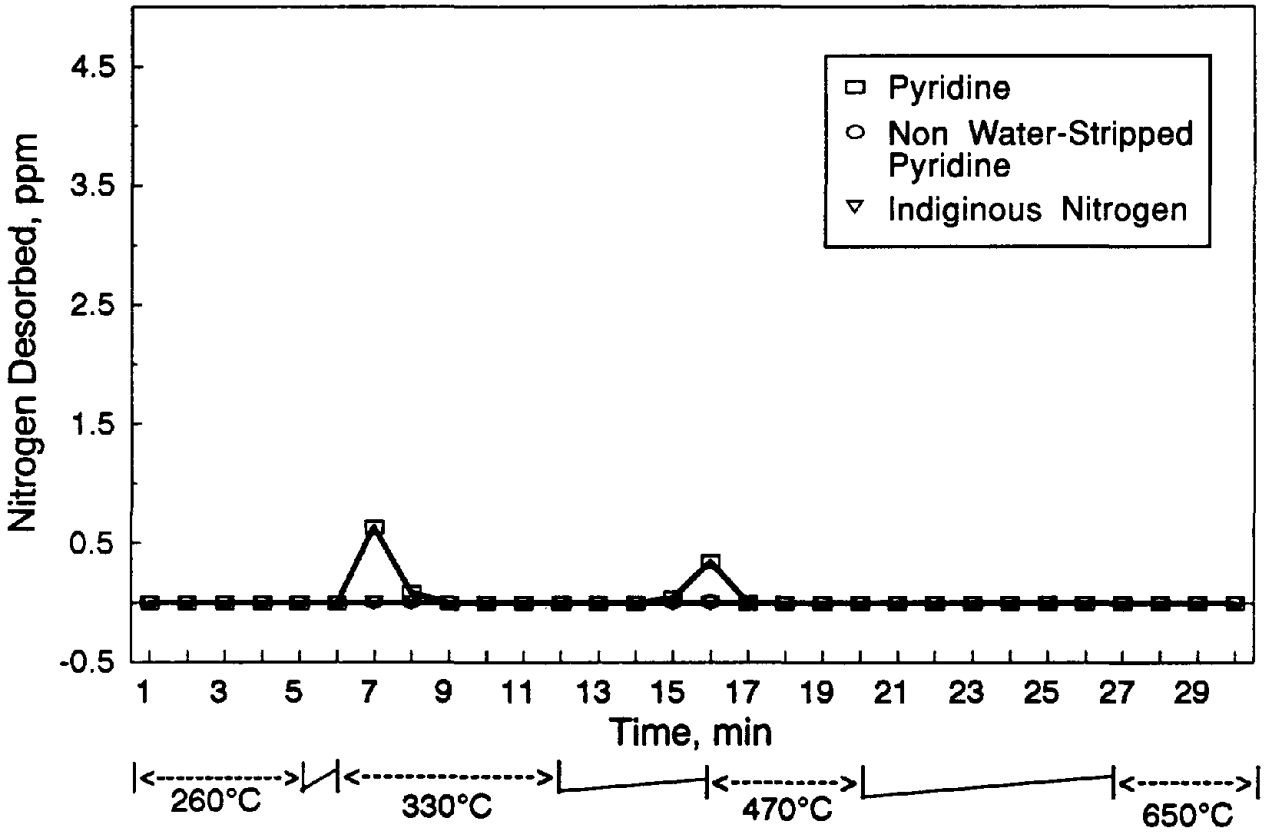

Figure 5-53. Thermal desorption characteristics of nitrogen-containing compounds from 70-80 mesh Virginia Lottman aggregate.

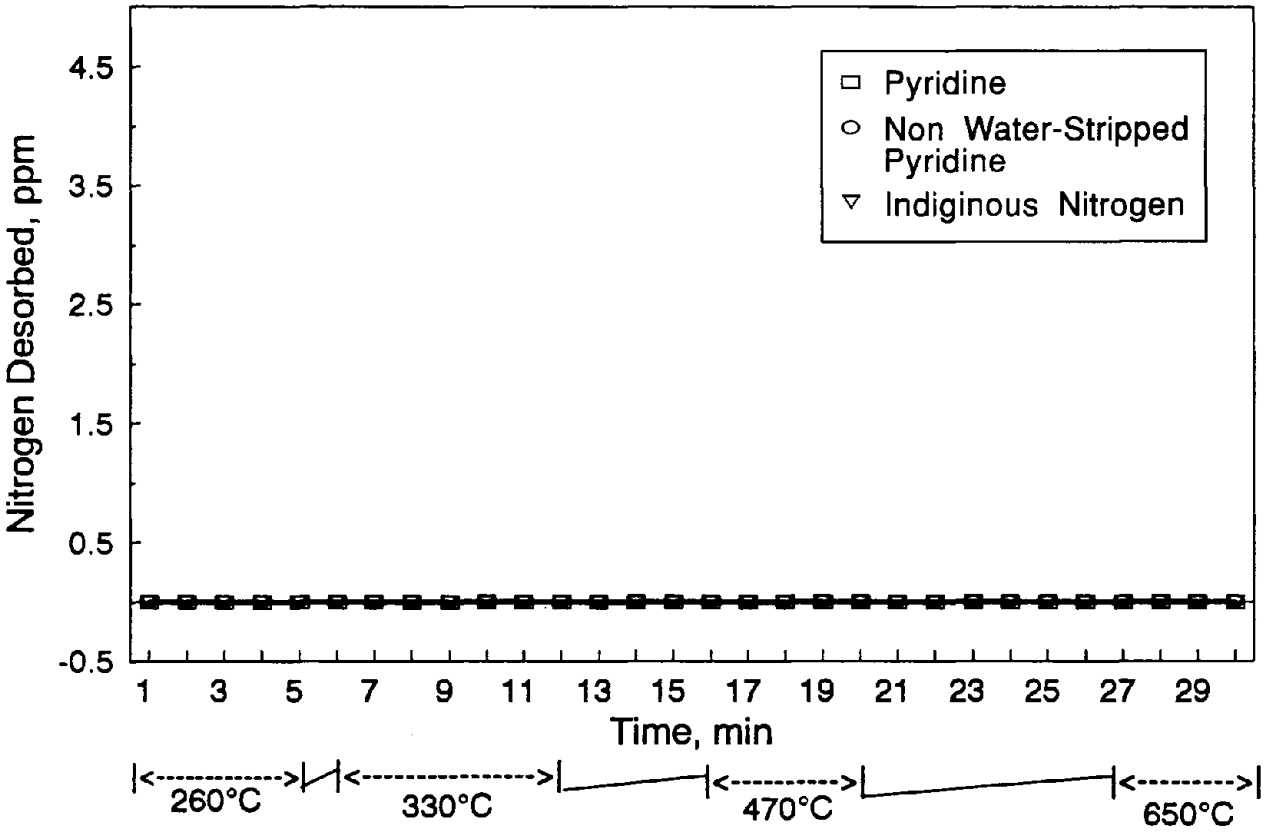

Figure 5-54. Thermal desorption characteristics of nitrogen-containing compounds from 70-80 mesh Georgia Lottman aggregate.

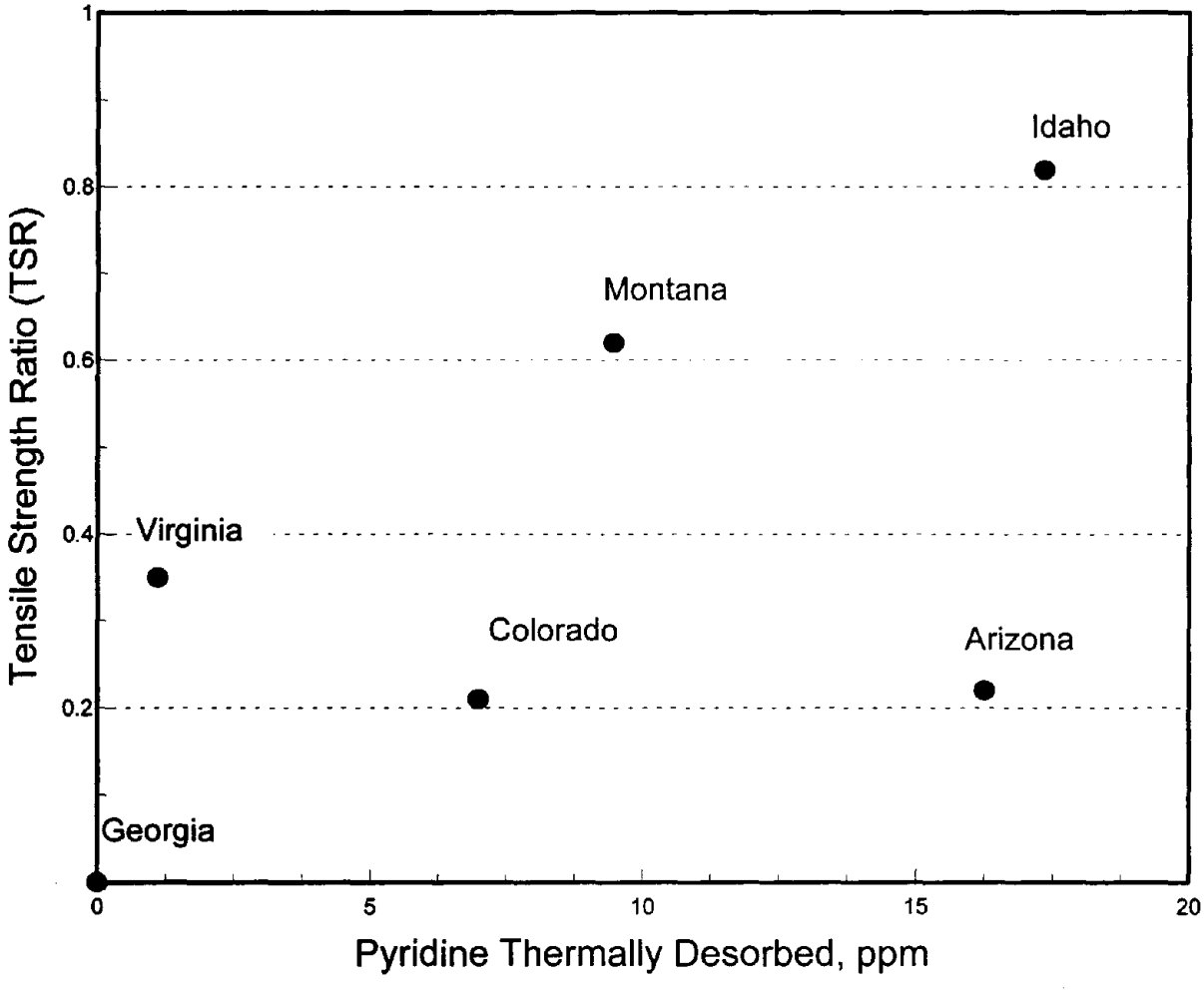

Figure 5-55. Correlation of Lottman II TSR data and pyridine thermally desorbing 470-650°C. R-squared value is 0.50.

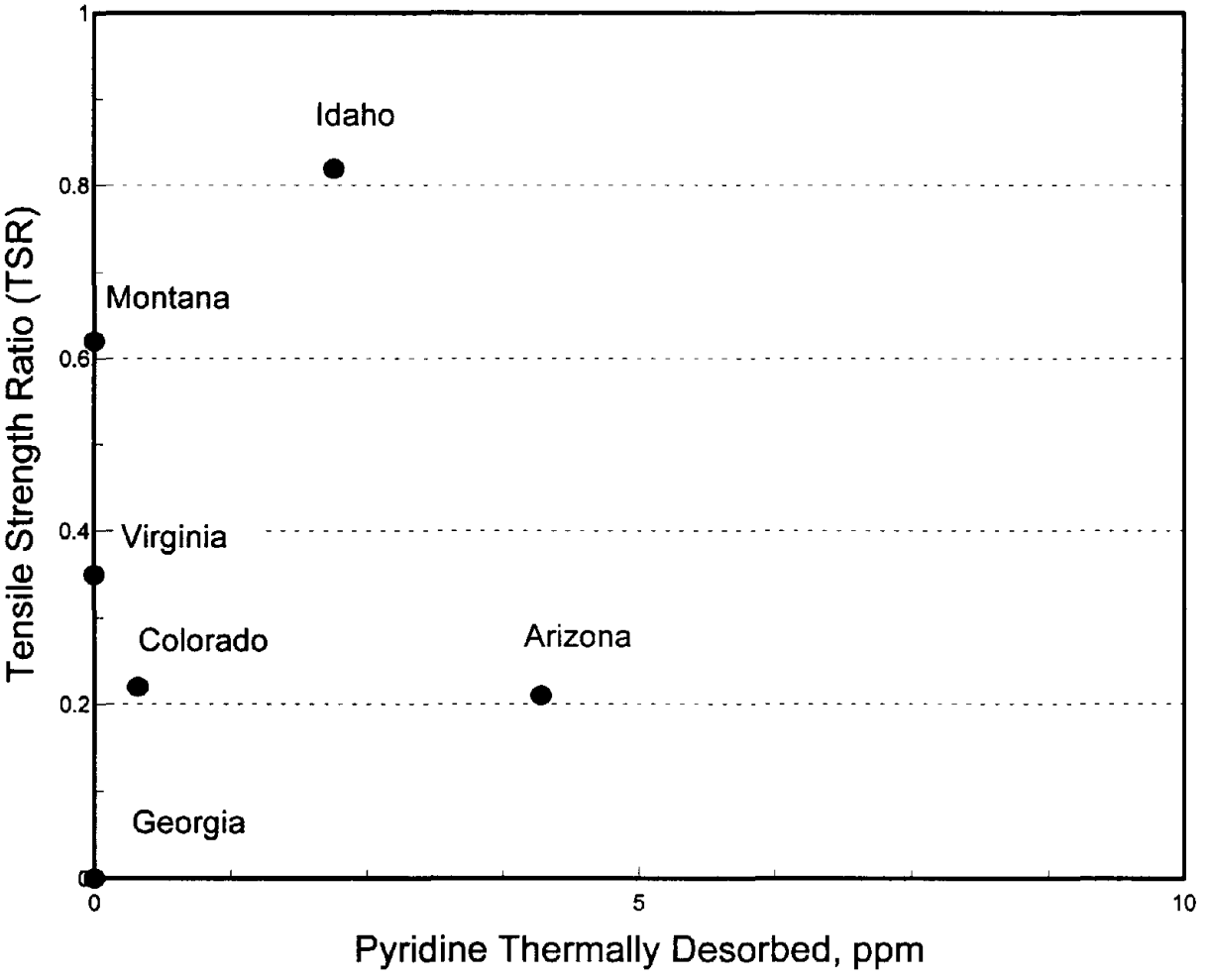

Figure 5-56. Correlation of Lottman II TSR data and pyridine/water washed sample desorbing 470-650°C. R-squared value is 0.01.

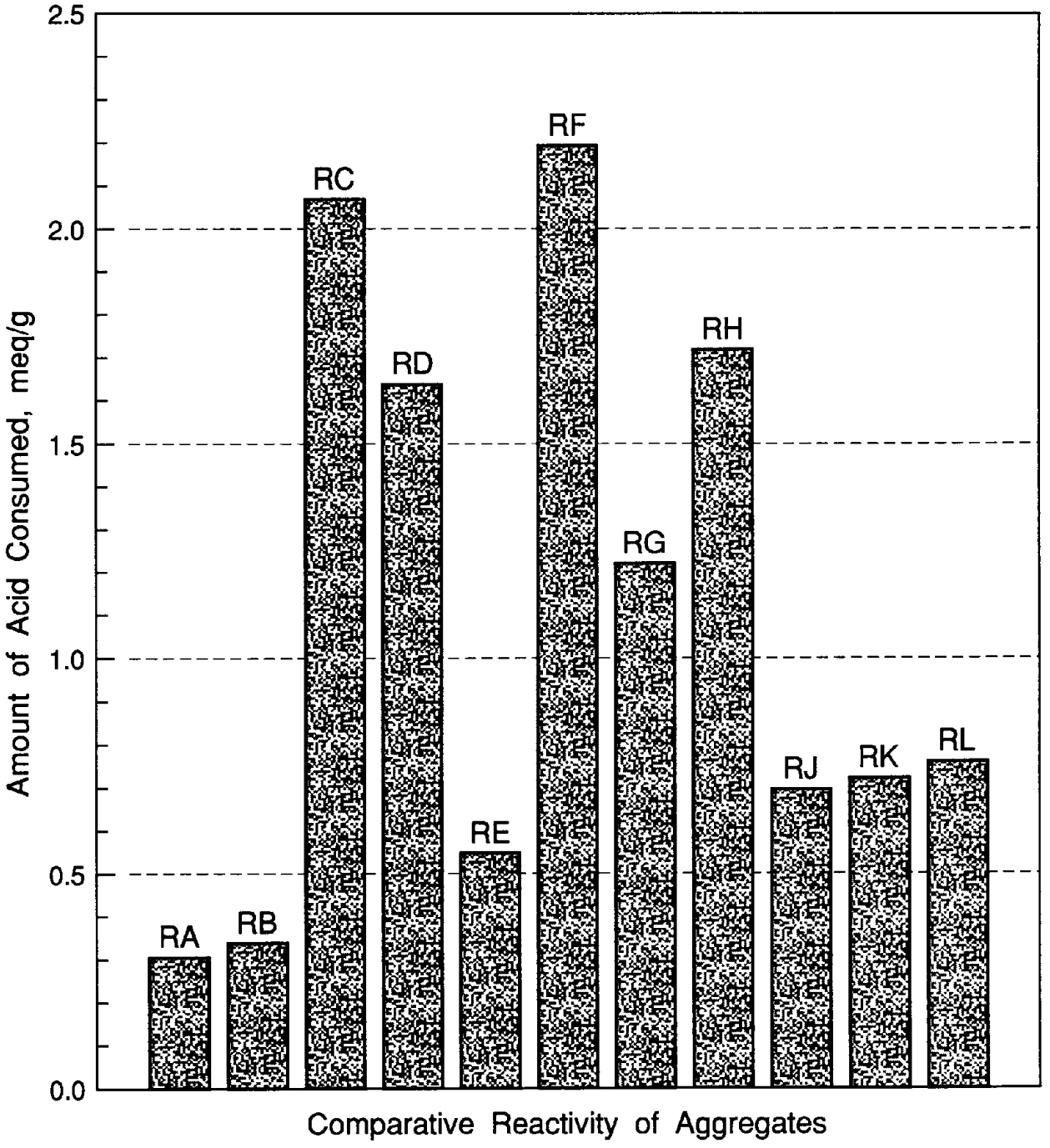

Figure 5-57. Meq/g of Indole-3-acetic acid consumed after reaction with 5 grams of 11 different SHRP aggregates (80-100 mesh) for 2 days.

REFERENCES

Anderson, D. A., D. W. Christensen, H. U. Bahia, R. Dongre, M. G. Sharma, C. E. Antle, and J. Button, 1994, *SHRP-A-369, Binder Characterization and Evaluation, Volume 3: Physical Characterization.* Strategic Highway Research Program, National Research Council, Washington D.C., p. 195.

Anderson, D. A., M. Marasteanu, C. Antle, and T. Ruscitti, Relationship of SHRP Asphalt Binder Properties to Performance," Final Report, June 30, 1995. Submitted to Western Research Institute as part of Federal Highway Administration Contract DTFH61-92C-00170.

Ando, I., T. Yamanobe, T. Sorita, T. Komoto, H. Sato, K. Deguchi, and M. Imanari, 1984, Conformation of Cyclic Paraffins and Polyethylene in the Solid State As Studied by ^{13}C CP/MAS NMR. *Macromolecules*, 17(10): 1955.

ASTM, 1992, *Annual Book of ASTM Standards, Equilibrium Moisture of Coal at 96 to 97 Percent Relative Humidity and 30°C, D 1412*, American Society for Testing and Materials: Philadelphia, PA.

Bahia, H. U., and D. A. Anderson, 1992, Physical Hardening of Paving Grade Asphalts as Related to Compositional Characteristics. *American Chemical Society Division Fuel Chemistry Preprints*, 37(3): 1397.

Baker, J. C., P. J. R. Uwins, and I. D. R. Mackinnon, 1992, ESEM Study of Authigenic Chlorite Acid Sensitivity in Sandstone Reservoirs. *Journal of Petroleum Science & Engineering*, 8: 269-277.

Bhurke, A., E. E. Shin, and L. T. Drzal, Fracture Morphology and Fracture Toughness Measurement of Polymer Modified Asphalt, Preprint No. 970942. 76th Annual Meeting, Transportation Research Board, January 12-16, 1997, Washington, D. C.

Branthaver, J. F., J. C. Petersen, R. E. Robertson, J. J. Duvall, S. S. Kim, P. M. Harnsberger, T. Mill, E. K. Ensley, F. A. Barbour, and J. F. Schabron, 1993a, *SHRP-A-368, Binder Characterization and Evaluation, Volume 2: Chemistry.* Strategic Highway Research Program, National Research Council, Washington, D. C.

Branthaver, J. F., J. C. Petersen, R. E. Robertson, J. J. Duvall, S. S. Kim, P. M. Harnsberger, T. Mill, E. K. Ensley, F. A. Barbour, and J. F. Schabron, 1993b, *SHRP-A-368, Binder Characterization and Evaluation, Volume 2: Chemistry.* Strategic Highway Research Program, National Research Council, Washington, D.C., p. 173.

Branthaver, J. F., J. C. Petersen, R. E. Robertson, J. J. Duvall, S. S. Kim, P. M. Harnsberger, T. Mill, E. K. Ensley, F. A. Barbour, and J. F. Schabron, 1993c, SHRP-A-368, *Binder Characterization and Evaluation, Volume 2: Chemistry.* Strategic Highway Research Program, National Research Council, Washington, D.C., p. 154.

Branthaver, J. F., J. C. Petersen, R. E. Robertson, J. J. Duvall, S. S. Kim, P. M. Harnsberger, T. Mill, E. K. Ensley, F. A. Barbour, and J. F. Schabron, 1993d, *SHRP-A-368, Binder Characterization and Evaluation, Volume 2: Chemistry*. Strategic Highway Research Program, National Research Council, Washington, D.C., p. 77-85.

Branthaver, J. F., J. C. Petersen, R. E. Robertson, J. J. Duvall, S. S. Kim, P. M. Harnsberger, T. Mill, E. K. Ensley, F. A. Barbour, and J. F. Schabron, 1993e, *SHRP-A-368, Binder Characterization and Evaluation, Volume 2: Chemistry*. Strategic Highway Research Program, National Research Council, Washington, D. C., p. 307.

Brown, A. B., J. W. Sparks, and F. M. Smith, 1957, Steric Hardening of Asphalts. *Proceedings, Association of Asphalt Paving Technologists*, 26: 486-494.

Bruch, M. D., ed., 1996, *NMR Spectroscopy Techniques*, Practical Spectroscopy Series, Chapter 9, Vol. 21. Marcel Dekker, Inc., New York.

Cameron, R. E., 1994, Environmental SEM: Principles and Applications. *USA Microscopy and Analysis*, May 1994: 17-19.

Campbell, P. G., J. R. Wright, and P. B. Bowman, 1962, The Effect of Temperature and Humidity on the Oxidation of Air-Blown Asphalts. *Materials Research and Standards*, p. 988-995.

Chang, S. J., J. R. Olsen, and P. C. Wang, 1989, NMR Imaging of Internal Features in Wood. *Forest Products Journal*, 39: 43-49.

Claudy, P., J. M. Letoffe, F. Rondelez, L. Germanaud, G. King, and J. P. Planche, 1992, A New Interpretation of Time-Dependent Physical Hardening in Asphalt Based on DSC and Optical Thermoanalysis. *American Chemical Society Division of Fuel Chemistry Preprints*, 37(3): 1408.

Cofer, G. P., J. M. Brown, and G. A. Johnson, 1989, In Vivo Magnetic Resonance Imaging at 5 μm. *Journal of Magnetic Resonance*, 83: 608.

Cominsky, R. J., J. S. Moulthrop, W. E. Elmore, and T. W. Kennedy, 1989, *SHRP-IR-A-89-002, SHRP Materials Reference Library Asphalt Selection Process*. Strategic Highway Research Program, National Research Council, Washington, D. C., 31 p.

Coombs, C. E., and R. N. Traxler, 1937, Rheological Properties of Asphalts IV, Observations Concerning the Anomalous Flow Characteristics of Air-Blown Asphalts. *Journal of Applied Physics*, 8: 291-296.

Critchfield, F. E., and E. T. Bishop, 1961, Water Determination by Reaction with 2,2-Dimethoxypropane. *Analytical Chemistry*, 33: 1034-1035.

Curtis, C. W., K. Ensley, and J. Epps, 1993, *SHRP-A-341, Fundamental Properties of Asphalt-Aggregate Interactions Including Adhesion and Adsorption.* Strategic Highway Research Program, National Research Council, Washington, D. C.

Daly, W. H., Z. Qiu, and I. Negulescu, 1996, Differential Scanning Calorimetry Study of Crystallinity of Asphalts. *Transportation Research Record* 1535, 54.

Danilatos, G. D., 1988, Foundations of Environmental Scanning Electron Microscopy, *Advances in Electronics and Electron Physics*, 71: 109-250.

Doehne, E., and D. C. Stulik, 1990, Applications of the Environmental Scanning Electron Microscope to Conservation Science. *Scanning Microscopy*, 4: 275-286.

Ege, S. N., 1989, *Organic Chemistry.* D. C. Heath and Company, Toronto, p. 50.

Ellingson, W. A., J. L. Ackerman, L. Garrido, P. S. Wong, and S. Gronemeyer, 1988, *Development of Nuclear Magnetic Resonance (NMR) Imaging Technology for Advanced Ceramics, ANL-87-53*, Argonne National Laboratory, prepared for U. S. Department of Energy, November 1988.

Ensley, E. K., 1975, Multilayer Adsorption with Molecular Orientation of Asphalt on Mineral Aggregate and Other Substrates. *Journal of Applied Chemistry and Biotechnology*, 25: 671-682.

Filatov, S. K., E. N. Kotelnikova, and E. A. Aleksandrova, 1985, High Temperature Crystal Chemistry of Normal Odd Paraffins. *Zeitschrift für Kristallographic*, 172: 35. Koenig, J. L., 1992, *Spectroscopy of Polymers*, Chapter 9. American Chemical Society, Washington, D. C.

Firth, C. H., V. Wagh, and A. R. Tarrer, 1993, Characterization of Limestone Aggregates Via Chemical Reactivity, Part V, Chapter 14. In *SHRP-A-341, Fundamental Properties of Asphalt-Aggregate Interactions Including Adhesion and Absorption*, SHRP A-003B Final Report. Strategic Highway Research Program, National Research Council, Washington, D. C.

Folland, P., and H. Anfindsen, 1996, Electrical Conductivity of Asphaltenes in Organic Solvents. *Fuel Science and Technology International*, 14(1&2): 101-115.

Granick, S., 1991, Motions and Relaxations of Confined Liquids. *Science*, 253: 1374-1379.

Green, J. B., S. K.-T. Yu, C. D. Pearson, and J. W. Reynolds, 1993, Analysis of Sulfur Compound Types in Asphalt. *Energy and Fuels*, 7: 119-126.

Henniker, J. C., 1949, The Depth of the Surface Zone of a Liquid. *Reviews of Modern Physics*, 21(2): 322-341.

Hwang, C. L., M. L. Wang, and S. Miao, 1993, Proposed Healing and Consolidation Mechanisms of Rock Salt Revealed by ESEM. *Microscopy Research and Technique*, 25: 456-464.

Jemison, H. B., B. L. Burr, R. R. Davison, J. A. Bullin, and C. J. Glover, 1992, Application and Use of the ATR, FT-IR Method to Asphalt Aging Studies. *Fuel Science and Technology International*, 10(4-6): 795-808.

Koenig, J. L., 1991, Application of NMR Imaging to Polymers. In *Solid State NMR of Polymers*, Mathias, L. J., ed. Plenum Press, New York, p. 61-79.

Kumler, W. D., 1940, Figures in Thin Layers of Grease and Viscous Liquids. *Journal of Physical Chemistry*, 44: 612-618.

Labib, M. E., 1992, Asphalt-Aggregate Interactions and Mechanisms for Water Stripping. *American Chemical Society Division of Fuel Chemistry Preprints*, 37(3): 1472.

Lottman, R. P., and D. L. Johnson, 1970, Pressure-Induced Stripping in Asphaltic Concrete. In *Asphalt Adhesion and Interfacial Phenomena*, Highway Research Record Number 340. Highway Research Board Division of Engineering, National Research Council, National Academy of Sciences-National Academy of Engineering, Washington, D. C., p. 13-28.

Luder, W. F., and S. Zuffanti, 1961, *The Electronic Theory of Acids and Bases*. Dover Publications, Inc., New York, p. 61.

Mack, C., 1957, Physical Properties of Asphalts in Thin Films. *Industrial Engineering Chemistry*, 49: 422-427.

Mandelkern, L., 1993, The Crystalline State. In *Physical Properties of Polymers*, Chapter 4. American Chemical Society, Washington, D. C.

Marek, C. R., and M. Herrin, 1968, Tensile Behavior and Failure Characteristics of Asphalt Cements in Thin Films. *Proceedings, Association of Asphalt Paving Technologists*, 37: 386-421.

Netzel, D. A., T. F. Turner, F. P. Miknis, J. C. Wallace, C. H. Butcher, J. M. Mitzel, and R. J. Hurtubise, 1996, Use of 2,2-Dimethoxypropane and ^{1}H NMR to Distinguish and Quantify the External and Internal Sorbed Water in Coals. *Energy and Fuels*, 10(2): 371-377.

Nguyen, T., E. Byrd, and J. Seiler, 1994, Development of a Method for Measuring Water-Stripping Resistance of Asphalt/Siliceous Aggregate Mixtures, Annual Progress Report 1. In *Emerging Concepts and Products for Highway Systems*, NCHRP IDEA. National Research Council, Washington, D. C., p. 18-22.

Petersen, J. C., 1967, An Infra-red Study of Hydrogen Bonding in Asphalt. *Fuel*, 46(4&5): 295-305.

Petersen, J. C., 1984, Chemical Composition of Asphalts as Related to Asphalt Durability: State of the Art. *Transportation Research Record* 999, 13-30.

Petersen, J. C., and H. Plancher, 1997, Model Studies and Interpretive Review of the Competitive Adsorption and Water Displacement of Asphalt Chemical Functionalities on Mineral Aggregate Surfaces, submitted to *Petroleum Science and Technology*.

Petersen, J. C., H. Plancher, E. K. Ensley, R. L. Venable, and G. Miyake, 1982, Chemistry of Asphalt-Aggregate Interaction: Relationship with Pavement Moisture-Damage Prediction Test. *Transportation Research Record* 843, 95-103.

Petersen, J. C., R. E. Robertson, J. F. Branthaver, P. M. Harnsberger, J. J. Duvall, S. S. Kim, D. A. Anderson, D. W. Christensen, H. U. Bahia, R. Dongre, C. E. Antle, M. G. Sharma, J. W. Button, and C. J. Glover, 1994, *SHRP-A-370, Binder Characterization and Evaluation, Volume 4: Test Methods*. Strategic Highway Research Program, National Research Council, Washington, D. C., 479 p.

Plancher, H., 1993, Moisture Sensitivity Evaluations by the Freeze-thaw Pedestal Test, Chapter 7. In *SHRP-A-341, Fundamental Properties of Asphalt-Aggregate Interactions Including Adhesian and Absorption*, SHRP A003B Final Report. Strategic Highway Research Program, National Research Council, Washington, D. C.

Plancher, H., S. M. Dorrence, and J. C. Petersen, 1977, Identification of Chemical Types in Asphalts Strongly Adsorbed at the Asphalt-Aggregate Interface and Their Relative Displacement by Water. *Proceedings, Association of Asphalt Paving Technologists*, 46: 151-175.

Plancher, H., G. Miyake, R. C. Venable, and J. C. Petersen, 1980, A Simple Laboratory Test to Indicate the Susceptibility of Asphalt-Aggregate Mixtures to Moisture Damage During Repeated Freeze-Thaw Cycling. *Canadian Technical Asphalt Association*, XXV: 246-262.

Plancher, H., F. A. Reid, and J. F. Branthaver, 1993, Studies on Isothermal Reversible Age-Hardening of SHRP Asphalts, Presented at the Northwest Regional Meeting of the ACS, Laramie, WY, June 19, 1993.

Podoll, R. T., C. H. Becker, and K. C. Irwin, 1991, Surface Analysis by Laser Ionization of the Asphalt-Aggregate Bond. Phase 2 Progress Report for Contract No. SHRP-87-AIIR-07, 63 p.

Rothwell, W. P., D. R. Holocek, and J. A. Kershaw, 1984, NMR Imaging: Study of Fluid Absorption by Polymer Composites. *Journal of Polymer Science, Polymer Letters to the Editor*, 22: 241.

Rozeveld, S. J., E. E. Shin, A. Bhurke, L. France, and T. Drzal, Network Morphology of Straight and Polymer Modified Asphalt Cements, Preprint No. 970850. 76th Annual Meeting, Transportation Research Board, January 12-16, 1997, Washington, D. C.

Sarkar, S. N., E. W. Wooten, and R. A. Komoroski, 1991, NMR Imaging of Water in Model Porous Materials. *Applied Spectroscopy*, 45: 619-625.

Scholz, T. V., and S. F. Brown, 1996, Rheological Characteristics of Bitumen in Contact with Mineral Aggregate. *Journal, Association of Asphalt Paving Technologists*, 65: 357-384.

Scott, J. A. N., 1978, Adhesion and Disbonding Mechanisms of Asphalt Used in Highway Construction and Maintenance. *Proceedings, Association of Asphalt Paving Technologists*, 47: 19-48.

Shriver, D. F., P. W. Atkins, and C. H. Langford, 1990, *Inorganic Chemistry*. W.H. Freeman and Company, N Y, p. 170-176.

Siffert, B., P. Rageul, and E. Papirer, 1996, Acid-base Characteristics of Asphaltenes Isolated from Mechanical Sheared Oil Distillation Residues. *Fuel*, 75(14): 1625-1628.

Stewart, M. J., W. L. Jarrett, L. J. Mathias, R. G. Alamo, and L. Mandelkern, 1996, Thermally Induced Molecular Motion and Premelting in the Solid State of *n*-Hexatriacontane. *Macromolecules*, 29(14): 4963.

Tanabe, K., M. Misono, Y. Ono, and H. Hattori, 1989, *New Solid Acids and Catalytic Properties*. (Delmon, B., and J. T. Yates, eds.), Studies in Surface Science and Catalysis, Vol. 51, Elsevier, Tokyo, p. 1-3.

Tarrer, A. R., and V. P. Wagh, 1992, Innovative Tests to Predict the Strength and Type of Asphalt-Aggregate Bonds. *Fuel Science and Technology International*, 10(4-6): 457-474.

Terrel, R. L., and J. W. Shute, 1989, SHRP-A/IR-89-003, Summary Report on Water Sensitivity. Strategic Highway Research Program, National Research Council, Washington, D. C.

Traxler, R. N., and C. E. Coombs, 1936, The Colloidal Nature of Asphalt as Shown by its Flow Properties. *Journal of Physical Chemistry*, 40: 1133-1147.

Traxler, R. N., and C. E. Coombs, 1937, Development of Internal Structure in Asphalts with Time. *Proceedings of the American Society of Testing Materials*, 37(II): 549-557.

Traxler, R. N., and H. E. Schweyer, 1936, Increase in Viscosity of Asphalts With Time. *Proceedings of the American Society of Testing Materials*, 36 (II): 544-550.

Traxler, R. N., H. E. Schweyer, and J. W. Romberg, 1944, Rheological Properties of Asphalt. *Industrial and Engineering Chemistry*, Sept. 1944: 823-829.

Uwins, P. J. R., J. C. Baker, and I. D. R. Mackinnon, 1993, Imaging Fluid/Solid Interactions in Hydrocarbon Reservoir Rocks. *Microscopy Research and Technique*, 25: 465-473.

Webb, A. G., K. Motsegood, and R. B. Clarkson, 1993, NMR Imaging Studies of Coal Samples Using Solvent Permeation. *Fuel*, 72: 1235-1237.

Weisenberger, L. A., and J. L. Koenig, 1991, NMR Investigations of Case II Diffusion in Polymers. In Mathias, L. J., ed., *Solid State NMR of Polymers*. Plenum Press, New York, p. 377-386.

Williams, D., D. N. Little, and R. L. Lytton, 1997, The Influence of Asphalt Surface Energies on Microcrack Growth and Healing. 34th Annual Meeting, Petersen Asphalt Research Conference, July 14-16, 1997, Laramie, Wyoming.

CHAPTER 6: THE EVALUATION OF MODIFIED ASPHALTS

SYNOPSIS

In this chapter the use of modified asphalts is addressed. In the first section the pavement performance and environmental impact of a shale oil-modified asphalt test strip are compared with those of a polymer-modified asphalt control strip. With regards to this first section, the reader is reminded that the final report for this activity was delivered to FHWA for review in December 1998. The work is fully described in that document. However, a discussion of some of the more interesting conclusions is presented here in this report. In the second section of this chapter, the impact of several variables that are related to the use of crumb rubber (CR) in asphalt are evaluated. In addition, the component in asphalt that is involved in the CR-asphalt interaction is elucidated.

A polymer-modified control strip (PBA-6a) and a shale oil-modified test strip (SOMAT) were constructed in Grand Teton National Park. The control strip has four sections (C1, C2, C3, and C4) and the test strip has two sections (S1 and S2) that were monitored for performance during this project. The specification testing for the two pavements was conducted by Western Federal Lands Highway Division (WFLHD). They are being monitored for pavement performance and environmental impact using the SHRP developed- and AASHTO-approved test procedures as appropriate. According to the SHRP Superpave® guidelines, the control pavement is a PG 70-22 and the test pavement is a PG 64-22. At 98 percent design reliability, the grade that is recommended in this area of Wyoming is PG 52-46. Thus, it appears the two pavements do not satisfy the low-temperature (cracking) requirement, being too stiff, but exceed the high-temperature (rutting) requirement. Consequently, both pavements may be susceptible to thermal cracking.

The continuing monitoring of the two different pavement sections has demonstrated that, based upon the high-temperature PG's, the extent of rutting observed in the two different sections does not exceed what would be normally expected, usually less than 0.25 cm (0.1 in). Cracking was observed in both pavement sections after the second winter (1994-1995). However, the control sections are exhibiting significantly less cracking than the test sections. This is surprising considering both asphalts have the same low-temperature specification, PG -22. Apparently, the addition of the polymer (Kraton® D 1184, a styrene-butadiene branched copolymer) to the control asphalt provides protection with respect to cracking and rutting that may not be measured using the SHRP grading procedures.

A continuing environmental monitoring program is also associated with the PBA-6a and SOMAT pavements that were laid in Grand Teton National Park. The results indicate that, during the laying of the two pavements, neither paving operation gave rise to exposures that exceeded the time-weighted average permissible exposure limits established by the Occupational Safety and Health Administration (OSHA) for the analyzed compounds. In addition, the analysis of the hot mixes demonstrated that no significant differences exist between the two materials, and they easily passed the Toxicity Characteristic Leaching

Procedure (TCLP) for toxicity. In the years following paving, the analysis of soil samples obtained adjacent to the two pavements resulted in the identification and quantification of a few hazardous compounds. However, rational explanations could be provided that did not involve leaching from the pavements. These explanations included: the compounds were also present in the blanks, they were also present in the baseline samples, or the presence of the compounds could be rationalized because either they are not normally present in petroleum feedstocks and/or they could be derived from an existing structure near the sampling site.

The impact of the use of CR in asphalt is also evaluated in this chapter. It was determined that there is a direct relationship between the amount of CR in the asphalt and the rheological properties, and also that the method of CR preparation has no impact on these rheological properties. Thus, it was concluded that the nature of the interaction between the CR and the asphalt is dependent on the asphalt or some component(s) in the asphalt. Subsequently, it was determined that the acid component in asphalt is involved in the CR-asphalt interaction, and the extent of the interaction is dependent upon the acid amount, the acid type, the mix temperature, and the time at the mix temperature.

The behavior of natural tire rubber was found to be different from that of CR, which is a mixture of natural and synthetic tire rubber. Natural rubber was found to dissolve in all asphalts tested, and the changes in the rheological properties were different from those imparted by CR. It was also shown that the rheological properties of the CRMA changed, sometimes dramatically, during the hours of storage and handling after mixing and at relatively low temperatures of about 150°C (302°F). These rheological changes during the hours following mixing could possibly change the grade of the modified binder. Thus, a load of CRMA stored for a particular paving project could have quite variable rheological properties depending on when it is used in the mixing and paving operation. From model compound studies, the changes in the rheological properties of the CRMA were found to be dependent on the type and amount of carboxylic acid and the mix temperature.

NMR imaging is also applied in the study of CR and asphalt. Exploratory NMR images were acquired on relatively large pieces of natural and styrene-butadiene tire rubber immersed in asphalt. These measurements demonstrated the feasibility of using NMR imaging to study different interactions between crumb rubbers and asphalt, such as swelling by asphalt molecules, possible dissolution of rubber components in asphalt, and devolatilization and cross-linking in rubber when heated at mix temperatures of 170°C (338°F).

SHALE OIL-MODIFIED ASPHALT TEST STRIP

In the early 1980's, scientists at WRI discovered that using Western shale oil as an asphalt modifier mitigated the onset of moisture damage in asphalt pavements. As a consequence of this discovery, a patent was granted to WRI in 1982 [Plancher and Petersen 1982]. In the years since, the New Paraho Corporation of Highlands Ranch, Colorado, has been licensed to use the concept and process for the production of an asphalt modifier. Over the past several years, 14 different pavements that incorporate the use of a shale oil-derived modifier

have been constructed in 5 States in the United States, 7 of which are monitored as test pavements. The States where the pavements are located include Wyoming, Colorado, Utah, Texas, and Michigan. In the construction of the test strips, the only notable difference from the normal paving procedures is that the asphalt binder contains 10 to 15 mass percent of the shale oil modifier (SOM). To date, the results of field evaluations of the previous test strips indicate that they are less susceptible to moisture damage when compared with conventional petroleum asphalts that are laid in the immediate vicinity of the SOMAT test strips [Lukens and Fox 1993].

Stripping of asphalts from aggregates and oxidative aging are continuing processes that impact the mechanisms that lead to the failure of asphalt concrete pavements. The mechanisms that result in the failure of asphalt concrete pavements include low temperature (thermal) cracking, fatigue cracking (alligator cracks), and permanent deformation (rutting and shoving). Thermal cracking is presumed to be independent of traffic load, whereas fatigue cracking and permanent deformation are dependent upon traffic load. The evaluation of the onset of these three modes of failure is fairly simple, i.e., by visual inspection. Moisture damage and aging are evaluated as they manifest themselves in these forms of failure. Recent information indicates that aging and rheological data obtained from asphalt recovered from cores taken during the earlier years of service can be used to predict the onset of distress [Lukens and Fox 1993]. In addition, the Lottman test or other procedures that involve water immersion followed by physical (mechanical) testing [Terrel and Shute 1989] can be used to evaluate moisture damage of laboratory cores and cores taken from pavements. It should also be noted that moisture damage can result in loss of structural strength of the pavement and subsequent pavement failure without the actual occurrence of visual stripping of the asphalt from the aggregate.

In light of the apparent success as demonstrated by the previously constructed SOMAT test strips, Congress mandated the construction and evaluation of a shale oil-modified asphalt test strip as described in the Intermodal Surface Transportation Efficiency Act (ISTEA) of 1991, Section 6016(d). The purpose of the test strip, as described in Section 6016(e), is to demonstrate and evaluate the unique energy and environmental advantages of using SOMAT under extreme climatic conditions. Upon the reconstruction of a portion of U.S. Highway 89 located in Grand Teton National Park and the completion of the monitoring program in 1998, this Congressional mandate will have been fulfilled.

The principal reason for the reconstruction of U.S. Highway 89 north of Jackson, Wyoming, is because the useful life of the original pavement is nearing an end as demonstrated by extensive cracking and projected increased traffic demands. This reconstruction from the south boundary of Grand Teton National Park to the east boundary of the park, a distance of 44.82 km (27.85 miles), is occurring in stages as funds for the work become available. The location of the reconstruction effort that was conducted during the 1993 construction season was from 26.39 to 35.18 km (16.40 to 21.86 miles) north of the south boundary of the park. In addition to age, the action of frost heaving has also contributed to the observed pavement failure. During the reconstruction of that portion of the highway contained in the park, those areas that were susceptible to frost heaving were dug out and rebuilt. The frost heaving was considered to be caused by poor drainage and moisture expansion in the subgrade [Heitzman

1984]. It should be noted that the control (PBA-6a) and test (SOMAT) sections, which are the subject of this study, are not located over any of the dug out portions of the reconstruction project.

The monitoring program that is being conducted on the control, which is constructed using a polymer-modified asphalt (Kraton® D 1184, a styrene-butadiene branched copolymer manufactured by Shell Chemical Company), and test sections in Grand Teton National Park is not scheduled to be completed until December 1998. At that time a final report will be delivered to the Federal Highway Administration (FHWA) that discusses all of the data collected. What is presented here in Volume I of this report is a discussion of some of the more pertinent data that have been obtained through April 1997. Where appropriate, conclusions are presented that appear to be valid at this time. A thorough discussion of the baseline data is contained in a topical report that was delivered to FHWA in December 1995 [Thomas and Harnsberger 1995]. In addition, information regarding comparisons of SOMAT with other polymer-modified asphalts is contained in a report published in 1996 [Thomas et al. 1996]. The emphasis of the discussion that follows is placed upon relating the observed field performance of the pavement sections to the chemical and physical properties of the original asphalt and the recovered cores. In addition, a summary of the environmental monitoring effort is included for completeness. A more thorough discussion of the baseline environmental results is contained in a report delivered to FHWA in May 1994 [WRI 1994].

SHRP (AASHTO) Testing and Evaluation of Original Paving Materials

Since the planning and construction of the pavement was carried out before the SHRP asphalt grading procedures had been finalized and adopted by AASHTO, the design of the pavement was conducted using the Hveem procedures by the Western Federal Lands Highway Division (WFLHD) of the FHWA. However, the evaluation being conducted at WRI of the performance of the pavement sections is based upon the new SHRP procedures. Consequently, the testing of the binders from the project was conducted using SHRP procedures [AASHTO 1994]. According to the SHRP Superpave® binder selection software [SUPERPAVE 1995], the grade of binder that is recommended for the project site, based on 98 percent reliability, varies from PG 52-52 at Moran Junction, Wyoming, to PG 52-46 at Moose, Wyoming. Since the recommended high-temperature grade was the same in both cases, the binders were initially tested assuming they would satisfy the PG 52 requirements. For the low- and mid-temperature measurements, it was decided that the best approach would be to perform measurements at several temperatures that would span the range of all of the low-temperature grades for a PG 52 asphalt. This decision resulted in dynamic shear measurements being made in the range from 25 to 7°C (77 to 45°F) and bending beam measurements being made in the range from 0 to -36°C (32 to -33°F). The results of the mid-temperature measurements provide information with regard to fatigue cracking potential, whereas the results of the low-temperature measurements are related to the thermal cracking potential of the binder.

Based upon these initial tests, the SOMAT binder would be graded as a PG 52-16 because of the mid-temperature rheological properties, whereas the PBA-6a binder would be graded as a PG 52-22 because of the m-value. However, since both binders were determined to

be considerably stiffer at 52°C (126°F) than required, it seemed reasonable to investigate what the maximum range of grade each binder could pass. Since it was already planned to characterize both binders using rheological measurements from 0 to 70°C (32 to 158°F) at 10°C (18°F) intervals, it was decided that these data could be used to predict what grade each binder material could pass. The results of these experiments showed the PBA-6a binder was a PG 70-22 and the SOMAT was a PG 64-22. In this case, both of the binders low-temperature grade is determined by the m-value.

As was mentioned above, previous test strips constructed with SOMAT have shown dramatic improvements with respect to moisture susceptibility when compared with the performance of more conventional petroleum-derived asphalts. Similar results have also been obtained from laboratory tests [Lukens and Plummer 1988]. To evaluate the future performance of the test pavements with respect to moisture damage, the hot mixes used in the construction of the SOMAT and PBA-6a pavements were compacted into slabs and then tested using the Hamburg wheel tracking device by personnel at the Colorado Department of Transportation (CDOT). The test, as originally devised, involves the passage of a steel wheel over a slab of asphalt concrete immersed in a water bath at a temperature of 50°C (122°F) for a total of 20,000 passes. The sample is considered to have passed the test if the rut that develops is less than 4 mm (0.16 in) in depth. These conditions are considered to be too severe for many of the pavements in Colorado [Aschenbrener et al. 1994] and also Wyoming. Consequently, the test temperature recommended by CDOT for the pavements in Grand Teton National Park is 40°C (104°F), and the rut depth is required to be not more than 10 mm (0.39 in). The results of testing the two compacted hot mixes demonstrated that both materials passed, but the SOMAT rutted at a faster rate than the PBA-6a material (2.2 vs 1.4 mm at 40°C [0.09 vs 0.06 in at 104°F]). The test was also conducted at 45°C (113°F), and the results demonstrated that the two materials still passed at these more severe conditions. The rut depths in this case were 4.6 and 1.4 mm (0.18 and 0.06 in), respectively. The stripping inflection point could not be determined for these samples because stripping of the asphalt did not occur during the test. The stripping inflection point is defined as the intersection of the creep slope (rutting) and the stripping slope (the severity of moisture damage) and is related to a material's ability to resist moisture damage [Aschenbrener et al. 1994].

In addition to testing reconstructed slabs with the Hamburg wheel tracking device, cores from the control and test sections were evaluated with respect to moisture susceptibility using SHRP Protocol P05 (modified Lottman test). The results of this testing of the baseline core samples indicated that the TSR of the control cores was greater (0.84) than that for the test cores (0.74). Based on these data, the conclusion is that the control sections will be less susceptible to moisture damage than the test sections. However, this neglects the fact that the indirect tensile strength of the *wet* test cores averages 474 kPa, while that for the *dry* control cores averages 427 kPa.

During the reconstruction of the pavement during the 1993 construction season, WFLHD required numerous analytical tests to be conducted on the paving materials and cores taken from the new pavement. A summary of these results is discussed here. The weight percentage of asphalt extracted from four loose mix samples obtained during the paving of the

highway with PBA-6a averaged 5.49 mass percent, while the percentage of asphalt extracted from two samples obtained during the paving of the highway with SOMAT averaged 5.61 mass percent. The mix design conducted by the WFLHD and contained in the job mix formula stipulated that the asphalt content be 5.66 mass percent for both pavement sections. In general, the results of the sieve analysis of the aggregate obtained from samples showed that the specifications required for this project were satisfied. Shown in figure 6-1 is a 0.45 power curve of the average of the 12 cores that were taken from the control (8) and test (4) sections by Nichols Consulting Engineers (NCE) of Reno, Nevada, for analysis. In figure 6-2 are the results for the six loose mix samples taken from the control (4) and test (2) sections by WFLHD. Included in figure 6-1 is the location of the restricted zone and the control points as recommended by Superpave®, while in figure 6-2 is shown the allowable tolerances from the target values as stipulated in the job mix formula. Several points are noted regarding the data presented in the figures. First, the average gradation of the aggregate for the control and test materials depicted in both figures is very similar. In only one case was the gradation of the aggregate in 1 of the 12 cores taken by NCE not within the specifications required by WFLHD in the job mix formula. In that case, the percentage of the material passing the 12.50, 9.50, and 4.75 mm (½ and 3/8 in and No. 4) sieves was above the limit, indicating that the gradation was finer than required. However, plotting the data on a 0.45 power curve (figure 6-1) demonstrated that the gradation did not deviate beyond the control points recommended by Superpave®. This particular core was obtained adjacent to control section C4 where no unusual distress has been observed to date. Second, it should be noted that, apparently because of a difference in the sieve sizes used in the vicinity of the restricted zone, the gradation passes through the restricted zone for the NCE data (see figure 6-1). If the gradation enters the restricted zone, this normally indicates the mix may be prone to permanent deformation [Asphalt Institute 1995a]. However, this has not been observed in the field to date. The topic of permanent deformation will be discussed again later in this section. In figure 6-2 are presented the results of sieve analysis of the cores taken by WFLHD. However, in this case the comparison is made with the requirements of the job mix formula. As shown in the figure, the average gradation of the WFLHD cores is within the limits established by the job mix formula.

The sand equivalent (AASHTO T 176) for the cold aggregate feed samples used in the preparation of the PBA-6a hot mix used in the control sections averaged 52 percent, while the sand equivalent for the SOMAT samples averaged 57 percent. The percent of fractured faces (FLH; T-507, which are determined visually) in the aggregate feed used for the preparation of the PBA-6a hot mix averaged 97.3 percent, while the percentage for the SOMAT samples averaged 97.1 percent. Thus, the minimum requirements normally established for these two properties (35 percent and 90 percent, respectively) were exceeded [Roberts et al. 1991].

The bulk specific gravity and the degree of compaction of core samples taken from the new pavement constructed with PBA-6a hot mix in the control sections averaged 2.183 and 91.8 percent, respectively. The same properties determined for core samples taken from the new pavement constructed with SOMAT averaged 2.187 and 92.0 percent, respectively. These values also met the requirements established by FHWA. The theoretical maximum density of the hot mixes was 2.377 and 2.384, respectively.

Continued Monitoring of the Pavement Sections

To evaluate the performance of the pavement sections with time, cores were obtained from the control and test sections in 1994 and in 1995. Cores will also be obtained from these same sections in 1998 when the monitoring period is completed. In figures 6-3 and 6-4 are shown the results of field aging on the rheological and spectroscopic properties of the two asphalts. When placed into service, all asphalts begin to age, i.e., they become stiffer. There are several causes for the observed increasing stiffness with time of asphalts. These causes include steric hardening (structuring of the molecules), oxidation (chemical aging), volatilization of "light ends," etc. The net result of these processes is an increase in the rheological properties of the asphalts. Based upon the format of Glover and his co-workers [Lau et al. 1992], a plot of carbonyl absorbance versus G*/sin delta for the two binders is shown in figure 6-3. These preliminary data indicate and confirm what has been observed by personnel at WRI and others — as a pavement ages the stiffness increases, and the stiffness is directly proportional to the carbonyl content of the binder. A plot of the G*sin delta for the field-aged binders recovered immediately after construction in September 1993 and after 1 and 2 years of service is shown in figure 6-4. The G*sin delta values at 25°C (77°F) for the binders extracted from cores obtained from the PBA-6a control sections are lower than those for the SOMAT test sections, indicating that the test pavement may be more susceptible to fatigue cracking than the control pavement. G*sin delta for both binders increased rapidly during the first year in service, but now appears to have leveled off. This will be verified when the cores taken in 1998 are analyzed. In addition, notice that the rate of change in G*sin delta for both asphalts appears to be comparable, demonstrating that both pavements are aging at about the same rate. The data were collected at 25°C (77°F) because at this temperature both binders met the specification limit of not exceeding 5000 kPa during original grading.

Presented in table 9-2 in Volume II are the indirect tensile strength data for unconditioned (dry) and conditioned (wet) cores taken from the control and test pavements for 1993 through 1995. The ratio of the values (wet/dry) is a measure of the moisture susceptibility of the cores. It should be recalled that the TSR's of the baseline cores indicated that the control sections would be less susceptible to moisture damage than the test sections. As shown in table 9-2 of Volume II, the TSR values for the cores from the control and test sections are now comparable, indicating that both asphalts are providing equivalent protection from moisture damage. Notice that the tensile strength of the dry and wet cores increases significantly during the first year of service for both asphalts. But, during the second year of service, the increase in tensile strength of the dry and wet cores from the control sections is not as dramatic. However, the increase is again significant for the dry and wet cores from the test sections. A plot of the indirect tensile strength (wet) versus the percentage of air voids of the cores taken in 1993, 1994, and 1995 is shown in figure 6-5 of this volume. From the figure it can be concluded: (1) the air void content of the cores from the control sections (PBA-6a) is greater than that for the test sections (SOMAT), possibly indicating that it is harder to compact a polymer-modified asphalt than a non-polymer-modified asphalt; (2) the wet strength of the materials increases with time due to aging of the binder; and (3) the wet strength of the cores taken from the test sections is higher than that for the cores taken from the control sections. Confirmation of the trends

depicted in figure 6-5 (this volume) should be validated when the data for the cores taken in 1998 are available.

The moisture susceptibility of the pavement sections was also evaluated by personnel at CDOT using their Hamburg wheel tracking device. In 1995 cores measuring 25.4 cm (10 in) in diameter were taken from the control and test sections. The results of testing these samples demonstrated that both materials passed, but, in this case, the cores from the PBA-6a sections rutted at a slightly faster rate than those from the SOMAT sections. The average rut depth after 20,000 passes was 2.7 mm (0.11 in) for the SOMAT cores and 3.5 mm (0.14 in) for the PBA-6a cores. The test was conducted at 40°C (104°F), and for a sample to pass the test, the rut depth has to be less than 10 mm (0.39 in). As reported earlier, the stripping inflection point could not be determined for these samples because stripping of the asphalt did not occur during the test.

The resilient modulus of cores taken from the control and test sections was determined. The data for 1993 and 1995 are shown in tables 9-3 and 9-4 in Volume II. In general, the instantaneous and total resilient moduli for the cores taken from the test (SOMAT) sections, S1 and S2, are greater than those for the cores taken from the control (PBA-6a) sections, C1 and C2, at the three temperatures investigated (5, 25, and 40°C [41, 77, and 104°F]). In addition, the indirect tensile strengths of the cores taken from the test sections are greater than those for the cores taken from the control sections. These data parallel what was obtained from the moisture susceptibility studies, that is, the SOMAT asphalt concrete is stronger than the PBA-6a asphalt concrete.

In addition to determining the chemical and physical properties of cores taken from the control and test sections, the ride performance of the sections was evaluated by conducting transverse and longitudinal profiles and distress surveys. The extent of rutting is obtained from the transverse profile data, and the extent of cracking that has occurred in the sections is obtained from the distress surveys. Shown in figure 6-6 of this volume is the transverse profile data for sections C1 and S1. Notice that there continue to be changes in the elevation profiles of the pavement sections during the succeeding years. The compaction that is observed at about 90 and 275 cm (3 and 9 ft) reflects the initial and gradual compaction that occurs in the wheelpaths due to the impact of traffic. The maximum compaction observed in 1996 is in the right wheelpath and is about 0.06 cm (0.02 in) for section C1 and 0.21 cm (0.08 in) for section S1. The amount of compaction that is observed for section S1 is what is normally observed after 2 to 3 years of service [Roberts et al. 1991]. However, with respect to section C1 the amount of compaction is below normal. This is probably because the addition of the polymer to the binder has imparted some resiliency to the pavement structure. In addition, the control pavement is graded at a PG 70-22; while the test pavement is graded at a PG 64-22. Thus, the control pavement is stiffer than the test pavement. However, the grade recommended for this area of Wyoming is PG 52-46; thus, both pavements exceed the high temperature specification. It is also evident from the figure that the initial compaction of both pavements is about completed. Finally, the reader is cautioned that the visual magnitude of the observed "ruts" is the result of the different scales used in the figure to represent the vertical and horizontal dimensions. Thus, they are not as serious as they appear.

In figures 6-7 and 6-8 of this volume are shown the contour maps produced from the transverse profile data collected in 1996 for these same two sections. The vertical lines at 90 and 275 cm (3 and 9 ft) on both figures denote the resulting wheelpath for a vehicle having a 183-cm- (6-ft-) wide wheel spacing, i.e., a large truck. The contour lines, especially in the right wheelpaths for both figures, demonstrate that compaction is occurring along these lines as a result of the weight of trucks passing over these sections.

Cracking was not observed in any of the sections until after the second winter (in August 1995). The cause of these cracks can, of course, be either thermal and/or reflection. In fact, in two cases cracks visually located in sections S1 and S2 are indeed due to reflection. Shown in figures 6-9 and 6-10 (this volume) are crack maps for sections C1 and S1, which are adjacent to each other on the highway. The reader is referred to figure 9-2 in Volume II for an orientation of the monitored sections. (Section S1 was surveyed against the traffic flow in 1995; that is why the length measurement is in the same direction as in C1.) It is evident from the data that the test section, S1, is more prone to cracking than the control section, C1, and the severity of cracking increased significantly in S1 from August 1995 to August 1996. The fact that the test section is more prone to cracking than the control section is surprising since the low temperature specification for the two pavements is the same, PG -22. In addition, the indirect tensile strength of cores taken from the two pavements shows that the test pavement is stronger than the control pavement (see tables 9-2, 9-3, and 9-4 in Volume II). However, the binder used to construct the control pavement contains 5 percent Kraton® D 1184 . This elastomer is a styrene-butadiene branched copolymer ($[SB]_n$) that is known to exhibit thermoplastic character at elevated temperatures and provides a three-dimensional network at low temperatures [Isacsson and Lu 1995]. Thus, the use of this additive in conventional asphalts provides for increased resistance to rutting at elevated temperatures and increased toughness at low temperatures, i.e., protection against thermal cracking. Consequently, it would appear that the bending beam data (TP1) did not distinguish this difference between the polymer-modified asphalt (PBA-6a) and the shale oil-modified asphalt (SOMAT). Finally, the reader is reminded that the use of SOMAT as an additive in conventional asphalts and, for that matter, Kraton® in certain cases is for protection from moisture damage rather than from other forms of distress [Plancher and Petersen 1982]. However, the loss of pavement strength from moisture damage can be a major contributor to pavement rutting.

The results of some field tests have indicated that with regard to rutting and thermal cracking, the use of SOMAT provides better protection when compared with conventional asphalts and provides comparable protection when compared with polymer-modified asphalts [Lukens and Plummer 1988]. However, in these field tests the low temperatures experienced, e.g., in Utah, may not have been as severe as those experienced north of Jackson, Wyoming. In addition, the reader is reminded that the low-temperature grade of the two asphalts is PG -22; while that recommended for this area of Wyoming is PG -46 to -52. It is suggested that if the low-temperature grade of SOMAT had been lower, it probably would have been more resistant to thermal cracking.

In addition to ride performance data, climatic data are also being collected for the area near the construction site. The climatic data consists of maximum and minimum temperatures,

amount of precipitation as rain or snow, and snow depth for Jackson, Moose, and Moran, Wyoming. The location of the control and test pavement sections is between Moose and Moran with the construction site being closest to Moran. As mentioned above, the SHRP grade of the pavement sections is PG 70-22 (control) and PG 64-22 (test). The low-temperature specification implies that the pavement sections are protected from thermal cracking down to a temperature of -22°C (-7.6°F). From the minimum air temperature data, the minimum daily pavement temperatures were calculated [Asphalt Institute 1995b]. The number of times the pavement temperature went below -22°C (-7.6°F) was then determined from the Moran temperature data and is presented in table 6-1 (this volume). It is interesting to note that cracking was not observed until after the winter of 1994-1995. It was during this winter season that the number of potential thermal cracking events, as defined by the number of times the pavement temperature went below the low-temperature PG, more than tripled from those of the preceding winter season. If the asphalts are graded using a continuous grading procedure (here referred to as a continuous performance grade [CPG]), then the low-temperature grades become CPG -26 for the control and CPG -24 for the test asphalt. From this revised data it appears the control asphalt may have been less susceptible to the low pavement temperatures than the test asphalt.

Summary of the Environmental Analyses

The environmental monitoring effort associated with the test pavements in Grand Teton National Park is divided into three phases. These include: (1) baseline studies of the chemical characteristics of the soil near the test and control sections, (2) ambient air monitoring during pavement construction and chemical evaluation of the two hot mixes (SOMAT and PBA-6a) with respect to the presence of potentially hazardous compounds, and (3) continued environmental monitoring of soil near the pavement sections after construction was completed.

After the completion of a comprehensive site survey, appropriate sampling locations were chosen. Eight soil samples were taken near the test sections, and six samples were taken near the control sections. These samples were analyzed for the metals listed as hazardous in the Resource Conservation and Recovery Act and the volatile and semivolatile organic compounds that are listed as hazardous by the U.S. Environmental Protection Agency and are analyzed for in its Contract Laboratory Program. The analytical results conclusively demonstrate that the baseline samples did not contain any of the hazardous compounds for which analyses were performed. Thus, the sample locations that were chosen are suitable as baseline references for the Phase 3 work.

As part of Phase 2, four ambient air samples obtained during the SOMAT paving, four ambient air samples obtained during the control paving, and one method blank were analyzed for volatiles. The analytical results indicate that neither paving operation gave rise to concentrations that exceed the time-weighted average permissible exposure limits (TWA PEL's) established by the OSHA for the hazardous compounds tested. In addition, samples of the SOMAT and control hot mixes were analyzed for metals, volatiles, and semivolatiles. The analytical results revealed the presence of some compounds, but no significant differences exist between the analyte compositions of the two hot mixes. Phase 2 also included extraction of the

two hot mixes according to the TCLP. The resulting TCLP extracts were analyzed for metals, volatiles, and semivolatiles. Only very low concentrations of some compounds were detected in the extracts, and, as a result, the hot mixes easily passed TCLP testing for toxicity. Phase 2 demonstrated that the environmental impact of the SOMAT paving operation, as measured by the parameters tested, appears to be no different than that of the control paving operation. A more detailed discussion of the results of the baseline environmental monitoring effort (Phases 1 and 2) is contained in a report that was delivered to FHWA [WRI 1994].

Phase 3 of this effort concerns the continued monitoring of the soil near the pavement sections through 1998. Consequently, soil samples were taken in 1994 and 1995 in the same locations as in Phase 1. These soil samples were analyzed for the same volatiles, semivolatiles, and metals as in Phase 1. The results of these analyses showed that no hazardous compounds have leached from the pavements. The compounds that were identified and quantified in the soil samples at above the detection limit of the methods were found to be also present in the blanks, were also present in the baseline samples, or a rational explanation could be provided that did not involve leaching of the compounds from the pavements. For example, the compounds are either not normally present in petroleum feedstocks and/or they could be derived from an existing structure near the sampling site. A more detailed discussion of the environmental monitoring that is being conducted adjacent to the pavement sections is contained in a report that was delivered at the annual Transportation Research Board meeting in January 1997 [Thomas et al. 1997].

Table 6-1. An accounting of the number of times the low-temperature limit has been exceeded.

Winter season	PG -22	CPG[1] -26 (control)	CPG -24 (test)
1993-1994	3	0	1
1994-1995	9	4	6
1995-1996	8	4	8

[1] CPG means continuous performance grade.

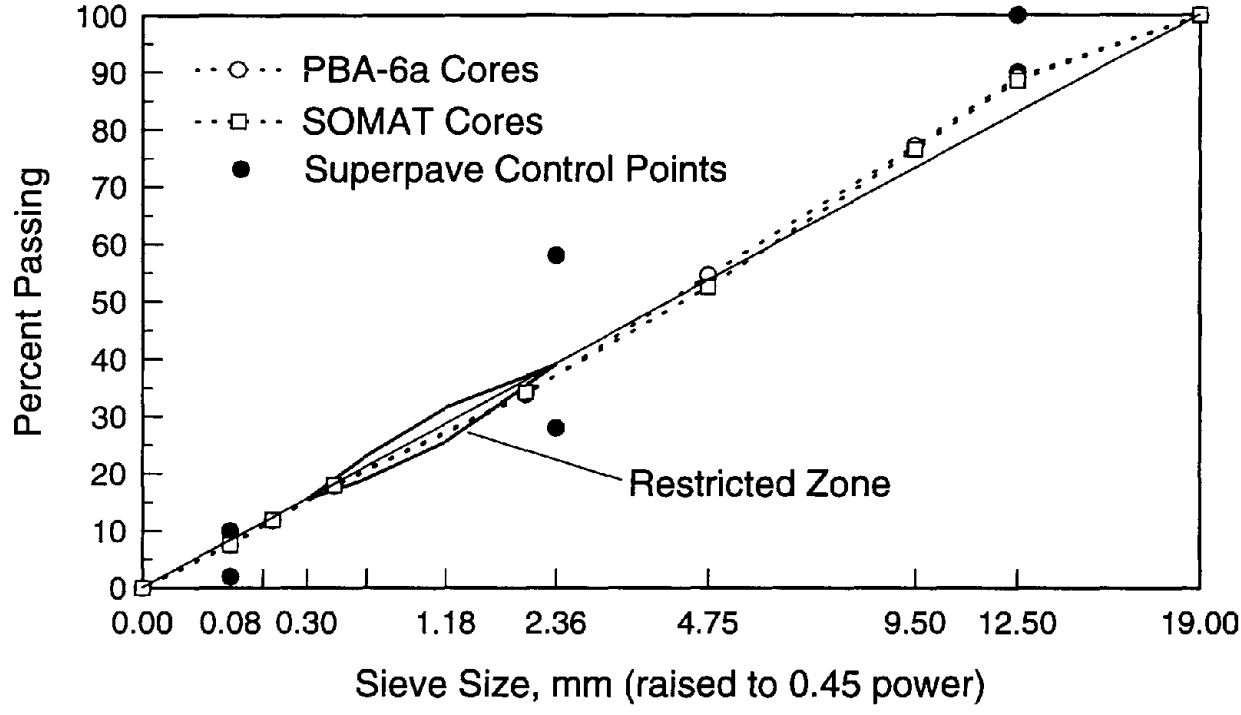

Figure 6-1. Aggregate grading chart for the averages of the two mixes used in Grand Teton National Park (NCE data). (The Superpave® gradation requirements are shown.)

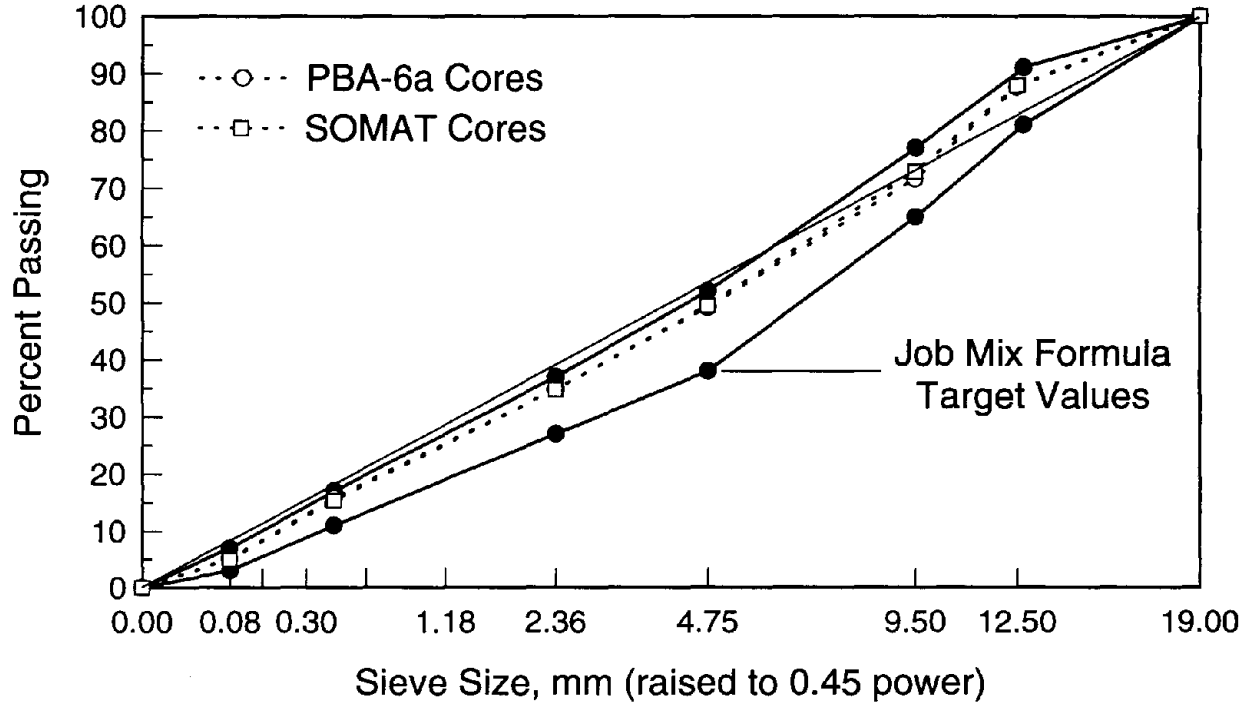

Figure 6-2. Aggregate grading chart for the averages of the two mixes used in Grand Teton National Park (WFLHD data). (The job mix formula target values are shown.)

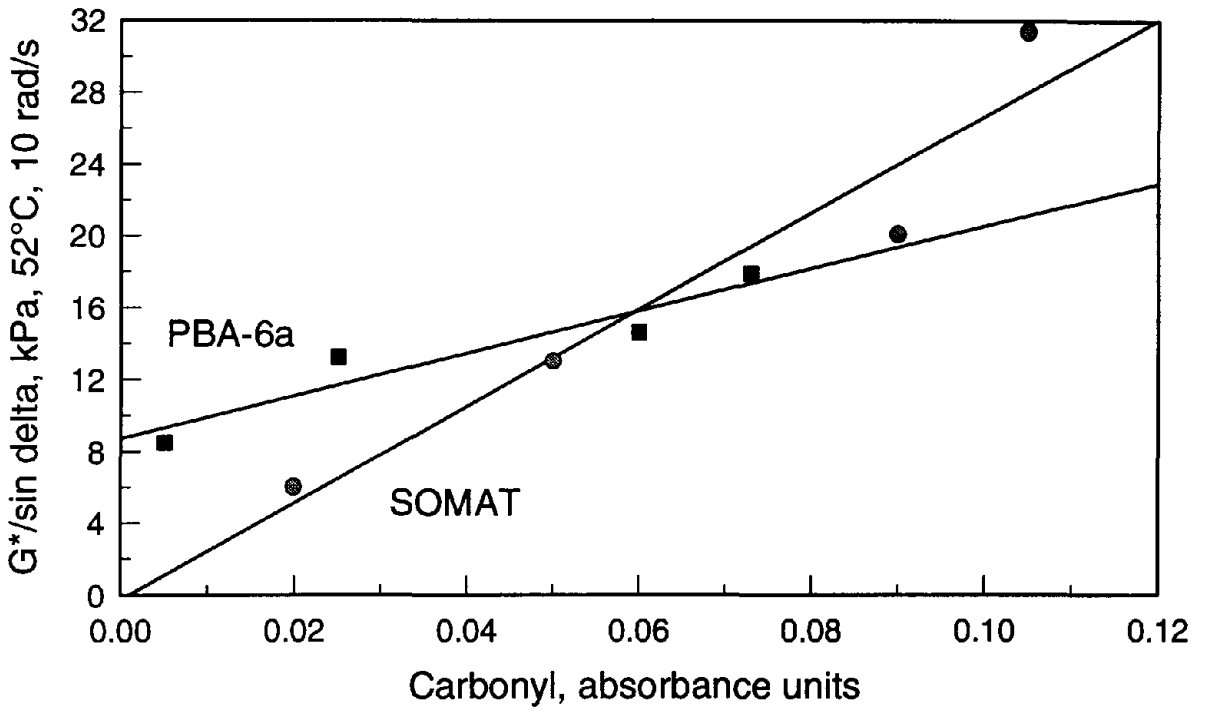

Figure 6-3. A plot showing the relationship between oxidation with time (in-service aging) and a rheological property of the asphalts.

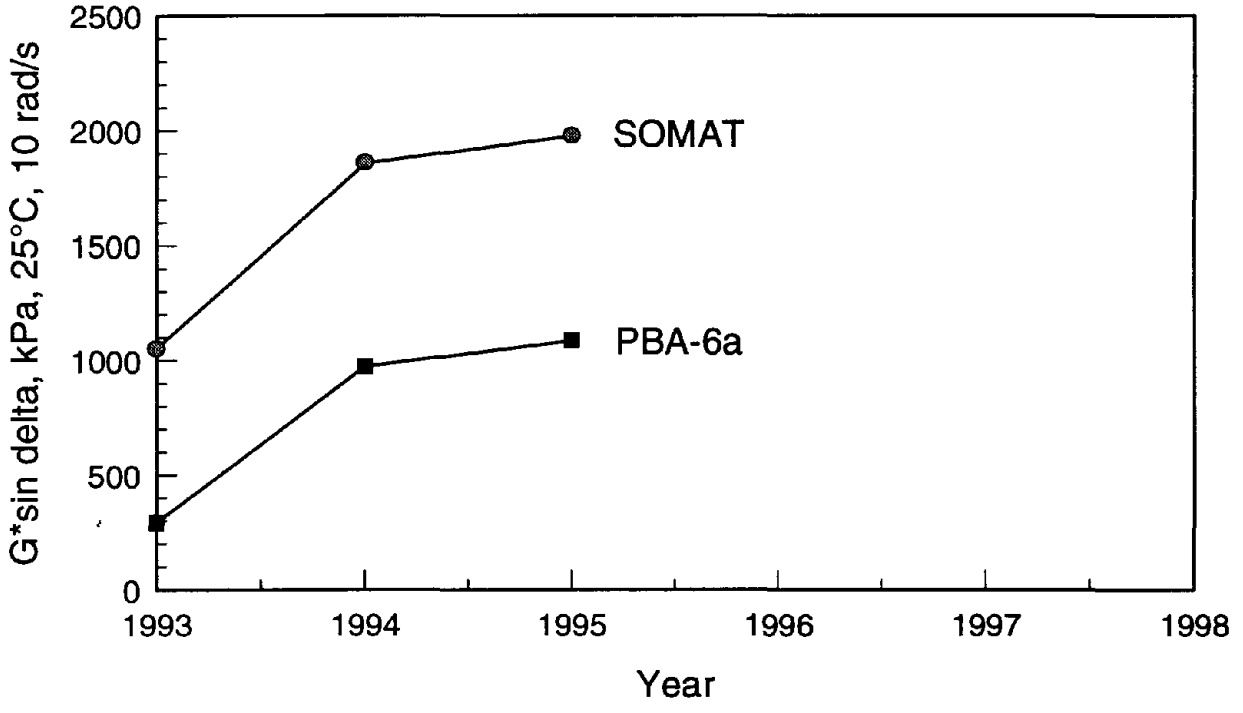

Figure 6-4. A plot of the change in G*sin delta of the asphalts versus time in service.

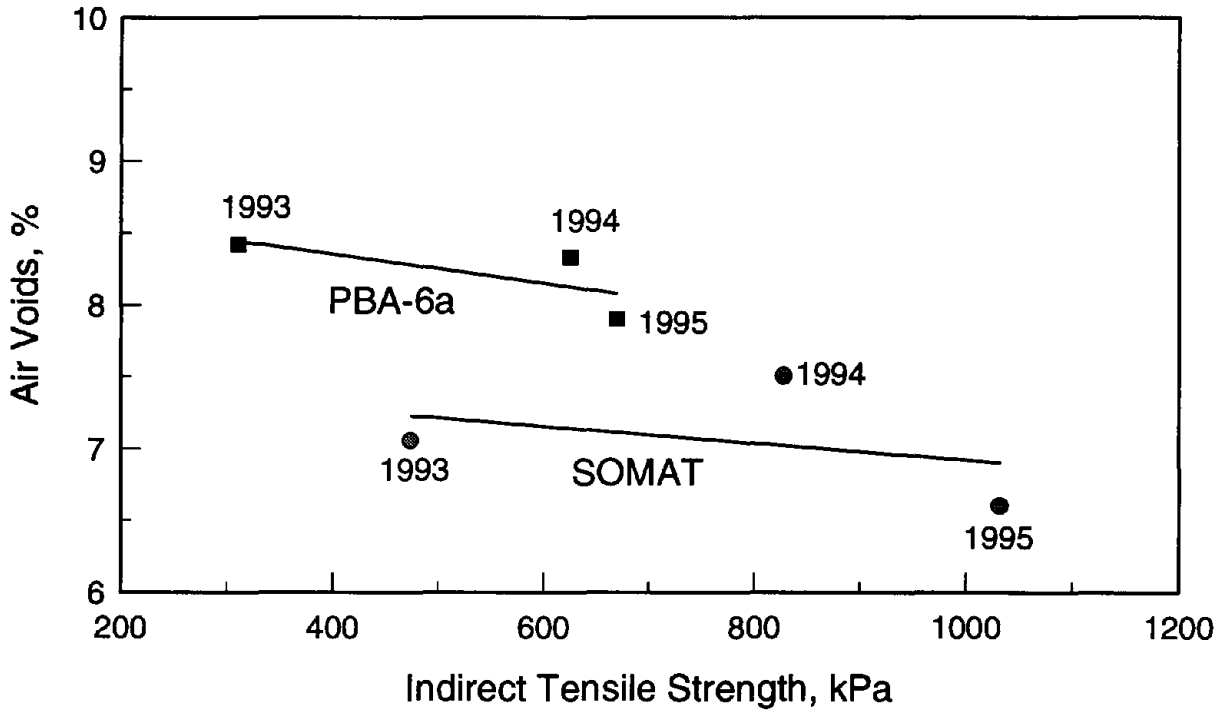

Figure 6-5. The indirect tensile strength (wet) versus the percentage of air voids for cores taken from sections of the two pavements.

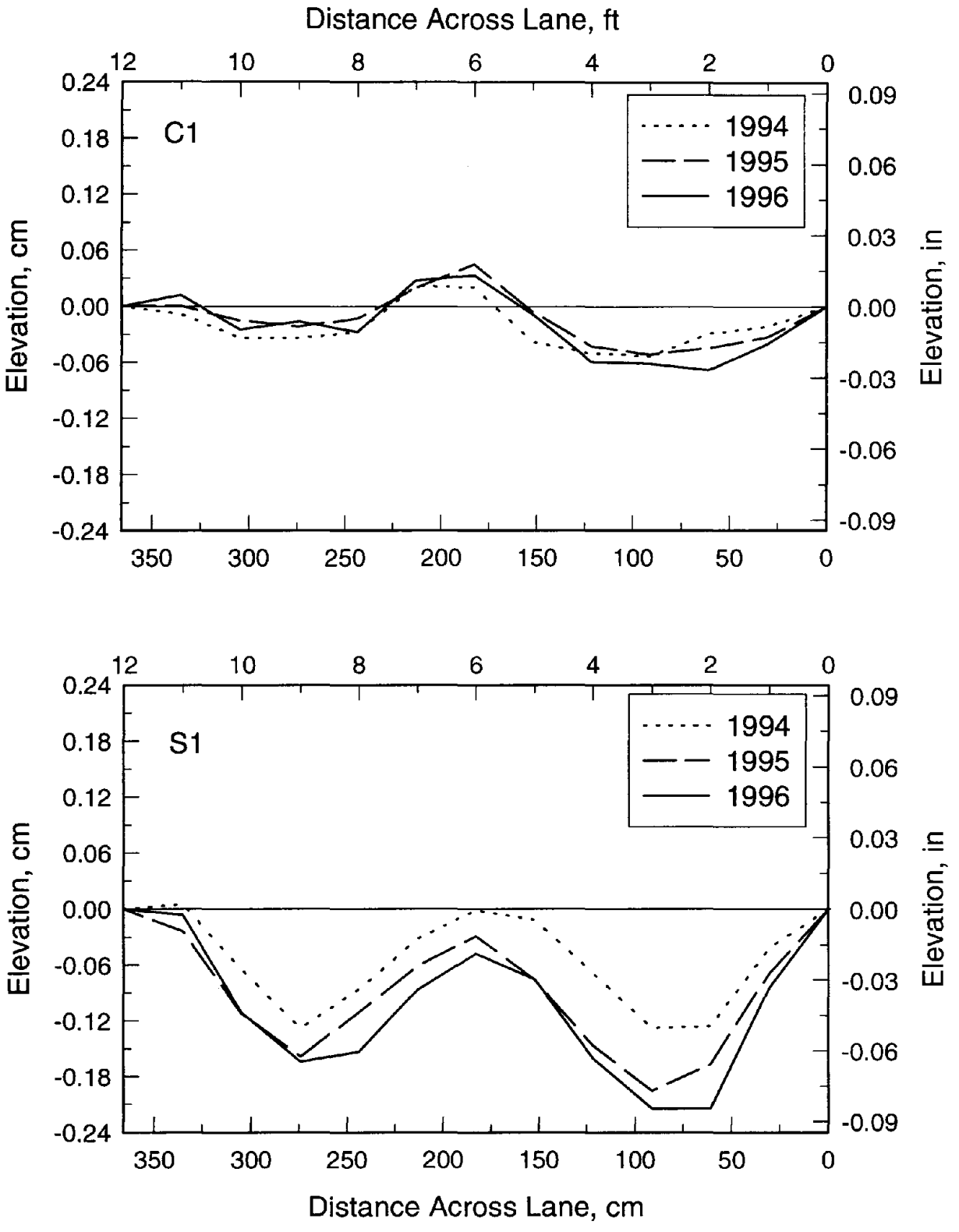

Figure 6-6. Average elevation change from the base (1993) for sections C1 and S1 of U.S. 89.

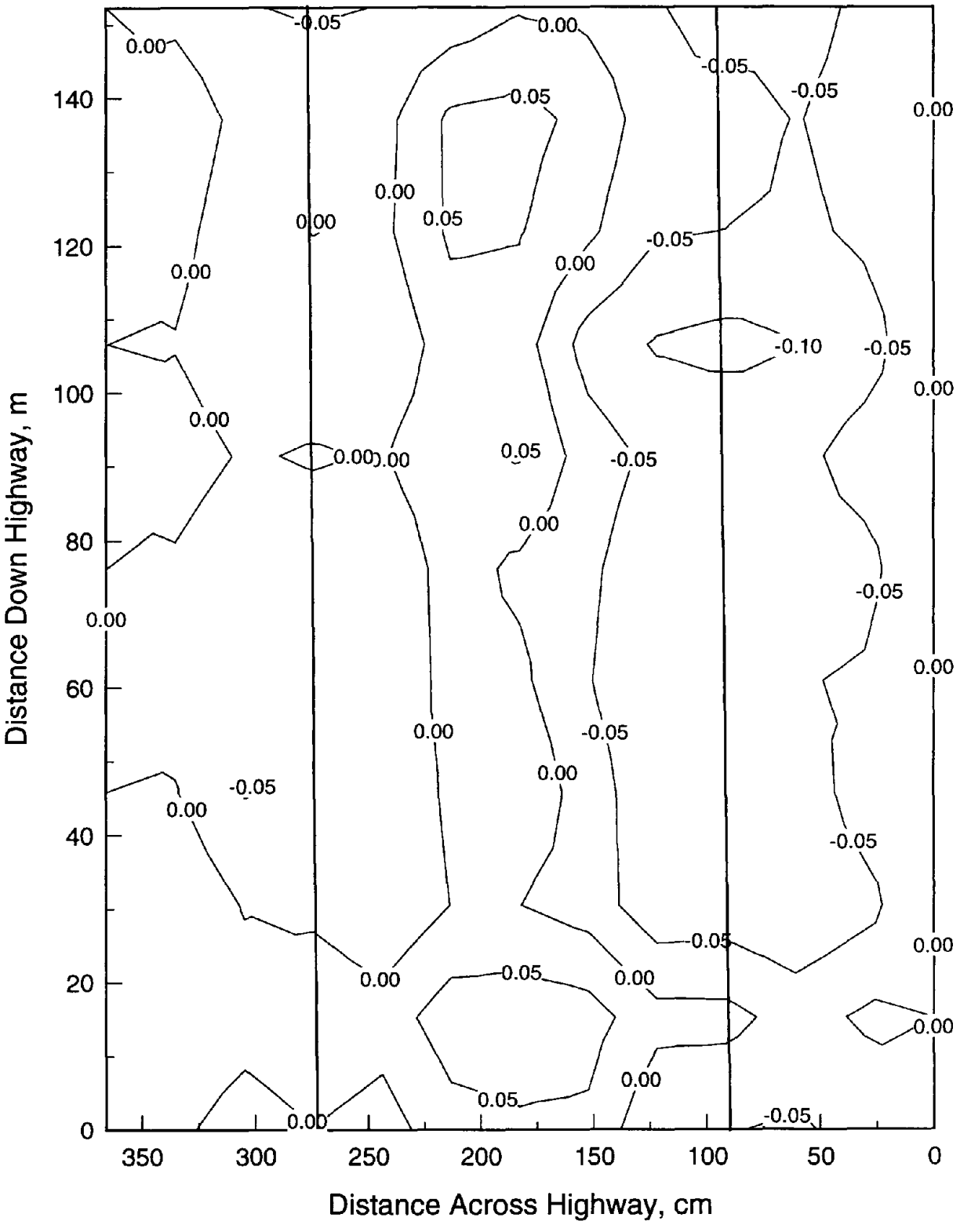

Figure 6-7. Contour map showing the change in elevation in centimeters for section C1 of U.S. Highway 89 (Base to 1996). The verticle lines denote a 1.8-m (6-ft) wheelpath.

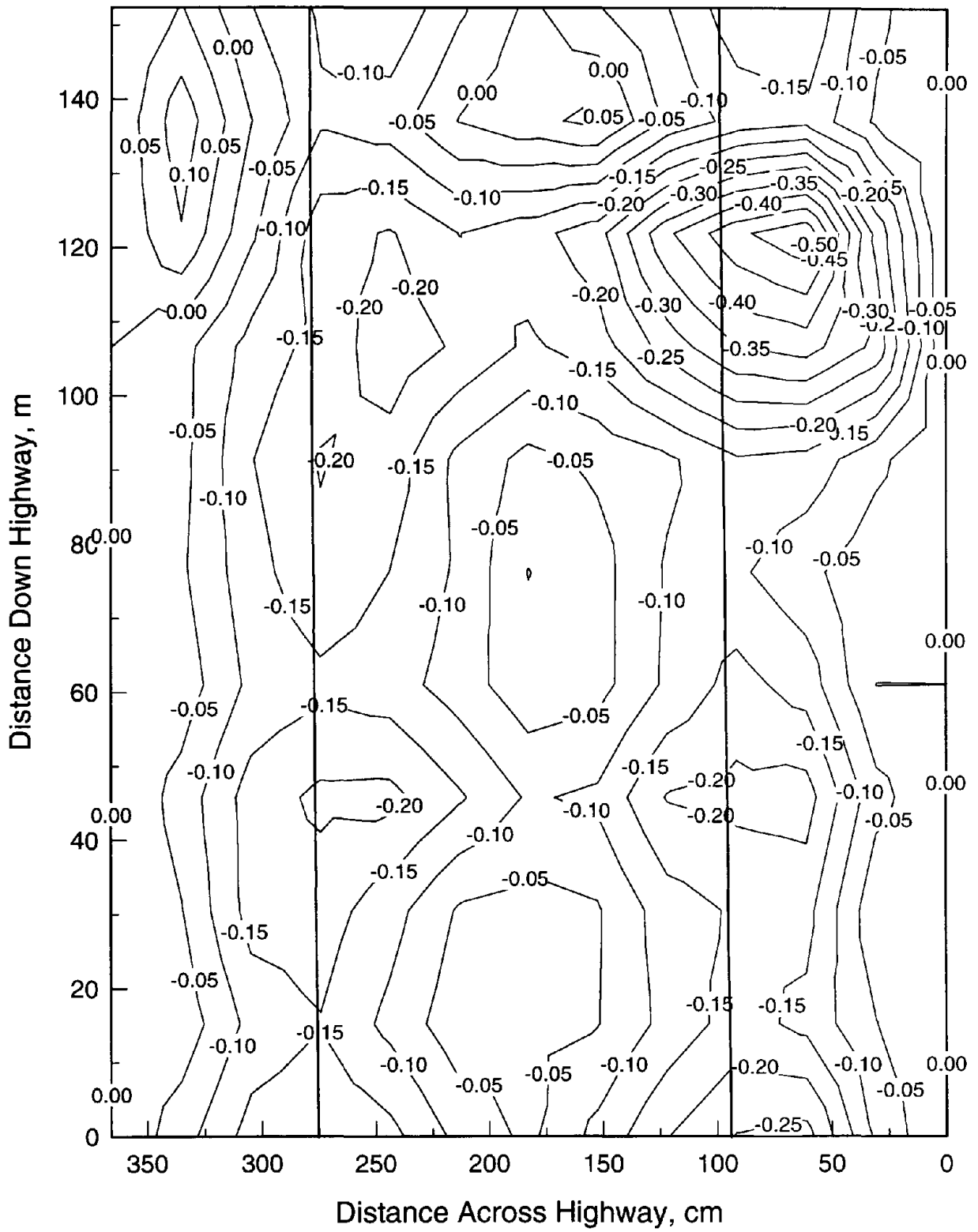

Figure 6-8. Contour map showing the change in elevation in centimeters for section S1 of U.S. Highway 89 (Base to 1996). The verticle lines denote a 1.8-m (6-ft) wheelpath.

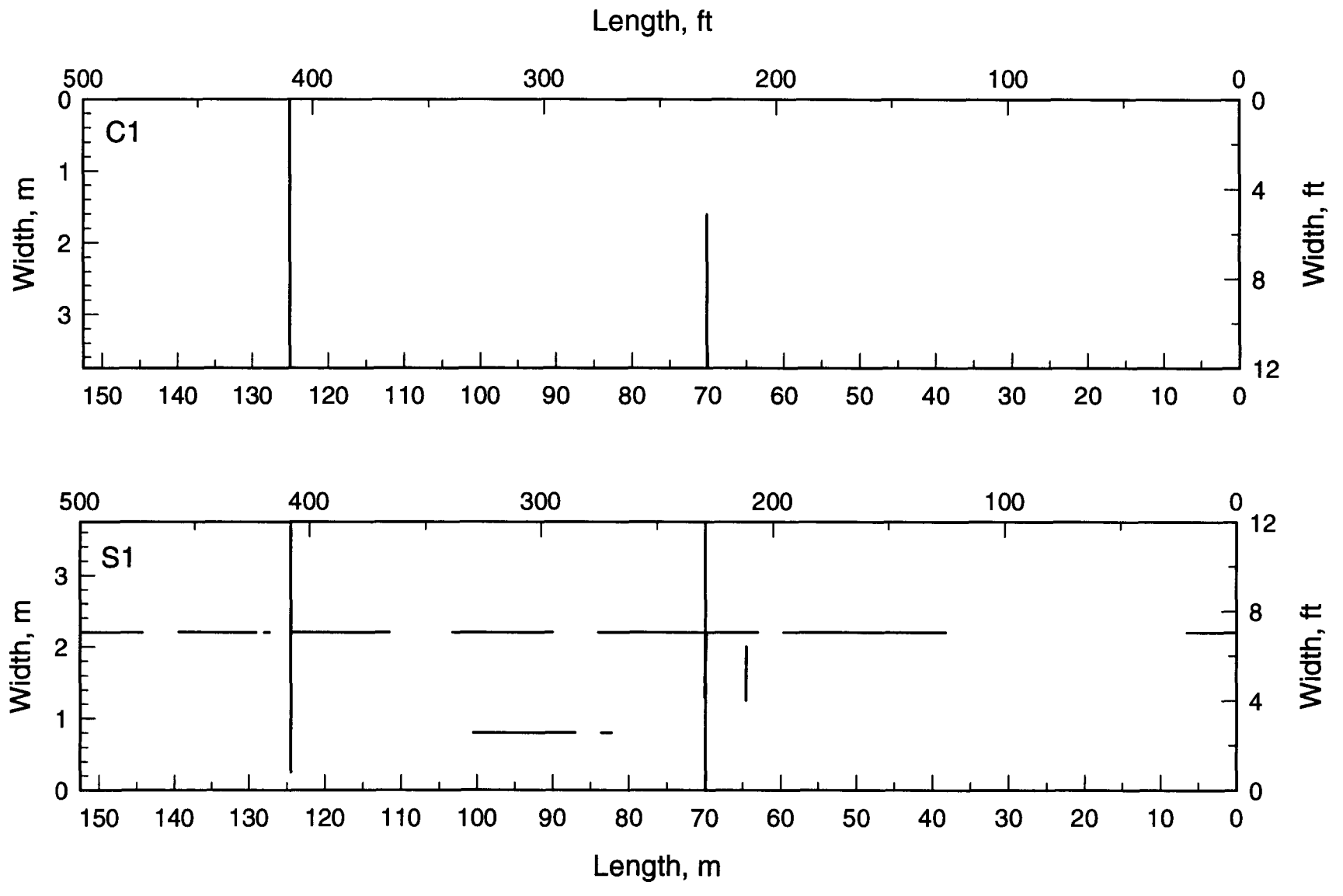

Figure 6-9. Crack map for sections C1 and S1, 1995 (C1 is in the southbound and S1 is in the northbound lane).

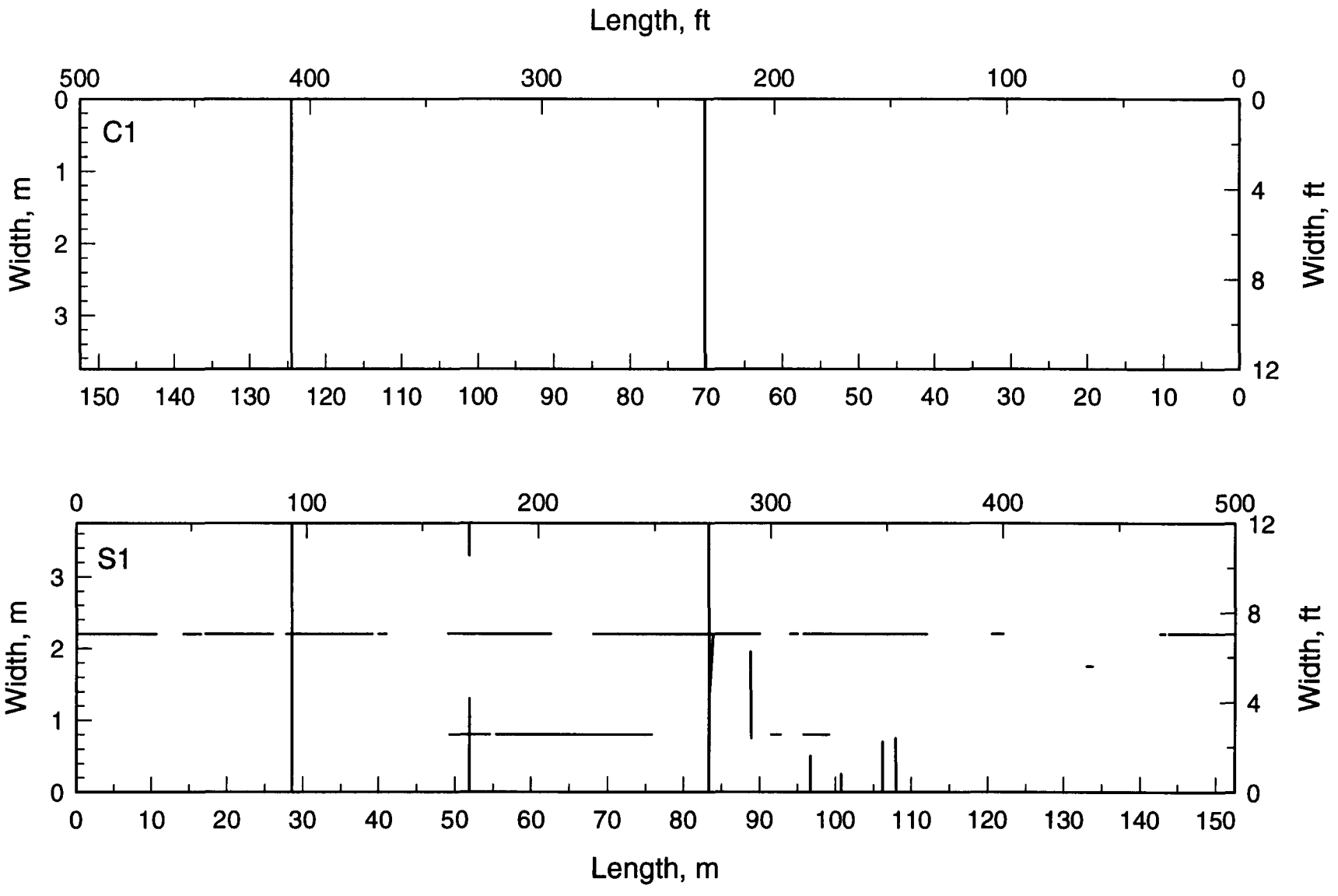

Figure 6-10. Crack map for sections C1 and S1 for 1996 (C1 is in the southbound and S1 is in the northbound lane).

CRUMB RUBBER MODIFIED ASPHALT

Evaluation of Variables that Are Related to the Use of Crumb Rubber

Understanding the behavior of CRMA became very important with the passage of the ISTEA in 1991, which required the States use certain amounts of CR from used tires in pavement construction. At that point in time, CRMA was being used by California, Arizona, and Florida. Each State used its own recipe for mixing CRMA. The rheological properties of the CRMA were unpredictable, and the rheological properties of each combination of asphalt and crumb rubber modifier (CRM) varied widely from other asphalt and CRM combinations. Opinion was divided on whether the CR was inert in asphalt, acting only as filler, whether it dissolved completely due to the action of the aromatic oils present in asphalt, or whether CR dissolved partially. The purpose of this study was to describe the interaction of asphalt and CR systematically. Could the rheological properties of CRMA be predicted based on the type of CRM, type of asphalt, CR particle size, CR particle content, temperature of mixing, speed of mixing, and/or time of mixing?

CR can be incorporated into asphalt concrete by two methods. The wet process, defined as "any method that adds the CRM to the asphalt cement prior to incorporating the binder in the asphalt paving project" and the dry process, defined as "any method of adding CRM directly into the hot-mix asphalt mix process, typically pre-blending the CRM with the heated aggregate" [FHWA 1992]. The dry process shows very little interaction of CR and asphalt while the wet process shows moderate to large interactions. In this study, the effort was concentrated entirely on the wet process.

The study began with an effort to control as many mixing variables as possible, i.e., the size of the CR particles, the temperature of mixing, the time of mixing, and the speed of mixing. The effect of CR concentration on CRMA rheological properties was the first variable examined. CR was obtained from several producers to determine if major differences in rheological properties occurred among CR producers. The study began with 425 to 180 μm (-40+80 mesh) CR from four different producers and, as a control, ground Teflon®. The Teflon® was added as a control to demonstrate what changes in rheological properties would occur when asphalt was mixed with an inert material of the same size and general shape as the CR. Each CR was given a number and mixed in various concentrations with three different asphalts. The asphalts, AAD-1, AAG-1, and AAM-1, were selected because they represent extremes in chemical composition as described in chapter 3. Asphalts AAD-1 and AAG-1 have large amounts of polar compounds and are relatively low in number-average molecular weight. Asphalt AAG-1 was lime-treated. It is low in sulfur content. Asphalt AAD-1 is a high sulfur asphalt. Asphalt AAM-1 is low in sulfur, has relatively few polar compounds, and is a high molecular weight asphalt. The mixing parameters were set at a mix temperature of 175°C (347°F) for 1 hour. These parameters were suggested for mixing CR and asphalt [FHWA 1992]. Three concentrations of CRMA were prepared: 6, 12, and 18 percent by total weight of binder. The rheological properties of asphalts AAD-1, AAG-1, and AAM-1 were measured along with the CRMA's and control.

Measurements and calculations of the rheological properties were performed using a DSR. When analyzing asphalts, the DSR is run in an oscillatory mode, which supplies a periodic deformation at a given frequency, ω. The DSR can calculate several material constants including the magnitude of the complex modulus, $|G^*|$, the loss or phase angle, δ, the storage modulus, G', and the loss modulus, G''. These rheological properties (or material constants) are related to one another, and given any two properties, the others can be calculated. The complex modulus, $G^*(\omega)$, is a complex function of frequency, as shown in equation 6-1,

$$G^*(\omega) = \frac{\sigma_0}{\epsilon_0} e^{i\delta} = G' + iG'' \tag{6-1}$$

where δ is the loss angle at a given frequency, σ_0 is the stress amplitude at a given frequency , and ϵ_0 is the strain amplitude at a given frequency. The loss or phase angle, δ, is a function of the internal friction of the material. A purely elastic material will have a loss angle of 0°, while a purely viscous material will have a loss angle of 90°. The $|G^*|$ is, as its name implies, the magnitude of the vector $G^*(\omega)$ and is found using equation 6-2.

$$|G^*| = \sqrt{G'^2 + G''^2} \tag{6-2}$$

The real part of the complex modulus, G', is known as the storage modulus, and is associated with energy storage and release (recoverable deformation) during periodic deformation. The imaginary part of the complex modulus, G'', is known as the loss modulus and is associated with the dissipation of energy and its transformation into heat. G' and G'' can be found using equations 6-3 and 6-4.

$$G' = |G^*| \cos \delta \tag{6-3}$$

$$G'' = |G^*| \sin \delta \tag{6-4}$$

The ratio G''/G', or $\tan \delta$, is widely used as a measure of the damping capacity of viscoelastic materials [Findley et al. 1989; Rosen 1993]. For a complete description of the relationships the reader is referred to Findley et al. [1989].

The results from the first series of CR concentration experiments showed that as the percentage of CRM was increased, the rheological properties of the CRMA changed directly with increasing CR amounts. Figure 6-11 shows the effect of increasing CRM percent in asphalt AAD-1 on G* as a function of temperature. AAG-1 and AAM-1 exhibit the same behavior. The change in the rheological properties depended mainly on the asphalt used in the mixture. Mixtures of a particular binder with CRM from various sources showed slightly different properties, but these differences were small when compared with the differences between asphalts (see figure 6-12). Also, this experiment showed the effects of an inert material (Teflon®) on the CRMA. The Teflon® mixtures showed very little change in rheological properties (see figure 6-13). These results showed unquestionably that CR is not inert in asphalt, and that there is an interaction occurring between the CR and asphalt. At this point in

the study it became apparent that the various CRM's exhibited much the same behavior. To simplify the task, the next experiments were designed to concentrate work on two of the CRM's. This was started by looking at the CR's that represent the extremes in rheological behavior in all the asphalts. The difference between these extremes was small relative to the differences in the asphalts used in the mixes (see figure 6-13). Also, at this time, the question of the effect of CR preparation arose. Is there a difference between ambient-ground CR and cryogenically ground CR? Hence, a cryogenically ground 425 to 180 μm (-40+80 mesh) CR was added to the experiment to determine if the method of preparation of CR had an effect on the rheological properties of CRMA. It was found that the rheological properties of CRMA prepared with the cryogenically ground rubber did not differ from the other CR's used in this experiment, i.e., the rheological properties fell between the CR's that had been chosen as the extremes of rheological behavior (see figure 6-13). This experiment demonstrated that the major factor in the final CRMA rheological properties was the asphalt used in the mixture and that there was an interaction between the CR and the asphalt. Now that it was clear that there was an interaction between the asphalt and the CR, the next step was to determine the nature of the interaction. More than that, the question became: What component(s) in the asphalts were interacting with the CR?

The next experiment was designed to investigate the interaction of CR and asphalt over time and to try to uncover the nature of the CR-asphalt interaction. CRMA samples were prepared using 12 percent by weight of total binder of CRM1 or CRM4 (these materials are commercially available CR's from two suppliers) and each of the three test asphalts, AAD-1, AAG-1, and AAM-1. Large samples of these mixtures were prepared by mixing, at 175°C (347°F) for 1 hour, and then a small sample of each mixture was removed for testing while the remainder of each CRMA was stored under argon in ovens set at 0, 100, and 200°C (32, 212, and 392°F). Each set of CRMA's had a corresponding control mixture. The control mixtures consisted of the unmodified asphalt put through the mix procedure and stored with the CRMA's. The control samples contained no CR, and these samples were prepared to ensure that any changes measured were due to the interaction of the CRM and asphalt and not to aging or hardening of the asphalts themselves.

The control mixtures stored at 0, 100, and 200°C (32, 212, and 392°F) showed little change in rheological properties over the entire storage temperature range for all the asphalts tested. In figures 6-14 through 6-16 it is clear that storage at a temperature of 0°C (32°F) caused no changes in the rheological properties of the CRMA's. Storage temperatures of 100 and 200°C (212 and 392°F) produced varying amounts and directions of rheological change depending on the storage temperature, time at storage temperature, and the type of asphalt. Nothing could be said about the effect of particle size since all mixtures used the same particle size of 425 to 180 μm (-40+80 mesh). Observation of significant amounts of swelling in neat asphalt at any of the storage temperatures and times proved to be impossible. Realizing that swelling may be significant, an NMR experiment was initiated to elucidate the importance of swelling. The results show that swelling is an important part of the CR interaction with asphalt. This is discussed in more detail later in this section. It is most likely that fine particles of CR "dissolve" at a rate similar to their swelling rate so that one cancels the other. Thus, the overall appearance changes very little when CR contacts asphalt. The rheological data for CRMA's

stored at 100°C (212°F) show a change in properties; there is an increase in |G*|, especially at a storage time of 1,000 hours. However, storage at 200°C (392°F) decreased |G*| in the AAD-1 and AAM-1 mixtures (figures 6-14 and 6-16) while the AAG-1 mixtures showed little change for the first 24 hours (figure 6-15).

The behavior of the mixtures of CR and asphalt AAG-1 led to the examination of the behavior of asphalt ABD. Asphalt ABD is from the same crude source as AAG-1, but is not lime treated. Asphalt ABD was mixed with CRM using the same mix procedure as the other samples. When the 200°C (392°F), 144-hour storage sample was removed for testing, it was observed that this sample appeared different from previous samples. With the test samples of the other CRMA's, the CR was visible in the mixture, i.e., when spread on a microscope slide, individual particles of CR were visible to the unaided eye. When viewed through a microscope (10X) the individual particles appeared as feathered or string-like particles. However, in the case of the CRM-ABD mixture there were no particles visible to the unaided eye. The experiment was repeated. A sample of the mixture was spread on a slide and viewed through a microscope. In the CRM-ABD mixture the particles appeared to be quite different. There were no feathered or string-like particles, only very small, sharp-edged particles. Next, another sample of ABD and CR using the same mix procedure was prepared. This sample was stored in an oven at 200°C (392°F) and monitored each day. After 120 hours (5 days), the sample had the appearance of neat asphalt. To the unaided eye it appeared smooth and shiny. Again, when viewed under the microscope, the small, sharp-edged particles were present. It appeared the CR had dissolved in the asphalt. Since dissolution of CR in asphalt AAG-1 had never been observed, and AAG-1 is lime treated to neutralize the high acid content, it was suspected the acids present in ABD (carboxylic acid 0.025 mol/L [SHRP 1993]), were somehow promoting interaction with the CR. This experiment was repeated using asphalt AAK-2, which is also high in carboxylic acids (0.023 mol/L [SHRP 1993]), with the same results after 192 hours (8 days). Next, the acid fraction from asphalt ABD was removed, using IEC [SHRP 1993], and the acid fraction added to AAM-1. CR was mixed with acid-free ABD and acidified AAM-1 and stored at 200°C (392°F) in an oven for several hours. After several days, the acid-free ABD and CR mixture showed no signs of interaction. CR particles were still visible in the acid-free ABD mixture. However, the acid-enriched AAM-1 and CR mixture had the appearance of a neat asphalt, smooth and shiny with no apparent particles. This was sufficient evidence for the involvement of carboxylic acids as the active component or a marker of the active component to begin a series of controlled acid-doping experiments. The next experiment involved the doping of two low carboxylic-acid asphalts (AAB-1 and AAM-1) with various pure carboxylic acids. The acids included 9-anthranoic acid, stearic acid, and cholic acid, each at three concentrations of 0.01, 0.02, and 0.03 molar. All combinations of acid-doped asphalts were then mixed with -425 μm (-40 mesh) CRM and -425 μm (-40 mesh) natural tire rubber and stored at 156 and 200°C (313 and 392°F). Rheological measurements were taken at various times. Suitable control samples were prepared and rheological measurements were taken for comparison to the acid-doped CRMA samples.

As the acid-doping experiments were begun, the need to determine behavioral differences between natural and synthetic CRM arose. Some of the States using CRM required that a percentage of the CR be natural tire rubber (NR). An attempt was made to obtain samples

of NR. Several of the samples supplied as NR were found to be, as are most CRM's, a mixture of natural and synthetic tire rubber. Solid-state NMR spectroscopy was used to determine the ratio of natural and synthetic tire rubber in each sample. The differences in natural and synthetic tire rubber are shown in figures 6-17a and 6-17b. After several attempts, it was verified that one sample was approximately 100 percent NR. This NR was hand stirred with several asphalts of varying carboxylic acid content. The samples were split, and one group of samples was placed in an oven at 200°C (392°F), while the second group was placed in an oven at 156°C (313°F). As can be seen in tables 6-2 and 6-3, the NR dissolved in all asphalts tested. CRMA prepared with 100 percent NR shows an increase in |G*| at 0, 25, and 60°C (32, 77, and 140°F). Data from this experiment led to the hypothesis that there are two different mechanisms involved in the interaction of CRM and asphalt. The first mechanism involves the interaction of NR and asphalt and appears to depend on the solubility parameter of the two materials. The second involves the interaction of synthetic tire rubber and asphalt and appears to depend on the carboxylic acid content of the asphalt.

If the NR dissolved in asphalt, why did the shear moduli of CRMA's made with NR increase over all test temperatures (0, 25, and 60°C/32, 77, and 140°F)? With the dissolution of NR into asphalt, the molecular size distribution (MSD) of the reacted/dissolved rubber with respect to that of the CRMA was a relevant question. It was decided that HPLC/SEC should be an appropriate technique to determine the MSD of the reacted/dissolved rubber. Figures 6-18 and 6-19 show chromatograms for mixtures ABD-NR and AAB-1-NR stored for various time periods at 200°C (392°F). In figure 6-18, chromatograms for the AAB-1-NR mixture show that heating this CRMA leads to an increase in the large molecular size region of the chromatogram; that is, a peak is now seen at the front edge of the chromatogram that was not present prior to heating. Figure 6-19 shows that heating the ABD-NR mixture for as little as 1 hour has made a significant change in the very large molecular size region of the chromatogram. The differences in the rate of dissolution in the two asphalts may be due to the fact that asphalt ABD is a high carboxylic-acid asphalt while AAB-1 is a low carboxylic-acid asphalt. Further heating of the mixtures gradually fills in the area between the front peak and the rest of the chromatogram. This suggests that the rubber particles break down to initially yield a relatively large molecular-sized material (the increase in |G*| may be the result of this), followed by further breakdown into smaller molecular-sized material (the subsequent decrease in |G*| at longer heating times).

The HPLC/SEC technique was also used to investigate the interaction of asphalt and synthetic CR. Figures 6-20 and 6-21 show the corresponding chromatograms for CRM4 (a blend of NR and synthetic tire rubbers) mixed with asphalts AAB-1 and ABD, respectively. The chromatograms obtained for AAB-1-CRM4 (figure 6-20) show that for the first 48 hours of heating a peak formed in the very large molecular-sized region that diminishes on further heating until it is only a shoulder after 192 hours of heating. A shoulder at this same point is also present in the chromatogram of the neat asphalt (figure 6-22) and in the asphalt-NR mixture. However, this shoulder diminished in size after 24 hours of heating in the neat asphalt. In fact, the chromatograms for both AAB-1 CRM's are almost identical after 168 hours of heating. These results show that the two CR's react differently in the same asphalt and that materials form in the CRMA's that do not form in the asphalt itself during the same heating process. The chromatograms for ABD-CRM4 (figure 6-21) show that the 0 and 1-hour

chromatograms are virtually identical, while the leading edge peak of the 24-hour chromatogram and those for longer storage times show that CRM4 does not begin to break down as early as NR breaks down as a function of storage time in ABD (figure 6-19). The chromatograms for the two CRM's are similar after 48 hours of heating, and a comparison with figure 6-23 shows that the material added during storage at 200°C (392°F) to the front part of the chromatogram comes from the CR's and not from the asphalt.

The nature of the relationships among the rheological properties requires that data be plotted carefully. In many cases, plots of the magnitude of the complex modulus, $|G^*|$, against the run temperatures or storage times indicated very little change in the rheological properties of the CRMA (figure 6-24). The same can be said of plots using the magnitude of the dynamic viscosity, ($|\eta^*| = |G^*|/\omega$). Other combinations of G', G'', $|G^*|$, and δ plotted against the storage time or run temperature each add to the understanding of the process (figures 6-25 and 6-26). To gain an understanding of how each of the properties changed relative to one another, the best methods found were to plot the loss modulus, G'', against the storage modulus, G', and the magnitude of the complex modulus, $|G^*|$, against the loss angle, δ.

The results of the acid-doping experiments were quite surprising. It was speculated that the amount of carboxylic acid present in the asphalt determined the amount of interaction, but the results showed that not only was it the amount of carboxylic acid but also the type of carboxylic acid was important. Figures 6-25 through 6-28 show the results of the experiments. Asphalt AAM-1 mixtures show the same general trends as asphalt AAB-1 mixtures. The addition of carboxylic acids to asphalts AAB-1 and AAM-1 produces varying amounts of rheological change in the CR mixture. Figure 6-25 shows the effects of the various types of carboxylic acids on CRMA's prepared with AAB-1 and CRM4. The results for each carboxylic acid can be found grouped together with the exception of those of the 1-hour mixtures. The grouping of the mixtures by carboxylic acid type is more pronounced in those samples stored at 156°C (313°F) than those stored at 200°C (392°F) (figure 6-26). The interaction is acid type and temperature dependent. The rheological changes occur at a fairly low temperature in a relatively short time. The most rapid change in rheological properties occurs in the first 24 hours and the amount of change depends on the type of carboxylic acid present in the asphalt (figures 6-27 and 6-28).

The addition of carboxylic acids to asphalts AAB-1 and AAM-1 produces varying amounts of rheological change in the CRMA [Tauer and Robertson 1996]. At 200°C (392°F), the interaction proceeds more rapidly, resulting in a reduction in rheological properties. In some instances, the CR has been degraded to a point where the CRMA properties are similar to the neat asphalt, notably where stearic acid has been added. The 9-anthranoic acid, however, seems to protect the CR from degradation. The rheological properties of the CRMA are maintained and even increased in value with time. However, it should be noted that each of the carboxylic acids produce changes in the rheological properties at different rates, and a mixture tested immediately after mixing will have different properties than one tested 6 hours after mixing.

The data presented above indicate that the properties of CRMA change with time, and consequently, the grade originally determined for the modified binder may change to the extent

that the resultant grade may no longer be acceptable for a paving project. In addition, it may imply that when a designated load of CRMA hot mix is being used in a paving project, the properties of the new pavement may vary along the job site. The reader is cautioned that neither the older AC grading system nor the new SHRP PG system have a provision that addresses the carboxylic acid content of the binder. This lack of consideration of the chemistry that controls the final CRMA product quality clearly constitutes a "hole" in any blind-to-source selection (speculation) process.

At the time this report was written, a series of CRM experiments in cooperation with Oregon State University (OSU) have been completed. These experiments are in support of a user's manual for CRM asphalts, which will be prepared under a separate contract. They include varying the CR particle size and concentration and varying the mix time and temperature.

Nuclear Magnetic Resonance Imaging of Crumb Rubber Modified Asphalt

Tire rubbers consist of complex mixtures of elastomers (natural and synthetic rubber), curatives (sulfur, peroxides, etc.), cure-system activators (e.g., stearic acid), fillers and reinforcing agents (carbon black, fibers, etc.), process oils, plasticizer(s), and other additives (antioxidants, antiozonents, etc.). Likewise, asphalts are complex mixtures of chemical compounds, consisting functionally of such compound classes as strong and weak acids, strong and weak bases, neutral compounds, and amphoterics. Therefore, there are questions about what happens when these complex materials are blended at mix temperatures (~170°C/338°F). For example, does finely ground tire rubber (CR) dissolve in the asphalt, does it swell in the asphalt, do volatile components (extender oils, plasticizers) in the rubber migrate into the asphalt, and how might these reactions influence the rheological properties of the mixture?

One method to study these possible interactions is NMR imaging. Because of the sensitivity of the hydrogen nucleus in NMR and because of its favorable relaxation times, water is the fluid most often imaged. However, in favorable circumstances, NMR imaging methods can be employed for imaging solid materials such as elastomers. Sarkar and Komoroski [1992] used NMR imaging to study the morphology and defects in tire composites and the dispersion of carbon black in sections of tire tread. Chang and Komoroski [1989] used NMR imaging to detect voids, gaps, and foreign particles in elastomers. Blumler and Blumich [1991] used NMR imaging to study aging and phase separation in elastomers and obtained the kinetics of the aging reaction using these techniques. In addition, inhomogeneities in NR were detected and characterized. NMR imaging has also been employed in other non-medical applications such as studying fluids in porous rocks [Sarkar et al. 1991], ceramics [Ellingson et al. 1988], wood [Chang et al. 1989], solvent diffusion in polymers [Weisenberger and Koenig 1991; Grinstead and Koenig 1992], bonding of adhesives [Koenig 1991], and coals [French et al. 1991; Hou et al. 1995; Webb et al. 1993]. Komoroski [1993] has written a recent review of non-medical applications of NMRI. Some work has been done using NMR imaging in asphalt research [Miknis and Netzel 1996; Miknis and Pauli 1997].

Although the CR mandate of ISTEA has been removed, there is still sufficient interest to more fully understand the compatibility and physicochemical interactions of asphalt and CR materials. In this section, some preliminary results on the use of NMR imaging to study asphalt-CR mixtures are presented.

Natural tire rubber and styrene-butadiene tire rubber samples were obtained from Rouse Rubber Industries, Inc. The NR samples were conical in shape (~8 mm dia. x ~10 mm height/0.31 x 0.39 in) and sat on a circular base (16 mm dia. x 2 mm height/0.63 x 0.08 in). The styrene-butadiene samples had the shape of a triangular prism (~16 mm base x ~8 mm height x ~10 mm length/0.63 x 0.31 x 0.39 in). In the NMR images, the areas of these shapes were computed using a Cal Comp Drawing Board II hand-held digitizer. The reader is reminded that the size of the samples used in this imaging study is large compared with the CR used in the wet process study.

The natural rubber and styrene-butadiene samples were epoxy glued to the bottom of 23 mm (0.90 in) OD glass vials. The reason for this was to prevent their floating and moving during heating in the asphalt and to ensure that images taken after the heating experiments were made at the same sample orientation. The vials were then placed in 25 mm (0.98 in) (OD) glass tubes. The tubes were inserted into the MRI probe and were positioned in the probe using O rings such that the cross-sections to be imaged were contained in the experimental FOV.

Two sets of samples of each rubber were made. One set was used for heating experiments in the absence of asphalt; the other set was used for heating experiments in the presence of asphalt. The asphalt (ABD) chosen for study was derived from a crude oil from the San Joaquin valley in California and has a relatively high carboxylic acid content of 0.025 mol/L. Carboxylic acid-enriched asphalts have been shown to dissolve different rubber materials when heated to 200°C (392°F) for extended periods of time [Tauer and Robertson 1996]. The asphalt was heated and then poured into the glass vials such that the rubber samples were several millimeters below the level of the asphalt.

Each sample was heated repeatedly in an oven, which was set at 170°C (338°F) for periods of 1, 2, 4, 8, 12, 24, and 48 hours. Cumulatively, this corresponded to heating times of 1, 3, 7, 15, 27, 51, and 99 hours. Between the different heating periods, images were recorded while the sample cooled and after the sample was at room temperature. A temperature of 170°C (338°F) corresponds closely to the temperature at which the paving industry produces asphalt-rubber binders [Billiter et al. 1996].

A comprehensive discussion of the theory of NMR and NMR imaging is beyond the scope of this report. Some discussion of NMR methods is included in chapter 3 and in chapter 5 of this volume. Details of the method are provided in Netzel et al.[1998]. NMR imaging experiments were carried out at a nominal proton resonance frequency of 200 MHz using a Chemagnetics/Otsuka Electronics microimaging probe. For elastomeric and viscous materials, the relaxation times of the protons are generally too short for conventional spin echo imaging. Consequently, a three-dimensional imaging technique was used.

Images using the three-dimensional method were acquired using an echo time of 2 ms, a pulse delay of 0.5 s, a free induction decay size of 256 data points, 64 phase encodes, 20 acquisitions, and a gradient strength of 70 G/cm. Eight 3-mm (0.12-in) thick slices were obtained in an FOV of 22 mm (0.87 in). The measuring time was ~1.4 hours for these experiments. Images taken during cooling were acquired under the same conditions, except that two acquisitions were made. These images were acquired in ~8.5 minutes. All images were recorded in the XZ plane, where the z axis is the direction of the magnetic field and also corresponds to the cylindrical axis of the glass vial.

Images of natural tire rubber (figure 6-29) and styrene-butadiene tire rubber (figure 6-30) in the absence and presence of asphalt were acquired before and after heating and during cooling using the three-dimensional technique. NMR images of the protons in asphalt are not obtained at room temperature because the lack of molecular mobility (high viscosity) shortens the NMR relaxation times such that the NMR signal decays away before any spin echoes can be formed. This is the reason that three-dimensional imaging was used. Only the protons in the rubber are imaged at room temperature. In all cases, only the fifth slice of an image set of eight slices is shown. This slice corresponds to a 3-mm (0.12-in) thick slice through the center of the sample in the XZ plane.

In figure 6-29, the set of four images at the top are for the natural tire rubber heated at 170°C (338°F) for 0 (unheated), 2, 8, and 24 hours in the absence of asphalt. The middle set of four images are for another natural tire rubber sample heated for the same time periods, but in the presence of asphalt. These images were recorded when the sample returned to room temperature after having been heated at 170°C (338°F) for the different periods of time. The bottom set of four images was acquired while the asphalt treated sample was cooling to room temperature. Analogous sets of images were acquired for styrene-butadiene CR treated in the same manner and are shown in figure 6-30.

The intensity of the NMR images decreases with increased time of heating. This is true for both the natural tire rubber and styrene-butadiene tire rubber heated in the presence and absence of asphalt (figures 6-29 to 6-31). However, the loss of signal is more evident for every tire rubber that was heated in asphalt and more so for styrene-butadiene compared with natural rubber. From an NMR perspective, loss of signal intensity is indicative that the rubber became more rigid in the asphalt and as a result, the relaxation times became shorter. This could happen, for example, if oils and plasticizers were driven from the rubber and/or cross-linking reactions occurred as a result of heating. Another reason for the loss of signal intensity could be that the rubber had dissolved in the asphalt, and the only signal remaining was due to the undissolved material. Others [Tauer and Robertson 1996; Billiter et al. 1996] have shown that, depending on asphalt-crude oil source, CR particles dissolve in asphalt when heated at elevated temperatures (170-200°C/338-392°F) for extended periods of time.

NR and styrene-butadiene rubber samples that were heated in the absence of asphalt undergo changes in structure and become more rigid. This was apparent both from the hardness of the rubber samples after heating, and the fact that the rubber samples were impervious to solvents, such as chloroform, after heating (i.e., did not swell in solvents). The apparent change

in the physical state of the rubber could be due to oxidation at the rubber surface and/or devolatilization and cross-linking reactions in the rubber.

The real effect of asphalt on the pieces of tire rubber when heated in the presence of asphalt is quite clear in the lower sets of four images in figures 6-29 and 6-30. These images were acquired during cooling and show that the rubber had not dissolved, but had swelled. In fact, the natural tire rubber has swelled to about two times its normal size (figures 6-29 and 6-32). The images of the swollen rubber could be reproduced by simply reheating the sample for 10 minutes after it had been at room temperature and re-imaging the sample. These images clearly indicate that the loss of signal in the middle sets of images is not due to dissolution of the rubber. This experiment was intentionally designed to use pieces of tire rubber with a very small surface-to-mass ratio to minimize dissolution and to image swelling behavior. Swelling is nearly impossible to image with finely ground CR. The images of the swollen rubber also negate the notion that the rubber had undergone more cross-linking and became more rigid when heated in the asphalt.

A possible explanation of the swelling could be migration of low molecular weight components of asphalts into rubber during heating. Valkering et al. [1992] have shown that maltenes from asphalt cause considerable swelling in styrene-butadiene-styrene block copolymer/asphalt blends. This exchange might also account for the loss of signal at room temperature if the relaxation times of the rubbers took on those of the asphalt components.

There was little or no swelling of the rubber samples when heated in the absence of asphalt. This is seen by the top set of images in figures 6-29 and 6-30. The lack of swelling was also verified visually immediately after the samples were removed from the oven. Thus, the swelling of the rubber appears to be caused by solvent penetration of components of the asphalt, possibly maltene components as described above, into the rubber. Loss of the extender oils in rubber could also account for some of the rigidity and brittleness exhibited by the rubber samples after heating in the absence of asphalt.

One reason for imaging the samples at elevated temperatures is that the NMR relaxation times are lengthened at higher temperatures so that protons that do not image at room temperature might be imaged at the higher temperature. In the lower sets of images in figures 6-29 and 6-30, signals from the heated asphalt can be seen as the light contrast surrounding the rubber samples. In figure 6-30 b, c, and d, the signal at the bottom of the triangularly shaped styrene-butadiene rubber is actually the top of the asphalt layer. This is an artifact in the images caused by positioning the sample in the image probe, such that the FOV was not large enough to encompass the sample. The temperature at which the images are acquired during the cooling phase is not known because the NMRI probe is not capable of variable temperature measurements. By convention, the samples were allowed to set for 3 minutes after they were removed from the oven and then were put into the NMR probe. Images were then acquired using the same conditions as before, except only two acquisitions were obtained.

Applications of NMR imaging to study polymer-modified asphalts are in their infancy. In this study, exploratory NMR images were acquired on relatively large pieces of natural and

styrene-butadiene rubber alone and immersed in asphalt. These measurements demonstrated the feasibility of using NMR imaging to study different interactions between CR's and asphalt, such as swelling by asphalt molecules, possible dissolution of rubber components in asphalt, and devolatilization and cross-linking in rubber when heated at mix temperatures of 170°C (338°F).

Table 6-2. Asphalt and natural tire rubber storage time at 200°C.

Asphalt	Storage time, hr						
	1	24	48	72	96	168	192
AAB-1		Dissolved	Dissolved	Dissolved	Dissolved	Dissolved	Dissolved
AAD-1		Dissolved	Dissolved	Dissolved	Dissolved	Rubber chunks form	Skin dissolved
AAF-1	Dissolved	Dissolved	Dissolved	Dissolved	Dissolved	Partial skin develops	Dissolved
AAG-1		Dissolved	Dissolved	Dissolved	Dissolved	Dissolved	Dissolved
ABM-1		Dissolved	Dissolved	Dissolved	Dissolved	Dissolved	Dissolved
AAK-1	Dissolved	Dissolved	Dissolved	Dissolved	Dissolved	Dissolved	Dissolved
AAK-2		Dissolved	Dissolved	Dissolved	Dissolved	Partial skin develops	Dissolved
AAM-1	Dissolved	Dissolved	Dissolved	Dissolved	Dissolved	Partial skin develops	Dissolved
ABD	Dissolved	Dissolved	Dissolved	Dissolved	Dissolved	Dissolved	Dissolved

Table 6-3. Asphalt and natural tire rubber storage time at 156°C.

Asphalt	Storage time, hr						
	1	24	48	72	96	168	192
AAB-1		Partially dissolved	Partially dissolved	Partially dissolved	Partially dissolved	Rubber ball forms	Dissolved
AAD-1		Partially dissolved	Skin forms	Dissolved	Dissolved	Rubber chunks form	Skin dissolved
AAF-1		Partially dissolved	Partially dissolved	Partially dissolved	Partially dissolved	Partially dissolved	Dissolved
AAG-1		Partially dissolved	Partially dissolved	Partially dissolved	Partially dissolved	Dissolved	Dissolved
ABM-1		Partially dissolved	Partially dissolved	Partially dissolved	Partially dissolved	Dissolved	Dissolved
AAK-1		Partially dissolved	Partially dissolved	Partially dissolved	Partial skin forms	Skin covers sample	Skin thickens
AAK-2		Partially dissolved	Partially dissolved	Partially dissolved	Partially dissolved	Dissolved	Dissolved
AAM-1		Partially dissolved	Partially dissolved	Partially dissolved	Partially dissolved	Partially dissolved	Partially dissolved
ABD		Partially dissolved	Partially dissolved	Partially dissolved	Partially dissolved	Partially dissolved	Partially dissolved

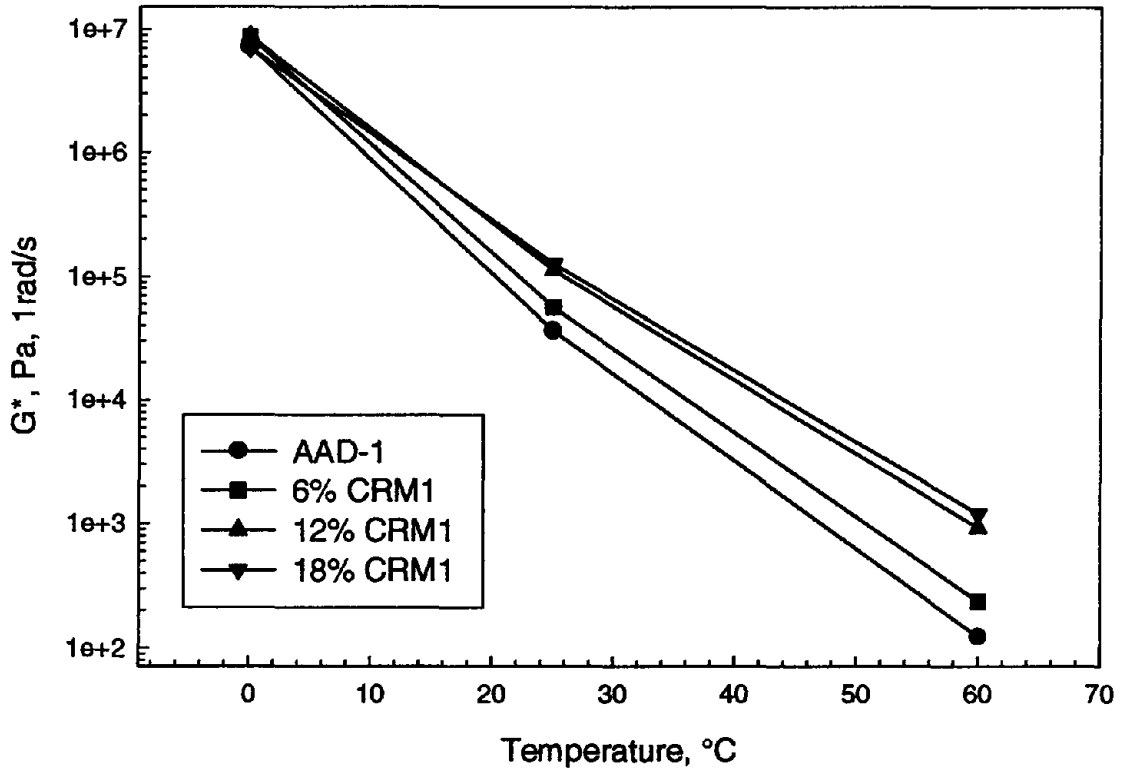

Figure 6-11. Asphalt AAD-1 and CRM1 at 6, 12, and 18% by total weight of binder.

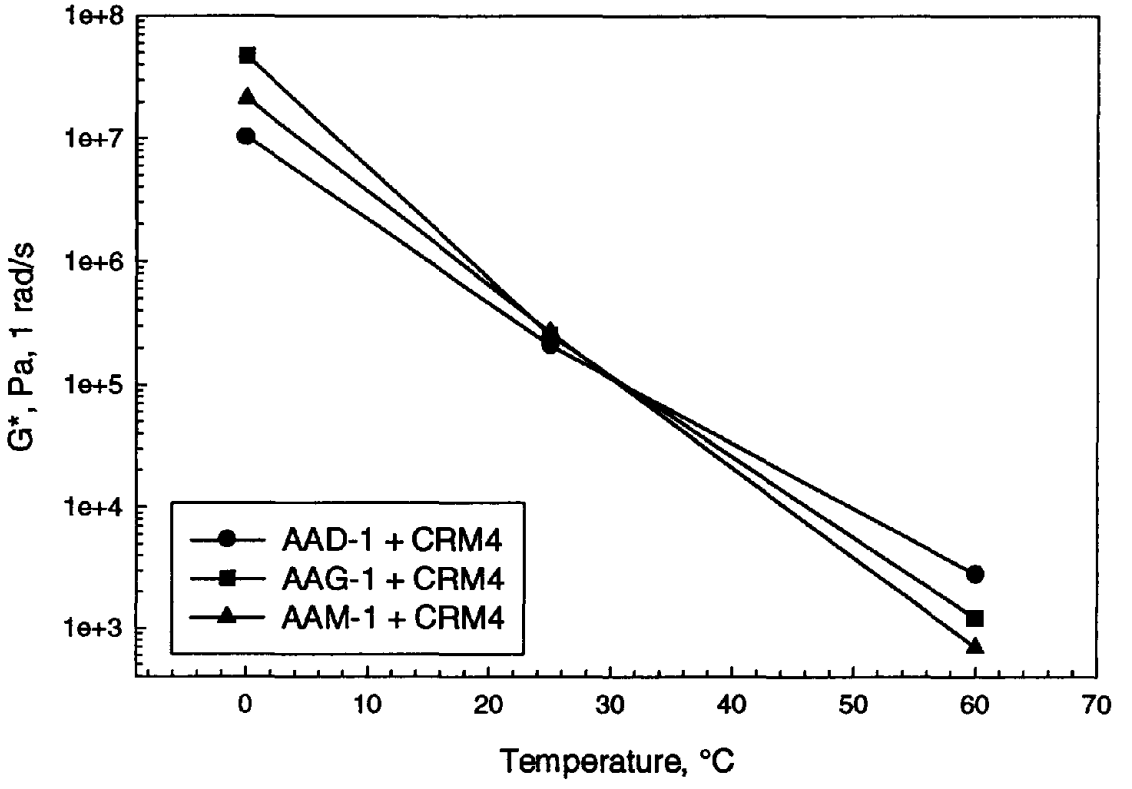

Figure 6-12. Asphalts AAD-1, AAG-1, and AAM-1 with 18% CRM4 by total weight of binder.

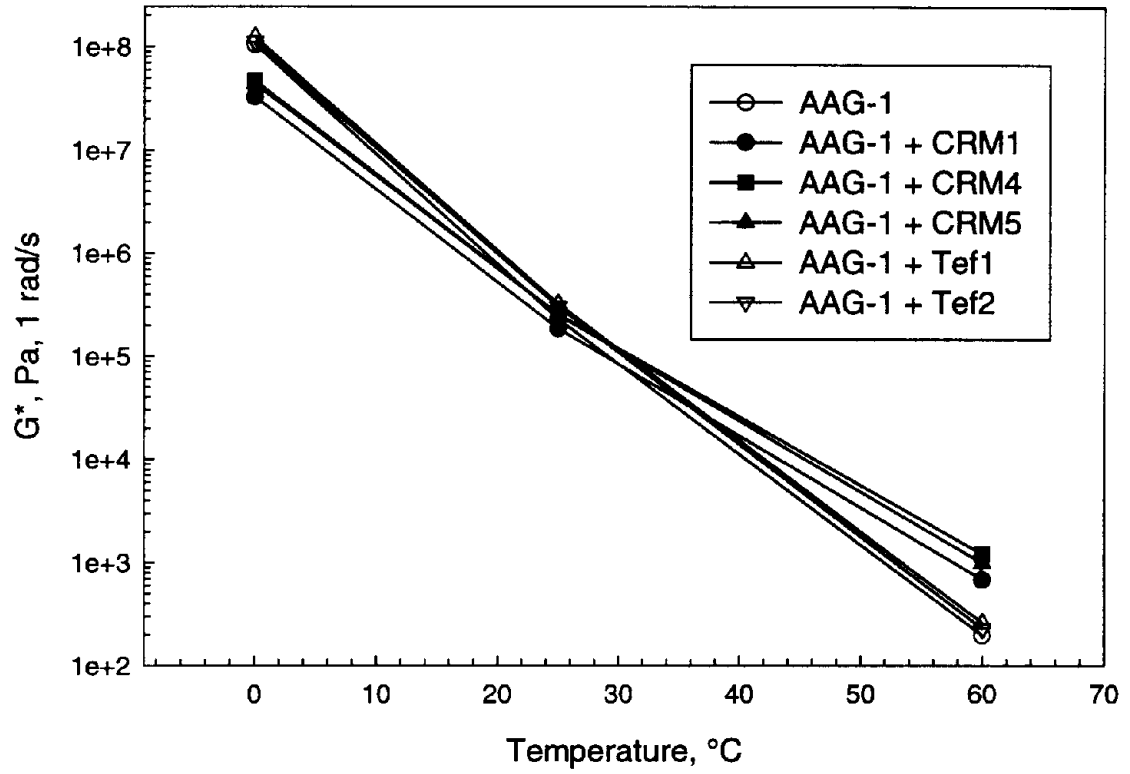

Figure 6-13. Asphalt AAG-1 and 18% CRM's or Teflon by total weight of binder.

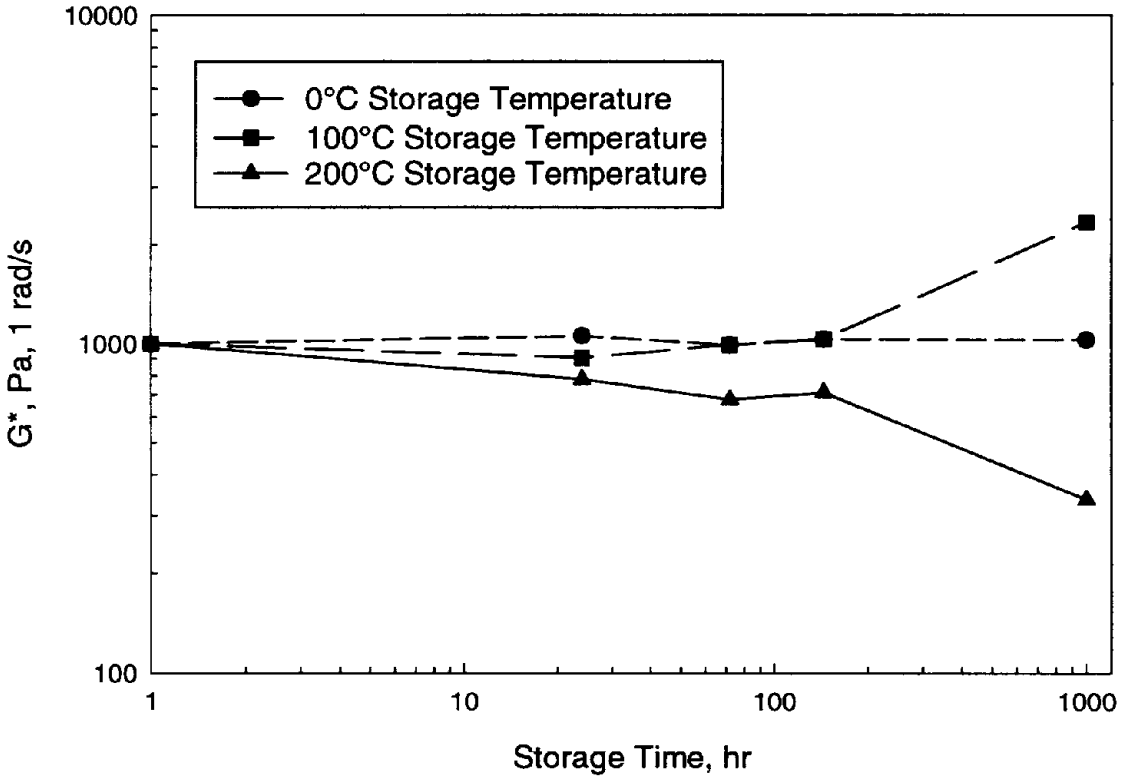

Figure 6-14. Asphalt AAD-1 and 12% CRM1 by total weight of binder, 60°C data.

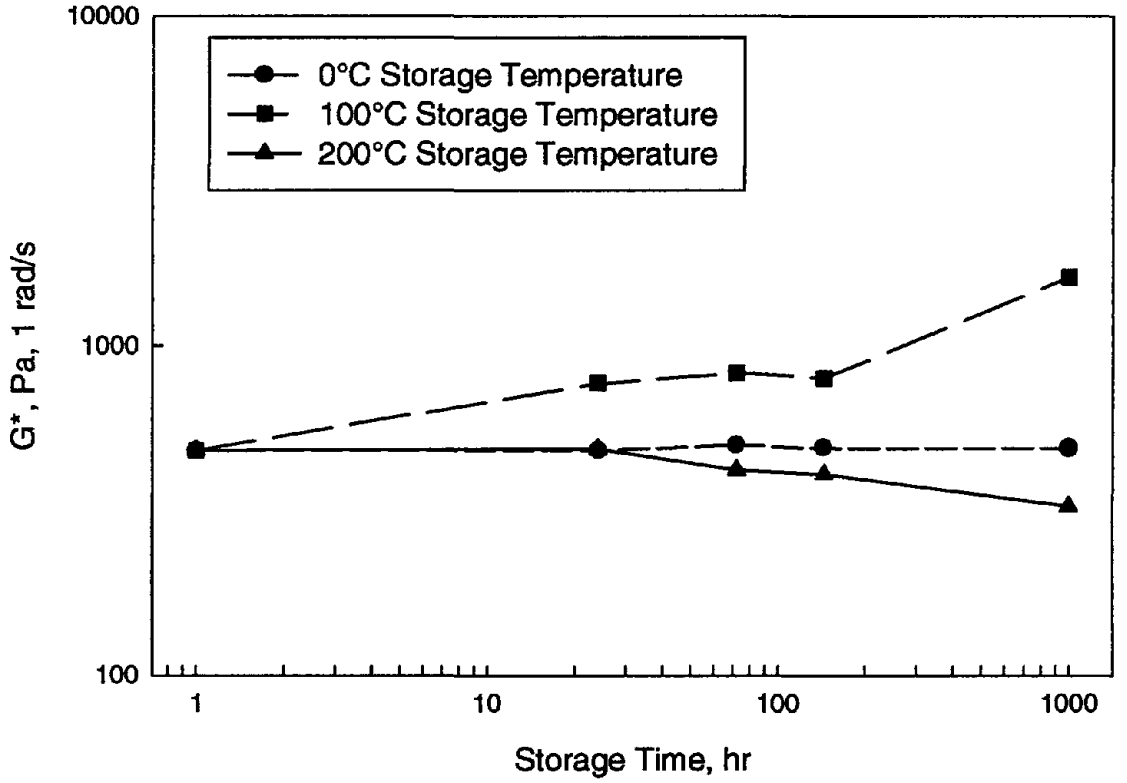

Figure 6-15. Asphalt AAG-1 and 12% CRM1 by total weight of binder, 60°C data.

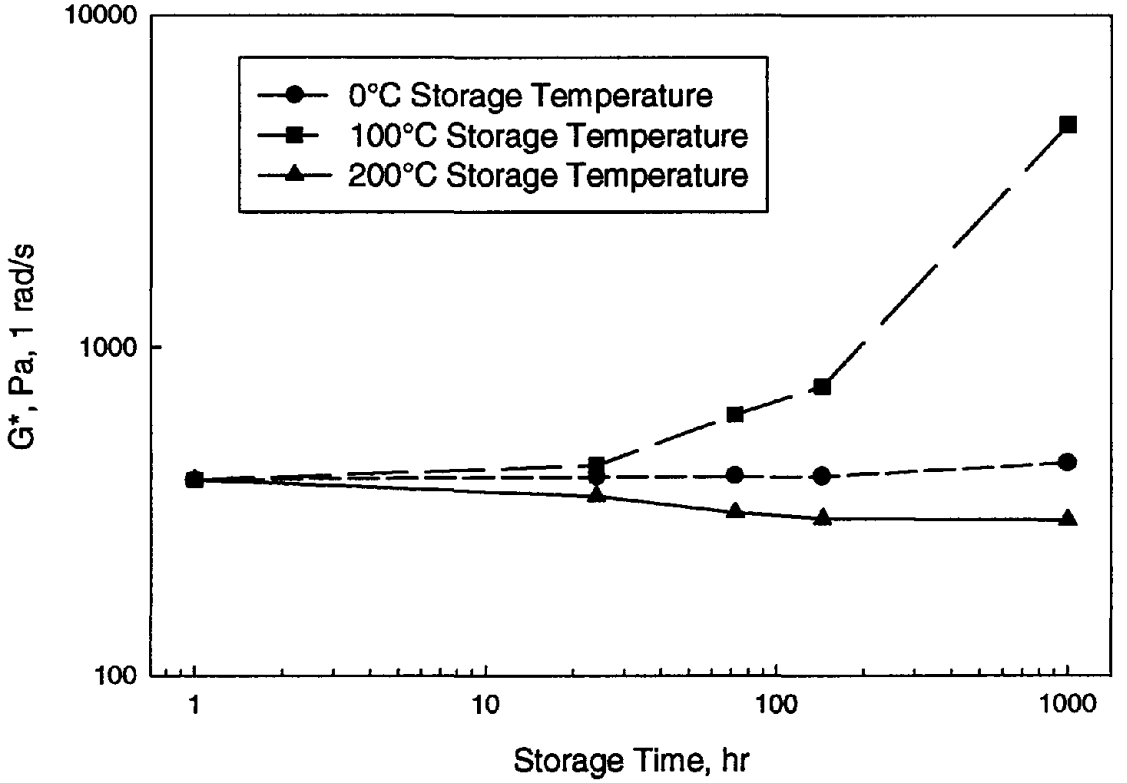

Figure 6-16. Asphalt AAM-1 and 12% CRM1 by total weight of binder, 60°C data.

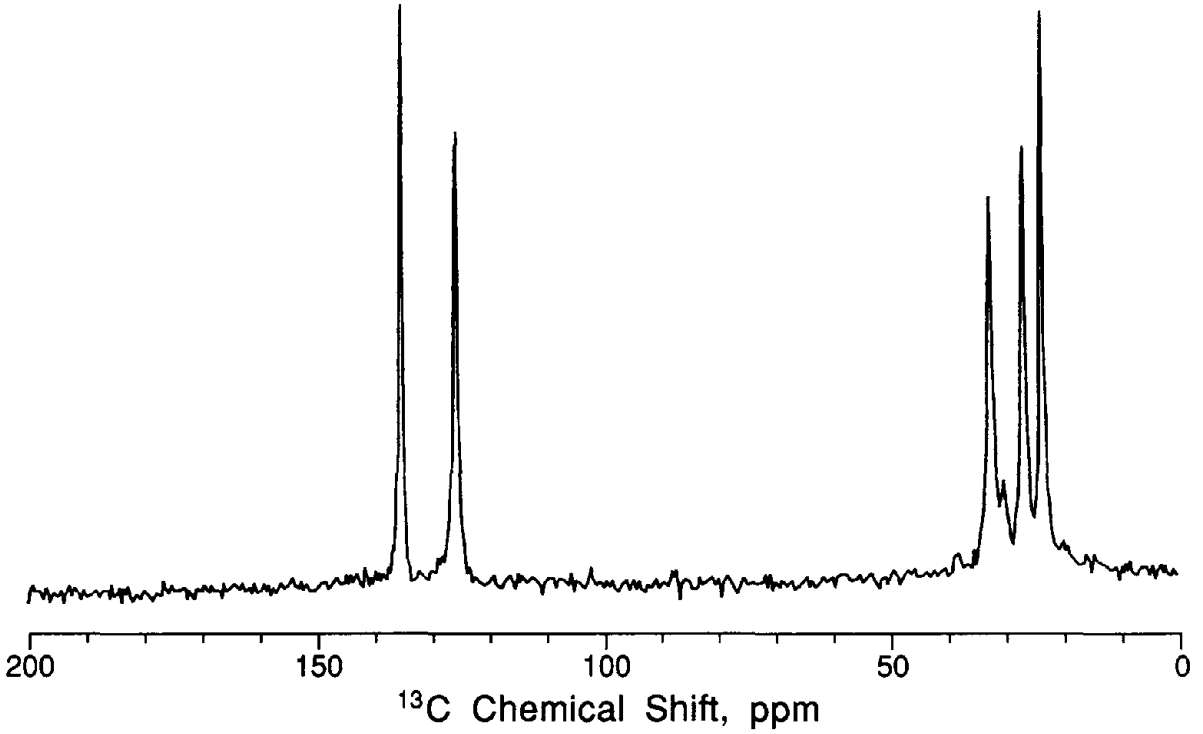

Figure 6-17a. NMR spectra of natural tire rubber.

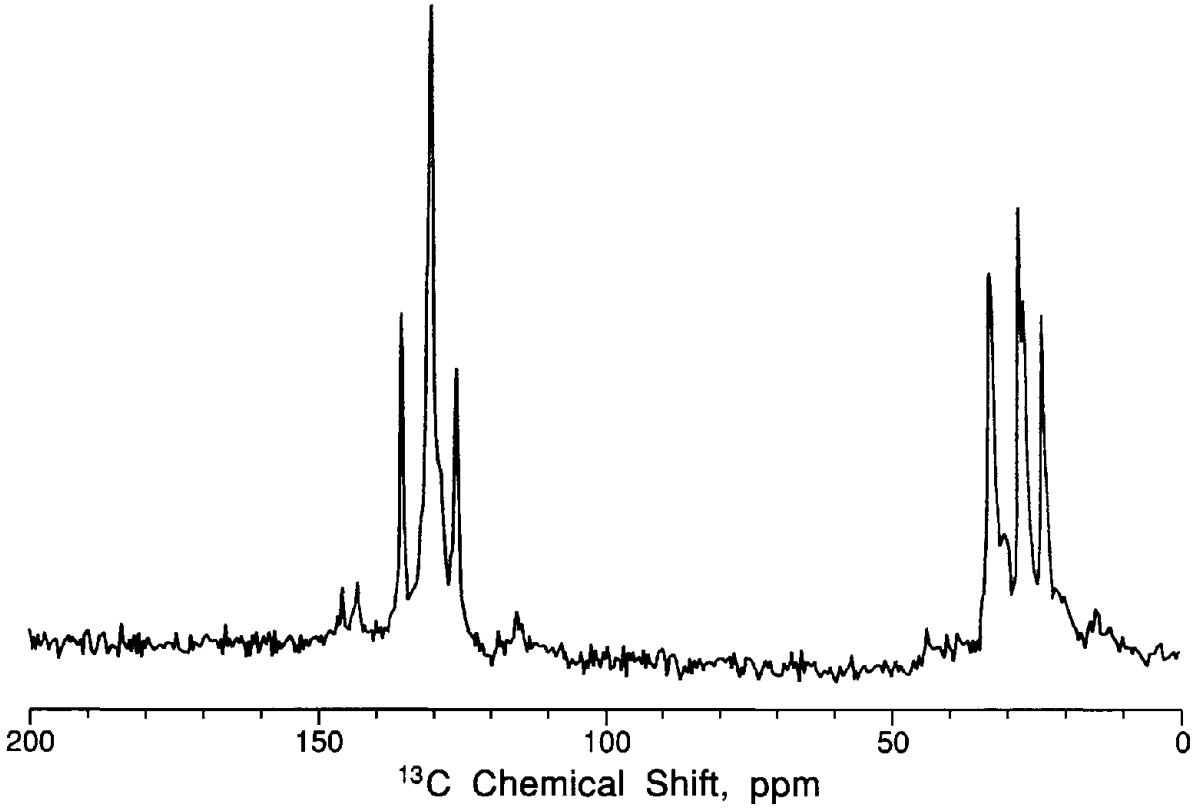

Figure 6-17b. NMR spectra of CRM rubber.

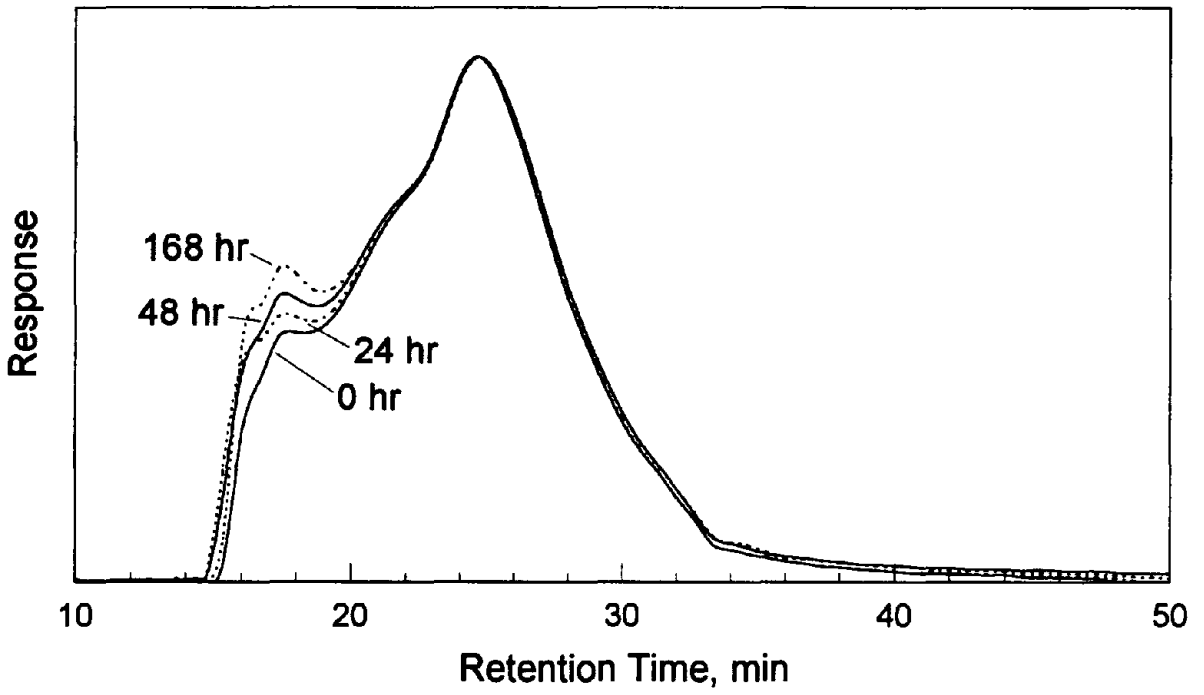

Figure 6-18. HPLC/SEC DRID chromatograms of core asphalt AAB-1 with NR, heated for various times.

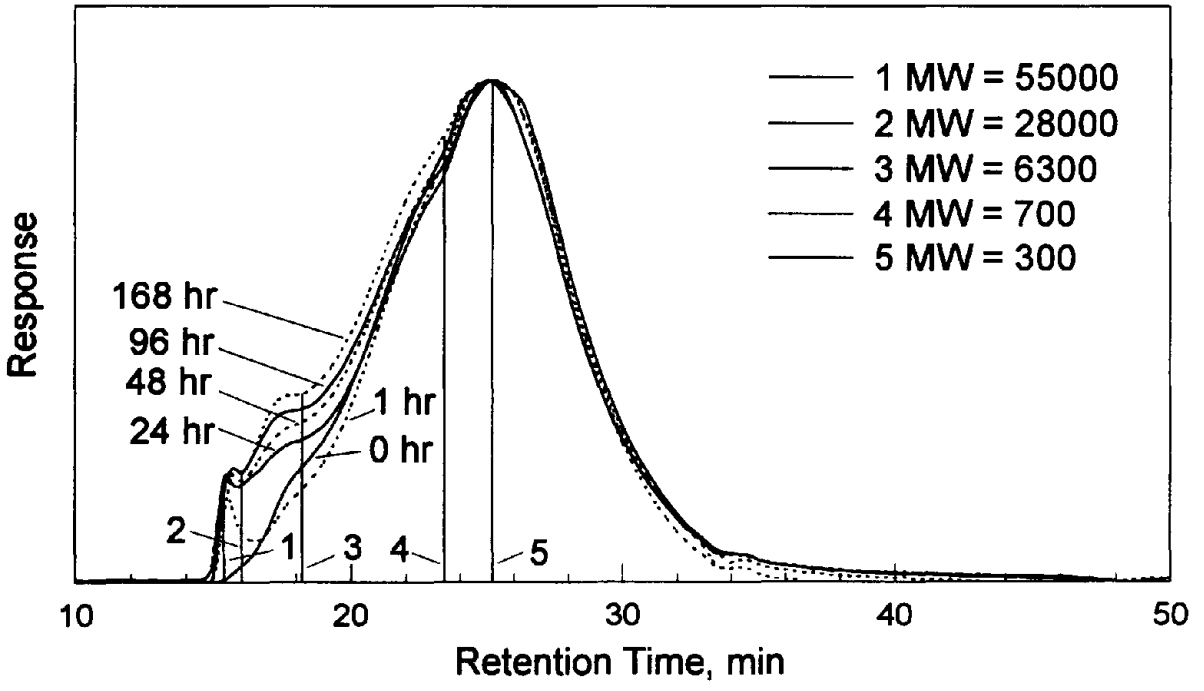

Figure 6-19. HPLC/SEC DRID chromatograms of asphalt ABD with NR, heated for various times.

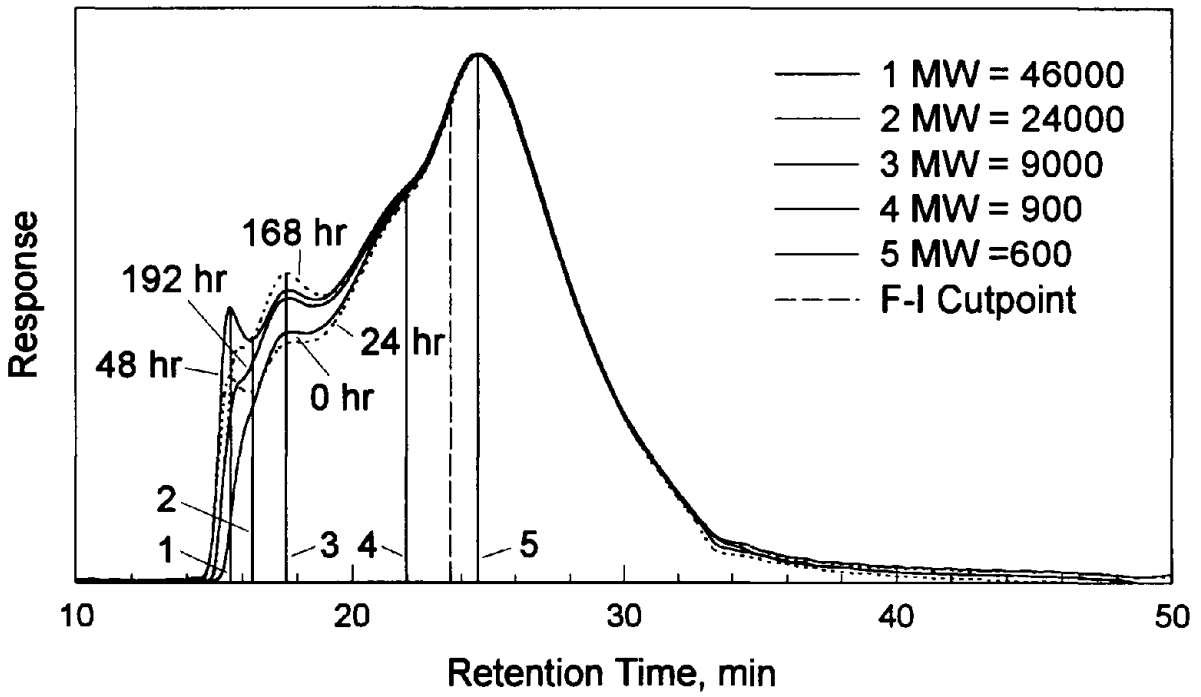

Figure 6-20. HPLC/SEC DRID chromatograms of core asphalt AAB-1 with CRM4, heated for various times.

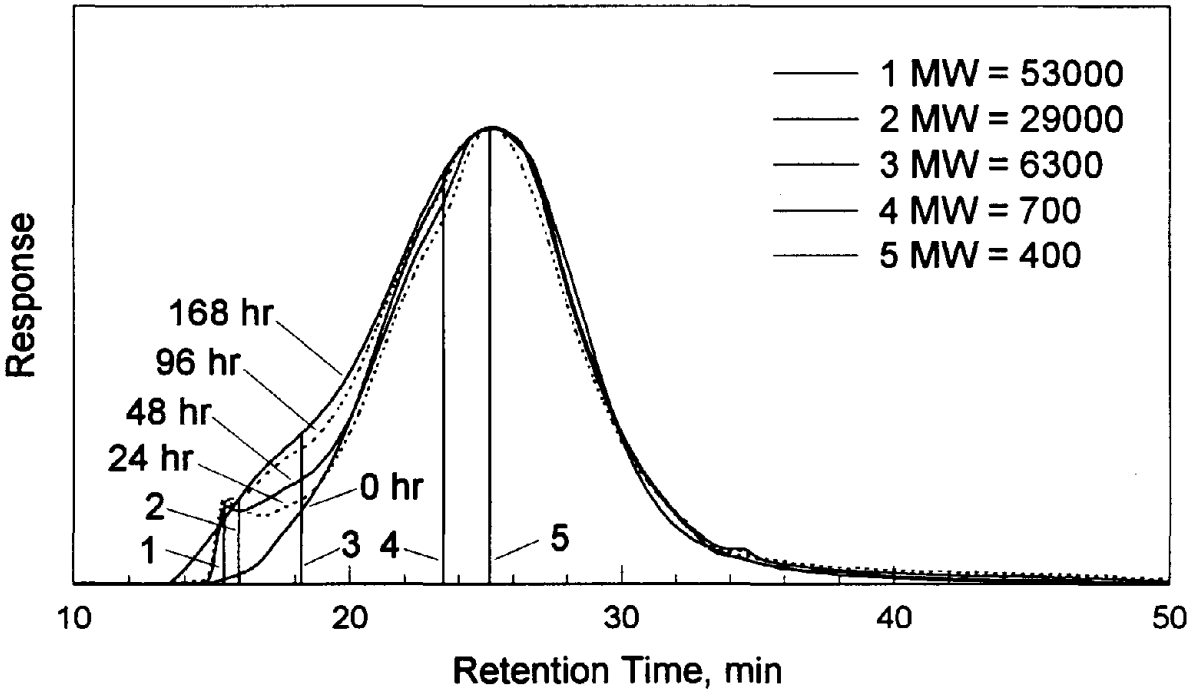

Figure 6-21. HPLC/SEC DRID chromatograms of asphalt ABD with CRM4, heated for various times.

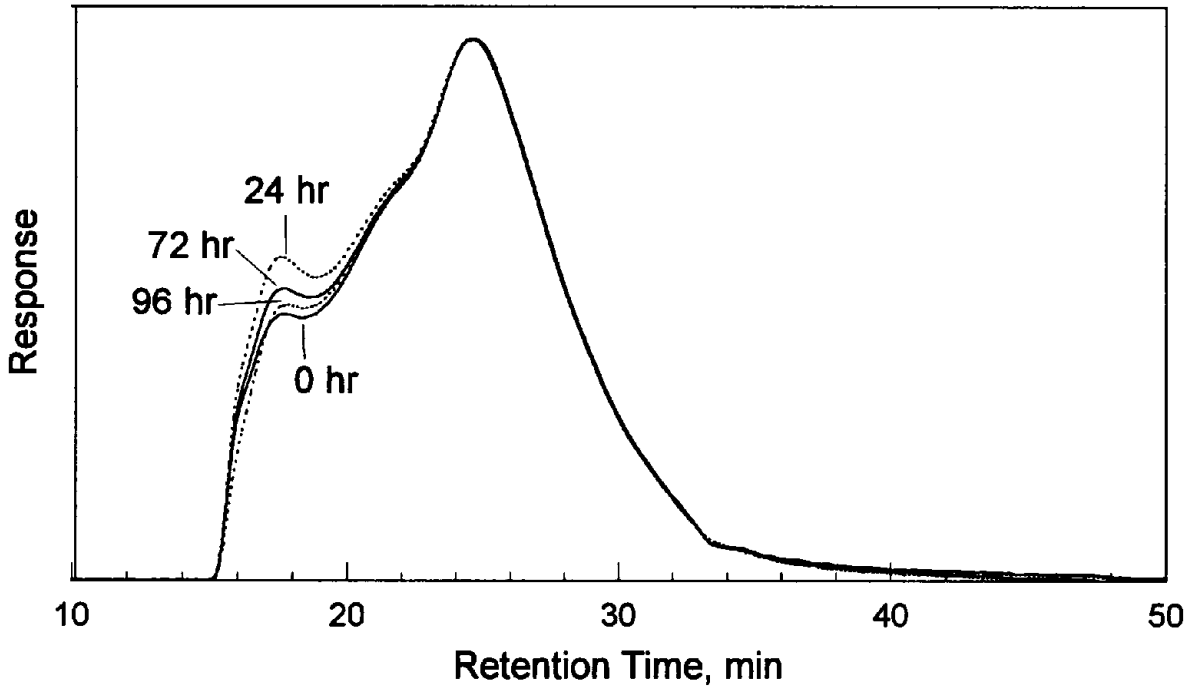

Figure 6-22. HPLC/SEC DRID chromatograms of unmodified core asphalt AAB-1, heated for various times,.

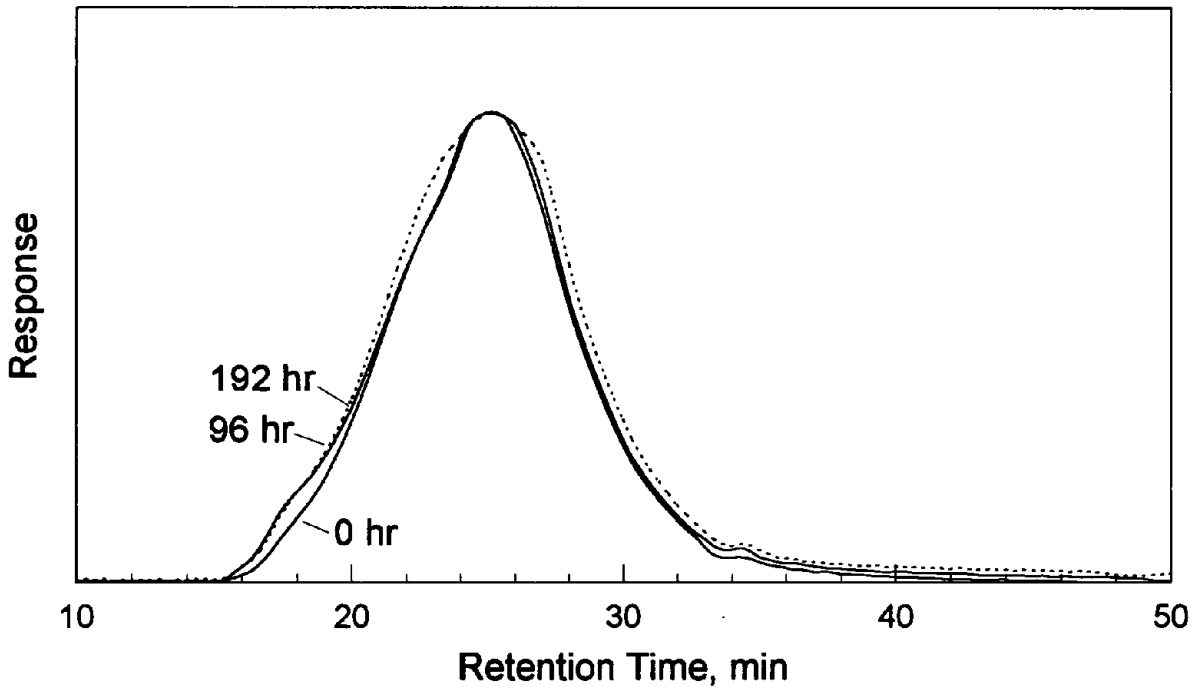

Figure 6-23. HPLC/SEC DRID chromatograms of unmodified asphalt ABD, heated for various times.

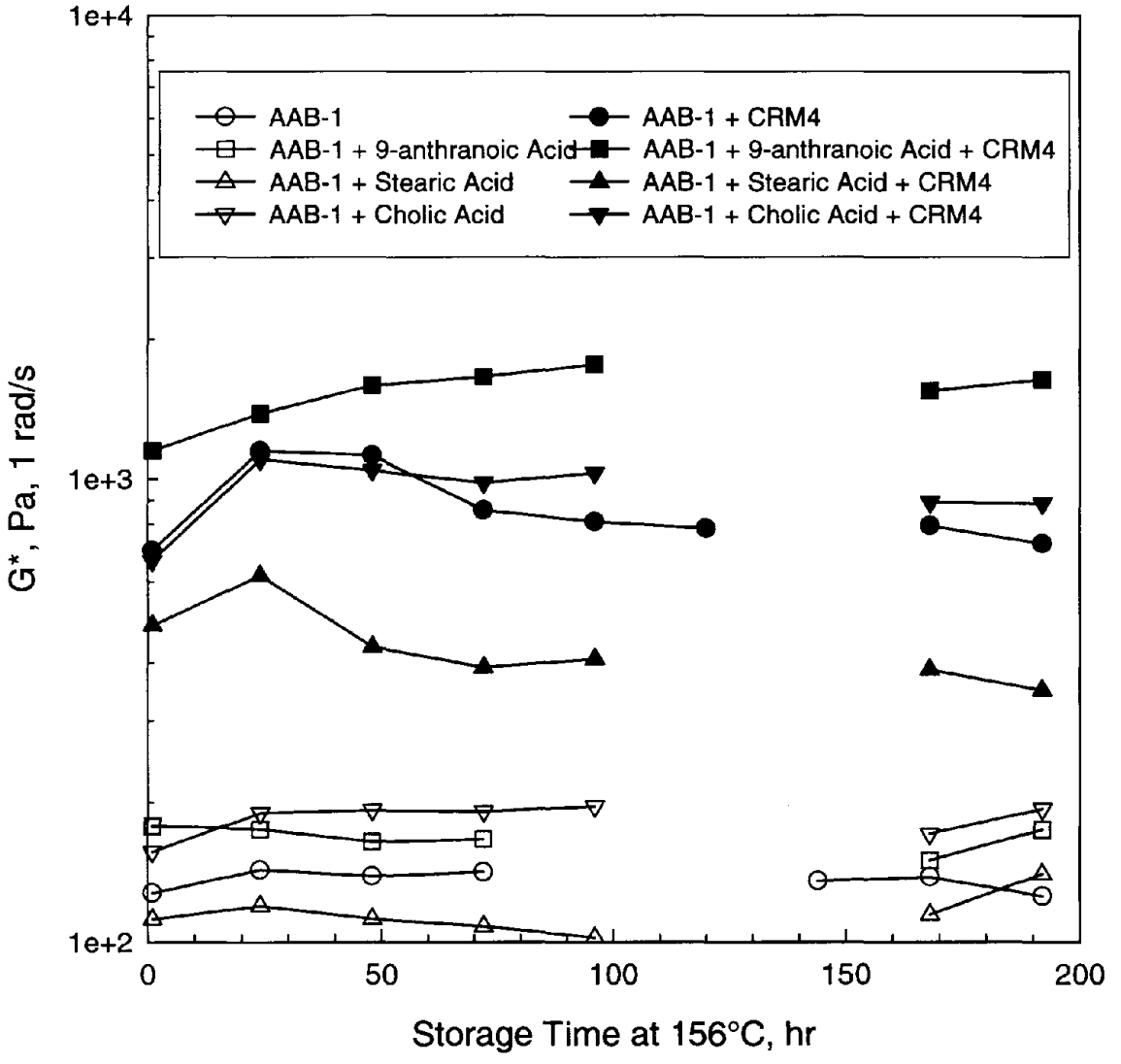

Figure 6-24. Shear modulus for asphalt AAB-1, carboxylic acid-modified AAB-1, and CRMA's, 60°C data.

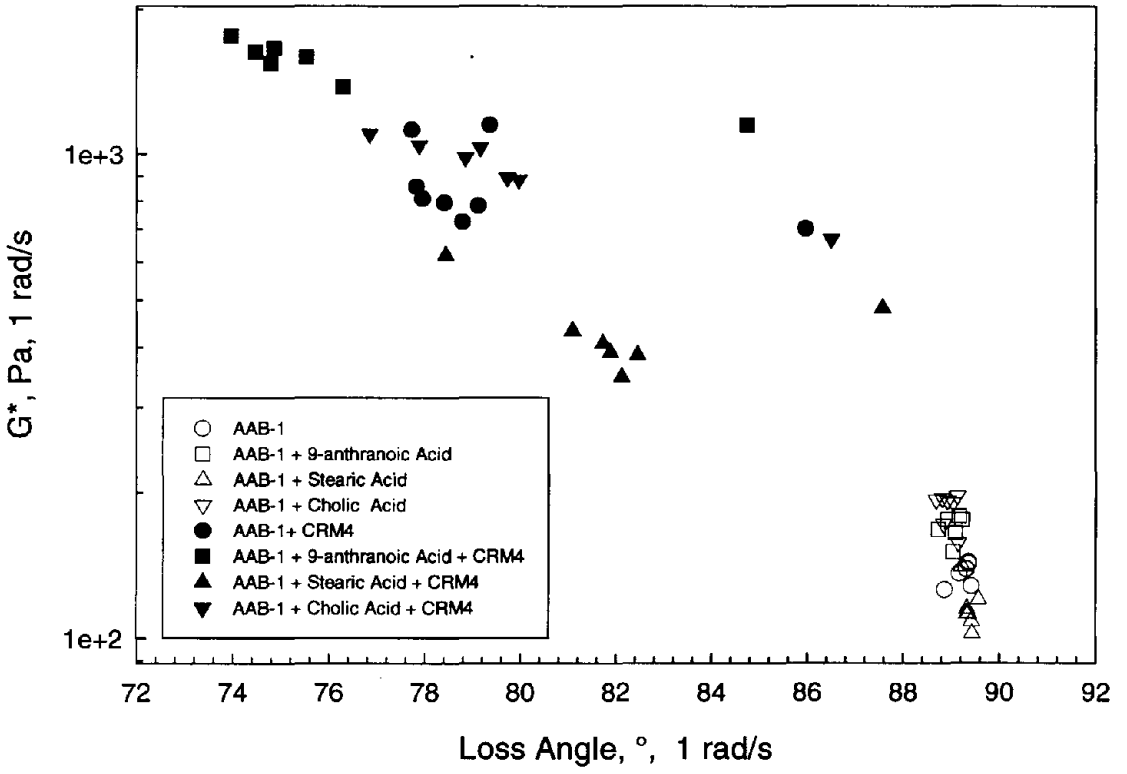

Figure 6-25. Asphalt AAB-1, carboxylic acid-modified AAB-1, and CRMA's stored at 156°C, data measured at 60°C.

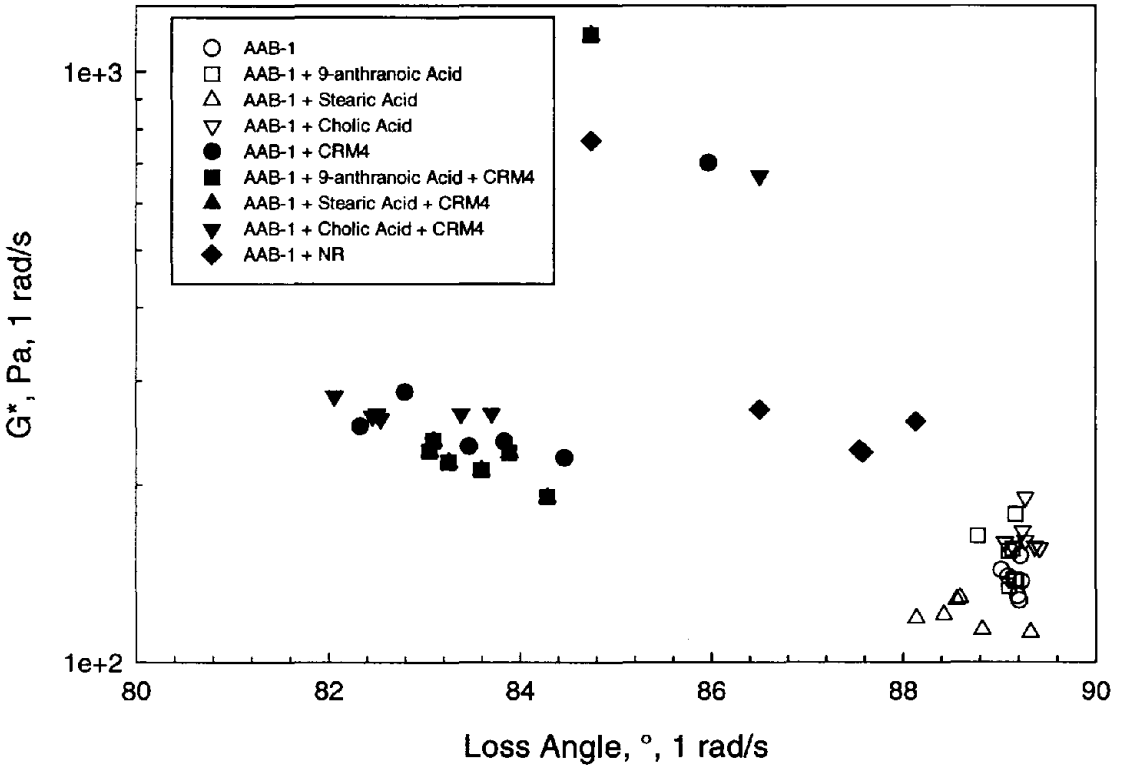

Figure 6-26. Asphalt AAB-1, carboxylic acid-modified AAB-1, and CRMA's stored at 200°C, data measured at 60°C.

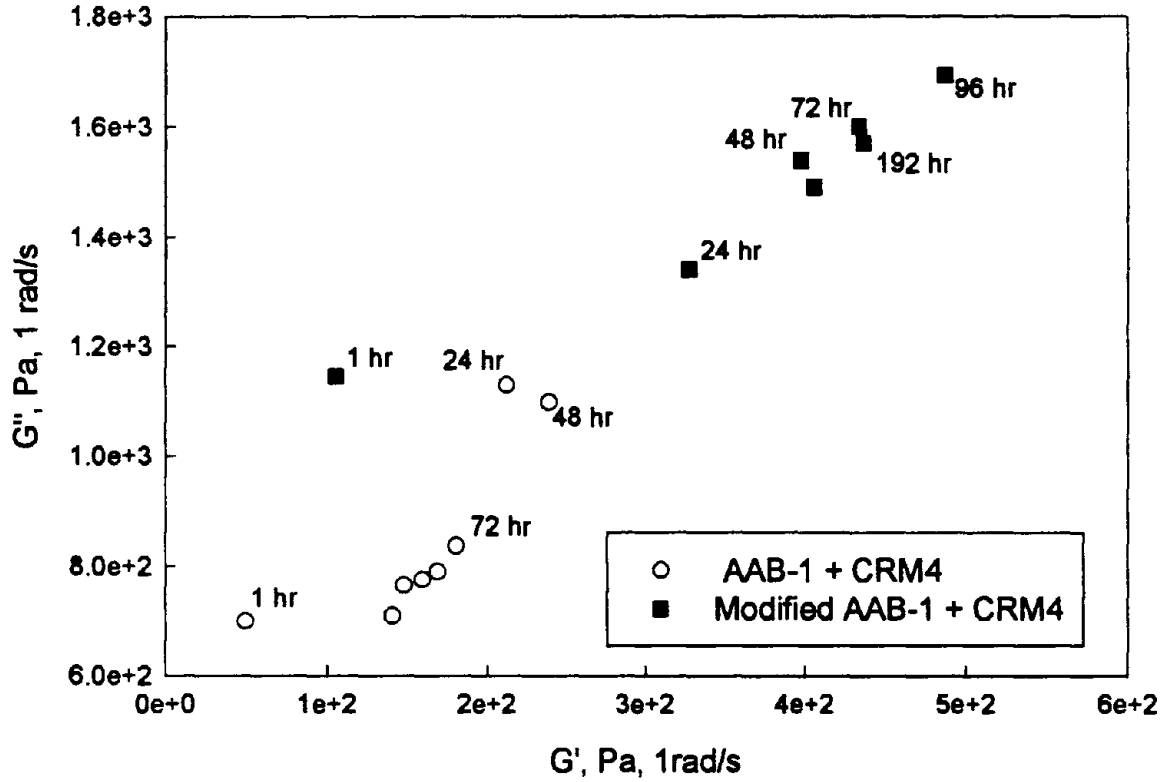

Figure 6-27. Asphalt AAB-1 with CRM4, and AAB-1 with CRM4 modified with 0.03 molar 9-anthranoic acid stored at 156°C, 60°C data.

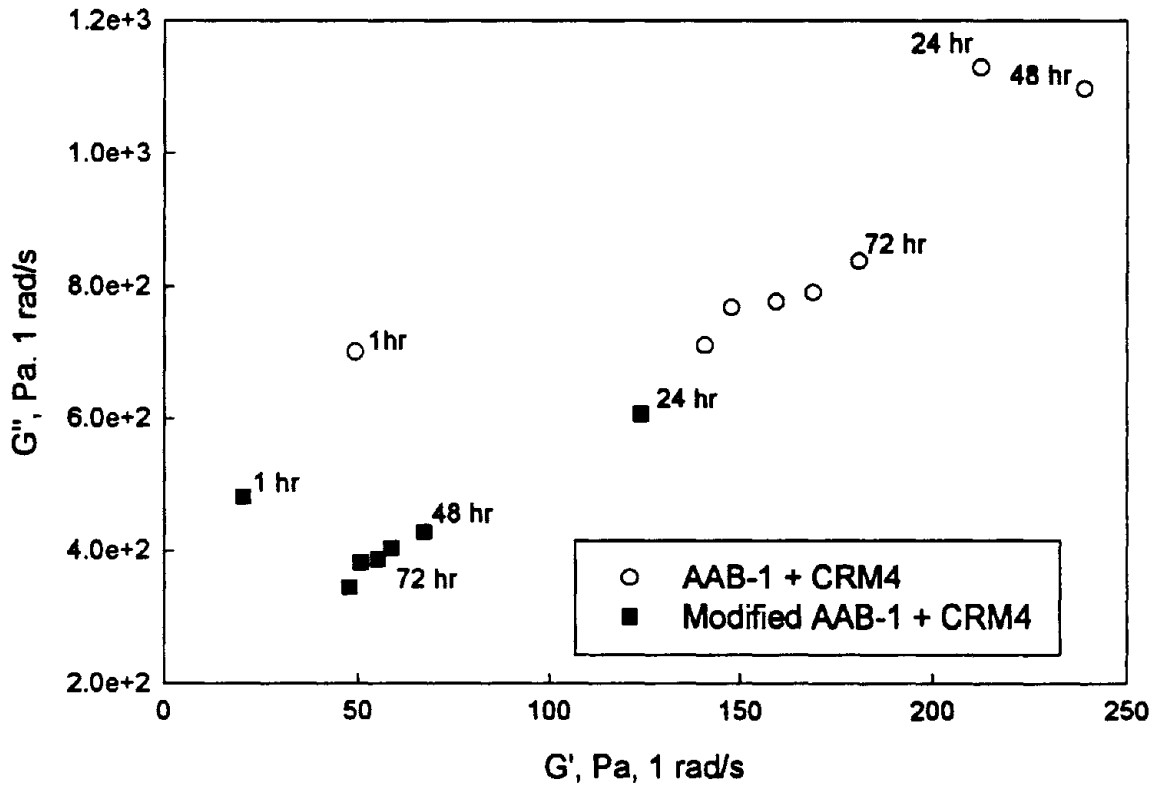

Figure 6-28. Asphalt AAB-1 with CRM4, and AAB-1 with CRM4 modified with 0.03 molar stearic acid stored at 156°C, 60°C data.

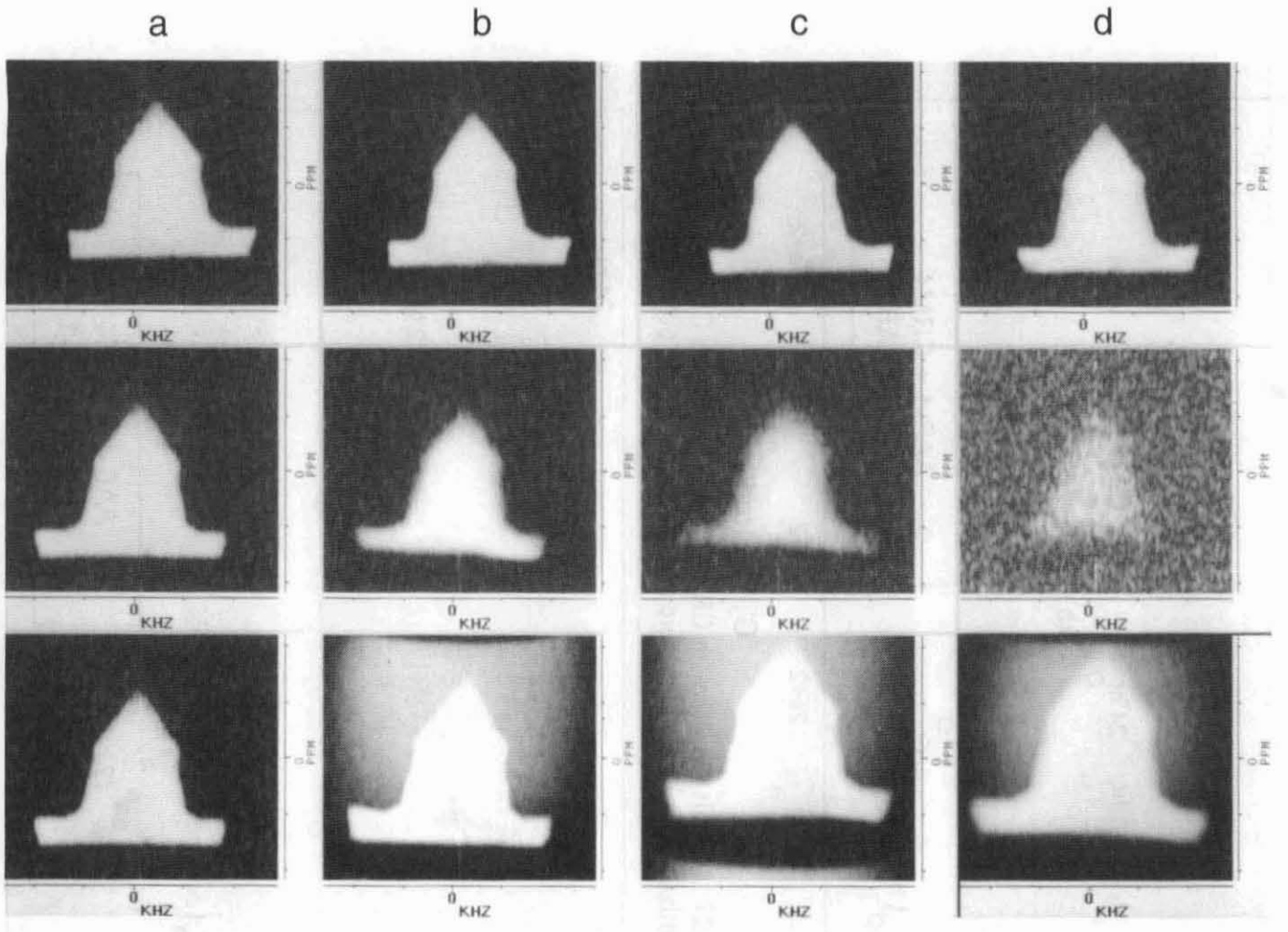

Figure 6-29. NMR images showing the cross-section of a conical piece of natural tire rubber taken after heating at 170°C for (a) 0, (b) 2, (c) 8, and (d) 24 hr. In the top set of four images, the natural rubber was heated in the absence of asphalt. In the middle set of four images, the natural rubber was heated in the presence of asphalt. Both sets of images were acquired when the sample was at room temperature. In the bottom set of four images, the natural rubber was heated in the presence of asphalt and imaged while the sample cooled to room temperature.

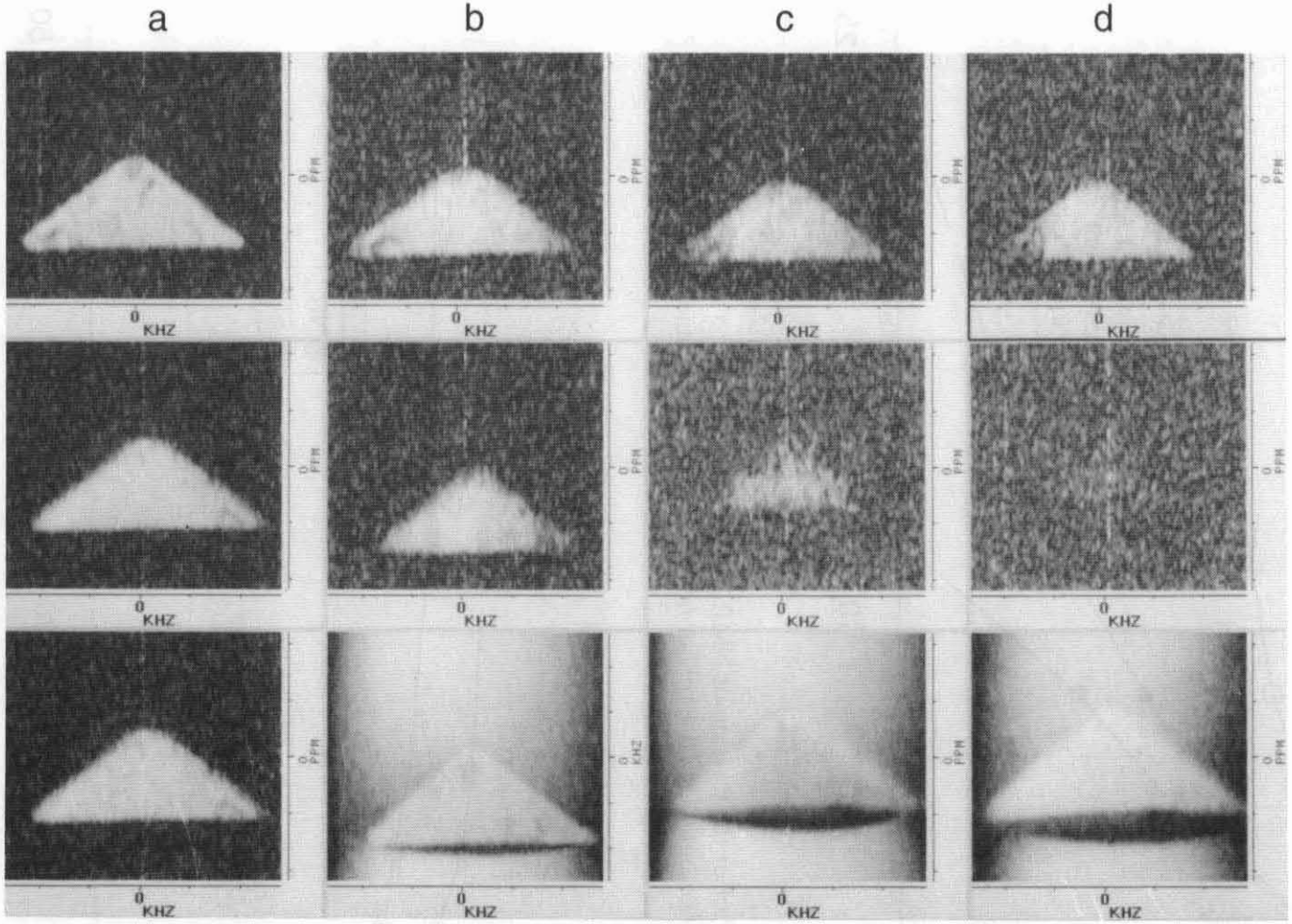

Figure 6-30. NMR images showing the cross-section of a triangular prism-shaped piece of styrene-butadiene tire rubber taken after heating at 170°C for (a) 0, (b) 2, (c) 8, and (d) 24 hr. In the top set of four images, the styrene-butadiene rubber was heated in the absence of asphalt. In the middle set of four images, the styrene-butadiene rubber was heated in the presence of asphalt. Both sets of images were acquired when the sample was at room temperature. In the bottom set of four images, the styrene-butadiene rubber was heated in the presence of asphalt and imaged while the sample cooled to room temperature.

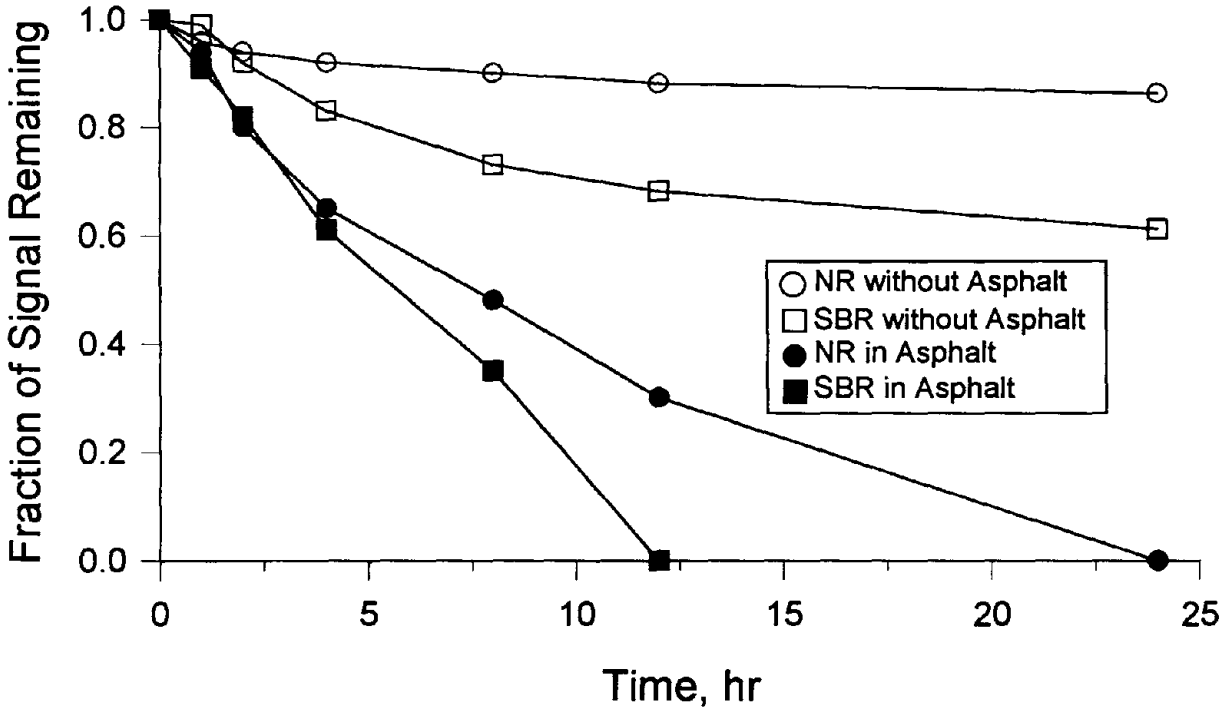

Figure 6-31. Plot of the fraction of NMR signal remaining versus time of heating for natural and styrene-butadiene tire rubber heated in the presence and absence of asphalt.

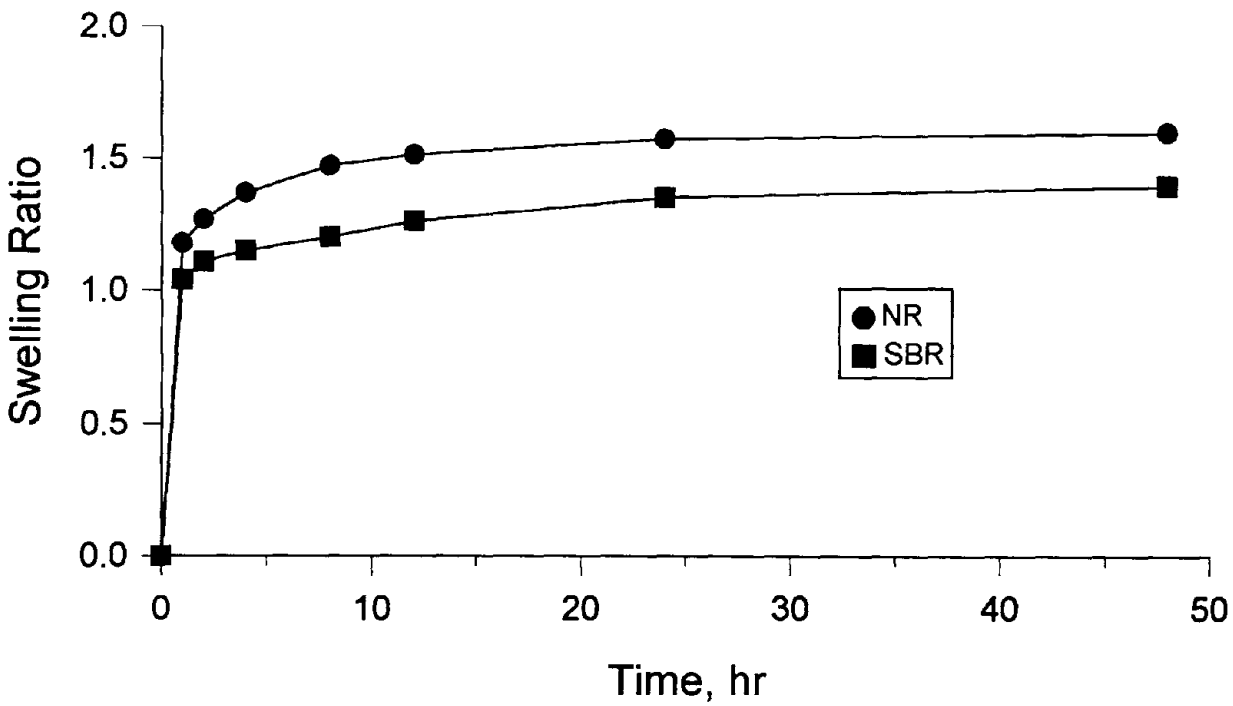

Figure 6-32. Plot of the swelling ratio versus time of heating for natural and styrene-butadiene tire rubber heated in the presence and absence of asphalt.

REFERENCES

AASHTO Provisional Standards, 1994, Standard Specification for Performance Graded Asphalt Binder, AASHTO Designation MP1, Edition 1A. AASHTO, Washington, D.C.

Aschenbrener, T., R. L. Terrel, and R. A. Zamora, 1994, Comparison of the Hamburg Wheel Tracking Device and the Environmental Conditioning System to Pavements of Known Stripping Performance. Colorado Department of Transportation, CDOT-DTD-R-94-1.

Asphalt Institute, 1995a, Superpave Level 1 Mix Design, SP-2. Asphalt Institute, Lexington, KY, p. 35.

Asphalt Institute, 1995b, Superpave Asphalt Binder Specification, SP-1. Asphalt Institute, Lexington, KY, p. 50.

Billiter, T. C., J. S. Chun, R. R. Davison, C. J. Glover, and J. Bullin, 1996, Investigation of the Curing Variables of Asphalt-Rubber Binder. *American Chemical Society Division of Fuel Chemistry Preprints*, 41(4): 1221-1226.

Blumler, P., and B. Blumich, 1991, Aging and Phase Separation of Elastomers Investigated by NMR Imaging. *Macromolecules*, 24: 2183-2188.

Chang, C., and R. A. Komoroski, 1989, NMR Imaging of Elastomeric Materials. *Macromolecules*, 22: 600-607.

Chang, S. J., J. R. Olsen, and P. C. Wang, 1989, NMR Imaging of Internal Features in Wood. *Forest Products Journal*, 39: 43-49.

Ellingson, W. A., J. L. Ackerman, L. Garrido, P. S. Wong, and S. Gronemeyer, 1988, Development of Nuclear Magnetic Resonance (NMR) Imaging Technology for Advanced Ceramics, ANL-87-53, Argonne National Laboratory, prepared for U. S. Department of Energy, November 1988.

Federal Highway Administration, 1992, FHWA-SA-92-022, State of the Practice - Design and Construction of Asphalt Paving Materials with Crumb Rubber Modifier, May 1992.

Findley, W. N., J. S. Lai, and K. Onaran, 1989, *Creep and Relaxation Of Nonlinear Materials With an Introduction to Linear Viscoelasticity*. Dover Publications, Inc., New York, NY, 371 p.

French, D. C., S. L. Dieckman, N. Gopalsami, and R. E. Botto, 1991, NMR Imaging a Chemical Microscope for Coal Analysis. *American Chemical Society Division of Fuel Chemistry Preprints*, 36(3): 1289-1294.

Grinstead, R. A., and J. L. Koenig, 1992, Study of Multicomponent Diffusion into Polycarbonate Rods Using NMR Imaging. *Macromolecules*, 25: 1229-1234.

Heitzman, M. A., 1984, Report of Investigation North/South Highway Grand Teton National Park (Teton County, Wyoming). Department of Transportation, Federal Highway Administration, Western Direct Federal Division, Geotechnical Report No. 22-84.

Hou, L., G. D. Cody, D. C. French, R. E. Botto, and P. G. Hatcher, 1995, Dynamic Detection of a Phase Transition for Illinois No. 6 Coal in Pyridine by Nuclear Magnetic Resonance Imaging (NMRI) and NMR Spectroscopy. *Energy and Fuels*, 9: 84-89.

Isacsson, U., and X. Lu, 1995, Testing and Appraisal of Polymer Modified Road Bitumens - State of the Art. *Materials and Structures*, 28: 139-159.

Koenig, J. L., 1991, Application of NMR Imaging to Polymers. In Mathias, L. J., ed., *Solid State NMR of Polymers*. Plenum Press, New York, p. 61-79.

Komoroski, R. A., 1993, Nonmedical Applications of NMR Imaging. *Analytical Chemistry*, 65: 1068A-1077A.

Lau, C. K., K. M. Lunsford, C. J. Glover, R. R. Davison, and J. A. Bullin, 1992, Reaction Rates and Hardening Susceptibilities as Determined from POV Aging of Asphalts. *Transportation Research Record* 1342, 50-57.

Lukens, L. A., and M. A. Plummer, 1988, Commercial Feasibility of Producing Shale Oil-Modified Asphalt. *Colorado School of Mines Quarterly*, 83(4): 108-114.

Lukens, L., and J. Fox, 1993, SOMAT - Technical Performance Characteristics, Annual Report. The New Paraho Corporation, Golden, CO.

Miknis, F. P., and D. A. Netzel, 1996, Use of Magnetic Resonance Imaging to Study Asphalt. *American Chemical Society Division of Fuel Chemistry Preprints*, 41(4): 1327-1331.

Miknis, F. P., and A. T. Pauli, 1997, Nuclear Magnetic Resonance Imaging Studies of Asphaltene Precipitation in Aged and Unaged Asphalts. *American Chemical Society Division of Fuel Chemistry Preprints*, 42(2): 374-380.

Netzel, D. A., F. P. Miknis, J. L. Soule, A. E. Taylor, and M. L. Serres, 1998, Solid-State ^{13}C NMR Studies of the Structure and Dynamics of Asphalts. In Youtcheff, J., ed., *Paving Asphalt Technology Handbook*, in preparation.

Plancher, H., and J. C. Petersen, 1982, Tertiary Nitrogen Heterocyclic Material to Reduce Moisture-Induced Damage in Asphalt-Aggregate Mixtures. U.S. Patent No. 4,325,738.

Roberts, F. L., P. S. Kandhal, E. R. Brown, D.-Y. Lee, and T. W. Kennedy, 1991, *Hot Mix Asphalt Materials, Mixture Design, and Construction.* NAPA Education Foundation, Lanham, MD, p. 109 and p. 416.

Rosen, S. L., 1993, *Fundamental Principals of Polymeric Materials*. John Wiley and Sons, Inc., New York, NY, 420 p.

Sarkar, S. N., and R. A. Komoroski, 1992, NMR Imaging of Morphology, Defects, and Composition of Tire Composites and Model Elastomer Blends. *Macromolecules*, 25: 1420-1426.

Sarkar, S. N., E. W. Wooten, and R. A. Komoroski, 1991, NMR Imaging of Water in Model Porous Materials. *Applied Spectroscopy*, 45: 619-625.

SHRP, 1993, *SHRP-A-368, Binder Characterization and Evaluation, Volume 2: Chemistry*. Strategic Highway Research Program, National Research Council, Washington, D. C.

SUPERPAVE Software, 1995, A Program for Determination of SHRP SUPERPAVE Asphalt Binder Grade from Weather Data, Version 2.0. PCS/Law Engineering, Beltsville, MD.

Tauer, J. E., and R. E. Robertson, 1996, Effects of Carboxylic Acids on the Rheological Properties of Crumb Rubber Modified Asphalt. *American Chemical Society Division of Fuel Chemistry Preprints*, 41(4): 1214-1220.

Terrel, R. L., and J. W. Shute, 1989, SHRP-A/IR-89-003, Summary Report on Water Sensitivity. Strategic Highway Research Program, National Research Council, Washington, D.C.

Thomas, K. P., and P. M. Harnsberger, 1995, Baseline Evaluation of the Properties of the SOMAT Test Strip in Grand Teton National Park. Draft of Topical Report delivered to FHWA.

Thomas, K. P., P. M. Harnsberger, R. E. Robertson, L. A. Lukens, and V. J. Peters, 1996, A Comparative Field Evaluation of Shale Oil-Modified Asphalt with Polymer-Modified Asphalts. *Transportation Research Record* 1545, 120-125.

Thomas, K. P., J. F. Rovani, and D. C. Lane, 1997, An Evaluation of the Impact of Shale Oil-Modified Asphalt (SOMAT) on the Environment. TRB, National Research Council, Washington, D.C., Preprint 970440.

Valkering, C. P., W. C. Wonk, and C. D. Whiteoak, 1992, Improved Asphalt Properties Using SBS Modified Bitumens. *Shell Bitumen Review*, 66: 9-11.

Webb, A. G., K. Motsegood, and R. B. Clarkson, 1993, NMR Imaging Studies of Coal Samples Using Solvent Permeation. *Fuel*, 72: 1235-1237.

Weisenberger, L. A., and J. L. Koenig, 1991, NMR Investigations of Case II Diffusion in Polymers. In Mathias, L. J., ed., *Solid State NMR of Polymers*. Plenum Press, New York, p. 377-386.

Western Research Institute, 1994, Environmental Monitoring and Testing Associated with the SOMAT Test Strip in Grand Teton National Park. Revised draft of Topical Report delivered to FHWA.

CHAPTER 7: PREDICTION OF FATIGUE IN PAVEMENT

UTILITY OF MICROMECHANICAL ANALYSIS TO ASPHALT CONCRETE PAVEMENT DESIGN

The phenomenon of a loss of strength in composite materials with repeated strain followed by a recovery of some part of the original strength with rest has been observed in numerous material combinations. Without rest, or with insufficient rest, the loss of strength exceeds the gain and eventually the composite fails by fatigue. Relaxation of the binder portion of a composite, starting with molecular motion of some sort, is the most obvious explanation. Molecular realignment of polars to form a stiffer binder (i.e., steric hardening), after molecular scrambling due to repeated strain, is one possible explanation. Flow of highly viscous binder to refill microcracks, formed during repeated strain, is another possible explanation. Probably both processes can occur and the portion contributed by each process is situation dependent.

AC in pavement has been observed to undergo loss and recovery of strength with heavy traffic and rest, much like other composites. It is reasonable to assume that the absolute amounts and rates of both loss and gain of strength depend upon the composition of the binder. Again, asphalts are binders having many different compositions, hence their behaviors relative to each other should be expected to differ. Certainly from a practical standpoint, AC roadways differ significantly in the amounts and rates at which fatigue damage appears, even when other variables appear quite similar.

The major objectives of this study were (1) to prove unequivocally that the phenomenon of loss and gain of strength, attributable to damage and healing, does occur in AC, (2) to develop a laboratory method to measure the phenomenon, (3) to develop a method to measure the phenomenon in roadways, and (4) to develop models to describe damage and healing. Particular attention was focused on elucidating the absolute amounts and rates of both damage and healing as a function of asphalt source. The next missions must be development of rapid analytical methodology and development of correlations between compositional features of asphalts and the observed major differences in amounts and rates of damage and healing.

The text that follows is a summary of four numbered items above. The complete work is described in four volumes by D. N. Little, R. L. Lytton, D. Williams, C. W. Chen, Y. R. Kim, H. J. Lee, and Y. Kim, *Microdamage Healing in Asphalt and Asphalt Concrete*, 1998; submitted to Western Research Institute as part of FHWA Contract DTFH61-92C-00170 for publication by FHWA.

The results of this research project have demonstrated several important matters that relate directly to asphaltic concrete pavement design and also show that microdamage and healing are directly related to the prediction of the appearance of the following distress types:

1. Fatigue damage (cracking) due to load and thermal stresses (and its delay due to healing).

2. Rutting.
3. Stripping and other forms of moisture damage.

Slowing these distress modes always improves:

1. Riding quality.
2. Safety (especially wet weather safety).
3. Life cycle costs (both agency and user).

Understanding these distress modes also relates directly to several important characteristics of mixture design and material selection for a given project. Specifically, the research results have direct application to:

1. Binder specification and selection.
2. Specification and selection of gradation, shape, and texture of aggregate particles for a mix.
3. Specification of types, amounts, and necessary dispersion of additives in providing a stiffer and tougher mix.
4. Specification of asphalt binder (or mastic) film thicknesses in mix design to reduce fracturing, promote healing, and retard rutting.

The material properties that are directly affected by findings in this research are:

1. Resilient modulus as it depends upon temperature and stress state.
2. Poisson's ratio as it also depends upon temperature and stress state.
3. The dependence of these properties on the rate of loading.
4. The susceptibility of these properties to deterioration due to repeated loads, moisture, and temperature.

The results of this research project also include a finite element program, which is set up to allow different amounts of microcracking and healing to occur in each element. The program used in this project is axisymmetric and is set up identically to the two-dimensional finite element program used in the SHRP A005 project to analyze the rate of change of dissipated energy and the reduction of stiffness of beam fatigue tests. The success of this approach in this project and in the SHRP A005 project shows that it can be used successfully to predict the growth of microcracks and healing in pavement structures acted upon by traffic and thermal stresses. The initial formation of microcracks at right angles to the major principal tensile stress or in the plane of the maximum shearing stress in an element of the finite element mesh dictates the behavior of that element from that point onward. The material in that element is orthotropic having its original elastic properties parallel to the cracks and reduced elastic properties at right angles to the plane of the cracks. The orientation of these crack planes changes from one element to the next based upon the original major tensile and shear stress orientations.

The following discussion is an overview of the way in which the findings of this research will (and should) affect the performance of AC pavements (distress, reliability, life

cycle costs, riding quality, and safety), the material properties of the AC under traffic, and the design of mixes to meet the performance standards that will be expected of new and rehabilitated pavements in the future.

First, consider microcracking and healing. Fatigue of asphalt pavements occurs in two sequential stages: crack initiation and crack propagation. Microcracking of these pavements and the healing of the microcracks during the rest periods between the larger load applications is what occurs during the crack initiation phase. Under repeated loading, and with insufficient healing to counteract it, microcracks will grow to a size at which crack propagation begins. This size has been estimated as 7.5 mm, or roughly the radius of the largest nominal size particle in the mix. The average beginning microcrack size is around 0.075 mm or around the size of the particles that pass the #200 sieve. They probably begin as small air bubbles in the mastic or at a flaw in the surface contact between the bitumen and the fine-grained particles.

Microcracks will always form and grow in any stress condition in which tension or shear stresses or both exist. This means that fatigue cracks can start anywhere: at the pavement surface, at the bottom of the asphalt layer, or in the middle of the layers where, in deep asphalt layers, the tensile stress is higher than at the bottom of the layer.

The microcracks can grow under the same stress conditions that cause the larger, visible cracks to propagate. These are commonly separated into three categories: mode I, tension; mode II, in-plane shear; and mode III, out-of-plane shear or the "tearing" mode. The stress conditions for all three models of microcrack growth and crack propagation are present on the pavement surface at the edge of the tire. Tension is imposed by the inward-directed tangential tire contact stresses. In-plane shear stress is imposed by the large, normal contact stresses beneath the tire wall. Out-of-plane shear stresses are imposed by the longitudinal tangential tire friction forces that drive the vehicle forward.

Within the pavement surface, tensile bending stresses are supplemented by shear stresses beneath the edge of the tire and these two together cause microcrack growth and crack propagation. Within a tire radius of the surface, the tensile stresses are replaced by compressive stresses and only shearing stresses are present to continue propagating the fatigue cracks upward.

In thermal fatigue, the entire process is tensile with microcracks forming at the surface initiating a visible crack, and then tensile stresses drive the crack downward. It is obvious that microcracks that have been initiated by load stresses can grow further by thermal stresses and vice versa.

One of the interesting things that has been revealed in this research is that the same material properties govern the growth of microcracks as control the propagation of the visible cracks and the same simple tests are needed to determine these properties. In fact, the simpler and more straightforward the test is; the better. In the case of microcrack growth and healing, a uniaxial tensile repeated load, strain-control test is best. Strain should be measured in the center of a test sample that is at least twice as tall as its diameter. There is no need (during testing) to

attempt to simulate the complicated stress patterns that are generated by tire contact stress patterns in real pavements. In any case, it is virtually impossible to do so. Instead, it is more efficient to concentrate on measuring the actual material properties that govern the growth and healing of the microcracks, and then use numerical computation methods to determine how these material properties affect the microcrack growth and crack propagation in pavements. For the first time in history, there are computer models available, and computers that have large enough memories and are fast enough to handle both microcrack growth and crack propagation in pavements. The material properties to use as input to these models can only be measured accurately in samples where a uniform stress and strain field is imposed upon the material. What is measured in such a test is a *pure material response,* which can be analyzed directly to determine the desired material property. This does not require the use of the same kind of computer program described above to analyze a sample with a non-uniform stress and strain distribution and infer material properties from the tests measurements by some form of inverse analysis.

Measuring material properties directly has several important advantages:

1. The tests are simpler.
2. The interpretation of test data is simpler.
3. It is easier to see which material properties are important and which are unimportant, and, of course, which are appropriate for use in specifications.

In the case of the growth and healing of microcracks, it has become apparent that both processes — *growth* and *healing* — are the result of the interplay of two material properties, namely, creep compliance and surface energy. In microcrack growth, a low tensile (and shear) compliance reduces the crack growth rate while a low-fracture surface energy accelerates the growth rate. In microcrack healing, a low compression (and shear) compliance reduces healing while a low healing surface energy accelerates the healing process. Furthermore, if the compressive compliance of the material changes during a rest period due to a softening of the structure of the asphalt (or mastic), then healing can be accelerated. Higher temperatures retard fracture and accelerate healing. Both tensile and compressive compliances are easy to measure and so are the cohesive surface energies of asphalts with and without additives. The compliances and surface energies are measured in separate tests.

The adhesive surface energies between aggregate and asphalt surfaces are somewhat more complicated, requiring vapor adsorption on to the aggregate surfaces. However, once they are measured, they never need to be measured again. The surface energies of aggregates change slightly with the size of the particles, becoming larger as the particle size decreases. These surface energies are always strongly affected by particle crushing.

According to modern theories of surface energies, both asphalt and aggregate surfaces are composed of "polar" and "non-polar" components. The polar components are further divided into "acidic" and "basic" components. All aggregates vary somewhat from one another in the magnitude of their polar and non-polar surface energy components. The largest difference is found between the basic components of aggregate surface energies. This large difference

between aggregate types is a major part of the explanation of how different mixtures retard fracture and promote healing.

These same modern theories of surface energies provide a means of calculating the work that is required to separate surfaces (cohesively or adhesively), and how the presence of water on the separating surfaces *increases* or *decreases* the work that is required. Some general observations on these works of separation are the following:

1. In the presence of water, some asphalts require more work and others require less work for *cohesive* fracture as compared to the condition where no water is present.

2. In the presence of water on a fracturing interface, adhesive fracture requires a reduced amount of work, i.e., the water assists in creating the fracture. The reduced level of work varies by large amounts from one aggregate-asphalt combination to another with no water present. The adhesive fracture of all aggregates from all asphalts requires positive work.

The second finding dramatically demonstrates the importance of the findings of this research for the understanding of *stripping* and points toward simple and straightforward tests and specifications for asphalt and aggregate combinations in mixtures to inhibit stripping. Absolute solubility of aggregate, of course, must be considered although this subject has been addressed numerous times previously.

Healing of fractured surfaces shows similar effects as follows: (1) The work of healing of cohesive fractures is sometimes positive and sometimes negative in the presence of water, whereas it is always positive where no water is present. (2) The work of healing adhesive fractures is always negative in the presence of water whereas it is always positive when no water is present.

Thus, water always assists in the process of *adhesive fracture* and always opposes *adhesive healing*. Its effects on cohesive fracture and healing vary greatly from one asphalt binder to another. At the present time there is no binder purchase specification that differentiates this behavior among binders.

The discussion presented in this overview shows that the fracture and healing testing and the analysis methods developed in this project are applicable to the determination of the materials' properties and to the prediction of crack initiation, material softening due to microcracking, and microcrack growth. Furthermore, moisture damage, in pavements acted upon by repeated traffic and weather stressing, affects fatigue life and can be treated as an extension of the growth of microcracks. Thus, the finite element model used in the analysis of test data is appropriate to use in predicting the fatigue performance of asphalt pavements.

There is an important property of granular materials, both bound and unbound, that affects both fatigue and rutting behavior. The property is its elastic volume change under load

and is due to the tendency of the larger aggregates to roll past one another when they are loaded. They then snap back to their original portion when they are unloaded. Under low confining pressures or high shearing stresses, the volume increases under load and this results in a measured Poisson's Ratio greater than 0.5. In some cases, Poisson's Ratio has been found to be upwards of 0.6 to 1.0 for unbound aggregates. In any case, the Poisson's Ratio has been found to be dependent upon the stress state of the material. In AC, the asphalt binder exercises internal restraint (like a confining pressure) upon the aggregates and only occasionally allows the Poisson's Ratio to rise above 0.5. When it does, it is usually at higher temperatures when the asphalt binder has a very low stiffness and exercises little restraint upon the aggregates.

In an asphalt pavement, at higher temperatures, most of the rutting occurs with a mixture that has the property of expanding under pressure with low confinement, (Poisson's Ratio greater than 0.5). The mixture directly beneath a tire load will build up its own lateral confining pressure, become much stiffer, and resist rutting very effectively. This Poisson's Ratio effect under low confining pressures depends upon the aggregate gradation, shape, and texture. This suggests a specification test of asphalt mixtures. At high in-service temperatures, make certain that the Poisson's Ratio under zero confining pressure is between 0.5 and 0.8. A proper combination of gradation shape, texture, and binder additives will ensure a Poisson's Ratio in that range. A value of greater than 0.8 will generate a lateral confining pressure sufficient to produce lateral shoving.

The ability of a mixture to expand under pressure with low confinement (or high shear stress) has a direct effect upon the formation and growth of microcracks. The higher the Poisson's Ratio, the more tensile stress is developed in the asphalt films that stretch between aggregate particles and the faster the microcracks will grow under repeated load.

This Poisson's Ratio property, termed "resilient dilatancy," is important in resisting rutting but is also instrumental in forming and growing microcracks. Thus, a proper mix design should take resilient dilatancy into account in selecting the aggregate gradation, shape, and texture and in selecting asphalt binder for its resistance to both cohesive and adhesive microfracture. Prediction of both rutting and fatigue in pavements must make use of how this "resilient dilatancy" varies with stress state and temperature.

Having shown how the products of this research impact the rate of appearance of fatigue (load and thermal), rutting, and stripping, it is now apparent how it also affects riding quality (related to the variance of rutting and rut depth), safety (related to the amount of water that can be trapped in a rut), reliability (related to the variance and, therefore, the quality assurance and control exercised on the as-constructed mix properties), and *life cycle costs* (also related to the as-constructed variances of the fatigue and rutting properties).

It is also apparent that the balance between compliance and surface energies, which must be maintained in a mix to resist fracture and promote healing, suggests that ranges of each should be specified and used as a basis for selection of asphalt-aggregate combinations for mixes for a particular project. The criteria include:

1. Tensile and shear compliance of the mix - dewetting (fracture) surface energies to resist fracture.
2. Compressive compliance of the mix - wetting (healing) surface energies to promote healing.

The compliances and surface energies should be measured at the lower temperatures, below 25°C (77°C), where fracture occurs and healing is needed. The faster healing mixes should be selected for the projects with higher traffic volumes. Mixes that heal more slowly but have the potential for enhanced healing with longer rest periods should be selected for projects with lower traffic volumes.

The effects of aggregate gradation, shape, and texture on the "resilient dilatancy" of a mix and its effects upon rutting and fatigue were discussed above. The test for the Poisson's Ratio under low confining pressure provides a simple but straight forward test of the aggregate characteristics as they contribute to the performance of the mix. This property, as it changes with stress state and temperature, is necessary to predict the performance of the pavements.

Additives to the binder or fines in the mastic may act as crack stoppers by providing reinforcement at the tips of microcracks. Acting in this way, they can produce a stiffer, stronger, and tougher mix. They can do this only if they are small enough (about the size of the average beginning microcrack size), well dispersed in the binder or mastic, and able to bond well adhesively to the asphalt, even when water is present.

Adhesive fracture is accelerated and adhesive healing is resisted when water is on the interface between aggregate (or fine) particles and asphalt. The importance of keeping water away from these interfaces, given the importance of additives or fines in improving mixture properties, cannot be over emphasized. Greater binder film thicknesses on these particles require water to diffuse farther to reach the interface, and this provides greater resistance to stripping. The effect of aggregate surface treatments (such as lime) or changing the adhesive surface energies to make them more resistant to stripping can be understood more readily and can point to specifications of aggregate surface energies (especially polar, basic) that provide acceptable resistance to stripping. Ranges of these aggregate surface energies must be combined with asphalt binder or mastic film thickness to produce specifications that are consistent with the findings of this research project.

Two damage models are offered in this study. One is the previously discussed microdamage model, which allows one to predict fatigue damage (including the effects advocated with healing) based on fundamental material properties. A two-dimensional finite element model is used to access crack growth and healing under realistic pavement stresses and *not* under unrealistic laboratory-induced stress states. A second model is a viscoelastic continuous damage model which, although more phenomenologized in nature, accounts for the effects of loadings and rest periods (healing) on the rate and level of damage of asphalt mixes.

The second model successfully predicts the damage growth in AC under monotonic (or non-cyclic) loading of varying strain rates. Furthermore, the model successfully accounts for

damage growth and recovery due to complex loading histories. The model can successfully account for both controlled-stress and controlled-strain modes of loading, and for randomly applied multi-level loading with different loading rates and varying durations of rest periods among loading cycles. Based on this constitutive model, a fatigue test protocol is presented, which is suitable for standard, specification-type testing. The test protocol employs a set of uniaxial tensile tests for viscoelastic characterization as well as the characterization of internal state functions representing the fatigue damage growth and microdamage healing in AC mixtures. Details of the constitutive model relating cyclic tensile loading to failure are given in the next section of this chapter. Therefore, two quite different approaches are offered to assess fatigue fracture: the micromechanics approach and the constitutive viscoelastic damage model. What is of particular significance is that both approaches require consideration of the effect of healing during rest periods to successfully predict pavement fatigue life.

If microdamage healing is an important consideration in design and analysis of asphalt pavements, it must be evident in actual pavements. A stress wave test was used in this study to determine whether or not microdamage healing can be detected in actual pavements. The analysis demonstrated that the stress wave test can effectively detect changes in structural responses in the asphalt pavement, namely, changes in stiffness. The study verified the recovery of stiffness following rest periods at the MnROAD project and at the FHWA Accelerated Loading Facility (ALF) at the Turner-Fairbank Highway Research Center in McLean, Virginia. It is significant to note that the study demonstrated a major reduction in the elastic modulus of the pavements evaluated during early stages of fatigue when no visible cracks were evident at the surface. The stiffness reduction was concluded to be related to microcrack initiation, propagation, and densification. Additional reduction of the elastic modulus near failure seemed to coincide with rapid propagation of surface cracks.

The most important finding using the stress wave concept is that healing does occur in pavements in the field during rest periods, which suggests that the performance and service life of the pavement will be increased if rest periods are introduced. A second important finding is that the stress wave analysis at the ALF facility demonstrated that fatigue damage under the tire edge due to shear stresses appears to be very significant. To accurately predict the fatigue performance of AC pavements, the fatigue damage growth under the tire wall due to shear stresses must be evaluated in addition to tensile cracks at the bottom of the AC pavement layer.

DEVELOPMENT OF A MECHANISTIC FATIGUE PREDICTION MODEL FOR AGING ASPHALT-AGGREGATE MIXTURES

The significance of aging in asphalt binders on fatigue performance of asphalt-aggregate mixtures has been well recognized and studied in the recent SHRP. The most realistic method of investigating the effect of aging is to subject asphalt-aggregate mixtures to aging conditions and measure physical properties of the aged mixtures. However, little work has been conducted on how to include the changes in mixture properties due to aging in the framework of constitutive modeling or fatigue performance modeling.

Recently, a uniaxial constitutive model of non-aging asphalt-aggregate mixtures has been developed as a result of the study under Task K entitled "Healing of Microcracks in Asphalt and Asphalt Concrete" in FHWA Contract No. DTFH61-92-C-00170. It employs the elastic-viscoelastic correspondence principle and damage parameter based on Schapery's work potential theory to model the stress-strain behavior of asphalt-aggregate mixtures under cyclic loading. This model is able to predict hysteretic stress-strain behavior of AC under different loading histories (monotonic vs. cyclic), varying rates of loading, different modes-of-loading (controlled-stress vs. controlled-strain), various stress/strain amplitudes, and the beneficial effects of healing during random rest periods.

It is analytically possible to include the effect of aging in the formulation of the current constitutive model using another time variable accounting for aging time. The major advantage of this approach is that the interaction between fatigue loading and aging can be realistically modeled, allowing more accurate evaluation of the effects of aging binders on mixture properties and fatigue performance of the mixtures. Accounting for the effect of aging on the fatigue damage growth and healing of asphalt-aggregate mixtures using fundamental damage mechanics principles is probably the best approach to realistically simulate the interaction between damage and aging that occur simultaneously in actual pavements.

The objectives for this research include:

1. Determine the viscoelastic properties of aged AC mixtures.

2. Develop a method to account for the effect of aging on viscoelastic material properties.

3. Establish an analytical framework for using the elastic-viscoelastic correspondence principle with the aging viscoelastic properties.

4. Verify the correspondence principle for the aged mixtures.

Watsonville granite aggregate and SHRP designated AAD-1 asphalt binder were used in this study. The rolling wheel compaction method was used to fabricate slabs from which six 10 cm (3.9 in) diameter by 20 cm (7.9 in) height cylindrical specimens were obtained.

Based on findings from the SHRP mixture aging study, four different levels of aging were simulated using the following approach:

1. Short term aging (STA): The loose, uncompacted mixture is conditioned at 135°C (275°F) for 4 hours and then compacted to a slab. This method is currently recommended.

2. Long term aging (LTA) Level 1: STA plus the specimens are conditioned at 85°C (185°F) for 2 days before testing.

3. Long term aging Level 2: STA plus the specimens are conditioned at 85°C (185°F) for 4 days before testing.

4. Long term aging Level 3: STA plus the specimens are conditioned at 85°C (185°F) for 8 days before testing.

A series of uniaxial tensile creep and recovery tests and complex modulus tests were performed on the specimens aged to the four different levels to determine how creep compliance, relaxation modulus, dynamic modulus, and phase angle change with aging. The creep and complex modulus tests were performed at five different temperatures, with the corresponding load levels low enough not to induce damage (material response remains in the linear viscoelastic range). Complex modulus testing was performed at five frequencies (2.5, 5, 10, 20, and 33 Hz).

In this research, creep compliance testing was performed and the relaxation modulus was predicted from it through the theory of linear viscoelasticity. The time-temperature superposition principle was used to horizontally shift creep curves at individual temperatures to the 25°C (77°F) reference temperature, developing the master creep curves. The shift factors remain constant regardless of aging level. Prony series representation was used to define creep compliance and relaxation modulus.

The slopes of both creep compliance and relaxation modulus decrease as the extent of aging increases. The long-time asymptotes occur at later times as well. The creep compliance values at short and long times decrease slightly with aging level and, correspondingly, the relaxation modulus values increase slightly.

Dynamic modulus and phase angle measurements show trends consistent with increased stiffness due to aging. Dynamic modulus values increase and phase angles decrease with continued aging.

One of the major parameters to be evaluated in the constitutive modeling is pseudo strain. The pseudo strain of an aging material in a uniaxial case (ε^R) is represented by the following hereditary integral (the term convolution integral is used only for a non-aging system)

$$\varepsilon^R = \frac{1}{E_R}\int_0^t E(t,\xi)\frac{d\varepsilon}{d\xi}d\xi \qquad (7\text{-}1)$$

where E_R = the reference modulus which is an arbitrary constant,
$E(t, \xi)$ = relaxation modulus, and
ε = uniaxial strain.

There are two time variables used in this integral, t and ξ. The variable t is the time elapsed since the specimen was fabricated and the time of interest for the analysis. The variable

ξ represents the loading time, and for computational purposes, it is simply a variable of integration.

Pseudo strains determined using (7-1) account for the viscoelasticity of the aging material and, therefore, simplify the modeling of damage evolution under cyclic loading. The relaxation modulus E(t, ξ) as a function of aging and loading times is determined by defining modified power law (MPL) coefficients with respect to aging time.

$$E(t,\xi) = E_0(t) + \frac{E_0(t) - E_\infty(t)}{(1 + \frac{\xi}{\tau_0(t)})^{n(t)}} \qquad (7\text{-}2)$$

A power relationship with aging time exists for E_0, E_∞, and n. The coefficient τ_0, the time constant, does not appear to follow any particular trend with respect to aging time, instead remaining fairly constant.

The relaxation modulus at different aging levels was predicted using (7-2) and an averaged value of τ_0. In general, there is a very good correlation between the measured and predicted values for the whole time range. The prediction is not as good at longer times, partially due to the logarithmic scale, but mostly as a result of the difficulties the MPL has in fitting that portion of the relaxation curve.

Cyclic tests in the linear viscoelastic range (i.e., no significant damage evolution) were performed to verify the applicability of pseudo strains, calculated from the aging relaxation modulus function, to eliminating time-dependence of the material for modeling purposes. The use of pseudo strains successfully eliminated the hereditary behavior of cyclic loading and was able to account for creep and relaxation effects during loading and rest periods for all four levels of aging.

CHAPTER 8: PREDICTION OF PERFORMANCE

SYNOPSIS

In this chapter, there is a discussion of four failure modes together with new test methods to predict the onset of each type of failure. The modes are low temperature (thermal) cracking, permanent deformation (rutting), moisture damage, and fatigue. The current model of asphalt structure and past experience are used in various degrees to explain each phenomenon. Following this is a description of one or more new or newly improved methods that should contribute to an improved classification of asphalts with respect to the expected performance in roadways. The emphasis is placed on physical properties of asphalt in a service environment. These are properties that cannot be measured in bulk asphalts because of composition-driven variability that appears as an asphalt is placed into a service environment.

INTRODUCTION

A conceptual, chemistry-based model of asphalt behavior has continued to evolve during this project and has become more detailed as research has progressed. There is an improved understanding of the effects of molecular size, polarity, molecular motions, and intermolecular associations on asphalt physical properties as well as an improved understanding of roadway service environmental effects on asphalt behavior. The latter includes the long term effects of water and oxygen and the effects of aggregate on thin films of asphalt. Some of the understanding is still qualitative, but an increasing portion is described by mathematical relationships that allow some prediction and extrapolation of asphalt behavior. As always, extrapolation is risky, but it can be a useful tool for examining the weaknesses and strengths of a given model and for planning future work. The goal of all this work, of course, is to understand how asphalt chemical composition and reactivity determine asphalt pavement failure or success and, further, to develop rapid methods that are applicable to tank asphalts to predict performance. By developing a model of asphalt performance based on chemical composition, the economic risk and uncertainty for the refiner are reduced. The refiner is increasingly having to rely on a variety of petroleum sources, and is asked to ensure more uniform, reliable, and better quality materials for the highway engineer who faces a constant demand for less performance variability in roads. In this chapter four modes of pavement failure are examined in light of the current understanding of asphalt behavior. These modes are thermal and fatigue cracking, moisture damage, and permanent deformation. At the end of each failure mode section, there are recommended procedures to be applied to asphalt to improve the prediction of its performance in roadways.

THERMAL CRACKING

Low-temperature cracking typically occurs during extreme low-temperature weather, usually within the first year or two after pavement construction. This failure mode can be

recognized by transverse cracks in the pavement caused by the inability of the asphalt binder to deform and reduce stress. As the temperature of an asphalt binder decreases, its specific volume decreases. At the glass transition temperature (T_g), large scale molecular motion is hindered by a "freezing in" of the system. This transforms the asphalt binder from a viscoelastic material to a brittle, amorphous solid. Since some reduction in specific volume occurs even below the glass transition temperature, internal stresses increase with decreasing temperature. In a roadbed, lateral stresses are usually relieved by shrinkage; however, longitudinally, the road length is effectively infinite, limiting shrinkage and stress relief. If the longitudinal stresses exceed the asphalt binder's strength, the transverse cracks typical of low temperature cracking appear. The problem is exacerbated by rapid cooling, which does not allow sufficient time for stress relaxation through molecular movement.

The current Superpave® low temperature grade for asphalts is based on the creep stiffness and creep rate of an oxidatively aged sample. The grade is specified as 10°C (18°F) lower than the temperature at which the creep stiffness, S, equals 300 MPa or the m-value (-log(S)/log(t)) equals 0.3, whichever temperature is greater. Meeting this low temperature specification is believed to provide reasonable assurance that low temperature cracking will be minimal as long as actual pavement temperatures stay within the historical range. Note that a specification measurement on an aged binder predicts performance for a low level of aging in the asphalt-aggregate mix (low temperature cracking usually occurs early in a pavement's lifetime). The utility of this approach suggests that oxidative aging at specification levels and aggregate content have limited influence on the low temperature pavement performance limit. This idea is supported by recent low temperature tests on neat and aged asphalts using bending beam rheometry, described in chapter 4, and DSC, described in chapter 3. Additional evidence is shown in chapter 3 by a strong correlation between the glass transition temperatures, determined by DSC, of neat asphalts and low temperature specifications of aged asphalts. The discussion in chapter 3 also details the control of solvent-like non-polar and weakly polar materials on the glass transition temperature of asphalts. The flexibility and mobility of aliphatic chains and the intermolecular interactions of weakly polar species combine to determine low temperature properties.

The importance of molecular flexibility on asphalt low temperature behavior is shown in the results of solid-state NMR studies on neat asphalts. NMR can not only measure the relative amounts of aromatic and aliphatic carbons, but it is also sufficiently sensitive to molecular segmental motions to determine the relative amounts of aliphatic carbons in flexible and rigid environments. Since asphalts contain ~ 70 percent aliphatic carbons [Jennings 1993], it might be assumed that the rheological properties of "tank" asphalts are dominated by the motions of these carbons. In polymer rheology, it is well known that rheological properties depend on the segmental and rotational motions of the aliphatic carbons [Mark et al. 1993]. Thus, a correlation should exist between the flexible aliphatic carbons in an asphalt and some of its rheological properties, although certainly the aromatic carbon and heteroatom content also influence rheological properties by restricting molecular motion.

The solid-state NMR dipolar dephasing technique was used to determine the type and fractional amount of motions (flexible) or lack thereof (rigid) of the aliphatic carbons in the

eight SHRP core asphalts. To correlate the flexible aliphatic carbon content for the different asphalts with their rheological properties, the mass percent of flexible aliphatic carbons in a whole asphalt must be known. This value is calculated from the product of the mass percent carbon (from elemental analysis), the fraction of all carbons that are aliphatic (from liquid-state NMR), and the fraction of aliphatic carbons that are flexible (from solid-state NMR). Table 8-1 lists the mass percent of carbon, the fraction of all carbons that are aliphatic, the fraction of aliphatic carbons that are flexible, and the mass percent of flexible aliphatic carbons for each of the SHRP core asphalts at 23°C (73.4°F). A temperature of 23°C (73.4°F) was chosen as a convenient temperature to make the above measurements. At very low temperatures, molecular motion is significantly slowed, and at higher temperatures all asphalts have similar and extensive molecular motions of the different carbon types.

Jung and Vinson [1993] reported a thermal stress restrained specimen test to evaluate the thermal cracking resistance of asphalt concrete mixtures. These authors determined the fracture temperature of 14 SHRP asphalts and found that their ranking of the asphalts compared favorably with a ranking based on the limiting stiffness temperature and the ultimate strain at failure of the asphalt. A plot of the fracture temperature determined by Jung and Vinson as a function of the of the flexible aliphatic carbon content is shown in figure 8-1. A fair correlation ($R^2 = 0.87$) exists for six of the asphalts, with AAF-1 and AAK-1 being outliers. The correlation shows that as the flexible carbon content in an asphalt increases, the fracture temperature decreases. Asphalt AAK-1 contains a high concentration of vanadium, which, being paramagnetic, interferes with NMR measurements. Asphalt AAF-1 is produced, in part, by solvent deasphaltening and has already been shown to behave anomalously in some thermal tests (see for example figures 3-30 and 3-40).

A similar correlation is possible with actual specification temperatures. Anderson et al. [1996] reported the results of low temperature specification measurements for SHRP core and extended-set asphalts. The limiting low temperature (T at S=300MPa or m=0.3, whichever is greater) from this data set is plotted as a function of the flexible aliphatic carbon content in figure 8-2. Again, there is a good correlation ($R^2 = 0.99$) with flexible aliphatic carbon content for six of the asphalts with the same two outliers. As expected, increasing flexible carbon content decreases the low temperature limit.

Clearly, increasing flexible aliphatic carbon content improves asphalt low temperature properties. Of course, improvement of low temperature behavior is only useful if high temperature properties are not adversely affected. An obvious method of increasing flexible carbon content is to change the distillation cut point to retain lower molecular weight species in the asphalt. This method is already used extensively to vary asphalt grades, but its success is strongly dependent on the petroleum composition and it does not consistently address both low and high temperature needs. Another idea is to increase flexible carbon content without lowering the average molecular weight. Increasing the degree of branching in aliphatic chains increases flexible carbon content, but does not necessarily affect molecular weight. It is possibly relevant that the asphalt with the highest flexible aliphatic carbon content is, disregarding AAK-1, AAA-1, an asphalt that comes from a petroleum source known to have undergone biodegradation, which increases the proportion of aliphatic branching. Asphalt

AAA-1 also has the lowest glass transition temperature (by DSC) of the eight SHRP core asphalts and the second lowest crystallizable fraction (after AAG-1). Aliphatic branching hinders crystallization.

Another analytical method that is providing insight into low temperature asphalt behavior is DSC in both conventional and modulated forms (DSC and MDSC). Chapter 3 contains a detailed description of the work that relates the molecular sizes and polarities of asphalt components to their glass transitions. The glass transition temperatures of all non-polar IEC neutrals are found to depend on their number average molecular weights. As polarity increases, glass transition temperatures increase. This is demonstrated with heptane maltenes, iso-octane maltenes, SEC Fraction-II fractions, and IEC weak neutrals (figure 3-41). Strongly polar, associating species are found to increase the glass transition temperature by an amount directly proportional to their mass fraction (or volume fraction) (figure 3-34). To a first approximation, all asphalts examined have the same proportionality constant for the effect of adding strongly polar, associating species. As a result of these investigations and the good correlation between glass transition temperatures and low temperature specification (figure 3-28), it was shown quantitatively that certain ion exchange-defined molecular types interact to influence low temperature asphalt properties. Weak acids plus weak amphoteric species have the largest effect, increasing the low temperature specification limit by over 3°C (5.4°F)/mass percent. Weak bases have an effect of about 1°C (1.8°F)/mass percent and strong acids and bases increase temperatures by less than 1°C (1.8°F)/mass percent. At the present time this predictive method requires the use of the MDSC instrument, which can acquire data in about 4 hours. The weak acids and amphoterics are determined by the fast IEC method, described in Volume II, method 5 that requires a few hours but has a complicated and tedious resin preparation step. The next step in this development will be to attempt to replace fast IEC values with NAPT values. NAPT values are acquired in 30-40 minutes per sample with a user friendly device (see Volume II, method 7). If this combination of two fast, user-friendly methods continues to prove to be successful at predicting low temperature specification values, it would be much faster than the current Superpave® method in that both operations (analyses) are conducted with tank asphalts.

MOISTURE DAMAGE

Although often overlooked or misdiagnosed, loss of tensile strength in pavement mixtures can be a primary contributor to pavement rutting and fatigue cracking. Research on the effects of water on asphalt performance and asphalt-aggregate interactions reported in chapter 5 shows that water does have an impact on performance and that this impact is both asphalt and aggregate dependent. It is accepted here as common knowledge that variations in aggregate cause variability in moisture sensitivity in AC. In this project, it has been shown that variation of asphalt source also contributes to variable moisture sensitivity. In asphalt-aggregate systems it appears that susceptibility to water stripping depends, at least in part, on the water solubility of the organic salts formed from the reaction of carboxylic acids in the asphalt with carbonates in the aggregate. High molecular weight magnesium and calcium salts are relatively hydrophobic (water repelling) and are very insoluble in water. Sodium salts, being more soluble

(and, in fact, being surfactants), lead to stripping. Further, it was shown, in pre-SHRP research, that carboxylic acids in asphalts hydrogen bond very strongly with the hydroxyl groups on siliceous aggregates, thus being highly concentrated on the aggregate surface. However, these hydrogen bonds are highly sensitive to disruption by water, thus accounting, at least in part, for the high sensitivity to moisture damage of pavement mixtures containing siliceous aggregates. Conversion of carboxylic acids of asphalts to insoluble salts (e.g., calcium) prior to use in pavement mixtures should prevent adsorption of the water-sensitive free acids on the aggregates in the first place.

Complicating the picture, in other tests described in chapter 5, water was shown to be incorporated into aged asphalts and to inhibit the normal hardening of the asphalts with time (steric hardening) and to reduce the tackiness or stickiness of asphalts. The decrease in steric hardening is more apparent in asphalts with high carboxylic acid contents, suggesting that water interferes with the polar molecular interactions that stiffen an asphalt with time. Water could thus contribute to early pavement failure by permanent deformation and, because of the loss of tackiness, by fatigue. One might also expect that a pavement laid under wet conditions would be tender and would not set properly. Since petroleum stocks vary widely in acid content, it is almost certain that asphalts from different sources will exhibit different moisture susceptibilities, even if graded the same by the Superpave® specification.

Although the effects of water are not completely understood, most appear detrimental to pavement performance. As expected from general principles of physical chemistry, water interacts or reacts most strongly with highly polar species in both aggregates and asphalts. Further work is needed, but it appears that selection of aggregates with high surface concentrations of calcium and magnesium will mitigate stripping. However, even if a good aggregate selection is made, there is a balance in the asphalt between the need for carboxylic acids for good aggregate binding and the sensitivity of carboxylic acids to water, resulting in poor performance. Ideally, all carboxylic acids might be bound to the aggregate as insoluble salts, leaving none susceptible to water. Alternatively, excess acids might be tightly bound into associations (asphaltenes and resins) surrounded and protected by a hydrophobic layer (neutrals). Protection from water might thus depend on the proper chemical component balance in the asphalt binder after taking into account interactions with the aggregate. Achievement of this "correct balance" in each and every asphalt batch, although desirable, would be operationally tedious, very expensive, and not at all practical. However, one additional specification that would be met easily would be to remove surface activity from *all* asphalts, at least to a first practical approximation. This is necessary because, as stated earlier, sodium and/or potassium salts of petroleum carboxylic acids show significant surface activity. When pavement containing surface active materials is wet and is subjected to the mechanical action of traffic, it is predictable that the surface activity of the sodium carboxylates (soaps) in the asphalt will help scrub the oil (asphalt) away from the rock the same way soaps and detergents (surface active agents) scrub oil from any surface.

The practical, perhaps conservative, solution to the above described historical problem is to convert all acidic materials in asphalt to water-insensitive (non-surface active) calcium salts at the time of production. This would require a lime treatment step at the refinery. Some

refineries do this today. The recommendation here is that conversion of acids to calcium salts be made a universal requirement. The method to ensure that all acids are converted to calcium salts is straightforward. The first step requires verification that no free acids remain, a half-hour procedure by either IR spectroscopy or by NAPT. The second step is to ensure that the total calcium content equals (or exceeds) the total sodium plus potassium chemical equivalent content. This can be achieved several ways. One example is by atomic absorption spectroscopy, which is an inexpensive, fast, and common technique available in most chemical analytical laboratories. A note of caution: what is recommended here is NOT equivalent to lime treatment of aggregate. The process recommended here reduces moisture susceptibility of the whole asphalt rather than just at the interface. Lime treatment of aggregate may still be desirable.

Separately, in chapter 3, the use of an ESEM has shown clearly that adhesion of asphalt to aggregate differs sharply with source after about 10 freeze-thaw cycles. Adhesion is not addressed by the Superpave® binder specification. While 10 days of freeze-thaw cycling is totally impractical as a specification method to determine the loss of adhesion, there is no particular evidence to say freeze-thaw cycling could not be speeded up to a more acceptable test requiring a few hours. This should be investigated. If the results of rapid freeze-thaw cycling are similar to the day-at-a-time freeze-thaw cycling, then a practical test to distinguish among adhesion levels should follow readily. A probable configuration is a measure of failure stress of a standardized asphalt-aggregate fixture fitted with a standard aggregate (mineral surface) after, say 10 rapid freeze-thaw cycles. While somewhat empirical, this addresses the same type of problem for asphalt alone (asphalt is the test material and the only variable) that the 15-cycle Lottman test does for whole concrete. The distinction of serviceability brought to the system by asphalt will have been measured.

PERMANENT DEFORMATION

This failure mode, sometimes called rutting, can result from base or subbase failure, pavement layers that are too thin for the applied loads, poor mix design, or from insufficient binder stiffness at high use temperatures. With better designed highways and with better mix designs, it is hoped that this failure mode will appear less frequently in the future. Proper design, however, does not dismiss the need for proper binder selection. The problem, as is often the case, is obtaining adequate high temperature performance while maintaining good low temperature properties.

The asphalt chemical and rheological models posed herein and the supporting research have shown that low temperature properties are controlled by the more fluid maltene or SEC Fraction-II solvent-type material in the asphalt. By adjusting the molecular weight and polarity of this solvent-like material, the low temperature performance limit of the asphalt can be varied. To get good (stiffer) high temperature properties while maintaining the low temperature properties, the polarity of the solvent material must increase as the asphalt temperature increases. This increasing polarity balances some of the normal reduction in viscosity as temperature is increased. The temperature-dependent release of polar species (resins) from

polar associations (asphaltenes) can accomplish this feat. Again, a proper balance of chemical species and molecular interactions is required to obtain an optimally performing asphalt binder. Now comes the question: Is there a fast, user-friendly (practical) method to predict the level of balance of polars and neutrals under roadway service conditions? Stated another way: Is there a practical method to predict high temperature stiffness under service conditions? Note that this says service conditions, which means a measure of stiffness of thin films of asphalt on aggregate, not stiffness of bulk asphalt. Two methods (aggregate sliding plate and mastic penetration) that address the above questions are reported in chapter 5 and both give similar results. The chemical composition of asphalt is responsible for significant variability of in-service stiffness, even for asphalts that are graded by Superpave® as being alike. While the sliding plate method is probably more informative, the mastic penetration test is simpler to conduct. However, either is sufficiently user-friendly that it could be made into a specification method rather easily. Scholz and Brown, AAPT [1996], have made a similar point using a rheometer fitted with an aggregate plate. The main point is that there is an aggregate-induced control of asphalt stiffness under service conditions. It is measurable by user-friendly methods.

Stiffness of asphalt in pavement is generally considered to affect rutting, as evidenced by incorporation of this idea into the Superpave® binder specification. If this is correct, it is recommended that a measure of in-service asphalt stiffness be made by one of the methods that simulates in-service conditions. Further, the simulated in-service stiffness (rather than bulk stiffness) should constitute the acceptance criterion for the high temperature specification. Clearly there would need to be a standard aggregate (mineral) selected to produce a universal test. However, there is another benefit to choosing asphalts by their in-service high temperature stiffness that could be implemented readily. In a majority of cases, the aggregate source for a particular job is specified well before asphalt is purchased. Therefore, asphalt selection could be made using the actual aggregate to be used in a job. Clearly, this would likely cause any given asphalt to be graded differently from one job site to another. This latter "additional benefit" may not be at all practical, but certainly a universal in-service asphalt thin-film stiffness gradation would be a very practical specification and would be more predictive of expected performance than the current method.

FATIGUE

Fatigue is perhaps the most difficult failure mechanism to define. No doubt there are many factors that contribute to loss of serviceability in roadways categorized under the general heading of fatigue. It goes without saying that an excessive traffic load for any given design will accelerate fatigue failure. Certainly, a loss of strength resulting from the action of moisture, essentially equivalent to underdesign, would result in fatigue and/or permanent deformation. However, the effects of water have already been discussed.

One material-related property that also most likely contributes to fatigue, especially in thin pavements, is the loss of flexibility that results from embrittlement. Chapter 4 discusses the subject of oxidation extensively. In that chapter it is clear that the physical property changes resulting from oxidative aging vary significantly with source. The propensity to oxidize and

age-harden to some maximum allowed value (not just the minimum value, which is part of the current specification) is readily predicted by two methods. The first is an extended PAV test; extended in aging time over what is called for in the current specification. However, that is too time consuming and a surrogate is needed. The reader is reminded that a faster version of the PAV using a microwave method is being investigated at the present time, but is not yet a proven method. The results of the microwave aging technique are described in Volume II, method 6. If it is successful, the microwave aging technique could become the method of choice. On the other hand, a fully developed, user-friendly, fast and operator-independent version of the Heithaus method, described in chapter 1 and in Volume II, method 1, has been developed. This method measures a level of compatibility (between polars and neutrals) within an asphalt. A high level of self-compatibility in asphalt has been shown to be resistant to hardening with oxidation. It is recommended here that such a test be applied to tank asphalts to predict the relative rate of embrittlement.

SUMMARY

Each of the above failure modes is driven by asphalt composition to a greater or lesser extent. The result is that asphalts graded alike by a set of bulk physical property measurements may still perform differently, because of differential changes that occur from bulk asphalt to asphalt in service conditions. New methods, to elucidate the differential changes that occur in bulk asphalts that are placed in service environments, have been posed throughout the previous chapters and summarized above. The next major effort is to validate the respective utility of each method when observed pavement distress is used as the "measuring stick" of performance. Thereafter, the significant predictors can be used to formulate performance prediction tests that add to the prediction capability of the current Superpave® binder specification.

Table 8-1. Amount of flexible aliphatic carbons in SHRP core asphalts at 23°C using cross polarization-magic angle spinning-dipole dephasing NMR (contact time = 0.5 ms).

Asphalt	Carbon, [1] mass %	Fraction of all carbons that are aliphatic[2] (f_{al}^{C})	Fraction of aliphatic carbons that are flexible (f_{al}^{C}, Flex)	Flexible aliphatic carbon, mass % of whole asphalt
AAA-1	84.2	0.721	0.59 (0.55) [3]	35.8 (33.1) [3]
AAB-1	82.3	0.688	0.58	32.6
AAC-1	86.5	0.722	0.53	33.2
AAD-1	81.6	0.766	0.54	33.7
AAF-1	84.5	0.672	0.48	27.1
AAG-1	85.6	0.710	0.47	28.6
AAK-1	80.7	0.738	0.61	36.4
AAM-1	86.7	0.741	0.49	31.6

[1,2] See reference [Jennings 1993]

[3] Values in parentheses are repeat experiments

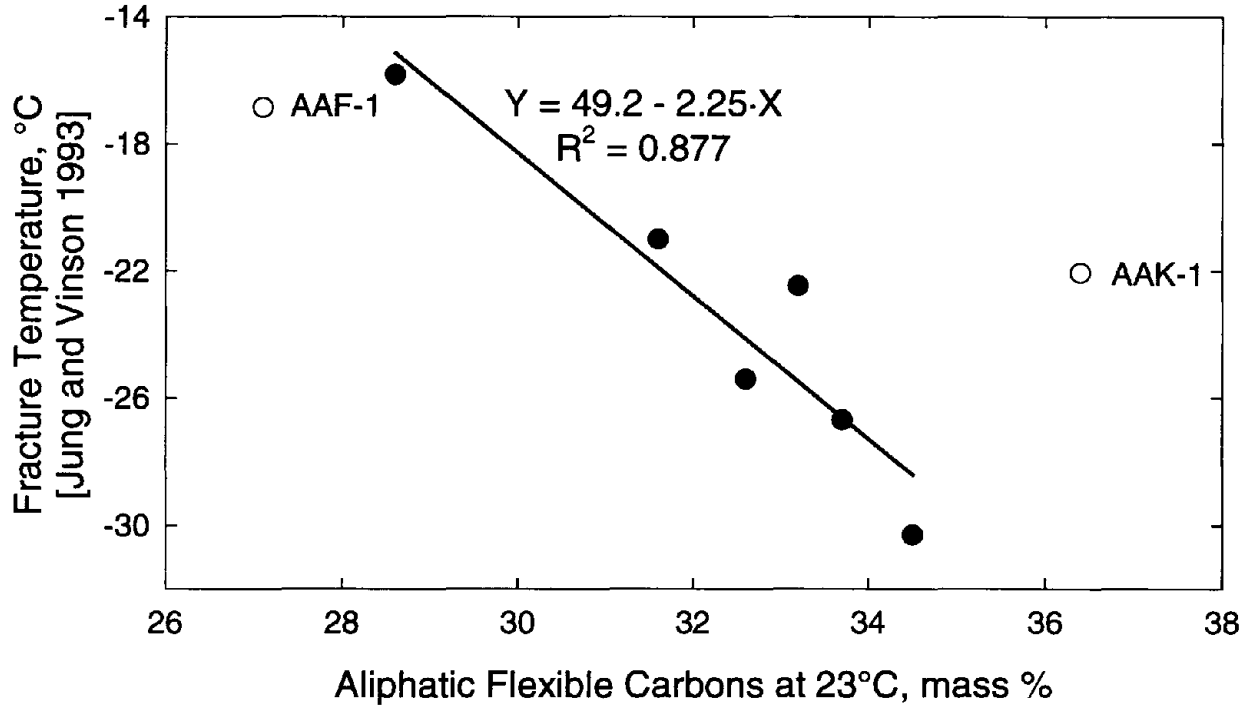

Figure 8-1. A plot of fracture temperature versus flexible aliphatic carbon content.

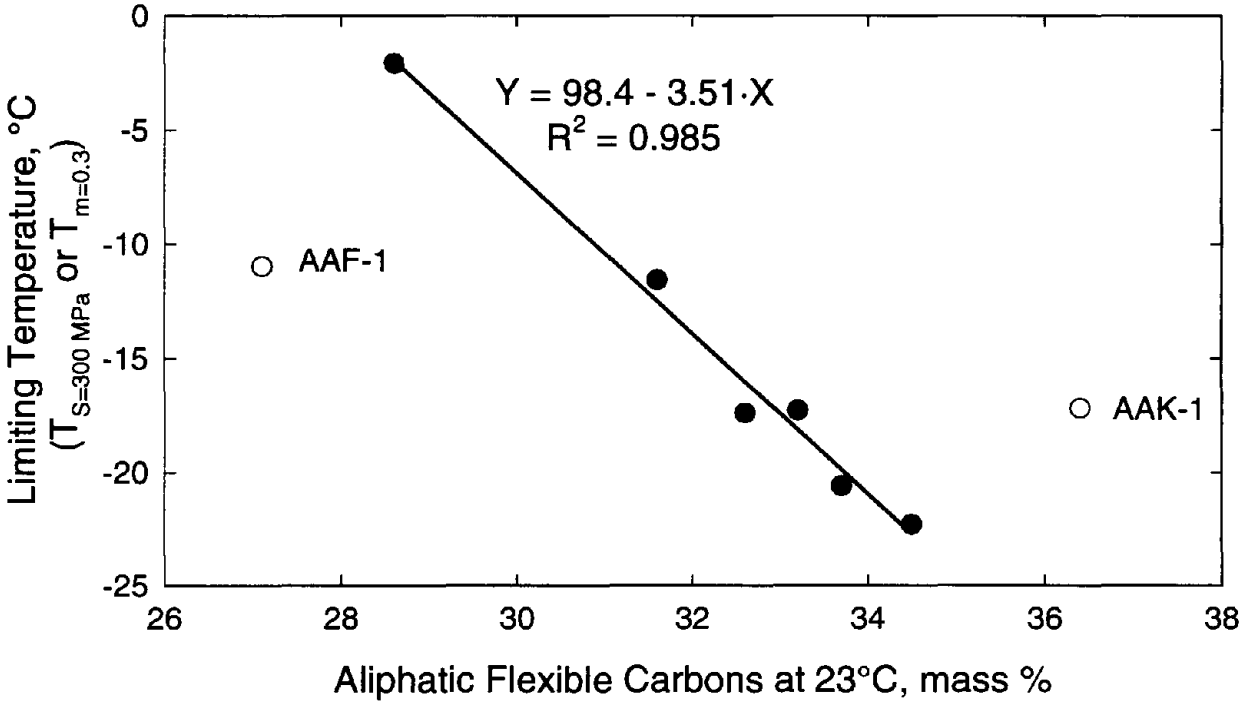

Figure 8-2. A plot of the limiting stiffness temperature versus flexible aliphatic carbon content.

REFERENCES

Anderson, D. A., M. Marasteanu, C. Antle, and T. Ruscitti, 1996, Relationship of SHRP Asphalt Binder Properties to Performance: Draft of Final Report, FHWA Contract DTFH-61-92-C-00170.

Jennings, P. W., 1993. In *SHRP-A-335, Binder Characterization and Evaluation by Nuclear Magnetic Resonance Spectroscopy*. Strategic Highway Research Program, National Research Council, Washington, D. C.

Jung, D., and T. S. Vinson, 1993, Thermal Stress Restrained Specimen Test to Evaluate Low-Temperature Cracking of Asphalt-Aggregate Mixtures. *Transportation Research Record* 1417, p. 12.

Mark, J. E., A. Eisenberg, W. W. Graessley, L. Mandelkern, E. T. Samulski, J. L. Koenig, and G. D. Wignall, 1993, *Physical Properties of Polymers*, 2nd Ed. American Chemical Society, Washington, DC, Chapter 3.

Scholz, T. V., and S. F. Brown, 1996, Rheological Characterization of Bitumen in Contact with Mineral Aggregate. *Journal of the Association of Asphalt Paving Technologists*, 65: 357-384.

CHAPTER 9: VALIDATION

The validation effort in this project is best understood as two rather specific approaches. The first effort was to apply performance predictive methods, developed during this project and the SHRP, to asphalts that had been collected during SHRP. The objective was to test, i.e., to confirm or refute the validity of various new performance predictive analyses (methods). Many methods were tested to a greater or lesser extent and the results are discussed in previous chapters. These validations are not reiterated here.

The second major effort is ongoing and is designed to use observed pavement performance as the "measuring stick" for the validity of performance prediction methods. The principal objective, of using real (observed) pavement performance for validation of newly developed predictive methods, is to elucidate how much influence the variations in asphalt composition exert on performance when asphalt is performing in actual service conditions. Ideally, one would like to compare a multiplicity of roadway sections that are totally alike, except for the source of asphalt. This will expose the composition-related performance characteristics that cannot be determined by physical property tests. Totally alike, except for asphalt source, means that all asphalts meet the same physical property grade (PG or other grading system) except that two, or preferably more than two, sources of asphalt are used in a continuous stretch of roadway, and each asphalt is used to build a well separated and well identified section of roadway. Further, totally alike means the aggregate composition and gradation, design, construction, traffic, age, and climate are "identical" for all sections. Further still, original samples of all asphalts used in such a roadway must be available. Original asphalt samples are needed, because any useful method must predict the expected performance from the point at which the asphalt is purchased, i.e., as the asphalt is delivered from the refinery (original material).

This type of validation effort is especially useful when correlating predictive methods with specific failures that are not readily confused with other types of failure. For example, low temperature cracking appears to be asphalt dependent. The data given in chapter 3 (physical hardening measured by NMR and modulated DSC indicate that significant changes in physical properties of asphalts occur very slowly. The ultimate physical property changes at low temperature in an actual roadway are likely to take several weeks to occur. Hence, materials classified by a rapid method such as the Superpave® binder specification (PG grade) may be graded alike but perform differently. On the other hand, it is possible that a readily measurable compositional property will predict the ultimate low temperature stiffness more accurately than a rapid physical property measurement. To continue this example, the ultimate low temperature stiffness appears to be predicted well by measuring the total crystallizable fraction of an asphalt as measured by MDSC. This method can be altered to allow total crystallization to occur rapidly, i.e., on the same scale of time as bending beam and direct tension measurements. Validation with "real world" samples is needed (and is in progress) to determine which method most accurately predicts observed performance. To summarize, this type of predictive methodology is being sought to predict variations in performance that are not distinguished by any bulk physical property measurement.

Samples of asphalts used in actual roadways (retained original samples) together with performance data are needed. These may best be characterized as LTTP, Special Pavement Section (SPS) experiment 9 [LTPP SPS-9] types of samples. Certainly the LTPP SPS-9 samples will be useful, but are too few to provide an adequate number of examples for effective validation. An effort was launched to find more sites that coincidentally meet the LTPP SPS-9 criteria, but which are not actual SPS-9 sites. To do this, the four LTPP Regional Contractors were employed to search for such sites, and original material supplies, in their four respective regions in the United States and Canada. Three appropriate sites were found by the Northeast LTPP Regional Contractor. All are in Canada. This effort is still in progress with the other three contractors. Separately, the Pennsylvania Transportation Institute was employed to search for the same types of sites in Europe. About six European sites that are appropriate for this study have been identified but, likewise, this search is still in progress. While there are numerous roadway test sites in the United States, Canada, and Europe, the limitation most frequently encountered is that samples of the original asphalts were discarded very soon after construction or were never collected at the construction site.

In summary, original asphalts with established performance histories (relative to each other) are needed to validate new methods that are believed to predict the onset of failure. Again, these "new methods" are to be applied to predict differences in actual roadway performance that cannot be predicted by current specification methods.